MAGNETOENCEPHALOGRAPHY: AN EMERGING NEUROIMAGING TOOL FOR STUDYING NORMAL AND ABNORMAL HUMAN BRAIN DEVELOPMENT

EDITED BY: Christos Papadelis, P. Ellen Grant, Yoshio Okada and Hubert Preissl

PUBLISHED IN: Frontiers in Human Neuroscience

frontiers Research Topics

frontiers

ISSN 1664-8714
ISBN 978-2-88919-658-6
DOI 10.3389/978-2-88919-658-6

About Frontiers

Frontiers is more than just an open-access publisher of scholarly articles: it is a pioneering approach to the world of academia, radically improving the way scholarly research is managed. The grand vision of Frontiers is a world where all people have an equal opportunity to seek, share and generate knowledge. Frontiers provides immediate and permanent online open access to all its publications, but this alone is not enough to realize our grand goals.

Frontiers Journal Series

The Frontiers Journal Series is a multi-tier and interdisciplinary set of open-access, online journals, promising a paradigm shift from the current review, selection and dissemination processes in academic publishing. All Frontiers journals are driven by researchers for researchers; therefore, they constitute a service to the scholarly community. At the same time, the Frontiers Journal Series operates on a revolutionary invention, the tiered publishing system, initially addressing specific communities of scholars, and gradually climbing up to broader public understanding, thus serving the interests of the lay society, too.

Dedication to Quality

Each Frontiers article is a landmark of the highest quality, thanks to genuinely collaborative interactions between authors and review editors, who include some of the world's best academicians. Research must be certified by peers before entering a stream of knowledge that may eventually reach the public - and shape society; therefore, Frontiers only applies the most rigorous and unbiased reviews.
Frontiers revolutionizes research publishing by freely delivering the most outstanding research, evaluated with no bias from both the academic and social point of view.
By applying the most advanced information technologies, Frontiers is catapulting scholarly publishing into a new generation.

What are Frontiers Research Topics?

Frontiers Research Topics are very popular trademarks of the Frontiers Journals Series: they are collections of at least ten articles, all centered on a particular subject. With their unique mix of varied contributions from Original Research to Review Articles, Frontiers Research Topics unify the most influential researchers, the latest key findings and historical advances in a hot research area! Find out more on how to host your own Frontiers Research Topic or contribute to one as an author by contacting the Frontiers Editorial Office: **researchtopics@frontiersin.org**

MAGNETOENCEPHALOGRAPHY: AN EMERGING NEUROIMAGING TOOL FOR STUDYING NORMAL AND ABNORMAL HUMAN BRAIN DEVELOPMENT

Topic Editors:
Christos Papadelis, Boston Children's Hospital, Harvard Medical School, USA
P. Ellen Grant, Boston Children's Hospital, Harvard Medical School, USA
Yoshio Okada, Boston Children's Hospital, Harvard Medical School, USA
Hubert Preissl, Institute for Diabetes Research and Metabolic Diseases, University Hospital of Tuebingen, Germany

Overview of the high-density BabyMEG system (Tristan Technologies Inc., San Diego, USA) that is especially designed for neonates, babies, and toddlers (0 to 3-years-old). The BabyMEG has a two-layers sensor array of 375 magnetometers (270 coils at the first layer; 105 coils at the second layer; 1 cm coil diameter, 16 mm spacing (center to center); coil-helmet gap 8 mm, nine reference channels, 52 cm helmet circumference) and is supported by a 100% liquid helium recycle system. It is located in the Neonatal Intensive Care Unit (NICU) area of Boston Children's Hospital.
Image by Christos Papadelis

Research on the human brain development has seen an upturn in the past years mostly due to novel neuroimaging tools that became available to study the anatomy and function of the developing brain. Magnetic Resonance Imaging (MRI) and Diffusion Tensor Imaging (DTI) are beginning to be used more frequently in children to determine the gross anatomy and structural connectivity of their brain. Functional MRI and Near-Infrared Spectroscopy (NIRS) determine the hemodynamics and electroencephalography (EEG) the electrophysiological functions of the developing human brain. Magnetoencephalography (MEG) complements EEG as the only other technique capable of directly measuring the developing brain electrophysiology. Although MEG

is still being used relatively rarely in pediatric studies, the recent development in this technology is beginning to demonstrate its utility in both basic and clinical neurosciences. MEG seems to be quite attractive for pediatric use, since it measures the human brain activity in an entirely passive manner without possessing any conceivable risk to the developing tissue. MEG sessions generally require minimal patient preparation, and the recordings are extremely well tolerated from children. Biomagnetic techniques also offer an indirect way to assess the functional brain and heart activity of fetuses in humans in utero by measuring the magnetic field outside the maternal abdomen. Magnetic field produced by the electrical activity in the heart and brain of the fetus is not attenuated by the vernix, a waxy film covering its entire skin. A biomagnetic instrument specifically designed for fetal studies has been developed for this purpose. Fetal MEG studies using such a system have shown that both spontaneous brain activity and evoked cortical activity can be measured from outside the abdomen of pregnant mothers. Fetal MEG may become clinically very useful for implementation and evaluation of intervention programs in at-risk populations. Biomagnetic instruments have also been developed for specifically measuring the brain activity in newborns, infants and older children. MEG studies have shown the usefulness of MEG for localizing active regions in the brain and also for tracking the longitudinal maturation of various sensory systems. Studies of pediatric patients are beginning to show interesting functional pathology in autism spectrum disorder, cerebral palsy, epilepsy and other types of neurological and psychiatric disorders (Down syndrome, traumatic brain injury, Tourette syndrome, hearing deficits, childhood migraine). In this eBook, we compile the state of the art MEG and other neuroimaging studies focused on pediatric population in both health and disease. We believe a review of the recent studies of human brain development using MEG is quite timely, since we are witnessing advances not only in the instrumentation optimized for the pediatric population, but also in the research based on various types of MEG systems designed for both human fetuses in utero and neonates and older children.

Citation: Papadelis, C., Grant, P. E., Okada, Y., Preissl, H., eds. (2015). Magnetoencephalography: An Emerging Neuroimaging Tool for Studying Normal and Abnormal Human Brain Development. Lausanne: Frontiers Media. doi: 10.3389/978-2-88919-658-6

Table of Contents

frontiers in Human Neuroscience

EDITORIAL
published: 11 March 2015
doi: 10.3389/fnhum.2015.00127

Editorial on emerging neuroimaging tools for studying normal and abnormal human brain development

Christos Papadelis[1,2]*, *P. Ellen Grant*[1,2,3], *Yoshio Okada*[1,2] and *Hubert Preissl*[4,5]

[1] BabyMEG/EEG facility, Fetal-Neonatal Neuroimaging and Developmental Science Center, Boston Children's Hospital, Boston, MA, USA, [2] Division of Newborn Medicine, Department of Medicine, Boston Children's Hospital, Harvard Medical School, Boston, MA, USA, [3] Department of Radiology, Boston Children's Hospital, Harvard Medical School, Boston, MA, USA, [4] fMEG Center, Institute for Medical Psychology and Behavioural Neurobiology, University of Tuebingen, Tuebingen, Germany, [5] Department of Obstetrics and Gynecology, University of Arkansas for Medical Sciences, Little Rock, AR, USA

Keywords: developmental disabilities, magnetoencephalography (MEG), pediatric neuroscience, pediatric neuroimaging, brain development

Research on human brain development has seen an upturn in the past few years due to increasing use of noninvasive neuroimaging tools for studying the anatomy and function of the developing brain. Here we gathered innovative studies of human brain function and development using magnetic resonance imaging (MRI), near infrared spectroscopy (NIRS) and magnetoencephalography (MEG) with experimental paradigms suitable for pediatric research. These modalities are without significant risk to the developing brain, generally require minimal patient preparation, and are well tolerated by children when performed by experienced teams. A review of recent studies of human brain development using these advanced neuroimaging tools is quite timely, since we are witnessing advances not only in the instrumentation optimized for the pediatric population, but also in research focused on the human fetuses in utero, neonates, and older children. MRI methods such volumetric T1 imaging and Diffusion Tensor Imaging (DTI) are being used more frequently in children to determine the gross anatomy and structural connectivity of the developing brain. Functional MRI and NIRS are being used to assess the hemodynamics of neurovascular responses and functional localization in development (Govindan et al., 2014; Horowitz-Kraus et al., 2014). MEG complements electroencephalography (EEG) as the only other technique capable of directly measuring the developing brain neural activity in an entirely passive manner with MEG being superior to EEG in its ability to localize activity during development. MEG and EEG can be used to assess electrophysiological functions of the developing human brain (Edgar et al., 2014). Findings from multiple neuroimaging methods can be combined to answer specific scientific questions regarding pediatric pathology (Brown et al., 2014; Hunold et al., 2014; Papadelis et al., 2014) or typical human brain development. Although MEG is still being used relatively rarely in pediatric studies, recent developments in this technology (Roberts et al., 2014) are beginning to demonstrate its utility in both the basic and clinical neuroscience of brain development (Edgar et al., 2014; Rezaie et al., 2014; Sowman et al., 2014; Taylor et al., 2014). Biomagnetic techniques also offer a direct noninvasive way to assess the functional brain and heart activity of human fetuses in utero. Unlike electric fields, magnetic fields produced by the electrical activity in the heart and brain of the fetus are not attenuated by the vernix, a waxy film covering its entire skin. Biomagnetic instruments specifically designed for fetal studies have been developed for this purpose. Fetal MEG studies using such a system have shown that both spontaneous brain activity and evoked cortical activity can be measured from outside the abdomen of pregnant mothers (Muenssinger et al., 2013). Fetal MEG and Magnetocardiography (MCG) may become clinically very useful for implementation and evaluation of intervention programs in at-risk populations. Biomagnetic instruments have also been developed for specifically measuring the brain activity in newborns,

OPEN ACCESS

Edited and reviewed by:
Hauke R. Heekeren, Freie Universität Berlin, Germany

***Correspondence:**
Christos Papadelis, christos.papadelis@childrens.harvard.edu

Received: *07 January 2015*
Accepted: *23 February 2015*
Published: *11 March 2015*

Citation:
Papadelis C, Grant PE, Okada Y and Preissl H (2015) Editorial on emerging neuroimaging tools for studying normal and abnormal human brain development. Front. Hum. Neurosci. 9:127. doi: 10.3389/fnhum.2015.00127

infants, and older children (Roberts et al., 2014). MEG studies have shown the usefulness of MEG for localizing active regions in the brain and also for tracking the longitudinal maturation of various sensory systems. Studies of pediatric patients are beginning to show interesting functional pathology in autism spectrum disorder (Doesburg et al., 2013; Edgar et al., 2014), cerebral palsy (Papadelis et al., 2014), epilepsy (Hunold et al., 2014; Khan et al., 2014; Tanaka and Stufflebeam, 2014), and other neurological and psychiatric disorders (Down syndrome, traumatic brain injury, Tourette syndrome, hearing deficits, childhood migraine) (Larson and Lee, 2014). The current research topic gathers studies from different research groups studying the human brain development by using advanced neuroimaging tools. Neuroimaging can offer critical information about both normal as well as abnormal human brain development. Most of the currently available tools are designed for adult use. Hardware and methods especially tailored for pediatric use remain under continual refinement. Issues relating to compliance are now mitigated by new software developments such as head motion tracking and motion correction. Such technological advancements to address specific issues germane to pediatric populations will likely promote wider adoption of neuroimaging for both clinical as well as research purposes.

References

Brown, T. T., Erhart, M., Avesar, D., Dale, A. M., Halgren, E., and Evans, J. L. (2014). Atypical right hemisphere specialization for object representations in an adolescent with specific language impairment. *Front. Hum. Neurosci.* 8:82. doi: 10.3389/fnhum.2014.00082

Doesburg, S. M., Vidal, J., and Taylor, M. J. (2013). Reduced theta connectivity during set-shifting in children with autism. *Front. Hum. Neurosci.* 7:785. doi: 10.3389/fnhum.2013.00785

Edgar, J. C., Lanza, M. R., Daina, A. B., Monroe, J. F., Khan, S. Y., Blaskey, L., et al. (2014). Missing and delayed auditory responses in young and older children with autism spectrum disorders. *Front. Hum. Neurosci.* 8:417. doi: 10.3389/fnhum.2014.00417

Govindan, R. B., Massaro, A. N., Andescavage, N. N., Chang, T., and du Plessis, A. (2014). Cerebral pressure passivity in newborns with encephalopathy undergoing therapeutic hypothermia. *Front. Hum. Neurosci.* 8:266. doi: 10.3389/fnhum.2014.00266

Horowitz-Kraus, T., Vannest, J. J., Gozdas, E., and Holland, S. K. (2014). Greater utilization of neural-circuits related to executive functions is associated with better reading: a longitudinal fMRI study using the verb generation task. *Front. Hum. Neurosci.* 8:447. doi: 10.3389/fnhum.2014.00447

Hunold, A., Haueisen, J., Ahtam, B., Doshi, C., Harini, C., Camposano, S., et al. (2014). Localization of the epileptogenic foci in tuberous sclerosis complex: a pediatric case report. *Front. Hum. Neurosci.* 8:175. doi: 10.3389/fnhum.2014.00175

Khan, S., Lefèvre, J., Baillet, S., Michmizos, K. P., Ganesan, S., Kitzbichler, M. G., et al. (2014). Encoding cortical dynamics in sparse features. *Front. Hum. Neurosci.* 8:338. doi: 10.3389/fnhum.2014.00338

Larson, E., and Lee, A. K. C. (2014). Potential use of MEG to understand abnormalities in auditory function in clinical populations. *Front. Hum. Neurosci.* 8:151. doi: 10.3389/fnhum.2014.00151

Muenssinger, J., Matuz, T., Schleger, F., Draganova, R., Weiss, M., Kiefer-Schmidt, I., et al. (2013). Sensitivity to auditory spectral width in the fetus and infant—an fMEG study. *Front. Hum. Neurosci.* 7:917. doi: 10.3389/fnhum.2013.00917

Papadelis, C., Ahtam, B., Nazarova, M., Nimec, D., Snyder, B., Grant, P. E., and Okada, Y. (2014). Cortical somatosensory reorganization in children with spastic cerebral palsy: a multimodal neuroimaging study. *Front. Hum. Neurosci.* 8:725. doi: 10.3389/fnhum.2014.00725

Rezaie, R., Narayana, S., Schiller, K., Birg, L., Wheless, J. W., Boop, F. A., and Papanicolaou, A. C. (2014). Assessment of hemispheric dominance for receptive language in pediatric patients under sedation using magnetoencephalography. *Front. Hum. Neurosci.* 8:657. doi: 10.3389/fnhum.2014.00657

Roberts, T. P. L., Paulson, D. N., Hirschkoff, E., Pratt, K., Mascarenas, A., Miller, P., et al. (2014). Artemis 123: development of a whole-head infant and young child MEG system. *Front. Hum. Neurosci.* 8:99. doi: 10.3389/fnhum.2014.00099

Sowman, P. F., Crain, S., Harrison, E., and Johnson, B. W. (2014). Lateralization of brain activation in fluent and non-fluent preschool children: a magnetoencephalographic study of picture-naming. *Front. Hum. Neurosci.* 8:354. doi: 10.3389/fnhum.2014.00354

Tanaka, N., and Stufflebeam, S. M. (2014). Clinical application of spatiotemporal distributed source analysis in presurgical evaluation of epilepsy. *Front. Hum. Neurosci.* 8:62. doi: 10.3389/fnhum.2014.00062

Taylor, M. J., Doesburg, S. M., and Pang, E. W. (2014). Neuromagnetic vistas into typical and atypical development of frontal lobe functions. *Front. Hum. Neurosci.* 8:453. doi: 10.3389/fnhum.2014.00453

Conflict of Interest Statement: The authors declare that the research was conducted in the absence of any commercial or financial relationships that could be construed as a potential conflict of interest.

frontiers in
HUMAN NEUROSCIENCE

ORIGINAL RESEARCH ARTICLE
published: 12 September 2014
doi: 10.3389/fnhum.2014.00725

Cortical somatosensory reorganization in children with spastic cerebral palsy: a multimodal neuroimaging study

Christos Papadelis[1,2]*†, Banu Ahtam[1,2†], Maria Nazarova[3,4], Donna Nimec[5], Brian Snyder[5], Patricia Ellen Grant[1,2,6] and Yoshio Okada[1,2]

[1] Fetal-Neonatal Neuroimaging and Developmental Science Center, Boston Children's Hospital, Harvard Medical School, Boston, MA, USA
[2] Division of Newborn Medicine, Department of Medicine, Boston Children's Hospital, Harvard Medical School, Boston, MA, USA
[3] Department of Neurorehabilitation and Physiotherapy, Research Center of Neurology, Moscow, Russia
[4] Centre for Cognition and Decision Making, Faculty of Psychology, Higher School of Economics, Moscow, Russia
[5] Department of Orthopaedic Surgery, Boston Children's Hospital, Harvard Medical School, Boston, MA, USA
[6] Department of Radiology, Boston Children's Hospital, Harvard Medical School, Boston, MA, USA

Edited by:
Hubert Preissl, University of Tübingen, Germany

Reviewed by:
Giancarlo Zito, San Giovanni Calibita Fatebenefratelli Hospital, Italy
Douglas Rose, Cincinnati Children's Hospital Medical Center and University of Cincinnati, USA

***Correspondence:**
Christos Papadelis, Boston Children's Hospital, Harvard Medical School, BabyMEG Facility, 9 Hope Avenue, Waltham, MA 02453, USA
e-mail: christos.papadelis@childrens.harvard.edu

† Christos Papadelis and Banu Ahtam are the co-first authors.

Although cerebral palsy (CP) is among the most common causes of physical disability in early childhood, we know little about the functional and structural changes of this disorder in the developing brain. Here, we investigated with three different neuroimaging modalities [magnetoencephalography (MEG), diffusion tensor imaging (DTI), and resting-state fMRI] whether spastic CP is associated with functional and anatomical abnormalities in the sensorimotor network. Ten children participated in the study: four with diplegic CP (DCP), three with hemiplegic CP (HCP), and three typically developing (TD) children. Somatosensory (SS)-evoked fields (SEFs) were recorded in response to pneumatic stimuli applied to digits D1, D3, and D5 of both hands. Several parameters of water diffusion were calculated from DTI between the thalamus and the pre-central and post-central gyri in both hemispheres. The sensorimotor resting-state networks (RSNs) were examined by using an independent component analysis method. Tactile stimulation of the fingers elicited the first prominent cortical response at ~50 ms, in all except one child, localized over the primary SS cortex (S1). In five CP children, abnormal somatotopic organization was observed in the affected (or more affected) hemisphere. Euclidean distances were markedly different between the two hemispheres in the HCP children, and between DCP and TD children for both hemispheres. DTI analysis revealed decreased fractional anisotropy and increased apparent diffusion coefficient for the thalamocortical pathways in the more affected compared to less affected hemisphere in CP children. Resting-state functional MRI results indicated absent and/or abnormal sensorimotor RSNs for children with HCP and DCP consistent with the severity and location of their lesions. Our findings suggest an abnormal SS processing mechanism in the sensorimotor network of children with CP possibly as a result of diminished thalamocortical projections.

Keywords: cerebral palsy, cortical reorganization, somatosensory processing, magnetoencephalography, MR tractography, resting-state functional MRI

INTRODUCTION

Cerebral palsy (CP) is a well-recognized group of motor and postural neurodevelopmental disorders beginning in early childhood and persisting through the lifespan. CP causes serious motor impairments often accompanied by disturbances of sensation and perception (Bax et al., 2005) and is the most common cause of physical disability in early childhood (Krageloh-Mann and Cans, 2009). Almost 3.6 out of every 1000 children born in the US suffer from CP and the prevalence of the disorder is on the rise worldwide (Yeargin-Allsopp et al., 2008). CP involves axonal and neuronal loss in cerebral white and gray matter, reduction in thalamocortical connections (Hoon et al., 2002, 2009; Thomas et al., 2005; Nagae et al., 2007), and comparable loss in subcortical structures (Volpe, 2009). Depending on the location, extent, and timing of the insult, clinical symptoms vary largely.

Spastic CP (SCP) is the most common form of CP that frequently alters the normal development of the somatosensory (SS) system. SCP is usually presented with increased muscle tone, hyperreflexia, and persistence of primitive reflexes (Tomlin, 1995). Aside from motor and postural impairments, children with SCP frequently experience sensory deficits such as altered tactile, proprioceptive, kinesthetic, and pain awareness (Van Heest et al., 1993; Cooper et al., 1995; Krumlinde-Sundholm and Eliasson, 2002; Sanger and Kukke, 2007; Wingert et al., 2009; Riquelme et al., 2011). Recent functional neuroimaging studies have reported altered SS processing in SCP individuals as measured by SS-evoked potentials or fields in terms of amplitude, morphology, frequency power, or somatotopy (Riquelme and Montoya, 2010; Kurz and Wilson, 2011; Teflioudi et al., 2011; Guo et al., 2012; Nevalainen et al., 2012; Pihko et al., 2014; Riquelme et al., 2014). In a recent

magnetoencephalography (MEG) study, Pihko et al. (2014) found that suppression and rebound of alpha and beta cortical activity to contralateral stimulation were smaller in the lesioned compared to the intact hemisphere in hemiplegic CP (HCP) children, while they did not find any difference between the hemispheres of typically developing (TD) children. A functional MRI study, which investigated tactile shape and grating discrimination, found decreased cortical activity in the parietal and frontal cortical SS regions of SCP compared to TD children (Wingert et al., 2010).

Anatomical neuroimaging studies using diffusion tensor imaging (DTI) have provided evidence of significant alterations in white matter fibers connecting to sensory cortex. These studies suggest that CP injuries might be reflective of disruption of sensory as well as motor connections. They also provide evidence of sensory and motor pathway involvement for the motor weakness in CP patients by showing that DTI measures reflect the degree of motor deficits (Hoon et al., 2002, 2009; Thomas et al., 2005; Trivedi et al., 2010). Two DTI studies observed more severe damage in the posterior white matter fibers connecting the thalamus to the sensory cortex than in the descending corticospinal tracts in children with periventricular leukomalacia (PVL) (Hoon et al., 2002) and SCP (Nagae et al., 2007), despite a history and clinical presentation consistent with motor tracts. Compared to TD children, children with CP have been reported to have decreased fractional anisotropy (FA) and increased apparent diffusion coefficient (ADC) values for the motor and sensory tracks (Trivedi et al., 2010); for the affected side of the corticospinal tract (Son et al., 2007; Yoshida et al., 2010); and for the tracks on the side ipsilateral to the periventricular lesion in corticospinal tract, corticobulbar tract, and superior thalamic radiation (Thomas et al., 2005).

Fundamental understanding of sensory function in CP children is extremely important, since SS input is an essential component of motor function, control, and development. Tactile inputs are used to localize and characterize the various qualities of touch, while cutaneous inputs contribute to proprioceptive information for coordinated motor actions (Dijkerman and de Haan, 2007). Both tactile and cutaneous inputs play an important role in the proprioceptive feedback for motor planning and execution (Wingert et al., 2008). Sensibility deficiencies have been correlated with diminished dexterity in the affected hand of CP children with spastic hemiplegia (Van Heest et al., 1993). It has been suggested that in CP there is a loss of coordinated messages from SS to motor areas (Burton et al., 2009), which may lead to deficits in motor coordination (Bax et al., 2005), fine and gross motor function (Himmelmann et al., 2006), and motor control (Ostensjo et al., 2004; Fowler and Goldberg, 2009). Deficits in the processing of SS information may also partially explain the tactile or motor deficits observed in this population (Wingert et al., 2008; Burton et al., 2009).

Somatosensory inputs are also important for the development of motor system; early learning in infants is driven largely by SS inputs. Moreover, the ability to process and utilize sensory information for motor planning control develops through the childhood (Riquelme and Montoya, 2010; Gordon et al., 2013). Thus, defective tactile/cutaneous feedback may worsen motor planning and performance (Gordon et al., 2013). CP children with even mild motor impairments have demonstrated more variable and redundant fingertip forces while adjusting to objects compared to TD, presumably, at least partly, due to imperfect proprioceptive feedback (Gordon et al., 2013). It is possible that there is also an opposite mechanism: deficits of spontaneous movements in CP infants (Prechtl, 1997; Prechtl et al., 1997; Hadders-Algra, 2004; Einspieler and Prechtl, 2005) may account for musculoskeletal tissue changes and thus contribute to aberrant sensory inputs to the brain (Coq et al., 2008). Understanding the pathophysiology mechanisms underlying the sensory impairments, specifically tactile, in CP children is essential to the design of effective therapeutic interventions.

In the present study, we investigated with three different neuroimaging modalities [pediatric MEG, DTI, and resting-state functional MRI (rs-fMRI)] whether SCP is associated with functional and anatomical abnormalities in the sensorimotor network. To our best knowledge, this is the first study that combines findings from multiple neuroimaging techniques for examining the anatomical and functional integrity of the SS and motor systems in children with SCP. Somatosensory-evoked fields (SEFs) in response to pneumatic stimulation of the fingertips were recorded with pediatric MEG and the underlying generators were localized by using minimum norm estimates (MNE) (Hamalainen and Ilmoniemi, 1994). MEG was used because it is able to elucidate the dynamic spatiotemporal characteristics of SS cortical activation (Lin et al., 2006a) with its excellent temporal and good spatial accuracy (Hämäläinen et al., 1993; Papadelis et al., 2009). So far, there are very few MEG studies reporting functional abnormalities in the SS cortex of CP children (Kurz and Wilson, 2011; Nevalainen et al., 2012; Pihko et al., 2014). With MEG, we tested our hypotheses that the SEFs will be abnormal and the primary cortical SS representation areas will present an altered somatotopy in the affected (or more affected) compared to the intact (or less affected) hemisphere of CP children, and compared to both hemispheres of TD children. The integrity of the thalamocortical tracts from thalamus to the pre-central and post-central gyri was examined in the same participants by using DTI. We expected a disruption in the thalamocortical tracts projecting from thalamus to the pre-central and post-central gyri in children with CP. The integrity of the sensorimotor resting-state network (RSN) functional architecture was also assessed by measuring spontaneous low-frequency fluctuations (<0.1 Hz) in the blood oxygen level-dependent (BOLD) signal by using an independent component analysis (ICA) method. We hypothesized that the cortical networks linked to areas within the SS and motor cortices would be either absent or at least abnormal in children with CP.

MATERIALS AND METHODS

PARTICIPANTS

Ten right-handed children participated in the study: four children with diplegic CP (DCP) (two males and two females, mean age: 11.8 years, SD 5.4 years), three children with HCP (two males and one female, mean age: 12.6 years, SD 5.8 years), and three age-matched TD children (one male and two females, mean age: 11.8 years, SD 5.2 years). CP patients were recruited from the Cerebral Palsy Clinic at Boston Children's Hospital (BCH), Harvard Medical School, according to the following inclusion criteria: (1) evaluation by a pediatric neurologist and diagnosis of DCP

or HCP, (2) absence of any genetic syndrome diagnosis, (3) no history of trauma or brain operation, and (4) classified as high-functioning in level I or II at the Gross Motor Function Classification System (GMFCS) (Palisano et al., 1997). TD comparison children had no history of neurological disorder or brain injury. None of the participants were under psychoactive or myorelaxant medications during the experiment. **Table 1** presents the demographic, clinical, and conventional MRI data for all participants. All participants were free of metallic objects or implant devices, and cooperative to understand and follow simple instructions. This study was approved by the local institutional review board and informed written consent was obtained from the parents of all participants.

MEG RECORDINGS

SEFs were elicited by tactile stimulation of the D1, D3, and D5 (thumb, middle, and little finger) of both hands. The stimuli were delivered through thin elastic membranes (with a diameter of 1 cm), surrounded by a plastic outer shell, which were attached to the distal, volar parts of the three digits. Membranes were inflated by an air pressure pulse through a rigid plastic tube (Somatosensory Stimulus Generator, 4D NeuroImaging Inc., San Diego, CA, USA) tapping gently the skin at the tip of each digit. The pressure of the tactile stimulator rose to 0.10 bar overpressure in 10 ms. Tactile stimuli were delivered to the three digits in a pseudorandom order with an interstimulus interval (ISI) of 1.5 ± 0.5 s. Each finger received in total 180 stimuli in three runs. Each run lasted ~6 min. The measurements were carried out in the BabyMEG Facility at BCH (Waltham, MA, USA). MEG signals were recorded inside a single-layer magnetically shielded room (MSR) (Imedco, Hägendorf, Switzerland) with a 76-axial gradiometers device (BabySQUID Tristan Technologies, Inc., San Diego, CA, USA). The sensor array in BabySQUID consists of 74 active gradiometers (10 mm pickup coil diameter, 30 mm baseline, and 12–14 mm coil center-to-coil center spacing) with a gap between each pickup coil and scalp of ~7–10 mm. The sensor array is ellipsoidal in shape with a radius of curvature of 7.5 cm along the coronal section, 10 cm along the sagittal section (Okada et al., 2006), and a depth of ~2 cm resulting in a coverage area of ~265 cm^2. The recording signal bandwidth was 0–341.33 Hz with a sampling rate of 1024 Hz. Vertical and horizontal electrooculograms (EOGs) and electrocardiogram (ECG) were simultaneously recorded using bipolar electrodes.

During the recordings, the children were comfortably lying down on the bed with the hemisphere contralateral to the stimulated hand placed on the headrest in such a way that the sensor array was covering the scalp area above the pre-central and post-central gyri. We focused our recordings on the contralateral hemisphere because previous evidence in CP children present that the SS representation remains in the hemisphere contralateral to the affected hand in contrast to the motor system (Gerloff et al., 2006; Staudt et al., 2006; Wilke and Staudt, 2009). The children kept their head still during the recordings with eyes open gazing at a fixation point on the wall. Prior to each run an anatomical coordinate system was defined by digitizing 15 points marked on the participant's face. More details about the followed coregistration procedure can be found in Papadelis et al. (2013).

MRI/DTI ACQUISITION

MRI data were collected with a 3-T Siemens Tim Trio MR scanner at BCH. The data from one child with DCP (DCP4) were excluded due to excessive motion artifact. The scans were performed without sedation or medication, while the children were awake. The imaging protocol consisted of structural and diffusion-weighted sequences. The structural sequence was a T1-weighted high-resolution magnetization-prepared rapid-acquisition gradient-echo (MPRAGE) acquisition, which used volumetric echo-planar imaging (EPI) navigators for real time motion correction [voxel size (mm) $= 1 \times 1 \times 1$; field of view (FOV) = 19.2–22.0 cm; echo time (TE) = 1.74 ms; repetition time (TR) = 2520 ms; flip angle = 7°]. The diffusion sequence (prescribed axially) used echo-planar (EP) readouts [voxel

Table 1 | Demographics and anatomical information.

Participant	Age	Gender	GMFCS	Affected side	Brain MRI
TD 1	12 years	F	N/A	N/A	Normal
TD 2	17 years	F	N/A	N/A	Normal
TD 3	6.5 years	M	N/A	N/A	Normal
HCP 1	17 years	M	2	Right	Chronic encephalomalacia due to left middle cerebral artery infarct
HCP 2	15 years	F	2	Left	Perinatal right periventricular white matter injury
HCP 3	6 years	M	1	Right	Subtle gliosis in the left central semiovale extending to the corona radiata
DCP 1	12 years 9 months	F	2	Both (right more)	Slight asymmetry of the left lateral ventricle
DCP 2	12 years	F	2	Both (right more)	Bilateral periventricular white matter injury
DCP 3	16 years	M	1	Both (left more)	No gross MRI abnormality
DCP 4	4 years 9 months	M	2	Both (right more)	Periventricular leucomalacia (PVL)[a]

[a] *MRI data were excluded due to excessive motion artifact. PVL diagnosis was given based on previous acquired MRI not available to this study.*

size (mm) = 2.0 × 2.0 × 2.0; FOV = 11–12.8 cm; TE = 88 ms; TR = 8320–10934 ms; flip angle = 90°; 30 gradient diffusion directions at $b = 1000$ s/mm^2; 10 acquisitions with $b = 0$ s/mm^2].

rs-fMRI RECORDINGS

The rs-fMRI data were collected with the same scanner at BCH after collecting the T1 and DTI sequences. The data from one child with DCP (DCP4) were excluded due to excessive motion artifact. The participants were asked to stay awake and keep their eyes open. The rs-fMRI sequence used EPI readouts with isotropic voxel sizes of 3 mm × 3 mm × 3 mm, whole brain coverage, TE = 30 ms, TR = 3 s, 47 axial slices, and 160 time series volumes.

ANALYSIS OF EVENT-RELATED MAGNETIC FIELDS

MEG data analysis was performed by using Brainstorm (Tadel et al., 2011), which is documented and freely available for download online under the GNU general public license[1]. The recorded MEG signals were visually inspected for possible artifacts and filtered offline in the frequency band of 1–100 Hz. Trials contaminated by prominent eye movements, blinks, or muscular activity were rejected. The remaining trials were then averaged (approximately 60 trials for each stimulation site) for each separate run from −100 to 400 ms relative to the stimulus onset. Grand averages across all runs were estimated per stimulation site for each participant. There was no significant difference in the number of useful trials between stimulation sites or groups ($p > 0.05$). The peak latency of the first cortical response was visually determined from the grand average butterfly plot for each site and each participant.

SOURCE LOCALIZATION ANALYSIS

An MRI-derived surface model of each participant's brain was initially estimated from the T1-weighted structural volumetric images by using FreeSurfer[2]. For the participant with no MRI, a template MRI from an age-matched child was used. The geometry of the gray–white matter surface was derived with an automatic segmentation algorithm to yield a triangulated model with approximately 270,000 vertices (Dale et al., 1999; Fischl et al., 1999, 2001). For computational purposes, the source space was obtained by decimating the original triangulation to a subset of vertices (~15,000 vertices) with an average of 5 mm distance between nearest dipoles. Each vertex represents a given source space point defined as an equilateral triangle in the tessellation of the cortical surface. To compute the forward model, the overlapping-sphere method was used for each participant that fits one local sphere for each sensor (Huang et al., 1999) and then derives the strength of a set of current dipoles located at the cortical surface. The distributed source model of the MEG signals was then estimated by using the MNE (Hamalainen and Ilmoniemi, 1994). MNE was selected because it does not require explicit *a priori* assumptions about the nature or number of source currents (Hamalainen and Ilmoniemi, 1994). It has been suggested to be the preferred method when analyzing multi-source SS-evoked activations compared to other inverse approaches (Lin et al., 2006a). Using distributed source analysis, the activation at each vertex was estimated at the peak of the first cortical response in the evoked fields obtained for each stimulus site and subject. During the computation of the inverse solution, we followed a previously described data analysis strategy (Hsiao et al., 2013): (i) the source orientations were constrained to be perpendicular to the cortical surface; (ii) a depth weighting algorithm was used to compensate for any bias affecting the superficial sources calculation (Lin et al., 2006b); and (iii) a regularization parameter, $\lambda^2 = 0.33$ was used to minimize numerical instability to reduce the sensitivity of the MNE to noise and to effectively obtain a spatially smoothed solution (Hamalainen and Ilmoniemi, 1994). The noise covariance matrix was computed from empty MSR recordings, which always preceded the actual recording sessions. MNE estimates were averaged across different runs after being coregistered in the same coordinate system. Regions of interest (ROIs) for the MEG analysis were selected as the global maxima of cortical activity at the peak of the first cortical response after the stimuli onset. These ROIs will be referred to from now on as MEG-defined ROIs. Each MEG-defined ROI consisted of 10 neighboring vertices surrounding the vertex with the global maximum activation at the peak of the first cortical response after the stimuli onset. The average size of MEG-defined ROIs was 0.792 ± 0.169 mm. The mean distance of the vertices defining the ROI from the central vertices was 3.4 ± 1.47 mm. Then, the exact location of each MEG-defined ROI was displayed on the anatomical MRI of each individual.

MRI-DEFINED ROIs

T1 and diffusion data were processed with Connectome Mapper (CMP) (Daducci et al., 2012) pipeline, which includes the use of several neuroimaging tools, such as the FreeSurfer[2]. The CMP-generated file ROI_HR_th.nii.gz was used to create volume files for thalamus, pre-central gyrus, and post-central gyrus using the mri_binarize command of FreeSurfer. All three volumes were checked and manually edited in FreeView to ensure correct segmentation. The three volumes and the T1 image were coregistered with the b0 image using 3D Slicer software[3]. The transformed volumes were then imported in TrackVis software[4] as ROIs. They will be referred to from now on as MRI-defined ROIs.

FIBER TRACTOGRAPHY

Diffusion data were processed with Diffusion Toolkit[5] using HARDI/Q-Ball imaging model and second order Runge Kutta propagation algorithm with an angle threshold of 45° and no FA threshold. Fiber tractography was performed with TrackVis software to create fiber tracks that pass through thalamus and post-central gyrus as well as thalamus and pre-central gyrus. Some spurious connections (<3%) were manually removed using TrackVis. Mean number of fibers as well as mean scalar measures of FA, ADC, axial diffusivity (AD), and radial diffusivity (RD) were derived for each fiber track. Data were analyzed separately for the two hemispheres identified as affected (or more affected) and intact (or less affected) hemispheres in CP children, and for right and left hemispheres for TD children.

[1] http://neuroimage.usc.edu/brainstorm
[2] http://surfer.nmr.mgh.harvard.edu/
[3] http://www.slicer.org
[4] http://www.trackvis.org
[5] http://www.trackvis.org/dtk/

RESTING-STATE fMRI

For the rs-fMRI analysis, we followed the same methodology as in Dehaes et al. (2013). Anatomical T1-weighted DICOM images were converted into a 3D NIFTI file format using the *mri_convert* command of FreeSurfer[2]. Then, the T1 image of each participant was manually oriented into Talairach space using the anterior commissure (AC) and posterior commissure (PC) landmarks using FreeView. Brain extraction tool (BET) was used to remove the non-brain tissue from the T1 image (Smith, 2002). Artifact detection for rs-fMRI raw data was performed using Artifact Rejection Tools (ART)[6]. All participants, except for one child with HCP who had three volumes affected by motion, were free of motion artifacts. After the removal of contaminated volumes, the remaining time series were converted into a 4D NIFTI volume file using *mri_convert* command of FreeSurfer. Slice timing correction was applied to the rs-fMRI data to correct for sampling offsets using the *slicetimer* command of FSL. The regression of motion signal was achieved using the *mcflirt* command of FSL (Jenkinson et al., 2002). Then, the rs-fMRI data were registered in the brain extracted structural T1-weighted image using the FSL's intensity-based affine registration tool, *flirt*[7] (Jenkinson et al., 2002). Before the statistical analysis, signal from cerebrospinal fluid (CSF) and white matter was regressed out.

For the statistical analysis, we used the Multivariate Exploratory Linear Optimized Decomposition into Independent Components (*melodic*) command of the FSL software, which allowed us to decompose the 4D rs-fMRI data sets into its spatial and temporal components with the use of ICA, which can be used to identify distinct RSNs (Beckmann and Smith, 2004). Number of components was not specified *a priori*. In this study, we have identified a sensorimotor RSN of all participants.

[6]http://www.nitrc.org/projects/artifact_detect
[7]www.fmrib.ox.ac.uk/fsl

RESULTS

CLINICAL DATA AND MRI

Table 1 describes the type of lesions in the HCP and DCP children. No gross MRI abnormality was observed in one DCP child. All CP participants had visible asymmetry on the FA maps on the corticospinal tracts. HCP1 had severe spastic paresis of the upper limb and moderately impaired tactile sensory function and proprioception. HCP3, DCP1, and DCP4 had mild paresis of the hand and normal sensory function. The rest of CP participants had no evidence of motor or sensory impairment.

DISTRIBUTED SOURCE ANALYSIS

Figure 1 shows the superimposed (butterfly) plots of the SEFs for a TD, an HCP, and a DCP child evoked by the tactile stimulation of right D1 and left D1, respectively. A weak reflection at ~30 ms was observed as the first cortical response after the stimulus onset, but only in four participants (two TD, one HCP, and one DCP) and only after few digits' stimulation: TD1: left hand D1 at 28 ms, D3 at 27 ms; TD2: right hand D1 at 32 ms, left hand D1 at 28 ms and D5 at 27 ms; HCP1: left hand D1 at 28 ms, D3 at 30 ms, D5 at 31 ms; DCP2: right hand D1 at 29 ms. The most prominent early deflection evoked by the tactile stimulation of D1, D3, and D5 of both hands was observed at around 40–50 ms (M50) in all TD (mean latency $\pm$ SD for D1: 42.62 ± 3.55 ms, D3: 43.82 ± 3.88 ms, and D5: 44.24 ± 4.6 ms) and all DCP children (mean latency $\pm$ SD for D1: 43.36 ± 4.1 ms, D3: 45.03 ± 4.5 ms, and D5: 45.06 ± 2.0 ms). For the lowest functioning HCP child (HCP1), the M50 was absent in the SEFs elicited from the stimulation of the D1, D3, and D5 of the paretic hand (see **Figure 1** for D1), while components at later latencies were present. Tactile stimulation of the non-paretic

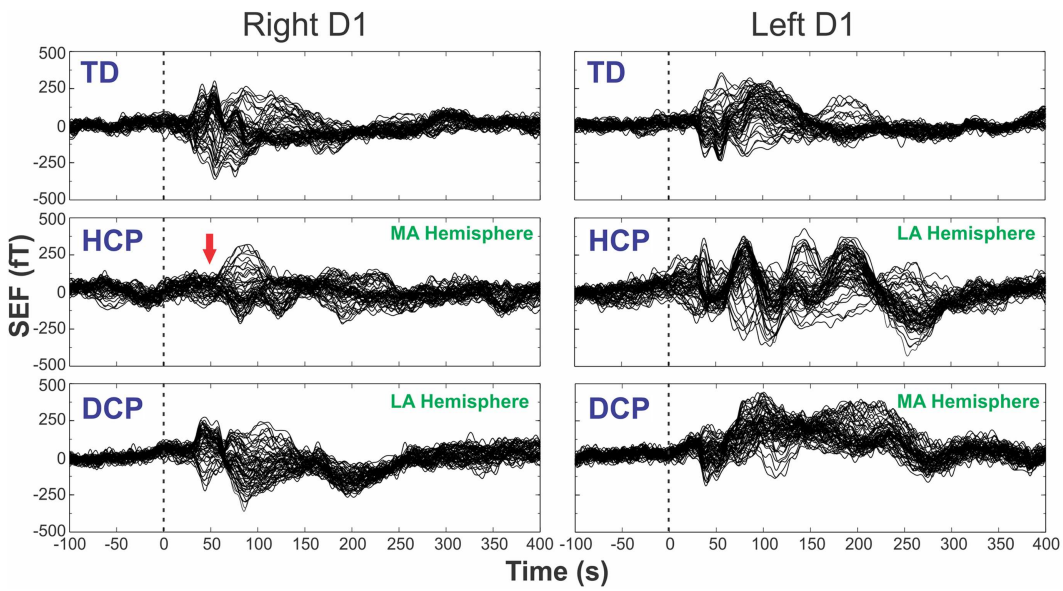

FIGURE 1 | SEFs evoked by the tactile stimulation of the right (left panels) and left (right panels) D1 from TD2, HCP1, and DCP3 children from −100 to 400 ms after the stimulus onset. Red arrow indicates the absence of the first cortical response in the HCP1 participant.

hand in the HCP children indicated altered SEFs in the later latencies. The M50 was present in the other two HCP children in both hemispheres. Isofield maps determined that the equivalent current dipoles (ECDs) for the components labeled as M30 presented an anterior ECD direction, while ECDs for the M50 components presented a posterior ECD direction.

Figure 2 shows the butterfly plots of the SEFs for TD1 (upper panel) and DCP2 (lower panel) child accompanied by the corresponding MNE solutions at the peak of M50. At this latency, distributed activations were also observed in the post-central and pre-central gyri and the parietal lobe contralateral to the stimuli for all TD and DCP children. **Figure 3** presents the M50 current sources (defined by maximal activities in the MNE maps) at the contralateral primary SS cortex (S1) for the stimulation of D1, D3, and D5 (both hands) for three representative participants from each group. Source analysis focused on the M50 that provided sufficient signal-to-noise (SNR) for reliable localization of the underlying generator. The M50 sources contralateral to the stimuli were located in the S1 area of the hand following a somatotopic order for both hands in all TD children (see **Figure 3** – upper panel for TD1), in all HCP children for the non-paretic hand (see **Figure 3** – middle panel – third column for HCP1), and in two DCP for the less paretic hand (see **Figure 3** – lower panel – third column for DCP2): D5 medial and superior to D3, and D3 medial and superior to D1. An altered somatotopy was observed for the more paretic hand in two DCP children, and in the non-paretic hand in one HCP child (HCP2): D3 was located more posterior and inferior to D1 (**Figure 3** – lower panel – second column for DCP2). Euclidean distances were markedly different among evoked activities in S1 between the TD group [mean distance ± SD (both hemispheres): for D1–D3: 7.38 ± 1.95 mm, for D3–D5: 6.89 ± 5.18 mm, for D1–D5: 8.18 ± 5.54 mm] and the HCP group for the more affected hand (mean distance ± SD: for D1–D3: 0.0 ± 0.00 mm, for D3–D5: 0.00 ± 0.00 mm, for D1–D5: 0.00 ± 0.00 mm) and the less affected hand (mean distance ± SD: for D1–D3: 12.95 ± 5.05 mm, for D3–D5: 10.58 ± 11.77 mm, for D1–D5: 21.47 ± 9.44 mm); Euclidean distances were markedly larger in the TD group compared to the HCP group for the more affected hemisphere and markedly shorter in the TD compared to the HCP for the less affected hemisphere. In the DCP children, Euclidean distances of S1 activities were markedly larger for both hemispheres compared to both hemispheres of the TD children. The Euclidean distances between activities within the contralateral S1 due to stimulation of D1, D3, and D5 for all participants are presented in **Table 2**.

TRACTOGRAPHY RESULTS

Figure 4 presents the thalamocortical tracks from thalamus to post-central gyrus (upper panel) and thalamus to pre-central gyrus (lower panel) for the same individuals as in **Figure 1**. The number of fibers between thalamus and post-central gyrus was not noticeably different between the two hemispheres in any of the participant groups (**Figure 5** – upper panel). Mean FA values for the thalamocortical fibers from thalamus to post-central gyrus were lower for the affected compared to the non-affected hemisphere in both CP groups and this difference was clearly visible in the HCP group (**Figure 5** – upper panel). Mean ADC, AD, and RD values for the thalamocortical fibers from thalamus to post-central gyrus were markedly higher for the affected than the non-affected hemisphere in both CP groups, where the difference was more pronounced in the HCP group (**Figure 5** – upper panel).

The mean number of fibers between thalamus and pre-central gyrus was higher in the non-affected hemisphere compared to the affected hemisphere in both CP groups and this difference was

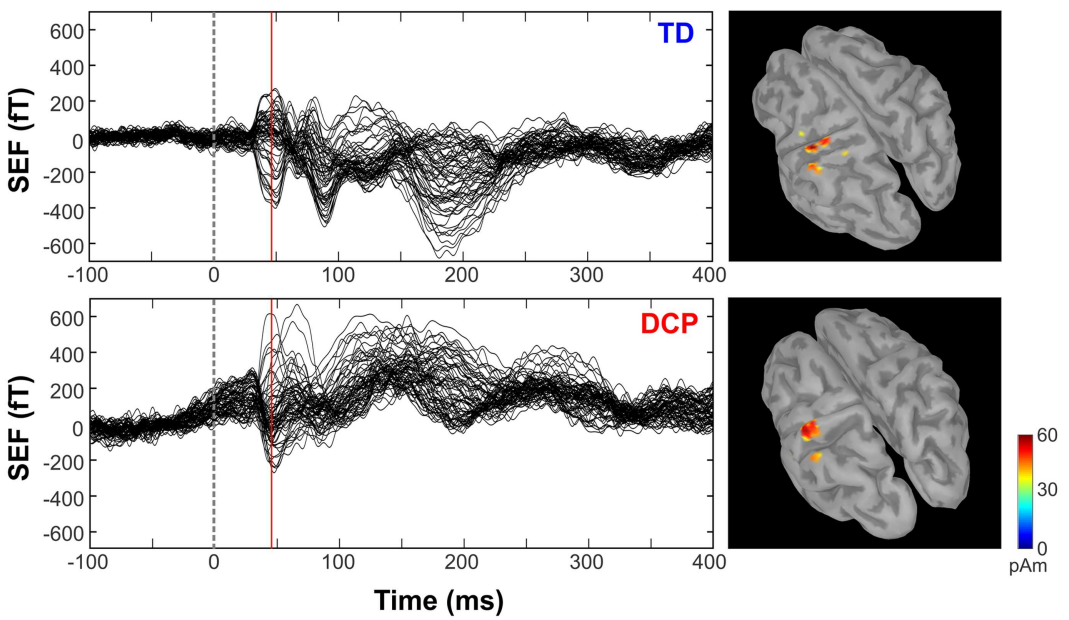

FIGURE 2 | Somatosensory-evoked fields evoked by the tactile stimulation of the right D1 (left panels) for TD1 and DCP2 (left hemisphere more affected) children respectively from −100 to 400 ms. MNEs (in pico ampere meter) overlaid on participant cortical surfaces at the peak of M50.

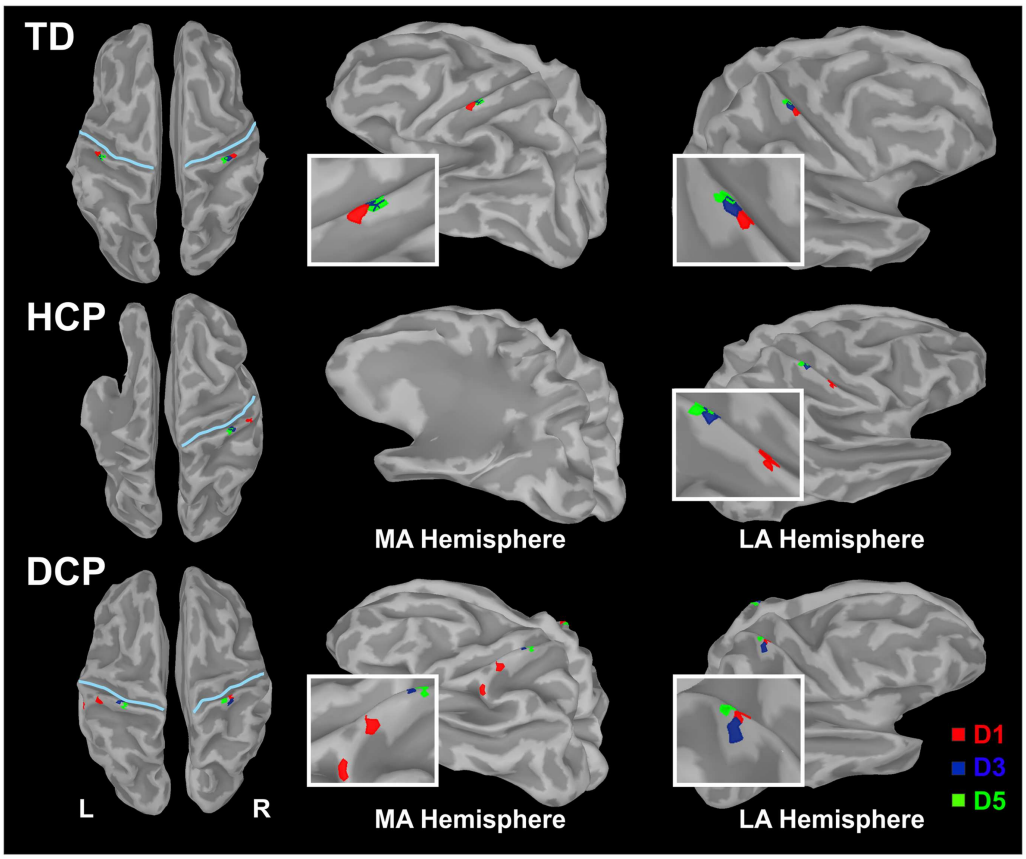

FIGURE 3 | Cortical responses in S1 at the peak of M50 for the tactile stimulation of D1, D3, and D5 of the right (left panel) and left (right panel) hands in the three representative participants (TD1, HCP1, and DCP2). Cortical responses were defined by the maxima MNEs elicited in the contralateral hemisphere. MA hemisphere, more affected hemisphere; LA, less affected hemisphere.

markedly larger in the HCP group (**Figure 5** – lower panel). Mean FA values for the fibers between thalamus and pre-central gyrus were lower for the affected compared to the non-affected hemisphere in both CP groups, where the difference was most visible in the HCP group (**Figure 5** – lower panel). Moreover, mean ADC, AD, and RD values of the thalamocortical fibers from thalamus to pre-central gyrus were higher for the affected than the non-affected hemisphere in both CP groups and the differences were always more pronounced in the HCP group (**Figure 5** – lower panel).

Mean diffusivity values for each individual in the three participant groups mostly followed the trend that we observed in the group averages for both fiber tracts (thalamus to post-central gyrus and thalamus to pre-central gyrus). Individual results are presented in **Tables 3** and **4**. The most striking result belonged to the HCP child (HCP1) with the large cortical lesion on the left hemisphere. For both fiber tracts, the mean ADC, AD, and RD values for this child's affected hemisphere was markedly increased compared to the non-affected hemisphere, while the mean FA values for the affected hemisphere was notably decreased than the non-affected hemisphere. Another interesting finding was of a DCP child (DCP3), whose left leg was affected and had a normal MRI of the brain according to the radiology report. Due to the left foot paresis, this child's right hemisphere was considered to be more affected; however, the results were not straightforward. For thalamus to post-central gyrus fiber tracts, this child's affected hemisphere did indeed had a lower mean FA value than the non-affected hemisphere like the rest of the CP children, however, for thalamus to pre-central gyrus fiber tracts, mean FA value was markedly higher for the affected hemisphere than the non-affected hemisphere unlike the rest of the CP children. The mean ADC, AD, and RD values for this child's affected hemisphere were lower compared to the non-affected hemisphere for both fiber tracts. Nevertheless, the differences between the mean diffusivity values of the two hemispheres in DCP3 were not too large.

rs-fMRI RESULTS

The number of spatially independent component maps ranged from 76 to 98 for the nine participants. We identified four ICA maps representing two anatomically distinct RSNs associated with the sensorimotor area. RSN1 and RSN2 were unilateral SS networks in the right or the left hemisphere, and RSN3 was a bilateral SS network. Both of these networks included activation in pre-central and post-central gyri, which are areas that represent the hand region in S1 and M1 in TD individuals (Liu et al., 2008).

RSN4 was a motor network that included activation in the midline and its surrounding areas, which are shown to represent the foot and leg region in TD individuals (Luft et al., 2002; Kapreli et al., 2006; Christensen et al., 2007). Similar patterns have been identified in previous RSN studies (Biswal et al., 1995; Beckmann et al., 2005; Liu et al., 2008). **Table 5** shows the RSNs identified for each participant.

Table 2 | Euclidean distances (in millimeter) for activities in S1.

Participant	D1–D3		D3–D5		D1–D5	
	RH	LH	RH	LH	RH	LH
TD1	7.79	7.82	7.79	14.85	0.00	7.56
TD2	9.42	3.72	10.50	1.00	14.77	3.72
TD3	7.13	8.44	4.35	2.87	12.11	10.96
Average	8.11	6.66	7.54	6.24	8.96	7.41
	MA	LA	MA	LA	MA	LA
HCP1	*	18.41	*	5.88	*	24.23
HCP2	0.00	8.44	0.00	23.97	0.00	29.24
HCP3	0.00	12.00	0.00	1.88	0.00	10.96
Average	0.00	12.95	0.00	10.58	0.00	21.47
	MA	LA	MA	LA	MA	LA
DCP1	5.15	–	–	–	–	–
DCP2	20.63	11.31	28.03	7.54	10.29	11.55
DCP3	8.34	31.49	9.94	6.54	16.44	25.17
DCP4	33.82	10.12	9.71	11.16	38.36	18.98
Average	16.98	17.64	15.89	8.41	21.69	18.56

**, Absent activity.*

–, No data.

All three SS ICA maps were present for each TD participant. Moreover, the bilateral SS network had a symmetrical pattern in all TD children. The most affected HCP participants did not have all of the three SS RSNs. HCP1, who had a large lesion in his left hemisphere did not have the left sided and the bilateral SS RSNs. HCP2 whose right hemisphere was affected, did not have separate SS RSNs for the right and left hemisphere and had an asymmetrical bilateral SS RSN where the left side activation was more widespread. HCP3 was the least affected child with HCP whose left hemisphere was affected. For him, we could find all the three SS RSNs. Nevertheless, his bilateral SS RSN was asymmetrical where the right hemisphere had a more widespread activity. We observed the fewest number of SS RSNs for the participants with DCP. DCP1 did not have either of the right and left SS RSNs, while her bilateral SS RSN was symmetrical. DCP2 did not have a right-sided SS RSN and her bilateral SS activity was larger on the left hemisphere. DCP3 did not have either of the right and left SS RSNs, and his bilateral SS RSN had symmetrical activity on both hemispheres.

The motor RSN was present in all nine participants. Within-group average results show that the localization of activity in the TD and HCP groups was similar and more restricted to the midline. However, the activity was stronger in the HCP group than in the TD group. On the other hand, the activity was more widespread in the DCP group than the other two participant groups, also covering the primary and secondary SS regions other than the motor region, a finding, which is similar to the one found in Burton et al. (2009).

DISCUSSION

Our preliminary multimodal neuroimaging findings suggest an abnormal SS processing mechanism in children with SCP. This mechanism could be the result of a possible reorganization process. Our results evident an altered SS mechanism as: (i) an

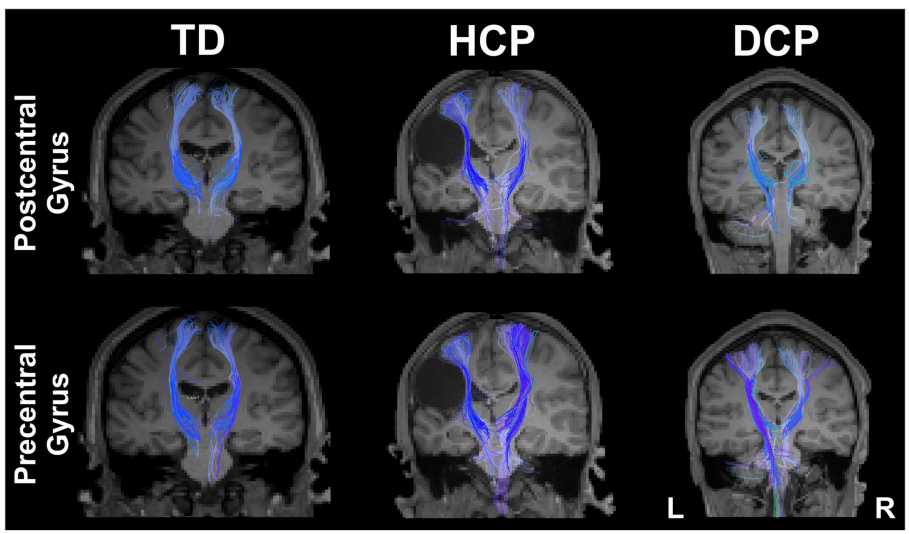

FIGURE 4 | Thalamocortical fibers projecting from thalamus to the post-central gyrus (upper panel) and from thalamus to pre-central gyrus (lower panel) for both sides of the brain for the same participants as in Figure 1 (TD2, HCP1, and DCP3 children).

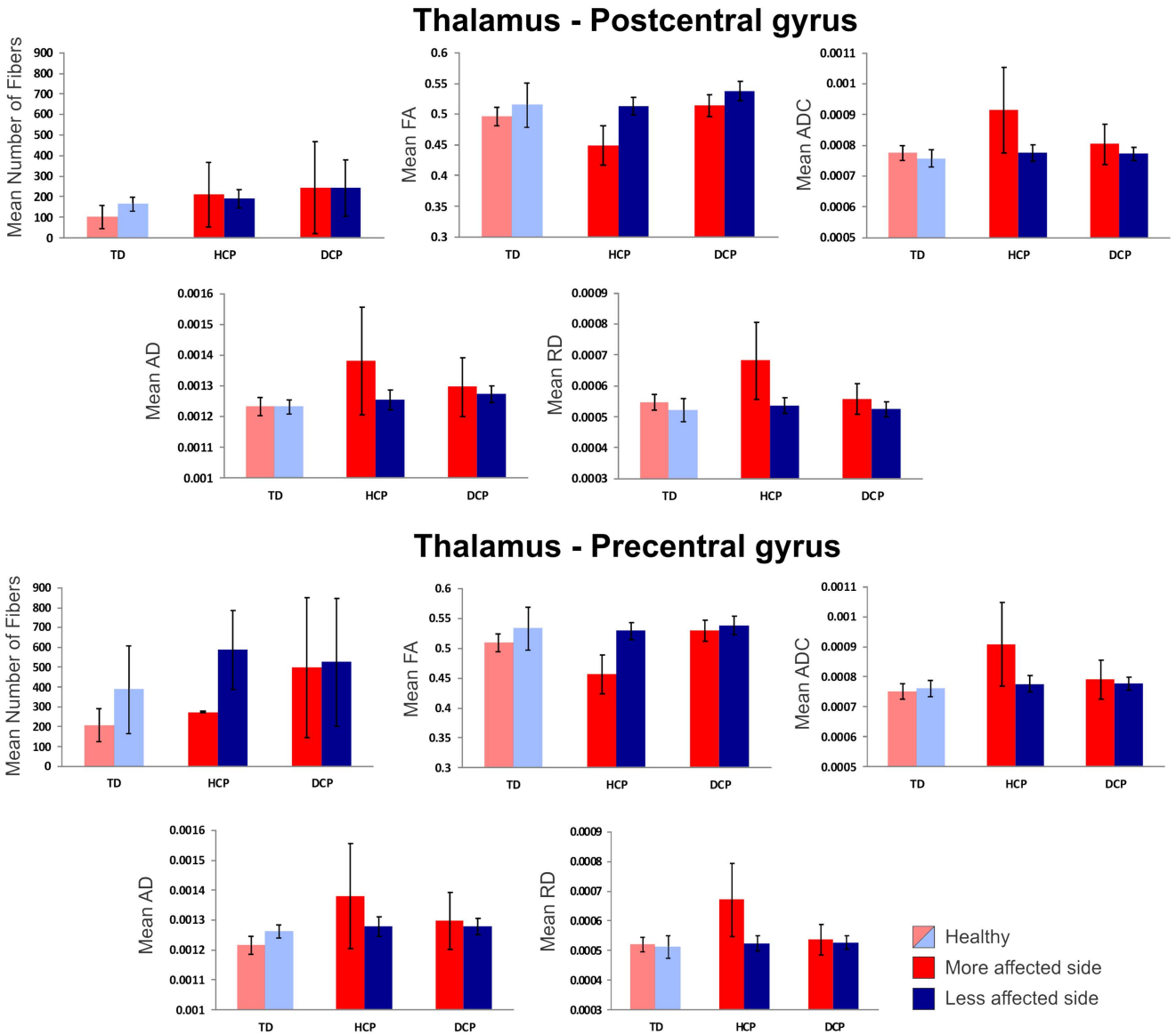

FIGURE 5 | Mean diffusivity values (±SD) for the thalamocortical fibers projecting from thalamus to post-central gyrus (upper panel) and thalamus to pre-central gyrus (lower panel) for all participants. Red indicates the affected (or more affected) hemisphere; blue indicates the intact (or less affected) hemisphere. Light red/blue indicate left and right hemisphere in TD.

altered morphology of the evoked responses elicited contralateral to the stimuli in both hemispheres of DCP and HCP children; (ii) an altered somatotopic representation of the hand areas in the contralateral S1 to the more paretic hand of two DCP children and to the non-paretic hand of one HCP child, (iii) markedly different Euclidean distances between S1 activities elicited by tactile stimulation of D1, D3, and D5 between the two hemispheres in the HCP children and between DCP and TD children for both hemispheres, and (iv) absent and/or abnormal sensorimotor RSNs for children with HCP and DCP. Functional abnormalities detected by MEG and rs-fMRI in CP children were supported by our DTI findings, which indicate structural deficits in the thalamocortical fibers projecting from thalamus to the pre-central and post-central gyri.

Functional alterations in the magnetic evoked responses observed here have also been previously reported after the tactile stimulation of fingers and after the electrical stimulation of the median nerve in HCP children with subcortical lesions (Nevalainen et al., 2012). These alterations include missing deflections, aberrant morphology, and different distances in the localized SEFs components between CP and TD patients. Such findings could be due to diminished thalamocortical projections from thalamus to S1 (Hoon et al., 2002; Lee et al., 2005) and/or subsequent aberrant functioning of cortical SS network. Our

Table 3 | DTI results from thalamus to post-central gyrus (mean values for the more affected and less affected hemispheres)[a].

Participant	NoF		FA		ADC		AD		RD	
	MA	LA	MA	LA	MA	LA	MA	LA	MA	LA
TD1	53	170	0.4798	0.4816	0.000804	0.000773	0.001262	0.001216	0.000575	0.000552
TD2	84	193	0.5101	0.5529	0.000757	0.000727	0.001203	0.001221	0.000535	0.000479
TD3	161	127	0.4969	0.5099	0.000765	0.000774	0.001231	0.001257	0.000531	0.000532
Average	99.3	163	0.4956	0.5148	0.000775	0.000758	0.001232	0.001231	0.000547	0.000521
HCP1	262	136	0.4142	0.5184	0.001075	0.000750	0.001582	0.001219	0.000821	0.000516
HCP2	30	215	0.4545	0.5233	0.000849	0.000771	0.001274	0.001260	0.000636	0.000526
HCP3	334	215	0.4789	0.4991	0.000818	0.000801	0.001285	0.001282	0.000692	0.000560
Average	209	189	0.4492	0.5136	0.000914	0.000774	0.001380	0.001254	0.000716	0.000534
DCP1	491	387	0.5169	0.5201	0.000850	0.000797	0.001367	0.001290	0.000592	0.000551
DCP2	52	110	0.4951	0.5505	0.000833	0.000768	0.001334	0.001288	0.000582	0.000508
DCP3	188	227	0.5299	0.5412	0.000729	0.000754	0.001188	0.001241	0.000499	0.000510
Average	244	241	0.5140	0.5373	0.000804	0.000773	0.001296	0.001273	0.000558	0.000523

[a]*NoF, number of fibers; FA, fractional anisotropy; ADC, apparent diffusion coefficient; AD, axial diffusivity; RD, radial diffusivity; MA, more affected hemisphere; LA, less affected hemisphere.*

Table 4 | DTI results from thalamus to pre-central gyrus (mean values for the more affected and less affected hemispheres)[a].

Participant	NoF		FA		ADC		AD		RD	
	MA	LA	MA	LA	MA	LA	MA	LA	MA	LA
TD1	135	188	0.4743	0.4946	0.000784	0.000777	0.001225	0.001239	0.000563	0.000546
TD2	187	627	0.5317	0.5699	0.000718	0.000731	0.001182	0.001250	0.000486	0.000471
TD3	298	345	0.5212	0.5347	0.000752	0.000777	0.001239	0.001296	0.000508	0.000518
Average	207	387	0.5091	0.5331	0.000751	0.000762	0.001215	0.001262	0.000519	0.000512
HCP1	273	533	0.3972	0.5283	0.001105	0.000779	0.001603	0.001278	0.000857	0.000530
HCP2	280	809	0.4864	0.5635	0.000814	0.000745	0.001276	0.001274	0.000584	0.000480
HCP3	271	421	0.4864	0.4949	0.000805	0.000803	0.001263	0.001284	0.000574	0.000560
Average	275	588	0.4567	0.5289	0.000908	0.000776	0.001381	0.001279	0.000672	0.000523
DCP1	848	829	0.4976	0.5304	0.000840	0.000788	0.001322	0.001295	0.000599	0.000535
DCP2	507	558	0.5506	0.5667	0.000786	0.000747	0.001344	0.001281	0.000507	0.000480
DCP3	141	188	0.5390	0.5168	0.000743	0.000796	0.001224	0.001257	0.000503	0.000565
Average	499	525	0.5291	0.5380	0.000790	0.000777	0.001297	0.001278	0.000536	0.000527

[a]*NoF, number of fibers; FA, fractional anisotropy; ADC, apparent diffusion coefficient; AD, axial diffusivity; RD, radial diffusivity; MA, more affected hemisphere; LA, less affected hemisphere.*

Table 5 | Somatosensory (SS) and motor RSNs.

Participant	Affected side	Components	SS right	SS left	SS bilateral	Motor
TD1	N/A	80	+	+	Symmetrical	+
TD2	N/A	76	+	+	Symmetrical	+
TD3	N/A	98	+	+	Symmetrical	+
HCP1	Right	81	+	−	−	+
HCP2	Left	89	−	−	Asymmetrical (left larger)	+
HCP3	Right	91	+	+	Asymmetrical (right larger)	+
DCP1	Both (right more)	94	−	−	Symmetrical	+
DCP2	Both (right more)	88	−	+	Asymmetrical (left larger)	+
DCP3	Both (left more)	79	−	−	Symmetrical	+

Euclidean distance results are in line with Nevalainen et al. (2012) that reported significant different distances between the representation areas of D1, D3, and D5 in the more affected hemisphere of HCP children compared to TD. Our most striking MEG finding was the altered somatotopy in the hemisphere contralateral to the most paretic hand in two DCP children and to the non-paretic hand in one HCP child. To our best knowledge, it is the first time that an altered somatotopic order is reported in CP.

In contrast with previous EEG and MEG studies (Teflioudi et al., 2011; Guo et al., 2012; Pihko et al., 2014), but in line with others (Nevalainen et al., 2012), we did not observe differences in latencies of the first prominent cortical response at M50 between the CP and TD children. Alterations in later deflections that were observed bilaterally in the DCP children likely reflect aberrant processing in the local cortical network after the arrival of the thalamocortical input to the cortex. Guo et al. (2012) reported delayed latencies for the first SEFs response in CP compared to TD children. Our group also observed similar findings in an adult CP patient with a large unilateral, prenatally acquired, periventricular brain lesion (Papadelis et al., 2012). On the other hand, other studies have reported the first cortical response at normal latencies after tactile stimulation of the paretic thumb of CP children with PVL, localized in its original topography in the Rolandic region of the affected hemisphere (Gerloff et al., 2006; Staudt et al., 2006; Wilke and Staudt, 2009). The contradictory findings between all these studies might be explained by the possible different timing of the insults in these patients. The maturational stage of the brain at the time of the insult determines the type of structural pathology and eventually the possible reorganization mechanism (Staudt, 2007).

One of our HCP children (HCP1) had a large lesion on his left hemisphere due to prenatal left middle cerebral artery infarct. For this child, the M50 component was absent from the SEFs in the contralateral hemisphere when the digits of the paretic hand were stimulated. Missing early cortical responses have been previously reported by Pihko et al. (2014) after the stimulation of the median nerve in CP children. There are two possible mechanisms that can explain our finding for the HCP1: (i) the primary SS representation of the paretic hand has been transferred to the contralesional hemisphere, ipsilateral to the stimulation due to damaged projections of the afferent thalamocortical fibers to S1, or (ii) the afferent thalamocortical SS projections had apparently "bypassed" the lesion and reached their original cortical destination area in the post-central gyrus, but the bypass caused a significant delay in the first cortical response that appeared later in time (see **Figure 1** – left middle panel). Unfortunately, the partial coverage of our system's sensor array does not allow us to conclude which mechanism was present but only to speculate. A previous study by Staudt et al. (2006) in hemiparetic patients has supported the later explanation as the most possible one. It was found that despite the large periventricular lesions of their patients, the S1 representation of the paretic hand was located in the Rolandic cortex of their affected hemisphere. They assumed that the outgrowing thalamocortical projections might have developed as a consequence of compensation after the insult. In our HCP1 patient, these axons may not have found their way to the preserved tissue around the periventricular defect and may project to the ipsilateral hemisphere. Although this is a plausible explanation, the exact timing of the insult remains unclear in all these studies. A later cortical response peaking at ~80 ms was observed in this child that was localized in the pre-central gyrus. This response was prolonged looking similar to components that occur at later latencies (~80–100 ms after stimulus onset) in the normal SS processing and probably reflects secondary processes in the SS cortex. The localization of this component in the pre-central gyrus might be explained by the missing secondary SS cortex in the lesioned hemisphere. Such a later component was also present in the TD and DCP children at the same latency (see **Figure 1**).

We further used two neuroimaging methods, namely DTI and rs-fMRI, that can help us disentangle this issue. Several previous studies have used DTI to investigate microstructural abnormalities responsible for motor weakness and disability in children with CP because conventional MRI is unable to detect subtle structural abnormalities (Lee et al., 2003). However, to our knowledge, no study yet reported the integrity of motor and sensory white matter pathway differences among TD, HCP, and DCP children. In our study, we found decreased FA values for the thalamocortical pathways in the affected (compared to the unaffected) hemisphere in children with CP, which may reflect a loss or disorganization of the structural barriers to molecular diffusion of water in these patients (Trivedi et al., 2010; Rai et al., 2013). Increased ADC values could be suggestive of increased extracellular water content due to gliosis and microscopic cystic changes emerging at the affected brain regions in CP children (Trivedi et al., 2010; Rai et al., 2013). In our findings, the increase in ADC values was accompanied by an increase both in AD and, primarily, RD. Studies have shown that while an increase in RD might be a sign of disorganized, demyelinated, dysmyelinated, and/or poorly myelinated axons (Song et al., 2002, 2005; Nair et al., 2005), an increase in AD is associated with axonal injury or damage, which causes a decrease in axonal density or caliber, finally resulting in an increase in the extra-axonal space allowing water molecules to move faster (Song et al., 2005; Sun et al., 2008; Kumar et al., 2010; Della Nave et al., 2011).

We found that children with HCP showed the most noticeable FA and ADC value differences between their affected and non-affected hemispheres for both of the pathways that we studied. The mean number of tracts was considerably higher for the non-affected hemisphere of HCP children compared to their affected hemisphere and to the healthy hemispheres of TD children. Although this change does not necessarily directly translate into an increase in the actual number of axons (Koerte et al., 2011), it may indicate a possible reorganization of the thalamus to the pre-central gyrus. Our finding is in parallel with previous studies, which showed that quadriplegic CP children were more affected (decreased mean FA and increased mean ADC in corticospinal tract) than DCP (Chang et al., 2012), and CP children with low gross motor function were more affected (lower number of fibers in corticospinal tract) than ones with high gross motor function (Rha et al., 2012).

Our DTI results indicate anatomical deficits in both the quality and quantity of thalamocortical fibers projecting from thalamus to the pre-central and post-central gyri. The diminished quality of the ascending thalamocortical fibers projecting from thalamus to the post-central gyrus may explain the observed abnormalities in

the SEFs. Our DTI findings also support the notion that anatomical deficits in the sensory pathways, in addition to the motor pathways, could be responsible for the pathophysiology of motor disability and weakness in children with CP. By extending the findings of previous studies, we show a clear difference in the sensory and motor pathways of children with HCP compared to DCP and TD children, as well as an indication of possible reorganization of the tracks from thalamus to pre-central gyrus in HCP children.

In order to test the functionality of the cortical SS network in CP children, we have also examined the sensorimotor RSNs in the three groups of children using an ICA method. For TD children, we managed to identify all the known SS and motor RSNs. HCP and DCP children showed absent and/or abnormal sensorimotor RSNs consistent with the severity and location of their lesions. Participants with HCP had absent or weak SS networks on their lesioned hemispheres while the intact hemisphere seemed to have stronger and more widespread activation (see **Figure 6**). Participants with DCP showed widespread activity for the motor RSN, extending to the SS cortices compared to the other participant groups, which is a similar finding as in Burton et al. (2009). The more widespread and/or stronger activity in participants with CP could be explained by disruptions to the somatotopic organizations in the SS cortices and the development of new and the strengthening of already existing intracortical connections (Marin-Padilla, 1997; Burton et al., 2009). The findings are in parallel with our DTI findings where the number of fibers for DCP children was low for the thalamus and post-central pathway but high for thalamus to pre-central pathway for both hemispheres.

METHODOLOGICAL LIMITATIONS

Magnetoencephalography findings were used to determine the S1 functionally for the DTI analysis. In all CP and TD children, S1 activity was localized within the post-central gyrus. Ideally, the MEG-defined ROIs should be used for the determination of ROIs in the DTI analysis. However, fiber tracking has limitations in determining the thalamocortical SS radiations and the motor tracts for the hand areas due to its well-known weakness to handle crossing fibers at the centrum semiovale level (Nowinski et al., 2012). Here, we were not able to reconstruct fibers passing from the MEG-defined ROIs to the thalamus. Therefore, for the DTI analysis, we considered the volume of the entire post-central gyrus as the ROI. Since our experimental setup did not involve any spontaneous movements from the participants, we were unable to determine the M1 functionally. Although MNE indicated cortical activity within the pre-central gyrus, this activity was not considered to be significant functionally. There is evidence that MNE solutions of even focal sources can extend across sulcal walls separated by only a few millimeters (Liu et al., 2002; Lin et al., 2006b; Hauk et al., 2011). The observed activity within the pre-central gyrus was probably due to the expansion of MNE solutions from the actual primary generator located within the post-central gyrus to more anterior locations. Since we were unable to functionally define the M1 by using our MEG data, we followed the most common practice to define it anatomically by choosing the volume of the entire pre-central gyrus as the ROI (Trivedi et al., 2010; Chang et al., 2012; Rha et al., 2012).

CONCLUSION

Even though our study is limited by the relatively small number of participants and the lack of statistical results, it is the first study that reports findings from multiple neuroimaging modalities in the same CP patients. Our functional and anatomical findings provide preliminary evidence of impaired SS processing in CP patients that are due to (i) diminished thalamocortical projections from thalamus to S1 (Hoon et al., 2002; Lee et al., 2005), and (ii) subsequent aberrant functioning of the cortical SS network.

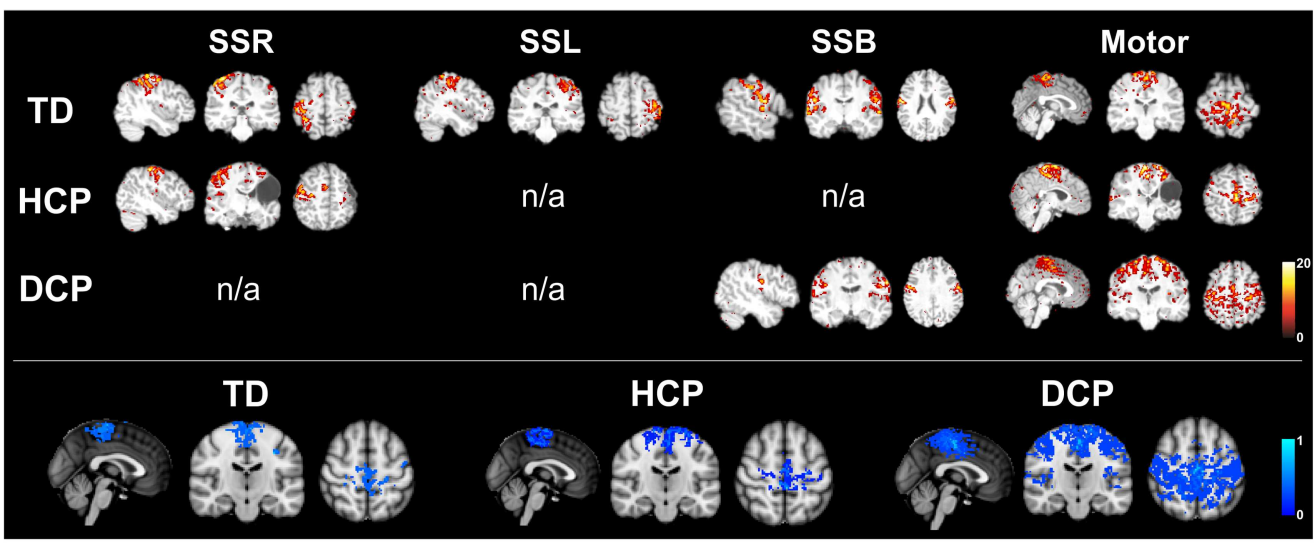

FIGURE 6 | Upper panel: RSNs for the same participants as in Figure 1 (TD2, HCP1, and DCP3 children). SSR, right somatosensory RSN; SSL, left somatosensory RSN; SSB, bilateral somatosensory RSN; motor, motor RSN (*z*-scores). Lower panel: mean motor RSN (lower panel) for the three groups of participants.

It should be noted though that our findings are limited due to the partial head coverage of our BabySQUID MEG system that does not allow simultaneous recordings of both hemispheres. Also, our small sample size prevents us from generalizing our conclusions to the general CP population. We conclude that motor and sensory pathways could both be important in the clinical outcome of children with CP and that the diminished connectivity in these pathways in the affected hemisphere, especially of children with HCP, could be indicative of a pathophysiological mechanism responsible for motor dysfunction (Yoshida et al., 2010; Lee et al., 2011). These results have important implications for the diagnosis and the rehabilitation of patients with CP. Such interventions should be applied early in life when the brain demonstrates the ability to plasticity, allowing it to readily reorganize in the face of injury (Johnston, 2009). Therefore, new approaches using innovative technologies that will identify early functional and structural deficits in the brain of children with PVL are needed.

ACKNOWLEDGMENTS

The authors would like to thank Chiran Doshi, MSc for his technical support with the data analysis and collection, Tapsya Nayak, MSc for her help with the data collection, Borjan Gagoski, Ph.D. for his help with the MRI sequences, Mathieu Dehaes, Ph.D., and Danielle Sliva, MA, for their help with rs-fMRI analysis.

REFERENCES

Bax, M., Goldstein, M., Rosenbaum, P., Leviton, A., Paneth, N., Dan, B., et al. (2005). Proposed definition and classification of cerebral palsy, April 2005. *Dev. Med. Child Neurol.* 47, 571–576. doi:10.1017/S001216220500112X

Beckmann, C. F., DeLuca, M., Devlin, J. T., and Smith, S. M. (2005). Investigations into resting-state connectivity using independent component analysis. *Philos. Trans. R. Soc. Lond. B Biol. Sci.* 360, 1001–1013. doi:10.1098/rstb.2005.1634

Beckmann, C. F., and Smith, S. M. (2004). Probabilistic independent component analysis for functional magnetic resonance imaging. *IEEE Trans. Med. Imaging* 23, 137–152. doi:10.1109/TMI.2003.822821

Biswal, B., Yetkin, F. Z., Haughton, V. M., and Hyde, J. S. (1995). Functional connectivity in the motor cortex of resting human brain using echo-planar MRI. *Magn. Reson. Med.* 34, 537–541. doi:10.1002/mrm.1910340409

Burton, H., Dixit, S., Litkowski, P., and Wingert, J. R. (2009). Functional connectivity for somatosensory and motor cortex in spastic diplegia. *Somatosens. Mot. Res.* 26, 90–104. doi:10.3109/08990220903335742

Chang, M. C., Jang, S. H., Yoe, S. S., Lee, E., Kim, S., Lee, D. G., et al. (2012). Diffusion tensor imaging demonstrated radiologic differences between diplegic and quadriplegic cerebral palsy. *Neurosci. Lett.* 512, 53–58. doi:10.1016/j.neulet.2012.01.065

Christensen, M. S., Lundbye-Jensen, J., Petersen, N., Geertsen, S. S., Paulson, O. B., and Nielsen, J. B. (2007). Watching your foot move – an fMRI study of visuomotor interactions during foot movement. *Cereb. Cortex* 17, 1906–1917. doi:10.1093/cercor/bhl101

Cooper, J., Majnemer, A., Rosenblatt, B., and Birnbaum, R. (1995). The determination of sensory deficits in children with hemiplegic cerebral palsy. *J. Child Neurol.* 10, 300–309. doi:10.1177/088307389501000412

Coq, J. O., Strata, F., Russier, M., Safadi, F. F., Merzenich, M. M., Byl, N. N., et al. (2008). Impact of neonatal asphyxia and hind limb immobilization on musculoskeletal tissues and S1 map organization: implications for cerebral palsy. *Exp. Neurol.* 210, 95–108. doi:10.1016/j.expneurol.2007.10.006

Daducci, A., Gerhard, S., Griffa, A., Lemkaddem, A., Cammoun, L., Gigandet, X., et al. (2012). The connectome mapper: an open-source processing pipeline to map connectomes with MRI. *PLoS ONE* 7:e48121. doi:10.1371/journal.pone.0048121

Dale, A. M., Fischl, B., and Sereno, M. I. (1999). Cortical surface-based analysis. I. Segmentation and surface reconstruction. *Neuroimage* 9, 179–194. doi:10.1006/nimg.1998.0395

Dehaes, M., Raschle, N. M., Sliva, D. D., Zuk, J., Drottar, M., Chang, M., et al. (2013). *Potential of Resting State Connectivity and Passive fMRI to Detect Precursors of Learning Disabilities in Infants: Preliminary Results with Infants at Familial Risk for Developmental Dyslexia.* Salt Lake City: The International Society for Magnetic Resonance in Medicine.

Della Nave, R., Ginestroni, A., Diciotti, S., Salvatore, E., Soricelli, A., and Mascalchi, M. (2011). Axial diffusivity is increased in the degenerating superior cerebellar peduncles of Friedreich's ataxia. *Neuroradiology* 53, 367–372. doi:10.1007/s00234-010-0807-1

Dijkerman, H. C., and de Haan, E. H. (2007). Somatosensory processes subserving perception and action. *Behav. Brain Sci.* 30, 189–201. doi:10.1017/S0140525X07001392 discussion 201-139,

Einspieler, C., and Prechtl, H. F. (2005). Prechtl's assessment of general movements: a diagnostic tool for the functional assessment of the young nervous system. *Ment. Retard. Dev. Disabil. Res. Rev.* 11, 61–67. doi:10.1002/mrdd.20051

Fischl, B., Liu, A., and Dale, A. M. (2001). Automated manifold surgery: constructing geometrically accurate and topologically correct models of the human cerebral cortex. *IEEE Trans. Med. Imaging* 20, 70–80. doi:10.1109/42.906426

Fischl, B., Sereno, M. I., and Dale, A. M. (1999). Cortical surface-based analysis. II: inflation, flattening, and a surface-based coordinate system. *Neuroimage* 9, 195–207. doi:10.1006/nimg.1998.0396

Fowler, E. G., and Goldberg, E. J. (2009). The effect of lower extremity selective voluntary motor control on interjoint coordination during gait in children with spastic diplegic cerebral palsy. *Gait Posture* 29, 102–107. doi:10.1016/j.gaitpost.2008.07.007

Gerloff, C., Bushara, K., Sailer, A., Wassermann, E. M., Chen, R., Matsuoka, T., et al. (2006). Multimodal imaging of brain reorganization in motor areas of the contralesional hemisphere of well recovered patients after capsular stroke. *Brain* 129, 791–808. doi:10.1093/brain/awh713

Gordon, A. M., Bleyenheuft, Y., and Steenbergen, B. (2013). Pathophysiology of impaired hand function in children with unilateral cerebral palsy. *Dev. Med. Child Neurol.* 55(Suppl. 4), 32–37. doi:10.1111/dmcn.12304

Guo, X., Xiang, J., Mun-Bryce, S., Bryce, M., Huang, S., Huo, X., et al. (2012). Aberrant high-gamma oscillations in the somatosensory cortex of children with cerebral palsy: a meg study. *Brain Dev.* 34, 576–583. doi:10.1016/j.braindev.2011.09.012

Hadders-Algra, M. (2004). General movements: a window for early identification of children at high risk for developmental disorders. *J. Pediatr.* 145, S12–S18. doi:10.1016/j.jpeds.2004.05.017

Hämäläinen, M., Hari, R., Ilmoniemi, R., Knuutila, J., and Lounasmaa, O. (1993). Magnetoencephalography – theory, instrumentation, and applications to noninvasive studies of the working human brain. *Rev. Mod. Phys.* 65, 1–93.

Hamalainen, M. S., and Ilmoniemi, R. J. (1994). Interpreting magnetic fields of the brain: minimum norm estimates. *Med. Biol. Eng. Comput.* 32, 35–42. doi:10.1007/BF02512476

Hauk, O., Wakeman, D. G., and Henson, R. (2011). Comparison of noise-normalized minimum norm estimates for MEG analysis using multiple resolution metrics. *Neuroimage* 54, 1966–1974. doi:10.1016/j.neuroimage.2010.09.053

Himmelmann, K., Beckung, E., Hagberg, G., and Uvebrant, P. (2006). Gross and fine motor function and accompanying impairments in cerebral palsy. *Dev. Med. Child Neurol.* 48, 417–423. doi:10.1017/S0012162206000922

Hoon, A. H. Jr., Lawrie, W. T. Jr., Melhem, E. R., Reinhardt, E. M., Van Zijl, P. C., Solaiyappan, M., et al. (2002). Diffusion tensor imaging of periventricular leukomalacia shows affected sensory cortex white matter pathways. *Neurology* 59, 752–756. doi:10.1212/WNL.59.5.752

Hoon, A. H. Jr., Stashinko, E. E., Nagae, L. M., Lin, D. D., Keller, J., Bastian, A., et al. (2009). Sensory and motor deficits in children with cerebral palsy born preterm correlate with diffusion tensor imaging abnormalities in thalamocortical pathways. *Dev. Med. Child Neurol.* 51, 697–704. doi:10.1111/j.1469-8749.2009.03306.x

Hsiao, F. J., Cheng, C. H., Chen, W. T., and Lin, Y. Y. (2013). Neural correlates of somatosensory paired-pulse suppression: a MEG study using distributed source modeling and dynamic spectral power analysis. *Neuroimage* 72, 133–142. doi:10.1016/j.neuroimage.2013.01.041

Huang, M. X., Mosher, J. C., and Leahy, R. M. (1999). A sensor-weighted overlapping-sphere head model and exhaustive head model comparison for MEG. *Phys. Med. Biol.* 44, 423–440. doi:10.1088/0031-9155/44/2/010

Jenkinson, M., Bannister, P., Brady, M., and Smith, S. (2002). Improved optimization for the robust and accurate linear registration and motion correction of brain images. *Neuroimage* 17, 825–841. doi:10.1006/nimg.2002.1132

Johnston, M. V. (2009). Plasticity in the developing brain: implications for rehabilitation. *Dev. Disabil. Res. Rev.* 15, 94–101. doi:10.1002/ddrr.64

Kapreli, E., Athanasopoulos, S., Papathanasiou, M., Van Hecke, P., Strimpakos, N., Gouliamos, A., et al. (2006). Lateralization of brain activity during lower limb joints movement. An fMRI study. *Neuroimage* 32, 1709–1721. doi:10.1016/j.neuroimage.2006.05.043

Koerte, I., Pelavin, P., Kirmess, B., Fuchs, T., Berweck, S., Laubender, R. P., et al. (2011). Anisotropy of transcallosal motor fibres indicates functional impairment in children with periventricular leukomalacia. *Dev. Med. Child Neurol.* 53, 179–186. doi:10.1111/j.1469-8749.2010.03840.x

Krageloh-Mann, I., and Cans, C. (2009). Cerebral palsy update. *Brain Dev.* 31, 537–544. doi:10.1016/j.braindev.2009.03.009

Krumlinde-Sundholm, L., and Eliasson, A. C. (2002). Comparing tests of tactile sensibility: aspects relevant to testing children with spastic hemiplegia. *Dev. Med. Child Neurol.* 44, 604–612. doi:10.1111/j.1469-8749.2002.tb00845.x

Kumar, A., Sundaram, S. K., Sivaswamy, L., Behen, M. E., Makki, M. I., Ager, J., et al. (2010). Alterations in frontal lobe tracts and corpus callosum in young children with autism spectrum disorder. *Cereb. Cortex* 20, 2103–2113. doi:10.1093/cercor/bhp278

Kurz, M. J., and Wilson, T. W. (2011). Neuromagnetic activity in the somatosensory cortices of children with cerebral palsy. *Neurosci. Lett.* 490, 1–5. doi:10.1016/j.neulet.2010.11.053

Lee, J. D., Park, H. J., Park, E. S., Oh, M. K., Park, B., Rha, D. W., et al. (2011). Motor pathway injury in patients with periventricular leukomalacia and spastic diplegia. *Brain* 134, 1199–1210. doi:10.1093/brain/awr021

Lee, S. K., Kim, D. I., Kim, J., Kim, D. J., Kim, H. D., Kim, D. S., et al. (2005). Diffusion-tensor MR imaging and fiber tractography: a new method of describing aberrant fiber connections in developmental CNS anomalies. *Radiographics* 25, 53–65. doi:10.1148/rg.251045085 discussion 66-58,

Lee, Z. I., Byun, W. M., Jang, S. H., Ahn, S. H., Moon, H. K., and Chang, Y. (2003). Diffusion tensor magnetic resonance imaging of microstructural abnormalities in children with brain injury. *Am. J. Phys. Med. Rehabil.* 82, 556–559. doi:10.1097/01.PHM.0000073830.15643.6A

Prechtl, H. F., Einspieler, C., Cioni, G., Bos, A. F., Ferrari, F., and Sontheimer, D. (1997). An early marker for neurological deficits after perinatal brain lesions. *Lancet* 349, 1361–1363. doi:10.1016/S0140-6736(96)10182-3

Lin, F. H., Belliveau, J. W., Dale, A. M., and Hamalainen, M. S. (2006a). Distributed current estimates using cortical orientation constraints. *Hum. Brain Mapp.* 27, 1–13. doi:10.1002/hbm.20155

Lin, F. H., Witzel, T., Ahlfors, S. P., Stufflebeam, S. M., Belliveau, J. W., and Hämäläinen, M. S. (2006b). Assessing and improving the spatial accuracy in MEG source localization by depth-weighted minimum-norm estimates. *Neuroimage* 31, 160–171. doi:10.1016/j.neuroimage.2005.11.054

Liu, A. K., Dale, A. M., and Belliveau, J. W. (2002). Monte Carlo simulation studies of EEG and MEG localization accuracy. *Hum. Brain Mapp.* 16, 47–62. doi:10.1002/hbm.10024

Liu, W. C., Flax, J. F., Guise, K. G., Sukul, V., and Benasich, A. A. (2008). Functional connectivity of the sensorimotor area in naturally sleeping infants. *Brain Res.* 1223, 42–49. doi:10.1016/j.brainres.2008.05.054

Luft, A. R., Smith, G. V., Forrester, L., Whitall, J., Macko, R. F., Hauser, T. K., et al. (2002). Comparing brain activation associated with isolated upper and lower limb movement across corresponding joints. *Hum. Brain Mapp.* 17, 131–140. doi:10.1002/hbm.10058

Marin-Padilla, M. (1997). Developmental neuropathology and impact of perinatal brain damage. II. White matter lesion of the neocortex. *J. Neuropathol. Exp. Neurol.* 56, 219–235. doi:10.1097/00005072-199703000-00001

Nagae, L. M., Hoon, A. H. Jr., Stashinko, E., Lin, D., Zhang, W., Levey, E., et al. (2007). Diffusion tensor imaging in children with periventricular leukomalacia: variability of injuries to white matter tracts. *AJNR Am. J. Neuroradiol.* 28, 1213–1222. doi:10.3174/ajnr.A0534

Nair, G., Tanahashi, Y., Low, H. P., Billings-Gagliardi, S., Schwartz, W. J., and Duong, T. Q. (2005). Myelination and long diffusion times alter diffusion-tensor-imaging contrast in myelin-deficient shiverer mice. *Neuroimage* 28, 165–174. doi:10.1016/j.neuroimage.2005.05.049

Nevalainen, P., Pihko, E., Maenpaa, H., Valanne, L., Nummenmaa, L., and Lauronen, L. (2012). Bilateral alterations in somatosensory cortical processing in hemiplegic cerebral palsy. *Dev. Med. Child Neurol.* 54, 361–367. doi:10.1111/j.1469-8749.2011.04165.x

Nowinski, W. L., Chua, B. C., Yang, G. L., and Qian, G. Y. (2012). Three-dimensional interactive and stereotactic human brain atlas of white matter tracts. *Neuroinformatics* 10, 33–55. doi:10.1007/s12021-011-9118-x

Okada, Y., Pratt, K., Atwood, C., Mascarena, A., Reineman, R., Nurminen, J., et al. (2006). BabySQUID: a mobile, high-resolution multichannel MEG system for neonatal brain assessment. *Rev. Sci. Instrum.* 77, 24301–24309. doi:10.1063/1.2168672

Ostensjo, S., Carlberg, E. B., and Vollestad, N. K. (2004). Motor impairments in young children with cerebral palsy: relationship to gross motor function and everyday activities. *Dev. Med. Child Neurol.* 46, 580–589. doi:10.1111/j.1469-8749.2004.tb01021.x

Palisano, R., Rosenbaum, P., Walter, S., Russell, D., Wood, E., and Galuppi, B. (1997). Development and reliability of a system to classify gross motor function in children with cerebral palsy. *Dev. Med. Child Neurol.* 39, 214–223. doi:10.1111/j.1469-8749.1997.tb07414.x

Papadelis, C., Chellamani, H., Ahtam, B., Doshi, C., Grant, E., and Okada, Y. (2013). Current and emerging potential for magnetoencephalography in pediatric epilepsy. *J. Pediatr. Epilepsy* 2, 73–85. doi:10.3233/PEP-13040

Papadelis, C., Leonardelli, E., Staudt, M., and Braun, C. (2012). Can magnetoencephalography track the afferent information flow along white matter thalamocortical fibers? *Neuroimage* 60, 1092–1105. doi:10.1016/j.neuroimage.2012.01.054

Papadelis, C., Poghosyan, V., Fenwick, P. B., and Ioannides, A. A. (2009). MEG's ability to localise accurately weak transient neural sources. *Clin. Neurophysiol.* 120, 1958–1970. doi:10.1016/j.clinph.2009.08.018

Pihko, E., Nevalainen, P., Vaalto, S., Laaksonen, K., Mäenpää, H., Valanne, L., et al. (2014). Reactivity of sensorimotor oscillations is altered in children with hemiplegic cerebral palsy: a magnetoencephalographic study. *Hum. Brain Mapp.* 35, 4105–4117. doi:10.1002/hbm.22462

Prechtl, H. F. (1997). State of the art of a new functional assessment of the young nervous system. An early predictor of cerebral palsy. *Early Hum. Dev.* 50, 1–11. doi:10.1016/S0378-3782(97)00088-1

Rai, Y., Chaturvedi, S., Paliwal, V. K., Goyal, P., Chourasia, A., Singh Rathore, R. K., et al. (2013). DTI correlates of cognition in term children with spastic diplegic cerebral palsy. *Eur. J. Paediatr. Neurol.* 17, 294–301. doi:10.1016/j.ejpn.2012.11.005

Rha, D. W., Chang, W. H., Kim, J., Sim, E. G., and Park, E. S. (2012). Comparing quantitative tractography metrics of motor and sensory pathways in children with periventricular leukomalacia and different levels of gross motor function. *Neuroradiology* 54, 615–621. doi:10.1007/s00234-011-0996-2

Riquelme, I., Cifre, I., and Montoya, P. (2011). Age-related changes of pain experience in cerebral palsy and healthy individuals. *Pain Med.* 15, 535–545. doi:10.1111/j.1526-4637.2011.01094.x

Riquelme, I., and Montoya, P. (2010). Developmental changes in somatosensory processing in cerebral palsy and healthy individuals. *Clin. Neurophysiol.* 121, 1314–1320. doi:10.1016/j.clinph.2010.03.010

Riquelme, I., Padrón, I., Cifre, I., González-Roldán, A. M., and Montoya, P. (2014). Differences in somatosensory processing due to dominant hemispheric motor impairment in cerebral palsy. *BMC Neurosci.* 15:10. doi:10.1186/1471-2202-15-10

Sanger, T. D., and Kukke, S. N. (2007). Abnormalities of tactile sensory function in children with dystonic and diplegic cerebral palsy. *J. Child Neurol.* 22, 289–293. doi:10.1177/0883073807300530

Smith, S. M. (2002). Fast robust automated brain extraction. *Hum. Brain Mapp.* 17, 143–155. doi:10.1002/hbm.10062

Son, S. M., Ahn, Y. H., Sakong, J., Moon, H. K., Ahn, S. H., Lee, H., et al. (2007). Diffusion tensor imaging demonstrates focal lesions of the corticospinal tract in hemiparetic patients with cerebral palsy. *Neurosci. Lett.* 420, 34–38. doi:10.1016/j.neulet.2007.04.054

Song, S. K., Sun, S. W., Ramsbottom, M. J., Chang, C., Russell, J., and Cross, A. H. (2002). Dysmyelination revealed through MRI as increased radial (but unchanged axial) diffusion of water. *Neuroimage* 17, 1429–1436. doi:10.1006/nimg.2002.1267

Song, S. K., Yoshino, J., Le, T. Q., Lin, S. J., Sun, S. W., Cross, A. H., et al. (2005). Demyelination increases radial diffusivity in corpus callosum of mouse brain. *Neuroimage* 26, 132–140. doi:10.1016/j.neuroimage.2005.01.028

Staudt, M. (2007). (Re-)organization of the developing human brain following periventricular white matter lesions. *Neurosci. Biobehav. Rev.* 31, 1150–1156. doi:10.1016/j.neubiorev.2007.05.005

Staudt, M., Braun, C., Gerloff, C., Erb, M., Grodd, W., and Krageloh-Mann, I. (2006). Developing somatosensory projections bypass periventricular brain lesions. *Neurology* 67, 522–525. doi:10.1212/01.wnl.0000227937.49151.fd

Sun, S. W., Liang, H. F., Cross, A. H., and Song, S. K. (2008). Evolving Wallerian degeneration after transient retinal ischemia in mice characterized by diffusion tensor imaging. *Neuroimage* 40, 1–10. doi:10.1016/j.neuroimage.2007.11.049

Tadel, F., Baillet, S., Mosher, J. C., Pantazis, D., and Leahy, R. M. (2011). Brainstorm: a user-friendly application for MEG/EEG analysis. *Comput. Intell. Neurosci.* 2011, 879716. doi:10.1155/2011/879716

Teflioudi, E. P., Zafeiriou, D. I., Vargiami, E., Kontopoulos, E., and Tsikoulas, I. (2011). Somatosensory evoked potentials in children with bilateral spastic cerebral palsy. *Pediatr. Neurol.* 44, 177–182. doi:10.1016/j.pediatrneurol.2010.11.001

Thomas, B., Eyssen, M., Peeters, R., Molenaers, G., Van Hecke, P., De Cock, P., et al. (2005). Quantitative diffusion tensor imaging in cerebral palsy due to periventricular white matter injury. *Brain* 128, 2562–2577. doi:10.1093/brain/awh600

Tomlin, P. I. (1995). *The Static Encephalopathies.* London: Times-Wolfe International.

Trivedi, R., Agarwal, S., Shah, V., Goyel, P., Paliwal, V. K., Rathore, R. K., et al. (2010). Correlation of quantitative sensorimotor tractography with clinical grade of cerebral palsy. *Neuroradiology* 52, 759–765. doi:10.1007/s00234-010-0703-8

Van Heest, A. E., House, J., and Putnam, M. (1993). Sensibility deficiencies in the hands of children with spastic hemiplegia. *J. Hand Surg. Am.* 18, 278–281. doi:10.1016/0363-5023(93)90361-6

Volpe, J. J. (2009). The encephalopathy of prematurity – brain injury and impaired brain development inextricably intertwined. *Semin. Pediatr. Neurol.* 16, 167–178. doi:10.1016/j.spen.2009.09.005

Wilke, M., and Staudt, M. (2009). Does damage to somatosensory circuits underlie motor impairment in cerebral palsy? *Dev. Med. Child Neurol.* 51, 686–687. doi:10.1111/j.1469-8749.2009.03332.x

Wingert, J. R., Burton, H., Sinclair, R. J., Brunstrom, J. E., and Damiano, D. L. (2008). Tactile sensory abilities in cerebral palsy: deficits in roughness and object discrimination. *Dev. Med. Child Neurol.* 50, 832–838. doi:10.1111/j.1469-8749.2008.03105.x

Wingert, J. R., Burton, H., Sinclair, R. J., Brunstrom, J. E., and Damiano, D. L. (2009). Joint-position sense and kinesthesia in cerebral palsy. *Arch. Phys. Med. Rehabil.* 90, 447–453. doi:10.1016/j.apmr.2008.08.217

Wingert, J. R., Sinclair, R. J., Dixit, S., Damiano, D. L., and Burton, H. (2010). Somatosensory-evoked cortical activity in spastic diplegic cerebral palsy. *Hum. Brain Mapp.* 31, 1772–1785. doi:10.1002/hbm.20977

Yeargin-Allsopp, M., Van Naarden Braun, K., Doernberg, N. S., Benedict, R. E., Kirby, R. S., and Durkin, M. S. (2008). Prevalence of cerebral palsy in 8-year-old children in three areas of the United States in 2002: a multisite collaboration. *Pediatrics* 121, 547–554. doi:10.1542/peds.2007-1270

Yoshida, S., Hayakawa, K., Yamamoto, A., Okano, S., Kanda, T., Yamori, Y., et al. (2010). Quantitative diffusion tensor tractography of the motor and sensory tract in children with cerebral palsy. *Dev. Med. Child Neurol.* 52, 935–940. doi:10.1111/j.1469-8749.2010.03669.x

Conflict of Interest Statement: The authors declare that the research was conducted in the absence of any commercial or financial relationships that could be construed as a potential conflict of interest.

Received: 14 May 2014; accepted: 28 August 2014; published online: 12 September 2014. Citation: Papadelis C, Ahtam B, Nazarova M, Nimec D, Snyder B, Grant PE and Okada Y (2014) Cortical somatosensory reorganization in children with spastic cerebral palsy: a multimodal neuroimaging study. Front. Hum. Neurosci. ***8****:725. doi: 10.3389/fnhum.2014.00725*

This article was submitted to the journal Frontiers in Human Neuroscience.

frontiers in
HUMAN NEUROSCIENCE

ORIGINAL RESEARCH ARTICLE
published: 21 August 2014
doi: 10.3389/fnhum.2014.00657

Assessment of hemispheric dominance for receptive language in pediatric patients under sedation using magnetoencephalography

Roozbeh Rezaie[1,2]*†, Shalini Narayana[1,2†], Katherine Schiller[2], Liliya Birg[2], James W. Wheless[2,3], Frederick A. Boop[2,4] and Andrew C. Papanicolaou[1,2]

[1] Department of Pediatrics, Division of Clinical Neurosciences, University of Tennessee Health Science Center, Memphis, TN, USA
[2] Neuroscience Institute, Le Bonheur Children's Hospital, Memphis, TN, USA
[3] Division of Pediatric Neurology, Department of Pediatrics, University of Tennessee Health Science Center, Memphis, TN, USA
[4] Department of Neurosurgery, University of Tennessee Health Science Center, Memphis, TN, USA

Edited by:
Christos Papadelis, Boston Children's Hospital – Harvard Medical School, USA

Reviewed by:
Kenji Kansaku, Research Institute of National Rehabilitation Center for Persons with Disabilities, Japan
Banu Ahtam, Boston Children's Hospital, USA

***Correspondence:**
Roozbeh Rezaie, Department of Pediatrics, Division of Clinical Neurosciences, University of Tennessee Health Science Center, 51 N. Dunlap Street, P320 Memphis, TN 38105, USA
e-mail: rrezaie@uthsc.edu

† Roozbeh Rezaie and Shalini Narayana have contributed equally to this work.

Non-invasive assessment of hemispheric dominance for receptive language using magnetoencephalography (MEG) is now a well-established procedure used across several epilepsy centers in the context of pre-surgical evaluation of children and adults while awake, alert and attentive. However, the utility of MEG for the same purpose, in cases of sedated patients, is contested. Establishment of the efficiency of MEG is especially important in the case of children who, for a number of reasons, must be assessed under sedation. Here we explored the efficacy of MEG language mapping under sedation through retrospective review of 95 consecutive pediatric patients, who underwent our receptive language test as part of routine clinical evaluation. Localization of receptive language cortex and subsequent determination of laterality was successfully completed in 78% ($n = 36$) and 55% ($n = 27$) of non-sedated and sedated patients, respectively. Moreover, the proportion of patients deemed left hemisphere dominant for receptive language did not differ between non-sedated and sedated patients, exceeding 90% in both groups. Considering the challenges associated with assessing brain function in pediatric patients, the success of passive MEG in the context of the cases reviewed in this study support the utility of this method in pre-surgical receptive language mapping.

Keywords: magnetoencephalography, non-invasive, language mapping, sedation, epilepsy, children

INTRODUCTION

Non-invasive assessment of hemispheric dominance for receptive language using magnetoencephalography (MEG) is now a well-established procedure used across several epilepsy centers in the context of pre-surgical evaluation of children and adults while awake, alert, and attentive. Specifically, localization of receptive language cortex and subsequent estimation of hemispheric dominance using MEG has most readily been achieved employing a recognition memory task for spoken words, based on hemispheric differences in the degree of activity in the temporo-parietal cortex (Breier et al., 1999; Papanicolaou et al., 2004, 2006). In particular, the reliability with which this protocol has been used to establish hemispheric dominance for receptive language in children has been shown in several normative, as well as clinical, cohorts. Moreover, the suitability of MEG language mapping protocols as an alternative to the Wada procedure have been addressed over the course of several validation studies, with concordance rates ranging from 87% in the study with largest sample to date (Papanicolaou et al., 2004) to 100% agreement in the first sub-sample of patients of the same series (Breier et al., 1999), with the rest of the studies reporting uniformly, high agreement (Breier et al., 2001; Maestú et al., 2002; Hirata et al., 2004; Bowyer et al., 2005; Merrifield et al., 2007; Doss et al., 2009; McDonald et al., 2009; Hirata et al., 2010; Findlay et al., 2012; Tanaka et al., 2013).

Nevertheless, establishment of the efficiency of MEG as a functional mapping tool is especially important in the case of children who, for a number of reasons (e.g., age; developmental delay; general anxiety), must be assessed under sedation, typically achieved through administration of one of the following agents: dexamedetomidine, etomidate, sevoflurane, midazolam, fentanyl, and more commonly- as is the case in our center- propofol (Szmuk et al., 2003; Balakrishnan et al., 2007; König et al., 2009). Given the observation by some that certain anesthetics may induce cerebral metabolic depression, and consequently affect cognitive function (Heinke and Schwarzbauer, 2002; Heinke et al., 2004), the feasibility of obtaining reliable brain activation patterns associated with higher cognitive processes, such as language, in sedated individuals requires further investigation, given the prominent role of MEG in pre-surgical functional mapping.

To date, the challenge of passively obtaining reliable language activation maps, under sedation, has been addressed in only a handful of studies, primarily using functional magnetic resonance imaging (fMRI). Specifically, it has been reported that children under propofol sedation exhibit patterns of left hemisphere activation in response to auditory linguistic stimuli comparable to those observed in non-sedated individuals (Souweidane et al., 1999; Gemma et al., 2009), with others reporting similar

patterns among sedated and non-sedated children during song, as well as speech, perception (Lai et al., 2012). Furthermore, the utility of passive language mapping with MEG has also been demonstrated recently in small series of cases, with the observation that patients undergoing subsequent resective surgery for epilepsy show no evidence of postoperative language deficits (Van Poppel et al., 2012).

In this report, we addressed whether the cortical mechanisms of linguistic processing of speech stimuli are sufficiently activated under sedation to allow for the determination of hemispheric dominance for receptive language. Specifically, we explored the efficacy of MEG language mapping under sedation through retrospective review of 95 consecutive pediatric patients, who underwent our receptive language protocol as part of routine clinical evaluation. If administration of anesthetic agents indeed results in the suppression of language related activity, we hypothesized that up to half of patients assessed under sedation would exhibit a departure from the higher incidence of left hemisphere dominance for language expected in non-sedated patients, similar to that of the general population.

MATERIALS AND METHODS

Ninety-five consecutive patients (46 non-sedated, 6–18 years of age; 49 sedated, 18 months–15 years of age) were identified through retrospective review of clinical evaluations performed at the Epilepsy Monitoring Unit of the Le Bonheur Comprehensive Epilepsy Program, Le Bonheur Children's Hospital, who underwent functional brain mapping with MEG between July 2012 and December 2013. The study was approved as a retrospective chart review by the Institutional Review Board of the University of Tennessee Health Science Center. Detailed workup for each patient included: (1) medical history and physical examination; (2) structural brain evaluation (e.g., MRI); (3) continuous scalp video electroencephalography (V-EEG) monitoring, (4) interictal scalp EEG/MEG, and (5) neuropsychological evaluation. Importantly, in cases where patients were of an appropriate age and/or behavioral difficulties did not impede cooperation, neuropsychological assessment of verbal skills was achieved using the following instruments: (1) Peabody Picture Vocabulary Test – Fourth Edition – (PPVT-4) to assess receptive vocabulary skills; (2) Boston naming test (BNT) to assess confrontational word retrieval; (3) *Verbal fluency* subtest of the Delis-Kaplan Executive Functioning System (D-KEFS) to assess semantic and phonemic fluency; (4) *Story memory* and *verbal learning* subtests of the Wide Range Assessment of Memory and Learning-Second Edition – (WRAML-2) to assess contextual and non-contextual verbal memory. Functional brain mapping with MEG was performed for each patient at the request of the referring epileptologist for further clinical evaluation. In addition to patients referred for evaluation of seizure disorder, six patients included in this retrospective review were admitted through the Le Bonheur Children's Hospital Neurosurgery Service for evaluation prior to a planned tumor resection, and two patients for planned resection of an arterio-venous malformation (AVM). These eight patients underwent the aforementioned workup, with the exception of video EEG and interictal scalp EEG/MEG. A summary of the clinical and demographic characteristics of all patients included in this review is presented in **Table 1**.

PROCEDURES

Induction of anesthesia

Sedation was administered according to the recently described protocol for the administration of general anesthesia during MEG (Birg et al., 2013). Initially, patients underwent pre-anesthetic evaluation by an anesthesiologist, which consisted of a review of medical history, and identification of contraindications for sedation (such as respiratory illness, fever, high blood pressure, and heart rate <60 beats/min). Patients did not receive any premedication prior to induction of intravenous (IV) sedation. General anesthesia was induced by propofol injection. The sedation was maintained by a propofol infusion rate of 2–10 mg/kg/h. Patients received oxygen via a nasal cannula. A blood pressure cuff and a pulse oximeter probe were placed on a lower extremity, away from the MEG sensors. All patients maintained spontaneous respiration. During breaks in the MEG data acquisition, the anesthesiologist/nurse titrated the anesthetic drugs and monitored the patient from outside the magnetically shielded room (MSR) scanner. The anesthesia machine and monitoring equipment were placed outside the MSR and extended breathing circuits, IV lines, and monitoring equipment were passed through a porthole in the MSR wall to the patient. The patient's EEG, electrocardiogram (ECG), arterial blood pressure, end-tidal CO_2, and temperature were monitored throughout the MEG testing.

Brain activation tasks

Localization of language specific cortex and subsequent determination of hemispheric dominance for receptive language was adapted from the continuous auditory word recognition protocol previously described by Papanicolaou et al. (2004) in a large-scale studies detailing specific procedures for determining hemispheric dominance for language functions using MEG. Immediately prior to the commencement of the MEG scan, patients instructed to "try to remember" a set of five words, deemed as targets. Depending on the patient's overall verbal memory capacity, the targets were presented once or twice. Subsequently, during the MEG scanning, the five target words were repeated in a different random order, mixed with a different set of 30 distractors (non-repeating words) in each of four blocks of stimuli. Stimuli were presented for 1 s, one at a time (with a randomly varied interstimulus interval of 2–3 s), and delivered binaurally via plastic tubes terminating in ear inserts at the patient's outer ear. Target words (*jump, please, little, drink,* and *good*) included 4 monosyllabic and one disyllabic word, and had a mean frequency in the Zeno et al. (1995) G6-7 corpus of 158 occurrences per million (range: 32–194 occurrences). A slightly higher proportion of distractors were disyllabic (40%) and the remaining monosyllabic, with a mean frequency of occurrence of 150 words per million in the same corpus (range: 18–820). During the procedure, patients were asked to lift their index finger of the dominant hand whenever they detect a repeated (one of the five targets) word. In the case of sedated patients, this protocol was modified to conform to a passive task given the state of

Table 1 | Clinical and demographic characteristics of patients having undergone receptive language mapping with and without sedation.

	Non-sedated	Sedated
N	46	49
Gender	24 M/23 F	21 M/28 F
Age range (Mean ± SD)	6–18 years (12.8 ± 3.4)	18 months–15 years (6.1 ± 3.2)
Handedness	37 Right/9 left	27 Right/15 left/7 undetermined
Chief complaint		
Symptomatic Partial Seizures	17	18
Symptomatic Generalized Seizures	3	15
Symptomatic Mixed Generalized Seizures	–	6
Cryptogenic Partial Seizures	9	–
Cryptogenic Mixed Seizures	1	4
Idiopathic Generalized Seizures	2	–
Idiopathic Mixed Generalized Seizures	3	–
Paroxysmal Events	6	3
Neuroepothelial Tumor	1	–
Ganglioglioma	2	–
Astrocytoma	1	–
Ependymoma	–	1
Cervical Medullary Tumor	–	1
Aterio-Venous Malformation (AVM)	1	1

the patients. Specifically, while the target words were presented immediately prior to commencement of the MEG scan, as was the case in non-sedated patients, sedated patient's overall verbal memory capacity was n ot assessed. Consequently, sedated patients were not required to respond to the occurrence of the target words, which excluded the possibility of assessment of their verbal memory performance.

Imaging procedures

Magnetoencephalography recordings were obtained with a whole-head neuromagnetometer array (4-D Neuroimaging, Magnes WH3600) equipped with 248 first-order magnetometer coils and housed in a magnetically shielded chamber. The position of the sensors relative to the patient's head was determined using five coils, three of which were anchored to the fiduciary points (nasion, left, and right periauricular points) and two on the forehead. The coils were activated briefly by passing a small current through them, at the beginning and then again at the end, of the recording session and their precise location in three-dimensional space was determined using a localization algorithm native to the recording system software. During the same process, the patient's head shape was digitized using a stylus for subsequent localization of activity sources. The magnetic flux measurements were digitized at 508 Hz, and filtered off-line with a band pass filter between 0.1 and 20 Hz, baseline corrected (150 ms pre-stimulus onset) to remove DC drifts, and subjected to a noise reduction algorithm that is part of the 4D-Neuroimaging software.

Structural MR images were obtained using either: (1) a sagittal T1-weighted 3D MPRAGE sequence acquired on a Siemens Verio scanner (Siemens AG, Munich, DE) equipped with a 32 channel head coil (176 slices, FOV 256 mm, voxel size 1.0 mm × 1.0 mm × 1.0 mm, $TE/TR = 2.6/2530$ ms, 512 × 512 matrix, Flip angle 7°); or (2) an axial T1-weighted 3D FSPGR sequence acquired on a GE Signa HDxt scanner (General Electric, Milwaukee, WI) equipped with an 8-channel head coil (220 slices, FOV 256 mm, voxel size 0.9 mm × 0.9 mm × 1.0 mm, $TE/TR = 3.7/8$ ms, 512 × 512 matrix, Flip angle 12°).

Data analysis procedures

Following filtering, single-trial MEG event-related field segments (ERFs) in response to 110–125 stimulus presentations were averaged and brain activity sources were modeled as single equivalent current dipoles (ECDs) and fitted independently at successive 2 ms intervals (Sarvas, 1987; Papanicolaou et al., 2004; Simos et al., 2005) using the 4D-Neuroimaging proprietary software. The algorithm searched for the source most likely to have produced the observed magnetic field distribution at a given point in time. For a given point in time, the ECD fitting algorithm was applied to the magnetic flux measurements obtained from a group of 34–38 magnetometers, always including both magnetic flux extrema. Source solutions were considered satisfactory if they were associated with a correlation coefficient of at least 0.9 between the observed and the "best" predicted magnetic field distribution, and occurred between 200–800 ms after stimulus onset to ensure

activity sources represent language-related activity, rather than modality-specific sensory activation (Simos et al., 1998; Szymanski et al., 2001; Halgren et al., 2002; Helenius et al., 2002). The location of each estimated dipolar source was determined with reference to a Cartesian coordinate system based on three fiducial points on the head (the nasion and external meatus of each ear), and subsequently approximated by co-registering these points to the patient's high-resolution anatomical MRI.

Receptive language cortex was identified by evoked activity sources computed during the late portion (>200 ms) of the ERF waveform, falling within fronto-temporal, temporo-parietal, and mesial temporal regions, for each hemisphere. Final laterality judgments for receptive language for MEG-derived activation maps were based on two criteria. First, a laterality index was calculated by comparing the number of acceptable late activity sources observed in the right and left hemispheric activation [$LI = (RH - LH)/(RH + LH)$], with a range from +1 to −1, with positive values indicating left hemispheric dominance and negative numbers indicating right hemispheric dominance. Index values between 0.1 and −0.1 were considered to be indicative of bilaterally symmetric activation. Second, determination of laterality also considered the spatial extent of activation, namely the degree to which dipolar sources associated with the late portion of the ERF waveform engaged association regions critical to supporting receptive language function.

RESULTS

Successful completion of laterality assessment for receptive language was achieved in 78% ($n = 36$) and 55% ($n = 27$) of non-sedated and sedated patients, respectively (**Table 2**). Across both groups of patients, cases with data deemed unusable for analysis was associated with several sources of artifact, including vagus nerve stimulator, ventriculoperitoneal shunt, orthodontic devices, excess epileptiform discharges, and environmental noise interfering with ambient recording environment.

Table 2 | Profiles of non-sedated and sedated patients included in final analysis and rationale for exclusion of cases not considered for laterality assessment.

	Non-sedated	Sedated
N	36/46 (78%)	27/49 (55%)
Gender	18 M/18 F	13 M/14 F
Age range (Mean ± SD)	6–18 years	18 months–11 years
Handedness	(13.2 ± 3.0)	(5.3 ± 2.8)
	32 Right/4 left	15 R/6 L/5 undetermined
Artifact source		
VNS	1	8
VP Shunt	–	1
Orthodontic Devices	2	1
Excessive Epileptiform Activity	2	–
Environmental Noise (e.g., Intraoperative MRI; Medical monitoring devices)	5	12

The number of total dipolar (activity) sources estimated between the two patient groups, across both hemispheres, did not significantly differ (mean ± SEM: 239 ± 28 in the sedated group vs. 244 ± 23 in non-sedated group, $p = 0.85$). Furthermore, a similar comparison at the hemispheric level revealed no significant differences between the two groups. On average (±SEM), the number of dipoles estimated in the left hemisphere was 287 ± 21 in the non-sedated group, and 273 ± 30 in the sedated group ($p = 0.7$), and in the right hemisphere it was 201 ± 23 in the non-sedated group, and 206 ± 24 in the sedated group ($p = 0.9$).

As summarized in **Table 3**, there was no significant difference in the proportion of non-sedated (91.6%) and sedated (92.6%) patients deemed to be left hemisphere dominant for receptive language (Fisher's exact test, $p = 0.636$). Moreover, among non-sedated and sedated individuals, two patients in each group were found to demonstrate bilateral representation for receptive language, with one patient in the non-sedated group also having been judged to be right hemisphere dominant. Characteristic brain activation profiles on the basis which laterality judgments for receptive language were made in non-sedated and sedate patients are displayed in **Figure 1**.

As mentioned earlier, the approach taken for making clinical judgments regarding hemispheric dominance for receptive language took into account both the conventional quantitative LI, as well as visual inspection of brain activation profiles to assess the spatial extent of activity within the left and right hemispheres. On the basis of this approach, it is noteworthy that across both non-sedated and sedated groups, final laterality judgments in 26 out of the 63 patients with data deemed usable for analysis exhibited a discord between the traditional LI scores and qualitative assessment of brain activation maps. In particular, among 12 patients with an LI score suggestive of bilateral language representation, consideration of the spatial distribution of activity sources rendered final laterality judgments as left hemisphere dominant for receptive language. Moreover, in 11 patients judged to be right hemisphere dominant for receptive language according to LI scores, nine were deemed to be left hemisphere dominant and two as bilateral. Furthermore, of three patients with LI scores indicating left hemisphere dominance, one was deemed to be right dominant and two as bilateral. Examples of cases where hemispheric differences in the spatial distribution of activity sources, primarily characterized by clusters of activity outside the primary auditory cortex, that resulted in reconsideration of final laterality judgments based solely on LI scores, are provided in **Figure 2**.

Table 3 | Judgments on hemispheric dominance for receptive language in non-sedated and sedated patients.

	Non-sedated	Sedated
Left hemisphere	33	25
Right hemisphere	1	0
Bilateral	2	2

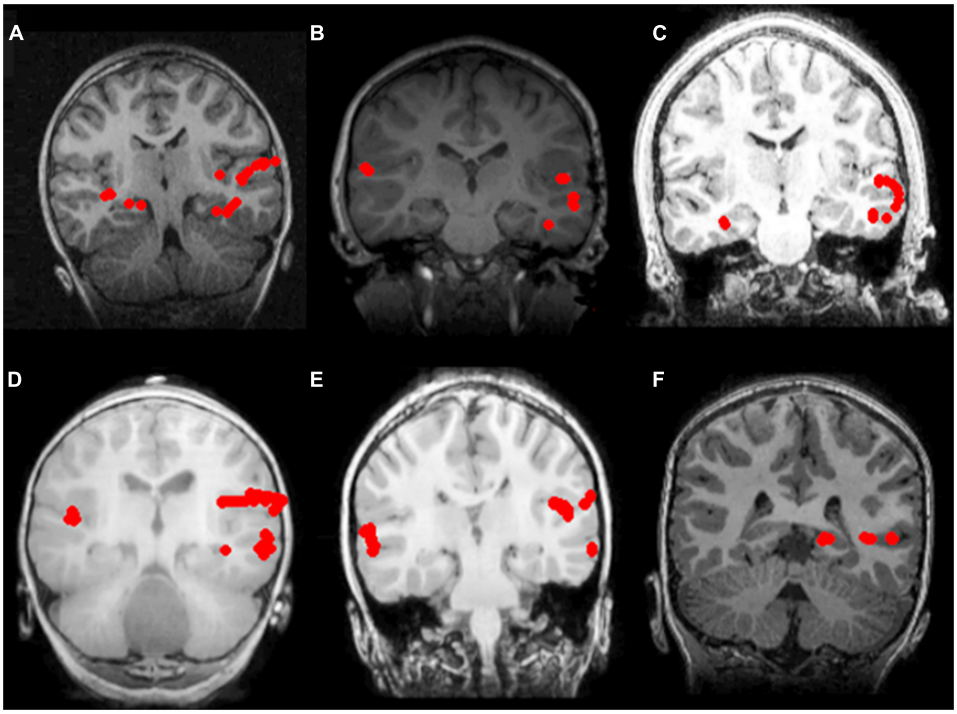

FIGURE 1 | Receptive language mapping with MEG with and without sedation. Language activity (dipolar) sources are represented as solid red circles projected onto the patients' MRI, displayed in radiological convention. Left hemispheric dominance for receptive language in patients evaluated without sedation **(A–C)**, and with sedation **(D–F)**. **(A)** 7 year-old female with symptomatic frontal lobe epilepsy; **(B)** 8 year-old female with ganglioglioma of the left temporal lobe; **(C)** 16 year-old male with symptomatic partial seizures of right temporal lobe origin; **(D)** 2 year-old male with cervical medullary tumor; **(E)** 6 year-old male with symptomatic epileptic spasms of right hemisphere origin; **(F)** 6 year-old male with symptomatic partial seizures of left temporal lobe origin.

DISCUSSION

In the present study, we evaluated the efficiency of MEG in establishing hemispheric dominance for receptive language in pediatric patients under propofol sedation, compared to patients assessed without sedation. Localization of receptive language cortex and subsequent determination of laterality was successfully achieved in 78 and 55% of non-sedated and sedated patients, respectively. While cases excluded from analysis were affected by similar sources of mechanical and/or biological artifact in both groups of patients, this was found to be more frequent in sedated patients, thus leading to smaller proportion of successful laterality assessments in this group. However, the proportion of patients deemed left hemisphere dominant for receptive language did not differ between non-sedated and sedated patients, exceeding 90% in both groups, overlapping with the accepted rate of incidence of left-lateralized individuals in the general population (Moser et al., 2011).

The relatively high rate of successful laterality assessments in both non-sedated and sedated patients, as well as similarities in the lateralization estimates between the two groups, make a strong case for the adoption of the passive receptive language mapping protocol discussed in the current study. For example, in cases where surgical intervention is warranted, either for treatment of intractable seizures or tumor resection, passive language mapping with MEG may be a suitable alternative to the Wada test and direct cortical stimulation mapping which, from a practical perspective, may be difficult to carry out in pediatric patients due to either age or inability to tolerate the demands posed by these procedures. Indeed, considering that in the present study sedation was administered to mitigate behavioral difficulties associated with developmental delay in a large number of patients, passive language mapping may in some cases better characterize the organization of linguistic processes, as opposed to more conventional language assessments that rely on patient cooperation. Nevertheless, in a broader context of the goal of the present study, it is worth noting that in patients where formal neuropsychological testing is feasible, performance on independent measures of linguistic ability may be accounted for by language profiles derived using MEG, as well as other neuroimaging modalities. For example, the capacity for verbal memory and receptive vocabulary skills assessed behaviorally may in fact reflect the spatiotemporal profile of receptive language function obtained using the present MEG protocol. However, despite these assessments being routine clinical practice in our center, the unavailability of complete neuropsychological data in the course of the chart review presented in this study made such a comparison difficult, and should be a point of consideration in future studies.

Though small in number, several studies have attempted to address the feasibility of obtaining functional brain maps in individuals under sedation. It has previously been argued by Heinke

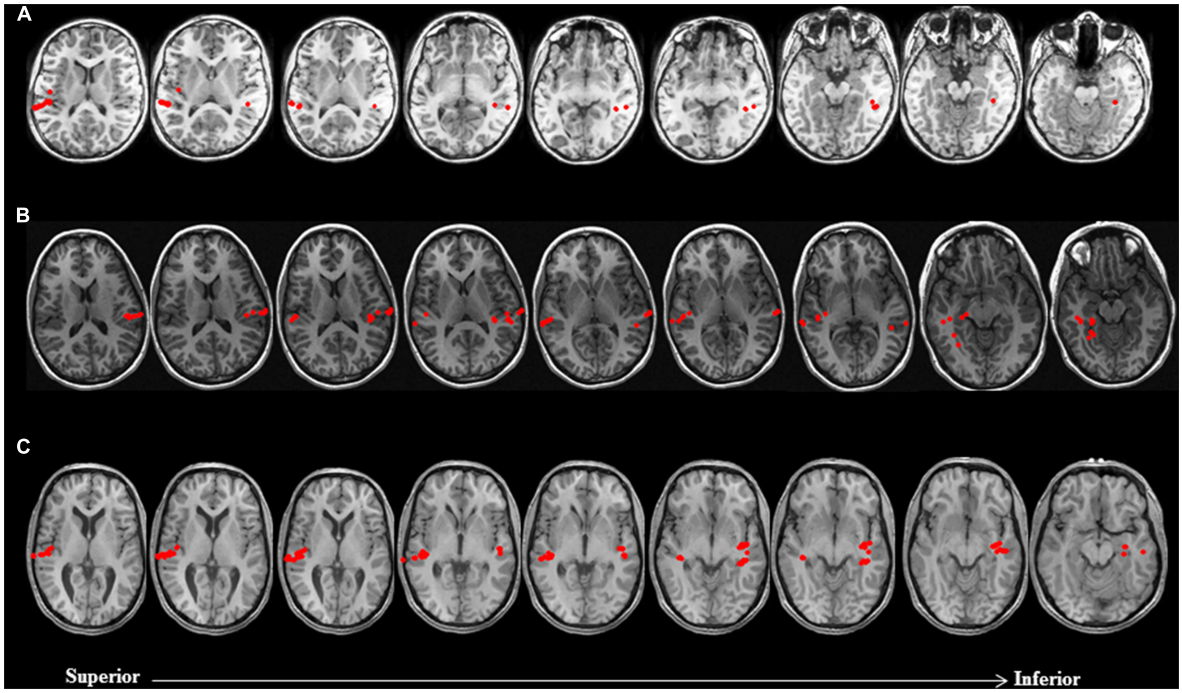

FIGURE 2 | Discordance between laterality judgments based on LI estimates and visual inspection of brain activation profiles in three non-sedated patients. Language activity (dipolar) sources are represented as solid red circles projected onto the patients' MRI, displayed in radiological convention. **(A)** 9 year-old female with symptomatic partial epilepsy of left temporal lobe origin was deemed to be right dominant for receptive language based on LI (−0.54). Visual inspection of brain activation profiles revealed despite a greater number of activity sources concentrated in the auditory cortex of the right hemisphere, posterior and mesial temporal engagement in the left hemisphere suggested that patient was left dominant for receptive language. **(B)** 14 year-old female with cryptogenic partial epilepsy of left temporal lobe origin was deemed to be left dominant for receptive language based on LI (0.43). Visual inspection of brain activation profiles revealed despite a greater number of activity sources concentrated in the auditory cortex of the left hemisphere, lateral and mesial temporal engagement in the right hemisphere suggested that patient was right dominant for receptive language. **(C)** 17 year-old male with idiopathic generalized seizures was deemed to have bilateral representation for receptive language based on LI (0). Visual inspection of brain activation profiles revealed despite an equal number of activity sources bilaterally, posterior middle and mesial temporal engagement in the left hemisphere suggested that patient was left dominant for receptive language.

and Schwarzbauer (2002) and Heinke et al. (2004) that anesthetic agents result in cerebral metabolic depression, potentially affecting brain responses to external stimulation. For example, the authors Heinke et al. (2004) reported dose-dependent effects of propofol on temporo-frontal regions involved in auditory language processing using passive fMRI in healthy volunteers, albeit these effects were most marked in frontal rather than temporal regions. Moreover, an fMRI study of controls by Davis et al. (2007) found that despite impairment of semantic and mnemonic processes at low levels of propofol sedation, perceptual processing of speech at even high levels of sedation is preserved, as characterized by engagement of temporal lobe regions previously implicated in receptive language processing.

The observations made in our study are consistent with the previous literature highlighting the utility of non-invasive techniques in identifying eloquent cortex among sedated patients (Papanicolaou et al., 2014). For example, using fMRI Souweidane et al. (1999) demonstrated consistent activation in left temporo-parietal and frontal regions in a group of eight children under propofol sedation, in response to passive auditory stimuli consisting of words and sentences, a pattern comparable to that derived in non-sedated subjects using a similar paradigm. Moreover, Gemma et al. (2009) compared the differential effects of propofol and midazolam on fMRI brain activation patterns during a passive listening task in 14 children, and reported that patients under propofol sedation exhibited primary auditory cortex activation patterns more similar to that observed in non-sedated adults. More recently, Lai et al. (2012) derived brain activation maps outlining cortical regions underlying speech and song perception in a group of low-functioning autistic children under light propofol sedation using passive auditory stimulation during fMRI. In addition, similar success was observed by Van Poppel et al. (2012) for the purpose of establishing hemispheric dominance for receptive language with MEG using a passive language mapping protocol in a series of 15 patients while under either sedation or during natural sleep (Stage I/II), three of whom exhibited no subsequent postoperative language deficits.

Given our criteria for determining hemispheric dominance in clinical practice, the findings from the present study also highlight the importance of the qualitative assessment of brain activation maps on an individual basis, as an adjunct to traditional quantitative estimates of laterality. Specifically, a large number of assessments based solely on the calculated LI, in either

group of patients in the present study, were not concordant with judgments based on visual inspection of activation profiles associated with receptive language processing. As evidenced by the cases reviewed here, recognizing the degree to which regions supporting linguistic processes are engaged is equally, if not more, important for identifying the dominant hemisphere, than only taking into account differences in the amount of activity sources between the hemisphere. An example of this scenario, and one encountered numerous times in our clinical assessments, is the observation that despite a greater distribution (but lower absolute count) of activity sources within one hemisphere, a greater number of activity sources concentrated in one region (e.g., auditory cortex) of the other hemisphere results in an LI that may not accurately reflect the organization of receptive language in a given individual. Indeed, considering the potential for functional reorganization in neurological patients, especially in the case of individuals with space-occupying lesions, a more subjective approach to assessing laterality for receptive language may be warranted.

Collectively, the findings from our large-scale retrospective review constitute an indication for the efficiency of MEG in establishing hemispheric dominance for receptive language in children under sedation. Considering the challenges associated with assessing brain function in pediatric patients, the success of passive MEG in the context of the cases reviewed in this study support the utility of this method in pre-surgical language mapping. Future studies incorporating a multimodal imaging framework may further highlight the efficiency of non-invasive methods for functional mapping in challenging pediatric populations.

ACKNOWLEDGMENTS

The authors would like to kindly acknowledge the support of the Neuroscience Institute- Le Bonheur Children's Hospital (http://www.lebonheur.org/our-services/neuroscience-institute/) for the work presented in this manuscript. The authors also wish to thank Dr. Abbas Babajani-Feremi and Dr. Bryan Potter for their helpful comments during the revision phase of the manuscript.

REFERENCES

Balakrishnan, G., Grover, K. M., Mason, K., Smith, B., Barkley, G. L., Tepley, N., et al. (2007). A retrospective analysis of the effect of general anesthetics on the successful detection of interictal epileptiform activity in magnetoencephalography. *Anesth. Analg.* 104, 1493–1497, table of contents. doi: 10.1213/01.ane.0000264084.12323.43

Birg, L., Narayana, S., Rezaie, R., and Papanicolaou, A. (2013). Technical tips: MEG and EEG with sedation. *Neurodiagn. J.* 53, 229–240.

Bowyer, S. M., Moran, J. E., Weiland, B. J., Mason, K. M., Greenwald, M. L., Smith, B. J., et al. (2005). Language laterality determined by MEG mapping with MR-FOCUSS. *Epilepsy Behav.* 6, 235–241. doi: 10.1016/j.yebeh.2004.12.002

Breier, J. I., Simos, P. G., Wheless, J. W., Constantinou, J. E., Baumgartner, J. E., Venkataraman, V., et al. (2001). Language dominance in children as determined by magnetic source imaging and the intracarotid amobarbital procedure: a comparison. *J. Child Neurol.* 16, 124–130. doi: 10.1177/088307380101600211

Breier, J. I., Simos, P. G., Zouridakis, G., Wheless, J. W., Willmore, L. J., Constantinou, J. E., et al. (1999). Language dominance determined by magnetic source imaging: a comparison with the Wada procedure. *Neurology* 53, 938–945. doi: 10.1212/WNL.53.5.938

Davis, M. H., Coleman, M. R., Absalom, A. R., Rodd, J. M., Johnsrude, I. S., Matta, B. F., et al. (2007). Dissociating speech perception and comprehension at reduced levels of awareness. *Proc. Natl. Acad. Sci. U.S.A.* 104, 16032–16037. doi: 10.1073/pnas.0701309104

Doss, R. C., Zhang, W., Risse, G. L., and Dickens, D. L. (2009). Lateralizing language with magnetic source imaging: validation based on the Wada test. *Epilepsia* 50, 2242–2248. doi: 10.1111/j.1528-1167.2009.02242.x

Findlay, A. M., Ambrose, J. B., Cahn-Weiner, D. A., Houde, J. F., Honma, S., Hinkley, L. B., et al. (2012). Dynamics of hemispheric dominance for language assessed by magnetoencephalographic imaging. *Ann. Neurol.* 71, 668–686. doi: 10.1002/ana.23530

Gemma, M., de Vitis, A., Baldoli, C., Calvi, M. R., Blasi, V., Scola, E., et al. (2009). Functional magnetic resonance imaging (fMRI) in children sedated with propofol or midazolam. *J. Neurosurg. Anesthesiol.* 21, 253–258. doi: 10.1097/ANA.0b013e3181a7181d

Halgren, E., Dhond, R. P., Christensen, N., Van Petten, C., Marinkovic, K., Lewine, J. D., et al. (2002). N400-like magnetoencephalography responses modulated by semantic context, word frequency, and lexical class in sentences. *Neuroimage* 17, 1101–1116. doi: 10.1006/nimg.2002.1268

Heinke, W., Kenntner, R., Gunter, T. C., Sammler, D., Olthoff, D., and Koelsch, S. (2004). Sequential effects of increasing propofol sedation on frontal and temporal cortices as indexed by auditory event-related potentials. *Anesthesiology* 100, 617–625. doi: 10.1097/00000542-200403000-00023

Heinke, W., and Schwarzbauer, C. (2002). In vivo imaging of anaesthetic action in humans: approaches with positron emission tomography (PET) and functional magnetic resonance imaging (fMRI). *Br. J. Anaesth.* 89, 112–122. doi: 10.1093/bja/aef155

Helenius, P., Salmelin, R., Richardson, U., Leinonen, S., and Lyytinen, H. (2002). Abnormal auditory cortical activation in dyslexia 100 msec after speech onset. *J. Cogn. Neurosci.* 14, 603–617. doi: 10.1162/089892902 60045846

Hirata, M., Goto, T., Barnes, G., Umekawa, Y., Yanagisawa, T., Kato, et al. (2010). Language dominance and mapping based on neuromagnetic oscillatory changes: comparison with invasive procedures. *J. Neurosurg.* 112, 528–538. doi: 10.3171/2009.7.JNS09239

Hirata, M., Kato, A., Taniguchi, M., Saitoh, Y., Ninomiya, H., Ihara, A., et al. (2004). Determination of language dominance with synthetic aperture magnetometry: comparison with the Wada test. *Neuroimage* 23, 46–53. doi: 10.1016/j.neuroimage.2004.05.009

König, M. W., Mahmoud, M. A., Fujiwara, H., Hemasilpin, N., Lee, K. H., and Rose, D. F. (2009). Influence of anesthetic management on quality of magnetoencephalography scan data in pediatric patients: a case series. *Paediatr. Anaesth.* 19, 507–512. doi: 10.1111/j.1460-9592.2009.02983.x

Lai, G., Pantazatos, S. P., Schneider, H., and Hirsch, J. (2012). Neural systems for speech and song in autism. *Brain* 135, 961–975. doi: 10.1093/brain/awr335

Maestú, F., Ortiz, T., Fernandez, A., Amo, C., Martin, P., Fernández, S., et al. (2002). Spanish language mapping using MEG: a validation study. *Neuroimage* 17, 1579–1586. doi: 10.1006/nimg.2002.1235

McDonald, C. R., Thesen, T., Hagler, D. J. Jr., Carlson, C., Devinksy, O., Kuzniecky, R., et al. (2009). Distributed source modeling of language with magnetoencephalography: application to patients with intractable epilepsy. *Epilepsia* 50, 2256–2266. doi: 10.1111/j.1528-1167.2009.02172.x

Merrifield, W. S., Simos, P. G., Papanicolaou, A. C., Philpott, L. M., and Sutherling, W. W. (2007). Hemispheric language dominance in magnetoencephalography: sensitivity, specificity, and data reduction techniques. *Epilepsy Behav.* 10, 120–128. doi: 10.1016/j.yebeh.2006.10.012

Moser, D. C., Papanicolaou, A. C., Swank, P., and Breier, J. I. (2011). Evidence for the solidarity of the expressive and receptive language systems: a retrospective study. *J. Int. Neuropsychol. Soc.* 17, 62–68. doi: 10.1017/S13556177 10001153

Papanicolaou, A. C., Pazo-Alvarez, P., Castillo, E. M., Billingsley-Marshall, R. L., Breier, J. I., Swank, P. R., et al. (2006). Functional neuroimaging with MEG: normative language profiles. *Neuroimage* 33, 326–342. doi: 10.1016/j.neuroimage.2006.06.020

Papanicolaou, A. C., Rezaie, R., Narayana, S., Choudhri, A. F., Wheless, J. W., Castillo, E. M., et al. (2014). Is it time to replace the Wada test and put awake craniotomy to sleep? *Epilepsia* 55, 629–632. doi: 10.1111/epi.12569

Papanicolaou, A. C., Simos, P. G., Castillo, E. M., Breier, J. I., Sarkari, S., Pataraia, E., et al. (2004). Magnetocephalography: a noninvasive alternative to the Wada procedure. *J. Neurosurg.* 100, 867–876. doi: 10.3171/jns.2004.100. 5.0867

Sarvas, J. (1987). Basic mathematical and electromagnetic concepts of the biomagnetic inverse problem. *Phys. Med. Biol.* 32, 11–22. doi: 10.1088/0031-9155/32/1/004

Simos, P. G., Breier, J. I., Zouridakis, G., and Papanicolaou, A. C. (1998). Identification of language-specific brain activity using magnetoencephalography. *J. Clin. Exp. Neuropsychol.* 20, 706–722. doi: 10.1076/jcen.20.5.706.1127

Simos, P. G., Sarkari, S., Castillo, E. M., Billingsley-Marshall, R. L., Pataraia, E., Clear, T., et al. (2005). Reproducibility of measures of neurophysiological activity in Wernicke's area: a magnetic source imaging study. *Clin. Neurophysiol.* 116, 2381–2391. doi: 10.1016/j.clinph.2005.06.019

Souweidane, M. M., Kim, K. H., McDowall, R., Ruge, M. I., Lis, E., Krol, G., et al. (1999). Brain mapping in sedated infants and young children with passive-functional magnetic resonance imaging. *Pediatr. Neurosurg.* 30, 86–92. doi: 10.1159/000028768

Szmuk, P., Kee, S., Pivalizza, E. G., Warters, R. D., Abramson, D. C., and Ezri, T. (2003). Anaesthesia for magnetoencephalography in children with intractable seizures. *Paediatr. Anaesth.* 13, 811–817. doi: 10.1046/j.1460-9592.2003.01159.x

Szymanski, M. D., Perry, D. W., Gage, N. M., Rowley, H. A., Walker, J., Berger, M. S., et al. (2001). Magnetic source imaging of late evoked field responses to vowels: toward an assessment of hemispheric dominance for language. *J. Neurosurg.* 94, 445–453. doi: 10.3171/jns.2001.94.3.0445

Tanaka, N., Liu, H., Reinsberger, C., Madsen, J. R., Bourgeois, B. F., Dworetzky, B. A., et al. (2013). Language lateralization represented by spatiotemporal mapping of magnetoencephalography. *AJNR Am. J. Neuroradiol.* 34, 558–563. doi: 10.3174/ajnr.A3233

Van Poppel, M., Wheless, J. W., Clarke, D. F., McGregor, A., McManis, M. H., Perkins, F. F. Jr., et al. (2012). Passive language mapping with magnetoencephalography in pediatric patients with epilepsy. *J. Neurosurg. Pediatr.* 10, 96–102. doi: 10.3171/2012.4.PEDS11301

Zeno, S. M., Ivens S. H., Millard, R. T., and Duvvuri R. (1995). *Educator's Word Frequency Guide*. Brewster, NY: Touchstone Applied Science Associates.

Conflict of Interest Statement: The authors declare that the research was conducted in the absence of any commercial or financial relationships that could be construed as a potential conflict of interest.

Received: 16 May 2014; accepted: 06 August 2014; published online: 21 August 2014.
Citation: Rezaie R, Narayana S, Schiller K, Birg L, Wheless JW, Boop FA and Papanicolaou AC (2014) Assessment of hemispheric dominance for receptive language in pediatric patients under sedation using magnetoencephalography. Front. Hum. Neurosci. ***8****:657. doi: 10.3389/fnhum.2014.00657*
This article was submitted to the journal Frontiers in Human Neuroscience.

frontiers in
HUMAN NEUROSCIENCE

ORIGINAL RESEARCH ARTICLE
published: 20 June 2014
doi: 10.3389/fnhum.2014.00447

Greater utilization of neural-circuits related to executive functions is associated with better reading: a longitudinal fMRI study using the verb generation task

Tzipi Horowitz-Kraus*, Jennifer J. Vannest, Elveda Gozdas and Scott K. Holland

Cincinnati Children's Research Foundation, Pediatric Neuroimaging Research Consortium, Cincinnati Children's Hospital Medical Center, Cincinnati, OH, USA

Edited by:
Christos Papadelis, Harvard Medical School, USA

Reviewed by:
Nadine Gaab, Harvard Medical School, USA
Panagiotis G. Simos, University of Crete, Greece

****Correspondence:***
Tzipi Horowitz-Kraus, Cincinnati Children's Research Foundation, Pediatric Neuroimaging Research Consortium, Cincinnati Children's Hospital Medical Center, Burnet Avenue 3333, Cincinnati, OH 45229-3039, USA
e-mail: tzipi.horowitz-kraus@cchmc.org

Introduction: Reading is an acquired-developmental ability that relies on intact language and executive function skills. Verbal fluency tasks (such as verb generation) also engage language and executive function skills. Performance of such tasks matures with normal language development, and is independent of reading proficiency. In this longitudinal fMRI study, we aim to examine the association between maturation of neural-circuits supporting both executive functions and language (assessed using verb generation) with reading proficiency achieved in adolescence with a focus on left-lateralization typical for language proficiency.

Methods: Normalized fMRI data from the verb generation task was collected from 16 healthy children at ages 7, 11, and 17 years and was correlated with reading scores at 17 years of age. Lateralization indices were calculated in key language, reading, and executive function-related regions in all age groups.

Results: Typical development was associated with (i) increasingly left-lateralized patterns in language regions (ii) more profound left-lateralized activation for reading and executive function-related regions when correlating with reading scores, (iii) greater involvement of frontal and parietal regions (in older children), and of the anterior frontal cortex (in younger children).

Conclusion: We suggest that reading and verb generation share mutual neural-circuits during development with major reliance on regions related to executive functions and reading. The results are discussed in the context of the dual-networks architecture model.

Keywords: development, dual-networks model, executive functions, fMRI, reading, verb generation

INTRODUCTION

The normal course of development involves continued improvement in higher-order cognitive abilities (e.g., executive functions), that originate in prefrontal cortex (PFC) (Diamond, 2002 for review). There is strong evidence supporting the continued anatomical and functional maturation of the PFC related to development of these skills (Sowell et al., 1999). The cognitive skills gathered under the umbrella term "Executive functions" include a wide range of conscious processes involved in monitoring and optimizing performance (Baddeley, 1986) such as error monitoring, selective attention to the relevant stimulus, inhibiting execution of undesired responses, working memory (WM) abilities (the ability to manipulate and maintain information), shifting, and fluency.

Fluency is part of the information processing component of executive functions and reflects the integrity of neural connections and the functional integration of frontal systems. Fluency can be evaluated by the speed, quantity, and quality of output (Anderson, 2002). Semantic verbal fluency ability is typically assessed either by semantic category fluency (generating members of a category) or by verb generation in response to auditory or visual nouns. Individuals performing a semantic category fluency task, exhibit activation of the left hemisphere regions related to language and articulation [inferior frontal gyrus (IFG), representing word retrieval; middle frontal gyrus (MFG) attributed to verbal WM, and supplementary motor area (SMA), which reflects attention and motor planning] (Paulesu et al., 1997; Hugdahl et al., 1999; Pihlajamaki et al., 2000; Gaillard et al., 2003) in both children and adults (Gaillard et al., 2003). The verb generation task also reflects semantic verbal fluency ability (Piatt et al., 1999). In this task, participants are presented with a noun, either auditorily or visually, and are asked to generate related verbs. Similar to semantic category fluency, the verb generation task has been found to activate several frontal regions [left and right IFG (BA 44, 45, 46, 47), and the left medial frontal gyrus (MFG) (BA 6, 8, 9)] as well as language regions in the brain [left and right medial temporal gyrus (BA 19/39, 21), right and left inferior temporal gyrus (ITG) (BA 19/37), and superior temporal gyrus (STG) (BA 22)] in participants aged 5–18 years of age (Holland et al., 2001, 2007; Karunanayaka et al., 2010, 2011). We have also documented developmental changes in lateralization of the language-network supporting the verb generation task in

both a cross-sectional (Holland et al., 2007) and a longitudinal study (Szaflarski et al., 2006). Specifically, the network becomes increasingly left-lateralized with age. Karunanayaka examined developmental changes in neurocognitive modules underlying the verb generation task using Independent Component Analysis (Karunanayaka et al., 2011). Two primary neurocognitive modules were identified in that work: (1) word processing [auditory (BA 22), and then phonological processing (BA 45/47, BA 44/45/46/9, and 39/40)] and; (2) word generation [the phonological information becomes associated with a semantic meaning (BA 30/35/19/27/39) a process that can engage visual imagery (BA 17)] (Karunanayaka et al., 2011). Although these regions were found to be active in the verb generation task from 5 to 18 years old, independent component analysis, and structural equation modeling revealed that the connections between STG and the IFG and within the frontal lobe itself (IFG and MFG) increase and become more left-lateralized from 5 to 18 years. This is in line with the timecourse of continued PFC maturation (Holland et al., 2001; Karunanayaka et al., 2011), and consistent with studies showing increased left-lateralization for verb generation from the age of 5 to 18 years (Holland et al., 2001). Utilizing this same large imaging and behavioral dataset, we can build on the previously published results from this task to explore the relationship between this developing circuitry underlying verb generation and reading skills.

Reading is also a linguistic ability, though unlike the phonological and semantic skills that underlie verbal fluency tasks, it must be explicitly acquired. Since reading is a phylogenetically new skill (roughly, 5000 years old), neuroscientists suggest that the brain uses regions, which are originally devoted to other cognitive functions and utilize them for gaining information from written symbols (see also Price, 2012; Vogel et al., 2013, 2014). Reading demands the translation of abstract graphemes (letters) into their corresponding spoken language sounds (phonemes) that format meaningful words (semantics). It therefore engages visual (cuneus and fusiform gyrus) (McCandliss et al., 2003), auditory/phonological (angular gyrus, STG) (Dehaene-Lambertz et al., 2002), and semantic brain regions (IFG) (Newman and Joanisse, 2011) mainly in the left hemisphere (Chiarello et al., 2009). An efficient synchronization of these processes is needed for fluent reading, which demands the engagement of the executive system (Breznitz, 2006). Behaviorally, reading performance has been suggested to correlate with executive function skills (Christopher et al., 2012; Kieffer et al., 2013; Booth et al., 2014). Many studies have focused on specific aspects of executive functions expected to be related to reading. For example, attention shifting and inhibition (Kieffer et al., 2013), WM, and speed of processing (Christopher et al., 2012), as well as verbal fluency (or verb generation ability), all were found to be correlated with reading ability (Snowling et al., 1997). These findings suggest a major role for executive functions in the reading process.

The neural architecture supporting executive function is described by the dual-networks top-down model (Dosenbach et al., 2008). This model proposed two cognitive control/executive functions networks with different neuroanatomical correlates. The first is the rapid adaptive control network, which is in charge of allocating attention to a cue; uses feedback to affect processing and involves a frontal–parietal circuit. The second network is the set-maintenance network that maintains task goals, which involves a cingulo-opercular circuit. The activation of these networks changes with development due to changes in connectivity between key elements within the network (Dosenbach et al., 2008). Both networks are engaged during reading (Ihnen et al., 2013), but only the functional connectivity between the fronto-parietal network and the fusiform gyrus was found to be positively correlated with reading skill and age (see Vogel et al., 2014).

In this current study, we aim to examine the relations between the maturation of neural networks supporting executive functions and language (during the verb generation task) and reading skill. We focus on the language-network described above (Holland et al., 2007; Karunanayaka et al., 2010, 2011), that includes reading regions related to word recognition (i.e., word form area, BA 37), and regions related to semantic WM (dorsolateral PFC; BA 9, anterior PFC; BA 10), which are part of the executive function network in the dual-network model (Dosenbach et al., 2008). To explore the role of early emerging language networks (Ahmad et al., 2003) in support of later acquired reading skills, we employed a novel longitudinal data analysis model that examines the association between brain activation in the verb generation task before reading skills have become automatic (as early as 7 years old) with reading scores at the age of 17 years. In this longitudinal study, children performed the fMRI verb generation task three times: before reading is fully acquired (7 years old, age range 5–8 years = T1), during acquisition of reading skills (11 years old, age range 9–14 years = T2) and after reading was mastered (17 years old, age range 15–19 years = T3). In typical language development, reading proficiency was found to be affected by the age of reading acquisition, an effect that was found to decrease with age (Zevin and Seidenberg, 2002). Also, a greater variety in strategies used for reading was found in younger individuals as compared to proficient older readers (Waters et al., 1984). We therefore examined the relationship between fMRI activation during verb generation, and reading scores achieved toward adulthood, at the age of 17 years (T3). We hypothesized that the verb generation task would show typical frontal, temporal, and occipital activation, with a trend toward left-lateralized activation with age. We also postulated that reading proficiency would be associated with left-lateralized activation in regions related to executive functions and reading; specifically in the frontal and occipital regions as reading is mastered (i.e., with development) (as was observed in Purcell et al., 2011). Lastly, we hypothesized that at T1 and T2 reading proficiency should be associated with greater activation (during verb generation) of regions in the cingulo-operculum network, because in younger children, maintaining focus on task goals and avoiding errors are of primary importance as reading skills are being acquired. In adolescence, we hypothesized that reading proficiency should be associated with greater activation of the fronto-parietal network at T3 after reading is mastered because in mature, proficient readers, rapid adaptive control mechanisms have been developed and support reading.

MATERIALS AND METHODS

PARTICIPANTS

Sixteen children (eight boys, eight girls) were included in this longitudinal study. Children initially entered the study at the age of

5–8 years and then returned annually for brain imaging and neurocognitive testing. In the present analysis, we focus on imaging data acquired at three time points in the 10-year longitudinal study, when children were of a mean age of $7 \pm 0.1.03$ (T1), 11.53 ± 1.59 (T2), and 17.18 ± 1.27 (T3) years.

All the participants ($N = 16$) completed the verb generation task during fMRI at T1 and T2. In the last session (T3), only 15 participants completed the scan due to braces in 1 of the participants. However, reading measures were acquired from all 16 individuals at T3.

The study was approved by the Institutional Review Board. Informed consent was obtained from the child's parent or guardian and assent also obtained from subjects 8 years and older. Exclusion criteria were previous neurological illness, learning disability, head trauma with loss of consciousness, current or past use of psycho-stimulant medication, pregnancy, birth at 37 weeks gestational age or earlier, or abnormal findings at a routine neurological examination performed by an experienced pediatric neurologist. All participants were part of a parent study investigating normal language development in children and were considered "healthy" based on neurological, psychological, and structural measures (Holland et al., 2007; Szaflarski et al., 2012).

All participants were native English speakers. Fifteen were right-handed and one was left-handed according to the Edinburgh Handedness Inventory (Oldfield, 1971). All participants were pre-screened for any conditions, which would prevent an MRI scan from being acquired safely. Intelligence was measured using the age appropriate Wechsler intelligence scales upon entry to the study and again 2 and 4 years later as follows: Wechsler Preschool and Primary Scale of Intelligence (WPPSI-R, ages below 6 years) (Wechsler, 1989), Wechsler Intelligence Scale for Children – Third Edition (WISC-III, age 6–16 years) (Wechsler, 1991), and Wechsler Adult Intelligence Scale – Third Edition (WAIS-III, ages 17 years and above) (Wechsler, 1997). Reading was assessed at the third session (T3 at age 17 years) using the Woodcock–Johnson Letter–Word reading test (Woodcock et al., 2001). In this task, the participants were instructed to read as accurately as possible, a list of words written in English, increasing in degree of difficulty. The task was stopped by the administrator after six reading errors in a row.

fMRI PARADIGM

The fMRI paradigm consisted of a covert verb generation task as previously detailed (Holland et al., 2001, 2007)] using a 30-s on–off block design. All stimuli were presented using MacStim (White Ant Software, Melbourne, VIC, Australia). Stimuli were presented at a rate of one noun every 5 s, for six stimuli during each 30-s epoch. During the active epochs, the participants were asked to think of appropriate verbs such as "throw" or "kick" to aurally presented concrete nouns such as "ball." Typically children can think of two or three verbs associated with each noun during each response interval. They are instructed not to move the lips or mouth while covertly generating the verb responses. During the control epochs, participants were asked to bilaterally tap their fingers when they heard a modulated tone. The bilateral finger tapping task was chosen as the control for verb generation since the sensory–motor response to bilateral finger tapping as reported previously (Holland et al., 2001; Szaflarski et al., 2006b). In order to compare the control task to the auditory stimulation and response initiation on the verb generation task, the participants were instructed to sequentially tap the fingers to the thumbs on both hands simultaneously when they hear a tone, in a self-paced manner. Participants were asked to stop tapping after touching each finger to the thumb twice. This control task accomplished five objectives in a pediatric fMRI experiment. First the auditory cue using a tone to pace the finger tapping controls for the auditory stimulation in the verb generation task. Second, tapping fingers provided activation of the motor strip as reference data for each participant as well as a method for examining differences in developmental aspects of BOLD activation from the neurocognitive language paradigm vs. a motor paradigm that should not have very strong developmental influence over the age span tested (Schapiro et al., 2004). It also provided participants with a task to shift their attention away from generating verbs into the control epoch. In addition, paced sequential finger tapping requires motor planning and execution and serves as a control for these processes underlying verb generation task. Finally, this control task is used to provide an indirect measure of participants' compliance inside the scanner. Yuan et al. (2009) also explored the differences in head motion children during fMRI while performing finger tapping vs. verb generation and did not find a significant difference in motion for these two phases of the task: a key consideration for obtaining high quality fMRI in pediatric subjects. The difficulty level of the fMRI task was selected such that children as young as 5 years old would be readily able to perform the task.

In order to verify that the participants were attentive to the presented nouns during the scan, they were given a yes/no recognition test involving the 25 nouns and 25 distracters. This quiz consisted of a sheet with a list of nouns on it: nouns that were in the task, and foils that were not. Participants were told to mark the words that they remembered hearing during the verb generation task in the scanner.

Imaging

An MRI-compatible audio visual system was used for presentation of the stimuli. Details of the techniques used to obtain fMRI data from younger children, as well as the success rates, are given in Byars et al. (2002). EPI–fMRI scan parameters were TR/TE = 3000/38 ms, 125 kHz, FOV = 25.6 cm × 25.6 cm, matrix = 64 × 64, and slice thickness = 5 mm. Twenty-four slices were acquired, covering the entire cerebrum. One hundred ten whole-brain volumes were acquired (the first 10 were discarded during post-processing to insure image contrast at relaxation equilibrium) for a total scan time of 5 min 30 s. Techniques detailed elsewhere (Byars et al., 2002) were used to acclimatize the participants to the MRI procedure and render them comfortable inside the scanner. Soft head restraints were used to minimize head motion. In addition to the fMRI scans, whole-brain T1 weighted MP-RAGE scans were acquired for anatomical co-registration. All imaging was performed using a 3 T, head only MRI scanner (Bruker Medspec 30/60).

DATA ANALYSIS

Data were analyzed using Cincinnati Children's Hospital Image Processing Software (CCHIPS), written in IDL (Research Systems

Inc., Boulder, CO, USA). Image data were corrected for Nyquist ghosts and geometric distortion using multi-echo reference method (Schmithorst et al., 2001), and was motion-corrected using pyramid co-registration (Thevenaz et al., 1998): we performed three-dimensional ridged body transformation to align the volumes. This resulted in six motion parameters. These parameters were included as regressors in the first-level general linear model (GLM) analysis for each subject's data. To ensure that the level of motion did not differ across the three sessions, the mean motion was reported as well as included in an analysis of variance (ANOVA). We also used a within group t-test analysis to compare the motion levels between the task (when generating verbs) and the contrast conditions (when tapping fingers). In addition, time points with excessive motion were rejected from the post-processing pipeline. We used a mutual information cost function for rejecting motion corrupted frames of fMRI data as previously described for this same cohort of longitudinal subjects (Szaflarski et al., 2006). As mentioned in our previous studies, covert and overt verb generation resulted in the same head motion in this same cohort of children (Vannest et al., 2009). Although the data included in the current analysis are from a slightly different block-periodic version of the verb generation task, we did not find differences in head motion during the covert verb generation and finger tapping conditions (Yuan et al., 2009). All data met the criterion of median voxel displacement in the center of the brain <2 mm. The fMRI data were transformed into stereotaxic space (Talairach and Tournoux, 1988) using a linear affine transformation (see Muzik et al., 2000). The use of the Talairach standard for children aged 5 years and above has been shown to produce minimal errors in co-registration for group analysis. Consequently, we are confident that using the adult Talairach standard in the present study will not substantially alter the findings of the current study (Wilke et al., 2002; Altaye et al., 2008). Note that the imaging data for this study were acquired over a period of 12 years and that the methods for fMRI analysis have improved considerably over this period of time. After data acquisition on all participants was completed, 12 years after the longitudinal study began we processed all of the data from all participants specifically for this report using the analysis pipeline as described above.

GROUP ACTIVATION MAP

A GLM and random-effects analysis were used in order to detect the group activation for T1, T2, and T3 children for the contrast between conditions of verb generation > finger tapping contrast. Images of the t-maps generated by this first-level contrast were thresholded for visual inspection purposes to $p < 0.001$, corrected via Monte Carlo simulation using a cluster of 30 voxels (Forman et al., 1995).

Regression

We used regression in second level analyses in order to examine the association between reading scores from the "Letter–Word" subtest (from the Woodcock–Johnson battery) from the third session (T3) and fMRI activation during the verb generation task at T1–T3. Following the first-level computation of individual t-score maps for the verb generation > finger tapping contrast, whole-brain voxel-wise group maps, were computed using Spearman's rank-correlation coefficient. These maps were based on unthresholded t-maps from the first-level analysis and each subject's behavioral score included as a predictor of activation (e.g., "Letter–Word" subtest from the Woodcock–Johnson III). Images were thresholded to $p < 0.001$, uncorrected. Cluster size for each group was 35 voxels.

Lateralization index calculation

A lateralization index (LI) was also calculated for each subject in the three age groups based on the unthresholded individual z-score maps. The LI represents a relative hemispheric difference for an individual that is self-normalizing in terms of relative BOLD activity. Since this index is non-dimensional, it provides a convenient means of comparing groups of subjects across different scanning sessions. As noted later, the brain areas included for LI calculation were determined so that they were consistent across the groups while still conforming to the traditional standard of regions of interest (ROI) selection for language lateralization. Every effort was made to insure that the methodologies applied in the LI calculation of the three subject groups were compatible.

Several ROIs were chosen for the purpose of the current analysis using an LI toolbox implemented in CCHIPS. Language-network regions were defined for LI calculation based on the composite map of activation obtained from the fMRI verb generation task from all subjects at T3. First, we chose a frontal ROI corresponding to the traditional "Broca's area"; we retained all active voxels within and contiguous to this area, so the frontal ROI included the entire IFG (BA 44, 45, 47) and extensions into additional dorsolateral prefrontal regions, including portions of the MFG (BA 46, 48, 49) and precentral gyrus (BA 46). We also selected a temporal language ROI based on the traditional "Wernicke's area," defined functionally by the group activation map. This ROI extended from the temporal plane (BA 41, 42) inferiorly through the middle temporal gyrus (MTG) to the margin of the ITG (including portions of BA 22, 21, 37) but did not include posterior aspects (BA 22, 39). ROIs for the right hemisphere homologs were established by reflecting the coordinates to the right hemisphere.

Using the same approach, we defined ROIs for reading (fusiform gyrus, BA 37) and for executive functions (dorsolateral PFC, BA 9; and the anterior PFC, BA 10) (after Purcell et al., 2011). We retained all active voxels within and contiguous to these areas and defined them as two additional separate ROIs on the left and for the right hemisphere homologs based on the correlation map of activation obtained from the fMRI verb generation task correlated with the WJ-III reading scores from all subjects at T3.

Lateralization indexes for language-network regions were computed both for the composite t-maps and for the regression maps; the LIs for the reading and executive functions-related regions were then computed separately from the regression maps. Only voxels with z-scores greater than or equal to the mean z-score within an ROI for each individual subject were used in the calculation of LIs. Voxels above this mean z-score threshold were counted and an LI was defined as the difference in the number of activated voxels, summed independently for the left and right ROIs, divided by the sum total of active voxels in the left plus right ROI. According to this formula, a positive LI indicated left hemisphere lateralization and a negative number indicated right lateralization. These

LI values were used to construct the lateralization growth curves (a linear regression line).

RESULTS

NEUROPSYCHOLOGICAL TESTING

Neuropsychological testing results verified that the participants had normal to above average scores in reading and verbal abilities. Mean Wechsler verbal and non-verbal IQ remained stable during development. At T1: verbal scaled IQ = 115.9 ± 9.23 (range = 104–139), non-verbal scaled IQ = 112.9 ± 12.23 (range = 96–130), at T3: verbal scaled IQ = 109.75 ± 0.37 (range = 99–139), non-verbal scaled IQ = 114.91 ± 14.71 (range = 95–123).

VERB GENERATION – POST-SCANNING MEASUREMENT

The average number of correct responses for the verb generation post-test outside the scanner at T2 and T3 were 12.4/25 ± 3.6 and 15.05/25 ± 2.4, respectively. Range of possible scores is 0–25 correct choices.

RANDOM-EFFECTS ANALYSIS

The statistical parameter maps for verb generation > finger tapping for T1–T3 in the longitudinal cohort shown in **Figures 1–3** are consistent with previous studies using this task (Holland et al., 2007; Szaflarski et al., 2012). While there are many areas of activation that are common across ages in the cohort, there are also variations.

T1 children

Significant activation was found in the left and right insula (BA 13) and left IFG (BA 13, 9), left fusiform gyrus (BA 20), left STG (BA 22), left MTG (BA 21), left superior frontal gyrus (SFG) (BA 6), left cingulate gyrus (BA 32), left thalamus, right precentral gyrus (BA 6), and left and right parahippocampal gyrus. Talairach coordinates of cluster centroids are listed in **Table 1** (see **Figure 1**).

T2 children

Significant activation was observed in the left and right MFG (BA 46, 9, 10), left IFG (BA 47), left MTG (BA 21, 22), right IFG (BA 13), and left anterior cingulate (BA 32). Talairach coordinates of cluster centroids are listed in **Table 1** (see **Figure 2**).

T3 children

Significant activation was observed in the left STG (BA 22), left MFG (BA 46, 9, 8), left parahippocampal gyrus (BA 36), left (BA 13) and right IFG (BA 47), and right cuneus (BA 30). Talairach coordinates of cluster centroids are listed in **Table 1** (see **Figure 3**).

REGRESSION ANALYSIS MAPS

Regression analyses maps using the "Letter–Word" standard scores from the Woodcock–Johnson III at T3 as a predictor, revealed significant positive correlations with the contrast of verb generation > finger tapping in the children at three different age points.

T1 children

A significant positive correlation was observed in the left insula (BA 13), left and right MFG (BA 8, 6), left posterior cingulate (BA 30), left anterior cingulate (BA 24), left thalamus, right precentral gyrus (BA 44), right superior temporal lobe (BA 41), right MTG (BA 37), right cuneus (BA 7), and right posterior cingulate (BA 23, 30). Talairach coordinates of cluster centroids are listed in **Table 2** (see **Figure 4**).

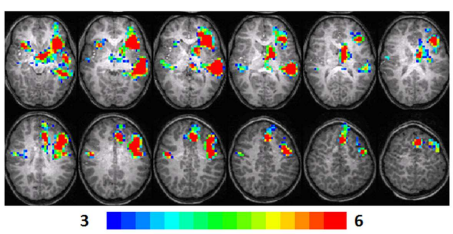

FIGURE 1 | Composite fMRI activation maps for the verb generation (verb generation > finger tapping) in T1 children ($N = 16$). The contrast is significant at $p < 0.001$ (corrected), slice thickness is 5 mm for these contiguous slices. Slices range from $z = 13$ to 24 in the Talairach frame. Cluster size is 30 voxels. Higher significance is indicated in hotter color (t threshold ranged from 3 to 6, see scale in the bottom of the figure). Figure is presented in a radiological orientation (L = R, R = L).

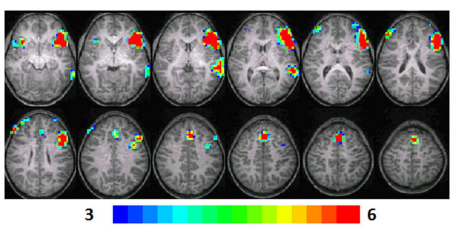

FIGURE 2 | Composite fMRI activation maps for the verb generation (verb generation > finger tapping) in T2 children ($N = 16$). The contrast is significant at $p < 0.001$ (corrected), slice thickness is 5 mm for these contiguous slices. Slices range from $z = 13$ to 24 in the Talairach frame. Cluster size is 30 voxels. Higher significance is indicated in hotter color (t threshold ranged from 3 to 6). Figure is presented in a radiological orientation (L = R, R = L).

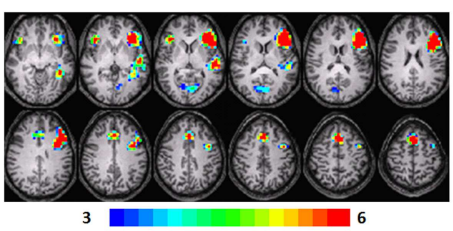

FIGURE 3 | Composite fMRI activation maps for the verb generation (verb generation > finger tapping) in T3 children ($N = 15$). The contrast is significant at $p < 0.001$ (corrected), slice thickness is 5 mm for these contiguous slices. Slices range from $z = 13$ to 24 in the Talairach frame. Cluster size is 30 voxels. Higher significance is indicated in hotter color (t threshold ranged from 3 to 6). Figure is presented in a radiological orientation (L = R, R = L).

Table 1 | Group composite contrast (verb generation > finger tapping) in T1, T2, and T3 participants.

Region	BA	Cluster size	Cluster centroid		
			X	*Y*	*Z*
T1 CHILDREN					
Left insula	13	133	−30	22	0
Left inferior frontal gyrus	13	66	−34	27	14
	9	150	−39	8	29
Left superior temporal gurus	22	155	−51	−24	3
Left middle temporal gyrus (sub-cluster)	21	26	−48	−36	−5
Left fusiform gyrus (sub-cluster)	20	22	−44	−37	−10
Left superior frontal gyrus	6	32	−8	15	57
Left parahippocampal gyrus		202	−26	2	−15
left thalamus		142	−8	15	57
Left cingulate gyrus	32	64	−7	22	39
Right precentral gyrus (frontal lobe)	6	41	42	−7	30
Right parahippocampal gyrus		224	26	4	−18
Right insula	13	48	42	−18	13
T2 CHILDREN					
Left middle frontal gyrus	46	15	−38	46	15
Left middle frontal gyrus (sub-cluster)	9	63	−43	12	27
Left inferior frontal gyrus (sub-cluster)	47	88	−40	18	−13
	13	345	−44	23	7
Left middle temporal gyrus	22	94	−60	−35	5
Left middle temporal gyrus (sub-cluster)	21	21	−58	−35	−13
Left anterior cingulate	32	91	−2	19	40
Right inferior frontal gyrus	13	69	38	13	−13
Right middle frontal gyrus	10	52	40	38	22
T3 CHILDREN					
Left parahippocampal gyrus (limbic lobe)	36	82	−39	−37	−6
Left superior temporal gyrus	22	87	−47	−22	4
Left inferior frontal gyrus	13	284	−38	24	8
Left middle frontal gyrus (sub-cluster)	9	78	−38	14	26
	6	28	−37	4	40
Right middle frontal gyrus	8	158	0	19	43
Right cuneus	30	56	1	−68	7
Right Inferior frontal gyrus	47	44	37	23	1

T2 children

A significant positive correlation was observed in left and right fusiform gyri (BA 37, 19), left STG (BA 41), left anterior cingulate (BA 32), and the MFG (BA 10). In the right side, a significant correlation was observed in the caudate, hypothalamus, and hippocampus. Talairach coordinates of cluster centroids are listed in **Table 2** (see **Figure 5**).

T3 children

A significant positive correlation was observed in the left STG (BA 41, 38), left MFG (BA 9, 10), left insula (BA 13), left fusiform gyrus (BA 20), left parahippocampal gyrus (BA 34), and the left precuneus (BA 7) and cuneus (BA 18). A significant correlation was also observed in the right MFG (BA 6), precuneus (BA 31), posterior cingulate (BA 30), and lingual gyrus (BA 18). Talairach coordinates of cluster centroids are listed in **Table 2** (see **Figure 6**).

AGE-RELATED CHANGES IN LATERALIZATION

In **Figure 7** the LI for each group is plotted as a function of age (for T1, T2, and T3) for frontal and temporal language-network ROIs illustrated in the composite maps in **Figures 1–3**. A significant age-related increased left-lateralization was found for the frontal ROI (i.e., "Broca") ($R^2 = 0.92$). Although we observed a leftward lateralization trend in the temporal region as well (i.e., "Wernicke"), age-related change in this posterior ROI was more modest ($R^2 = 0.02$). Results suggest that age accounted for as much as 92% of individual variance in LI in the activation in Broca and for 2% of individual variance *N* LI in the activation in Wernicke. See upper part of **Figure 7**.

An examination of the language ROIs from the regression maps with reading scores in **Figures 4–6**, revealed increased left-lateralization along development as shown in the lower panel of **Figure 7** for the frontal (green triangles, $R^2 = 0.99$) and temporal (red squares, $R^2 = 0.9$) language-network ROIs. Greater

Table 2 | Regression analysis of MRI data from the verb generation task at T1, T2, and T3 participants with Letter–Word reading standard scores at T3.

Region	BA	Cluster size	Cluster centroid		
			X	*Y*	*Z*
T1 CHILDREN					
Left posterior cingulate	30	32	−19	−58	17
Left insula	13	25	−41	−20	26
Left middle frontal gyrus (frontal lobe)	8	33	−27	20	42
Left thalamus		41	−9	−20	7
Left anterior cingulate cortex	24	35	−1	15	20
Right middle frontal gyrus (frontal lobe)	6	37	7	−4	56
Right precentral gyrus (frontal lobe) (sub-cluster)	44	20	46	5	10
Right inferior frontal gyrus (frontal lobe) (sub-cluster)	9	17	47	3	26
Right posterior cingulate (limbic system)	23	9	7	−51	25
Right posterior cingulate (sub-cluster)		55	10	−60	17
Right posterior cingulate (sub-cluster)	30	14	20	−54	10
Right transverse temporal gyrus (A1)	41	72	44	−25	12
Right superior temporal gyrus (sub-cluster)	41	9	46	−38	15
Right middle temporal gyrus	37	57	49	−58	5
Right cuneus (occipital lobe)	7	51	9	−66	30
T2 CHILDREN					
Left fusiform gyrus (temporal lobe)	37	48	−43	−50	−10
Left superior temporal gyrus (sub-cluster)	41	20	−38	−42	5
Left anterior cingulate	32	47	−5	31	20
Left middle frontal gyrus	10	36	−9	50	5
Left fusiform gyrus (occipital lobe)	19	40	−38	−73	−12
Right caudate (temporal lobe)		25	36	−30	−5
Right culmen (anterior) (sub-cluster)		25	25	−29	−25
Right hypothalamus		37	1	−2	−10
Right hippocampus (temporal lobe) (sub-cluster)		17	34	−29	−10
Right fusiform gyrus (occipital lobe)	19	35	34	−77	−12
T3 YEAR OLD CHILDREN					
Left superior temporal gyrus (temporal lobe)	38	44	−39	14	−22
Left fusiform gyrus (temporal Lobe)	20	96	−36	−38	−15
Left parahippocampal gyrus (limbic lobe)	34	41	−16	−7	−18
Left superior temporal gyrus	41	111	−44	−37	4
Left insula	13	100	−37	−20	9
Left insula (sub-cluster)	13	44	−35	−13	14
Left middle frontal gyrus (frontal lobe)	10	86	−37	37	9
Left middle frontal gyrus	9	97	−33	15	27
Left cuneus (occipital lobe)	18	58	−6	−76	23
Left precuneus (parietal lobe, sub-cluster)	7	16	−19	−55	56
Right medial frontal gyrus (frontal lobe)	6	81	6	−19	53
Right precuneus	31	76	18	−74	28
Right posterior cingulate	30	75	31	−74	12
Right lingual gyrus (occipital lobe)	18	72	17	−54	5

age-related changes in lateralization, were found for the reading regions as well (turquoise X, fusiform gyrus; $R^2 = 0.97$), and for the executive functions regions (purple X, BA 9: $R^2 = 0.83$, BA 10: $R^2 = 0.96$). See lower part of **Figure 7**. Results suggest that age and reading proficiency accounted for 99% of individual variance in LI in the activation in Broca and for 90% of individual variance in LI in the activation in Wernicke. It also emphasized that age and reading proficiency accounted for 97% of individual variance in LI in the activation in the Fusiform gyrus and for 83 and 96% of individual variance in LI in the activation in executive functions regions (BA 9 and 10, respectively). These findings indicate that those regions positively correlated with reading scores became more left-lateralized with age. This was true for functionally defined regions of significant correlation for reading scores

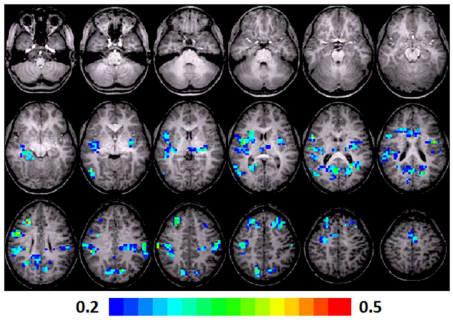

FIGURE 4 | Regression maps showing a positive correlation for activation during verb generation scans in T1 with the Letter–Word score from the Woodcock–Johnson III ($N = 16$) in T3. All activated pixels meet significance threshold of $p < 0.05$, corrected. Slices range from $z = 7$ to 24 in the Talairach frame. Cluster size is 35 voxels. Higher significance is indicated in hotter color (r value ranged from 0.2 to 0.5, see scale in the bottom of the figure). Figure is presented in a radiological orientation (L = R, R = L).

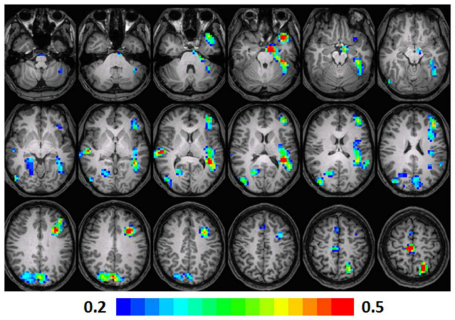

FIGURE 6 | Regression maps showing a positive correlation for activation during verb generation scans from T3 and the Letter–Word score from the Woodcock–Johnson III ($N = 15$) at T3. The activated pixels meet significance at $p < 0.001$, uncorrected, higher significance is indicated by hotter color. Slices range from $z = 7$ to 24 in the Talairach frame. Cluster size is 35 voxels. Higher significance is indicated in hotter color (r value ranged from 0.2 to 0.5). Figure is presented in a radiological orientation (L = R, R = L).

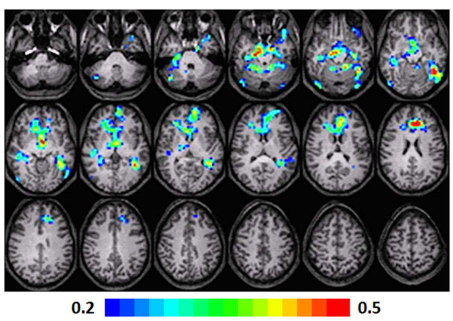

FIGURE 5 | Regression maps showing a positive correlation for activation during verb generation scans at T2 and the Letter–Word score from the Woodcock–Johnson III ($N = 16$) from T3. All activated pixels meet significance threshold of $p < 001$ uncorrected. Slices range from $z = 7$ to 24 in the Talairach frame. Cluster size is 35 voxels. Higher significance is indicated in hotter color (r value ranged from 0.2 to 0.5). Figure is presented in a radiological orientation (L = R, R = L).

and brain activation as well as for regions that were active in the first level analysis in Broca and Wernicke's areas. The fact that this lateralization trend is similar for all of these regions (slope of LI vs. time in the range of 0.37–0.59) suggests that these regions are all connected in support of reading and language skill and are developing at a similar pace, even though the regression coefficient is not significant for the primary regions.

DISCUSSION

In the current study, we aim to examine the relationship between reading proficiency and the maturation of neural networks related to executive functions and language, using the verb generation task. The verb generation task draws on language and executive skills that improve during development (Missier and Crescentini, 2011) and correlate with reading ability (Snowling et al., 1997); thus, we were able to study participants in the youngest group (T1) who entered the study before they formally acquired reading skills or before reading was fully acquired, and examine activation in regions supporting language and executive skills without requiring a reading task.

In line with our hypothesis, our results demonstrate a trend of more left-lateralized activation during the verb generation task from T1 to T3. In other words, age was found to account for the increasing left LI in language-related regions. Specifically, we observed increasingly leftward lateralization of the inferior/middle frontal region with development, as reported previously in a superset including the participants of the current analysis (Holland et al., 2001, 2007). This trend was less robust in the temporal language region, as previously observed, due to a weaker reliance on auditory–phonological-related regions during this task (Holland et al., 2007). A similar trend of left-lateralized activation with development was observed by Gaillard et al. (2000) while administering the verb generation task to participants age 10.7 and 28.7 years. This developmental shift to the left hemisphere for linguistic tasks was also reported in other studies (Szaflarski et al., 2006a) and reflects the specialization of the left hemisphere for language. These results are not confounded by differences in motion across age or between the different task conditions (i.e., generating verbs vs. tapping fingers). Although the head motion data were regressed out of the analysis, the absence of the effect of age on motion level, confirms that these findings of increased left-lateralization with age are not because of motion differences (see also Gaillard et al., 2003).

The main goal of the current study was to identify the developmental changes in the activation of the neural circuitry supporting language and executive functions (during the verb generation task in T1, T2, and T3) corresponding to proficient reading at T3. Our results confirm our second hypothesis: reading proficiency was found to be associated with left-lateralized activation in regions related to language and profound left-lateralization in executive functions (BA 9, 10) and reading (BA 37). In general, greater reading scores in T1 were associated with a bilateral

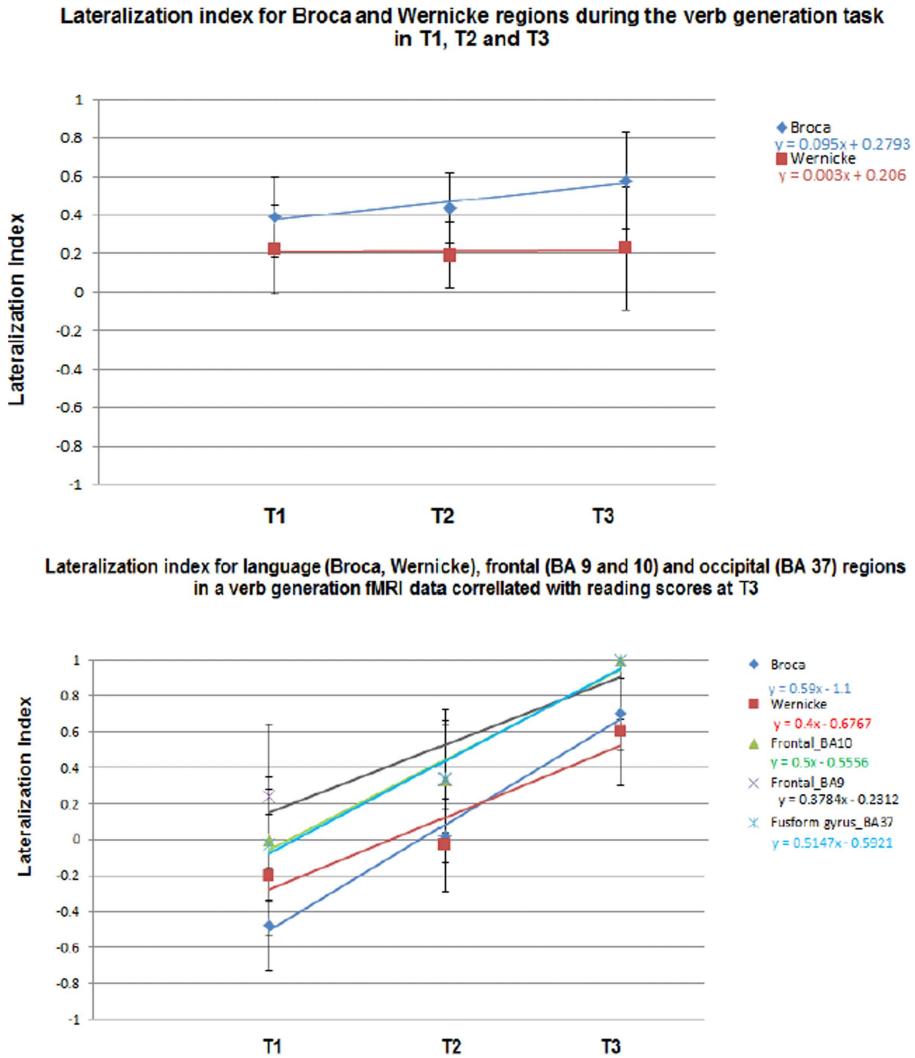

FIGURE 7 | Lateralization index (LI) for the composite (upper) and the regression maps (lower). LI was calculated on language-related regions (Broca and Wernicke) in the composite maps in T1–T3. LI was also calculated on language (Broca and Wernicke), executive functions (dorsolateral prefrontal cortex, anterior prefrontal cortex), and reading regions (fusiform gyrus). Standard deviations representing the distribution of individual LIs are indicated.

and more widespread brain activity, in addition to the "classical" reading regions. This involved the right STG and MTG, which are related to phonology and bilateral activation of production and semantic-related regions such as the insula. These findings extend our previous results (Holland et al., 2001, 2007) by showing that age and reading proficiency account for increasing left-lateralization in regions related to language, reading, and executive functions. This is in line with findings suggesting lesser reliance on phonological and semantic processes and greater reliance on orthographic processes during reading proficiency (Ehri, 2005), and neuroimaging findings of greater left-lateralization during reading along development (Turkeltaub et al., 2003). With age, the association of greater reading scores and brain activation in the verb generation task was found to be more specific to executive functions and reading-related regions. At T2 and T3, greater reading scores were associated with more leftward LI for language-related regions (frontal and temporal) than at T1, but even more leftward LI scores for frontal and occipital regions related to executive functions and reading, respectively. Since better reading is associated with greater reliance on word recognition (i.e., "orthographic route") and less on decoding (i.e., "phonological route"), these results might demonstrate the decreased role of language regions (i.e., phonology–auditory route) and the increased role of the orthography–visual route in reading development (for more information see Coltheart et al., 2001; dual route model).

Positive correlation of word reading scores and the activation of the fusiform gyrus was observed only in T2 and T3, whereas children in the T1 group showed greater right cuneus and left precuneus activation. We suggest that because younger age children have not reached reading proficiency and the mental lexicon

Table 3 | Motion measures, mean, and standard deviation (SD) for children at T1, T2, and T3.

	Mean (SD) (total: generating verbs and tapping fingers)	Mean (SD) (generating verbs)	Mean (SD) (tapping fingers)	*t* Test (generating verbs vs. tapping fingers) (ns)
T1 children	0.3 (0.22)	0.33 (0.22)	0.3 (0.21)	0.38
T2 children	0.39 (0.36)	0.43 (0.53)	0.37 (0.22)	0.26
T3 children	0.33 (0.3)	0.32 (0.31)	0.34 (0.3)	0.43

Means and standard deviations (SDs) for motion measures for the total task (generating verbs and finger tapping), the task condition (generating verbs), and for the contrast condition (finger tapping) across the different age groups. No significant differences were found between the different age groups for the total motion parameter as well as between the task and contrast conditions (left column).

has not fully been established, there is heavier load on regions related to phonological processing (e.g., STG, MTG) and less on regions related specifically to automatic word recognition (e.g., fusiform gyrus) earlier in development. At T2, children are using orthographic processing regions as they become more proficient readers (Ehri, 2005) and therefore show a correlation between reading proficiency with bilateral fusiform gyri activation. Finally, left sided fusiform gyrus activation is observed at T3, as expected from proficient and automatic readers (van der Mark et al., 2011). The activation of the fusiform gyrus, lingual gyrus, and other occipital regions may be related to visual imagery during the verb generation task (see also Karunanayaka et al., 2011). This process was also found to correspond to greater reading proficiency (Horowitz-Kraus et al., 2013).

Note that the ANOVA we performed to assess the effect of age on motion did not reveal significant age differences [$F(3,45) = 0.48$, $p > 0.05$]. Namely, the level of motion did not differ across the age points. No significant differences were found within groups either, suggesting that motion level for the task and contrast conditions was relatively equal (see **Table 3**).

The frontal lobe matures with age, along with concomitant improvements in executive functions (Segalowitz and Davies, 2004). Giedd observed that gray and white matter maturation, which includes completion of myelination and synaptic pruning, in the parietal and frontal regions peaks at 16 years old, so the cognitive abilities centered in these regions are mature as well (Giedd et al., 1999). Some later findings point at an inverse relationship between cortical gray matter density reduction and brain growth primarily in the superior frontal regions that control executive functioning even in 30-year-old adults (Sowell et al., 2001). Executive functions, which support inhibition, WM, planning, and attention, likely develop throughout adolescence together with the maturation of the frontal and parietal cortices (Casey et al., 2000; Luna et al., 2010).

Since our sample is children in the age range of 7–17 years, frontal lobe maturation is still in progress, and verb generation may demand a reliance on different neural-circuits related to executive functions for T1 and T2 children as compared to T3. We hypothesized that the fronto-parietal network may be more engaged in older children, and our finding of greater left frontal and parietal (precuneus) activation correlated with reading proficiency at T3 supports this hypothesis. As suggested by the dual-networks model, the fronto-parietal network may be in charge of rapid adaptive control and attention allocation, which are part of executive functions (Dosenbach et al., 2008). This network has been previously found to correlate with higher reading scores (Vogel et al., 2014). As adolescents become proficient readers, rapid monitoring is required to process the written stimuli in order to achieve fluent reading. This same rapid control mechanism that contributes to fluent reading is also engaged to a greater degree during verb generation in those participants who are the most proficient readers. The cingulo-opercular network, supporting maintenance of task goals and error monitoring, is also observed, in part, at T3: the insula was also positively correlated with higher reading scores.

We also found that the cingulo-opercular network was more engaged in younger children; there was activation of the insula at T1 and of the anterior cingulate cortex at T1 and T2. These results suggest that greater task maintenance and error monitoring is needed by younger children – as they perform the verb generation task, semantic associations among words are not as well-established, and selecting appropriate responses involves greater resources. This is consistent with a previous finding from the verb generation task when nouns presented to the participants involved greater conflict and the need for more attentional resources to resolve this conflict (Barch et al., 2000).

The activation of the anterior cingulate cortex in T1 and T2 was also positively correlated with higher reading scores at the age of 17 years (T3). This suggests that children who go on to become more proficient readers engage this region to a greater degree even early in development. Before reading becomes automatic, there are several competing representations of new words as they are encountered, until the orthographic route becomes stable (Coltheart et al., 2001; dual route model). Young children who devote increased resources to resolving these conflicting representations may ultimately become better readers, suggesting that, more generally, executive functions play a role in the reading acquisition process. We suggest that by adolescence, as linguistic and executive abilities increase, conflict may decrease, resulting in the absence of activation in the anterior cingulate cortex in the verb generation task at T3. The anterior cingulate cortex also supports error detection and is active when making reading errors (Horowitz-Kraus and Breznitz, 2008), and the absence of association between reading ability and the activation in this region at T3 years might be due to less error detection activation during the verb generation task as well as in reading and less need for set-maintenance during these processes, which become automatic. Vogel et al. (2013) found no developmental changes in fronto-parietal and cingulo-opercular networks when examining these networks using resting-state functional connectivity. Our regression maps as well as the LI values from the frontal ROIs suggest that while these executive functions networks remain equally active across development, when examining a specific task; one network may be more active than another at different developmental stages.

To conclude, our results support the utilization of language and executive functions regions for development of proficient reading. These domains also have a differential role of executive functions in reading development: greater role of the set-maintenance network before reading becomes automatic (T1 and T2) and greater activation of the rapid, adaptive control network when reading becomes proficient. Our results strengthen previous studies, which pointed at the crucial role of executive functions in the reading process, highlighting the differential need in sub-components of executive functions along development. Clinically, the results provide neuro-functional support for the importance of intact executive functions in future reading development, by means of early diagnosis and intervention, especially among populations with reading impairments (dyslexia, attention deficit hyperactive disorder). These conclusions should be taken in the context of the current study's limitations: (1) We did not acquire fMRI data during a reading task, so we cannot compare the regression maps with reading scores and verb generation to actual activation during reading in the same participants; (2) there is a reading exposure at 7 years old (and especially since the age range of this group was relatively wide) so the youngest group of participants is not completely "naïve" to reading. Adding to this ambiguity in the sample is the lack of assessment of reading ability at the younger age points. An additional study enrolling children younger than 7 years old should be done to verify whether the same phenomenon exists also in a younger age. (3) We did not assess the verb generation ability after the scan at 7 years old since the children were too young. (4) The only reading measure that was used in the current study was a word reading task. Although word reading is highly related to reading comprehension, these two abilities rely on different basic cognitive abilities (see Christopher et al., 2012 for more information) as well as different white matter tracts (Horowitz-Kraus et al., 2013). Also, whereas an untimed word reading task, as was used in the current study involves phonological and orthographical processing, a timed word recognition task relies additionally on speed of processing (see Wolf and Bowers, 1999; Hart et al., 2010). Therefore, a correlation of the fMRI data from the verb generation task with a timed word reading task may result in less activation of phonological-related regions (e.g., STG). A future study should look at the longitudinal difference in the fMRI verb generation correlates with these two measures. Despite these limitations, it is important to note that there are only a few studies assessing the relationship between executive functioning and reading and the current study is the first to do so longitudinally. Therefore, our findings (regional correlation of later reading abilities with early fMRI results) offer the possibility of a novel predictive biomarker for future reading ability.

ACKNOWLEDGMENTS

The authors would like to thank Dr. Mekibib Altaye, Ph.D., Department of Biostatistics and Epidemiology, Cincinnati Children's Hospital Medical Center, for his major contribution. This study was supported by a grant from the U.S. National Institute of Health NIH grant R01-HD38578.

REFERENCES

Ahmad, Z., Balsamo, L. M., Sachs, B. C., Xu, B., and Gaillard, W. D. (2003). Auditory comprehension of language in young children: neural networks identified with fMRI. *Neurology* 60, 1598–1605. doi:10.1212/01.WNL.0000059865.32155.86

Altaye, M., Holland, S. K., Wilke, M., and Gaser, C. (2008). Infant brain probability templates for MRI segmentation and normalization. *Neuroimage* 43, 721–730. doi:10.1016/j.neuroimage.2008.07.060

Anderson, P. (2002). Assessment and development of executive function (EF) during childhood. *Child Neuropsychol.* 8, 71–82. doi:10.1076/chin.8.2.71.8724

Baddeley, A. (1986). Modularity, mass-action and memory. *Q. J. Exp. Psychol. A* 38, 527–533. doi:10.1080/14640748608401613

Barch, D. M., Braver, T. S., Sabb, F. W., and Noll, D. C. (2000). Anterior cingulate and the monitoring of response conflict: evidence from an fMRI study of overt verb generation. *J. Cogn. Neurosci.* 12, 298–309. doi:10.1162/089892900562110

Booth, J. N., Boyle, J. M. E., and Kelly, S. W. (2014). The relationship between inhibition and working memory in predicting children's reading difficulties. *J. Res. Read.* 37, 84–101. doi:10.1111/1467-9817.12011

Breznitz, Z. (2006). *Fluency in Reading: Synchronization of Processes.* Mahwah, NJ: Lawrence Erlbaum and Associates.

Byars, A. W., Holland, S. K., Strawsburg, R. H., Bommer, W., Dunn, R. S., Schmithorst, V. J., et al. (2002). Practical aspects of conducting large-scale functional magnetic resonance imaging studies in children. *J. Child Neurol.* 17, 885–890. doi:10.1177/08830738020170122201

Casey, B. J., Giedd, J., and Thomas, K. M. (2000). Structural and functional brain development and its relation to cognitive development. *Biol. Psychol.* 54, 241–257. doi:10.1016/S0301-0511(00)00058-2

Chiarello, C., Welcome, S. E., Haldeman, L. K., Towler, S., Julagay, J., Otto, R., et al. (2009). A large-scale investigation of lateralization in cortical anatomy and word reading: are there sex differences? *Neuropsychology* 23, 210–222. doi:10.1037/a0014265

Christopher, M. E., Miyake, A., Keenan, J. M., Pennington, B., DeFries, J. C., Wadsworth, S. J., et al. (2012). Predicting word reading and comprehension with executive function and speed measures across development: a latent variable analysis. *J. Exp. Psychol. Gen.* 141, 470–488. doi:10.1037/a0027375

Coltheart, M., Rastle, K., Perry, C., Langdon, R., and Ziegler, J. (2001). DRC: a dual route cascaded model of visual word recognition and reading aloud. *Psychol. Rev.* 108, 204–256. doi:10.1037/0033-295X.108.1.204

Dehaene-Lambertz, G., Dehaene, S., and Hertz-Pannier, L. (2002). Functional neuroimaging of speech perception in infants. *Science* 298, 2013–2015. doi:10.1126/science.1077066

Diamond, A. (2002). "Normal development of prefrontal cortex from birth to young adulthood: cognitive functions, anatomy, and biochemistry," in *Principles of Frontal Lobe Function*, eds D. T. Stuss and R. T. Knight (New York, NY: Oxford University Press), 466.

Dosenbach, N. U. F., Fair, D. A., Cohen, A. L., Schlaggar, B. L., and Peterson, S. E. (2008). A dual-networks architecture of top-down control. *Trends Cogn. Sci.* 12, 99–105. doi:10.1016/j.tics.2008.01.001

Ehri, L. C. (2005). "Development of sight word reading: phases and findings," in *The Science of reading: A handbook*, eds M. J. Snowling and C. Hulme (Oxford: Blackwell), 135–145.

Forman, S. D., Cohen, J. D., Fitzgerald, M., Eddy, W. F., Mintun, M. A., and Noll, D. C. (1995). Improved assessment of significant activation in functional magnetic resonance imaging (fMRI): use of a cluster-size threshold. *Magn. Reson. Med.* 33, 636–647. doi:10.1002/mrm.1910330508

Gaillard, W. D., Hertz-Pannier, L., Mott, S. H., Barnett, A. S., LeBihan, D., and Theodore, W. H. (2000). Functional anatomy of cognitive development: fMRI of verbal fluency in children and adults. *Neurology* 54, 180–185. doi:10.1212/WNL.54.1.180

Gaillard, W. D., Sachs, B. C., Whitnah, J. R., Ahmad, Z., Balsamo, L. M., Petrella, J. R., et al. (2003). Developmental aspects of language processing: fMRI of verbal fluency in children and adults. *Hum. Brain Mapp.* 18, 176–185. doi:10.1002/hbm.10091

Giedd, J. N., Blumenthal, J., Jeffries, N. O., Castellanos, F. X., Liu, H., Zijdenbos, A., et al. (1999). Brain development during childhood and adolescence: a longitudinal MRI study. *Nat. Neurosci.* 2, 861–863. doi:10.1038/13158

Hart, S. A., Petrill, A. A., and Thompson, L. A. (2010). A factorial analysis of timed and untimed measures of mathematics and reading abilities in school aged twins. *Learn Individ. Differ.* 20, 63–69. doi:10.1016/j.lindif.2009.10.004

Holland, S. K., Plante, E., Byars, A. W., Strawsburg, R. H., Schmithorst, V. J., and Ball, W. S. (2001). Normal fMRI brain activation patterns in children performing a verb generation task. *Neuroimage* 14, 837–843. doi:10.1006/nimg.2001.0875

Holland, S. K., Vannest, J. J., Mecoli, M., Jacola, L. M., Tillema, J., Karunanayaka, P. R., et al. (2007). Functional MRI of language lateralization during development in children. *Int. J. Audiol.* 46, 533–551. doi:10.1080/14992020701448994

Horowitz-Kraus, T., and Breznitz, Z. (2008). An error detection mechanism in reading among dyslexic and regular readers – an ERP study. *Clin. Neurophysiol.* 119, 2238–2246. doi:10.1016/j.clinph.2008.06.009

Horowitz-Kraus, T., Wang, Y., and Holland, S. K. (2013). *The (Hidden) Role of the Right Hemisphere in Reading Comprehension: A DTI Study*. Seattle: Organization of Human Brain Mapping.

Hugdahl, K., Lundervold, A., Ersland, L., Smienoll, A. I., Sundberg, H., Barndon, R., et al. (1999). Left frontal activation during a semantic categorization task: an fMRI study. *Int. J. Neurosci.* 99, 49–58. doi:10.3109/00207459908994312

Ihnen, S. K. Z., Petersen, S. E., and Schlaggar, B. L. (2013). Separable roles for attentional control sub-systems in reading tasks: a combined behavioral and fMRI study. *Cereb. Cortex*. doi:10.1093/cercor/bht313

Karunanayaka, P., Schmithorst, V. J., Vannest, J., Szaflarski, J. P., Plante, E., and Holland, S. K. (2010). A group independent component analysis of covert verb generation in children: a functional magnetic resonance imaging study. *Neuroimage* 51, 472–487. doi:10.1016/j.neuroimage.2009.12.108

Karunanayaka, P., Schmithorst, V. J., Vannest, J. J., Szaflarski, J. P., Plante, E., and Holland, S. K. (2011). A linear structural equation model for covert verb generation based on independent component analysis of fMRI data from children and adolescents. *Front. Syst. Neurosci.* 5:1–15. doi:10.3389/fnsys.2011.00029

Kieffer, M. J., Vukovic, R. K., and Berry, D. (2013). Roles of attention shifting and inhibitory control in fourth-grade reading comprehension. *Read. Res. Q.* 48, 333–348. doi:10.1002/rrq.54

Luna, B., Padmanabhan, A., and O'Hearn, K. (2010). What has fMRI told us about the development of cognitive control through adolescence? *Brain Cogn.* 72, 101–113. doi:10.1016/j.bandc.2009.08.005

McCandliss, B. D., Cohen, L., and Dehaene, S. (2003). The visual word form area: expertise for reading in the fusiform gyrus. *Trends Cogn. Sci.* 7, 293–299. doi:10.1016/S1364-6613(03)00134-7

Missier, F. D., and Crescentini, C. (2011). Executive control of retrieval in noun and verb generation. *Cogn. Syst. Res.* 12, 45–55. doi:10.1016/j.cogsys.2010.01.001

Muzik, O., Chugani, D. C., Juhasz, C., Shen, C., and Chugani, H. T. (2000). Statistical parametric mapping: assessment of application in children. *Neuroimage* 12, 538–549. doi:10.1006/nimg.2000.0651

Newman, R. L., and Joanisse, M. F. (2011). Modulation of brain regions involved in word recognition by homophonous stimuli: an fMRI study. *Brain Res.* 1367, 250–264. doi:10.1016/j.brainres.2010.09.089

Oldfield, R. C. (1971). The assessment and analysis of handedness: the Edinburgh inventory. *Neuropsychologia* 9, 97–113. doi:10.1016/0028-3932(71)90067-4

Paulesu, E., Goldacre, B., Scifo, P., Cappa, S., Gilardi, M. C., Castiglioni, D. P., et al. (1997). Functional heterogeneity of left inferior frontal cortex as revealed by fMRI. *Neuroreport* 8, 2011–2016. doi:10.1097/00001756-199705260-00042

Piatt, L. A., Fields, J. A., Paolo, A. N., and Troester, A. I. (1999). Action (verb naming) fluency as an executive function measure: convergent and divergent evidence of validity. *Neuropsychologia* 37, 1499–1503. doi:10.1016/S0028-3932(99)00066-4

Pihlajamaki, M., Tanila, H., Hanninen, T., Kononen, M., Laakso, M., Partanen, K., et al. (2000). Verbal fluency activates the left medial temporal lobe: a functional magnetic resonance imaging study. *Ann. Neurol.* 47, 470–476. doi:10.1002/1531-8249(200004)47:4<470::AID-ANA10>3.0.CO;2-M

Price, C. J. (2012). A review and synthesis of the first 20 years of PET and fMRI studies of heard speech, spoken language and reading. *Neuroimage* 62, 816–884. doi:10.1016/j.neuroimage.2012.04.062

Purcell, J. J., Napoliello, E. M., and Eden, G. F. (2011). A combined fMRI study of typed spelling and reading. *Neuroimage* 55, 750–762. doi:10.1016/j.neuroimage.2010.11.042

Schapiro, M. B., Schmithorst, V. J., Wilke, M., Byars, A. W., Strawsburg, R. H., and Holland, S. K. (2004). BOLD fMRI signal increases with age in selected brain regions in children. *Neuroreport* 15, 2575–2578. doi:10.1097/00001756-200412030-00003

Schmithorst, V. J., Dardzinski, B. J., and Holland, S. K. (2001). Simultaneous correction of ghost and geometric distortion artifacts in EPI using a multiecho reference scan. *IEEE Trans. Med. Imaging* 20, 535–539. doi:10.1109/42.929619

Segalowitz, S. J., and Davies, P. L. (2004). Charting the maturation of the frontal lobe: an electrophysiological strategy. *Brain Cogn.* 55, 116–133. doi:10.1016/S0278-2626(03)00283-5

Snowling, M., Nation, K., Moxham, P., Gallagher, A., and Frith, U. (1997). Phonological processing skills of dyslexic students in higher education: a preliminary report. *J. Res. Read.* 20, 31–41. doi:10.1111/1467-9817.00018

Sowell, E. R., Thompson, P. M., Holmes, C. J., Jernigan, T. L., and Toga, A. W. (1999). In vivo evidence for post-adolescent brain maturation in frontal and striatal regions. *Nat. Neurosci.* 2, 859–861. doi:10.1038/13154

Sowell, R. S., Thompson, P. M., Tessner, K. D., and Toga, A. W. (2001). Mapping continued brain growth and gray matter density reduction in dorsal frontal cortex: inverse relationships during postadolescent brain maturation. *J. Neurosci.* 21, 8819–8829.

Szaflarski, J. P., Altaye, M., Rajagopal, A., Eaton, K., Meng, X., Plante, E., et al. (2012). A10-year longitudinal fMRI study of narrative comprehension in children and adolescents. *Neuroimage* 63, 1188–1195. doi:10.1016/j.neuroimage.2012.08.049

Szaflarski, J. P., Holland, S. K., Schmithorst, V. J., and Byars, A. W. (2006a). fMRI study of language lateralization in children and adults. *Hum. Brain Mapp.* 27, 202–212. doi:10.1002/hbm.20177

Szaflarski, J. P., Schmithorst, V. J., Altaye, M., Byars, A. W., Ret, J., Plante, E., et al. (2006b). A longitudinal functional magnetic resonance imaging study of language development in children 5 to 11 years old. *Ann. Neurol.* 59, 796–807. doi:10.1002/ana.20817

Szaflarski, J. P., Schmithorst, V. J., Altaye, M., Byars, A. W., Ret, J., Plante, E., et al. (2006). A longitudinal functional magnetic resonance imaging study of language development in children 5 to 11 years old. *Ann. Neurol.* 59, 796–807. doi:10.1002/ana.20817

Talairach, J., and Tournoux, P. (1988). *Co Planar Stereotaxic Atlas of the Human Brain*. New York: Thieme Medical Publishers.

Thevenaz, P., Ruttimann, U. E., and Unser, M. (1998). A pyramid approach to subpixel registration based on intensity. *IEEE Trans. Image. Process* 7, 27–41. doi:10.1109/83.650848

Turkeltaub, P. E., Gareau, L., Flowers, D. L., Zeffiro, T. A., and Eden, G. F. (2003). Development of neural mechanisms for reading. *Nat. Neurosci.* 6, 767–773. doi:10.1038/nn1065

van der Mark, S., Klaver, P., Bucher, K., Maurer, U., Schulz, E., Brem, S., et al. (2011). The left occipitotemporal system in reading: disruption of focal fMRI connectivity to left inferior frontal and inferior parietal language areas in children with dyslexia. *Neuroimage* 54, 2426–2436. doi:10.1016/j.neuroimage.2010.10.002

Vannest, J. J., Karunanayaka, P. R., Altaye, M., Schmithorst, V. J., Plante, E. M., Eaton, K. J., et al. (2009). Comparison of fMRI data from passive listening and active-response story processing tasks in children. *J. Magn. Reson. Imaging* 29, 971–976. doi:10.1002/jmri.21694

Vogel, A. C., Church, J. A., Power, J. D., Miezin, F. M., Petersen, S. E., and Schlaggar, B. L. (2013). Functional network architecture of reading-related regions across development. *Brain Lang.* 125, 231–243. doi:10.1016/j.bandl.2012.12.016

Vogel, A. C., Petersen, S. E., and Schlaggar, B. L. (2014). The VWFA: it's not just for words anymore. *Front. Hum. Neurosci.* 8:1–10. doi:10.3389/fnhum.2014.00088

Waters, G. S., Seidenberg, M. S., and Bruck, M. (1984). Children's and adults' use of spelling-sound information in three reading tasks. *Mem. Cogn.* 12, 293–305. doi:10.3758/BF03197678

Wechsler, D. (1989). *Wechsler Preschool and Primary Scale of Intelligence-Revised*. San Antonio, TX: Psychological Corporation.

Wechsler, D. (1991). *Wechsler Intelligence Scale for Children*, 3rd Edn. San Antonio, TX: Psychological Corporation.

Wechsler, D. (1997). *Wechsler Adult Intelligence Scale*, 3rd Edn. San Antonio, TX: Psychological Corporation.

Wilke, M., Schmithorst, V. J., and Holland, S. K. (2002). Assessment of spatial normalization of whole-brain magnetic resonance images in children. *Hum. Brain Mapp.* 17, 48–60. doi:10.1002/hbm.10053

Wolf, M., and Bowers, P. G. (1999). The double deficit hypothesis for the developmental dyslexia. *J. Educ. Psychol.* 91, 415–438.

Woodcock, R., McGrew, K., and Mather, N. (2001). *Woodcock-Johnson III Tests of Cognitive Abilities*. Itasca, IL: Riverside.

Yuan, W., Altaye, M., Ret, J., Schmithorst, V., Byars, A. W., Plante, E., et al. (2009). Quantification of head motion in children during various fMRI language tasks. *Hum. Brain Mapp.* 30, 1481–1489. doi:10.1002/hbm.20616

Zevin, J. D., and Seidenberg, M. S. (2002). Age of acquisition effects in word reading and other tasks. *J. Mem. Lang.* 47, 1–29. doi:10.1016/j.cognition.2008.08.004

Conflict of Interest Statement: The authors declare that the research was conducted in the absence of any commercial or financial relationships that could be construed as a potential conflict of interest.

Received: 30 November 2013; accepted: 02 June 2014; published online: 20 June 2014.

Citation: Horowitz-Kraus T, Vannest JJ, Gozdas E and Holland SK (2014) Greater utilization of neural-circuits related to executive functions is associated with better reading: a longitudinal fMRI study using the verb generation task. Front. Hum. Neurosci. ***8****:447. doi: 10.3389/fnhum.2014.00447*

This article was submitted to the journal Frontiers in Human Neuroscience.

frontiers in
HUMAN NEUROSCIENCE

REVIEW ARTICLE
published: 18 June 2014
doi: 10.3389/fnhum.2014.00453

Neuromagnetic vistas into typical and atypical development of frontal lobe functions

Margot J. Taylor [1,2,3,4,5] ****, Sam M. Doesburg*** [1,2,3,4] ***and Elizabeth W. Pang*** [2,5,6]

[1] *Department of Diagnostic Imaging, Hospital for Sick Children, Toronto, ON, Canada*
[2] *Neuroscience and Mental Health Program, Hospital for Sick Children Research Institute, Toronto, ON, Canada*
[3] *Department of Medical Imaging, University of Toronto, Toronto, ON, Canada*
[4] *Department of Psychology, University of Toronto, Toronto, ON, Canada*
[5] *Department of Paediatrics, University of Toronto, Toronto, ON, Canada*
[6] *Division of Neurology, Hospital for Sick Children, Toronto, ON, Canada*

Edited by:
Christos Papadelis, Harvard Medical School, USA

Reviewed by:
Giancarlo Zito, 'S. Giovanni Calibita' Fatebenefratelli Hospital, Italy
James Christopher Edgar, Children's Hospital of Philadelphia, USA

****Correspondence:***
Margot J. Taylor, Diagnostic Imaging, Hospital for Sick Children, 555 University Avenue, Toronto, ON, Canada M5G 1X8
e-mail: margot.taylor@sickkids.ca

The frontal lobes are involved in many higher-order cognitive functions such as social cognition executive functions and language and speech. These functions are complex and follow a prolonged developmental course from childhood through to early adulthood. Magnetoencephalography (MEG) is ideal for the study of development of these functions, due to its combination of temporal and spatial resolution which allows the determination of age-related changes in both neural timing and location. There are several challenges for MEG developmental studies: to design tasks appropriate to capture the neurodevelopmental trajectory of these cognitive functions, and to develop appropriate analysis strategies to capture various aspects of neuromagnetic frontal lobe activity. Here, we review our MEG research on social and executive functions, and speech in typically developing children and in two clinical groups – children with autism spectrum disorder and children born very preterm. The studies include facial emotional processing, inhibition, visual short-term memory, speech production, and resting-state networks. We present data from event-related analyses as well as on oscillations and connectivity analyses and review their contributions to understanding frontal lobe cognitive development. We also discuss the challenges of testing young children in the MEG and the development of age-appropriate technologies and paradigms.

Keywords: faces, inhibition, language, connectivity, ASD, preterm, developmental cognitive neuroscience, magnetoencephalography

Social function, executive processes, and speech are all complex cognitive processes that rely on the intact development and function of the frontal lobes. This paper will review, in turn, magnetoencephalography (MEG) studies addressing each of these three processes in typical development. Then, we will describe two clinical conditions – children with autism spectrum disorder (ASD) and children born very preterm – where these processes consistently, and differentially, follow an altered developmental trajectory. We will review our neuroimaging results that explored the involvement of the underlying neural bases of difficulties or dysfunction experienced in these domains. This contrast between typical and atypical development allows us a better understanding of which neural mechanisms are recruited, and at which stage of processing, to facilitate successful cognitive processing, and, it offers insight into how these mechanisms are compromised in clinical populations who experience difficulties in frontal lobe functions.

SOCIAL COGNITION

Social cognitive function refers to the capacity to adjust and manage successfully in social settings, which relies on executive abilities and on intact frontal lobe structure and function. Current models conceptualize executive processes as dependent on a network of frontal lobe regions with strong reciprocal connections to subcortical and parietal areas (Elliott, 2003). The frontal lobes are among the last brain regions to develop, and they play a critical role in executive abilities (Shaw et al., 2008). The maturation of social cognition parallels the development of the frontal lobes. Social cognitive functions have been strongly linked with medial prefrontal and anterior cingulate cortex (Bush et al., 2000; Radke et al., 2011; Telzer et al., 2011), which are inter-connected with dorsolateral and inferior frontal regions with connections to the superior temporal sulcus (STS) (Carter and Pelphrey, 2008; Kramer et al., 2010) and subcortical regions including the basal ganglia and amygdala (e.g., Satpute and Lieberman, 2006). This cognitive network is activated by a range of social and emotional tasks, including social judgment, facial affect, inhibition (Go/No-go), and empathy protocols. Disturbances of frontal lobe development can have severe consequences for the maturation of executive functions (Powell and Voeller, 2004). The present review focuses on the contribution of MEG for the study of frontal lobe function maturation and its relation to cognitive abilities, with a particular focus on executive functions and social cognition in both typically and atypically developing populations. We place

specific emphasis on the development of emotional processing and inhibition, as well as the use of MEG to investigate network connectivity involving frontal lobe systems.

DEVELOPMENT OF EMOTIONAL FACE PROCESSING

The human face plays a vital role in human social interactions. Faces convey a tremendous amount of information, and the ability to differentiate and recognize faces/individuals and their emotional content has an extended developmental course through adulthood [see Kolb et al. (1992) for review]. Although posterior brain areas are crucial for face processing, frontal cortices play a critical role in deciphering the social significance of facial expressions and in allocating appropriate attention. Thus, emotional facial perception involves a distributed network that includes the amygdala, frontal lobes, anterior cingulate, STS, and fusiform gyri (McCarthy et al., 1999; Allison et al., 2000; Haxby et al., 2000; Adolphs et al., 2002; Kilts et al., 2003).

Numerous neuroimaging studies have investigated face processing in adults; however, knowledge regarding the developmental course of such abilities remains scant. Differences in frontal activation between adolescents and adults have been reported in fMRI in emotional regulation tasks (Burnett et al., 2009; Passarotti et al., 2009), as well as in tasks of emotional self-regulation and empathy (Lamm and Lewis, 2010). The timing of brain processing in the development of emotional face perception throughout childhood and adolescence has been determined with event-related potentials (ERPs), with the early emotion-specific responses emerging only in adolescence (Batty and Taylor, 2006; Miki et al., 2011). Due to its uniquely good combination of spatial and temporal resolution, MEG has been able to contribute tremendously to our understanding of the spatiotemporal dynamics underlying the processing of faces (Taylor et al., 2008, 2010, 2011a,b, 2012). With emotional faces in an explicit recognition task, early frontal activation that reflected implicit emotional processing was observed, whereas later insula and fusiform activity was found to be related to explicit emotional recognition (Bayle and Taylor, 2010).

Spatiotemporal dynamics of implicit brain processing of happy and fearful facial emotions has been established in adults using MEG (Hung et al., 2010). In this study, faces were presented rapidly and concurrently with a scrambled pattern, one on each side of a central fixation cross. Participants were instructed to respond to the scrambled image, thus not orienting attention to the face stimuli. This implicit emotional processing task revealed rapid activation of left amygdala at 100 ms for fearful compared with emotionally neutral faces. Increases in activity were observed concurrently in the dorsal ACC. The fast amygdala–ACC activation suggested a specialized frontal–limbic network, which may be responsible for facilitating responses to a potential threat. This study also confirmed that MEG source analyses could accurately measure both the location and time course of neurocognitive events in deep brain structures (e.g., Moses et al., 2007, 2009), as validated with simulated and real data analyses (Quraan et al., 2011; Mills et al., 2012).

This MEG protocol has also been used to investigate the development of neural activations associated with the implicit processing of fearful and happy facial emotions using school-aged children (7–10 years) and young adolescents (12–15 years) (Hung et al., 2012). Right lateralized amygdala activation to both happy and fearful faces was observed for the school-age children, whereas ACC activation did not reach statistical significance. In the young adolescent group, the pattern of neural activation similar to that observed in adults, left amygdala and ACC activation, was detected only during the perception of fearful faces. The results indicate that the processing of emotions first engaged the earlier-maturing amygdala, but was non-specific with respect to the emotion, and by the teenage years implicated the later-developing ACC. The maturational shift in the lateralization of amygdala responses sensitive to the fearful faces was intriguing, suggesting a shift from the more reflexive processing of the right amygdala to the elaborative processing typical of the left amygdala (e.g., Costafreda et al., 2008) with age. These results also inform our present views regarding the development of functional specialization of fear perception throughout childhood. Specifically, these findings indicate that this is a late-developing process involving the frontal–limbic emotion system, consistent with behavioral data on later maturation of recognition of negative emotions (De Sonneville et al., 2002; Herba and Phillips, 2004; Thomas et al., 2007).

EXECUTIVE FUNCTIONS: INHIBITION ABILITIES AND IMAGING STUDIES

Inhibition plays a vital role in social cognition, as inhibition of context-inappropriate behavior is critical for successful social functioning. Behavioral studies of inhibition indicate improvements in inhibitory control throughout childhood and adolescence (Luna et al., 2004). Presently, it is understood that inhibitory control is supported by a distributed network of brain areas, in which frontal cortex plays a pivotal role (Rubia et al., 2007).

Studies using fMRI in adults have identified brain regions underlying inhibition, which include striatal and thalamic structures, motor areas, anterior cingulate, parietal lobes, and the inferior and dorsolateral frontal gyri (Rubia et al., 2001; Watanabe et al., 2002; Mostofsky and Simmonds, 2008). Frontal cortex has been demonstrated to be critical for inhibitory control in studies that used Go/No-go tasks where comparisons were made between the activations during No-go (successful response inhibition) and Go trials (response execution) [see review in Dillon and Pizzagalli (2007)]. Brain imaging findings from Go/No-go paradigms in typical development have yielded variable results, yet have demonstrated a role for dorsolateral and inferior frontal regions in inhibition, although activation of this region is not reliably reported in children (e.g., Durston et al., 2002; Tamm et al., 2004; Rubia et al., 2007).

Fewer MEG studies of inhibitory control have been conducted. Our research group used MEG to investigate the maturation of spatiotemporal brain dynamics of inhibition in adolescence and early adulthood. We employed a visual Go/No-go task that included a baseline condition with many more No-go than Go trials, allowing us to compare the No-go trials between the two conditions, thereby avoiding contamination of MEG activity from motor responses (Vidal et al., 2012), seen in studies that contrast Go with No-go trials. The stimuli and sample series of stimuli from this paradigm are presented in **Figure 1**. Right-frontal activity beginning as early as 200 ms was observed in adults in the inhibition condition. Similar results were also reported in a prior ERP study (Bokura et al., 2001). Relative to adults, adolescents exhibited

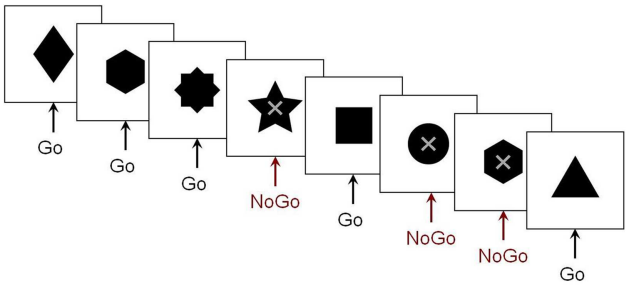

FIGURE 1 | The Go/No-go protocol. Example of the stimulus sequence in the Go/No-go paradigm from our research group. Subjects were instructed to respond as quickly as possible to the variously shaped stimuli, but to withhold this pre-potent response on trials where an "X" was superimposed on the stimulus.

delayed frontal responses, which were also bilateral (Vidal et al., 2012). The low percentage (7%) of Go trials in the control condition, however, raised the prospect that the observed pattern of results may be attributable to an oddball effect. To address this potential confound, a follow-up study was run which included two variants of this paradigm: the frequencies of Go to No-go trials were reversed for the experimental (67:33%) and control (33:66%) conditions.

We examined spatiotemporal MEG dynamics in 15 adolescents and 15 adults using this more classic Go/No-go task. Comparison of brain activation during No-go trials using vector event-related beamformer revealed increased recruitment of right inferior frontal gyrus in adults (BA 45, at 200–250 ms), but bilateral and delayed activation of similar brain regions in adolescents (BA 45/9, at 250–300 ms) (**Figure 2**). Activation in the adolescent group was also observed in the right temporal (BA 21) and inferior parietal (BA 40) regions on inhibition trials. These additional activations may reflect increased recruitment of attentional processes (Durston et al., 2002; Hampshire et al., 2010). Delayed activation of frontal cortex, in concert with additional brain activation indicative of increased attentional demands (Vidal et al., 2012), indicate that brain networks mediating inhibitory control are not yet fully mature in adolescence.

LANGUAGE PROCESSING: NEURAL CONTROL OF SPEECH PRODUCTION IN TYPICAL DEVELOPMENT

Speech production is a complex human behavior that requires the integration of articulatory control and oromotor control structures. Both non-speech mouth movements and speech-related mouth movements require the coordination of similar muscles and, presumably, similar neural pathways; however, the intentions behind the movements are different. Neuroimaging studies, primarily using fMRI, have compared the frontal cortical activation patterns during speech and non-speech oromotor tasks and report that the former was associated with more activation in left primary motor cortex, and the latter with bilateral and symmetric cortical activations (Wildgruber et al., 1996). It has been suggested that the motor cortex provides a common bilateral structural network for basic vocal motor tasks on which a left-lateralized functional network involved in the production of complex vocal behaviors, including speech and language production, is overlaid (Simonyan et al., 2009).

The spatiotemporal dynamics of speech production in humans can be studied with MEG. Thus far, MEG applications have been limited primarily to the study of language comprehension [for a review see Salmelin (2007)] as speech production generates high-magnitude artifacts that overwhelm the MEG signal. Various approaches have been used to address this challenge including the development of silent, covert, or imagined speech and language tasks (Dhond et al., 2001; Nishitani and Hari, 2002; Ihara et al., 2003; Vihla et al., 2006; Kato et al., 2007; Breier and Papanicolaou, 2008; Liljeström et al., 2009; Wheat et al., 2010; Pang et al., 2011). While silent tasks have addressed the significant artifact problem, they have unfortunately, also limited the study of the oromotor planning and motor control involved in speech and language production.

A few studies have examined overt speech and language production by using a subtraction method to remove the artifacts (Salmelin et al., 1994) or examining the neural responses prior to the onset of actual movements (Herdman et al., 2007; Carota et al., 2010). Another strategy has been to filter out high-frequency muscle-related activity and focus only on the 20 Hz beta-band motor responses to elucidate the neural regions involved in verbal and non-verbal lip, tongue (Salmelin et al., 1994), and mouth movements (Saarinen et al., 2006). As well, our group has used a spatial filtering approach to suppress artifacts from oromotor structures and have identified the sequence of neural activations involved in a simple oromotor task compared to a simple phoneme production task (Memarian et al., 2012). The successful application of this method in a control group allows us to use this approach in the examination of children with oromotor control and speech and language production difficulties.

MEG INVESTIGATIONS OF FRONTAL LOBE FUNCTIONS IN AUTISM SPECTRUM DISORDER

Autism spectrum disorder is associated with abnormal social reciprocity, an intense desire for sameness, atypical use of language, and difficulties with speech. Difficulties with executive functions are prevalent in ASD, and poor social skills are present even when communication and cognitive abilities are high (Frith, 2004).

Numerous studies have identified atypicalities in brain development in ASD. How such alterations in neural development lead to symptoms and cognitive problems associated with ASD, however, remains poorly understood. Research from our group with children aged 6–14 years showed a trend for decreasing gray matter throughout childhood and early adolescence in typical children, but this pattern was not seen in children with ASD (Mak-Fan et al., 2012). Children with ASD also showed age-related atypical alterations in white matter, particularly in long-range fibers and areas linked to social cognition (Cheng et al., 2010; Shukla et al., 2011; Mak-Fan et al., 2013). The most reliably reported differences in brain volumes in ASD are in the frontal lobes, particularly in dorsolateral and medial frontal cortices (Carper and Courchesne, 2005), brain regions involved in social cognition (Lewis et al., 2011; Telzer et al., 2011). More recently, there has been tremendous interest in measures of functional and structural connections in the brain (e.g., Just et al., 2007, 2012; Müller et al., 2011; Travers et al.,

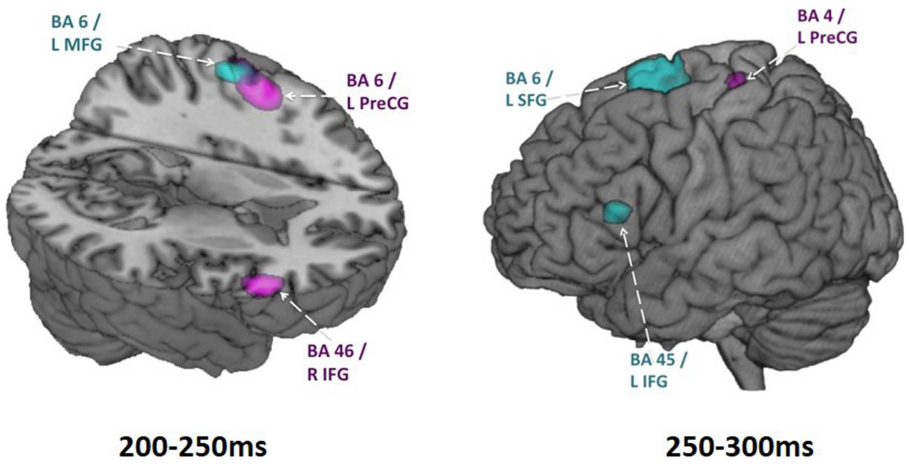

FIGURE 2 | Adolescent vs. adult inhibition activity. Within group activations overlaid on brain images for time windows from 200 to 250 ms (on the left) and 250 to 300 ms (on the right). Inhibition condition > baseline condition, in adults is shown in magenta ($p < 0.005$, uncorr.) and in adolescents shown in blue ($p < 0.005$, uncorr.). Note particularly the earlier right IFG activation in adults and the later left IFG activation in adolescents. These analyses were conducted using vector beamforming on no-go trials that either did or did not (baseline) require inhibitory control. Beamforming was conducted on successive 50 ms windows from 200 to 400 ms. In this figure, the images from the baseline condition were subtracted from the inhibition condition for each group.

2012; Schäfer et al., 2014), with studies finding that children with autism may have poorer long-range connectivity, which would negatively impact their ability to integrate information required for social interactions. Recent research from our group has demonstrated reduced MEG long-range theta-band coherence in children with ASD during the performance of an executive set-shifting task (Doesburg et al., 2013a). This reduced task-dependent synchronization included connections between frontal regions and a distributed network of brain regions, consistent with the view that poor executive ability in ASD may be linked with the inability of frontal structures to marshal coordinated activity among brain regions to support task performance.

SOCIAL COGNITION DEFICITS IN ASD AS ASSESSED USING EMOTIONAL FACES

The ability to perceive, recognize, and interpret emotional information in faces is critical for social interaction and communication. Impaired social interaction is considered to be a hallmark of ASD. Accordingly, studies designed to understand the bases for emotional face processing deficits in ASD play an important role in establishing the biological underpinnings of cognitive and social deficits in this group. Behavioral studies have consistently reported difficulties with face processing in children with ASD, and this population has also been shown to exhibit poor eye contact (Hobson and Lee, 1998) as well as a reduced tendency to look at the faces of others (Langdell, 1978). Prior work investigating neural responses to emotional faces in ASD have demonstrated activation of brain regions implicated in social cognition, including medial prefrontal and STS regions (Pierce et al., 2001; Pelphrey et al., 2007; Wang et al., 2007). ERP studies have also demonstrated that early responses to emotional faces in children with ASD were delayed and smaller (Wong et al., 2008; Batty et al., 2011). Such findings underscore the importance of MEG, as its uniquely good combination of spatial and temporal resolution permits accurate mapping of altered spatiotemporal dynamics in clinical child populations.

Using an implicit face processing paradigm in MEG (**Figure 3**), we investigated neural processing during the perception of happy and angry faces in adolescents with and without ASD. We chose angry instead of fearful faces, as this is a more commonly experienced emotion during childhood (Todd et al., 2012). In this study, emotional faces, adapted from the NimStim Face Stimulus Set (Tottenham et al., 2009), and scrambled images were presented concurrently on either side of a central fixation cross for 80 ms to adolescents with and without ASD; participants responded as quickly as possible indicating the side of the scrambled faces. Event-related beamforming analyses were performed on early MEG activation (60–200 ms). This revealed distinct brain activation patterns in response to happy and angry faces, which also differed between groups. We found significant group differences between the adolescents with and without ASD starting as early as 120–160 ms in source localized analyses, including greater left frontal activity in ASD, expressed particularly for angry faces.

We also examined connectivity with these data as inter-regional phase locking is a neurophysiological mechanism of communication among brain regions implicated in cognitive functions. When completed in task-based studies, these measures reflect the connectivity underlying task performance. Thus, we investigated inter-regional MEG phase synchronization during the perception of the emotional faces in this task. We found significant task-dependent increases in beta synchronization. However, beta-band inter-regional phase locking in the group of adolescents with ASD was reduced compared to controls during the presentation of angry faces. This decreased activity was seen in a distributed network involving the right fusiform gyrus and insula (**Figure 4**). This

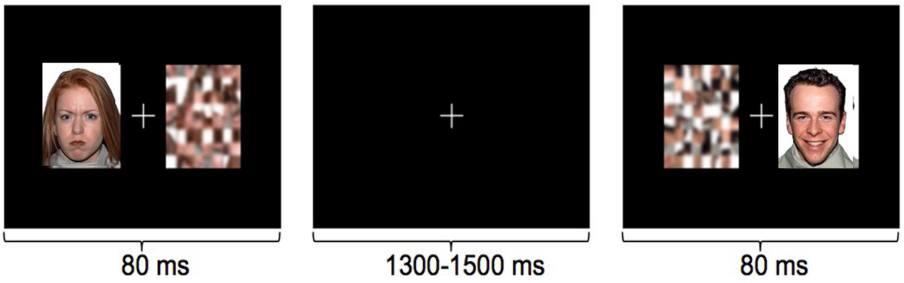

FIGURE 3 | Examples of the stimuli in the implicit emotional faces task. Angry, happy, or neutral faces were presented to the left or right of fixation, with their matched scrambled faces. Participants responded with a left or right button press, as quickly as possible, to indicate the side of the scrambled pattern.

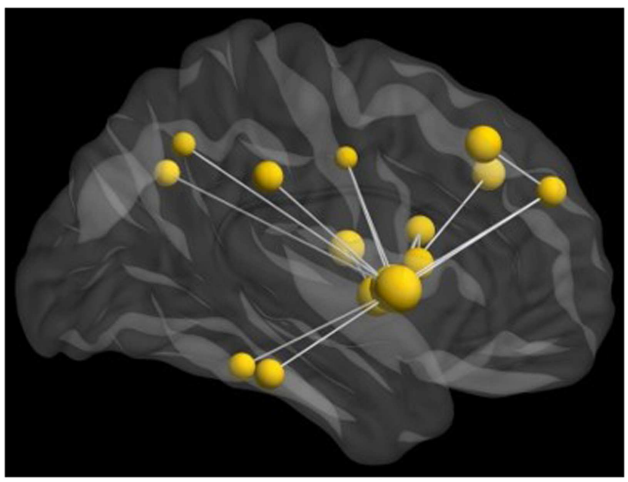

FIGURE 4 | Network of reduced beta-band connectivity seen in adolescents compared to matched controls during the implicit processing of angry faces. The hub of this network was in the right insula, with connections notably to the fusiform gyrus and frontal lobes. For this analysis, data from seed regions were reconstructed using beamformer analysis. Data were then filtered into physiologically relevant frequency ranges, time series of instantaneous phase values were obtained using the Hilbert transform, and inter-regional phase locking was calculated using the phase lag index [PLI; see (Stam et al., 2007)].

network also included activation in the right superior medial and dorsolateral frontal gyri; right fusiform and right supramarginal gyri; and right precuneus, left middle frontal, left insula, and left angular gyri.

Graph analysis of the connectivity in the beta-band, with the hub region of the right insula, revealed reduced task-dependent connectivity clustering, strength, and eigenvector centrality in adolescents with ASD compared to controls. Beta-band coherence has been suggested to be particularly important for long-range communication among brain regions, and these results suggest that reduced recruitment of this network, involving the limbic and frontal areas in the adolescents with ASD impacts their ability to integrate emotional information, particularly for angry faces.

In contrast, no significant differences were found in MEG responses to happy faces. These results are consistent with behavioral findings showing that high functioning ASD participants perform comparably to controls on tasks involving happy faces, but experience pronounced difficulties with processing angry faces (Kuusikko et al., 2009; Rump et al., 2009; Farran et al., 2011).

These findings are also in keeping with a broader literature reporting differences in functional connectivity between participants with and without ASD (e.g., Just et al., 2012; Khan et al., 2013) and suggest that these reductions in long-range task-dependent connectivity may be a factor in the social cognitive difficulties common in ASD.

DIFFICULTIES WITH INHIBITORY CONTROL IN ASD

Individuals with ASD often experience problems with inhibitory control, and this likely contributes to emotional outbursts and inappropriate social behavior commonly seen in this population. Inhibitory control has a protracted maturational course (Luna et al., 2010; Vidal et al., 2012). As such, investigation of these processes in adolescents with ASD is important, as this is a period when youths are adapting to increasing social demands. Moreover, it has been proposed that deficits in inhibitory control worsen with increasing age in ASD (Luna et al., 2004).

Several previous studies have investigated the neural underpinnings of inhibition difficulties ASD. For example in fMRI, adults with ASD have been shown to express greater left frontal activity (Schmitz et al., 2006), reduced anterior cingulate activity (Kana et al., 2007), together with atypical timing in the recruitment of frontal cortex. Since inhibitory control largely depends on the slowly maturing frontal lobes, the results from these studies in adults with ASD may not be generalizable to a younger population. Few neuroimaging investigations have been carried out during adolescence in ASD, when adult patterns of neural activity supporting inhibitory control are being established.

To elucidate the maturation of inhibitory control in ASD, we recorded MEG while adolescents with ASD and age- and sex-matched controls performed a Go/No-go task (Vara et al., 2014) (see **Figure 1**). Participants were instructed to respond to Go stimuli and withhold responses to No-go stimuli (as described above). During inhibitory control, adolescents with ASD primarily recruited frontal regions, whereas typically developing controls showed bilateral frontal activation together with activation in temporal and parietal regions (**Figure 5**).

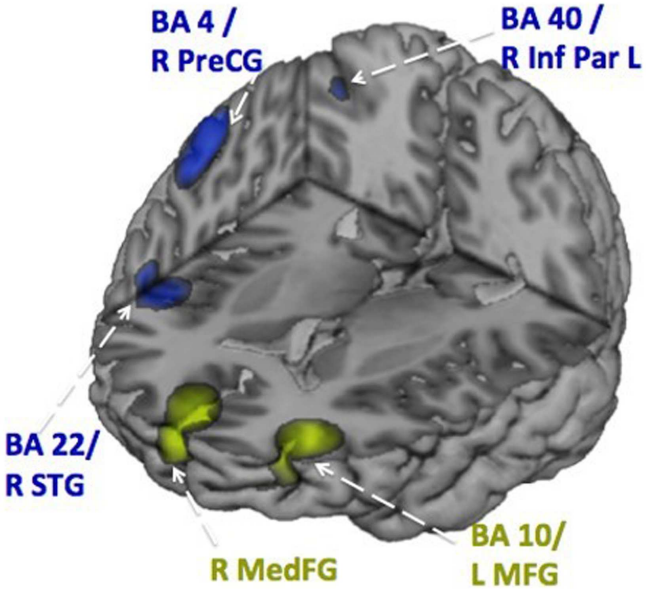

FIGURE 5 | Activation patterns during inhibition. Distributed activation patterns at 350–400 ms in the adolescents with ASD (in green) and the age-matched typically developing adolescents (in blue) showing that control adolescents used a wider network, that also involved temporal lobe activation, than adolescents with ASD. These data were analyzed with vector beamforming as described in **Figure 2**.

Results from this study suggest that inhibitory control is atypical in adolescents with ASD, whose false alarm rate was also higher than the control group, demonstrating poorer inhibitory control behaviorally. Also, patterns of the inhibition-related MEG activity in the adolescents with ASD exhibited different spatiotemporal neural processing than their matched controls. More extensive frontal activity was found in adolescents with ASD, which may be due to reduced long-range connectivity as well as increased short-range connectivity, or local over-connectivity (Belmonte et al., 2004).

ATYPICAL OROMOTOR CONTROL AND SPEECH PRODUCTION IN ASD

While ASD is characterized by deficits, most notably in the realm of social cognition, children with ASD have a variety of speech and language difficulties, the neurobiology of which is not well understood. We used MEG to examine a group of children with ASD as they completed several oromotor speech tasks to explore the neural regions implicated in the control and execution of these functions.

A group of children with ASD and a group of age- and sex-matched controls completed three increasingly complex oromotor and speech tasks in the MEG. These tasks included a simple motor task (open and close the mouth), a simple speech task (speak the phoneme/pa/), and a simple speech sequencing task (speak the phonemic sequence/pa-da-ka/). Beamforming analyses identified neural sources of interest which were then interrogated to generate the time courses of activation for the ASD and control groups. The peaks of activation were identified in each participant, and the latency and magnitude of prominent peaks were submitted to statistical testing.

Figures 6 and **7** show the time courses where significant differences were observed in magnitude and latency, respectively, between the ASD and control groups, in three frontal areas and one temporal region (Pang et al., 2013). In the simple oromotor task, the children with ASD showed greater activation in right hemisphere motor control areas (BA 4) and the middle frontal gyrus, a motor planning area (BA 9), together with delayed activation in right hemisphere motor planning areas (BA 6). In the phoneme production task, the children with ASD showed delayed activation in left frontal language control areas (BA 47). In the sequencing task, the ASD group showed greater activation in right hemisphere motor control (BA 4) and right hemisphere sequencing (BA 22) areas. As well, for the sequencing task, the children with ASD showed higher and delayed activations in the left insula (BA 13), an area known to be involved in sensorimotor integration (Hesling et al., 2005).

These results fit with reports of difficulties with oromotor control and challenges with more complex speech patterns in children with ASD. In summary, we observed atypical neural activation in frontal areas associated with motor control, speech production, and speech sequencing. These were characterized by an unusual pattern of laterality (mostly in the right hemisphere), with higher magnitude and delayed activations. It is likely that these neurophysiological abnormalities underlie some of the speech/language difficulties observed in this cohort and may contribute to the speech and language deficits frequently experienced in children with ASD.

MEG STUDIES OF FRONTAL LOBE DEVELOPMENT IN PRETERM CHILDREN

A large and growing number of children are now being born prematurely. Although the survival rate of these tiny infants has improved significantly due to advances in neonatal care, the morbidity rate has not changed and developmental difficulties are becoming increasingly noted (Roberts et al., 2010). Injuries to developing white matter systems are frequent in this group (Khwaja and Volpe, 2008) and even in the absence of injury on conventional MR imaging, atypical development of white matter has been reported (Anjari et al., 2007; Dudink et al., 2007). This has resulted in increasing interest in the relation between brain network connectivity and cognitive outcome in preterm children. The development of frontal lobe systems is of particular interest, as children born preterm often experience selective developmental difficulties with executive abilities, even when intelligence is broadly normal (Anderson Doyle, 2004; Marlow et al., 2007; Mulder et al., 2009).

Considerable investigation into relations between cognitive outcomes and atypical structural and functional brain development has been carried out using MRI [see Hart et al. (2008), Ment et al. (2009), Miller and Ferriero (2009)]. More recently, MEG has begun to emerge as a modality for imaging atypical development in preterm-born children. Early somatosensory responses have been shown to be atypical in preterm infants (Nevalainen et al., 2008), and these alterations are associated with illness severity (Rahkonen et al., 2013). Task-dependent MEG responses have been shown

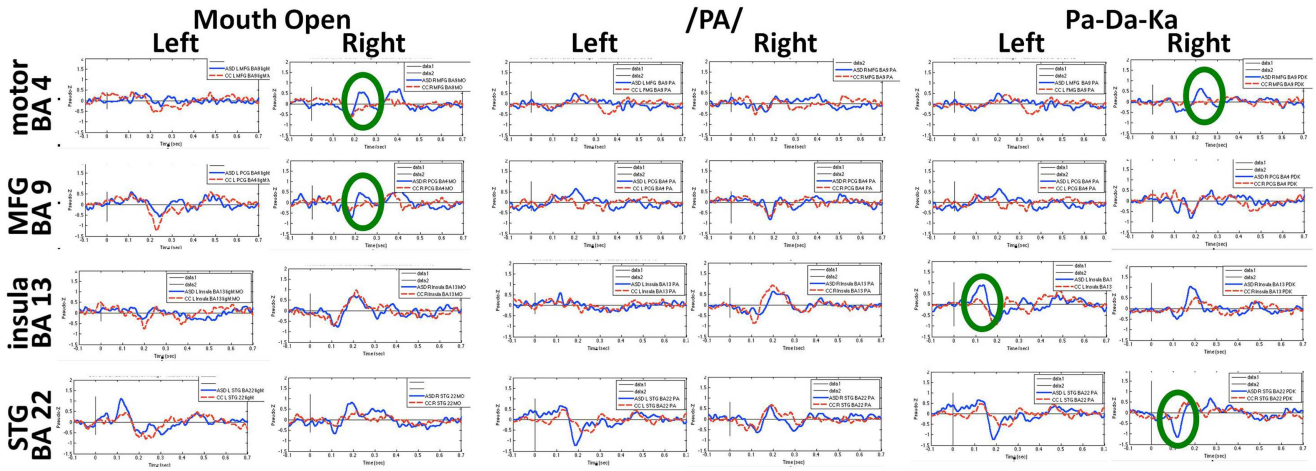

FIGURE 6 | Time courses of activations used in magnitude analyses for each speech production condition. Circles indicate neural locations where statistically significant differences were seen in the peak magnitude between children with autism (blue line) and control children (red line). These data for Figures 6 and 7 were analyzed with synthetic aperture magnetometry beamforming (Robinson and Vrba, 1999; Vrba and Robinson, 2001), and peak activation in regions of interest (based on nine *a priori* regions identified from canonical expressive language areas, plus each homologous region) were computed and averaged by group, and then the magnitude (amplitudes) and latency analyzed for each participant and submitted to paired *t*-tests and corrected for multiple comparisons.

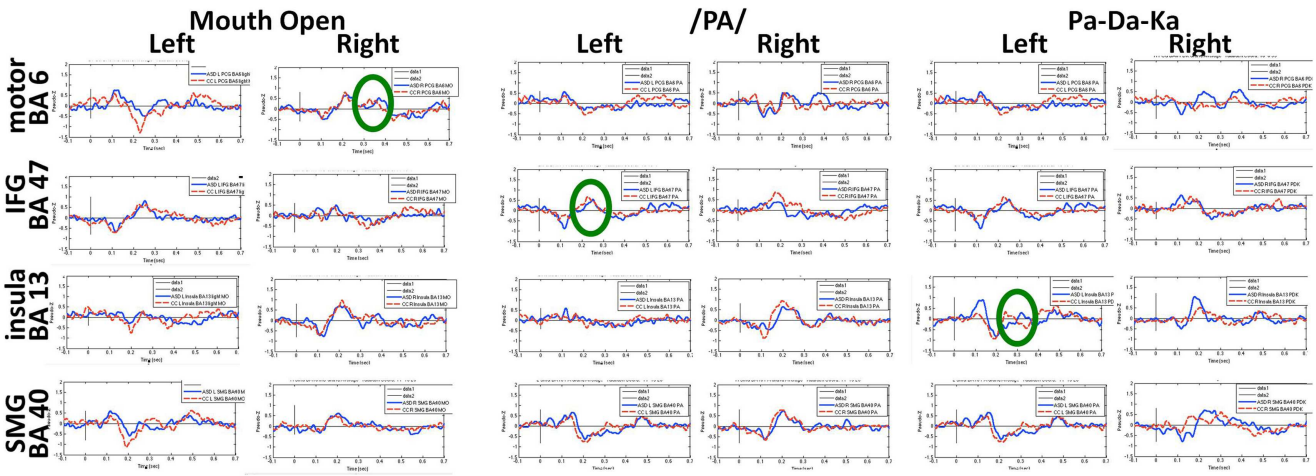

FIGURE 7 | Time courses of activations used in latency analyses for each speech production condition. Circles indicate neural locations where statistically significant differences were seen in the peak latencies between children with autism (blue line) and control children (red line).

to be atypical in children and adolescents born prematurely and are associated with cognitive outcome (Frye et al., 2010; Doesburg et al., 2011a). MEG imaging had also been shown to be effective for revealing relations between specific aspects of adverse neonatal brain development, spontaneous brain activity, and school-age cognitive outcome in particular domains in preterm-born children (Doesburg et al., 2013b).

Magnetoencephalography has also been shown to be of specific relevance for understanding atypical development of frontal lobe systems in children born preterm. Frye et al. (2010) demonstrated altered frontal lobe activation during language processing in preterm-born adolescents, which was interpreted as compensatory top–down control from prefrontal cortical regions. Visual short-term and working memory retention has been demonstrated to recruit increased phase coherence between frontal and posterior brain regions in multiple frequency ranges, with alpha-band oscillations playing a pivotal role in task-dependent coupling (Palva et al., 2005, 2010a,b). This pattern of task-dependent network coherence is also robust in school-age children (Doesburg et al., 2010a; **Figure 8A**). In contrast, school-age children born very preterm exhibit reduced inter-regional coherence and atypical regional activation during visual short-term memory retention

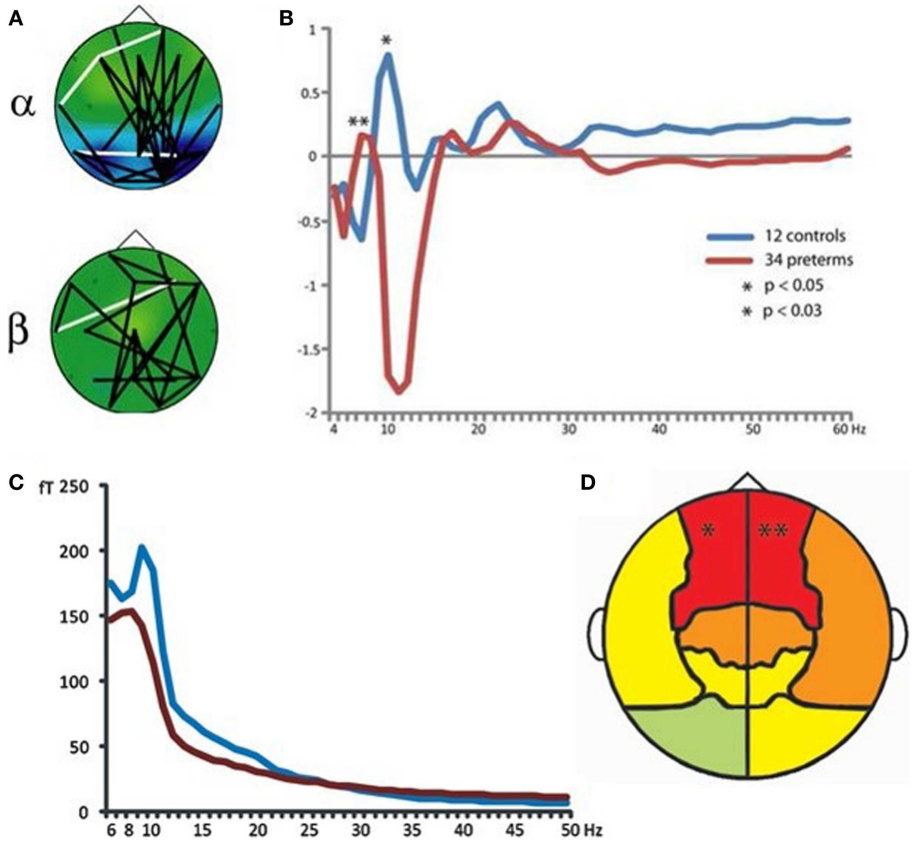

FIGURE 8 | Atypical neural oscillations in very preterm children. **(A)** Increased long-range phase synchrony during short-term memory retention in typically developing controls. **(B)** Altered long-range synchronization during memory retention in very preterm children, suggesting that alpha-band connectivity may be slowed toward the theta frequency range. **(C)** Slowing of spontaneous MEG oscillations in very preterm children (blue line represents typically developing controls; red line represents preterm children). **(D)** Regional analysis of oscillatory slowing in very preterm children indicates involvement of frontal lobes. For these analyses, bandpass filtering and the Hilbert transform were used to obtain phase and amplitude values for each frequency and sensor. Long-range phase synchronization was indexed using phase locking values [PLVs; see (Lachaux et al., 1999)].

(Cepeda et al., 2007; Doesburg et al., 2010b, 2011a). This was manifest as reduced task-dependent inter-regional synchronization in preterm children, which was correlated with cognitive outcome in this group (Doesburg et al., 2011a). Close inspection of the spectral signature of task-dependent connectivity suggested that alpha coherence might be slowed in preterm children, as inter-hemispheric phase synchronization was significantly reduced at alpha frequencies, but increased in the theta range (**Figure 8B**).

Analysis of the resting-state MEG activity has also indicated that spontaneous alpha oscillations are slowed toward the theta range, and that this effect is maximal at sensors located over frontal cortex (Doesburg et al., 2011b; **Figures 8C,D**). Subsequent analysis of slowing of alpha oscillations in preterm children confirmed the involvement of prefrontal cortical regions (Doesburg et al., 2013c). Taken together with results from task-dependent network coherence, these findings suggest that atypical oscillatory activity in frontal lobe systems may lead to reduced ability to recruit network coherence supporting cognitive abilities. In this view, selective developmental difficulties with executive abilities prevalent in preterm-born children may be in part attributable to the inability of frontal lobe systems to recruit task-dependent inter-regional communication, mediated by neuronal synchronization. This perspective is supported by observations that alterations in both spontaneous and task-dependent alpha oscillations are associated with poor cognitive outcome in children born prematurely (Doesburg et al., 2011a, 2013b,c).

PRACTICAL CONSIDERATIONS FOR CONDUCTING DEVELOPMENTAL MEG STUDIES

We have reviewed the contribution of MEG imaging for investigation of typical and atypical development in frontal lobe systems. Many of the studies reviewed demonstrate dramatic changes in the timing, location, and in connectivity, which continue throughout childhood, adolescence, and early adulthood, underscoring the utility of MEG for understanding the evolution of neural processes underlying cognitive abilities. Successful conduction of MEG imaging in children, however, requires several practical considerations, which we review here. The reader is referred to Pang (2011) for a detailed discussion.

The most common technical challenge to overcome when conducting MEG research with children is that of movement artifact. Although voluntary head and eye movements are reduced through training, researchers should be aware that tasks may need to be lengthened and trial numbers increased to allow for rejection of trials containing these artifacts. Moreover, MEG research in atypically developing child populations often requires a more liberal movement threshold, relative to what is typical for normative adult studies, in order to strike an appropriate balance between artifact-free recordings and an unbiased sample. New MEG systems with continuous head localization hold good promise for correcting for head movements, but these solutions may only be valid within a small range of movement and may not be able to correct appropriately for the movements of an agitated, hyperactive, or uncooperative child. Moreover, the impact of head motion correction techniques on more recently introduced analysis approaches has not yet been fully tested.

Magnetoencephalography helmets designed for recording from children improve issues with head movement, as there is less room for participants to move. These child-sized MEG systems also place the sensors much closer to the surface of the head, resulting in significant improvement to the signal to noise ratio. In an attempt to have the child feel less enclosed, however, these systems do not always have adequate coverage over the anterior aspect of the head for recording or analysis of frontal lobe activity. Also, institutions using these systems still require an adult MEG as the helmets of these pediatric systems would not accommodate pre-teen or teenaged participants.

In the studies described in this review from our research group, we have primarily relied on participant training to mitigate the influence of head movement on MEG recordings. The team members responsible for running the studies are trained to ensure that all participants understand the importance of staying still and spend considerable effort gaining and maintaining positive rapport with and cooperation from the children. Moreover, subjects are monitored throughout recording and reminded to remain as still as possible whenever necessary. Participants are also offered breaks as needed. Testing all children lying down, supine in the MEG, applying padding into the dewar to stabilize the head, as well as covering the child with a blanket to reduce body movement and thus head movement also facilitates cleaner recordings.

Task design is another critical consideration in developmental MEG studies. Experimental paradigms need to be age-appropriate, simple, understandable, engaging, and quick. One effective strategy is to first successfully implement an adult version of a protocol, usually adapted from a standard experimental neuropsychological test, and to subsequently pare the task down to its core features. Using colorful and child-friendly versions of these tasks is critical to maintain task performance long enough to obtain a sufficient number of MEG trials for subsequent reliable data analyses.

Taking these various considerations into account significantly reduces problems associated with MEG recordings in children, including clinical populations, allowing cognitive studies to be successfully completed. In our experience, the examination of cognitive functions using MEG is feasible in children as young as 4 years of age. For the youngest participants and clinical populations, the MEG is a much easier neuroimaging environment, as it is totally silent and less daunting than an MRI.

SUMMARY

We review MEG investigations of several frontal lobe functions associated with typical and atypical development – in social cognition, executive function, and speech – as well as network connectivity involving frontal lobe systems. This research highlights the complex and protracted developmental trajectory of frontal lobe systems, as well as the unique contribution that MEG can make to this field as a non-invasive neurophysiological imaging modality with a uniquely good combination of spatial and temporal resolution. We present some examples of atypical frontal lobe development, with relation to problems with cognitive development, in children with ASD and children born very preterm from a neuromagnetic imaging perspective. Finally, practical considerations for MEG imaging in clinical child populations and typically developing children are discussed. We believe that the range of applications briefly reviewed here highlight the promise of MEG for the comprehensive elucidation of typical and atypical development of frontal lobe processing and its relation to complex cognitive functions.

REFERENCES

Adolphs, R., Damasio, H., and Tranel, D. (2002). Neural systems for recognition of emotional prosody: a 3-D lesion study. *Emotion* 2, 23–51. doi:10.1037/1528-3542.2.1.23

Allison, T., Puce, A., and McCarthy, G. (2000). Social perception from visual cues: role of the STS region. *Trends Cogn. Sci.* 4, 267–278. doi:10.1016/S1364-6613(00)01501-1

Anderson, P. J., Doyle, L. W., and Victorian Infant Collaborative Study Group. (2004). Executive functioning in school-aged children who were born very preterm or with extremely low birth weight in the 1990s. *Pediatrics* 114, 50–57. doi:10.1542/peds.114.1.50

Anjari, M., Srinivasan, L., Allsop, J. M., Hajnal, J. V., Rutherford, M. A., Edwards, A. D., et al. (2007). Diffusion tensor imaging with tract-based spatial statistics reveals local white matter abnormalities in preterm infants. *Neuroimage* 35, 1021–1027. doi:10.1016/j.neuroimage.2007.01.035

Batty, M., Meaux, E., Wittemeyer, K., Roge, B., and Taylor, M. J. (2011). Early processing of emotional faces in children with autism. *J. Exp. Child. Psychol.* 109, 430–444. doi:10.1016/j.jecp.2011.02.001

Batty, M., and Taylor, M. J. (2006). The development of emotional face processing during childhood. *Dev. Sci.* 9, 207–220. doi:10.1111/j.1467-7687.2006.00480.x

Bayle, D. J., and Taylor, M. J. (2010). Attention inhibition of early cortical activation to fearful faces. *Brain Res.* 1313, 113–123. doi:10.1016/j.brainres.2009.11.060

Belmonte, M. K., Allen, G., Beckel-Mitchener, A., Boulanger, L. M., Carper, R. A., and Webb, S. J. (2004). Autism and abnormal development of brain connectivity. *J. Neurosci.* 24, 9228–9231. doi:10.1523/JNEUROSCI.3340-04.2004

Bokura, H., Yamaguchi, S., and Kobayashi, S. (2001). Electrophysiological correlates for response inhibition in a Go/NoGo task. *Clin. Neurophysiol.* 112, 2224–2232. doi:10.1016/S1388-2457(01)00691-5

Breier, J. I., and Papanicolaou, A. C. (2008). Spatiotemporal patterns of brain activation during an action naming task using magnetoencephalography. *J. Clin. Neurophysiol.* 25, 7–12. doi:10.1097/WNP.0b013e318163ccd5

Burnett, S., Bird, G., Moll, J., Frith, C., and Blakemore, S. J. (2009). Development during adolescence of the neural processing of social emotion. *J. Cogn. Neurosci.* 21, 1736–1750. doi:10.1162/jocn.2009.21121

Bush, G., Luu, P., and Posner, M. I. (2000). Cognitive and emotional influences in anterior cingulate cortex. *Trends Cogn. Sci.* 4, 215–222. doi:10.1016/S1364-6613(00)01483-2

Carota, F., Posada, A., Harquel, S., Delpuech, C., Bertrand, O., and Sirigu, A. (2010). Neural dynamics of the intention to speak. *Cereb. Cortex* 20, 1891–1897. doi:10.1093/cercor/bhp255

Carper, R. A., and Courchesne, E. (2005). Localized enlargement of the frontal cortex in early autism. *Biol. Psychiatry* 57, 126–133. doi:10.1016/j.biopsych.2004.11.005

Carter, E. J., and Pelphrey, K. A. (2008). Friend or foe? Brain systems involved in the perception of dynamic signals of menacing and friendly social approaches. *Soc. Neurosci.* 3, 151–163. doi:10.1080/17470910801903431

Cepeda, I. L., Grunau, R. E., Weinberg, H., Herdman, A. T., Cheung, T., Liotti, M., et al. (2007). Magnetoencephalography study of brain dynamics in young children born extremely preterm. *Int. Congr. Ser.* 1300, 99–102. doi:10.1016/j.ics.2006.12.090

Cheng, Y., Chou, K. H., Chen, I. Y., Fan, Y. T., Decety, J., and Lin, C. P. (2010). Atypical development of white matter microstructure in adolescents with autism spectrum disorders. *Neuroimage* 50, 873–882. doi:10.1016/j.neuroimage.2010.01.011

Costafreda, S. G., Brammer, M. J., David, A. S., and Fu, C. H. Y. (2008). Predictors of amygdala activation during the processing of emotional stimuli: a meta-analysis of 385 PET and fMRI studies. *Brain Res. Rev.* 58, 57–70. doi:10.1016/j.brainresrev.2007.10.012

De Sonneville, L. M. J., Vershoor, C. A., Njiokiktjien, C., Veld, V. O. H., Toorenaar, N., and Vranken, M. (2002). Facial identity and facial emotions: speed, accuracy and processing strategies in children and adults. *J. Clin. Exp. Neuropsychol.* 24, 200–213. doi:10.1076/jcen.24.2.200.989

Dhond, R. P., Buckner, R. L., Dale, A. M., Marinkovic, K., and Halgren, E. (2001). Spatiotemporal maps of brain activity underlying word generation and their modification during repetition priming. *J. Neurosci.* 21, 3564–3571.

Dillon, D. G., and Pizzagalli, D. A. (2007). Inhibition of action, thought, and emotion: a selective neurobiological review. *Appl. Prev. Psychol.* 12, 99–114. doi:10.1016/j.appsy.2007.09.004

Doesburg, S. M., Herdman, A. T., Ribary, U., Cheung, T., Moiseev, A., Weinberg, H., et al. (2010a). Long-range synchronization and local desynchronization of alpha oscillations during visual short-term memory retention in children. *Exp. Brain Res.* 201, 719–727. doi:10.1007/s00221-009-2086-9

Doesburg, S. M., Ribary, U., Herdman, A. T., Cheung, T., Moiseev, A., Weinberg, H., et al. (2010b). Altered long-range phase synchronization and cortical activation in children born very preterm. *IFMBE Proc.* 29, 250–253. doi:10.1007/978-3-642-12197-5_57

Doesburg, S. M., Ribary, U., Herdman, A. T., Miller, S. P., Poskitt, K. J., Moiseev, A., et al. (2011a). Altered long-range alpha-band synchronization during visual short-term memory retention in children born very preterm. *Neuroimage* 54, 2330–2339. doi:10.1016/j.neuroimage.2010.10.044

Doesburg, S. M., Ribary, U., Herdman, A. T., Moiseev, A., Cheung, T., Miller, S. P., et al. (2011b). Magnetoencephalography reveals slowing of resting peak oscillatory frequency in children born very preterm. *Pediatr. Res.* 70, 171–175. doi:10.1038/pr.2011.396

Doesburg, S. M., Vidal, J., and Taylor, M. J. (2013a). Reduced theta connectivity during set-shifting in children with autism. *Front. Hum. Neurosci.* 7, 785. doi:10.3389/fnhum.2013.00785

Doesburg, S. M., Chau, C. M., Cheung, T. P., Moiseev, A., Ribary, U., Herdman, A. T., et al. (2013b). Neonatal pain-related stress, functional cortical activity and school-age cognitive outcome in children born at extremely low gestational age. *Pain* 154, 2475–2483. doi:10.1016/j.pain.2013.04.009

Doesburg, S. M., Moiseev, A., Herdman, A. T., Ribary, U., and Grunau, R. E. (2013c). Region-specific slowing of alpha oscillations is associated with visual-perceptual abilities in children born very preterm. *Front. Hum. Neurosci.* 7, 791. doi:10.3389/fnhum.2013.00791

Dudink, J., Lequin, M., van Pul, C., Buijs, J., Conneman, N., van Goudoever, J., et al. (2007). Fractional anisotropy in white matter tracts of very-low-birth-weight infants. *Pediatr. Radiol.* 37, 1216–1223. doi:10.1007/s00247-007-0626-7

Durston, S., Thomas, K. M., Yang, Y., Ulu, A. M., Zimmerman, R. D., and Casey, B. J. (2002). A neural basis for the development of inhibitory control. *Dev. Sci* 4, 9–16. doi:10.1111/1467-7687.00235

Elliott, R. (2003). Executive functions and their disorders. *Br. Med. Bull.* 65, 49–59. doi:10.1093/bmb/65.1.49

Farran, E. K., Branson, A., and King, B. J. (2011). Visual search for basic emotional expressions in autism: impaired processing of anger, fear, and sadness, but a typical happy face advantage. *Res. Autism Spect. Dis.* 5, 455–462. doi:10.1016/j.rasd.2010.06.009

Frith, U. (2004). Emanuel Miller lecture: confusions and controversies about Asperger syndrome. *J. Child Psychol. Psychiatry* 45, 672–686. doi:10.1111/j.1469-7610.2004.00262.x

Frye, R. E., Malmberg, B., McLean, J., Swank, P., Smith, K., Papanicolaou, A., et al. (2010). Increased left prefrontal activation during an auditory language task in adolescents born preterm at high risk. *Brain Res.* 1336, 89–97. doi:10.1016/j.brainres.2010.03.093

Hampshire, A., Chamberlain, S. R., Monti, M. M., Duncan, J., and Owen, A. M. (2010). The role of the right inferior frontal gyrus: inhibition and attentional control. *Neuroimage* 50, 1313–1319. doi:10.1016/j.neuroimage.2009.12.109

Hart, A. R., Whitby, E. W., Griffiths, P. D., and Smith, M. F. (2008). Magnetic resonance imaging and developmental outcome following preterm birth: review of current evidence. *Dev. Med. Child Neurol.* 50, 655–663. doi:10.1111/j.1469-8749.2008.03050.x

Haxby, J. V., Hoffman, E. A., and Gobbini, M. I. (2000). The distributed human neural system for face perception. *Trends Cogn. Sci.* 4, 223–233. doi:10.1016/S1364-6613(00)01482-0

Herba, C., and Phillips, M. (2004). Annotation: development of facial expression recognition from childhood to adolescence: behavioural and neurological perspectives. *J. Child Psychol. Psychiatry* 45, 1185–1198. doi:10.1111/j.1469-7610.2004.00316.x

Herdman, A. T., Pang, E. W., Ressel, V., Gaetz, E., and Cheyne, D. (2007). Task-related modulation of early cortical responses during language production: an event-related synthetic aperture magnetometry study. *Cereb. Cortex* 17, 2536–2543. doi:10.1093/cercor/bhl159

Hesling, I., Clement, S., Bordessoules, M., and Allard, M. (2005). Cerebral mechanisms of prosodic integration: evidence from connected speech. *Neuroimage* 24, 937–947. doi:10.1016/j.neuroimage.2004.11.003

Hobson, R. P., and Lee, A. (1998). Hello and goodbye: a study of social engagement in autism. *J. Autism Dev. Disord.* 28, 117–127. doi:10.1023/A:1026088531558

Hung, Y., Smith, M. L., Bayle, D. J., Mills, T., and Taylor, M. J. (2010). Unattended emotional faces elicit early lateralized amygdala-frontal and fusiform activations. *Neuroimage* 50, 727–733. doi:10.1016/j.neuroimage.2009.12.093

Hung, Y., Smith, M. L., and Taylor, M. J. (2012). Development of ACC-amygdala activations in processing unattended fear. *Neuroimage* 60, 545–552. doi:10.1016/j.neuroimage.2011.12.003

Ihara, A., Hirata, M., Sakihara, K., Izumi, H., Takahashi, Y., Kono, K., et al. (2003). Gamma-band desynchronization in language areas reflects syntactic process of words. *Neurosci. Lett.* 339, 135–138. doi:10.1016/S0304-3940(03)00005-3

Just, M. A., Cherkassky, V. L., Keller, T. A., Kana, R. J., and Minshew, N. J. (2007). Functional and anatomical cortical underconnectivity in autism: evidence from an fMRI study of an executive function task and corpus callosum morphometry. *Cereb. Cortex* 17, 951–961. doi:10.1093/cercor/bhl006

Just, M. A., Keller, T. A., Malave, V. L., Kana, R. K., and Varma, S. (2012). Autism as a neural systems disorder: a theory of frontal-posterior underconnectivity. *Neurosci. Biobehav. Rev.* 4, 1292–1313. doi:10.1016/j.neubiorev.2012.02.007

Kana, R. K., Keller, T. A., Minshew, N. J., and Just, M. A. (2007). Inhibitory control in high-functioning autism: decreased activation and underconnectivity in inhibition networks. *Biol. Psychiatry* 62, 198–120. doi:10.1016/j.biopsych.2006.08.004

Kato, Y., Muramatsu, T., Kato, M., Shintani, M., and Kashima, H. (2007). Activation of right insular cortex during imaginary speech articulation. *Neuroreport* 18, 505–509. doi:10.1097/WNR.0b013e3280586862

Khan, S., Gramfort, A., Shetty, N. R., Kitzbichler, M. G., Ganesan, S., Moran, J. M., et al. (2013). Local and long-range functional connectivity is reduced in concert in autism spectrum disorders. *Proc. Natl. Acad. Sci. U.S.A.* 110, 3107–3112. doi:10.1073/pnas.1214533110

Khwaja, O., and Volpe, J. J. (2008). Pathogenesis of cerebral white matter injury of prematurity. *Arch. Dis. Child. Fetal Neonatal Ed.* 93, F153–F161. doi:10.1136/adc.2006.108837

Kilts, C. D., Egan, G., Gideon, D. A., Ely, T. D., and Hoffman, J. M. (2003). Dissociable neural pathways are involved in the recognition of emotion in static and dynamic facial expressions. *Neuroimage* 18, 156–168. doi:10.1006/nimg.2002.1323

Kolb, B., Wilson, B., and Taylor, L. (1992). Developmental changes in the recognition and comprehension of facial expression: implications for frontal lobe function. *Brain Cogn.* 20, 74–84. doi:10.1016/0278-2626(92)90062-Q

Kramer, U. M., Mohammadi, B., Donamayor, N., Samii, A., and Munte, T. F. (2010). Emotional and cognitive aspects of empathy and their relation to social cognition – an fMRI-study. *Brain Res.* 1311, 110–120. doi:10.1016/j.brainres.2009.11.043

Kuusikko, S., Haapsamo, H., Jansson-Verkasalo, E., Hurtig, T., Mattila, M. L., Ebeling, H., et al. (2009). Emotion recognition in children and adolescents with autism

spectrum disorders. *J. Autism Dev. Disord.* 39, 938–945. doi:10.1007/s10803-009-0700-0

Lachaux, J. P., Rodriguez, E., Martinerie, J., and Varela, F. J. (1999). Measuring phase synchrony in brain signals. *Hum. Brain Mapp.* 8, 194–208. doi:10.1002/(SICI)1097-0193(1999)8:4<194::AID-HBM4>3.0.CO;2-C

Lamm, C., and Lewis, M. D. (2010). Developmental change in the neurophysiological correlates of self-regulation in high- and low-emotion conditions. *Dev. Neuropsychol.* 35, 156–176. doi:10.1080/87565640903526512

Langdell, T. (1978). Recognition of faces: an approach to the study of autism. *J. Child Psychol. Psychiatry* 19, 225–268.

Lewis, P. A., Rezaie, R., Brown, R., Roberts, N., and Dunbar, R. I. (2011). Ventromedial prefrontal volume predicts understanding of others and social network size. *Neuroimage* 57, 1624–1629. doi:10.1016/j.neuroimage.2011.05.030

Liljeström, M., Hultén, A., Parkkonen, L., and Salmelin, R. (2009). Comparing MEG and fMRI views to naming actions and objects. *Hum. Brain Mapp.* 30, 1845–1856. doi:10.1002/hbm.20785

Luna, B., Garver, K. E., Urban, T. A., Lazar, N. A., and Sweeney, J. A. (2004). Maturation of cognitive processes from late childhood to adulthood. *Child Dev.* 75, 1357–1372. doi:10.1111/j.1467-8624.2004.00745.x

Luna, B., Padmanabhan, A., and O'Hearn, K. (2010). What has fMRI told us about the development of cognitive control through adolescence? *Brain Cogn.* 72, 101–113. doi:10.1016/j.bandc.2009.08.005

Mak-Fan, K., Morris, D., Anagnostou, E., Roberts, W., and Taylor, M. J. (2013). White matter and development in children with an autism spectrum disorder (ASD). *Autism* 7, 541–557. doi:10.1177/1362361312442596

Mak-Fan, K., Taylor, M. J., Roberts, W., and Lerch, J. P. (2012). Measures of cortical grey matter structure and development in children with autism spectrum disorder (ASD). *J. Autism Dev. Disord.* 42, 419–427. doi:10.1007/s10803-011-1261-6

Marlow, N., Hennessy, E. M., Bracewell, M. A., Wolke, D., and EPICure Study Group. (2007). Motor and executive function at 6 years of age after extremely preterm birth. *Pediatrics* 120, 793–804. doi:10.1542/peds.2007-0440

McCarthy, G., Puce, A., Belger, A., and Allison, T. (1999). Electrophysiological studies of human face perception. II: response properties of face-specific potentials generated in occipitotemporal cortex. *Cereb. Cortex* 9, 431–444. doi:10.1093/cercor/9.5.431

Memarian, N., Ferrari, P., MacDonald, M. J., Cheyne, D., De Nil, L. F., and Pang, E. W. (2012). Cortical activity during speech and non-speech oromotor tasks: a magnetoencephalography (MEG) study. *Neurosci. Lett.* 527, 34–39. doi:10.1016/j.neulet.2012.08.030

Ment, L. R., Hirtz, D., and Huppi, P. S. (2009). Imaging biomarkers of outcome in the developing preterm brain. *Lancet Neurol.* 8, 1042–1055. doi:10.1016/S1474-4422(09)70257-1

Miki, K., Watanabe, S., Teruya, M., Takeshima, Y., Urakawa, T., Hirai, M., et al. (2011). The development of the perception of facial emotional change examined using ERPs. *Clin. Neurophysiol.* 122, 530–538. doi:10.1016/j.clinph.2010.07.013

Miller, S. P., and Ferriero, D. M. (2009). From selective vulnerability to connectivity: Insights from newborn brain imaging. *Trends Neurosci.* 32, 496–505. doi:10.1016/j.tins.2009.05.010

Mills, T., Lalancette, M., Moses, S. N., Taylor, M. J., and Quraan, M. A. (2012). Techniques for detection and localization of weak hippocampal and medial frontal sources using beamformers in MEG. *Brain Topogr.* 25, 248–263. doi:10.1007/s10548-012-0217-2

Moses, S. N., Houck, J. M., Martin, T., Hanlon, F. M., Ryan, J. D., Thoma, R. J., et al. (2007). Dynamic neural activity recorded from human amygdala during fear conditioning using magnetoencephalography. *Brain Res. Bull.* 71, 452–460. doi:10.1016/j.brainresbull.2006.08.016

Moses, S. N., Ryan, J. D., Bardouille, T., Kovacevic, N., Hanlon, F. M., and McIntosh, A. R. (2009). Semantic information alters neural activation during transverse patterning performance. *Neuroimage* 46, 863–873. doi:10.1016/j.neuroimage.2009.02.042

Mostofsky, S. H., and Simmonds, D. J. (2008). Response inhibition and response selection: two sides of the same coin. *J. Cogn. Neurosci.* 20, 751–761. doi:10.1162/jocn.2008.20500

Mulder, H., Pitchford, N. J., Hagger, M. S., and Marlow, N. (2009). Development of executive function and attention in preterm children: a systematic review. *Dev. Neuropsychol.* 34, 393–421. doi:10.1080/87565640902964524

Müller, R. A., Shih, P., Keehn, B., Deyoe, J. R., Leyden, K. M., and Shukla, D. K. (2011). Underconnected, but how? A survey of functional connectivity MRI studies in autism spectrum disorders. *Cereb. Cortex* 21, 2233–2243. doi:10.1093/cercor/bhq296

Nevalainen, P., Pihko, E., Metsaranta, M., Andersson, S., Autti, T., and Lauronen, L. (2008). Does very premature birth affect the functioning of the somatosensory cortex? – A magnetoencephalography study. *Int. J. Psychophysiol.* 68, 85–93. doi:10.1016/j.ijpsycho.2007.10.014

Nishitani, N., and Hari, R. (2002). Viewing lips forms: cortical dynamics. *Neuron* 36, 1211–1220. doi:10.1016/S0896-6273(02)01089-9

Palva, J. M., Monto, S., Kulashekhar, S., and Palva, S. (2010a). Neuronal synchrony reveals working memory networks and predicts individual memory capacity. *Proc. Natl. Acad. Sci. U.S.A.* 107, 7580–7585. doi:10.1073/pnas.0913113107

Palva, S., Monto, S., and Palva, J. M. (2010b). Graph properties of synchronized cortical networks during visual working memory maintenance. *Neuroimage* 49, 3257–3268. doi:10.1016/j.neuroimage.2009.11.031

Palva, J. M., Palva, S., and Kaila, K. (2005). Phase synchrony among neuronal oscillations in the human cortex. *J. Neurosci.* 25, 3962–3972. doi:10.1523/JNEUROSCI.4250-04.2005

Pang, E. W. (2011). Practical aspects of running developmental studies in the MEG. *Brain Topogr.* 24, 253–260. doi:10.1007/s10548-011-0175-0

Pang, E. W., Valica, T., MacDonald, M. J., Oh, A., Lerch, J. P., and Anagnostou, E. (2013). Differences in neural mechanisms underlying speech production in autism spectrum disorders as tracked by magnetoencephalography (MEG). *Clin. EEG Neurosci.* 44, E117. doi:10.1177/1550059412471275

Pang, E. W., Wang, F., Malone, M., Kadis, D. S., and Donner, E. J. (2011). Localization of Broca's area using verb generation tasks in the MEG: validation against fMRI. *Neurosci. Lett.* 490, 215–219. doi:10.1016/j.neulet.2010.12.055

Passarotti, A. M., Sweeney, J. A., and Pavuluri, M. N. (2009). Neural correlates of incidental and directed facial emotion processing in adolescents and adults. *Soc. Cogn. Affect. Neurosci.* 4, 387–398. doi:10.1093/scan/nsp029

Pelphrey, K. A., Morris, J. P., McCarthy, G., and Labar, K. S. (2007). Perception of dynamic changes in facial affect and identity in autism. *Soc. Cogn. Affect. Neurosci.* 2, 140–149. doi:10.1093/scan/nsm010

Pierce, K., Muller, R. A., Ambrose, J., Allen, G., and Courchesne, E. (2001). Face processing occurs outside the fusiform 'face area' in autism: evidence from functional MRI. *Brain* 124, 2059–2073. doi:10.1093/brain/124.10.2059

Powell, K. B., and Voeller, K. K. (2004). Prefrontal executive function syndromes in children. *J. Child Neurol.* 19, 785–797. doi:10.1177/08830738040190100801

Quraan, M. A., Moses, S. N., Hung, Y., Mills, T., and Taylor, M. J. (2011). Detection and localization of evoked deep brain activity using MEG. *Hum. Brain Mapp.* 32, 812–827. doi:10.1002/hbm.21068

Radke, S., de Lange, F. P., Ullsperger, M., and de Bruijn, E. R. (2011). Mistakes that affect others: an fMRI study on processing of own errors in a social context. *Exp. Brain Res.* 211, 405–413. doi:10.1007/s00221-011-2677-0

Rahkonen, P., Nevalainen, P., Lauronen, L., Pihko, E., Lano, A., Vanhatalo, S., et al. (2013). Cortical somatosensory processing measured by magnetoencephalography predicts neurodevelopment in extremely low-gestational-age infants. *Pediatr. Res.* 73, 763–771. doi:10.1038/pr.2013.46

Roberts, G., Anderson, P. J., De Luca, C., and Doyle, L. W. (2010). Changes in neurodevelopmental outcome at age eight in geographic cohorts of children born at 22–27 weeks gestational age during the 1990s. *Arch. Dis. Child. Fetal Neonatal Ed.* 95, 90–94. doi:10.1136/adc.2009.165480

Robinson, S. E., and Vrba, J. (1999). "Functional neuroimaging by synthetic aperture magnetometry (SAM)," in *Recent Advances in Biomagnetism*, eds T. Yoshimoto, M. Kotani, S. Kuriki, et al. (Sendai: Tohoku University Press), 302–305.

Rubia, K., Russell, T., Overmeyer, S., Brammer, M. J., Bullmore, E. T., Sharma, T., et al. (2001). Mapping motor inhibition: conjunctive brain activations across different versions of go/no-go and stop tasks. *Neuroimage* 13, 250–261. doi:10.1006/nimg.2000.0685

Rubia, K., Smith, A. B., Taylor, E., and Brammer, M. (2007). Linear age-correlated functional development of right inferior fronto-striato-cerebellar networks during response inhibition and anterior cingulate during error-related processes. *Hum. Brain Mapp.* 28, 1163–1177. doi:10.1002/hbm.20347

Rump, K. M., Giovannelli, J. L., Minshew, N. J., and Strauss, M. S. (2009). The development of emotion recognition in individuals with autism. *Child Dev.* 80, 1434–1447. doi:10.1111/j.1467-8624.2009.01343.x

Saarinen, T., Laaksonen, H., Parviainen, T., and Salmelin, R. (2006). Motor cortex dynamics in visumotor production of speech and non-speech mouth movements. *Cereb. Cortex* 16, 212–222. doi:10.1093/cercor/bhi099

Salmelin, R. (2007). Clinical neurophysiology of language: the MEG approach. *Clin. Neurophysiol.* 118, 237–254. doi:10.1016/j.clinph.2006.07.316

Salmelin, R., Hari, R., Lounasmaa, O. V., and Sams, M. (1994). Dynamics of brain activation during picture naming. *Nature* 368, 463–465. doi:10.1038/368463a0

Satpute, A. B., and Lieberman, M. D. (2006). Integrating automatic and controlled processes into neurocognitive models of social cognition. *Brain Res.* 1079, 86–97. doi:10.1016/j.brainres.2006.01.005

Schäfer, C. B., Morgan, B. R., Ye, A. X., Taylor, M. J., and Doesburg, S. M. (2014). Oscillations, networks and their development: MEG connectivity changes with age. *Hum. Brain Mapp.* doi:10.1002/hbm.22547

Schmitz, N., Rubia, K., Daly, E., Smith, A., Williams, S., and Murphy, D. G. (2006). Neural correlates of executive function in autistic spectrum disorders. *Biol. Psychiatry* 59, 7–16. doi:10.1016/j.biopsych.2005.06.007

Shaw, P., Kabani, N. J., Lerch, J. P., Eckstrand, K., Lenroot, R., Gogtay, N., et al. (2008). Neurodevelopmental trajectories of the human cerebral cortex. *J. Neurosci.* 28, 3586–3594. doi:10.1523/JNEUROSCI.5309-07.2008

Shukla, D. K., Keehn, B., and Muller, R. A. (2011). Tract-specific analyses of diffusion tensor imaging show widespread white matter compromise in autism spectrum disorder. *J. Child Psychol. Psychiatry* 52, 286–295. doi:10.1111/j.1469-7610.2010.02342.x

Simonyan, K., Ostuni, J., Ludlow, C. L., and Horowitz, B. (2009). Functional but not structural networks of the human laryngeal motor cortex show left hemispheric lateralization during syllable but not breathing production. *J. Neurosci.* 29, 14912–14923. doi:10.1523/JNEUROSCI.4897-09.2009

Stam, C. J., Nolte, G., and Daffertshofer, A. (2007). Phase lag index: assessment of functional connectivity from multi-channel EEG and MEG with diminished bias from common sources. *Hum. Brain Mapp.* 28, 1178–1193. doi:10.1002/hbm.20346

Tamm, L., Menon, V., Ringel, J., and Reiss, A. L. (2004). Event-related FMRI evidence of frontotemporal involvement in aberrant response inhibition and task switching in attention-deficit/hyperactivity disorder. *J. Am. Acad. Child Adolesc. Psychiatry* 43, 1430–1440. doi:10.1097/01.chi.0000140452.51205.8d

Taylor, M. J., Bayless, S. J., Mills, T., and Pang, E. W. (2011a). Recognising upright and inverted faces: MEG source localisation. *Brain Res.* 1381, 167–174. doi:10.1016/j.brainres.2010.12.083

Taylor, M. J., Mills, T., and Pang, E. W. (2011b). The development of face recognition; hippocampal and frontal lobe contributions determined with MEG. *Brain Topogr.* 24, 261–270. doi:10.1007/s10548-011-0192-z

Taylor, M. J., Donner, E. J., and Pang, E. W. (2012). f MRI and MEG in the study of typical and atypical cognitive development. *Neurophysiol. Clin.* 42, 19–25. doi:10.1016/j.neucli.2011.08.002

Taylor, M. J., Mills, T., Smith, M. L., and Pang, E. W. (2008). Face processing in adolescents with and without epilepsy. *Int. J. Psychophysiol.* 68, 94–103. doi:10.1016/j.ijpsycho.2007.12.006

Taylor, M. J., Mills, T., Zhang, L., Smith, M. L., and Pang, E. W. (2010). "Face processing in children: novel MEG findings," in *IFMBE Proceedings*, Vol. 28, eds S. Supek and A. Susac (Berlin Heidelberg: Springer), 314–321.

Telzer, E. H., Masten, C. L., Berkman, E. T., Lieberman, M. D., and Fuligni, A. J. (2011). Neural regions associated with self control and mentalizing are recruited during prosocial behaviors towards the family. *Neuroimage* 58, 242–249. doi:10.1016/j.neuroimage.2011.06.013

Thomas, L. A., De Bellis, M. D., Graham, R., and LaBar, K. S. (2007). Development of emotional facial recognition in late childhood and adolescence. *Dev. Sci.* 10, 547–558. doi:10.1111/j.1467-7687.2007.00614.x

Todd, R. M., Evans, J. W., Morris, D., Lewis, M. D., and Taylor, M. J. (2012). The changing face of emotion: age related patterns of amygdala activation to salient faces. *Soc. Cogn. Affect. Neurosci.* 6, 12–23. doi:10.1093/scan/nsq007

Tottenham, N., Tanaka, J. W., Leon, A. C., McCarry, T., Nurse, M., Hare, T. A., et al. (2009). The NimStim set of facial expressions: judgments from untrained research participants. *Psychiatry Res.* 168, 242–249. doi:10.1016/j.psychres.2008.05.006

Travers, B. G., Adluru, N., Ennis, C., Tromp, D. P. M., Destiche, D., Doran, S., et al. (2012). Diffusion tensor imaging in autism spectrum disorder: a review. *Autism Res.* 5, 289–313. doi:10.1002/aur.1243

Vara, A. S., Pang, E. W., Doyle-Thomas, K. A., Vidal, J., Taylor, M. J., and Anagnostou, E. (2014). Is inhibitory control a "No-go" in adolescents with ASD? *Mol. Autism* 5, 6. doi:10.1186/2040-2392-5-6

Vidal, J., Mills, T., Pang, E. W., and Taylor, M. J. (2012). Response inhibition in adults and teenagers: spatiotemporal differences in the prefrontal cortex. *Brain Cogn.* 79, 49–59. doi:10.1016/j.bandc.2011.12.011

Vihla, M., Laine, M., and Salmelin, R. (2006). Cortical dynamics of visual/semantic vs. phonological analysis in picture confrontation. *Neuroimage* 33, 732–738. doi:10.1016/j.neuroimage.2006.06.040

Vrba, J., and Robinson, S. E. (2001). Signal processing in magnetoencephalography. *Methods* 25, 249–271. doi:10.1006/meth.2001.1238

Wang, A. T., Lee, S. S., Sigman, M., and Dapretto, M. (2007). Reading affect in the face and voice: neural correlates of interpreting communicative intent in children and adolescents with autism spectrum disorders. *Arch. Gen. Psychiatry* 64, 698–708. doi:10.1001/archpsyc.64.6.698

Watanabe, J., Sugiura, M., Sato, K., Sato, Y., Maeda, Y., Matsue, Y., et al. (2002). The human prefrontal and parietal association cortices are involved in NO-GO performances: an event-related fMRI study. *Neuroimage* 17, 1207–1216. doi:10.1006/nimg.2002.1198

Wheat, K. L., Cornelissen, P. L., Frost, S. J., and Hansen, P. C. (2010). During visual word recognition, phonology is accessed within 100 ms and may be mediated by a speech production code: evidence from magnetoencephalography. *J. Neurosci.* 30, 5229–5233. doi:10.1523/JNEUROSCI.4448-09.2010

Wildgruber, D., Ackermann, H., Klose, U., Kardatzki, B., and Grodd, W. (1996). Functional lateralization of speech production in the primary motor cortex: a fMRI study. *Neuroreport* 7, 2791–2795. doi:10.1097/00001756-199611040-00077

Wong, T. K., Fung, P. C., Chua, S. E., and McAlonan, G. M. (2008). Abnormal spatiotemporal processing of emotional facial expressions in childhood autism: dipole source analysis of event-related potentials. *Eur. J. Neurosci.* 28, 407–416. doi:10.1111/j.1460-9568.2008.06328.x

Conflict of Interest Statement: The authors declare that the research was conducted in the absence of any commercial or financial relationships that could be construed as a potential conflict of interest.

Received: 10 December 2013; accepted: 03 June 2014; published online: 18 June 2014.
Citation: Taylor MJ, Doesburg SM and Pang EW (2014) Neuromagnetic vistas into typical and atypical development of frontal lobe functions. Front. Hum. Neurosci. ***8****:453. doi: 10.3389/fnhum.2014.00453*
This article was submitted to the journal Frontiers in Human Neuroscience.

frontiers in
HUMAN NEUROSCIENCE

ORIGINAL RESEARCH ARTICLE
published: 06 June 2014
doi: 10.3389/fnhum.2014.00417

Missing and delayed auditory responses in young and older children with autism spectrum disorders

J. Christopher Edgar[1]*, Matthew R. Lanza[1], Aleksandra B. Daina[1], Justin F. Monroe[1], Sarah Y. Khan[1], Lisa Blaskey[1,2], Katelyn M. Cannon[1], Julian Jenkins III[1], Saba Qasmieh[1,2], Susan E. Levy[2] and Timothy P. L. Roberts[1]

[1] *Department of Radiology, Lurie Family Foundation MEG Imaging Center, The Children's Hospital of Philadelphia, Philadelphia, PA, USA*
[2] *Department of Pediatrics, The Children's Hospital of Philadelphia, Philadelphia, PA, USA*

Edited by:
Christos Papadelis, Harvard Medical School, USA

Reviewed by:
Sheraz Khan, Massachusetts General Hospital, USA
Elena V. Orekhova, Moscow State University of Psychology and Education, Russia
Elysa Jill Marco, University of California San Francisco, USA

****Correspondence:***
J. Christopher Edgar, Department of Radiology, Children's Hospital of Philadelphia, Wood Building, Suite 2115, 34th and Civic Center Boulevard, Philadelphia, PA 19104, USA
e-mail: edgarj@email.chop.edu

Background: The development of left and right superior temporal gyrus (STG) 50 ms (M50) and 100 ms (M100) auditory responses in typically developing (TD) children and in children with autism spectrum disorder (ASD) was examined. Reflecting differential development of primary/secondary auditory areas and supporting previous studies, it was hypothesized that whereas left and right M50 STG responses would be observed equally often in younger and older children, left and right M100 STG responses would more often be absent in younger than older children. In ASD, delayed neurodevelopment would be indicated via the observation of a greater proportion of ASD than TD subjects showing missing M100 but not M50 responses in both age groups. Missing M100 responses would be observed primarily in children with ASD with language impairment (ASD + LI) (and perhaps concomitantly lower general cognitive abilities).

Methods: Thirty-five TD controls, 63 ASD without language impairment (ASD − LI), and 38 ASD + LI were recruited. Binaural tones were presented. The presence or absence of a STG M50 and M100 was scored. Subjects were grouped into younger (6–10 years old) and older groups (11–15 years old).

Results: Although M50 responses were observed equally often in older and younger subjects and equally often in TD and ASD, left and right M50 responses were delayed in ASD − LI and ASD + LI. Group comparisons showed that in younger subjects M100 responses were observed more often in TD than ASD + LI (90 versus 66%, $p = 0.04$), with no differences between TD and ASD − LI (90 versus 76%, $p = 0.14$) or between ASD − LI and ASD + LI (76 versus 66%, $p = 0.53$). In older subjects, whereas no differences were observed between TD and ASD + LI, responses were observed more often in ASD − LI than ASD + LI. Findings were similar when splitting the ASD group into lower- and higher-cognitive functioning groups.

Conclusion: Although present in all groups, M50 responses were delayed in ASD. Examining the TD data, findings indicated that by 11 years, a right M100 should be observed in 100% of subjects and a left M100 in 80% of subjects. Thus, by 11 years, lack of a left and especially right M100 offers neurobiological insight into sensory processing that may underlie language or cognitive impairment.

Keywords: autism spectrum disorders, M50, M100, superior temporal gyrus, magnetoencephalography

INTRODUCTION

Autism spectrum disorders (ASD) are a set of developmental disorders characterized by social impairments, stereotypical behaviors, and deficits in communication. As a childhood disorder, an understanding of brain abnormalities in ASD requires an examination of brain processes in infants, toddlers, and young and older school-aged children with ASD. A growing number of electroencephalography (EEG) and magnetoencephalography (MEG) studies report auditory abnormalities in children with ASD. Findings include delayed superior temporal gyrus (STG) auditory 100 ms responses in children with ASD (Roberts et al., 2010), reduced 40 Hz auditory steady-state total power in children with ASD (Wilson et al., 2007), pre- and post-stimulus pure tone STG abnormalities in children with ASD (Edgar et al., 2013), and atypical hemispheric lateralization of

Abbreviations: ASD − LI, autism spectrum disorders without language impairment; ASD + LI, autism spectrum disorders with language impairment; CELF-4, clinical evaluation of language fundamentals – fourth edition; CHOP, Children's Hospital of Philadelphia; EEG, electroencephalography; MEG, magnetoencephalography; PRI, perceptual reasoning index; STG, superior temporal gyrus; TD, typically developing; VCI, verbal comprehension index.

auditory responses in children with ASD (Stroganova et al., 2013).

As reviewed below, EEG and MEG studies examining auditory processes in children with ASD differ from adult EEG and MEG studies, with some auditory components observed at a longer latency in children than adults, and some components more likely to be observed in children and not in adults, and vice versa. Building upon previous studies investigating the development of auditory responses in typically developing (TD) children (e.g., Ponton et al., 2002), the present study examined the development of STG auditory responses in children with ASD to determine if there was evidence for a developmental delay.

The text below reviews the literature on auditory responses in adults and children. Given that a primary goal of the present study is the use of MEG to examine left and right STG auditory responses in children with ASD, the tangential auditory responses best measured using MEG are a primary focus. [For EEG studies examining the development of auditory components due to radially oriented neurons on the lateral aspect of the STG, generally not detected using MEG, readers are directed to Ponton et al. (1999) and Ponton et al. (2002) and also to EEG studies examining these radially oriented auditory components in ASD (Bruneau et al., 1997; Orekhova et al., 2009; Stroganova et al., 2013)].

AUDITORY RESPONSES IN ADULTS

In adults, N100 (EEG) and M100 (MEG) are the most prominent deflections of the auditory event-related potential (EEG) or field (MEG), evolving with a peak latency of about 100 ms after stimulus onset (for a review see Hari, 1990). Näätänen and Picton (1987) argued that the electric N100 reflects contributions from five to six distinct cortical areas: dipoles in or near the primary auditory cortex, a frontal source, and early portions of the attention-related processing negativity and the mismatch negativity. Using BESA and VARETA to model the N100 sources, Picton et al. (1999) noted that although multiple brain regions contribute to N100, the major activity underlying the scalp-recorded N100 wave is located in the supratemporal plane. Because MEG does not detect activity from radial current configurations, M100 is well described as being generated by a pair of equivalent current dipoles (one in each hemisphere) located in the region of the planum temporale (e.g., Hari, 1990; Lutkenhoner and Steinstrater, 1998).

In adults, a smaller auditory response around 50 ms (EEG P1 or P50 and MEG M50) is also often seen. The relevant MEG literature points to STG as the M50 generator (e.g., Pelizzone et al., 1987; Reite et al., 1988; Mäkelä et al., 1994; Yoshiura et al., 1995; Huotilainen et al., 1998; Yvert et al., 2001). Investigators using either intraoperative electrocorticography (Ligeois-Chauvel et al., 1994) or chronic subdural electrodes (Lee et al., 1984) have reported that P50 is a near-field potential in the primary auditory cortex. The supratemporal origin is also supported by the scalp distribution of electrical potentials (Cohen, 1982) and by recordings from the pial surface over temporal and parietal lobes (Chatrian et al., 1960). Although it has been suggested that areas such as hippocampus (Goff, 1978; Waldo et al., 1994; Freedman et al., 1996), midbrain reticular (Erwin and Buchwald, 1986a,b), and midline brain regions (Kraus et al., 1992; Ninomiya et al., 1997) contribute to the scalp-recorded 50 ms response, the contribution from these non-STG sources is likely small. As an example, predicting EEG P50 Cz scalp-recorded activity from bilateral STG sources derived from whole-cortex MEG, Huang et al. (2003) showed that virtually all of the variance in P50 Cz in adult controls (96%) is accounted for by STG sources. In terms of the number of sources that could possibly contribute to EEG P50, the work by Grunwald et al. (2003) is also relevant, as they recorded directly from cortex. Examining 1270 subdural contacts, they did not observe 50 ms activity in the majority of cortical recording sites, concluding that "P50 is not generated in widespread cortical areas."

AUDITORY RESPONSES IN CHILDREN

Auditory responses in children differ from those observed in adults, with P50 more readily evoked in young children, and with P50 (P1) peak latency in children 5–6 years of age ~85–95 ms (Wunderlich and Cone-Wesson, 2006). P50 latency and amplitude decrease as a function of age (e.g., Paetau et al., 1995). Ponton et al. (2002) and Ceponiene et al. (2002) suggest that the attenuation in P50 amplitude as a function of age arises from the phase cancelation of the later parts of the P50 peak by the increasing magnitude of the N100 neural generators. Although less common in young children, when present, N100 appears around 100–150 ms (e.g., Satterfield et al., 1984; Bruneau et al., 1997; Ponton et al., 2000).

In older children, auditory responses become more complex and the components more defined, with an adult morphology typically observed around 10–12 years of age (Ponton et al., 2000), and thus with EEG N100 and MEG M100 auditory responses generally observed by late childhood and early adolescence (Ponton et al., 2000, 2002). There is conflicting evidence as to the effect of age on N100 amplitude. Some studies show that N100 amplitude increases with age (Bruneau et al., 1997; Ponton et al., 2000, 2002), whereas others have found no effect (e.g., Tonnquist-Uhlén, 1996; Ceponiene et al., 2002). Inter-stimulus interval (ISI) may account for study differences – in children, N100 generators require longer intervals to produce a large response given longer refractory periods in children than adults (e.g., Paetau et al., 1995; Rojas et al., 1998). The amplitude of a response occurring after the N100 and with the same general topography, N200, has an amplitude that is constant up to age 11 and then decreases (Ponton et al., 2002).

MISSING AUDITORY RESPONSES IN CHILDREN WITH ASD

In a preliminary report examining the presence or absence of left and right STG M100 responses, using a 1000 ms inter-trial interval, Khan et al. (2010) observed that M100 responses were observed more frequently in TD subjects than children with ASD. In particular, M100 responses were deficient especially in children with concomitant language impairment, and especially in the left-hemisphere. The present study further examined the occurrence of STG M50, M100, and M200, examining left and right STG responses, examining a larger population of TD and ASD children, and examining STG responses at a longer inter-trial interval (average 2,350 ms) to increase the possibility of observing auditory responses in young children. In addition, analyses were expanded to determine whether the "missing" M100 responses were unique to language impairment or were a pattern also observed in children with general intellectual impairments as indicated by lower IQ.

The following hypotheses were made:

1. Reflecting differential development of primary/secondary auditory cortex areas and supporting previous studies (e.g., Rojas et al., 1998; Yoshimura et al., 2012), whereas left and right M50 STG responses would be observed equally often in younger and older children, left and right M100 STG responses would more often be absent in younger than older children.
2. In ASD, delayed neurodevelopment would be indicated via the observation of a greater proportion of ASD than TD subjects showing missing M100 but not M50 responses in both age groups. Missing M100 responses would be observed primarily in children with ASD with language impairment (ASD + LI) (and perhaps concomitantly lower general cognitive abilities).

MATERIALS AND METHODS

SUBJECTS

Diagnoses of ASD were determined prior to recruitment based on the child's performance during clinical interviews, their documentation of DSM-IV criteria for ASD, and results from tests such as the Childhood Autism Rating Scale and the autism diagnostic observation schedule (ADOS). Advertisements through local newspapers and pediatric practices within the Children's Hospital of Philadelphia (CHOP) primary care network were utilized for recruitment of TD controls.

The subjects' first session at CHOP included clinical and diagnostic neuropsychological testing by a licensed child psychologist with expertise in autism (Lisa Blaskey) to ensure that all subjects met the minimum criteria for inclusion and to further confirm diagnoses of ASD, particularly by utilizing the ADOS, Social Responsiveness Scale (SRS), Krug Asperger's Disorder Index (KADI), and Social Communication Questionnaire (SCQ). For confirmation of the ASD diagnosis, all children had to exceed established cut-offs on both the ADOS and SCQ. Subjects one point below cut-off for ADOS scores were permitted entry into the study as long as they exceeded cut-offs on at least two parent questionnaires. In the rare event that diagnosis could not be confirmed via use of the ADOS and parent questionnaires alone, the autism diagnostic interview-revised (ADI-R) was administered to provide final clarification of diagnosis.

For testing language impairment, all subjects were evaluated with the clinical evaluation of language fundamentals – fourth edition (CELF-4). The ASD sample was divided into ASD without language impairment (ASD − LI) and ASD + LI groups. The ASD + LI group included subjects scoring at or below the 16th percentile (SS < 85) on the CELF-4 Core Language Index. All subjects scored at or above the 5th percentile (SS > 75) on the perceptual reasoning index (PRI) of the Wechsler Intelligence Scale for Children-IV (WISC-IV). The WISC-IV verbal comprehension index (VCI) was also obtained.

The total number of subjects included 35 TD and 101 ASD (63 ASD − LI, 38 ASD + LI). Although analyzing data from a different task, the present sample includes several, although not all, of the subjects reported in Roberts et al. (2010) (17 TD and 25 ASD). The study was approved by the CHOP IRB and all participants' families gave written consent.

AUDITORY STIMULI

Stimuli consisted of 1000 and 2000 Hz tones presented using Eprime v1.1. Tones were presented via a sound pressure transducer and sound conduction tubing to the subject's peripheral auditory canal via ear-tip inserts (ER3A, Etymotic Research, IL, USA). Prior to data acquisition, 1000 Hz tones of 300 ms duration and 10 ms rise time were presented binaurally and incrementally until reaching auditory threshold for each ear. Tones were presented at 45 dB sensation level above threshold. Each trial consisted of a 50 ms tone (S_1; randomly presented 1000 and 2000 Hz tones), an 800 ms ISI, a second 50 ms tone (S_2; randomly presented 1000 and 2000 Hz tones), and a 2350 ms (±100) inter-trial interval. A total of 120 tone pairs were presented. The present study reports on S_1 – the auditory response occurring after the long inter-trial interval and thus with the greatest recovery period. To obtain a response with sufficient trials, the S_1 average included 1000 and 2000 Hz tones.

MEG RECORDINGS

Magnetoencephalography data were obtained using a whole-cortex 275-channel system (VSM MedTech Inc., Coquitlam, BC, USA) in a magnetically shielded room. Prior to data acquisition, three head-position indicator coils were attached to the subject's scalp at the nasion, left-, and right-preauricular points, providing continuous specification on head position and orientation in relation to the MEG sensors. A movie (without sound) was displayed to prevent fatigue.

Electrodes were attached to the left and right clavicles for electrocardiogram recordings (ECG) and to the bipolar oblique (upper and lower left sites) for electro-oculogram recordings (EOG). A band-pass filter (0.03–150 Hz) was placed over the EOG, ECG, and MEG signals, which were then digitized at 1200 Hz with third order gradiometer environmental noise reduction over the MEG data.

MEG DATA ANALYSIS

Artifact correction was applied to remove eye-blink and cardiac activity (see Roberts et al., 2010) using BESA 5.2™. Epochs with artifacts other than blinks and heartbeats were rejected on the basis of amplitude and gradient criteria (amplitude >1200 fT/cm, gradients >800 fT/cm/sample). Artifact-free epochs (1000 + 2000 Hz tones) were then averaged according to stimulus type and filtered using a 1 Hz (6 dB/octave, forward) to 40 Hz (48 dB/octave, zero-phase) band-pass. Although group differences in the number of artifact-free trails were observed, $F(2, 133) = 8.82$, $p < 0.001$, the difference between groups in the mean number of trials was small: TD mean of 110 trials (range 83–119) = ASD − LI mean of 107 trials (range 86–119) > ASD + LI mean = 101 trials (range 81–116).

The presence or absence of M50, M100, and M200 responses in the left and right STG was determined by applying a standard source model transforming the raw MEG surface activity into brain space (MEG data co-registered to the Montreal Neurologic Institute averaged brain) using a model with multiple sources (Scherg and Berg, 1996). Specifically, the source model included left and right STG regional sources positioned at Heschl's gyrus and nine fixed regional sources modeling brain background activity and acting as probe sources for additional activity. Each

subject's eye-blink and heartbeat source vectors were included in the individual source models (Berg and Scherg, 1994).

To optimize the orientation of the standard STG sources, the left- and right-hemisphere dipoles were oriented at the maximum of the M100. Presence of a M100 was determined based on amplitude, latency, and hemisphere ingoing and outgoing flux topography (e.g., left-hemisphere ingoing anterior, outgoing posterior, and vice versa for the right-hemisphere). In particular, a M100 was scored if the magnetic flux topography were characteristic of the M100 response, was preceded by M50 (i.e., flux topography opposite M100), and followed by M200 (i.e., flux topography same as M100), and with source strength greater than baseline. In the present study, M50 was operationally defined as the first reversal in magnetic-field topography preceding M100 (or M200 if M100 not present). As reported below, in many subjects, a left- or right-hemisphere M100 response was not observed. For these subjects, left and right STG dipoles were oriented at the maximum of M50. If neither a M50 nor M100 was observed, the dipole was oriented at M200. Identification of auditory responses and orientation of the STG dipoles were done blind to group.

Of the subjects examined, 18 subjects (4 TD, 7 ASD − LI, 7 ASD + LI) did not have observable M50, M100, or M200 responses in the left- or right-hemisphere. Lack of an observable auditory response in these subjects was due to large metal artifact or poor compliance. Data from these subjects was excluded. Examining only the subjects with an identifiable auditory response, goodness-of-fit values (average from the start of M50 to M200) did not differ between the TD and ASD groups [TD = 94% (SD = 2.28), ASD = 93% (SD = 3.00); $p > 0.05$]. Examining all subjects, maximum head motion during the recording was greater in younger than older subjects [young = 1.5 cm (SD = 1.2), older = 0.92 (SD = 0.92), $p < 0.01$].

In subjects with usable data (with either a 50, 100, and 200 ms response and thus with clear evidence that the subject heard the tone), epochs were defined from the continuous recording: 500 ms before the first tone to 500 ms after the first tone. When a M50 or M100 response was observed, left and right M50 (35–120 ms) and M100 (80–185 ms) latency data were calculated from the largest point in the scoring windows using in-house MATLAB software after subtraction of prestimulus baseline activity. Given that in many subjects the M200 was of long duration and without a clear peak, M200 responses were simply scored as present or absent, with M200 defined as a sustained response occurring after the M100 interval (i.e., 80–185 ms) and showing a magnetic-field topography similar to M100.

STATISTICAL ANALYSES

Using IMB SPSS Statistics 20, *t*-tests examined group differences in age, CELF-4 scores, SRS, and IQ scores. For between-subject analyses, chi-square tests examined group differences in the presence or absence of a M50, M100, and M200 response (where an individual cell count was five or less, the Fisher Exact Test was used). For within-subject analyses, McNemar tests were used (McNemar, 1947). For analyses examining age differences, a median split separated subjects into younger (6–10 years old) and older (11–15 years old) groups. Finally, to examine if any ASD − LI versus ASD + LI missing M100 findings were specific to language impairment, using the PRI scores, the ASD group was also divided into a low and high IQ group (median split) and analyses re-run.

In the subset of subjects with a M50 or M100 response, repeated measures ANOVA examined group (TD, ASD − LI, ASD + LI), hemisphere, and group × hemisphere differences in latency. To examine how M50 and M100 latency differs as a function of group and age, hierarchical regression was run entering age first, diagnosis second, and their interaction last, with M50 or M100 latency as the dependent variable.

RESULTS

As shown in **Table 1**, groups did not differ in age. As expected, TD and ASD − LI subjects had significantly higher VCI and CELF-4 core language index scores than the ASD + LI subjects. As shown in **Table 1**, individuals with ASD − LI had higher PRI scores than individuals with ASD + LI.

M50

Collapsing across group and hemisphere, M50 responses were observed equally often in older (88.3%) and younger subjects (92.6%; $p = 0.27$). Collapsing across group and age, the presence or absence of M50 differed between the right (85.4%) and left-hemisphere (94.2%; McNemar $p = 0.02$). Given a significant difference between hemisphere but not age, simple effect analyses examined group differences for each hemisphere, collapsing across age group.

In the left-hemisphere, collapsing across age, no differences were observed between TD (91.7%) and ASD + LI (92.1%; Fisher $p = 1.0$), TD (91.7%) and ASD − LI (96.8%; Fisher $p = 0.35$), or ASD − LI (96.8%) and ASD + LI (92.1%; Fisher $p = 0.36$). In the right-hemisphere, collapsing across age, no differences were observed between TD (88.9%) and ASD + LI (81.6%; Fisher $p = 0.52$), TD (88.9%) and ASD − LI (85.7%; Fisher $p = 0.76$), or ASD − LI (85.7%) and ASD + LI (81.6%; $p = 0.58$). Splitting at the median head motion value, within each diagnostic age group, chi-square analyses showed that the presence or absence of M50 did not differ between individuals with more versus less head motion.

Table 2 (left column) shows the likelihood of observing a M50 for each group as a function of hemisphere. The Supplementary Material shows the likelihood of observing a M50 response in each group at each age.

M100

Collapsing across group and hemisphere, M100 responses were observed more often in older (89.4%) than younger subjects (77.5%; $p = 0.02$). Collapsing across group and age, the presence or absence of M100 did not differ between the right (85%) and left-hemisphere (77.9%; McNemar $p = 0.11$). Given a significant difference between age groups but no hemisphere difference, simple effect analyses examined group differences for each age group collapsing across hemisphere.

In younger subjects, collapsing across hemisphere, M100 responses were observed more often in TD (90%) than ASD + LI (66%; Fisher $p = 0.04$). No differences were observed between TD (90%) versus ASD − LI (76%; Fisher $p = 0.14$) or between ASD − LI (76%) and ASD + LI (66%; $p = 0.53$). In older subjects, collapsing across hemisphere, whereas no differences were

Table 1 | Age, language, and cognitive information for each group (means and SD), (a) comparing younger TD to ASD (total sample), (b) comparing older TD to ASD (total sample), (c) comparing younger ASD − LI to ASD + LI, (d) comparing older ASD − LI to ASD + LI.

Groups	Mean	SD	Mean	SD	Groups	Mean	SD	Mean	SD
(a) Younger	**TD ($N = 20$)**		**ASD ($N = 79$)**		**(b) Older**	**TD ($N = 16$)**		**ASD ($N = 34$)**	
Age	8.79	1.52	8.53	1.22	Age	13.46	1.58	13.07	1.33
PRI	108.95	15.5	104.37	16.98	PRI	108.75	12.94	102.88	14.94
VCI**	109.35	14.91	96.43	18.18	VCI	104	12.65	98.88	16.84
CELF**	109.36	12.41	86	21.74	CELF**	108.88	9.28	90.69	19.16
Groups	**Mean**	**SD**	**Mean**	**SD**	**Groups**	**Mean**	**SD**	**Mean**	**SD**
(c) Younger	**ASD − LI ($N = 45$)**		**ASD + LI ($N = 34$)**		**(d) Older**	**ASD − LI ($N = 23$)**		**ASD + LI ($N = 11$)**	
Age	8.74	1.25	8.26	1.15	Age	13.23	1.32	12.73	1.34
PRI**	110.84	16.09	95.79	14.26	PRI**	109.26	11.29	89.55	12.93
VCI**	107.69	11.19	81.53	14.59	VCI**	107.7	11.87	80.45	8.58
CELF**	101.26	10.87	65.35	14.37	CELF**	101.38	10.89	67.36	10.1

$^{**}p < 0.01$.

As noted in the Section "Materials and Methods," a median split separated subjects into younger (6–10 years old) and older (11–15 years old) groups.

Table 2 | Likelihood of observing a M50, M100, and M200 for each group as a function of age (young, older) for the left-hemisphere (left), right-hemisphere (right), and the average of the left- and right-hemisphere (average).

	N	M50			M100			M200		
		Left (%)	**Right (%)**	**Average (%)**	**Left (%)**	**Right (%)**	**Average (%)**	**Left (%)**	**Right (%)**	**Average (%)**
TD										
Young	20	84.2	94.7	89.5	90	95	92.5	100	100	100
Old	16	81.3	100.0	90.6	93.75	81.25	87.5	93.75	93.75	93.75
ASD − LI										
Young	42	73.8[a]	78.6	76.2[a]	95.24	78.57[a]	86.9[a]	100	95.24	97.6
Old	21	95.2[a]	95.2	95.2[a]	100	100[a]	100[a]	100	100	100
ASD + LI										
Young	28	60.7	75.0	66.1	96.43	78.57	87.5	100	96.48	98.2
Old	10	70.0	80.0	75.0	80	90	85	80	90	85

For M50, Fisher exact tests showed an effect of age only in ASD − LI (average young = 76.2%, older = 95.2%; Fischer $p = 0.01$).

[a]For M100, although a main effect of group was observed, Fisher tests showed an effect of age only in ASD − LI (average young = 86.9%, older = 100%, $p = 0.02$). For M200, Fisher exact tests showed a significant effect of age in ASD + LI (average young = 98.2%, older = 85%, $p = 0.05$).

observed between TD (91%) and ASD + LI (75%; Fisher $p = 0.24$), or between TD (91%) and ASD − LI (95%; Fisher $p = 0.64$), M100 responses were observed more often in ASD − LI (95%) than ASD + LI (75%; Fisher $p = 0.03$). Given similar differences in the presence/absence of M100 between TD versus ASD + LI and ASD − LI versus ASD + LI, the non-significant TD versus ASD + LI finding is likely due to a smaller *N* in the TD group. Splitting at the median head motion value, within each diagnostic age group, chi-square analyses showed that the presence or absence of M100 did not differ between individuals with more versus less head motion.

To assess if any of the missing M100 findings were specific to language impairment, the above analyses were re-run dividing the children with ASD into low and high PRI groups (median split). In younger subjects, collapsing across hemisphere, M100 responses were observed equally often in TD (88%) and PRI-high (78.2%; Fisher $p = 0.29$). Marginally significant differences were observed between TD (88%) versus PRI-low (70%; Fisher $p = 0.07$). No differences were observed between PRI-high (78.2%) and PRI-low (70%; $p = 0.33$). In older subjects, collapsing across hemisphere, no differences were observed between TD (91%) and PRI-high (91.3%; Fisher $p = 1.0$), between TD (91%) and PRI-low (86.4%; Fisher $p = 0.70$), or between PRI-high (91.3%) and PRI-low (86.4%; Fisher $p = 0.69$). Although not exactly the same, findings splitting children with ASD into low and high PRI groups were similar to findings splitting children with ASD into low and high CELF-4 groups. This is likely due to the fact that group membership remained largely unchanged. In particular, of the 25

ASD + LI subjects, 19 were in the lower half and 6 in the upper half of the PRI group, and of the 48 ASD − LI subjects, 9 were in the lower half and 39 in the upper half of PRI group.

Table 2 (middle column) shows the likelihood of observing a M100 for each group as a function of age (although when collapsing across group Fisher analyses showed a main effect of age, analyses show that at the group level a significant age differences was present only in ASD − LI). The Supplementary Material shows the likelihood of observing a M100 response in each group at each age.

M200

Collapsing across group and hemisphere, M200 responses were observed equally often in older (94.7%) and younger subjects (98.3%; Fisher $p = 0.13$). Collapsing across group and age, the presence or absence of M200 did not differ between the right (96.4%) and left-hemisphere (97.8%; McNemar $p = 0.69$). Given no significant differences between age or hemisphere, simple effect analyses examined group differences for each group collapsing across age and hemisphere.

No differences were observed between TD (97.2%) and ASD + LI (94.7%; Fisher $p = 0.68$), TD (97.2%) and ASD − LI (98.4%; Fisher $p = 0.62$), or ASD − LI (98.4%) and ASD + LI (94.7%; Fisher $p = 0.20$).

Table 2 (right column) shows the likelihood of observing a M200 for each group as a function of age. The Supplementary Material shows the likelihood of observing a M200 response in each group at each age.

M50 AND M100 LATENCY, HEMISPHERE, AND GROUP

ANOVAs examined hemisphere and group latency differences in the subjects with a M50 and M100 response. For M50, simple effect analyses of a main effect of group, $F(2, 107) = 4.59$, $p = 0.01$, showed marginally earlier responses in TD (67 ms) versus ASD − LI (74 ms; $p = 0.08$) and significantly earlier responses in TD versus ASD + LI (77 ms; $p = 0.01$). The ASD groups did not differ ($p = 0.74$). The main effect of hemisphere, $F(1, 107) = 0.11$, $p = 0.74$, and the hemisphere by group interaction, $F(2, 107) = 1.41$, $p = 0.25$, were not significant. Findings were unchanged re-running analyses with age as a covariate. The pattern of findings was unchanged splitting the ASD group based on PRI, with the earliest M50 latencies in TD, second earliest in the PRI-high group, and the longest in the PRI-low group (PRI-low and PRI-high groups did not differ).

For M100, a main effect of hemisphere, $F(1, 92) = 14.03$, $p < 0.001$, showed earlier responses in the right (119 ms) than left (126 ms). There was no main effect of group, $F(2, 92) = 1.42$, $p = 0.24$. Although the interaction term was not significant, given the right-hemisphere TD versus ASD group latency findings in Roberts et al. (2010), *post hoc* analyses separately examined the left- and right-hemisphere. As expected, although group M100 latency differences were not observed in the left-hemisphere, $F(1, 103) = 1.06$, $p = 0.31$, a significant group M100 latency difference observed in the right-hemisphere, $F(1, 92) = 4.87$, $p = 0.03$, indicated earlier M100 latencies in TD (112 ms, SD 18.61) versus ASD (121 ms, SD 19.34). Findings were unchanged re-running analyses with age as a covariate. Analyses also showed M100 right-hemisphere latency differences between TD and the combined PRI group and no right-hemisphere M100 latency differences between ASD PRI-low and PRI-high.

Table 3 shows M50 and M100 latency mean and standard deviation values for each group and hemisphere.

Table 3 | Latency values in subjects with an observed M50 or M100.

	N M50	M50 latency (ms) and SD	*N* M100	M100 latency (ms) and SD
CONTROLS				
Left STG	33	67 (15)[a]	29	122 (27)
Right STG	32	66 (15)[a]	34	114 (22)[+]
ASD − LI				
Left STG	61	76 (18)	51	121 (27)
Right STG	54	72 (15)	53	121 (21)
ASD + LI				
Left STG	35	76 (17)	26	131 (25)
Right STG	31	79 (19)	29	121 (19)

[a] *For M50, a main effect of group indicated earlier responses in TD versus ASD − LI and TD versus ASD + LI ($p = 0.01$). The ASD groups did not differ.*

[+] *Comparing TD to the combined ASD group, significant right-hemisphere M100 group differences were observed ($p = 0.03$).*

M50 AND M100 LATENCY AND AGE

For each hemisphere, to examine how M50 and M100 latency differs as a function of group and age, hierarchical regressions were run in which age was entered first, diagnosis second, and their interaction last, with M50 or M100 latency as the dependent variable. For M50, in both hemispheres the full regression model (age, group, interaction) accounted for considerable variance in M50 latency (left = 18%; right = 18%, p's < 0.001). Added first, age accounted for a significant 16% variance in left M50 latency ($p < 0.001$) and a significant 11% variance in right M50 latency ($p < 0.001$). Added second, group added a marginally significant 2% variance in left M50 latency ($p = 0.06$) and a significant 4% variance in right M50 latency ($p < 0.05$). The group × age interaction was not significant in either hemisphere (percent of variance <1%, ns). **Figure 1** scatter plots show associations between age and left and right STG M50 latency (upper row).

For M100, in both hemispheres, the full regression model (age, group, interaction) accounted for considerable variance in M100 latency (left = 29%; right = 29%, p's < 0.001). Added first, age accounted for a significant 28% variance in left M100 latency ($p < 0.001$) and a significant 25% variance in right M100 latency ($p < 0.001$). Added second, group added a non-significant 1% variance in left M100 latency ($p > 0.05$) and a marginally significant 3% variance in right M100 latency ($p = 0.07$). The group × age interaction was not significant in either hemisphere (percent of variance < 1%, ns). **Figure 1** scatter plots show associations between age and left and right STG M100 latency (bottom row).

Given greater head motion in younger than older individuals, analyses were re-run using max head motion determined over the course of the scan as a covariate. Findings remained unchanged for all analyses.

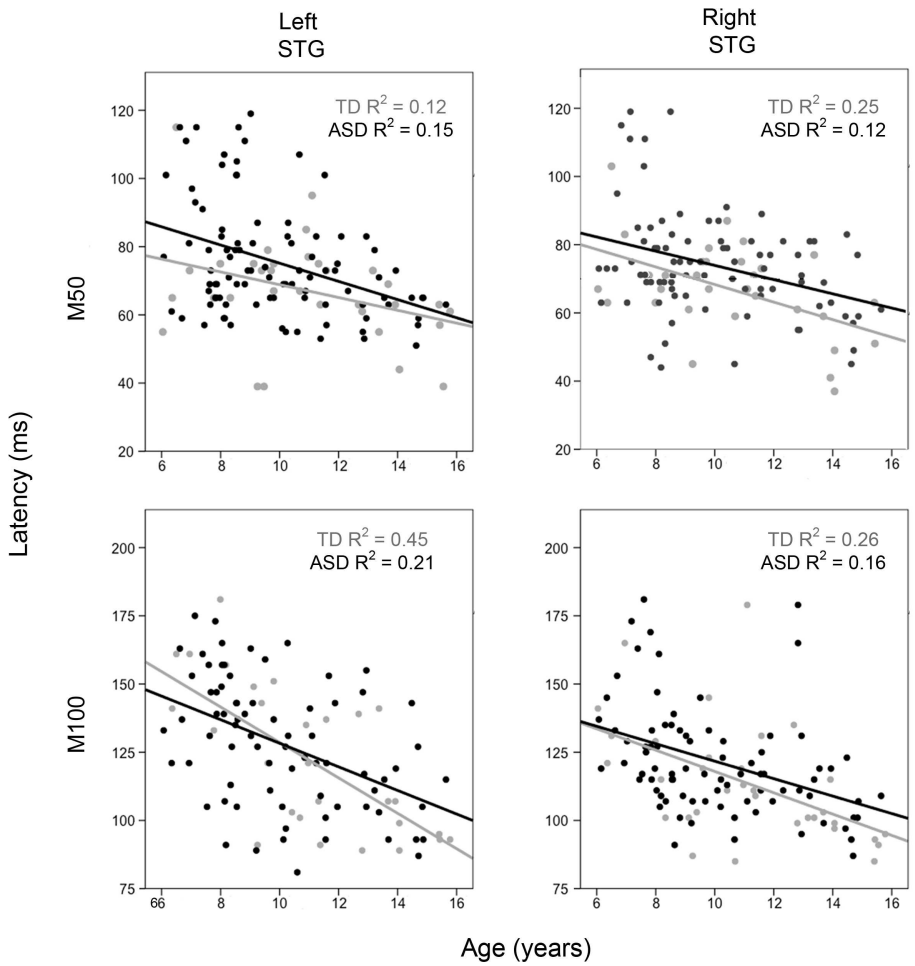

FIGURE 1 | Scatter plots showing associations between age and left and right M50 latency (upper row) and M100 latency (bottom row). Associations are shown for TD (light gray) and ASD (black). The *x* axis shows age and the *y* axis latency.

M50 AND M100 LATENCY AND CLINICAL MEASURES

Regression analyses with PRI or CELF-4 scores entered first, diagnosis second, and their interaction last, with M50 or M100 latency as the dependent variable, showed no associations between the two clinical measures and M50 or M100 latency scores.

SOURCE TIME COURSES

Grand average left and right STG source waveforms are shown for ASD (**Figure 2**) and TD (**Figure 3**) as a function of age. Given a smaller *N* in the TD group (and thus fewer subjects at a specific age), whereas grand average waveforms are shown for each ASD by year age group, grand averages were computed in 2-year steps for TD.

Examination of the left (solid line) and right (dotted line) waveforms in the TD groups shows even in the youngest TD subjects a distinct left and right STG M100 (also indicated in the above chi-square and Fisher analyses). Examination of the ASD − LI and TD plots shows that the left STG M100 appears later in time (i.e., close to the M200 in younger subjects), and only develops into a clearly distinct component in older subjects. For example, only in the 14- to 15-year-old TD group is the left M100 peak clearly distinct from M200. This is in contrast to the right M100, where even in the 6- to 7-year-old TD group, M100 is distinct from M200. With regard to hemisphere differences, the source waveforms suggest that only in the oldest ASD − LI and TD subjects is there, on average, similarity in latencies between the two hemispheres.

DISCUSSION

M50 AND M100 ABNORMALITIES IN ASD

Atypical auditory responses were observed in ASD. First, although STG M50 responses were observed in almost all subjects (replicating Ponton et al., 2002), M50 left and right responses were delayed by ~8 ms in ASD versus TD. Second, M100 responses were observed less often in ASD than TD; whereas a M100 response was observed in most younger and older TD controls, a M100 was missing in ~30% of the young and old ASD + LI subjects. Finally and perhaps unexpectedly, a significant age-dependent change in the presence of M100 was observed only in the ASD − LI subjects. As generally analogous findings were observed when dividing the

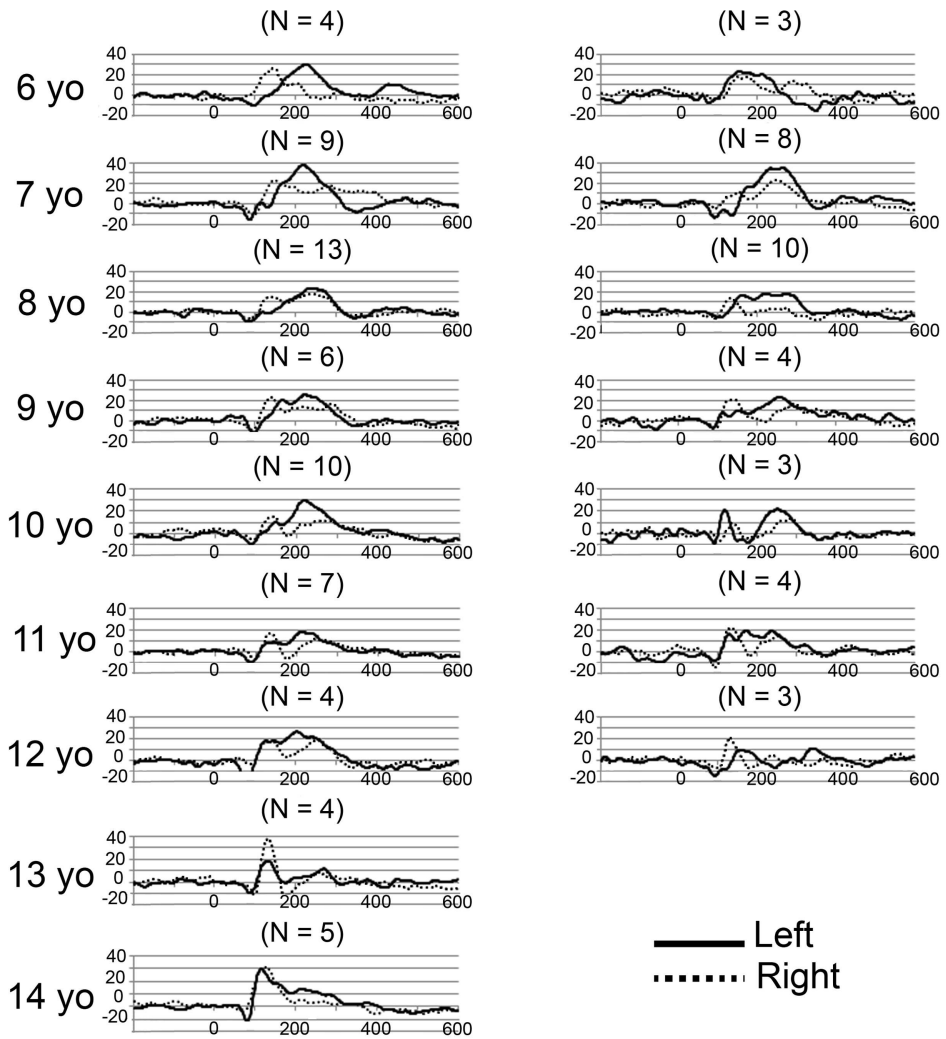

FIGURE 2 | Grand average left (solid) and right (dotted) STG source waveforms are shown for ASD as a function of age. The *x* axis shows time and the *y* axis source strength. Given the small numbers in many of the age groups, grand average waveforms without standard errors are plotted to show general trends in each age group.

ASD group by IQ, present findings cannot be uniquely interpreted as specific to language impairment and may instead be associated with general cognitive impairment.

In the present study, M50 responses were delayed bilaterally in children with ASD. This is in contrast to Roberts et al. (2010), where no M50 latency group differences were observed. Examination of **Table 2** in Roberts et al. (2010), however, does show non-significantly later M50 latencies in the ASD than TD group for most frequencies. The difference between the previous and present findings is likely due to differences in the tasks (with a longer inter-trial interval in the present study) as well as greater power in the present study, with a twofold increase in TD subjects (17 versus 35) and a fourfold increase in ASD subjects (25 versus 101).

Other studies using similar paradigms (i.e., an auditory task with a long inter-trial interval), however, have reported different group latency findings. Using a paired-click paradigm and examining P50 responses at electrode Cz, Orekhova et al. (2008) observed a main effect (i.e., collapsing across the first and second click) of earlier P50 latencies in children with ASD versus TD (3- to 8-year-olds). Examination of **Table 1** in Orekhova et al. indicates that the group P50 latency differences were most evident for the second click, with this perhaps accounting, in part, for study differences. Another difference is that whereas in the present study a high-pass filter of 1 Hz was applied, Orekhova et al. applied a 10 Hz high-pass filter. Kanno et al. (2000) and Yvert et al. (2001) have noted problems using a 10 Hz high-pass filter, showing in their studies that high-pass filters above 3 Hz produce artificial peaks in

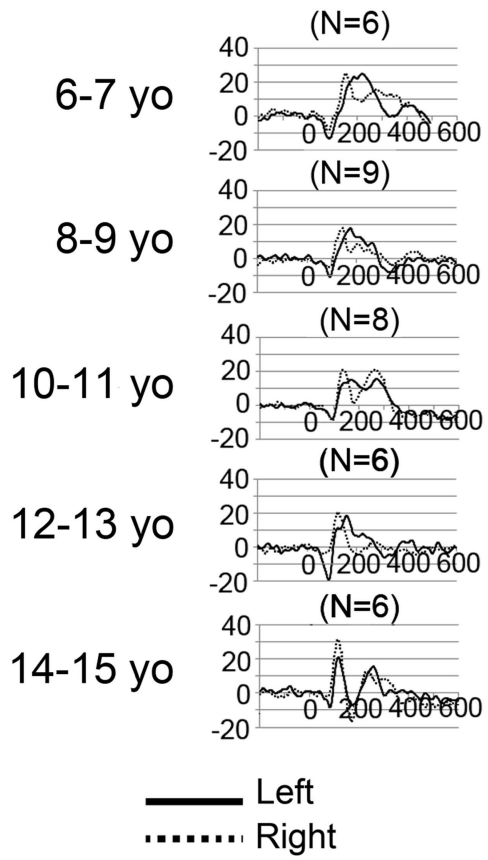

FIGURE 3 | Grand average left (solid) and right (dotted) STG source waveforms are shown for TD as a function of age. The *x* axis shows time and the *y* axis source strength. Given the small numbers in many of the age groups, grand average waveforms without standard errors are plotted to show general trends in each age group.

the P50 auditory response as well as distort the P50 electrical field topography. Finally, also using a paired-click task and examining P50 activity at electrode Cz, Oranje et al. (2013) observed non-significantly earlier P50 latencies in ASD versus TD (see **Table 3**). Given the above, additional studies are needed to replicate the present M50 group latency findings. In future studies, however, it is important to examine P50 activity in source rather than scalp space. As detailed in Edgar et al. (2003), given hemisphere differences in the strength, orientation, and latency of the left and right P50 auditory responses it is often not clear how to interpret findings associated with the multi-determined EEG Cz response (e.g., a response reflecting activity from, at least, left and right STG).

Whereas a delayed M50 could be considered a risk factor for ASD, present findings suggest that a missing M100 in younger children with ASD is a risk factor for language impairment, and in older ASD children a missing M100 is a marker for ASD with concomitant language impairment. It is important to note, however, that in addition to lower CELF-4 scores, the ASD + LI group also had lower PRI scores (a non-verbal IQ measure that minimizes emphasis on verbal skills) than the TD and ASD − LI groups. Thus, lower cognitive ability rather than language impairment likely account for the present findings and thus the hypothesis that language impairment would best predict missing M100 responses was not supported. Finally, *post hoc* analyses examining only the right-hemisphere showed significant right-hemisphere M100 latency delays in ASD + LI and ASD − LI versus TD (see **Table 3**). Thus, as in Roberts et al. (2010), present findings suggest that a delayed right-hemisphere M100 is common to ASD with and without language impairment.

The above M50 and M100 abnormalities in ASD may reflect distinct auditory cortex abnormalities. Development of deep layers (lower layer III to layer VI) in auditory cortex occurs between 6 months and 5 years of age (e.g., Ponton et al., 1999). In contrast, the superficial layers (upper layer III and layer II) continue to mature until about age 12 (Moore and Guan, 2001; Moore and Linthicum, 2007). Based on this, these researchers have hypothesized that the 50 ms auditory response reflects recurrent activation in layers III and IV, the termination zone of thalamo-cortical pathways that are almost fully developed in by age 6. M100, however, is observed less frequently in young children as generation of M100 likely reflects activation of cortical layers upper III and II, areas not fully developed until age 12 (e.g., Ponton et al., 1999, 2002; Ponton and Eggermont, 2001).

In the present study, observation of a M50 response in all groups likely reflects development of cortical layers III and IV, with the delayed M50 latency in both ASD groups perhaps indicating slower maturation of these layers, perhaps due to delayed myelination of thalamo-cortical pathways in ASD (Roberts et al., 2009, 2013). Lack of a M100 in the young ASD − LI and ASD + LI groups may indicate delayed maturation of layer II and upper layer III in ASD with abnormally decreased synchronization of afferent activity arriving at the synapses in layer II and upper layer III resulting in a greatly desynchronized M100 (Ponton and Eggermont, 2001). Whereas the finding of a missing M100 in younger but not older ASD − LI suggests delayed but continued maturation of layer II and upper layer III in ASD − LI, the lack of M100 in some older ASD + LI subjects indicates a more profound disruption of secondary auditory cortex areas in these subjects, perhaps never developing a fully functional set of superficial layer axons.

It may be, however, that M50 latency delays in ASD solely reflect M100 abnormalities. As reviewed in the Section "Introduction," Ponton et al. (2002) noted that during development, the magnitude of the earlier maturing tangential "50 ms" auditory response decreases as the magnitude of the later maturing tangential "100 ms" auditory response increases. Given this pattern, in the present study, whereas in the TD group a normally developing M100 responses could result in an earlier M50 response via "cancelation" of M50 activity via a increasingly dominant M100 response, in ASD a missing or abnormally developing M100 response could result in less "cancelation" of the M50 response and thus longer M50 latencies (even in the absence of abnormalities in layers III and IV). Longitudinal rather than cross-sectional studies are needed to understand the development of P50/M50 and N100/M100 auditory responses in order to better understand the present findings.

In any case, as described in Moore and Guan (2001), disruption in the development of STG auditory areas between the ages of 5 and 12 would lead to a failure to develop a meshwork of vertical and horizontal axons in the superficial layers, with axons in the superficial layer representing primarily (though not exclusively) corticocortical projections. Such disruptions could account for temporal lobe resting state abnormalities (Cornew et al., 2012) as well as the STG abnormalities observed in the present study. Given the possibility of a cascading effect, with early abnormalities increasingly distorting (or not allowing) normal development of upper cortical layers in some individuals with ASD, similar to the recommendations suggested for children with hearing impairments (e.g., Kral and Eggermont, 2007; Moore and Linthicum, 2007), present findings indicate the need for early treatment in ASD to increase the chance of normal development of auditory areas throughout childhood and adolescence.

M50 AND M100 LATENCY ASSOCIATIONS WITH AGE

Replicating previous studies (see Introduction), M50 and M100 latency decreased as a function of age. Present findings are also consistent with previous studies showing that the M100 develops "out of" the M200 response (Ponton et al., 1999, 2002), with present findings also indicating that the development of M100 as a component distinct from M200 occurs more slowly in the left-hemisphere. Studies examining hemisphere differences in even younger subjects are of interest to more fully understand the development of M100.

Although as noted in the Section "Introduction," there is strong evidence for a decrease in P50 latency as a function of age, using a paired-click paradigm similar to the paradigm used in the present study, age-related P50 latency findings using this paradigm have been mixed. Using the standard auditory paired-click paradigm (i.e., 500 ms ISI) and examining individuals from 1 to 65 years, Freedman et al. (1987) observed a negative correlation between Cz P50 latency and age for the entire population, with a rapid change in latency observed in children aged 1–8 years. Myles-Worsley et al. (1996) also observed earlier P50 latencies in a younger (10–14 years) versus older groups (15–19, 20–29, and 30–39 years). However, also using the standard paired-click paradigm and examining children, Rasco et al. (2000), Marshall et al. (2004), and Brinkman and Stauder (2007) did not observe associations between P50 latency and age. Similar to the previously noted ASD P50 Cz studies, a lack of an age-related P50 latency findings in Cz paired-click studies may be due to the examination of the multi-determined scalp P50 response (left and right STG activity) as well as in some of these studies the potentially problematic use of a 10 Hz high-pass filter to examine P50.

LIMITATIONS AND FUTURE DIRECTIONS

A potential limitation of the present study is that although the orientation of the STG dipoles was optimized for each subject, the STG dipoles were placed at standard locations rather than localized for each subject. This was necessary in the present study as M50 and/or M100 responses were not observed in some subjects; thus use of a standard source model allowed assessment of the primary question in the present study – determining the presence or absence of a left or right M50 and M100 STG response in children and adolescents with ASD.

As shown via examples in the Supplementary Material, although the estimated strength of the M50 and M100 response in some subjects could be inaccurate when using a standard source model, it is not likely that the latency estimate is inaccurate. In addition, present findings also show that in younger subjects M100 overlaps with M200. As such, whereas in young subjects localization of M100 would primarily reflect M200 generators, in older subjects M100 would reflect only M100 generators. Thus, in the present study, use of a standard model was not only necessary but also sufficient to examine the study questions.

Further considering the use of a standard model, present findings demonstrate a dilemma in this area of research: when examining M100 activity in individuals younger than ~13 years old, it is probably not possible to empirically determine whether localization of M100 in each subject provides more accurate information than the information provided by a standard source model (given the overlap between M100 and M200). Present findings also clearly indicate that developmental studies examining N100 activity at a single midline scalp site (e.g., Cz or Fz) are problematic as latency and amplitude measures at a single site in any individual could reflect activity from only a single hemisphere or, more likely, from some *a priori* unknown combination of M100 and M200 activity from each hemisphere. Indeed, Ponton et al. (2002) and Sussman et al. (2008) note that examining sensor data is problematic as the activity at any given sensor location reflects the weighted contribution of activity from different sources, each with potentially different maturation rates. Present findings suggest, however, that in older ASD − LI and TD subjects a single electrode EEG measure could be sufficient, as **Figures 2** and **3** suggest greater similarity in the left and right waveforms in these older subjects [although see Edgar et al. (2003) for a more detailed discussion of these issues].

It is possible that present findings could be improved via co-registering each subject to their own MRI and then using anatomical constraints (e.g., identifying each individuals left and right Heschl's gyrus) to place dipoles, a strategy that will be examined in future studies. Although possible in older children, as it is often not possible to obtain structural MR data in infants and young children, for some studies it will still be necessary to apply techniques to align MEG data to template MRIs. In future studies examining younger children, the use of whole-brain infant and young child MEG systems will be preferred, with a smaller helmet size providing optimal signal-to-noise in younger children (Roberts et al., 2014).

Other limitations are of note. First, although MEG provides excellent assessment of auditory activity on the surface of STG (i.e., tangential auditory activity), MEG does not easily detect radial sources. As such, studies using EEG (or simultaneous EEG + MEG) are needed to examine radially oriented STG auditory sources (e.g., see Ponton et al., 2002; Stroganova et al., 2013). Second, studies examining auditory responses in ASD using non-passive tasks are needed to assess the generalizability of the present findings. Third, in the present study, in some subjects, it was difficult to identify the M100 response with 100% certainty, especially in younger subjects where M100 just emerges from M200. As an example, as shown in **Figure 3** (TD subjects), the right STG grand

average waveforms (solid black) for the 6- and 7-year-olds show what could be a single M200 response, or a M200 preceded by a M100. In contrast, in **Figure 3**, the right STG grand average waveforms for the 10- and 11-year-olds show what is very clearly identified as a M100 followed by a M200. The source waveforms show that in young subjects it is intrinsically difficult to determine whether M100 is truly distinct from M200. Thus, in young ASD subjects, "follow-up" exams may be needed to monitor the development (or lack of development) of an M100 response. In the present study, M100 was scored as present if there was a peak with a rising and falling slope distinct from the M200, with a M100 magnetic-field topography, and with a latency between 80 and 185 ms. In the present study, in the few cases of ambiguous M100 determination, the final dichotomous assignment was determined by consensus review.

Finally, present findings as well as other studies indicate the need for longitudinal studies to more fully understand the development of auditory responses. For example, it has been reported that in some subjects, two M50 responses are observed. For example, using source modeling to examine left and right STG activity in children aged 7- to 16-years-old, Orekhova et al. (2013) observed in many subjects two components preceding the M100 response; a relatively low-amplitude response at ~65 ms (observed in ~50% of the subjects in the left-hemisphere and 75% of the subjects in the right-hemisphere) and a much more prominent later response with a M50 topography at ~100 ms. In the present study, M50 was defined as the first field reversal preceding M100 (or M200 if M100 not present). Although in the present study examination of the M50 latencies did not reveal a bi-modal distribution, additional longitudinal studies are needed to more fully examine the development of P50/M50 response(s).

CONCLUSION

Although almost all TD and ASD subjects had a M50 response, M50 responses were delayed in ASD than TD bilaterally. Although M100 latencies were longer in the left- than right-hemisphere in TD, this delay was not so pronounced such that even young TD subjects had an identifiable left and right M100 by 6 years of age. Whereas there was a significant increase in the presence of M100 responses in the older than younger ASD − LI group, many individuals in the older ASD + LI group had a missing M100. Examining the TD data, present findings indicate that by 11 years, a right M100 should be observed in 100% of subjects and a left M100 in 80% of subjects. Thus, by 11 years old, if a long inter-trial interval is used, lack of a left and especially right M100 offers neurobiological insight into abnormal sensory processing that may underlie language or cognitive impairment in ASD.

ACKNOWLEDGMENTS

This study was supported in part by NIH grant R01DC008871 (Timothy P. L. Roberts), NIH grant R01DC008871-02S1, a NIH grant K08 MH085100 (J. Christopher Edgar), Award number P30HD026979 from the Eunice Kennedy Shriver National Institute of Child Health and Human Development of the NIH, and grants from the Nancy Lurie Marks Family Foundation (NLMFF) and Autism Speaks. This research has been funded (in part) by a grant from the Pennsylvania Department of Health. The Pennsylvania Department of Health specifically disclaims responsibility for any analyses, interpretations, or conclusions. Dr. Roberts gratefully acknowledges the Oberkircher Family for the Oberkircher Family Chair in Pediatric Radiology at CHOP.

SUPPLEMENTARY MATERIAL

The Supplementary Material for this article can be found online at http://www.frontiersin.org/Journal/10.3389/fnhum.2014.00417/abstract

REFERENCES

Berg, P., and Scherg, M. (1994). A multiple source approach to the correction of eye artifacts. *Electroencephalogr. Clin. Neurophysiol.* 90, 229–241. doi:10.1016/0013-4694(94)90094-9

Brinkman, M. J. R., and Stauder, J. E. A. (2007). Development and gender in the P50 paradigm. *Clin. Neurophysiol.* 118, 1517–1524. doi:10.1016/j.clinph.2007.04.002

Bruneau, N., Roux, S., Guérin, P., Barthélémy, C., and Lelord, G. (1997). Temporal prominence of auditory evoked potentials (N1 wave) in 4-8-year-old children. *Psychophysiology* 34, 32–38. doi:10.1111/j.1469-8986.1997.tb02413.x

Ceponiene, R., Rinne, T., and Näätänen, R. (2002). Maturation of cortical sound processing as indexed by event-related potentials. *Clin. Neurophysiol.* 113, 870–882. doi:10.1016/S1388-2457(02)00078-0

Chatrian, G. E., Petersen, M. C., and Lazarte, J. A. (1960). Responses to clicks from the human brain: some depth electrographic observations. *Electroencephalogr. Clin. Neurophysiol.* 12, 479–489. doi:10.1016/0013-4694(60)90024-9

Cohen, M. M. (1982). Coronal topography of the middle latency auditory evoked potentials (MLAEPs) in man. *Electroencephalogr. Clin. Neurophysiol.* 53, 231–236. doi:10.1016/0013-4694(82)90028-1

Cornew, L., Roberts, T. P. L., Blaskey, L., and Edgar, J. C. (2012). Resting-state oscillatory abnormalities in autism spectrum disorders. *J. Autism Dev. Disord.* 42, 1884–1894. doi:10.1007/s10803-011-1431-6

Edgar, J. C., Huang, M. X., Weisend, M. P., Sherwood, A., Miller, G. A., Adler, L. E., et al. (2003). Interpreting abnormality: an EEG and MEG study of P50 and the auditory paired-stimulus paradigm. *Biol. Psychol.* 65, 1–20. doi:10.1016/S0301-0511(03)00094-2

Edgar, J. C., Khan, S. Y., Blaskey, L., Chow, V. Y., Rey, M., Gaetz, W., et al. (2013). Neuromagnetic oscillations predict evoked-response latency delays and core language deficits in autism spectrum disorders. *J. Autism Dev. Disord.* doi:10.1007/s10803-013-1904-x

Erwin, R., and Buchwald, J. S. (1986a). Mid latency auditory evoked responses: differential effects of sleep in the human. *Electroencephalogr. Clin. Neurophysiol.* 65, 383–392. doi:10.1016/0168-5597(86)90017-1

Erwin, R. J., and Buchwald, J. S. (1986b). Midlatency auditory evoked responses: differential recovery cycle characteristics. *Electroencephalogr. Clin. Neurophysiol.* 64, 417–423. doi:10.1016/0013-4694(86)90075-1

Freedman, R., Adler, L. E., Myles-Worsley, M., Nagamoto, H. T., Mille, C., Kisley, M., et al. (1996). Inhibitory gating of an evoked response to repeated auditory stimuli in schizophrenic and normal subjects: human recordings, computer simulation, and an animal model. *Arch. Gen. Psychiatry* 53, 1114–1121. doi:10.1001/archpsyc.1996.01830120052009

Freedman, R., Adler, L. E., and Waldo, M. (1987). Gating of the auditory evoked potential in children and adults. *Psychophysiology* 24, 223–227. doi:10.1111/j.1469-8986.1987.tb00282.x

Goff, W. R. (1978). "The scalp distribution of auditory evoked potentials," in *Evoked Electrical Activity in the Auditory Nervous System*, eds R. F. Naunton and C. Fernandez (New York, NY: Academic Press), 505–524.

Grunwald, T., Boutros, N. N., Perzer, N., von Oertzen, J., Fernandex, G., Schaller, C., et al. (2003). Neuronal substrates of sensory gating within the human brain. *Biol. Psychiatry* 53, 511–519. doi:10.1016/S0006-3223(02)01673-6

Hari, R. (1990). "The neuromagnetic method in the study of the human auditory cortex," in *Auditory Evoked Magnetic Fields and Potentials. Advances in Audiology*, Vol. 6, eds F. Grandori, M. Hoke, and G. Romani (Basel: Karger), 222–282.

Huang, M. X., Edgar, J. C., Thoma, R. J., Hanlon, F. M., Moses, S. N., Lee, R. R., et al. (2003). Predicting EEG responses using MEG sources in superior temporal gyrus reveals source asynchrony in patients with schizophrenia. *Clin. Neurophysiol.* 114, 835–850. doi:10.1016/S1388-2457(03)00041-5

Huotilainen, M., Winkler, I., Alho, K., Escera, C., Virtanen, J., Ilmoniemi, R. J., et al. (1998). Combined mapping of human auditory EEG and MEG

responses. *Electroencephalogr. Clin. Neurophysiol.* 108, 370–379. doi:10.1016/S0168-5597(98)00017-3

Kanno, A., Nakasato, N., Murayama, N., and Yoshimoto, T. (2000). Middle and long latency peak sources in auditory evoked magnetic fields for tone bursts in humans. *Neurosci. Lett.* 293, 187–190. doi:10.1016/S0304-3940(00)01525-1

Khan, S. Y., Edgar, J. C., Monroe, J. F., Cannon, K. M., Blaskey, L., Qasmieh, S., et al. (2010). Obtaining auditory M100 responses: success rates in children autism spectrum disorders. *IFMBE Proc.* 28, 401–404.

Kral, A., and Eggermont, J. J. (2007). What's to lose and what's to learn: development under auditory deprivation, cochlear implants and limits of cortical plasticity. *Brain Res. Rev.* 56, 259–269. doi:10.1016/j.brainresrev.2007.07.021

Kraus, N., McGee, T., Littman, T., and Nicol, T. (1992). Reticular formation influences on primary and non-primary auditory pathways as reflected by the middle latency response. *Brain Res.* 587, 186–194. doi:10.1016/0006-8993(92)90996-M

Lee, Y. S., Leuders, H., Dinner, D. S., Lesser, R. P., Hahn, J., and Klem, G. (1984). Recording of auditory evoked potentials in man using chronic subdural electrodes. *Brain* 107, 115–131. doi:10.1093/brain/107.1.115

Ligeois-Chauvel, C., Musolino, A., Badier, J. M., Marquis, P., and Chauvel, P. (1994). Evoked potentials recorded from the auditory cortex in man: evaluation and topography of the middle latency components. *Electroencephalogr. Clin. Neurophysiol.* 92, 414–421.

Lutkenhoner, B., and Steinstrater, O. (1998). High-precision neuromagnetic study of the functional organization of the human auditory cortex. *Audiol. Neurootol.* 3, 191–213. doi:10.1159/000013790

Mäkelä, J. P., Hämäläinen, M., Hari, R., and McEvoy, L. (1994). Whole-cortex mapping of middle-latency auditory evoked magnetic fields. *Electroencephalogr. Clin. Neurophysiol.* 92, 414–421. doi:10.1016/0168-5597(94)90018-3

Marshall, P. J., Bar-Haim, Y., and Fox, N. A. (2004). The development of P50 suppression in the auditory event-related potential. *Int. J. Psychophysiol.* 51, 135–141. doi:10.1016/j.ijpsycho.2003.08.004

McNemar, Q. (1947). Note on the sampling error of the difference between correlated proportions or percentages. *Psychometrika* 12, 153–157. doi:10.1007/BF02295996

Moore, J. K., and Guan, Y. L. (2001). Cytoarchitectural and axonal maturation in human auditory cortex. *J. Assoc. Res. Otolaryngol.* 2, 297–311. doi:10.1007/s101620010052

Moore, J. K., and Linthicum, F. H. Jr. (2007). The human auditory system: a timeline of development. *Int. J. Audiol.* 46, 460–478. doi:10.1080/14992020701383019

Myles-Worsley, M., Coon, H., Byerley, W., Waldo, M., Young, D., and Freedman, R. (1996). Developmental and genetic influences on the P50 sensory gating phenotype. *Biol. Psychiatry* 39, 289–295. doi:10.1016/0006-3223(95)00134-4

Näätänen, R., and Picton, T. W. (1987). The N1 wave of the human electric and magnetic response to sound: a review and an analysis of the component structure. *Psychophysiology* 24, 375–425. doi:10.1111/j.1469-8986.1987.tb00311.x

Ninomiya, H., Onitsuka, T., Chen, C. H., and Kinukawa, N. (1997). Possible overlapping potentials of the auditory P50 in humans: factor analysis of middle latency auditory evoked potentials. *Electroencephalogr. Clin. Neurophysiol.* 104, 23–30. doi:10.1016/S0168-5597(96)96026-8

Oranje, B., Lahuis, B., van Engeland, H., van der Gaag, R. J., and Kemner, C. (2013). Sensory and sensorimotor gating in children with multiple complex developmental disorders (MCDD) and autism. *Psychiatry Res.* 206, 287–292. doi:10.1016/j.psychres.2012.10.014

Orekhova, E. V., Butorina, A. V., Tsetlin, M. M., Novikova, S. I., Sokolov, P. A., Elam, M., et al. (2013). Auditory magnetic response to clicks in children and adults: its components, hemispheric lateralization and repetition suppression effect. *Brain Topogr.* 26, 410–427. doi:10.1007/s10548-012-0262-x

Orekhova, E. V., Stroganova, T. A., Prokofyev, A. O., Nygren, G., Gillberg, C., and Elam, M. (2008). Sensory gating in young children with autism: relation to age, IQ, and EEG gamma oscillations. *Neurosci. Lett.* 434, 218–223. doi:10.1016/j.neulet.2008.01.066

Orekhova, E. V., Stroganova, T. A., Prokofyev, A. O., Nygren, G., Gillberg, C., and Elam, M. (2009). The right hemisphere fails to respond to temporal novelty in autism: evidence from an ERP study. *Clin. Neurophysiol.* 120, 520–529. doi:10.1016/j.clinph.2008.12.034

Paetau, R., Ahonen, A., Salonen, O., and Sams, M. (1995). Auditory evoked magnetic fields to tones and pseudowords in healthy children and adults. *J. Clin. Neurophysiol.* 12, 177–185. doi:10.1097/00004691-199503000-00008

Pelizzone, M., Hari, R., Mäkelä, J. P., Huttunen, J., Ahlfors, S. W., and Hämäläinen, M. (1987). Cortical origin of middle-latency auditory evoked responses in man. *Neurosci. Lett.* 82, 303–307. doi:10.1016/0304-3940(87)90273-4

Picton, T. W., Alain, C., Woods, D. L., John, M. S., Scherg, M., Valdes-Sosa, P., et al. (1999). Intracerebral sources of human auditory-evoked potentials. *Audiol. Neurootol.* 4, 64–79. doi:10.1159/000013823

Ponton, C., Eggermont, J. J., Khosla, D., Kwong, B., and Don, M. (2002). Maturation of human central auditory system activity: separating auditory evoked potentials by dipole source modeling. *Clin. Neurophysiol.* 113, 407–420. doi:10.1016/S1388-2457(01)00733-7

Ponton, C., Eggermont, J. J., Kwong, B., and Don, M. (2000). Maturation of human central auditory system activity: evidence from multi-channel evoked potentials. *Clin. Neurophysiol.* 111, 220–236. doi:10.1016/S1388-2457(99)00236-9

Ponton, C. W., and Eggermont, J. J. (2001). Of kittens and kids: altered cortical maturation following profound deafness and cochlear implant use. *Audiol. Neurootol.* 6, 363–380. doi:10.1159/000046846

Ponton, C. W., Moore, J. K., and Eggermont, J. J. (1999). Prolonged deafness limits auditory system developmental plasticity: evidence from an evoked potentials study in children with cochlear implants. *Scand. Audiol. Suppl.* 51, 13–22.

Rasco, L., Skinner, R. D., and Garcia-Rill, E. (2000). Effect of age on sensory gating of the sleep state-dependent P1/P50 midlatency auditory evoked potential. *Sleep Res. Online* 3, 97–105.

Reite, M., Teale, P., Zimmerman, J., Davis, K., and Whalen, J. (1988). Source location of a 50 msec latency auditory evoked field component. *Electroencephalogr. Clin. Neurophysiol.* 70, 490–498. doi:10.1016/0013-4694(88)90147-2

Roberts, T. P., Khan, S. Y., Rey, M., Monroe, J. F., Cannon, K., Blaskey, L., et al. (2010). MEG detection of delayed auditory evoked responses in autism spectrum disorders: towards an imaging biomarker for autism. *Autism Res.* 3, 8–18. doi:10.1002/aur.111

Roberts, T. P., Paulson, D. N., Hirschkoff, E., Pratt, K., Mascarenas, A., Miller, P., et al. (2014). Artemis 123: development of a whole-head infant and young child MEG system. *Front. Hum. Neurosci.* 8:99. doi:10.3389/fnhum.2014.00099

Roberts, T. P. L., Khan, S. Y., Blaskey, L., Dell, J., Levy, S., Zarnow, D. M., et al. (2009). Developmental correlation of diffusion anisotropy with auditory-evoked response. *Neuroreport* 20, 1586–1591. doi:10.1097/WNR.0b013e3283306854

Roberts, T. P. L., Lanza, M. R., Dell, J., Qasmieh, S., Hines, K., Blaskey, L., et al. (2013). Maturational differences in thalamocortical white matter microstructure and auditory evoked response latencies in autism spectrum disorders. *Brain Res.* 1537, 79–85. doi:10.1016/j.brainres.2013.09.011

Rojas, D. C., Walker, J. R., Sheeder, J. L., Teale, P. D., and Reite, M. L. (1998). Developmental changes in the refractoriness of the neuromagnetic M100 in children. *Neuroreport* 9, 1543–1547. doi:10.1097/00001756-199805110-00055

Satterfield, J. H., Schell, A. M., Backs, R. W., and Hidaka, K. C. (1984). A crosssectional and longitudinal study of age effects of electrophysiological measures in hyperactive and normal children. *Biol. Psychiatry* 19, 973–990.

Scherg, M., and Berg, P. (1996). New concepts of brain source imaging and localization. *Electroencephalogr. Clin. Neurophysiol. Suppl.* 46, 127–137.

Stroganova, T. A., Kozunov, V. V., Posikera, I. N., Galuta, I. A., Gratchev, V. V., and Orekhova, E. V. (2013). Abnormal pre-attentive arousal in young children with autism spectrum disorder contributes to their atypical auditory behavior: an ERP study. *PLoS ONE* 8:e69100. doi:10.1371/journal.pone.0069100

Sussman, E., Steinschneider, M., Gumenyuk, V., Grushko, J., Lawson, K. (2008). The maturation of human evoked brain potentials to sounds presented at different stimulus rates. *Hear. Res.* 236, 61–79. doi:10.1016/j.heares.2007.12.001

Tonnquist-Uhlén, I. (1996). Topography of auditory evoked long-latency potentials in children with severe language impairment: the P2 and N2 components. *Ear Hear.* 17, 314–326. doi:10.1097/00003446-199608000-00003

Waldo, M., Cawthra, E., Adler, L. E., Dubester, S., Staunton, M., Nagamoto, H., et al. (1994). Auditory sensory gating, hippocampal volume, and catecholamine metabolism in schizophrenics and their siblings. *Schizophr. Res.* 12, 93–106. doi:10.1016/0920-9964(94)90067-1

Wilson, T. W., Rojas, D. C., Reite, M. L., Teale, P. D., and Rogers, S. J. (2007). Children and adolescents with autism exhibit reduced MEG steady-state gamma responses. *Biol. Psychiatry* 62, 192–197. doi:10.1016/j.biopsych.2006.07.002

Wunderlich, J. L., and Cone-Wesson, B. K. (2006). Maturation of CAEP in infants and children: a review. *Hear. Res.* 212, 212–223. doi:10.1016/j.heares.2005.11.008

Yoshimura, Y., Kikuchi, M., Shitamichi, K., Ueno, S., Remijn, G., Haruta, Y., et al. (2012). Language performance and auditory evoked fields in 2- to 5-year-old children. *Eur. J. Neurosci.* 35, 644–650. doi:10.1111/j.1460-9568.2012.07998.x

Yoshiura, T., Ueno, S., Iramina, K., and Masuda, K. (1995). Source localization of middle latency auditory evoked magnetic fields. *Brain Res.* 703, 139–144. doi:10.1016/0006-8993(95)01075-0

Yvert, B., Crouzeix, A., Bertrand, O., Seither-Preisler, A., and Pantev, C. (2001). Multiple supratemporal sources of magnetic and electric auditory evoked middle latency components in humans. *Cereb. Cortex* 11, 411–423. doi:10.1093/cercor/11.5.411

Conflict of Interest Statement: The Reviewer Elysa Jill Marco declares that despite having collaborated with the author Timothy P. L. Roberts on another project, the review process was handled objectively and no conflict of interest exists. The authors declare that the research was conducted in the absence of any commercial or financial relationships that could be construed as a potential conflict of interest.

Received: 01 December 2013; accepted: 23 May 2014; published online: 06 June 2014.
Citation: Edgar JC, Lanza MR, Daina AB, Monroe JF, Khan SY, Blaskey L, Cannon KM, Jenkins J III, Qasmieh S, Levy SE and Roberts TPL (2014) Missing and delayed auditory responses in young and older children with autism spectrum disorders. Front. Hum. Neurosci. ***8****:417. doi: 10.3389/fnhum.2014.00417*
This article was submitted to the journal Frontiers in Human Neuroscience.

frontiers in
HUMAN NEUROSCIENCE

ORIGINAL RESEARCH ARTICLE
published: 28 May 2014
doi: 10.3389/fnhum.2014.00354

Lateralization of brain activation in fluent and non-fluent preschool children: a magnetoencephalographic study of picture-naming

Paul F. Sowman[1,2]*, Stephen Crain[3], Elisabeth Harrison[3] and Blake W. Johnson[1]

[1] *Department of Cognitive Science, ARC Centre of Excellence for Cognition and its Disorders, Macquarie University, Sydney, NSW, Australia*
[2] *Perception and Action Research Centre (PARC), Faculty of Human Sciences, Macquarie University, Sydney, NSW, Australia*
[3] *Department of Linguistics, ARC Centre of Excellence for Cognition and its Disorders, Macquarie University, Sydney, NSW, Australia*

Edited by:
Christos Papadelis, Harvard Medical School, USA

Reviewed by:
Danilo Bzdok, Research Center Jülich, Germany
Banu Ahtam, Boston Children's Hospital, USA

****Correspondence:***
Paul F. Sowman, Department of Cognitive Science, ARC Centre of Excellence for Cognition and its Disorders, Macquarie University, 16 University Avenue, Sydney, NSW 2109, Australia
e-mail: paul.sowman@mq.edu.au

The neural causes of stuttering remain unknown. One explanation comes from neuroimaging studies that have reported abnormal lateralization of activation in the brains of people who stutter. However, these findings are generally based on data from adults with a long history of stuttering, raising the possibility that the observed lateralization anomalies are compensatory rather than causal. The current study investigated lateralization of brain activity in language-related regions of interest in young children soon after the onset of stuttering. We tested 24 preschool-aged children, half of whom had a positive diagnosis of stuttering. All children participated in a picture-naming experiment whilst their brain activity was recorded by magnetoencephalography. Source analysis performed during an epoch prior to speech onset was used to assess lateralized activation in three regions of interest. Activation was significantly lateralized to the left hemisphere in both groups and not different between groups. This study shows for the first time that significant speech preparatory brain activation can be identified in young children during picture-naming and supports the contention that, in stutterers, aberrant lateralization of brain function may be the result of neuroplastic adaptation that occurs as the condition becomes chronic.

Keywords: stuttering, magnetoencephalography, lateralization, source analysis, speech, preschool children, speech production, vocalization

INTRODUCTION

Stuttering is a disorder of speech fluency that presents itself between the ages of 2 and 4 years. In the preschool population, the incidence is approximately 5% and the prevalence in the general population is 1%.

An early and influential theory of the brain basis of stuttering holds that its underlying cause is anomalous hemispheric lateralization of the speech control centers. Specifically, Orton (1927) contends that, in contrast to fluent speakers, people who stutter (PWS) have bilateral representations for speech processes. In their schema, rather than a single dominant (left) hemisphere producing speech, in the person who stutters both hemispheres issue commands which, when not perfectly synchronized, cause the blocking and repetition of speech segments that characterize stuttering. Despite the substantial face validity of this hypothesis, extensive behavioral testing of motor behavior in stutterers provides scant support. Work in the 80s and 90s by Webster (1985, 1986) converged on the position that "*people who stutter have normal left hemisphere lateralization of the neural mechanisms for the control of speech and other forms of sequential movement*" (Webster, 1997), findings that concur with sodium amytal tests of cerebral dominance for speech and language in PWS. As described by Andrews et al. (1972) and Luessenhop et al. (1973), PWS respond to right- and left-sided carotid artery injections of sodium amytal in the same way as fluent speakers. Such direct evidence supports the contention that PWS have a normal pattern of hemispheric specialization for speech.

Despite such findings, the theory that abnormal speech control lateralization drives stuttering still has currency in the general discourse around stuttering (e.g., Kushner, 2012). The perpetuation of this idea is supported in part by the findings from brain imaging evidence that has emerged in the past 20 years (for review, see Brown et al., 2005). A common finding in a number of these studies is a shift of speech-related brain activity to the right hemisphere in adults who stutter. In their seminal PET study, Fox et al. (1996) report increased activation in the right hemisphere in a language task in developmental stutterers. This finding was subsequently replicated by Braun et al. (1997), who were able to differentiate between patterns of stuttered and fluent speech in the stutterers that they tested. Importantly, their results challenge the idea that abnormal laterality caused stuttering. By demonstrating that the left hemisphere was more active during the production of stuttered speech and the right more active with fluent speech, the authors were able to conclude that the primary dysfunction in stuttering is located in the left hemisphere. They further suggested that hyperactivation of the right hemisphere is therefore not the cause of stuttering, but rather a reflection of neuroplastic adaptation.

Such compensatory plasticity has a well-established precedent in the lesion literature where transference of function between hemispheres has been observed in (e.g., Weiller et al., 1995).

Following on from the early PET studies of stuttering, a subsequent fMRI investigation by Preibisch et al. (2003) showed that overactivity in the right frontal operculum in PWS was negatively correlated with stuttering. Furthermore, this overactivation was evident even when speech tasks were not required. Taken together, these observations support the idea that overactivation in the right hemisphere seen with functional neuroimaging in PWS reflects a compensatory mechanism rather than being a manifestation of abnormal cerebral dominance for speech control (e.g., Braun et al., 1997; Preibisch et al., 2003; Chang et al., 2008; Lu et al., 2010).

There is a missing piece in this puzzle that might help adjudicate between causal and reactive origins for hemispheric activation anomalies in stuttering. Given that stuttering emerges most commonly in the preschool years, observation of normal hemispheric laterality of brain activity during speech production would support the thesis that increases in the right hemispheric activation in adults who stutter are the result of compensatory mechanisms developed over a lifetime of stuttering. At present, there is no functional brain imaging evidence from children near the age of onset of stuttering. The present study was designed to provide such evidence.

MATERIALS AND METHODS

SUBJECTS

This study was conducted with the approval of the Macquarie University Human Ethics Committee #HE29MAY2009-R06572. Preschool children who stutter (CWS) were recruited by newspaper advertisement. All were examined by a highly experienced speech pathologist (Elisabeth Harrison) who has more than 20 years of experience in the diagnosis and treatment of stuttering, prior to their inclusion in the study. Twelve children who were positively diagnosed as stutterers (CWS) were included in the study. The stutterers as a group were typical of the wider population of preschool age CWS in terms of the severity of their stuttering, i.e., all were in the range of mild–moderately severe with severity ratings between 3 and 6 (1 = no stuttering, 2 = extremely mild stuttering, 10 = extremely severe stuttering). This was expected since the distribution of stuttering severity is positively skewed in both children and adults (Bloodstein and Ratner, 2008, p. 2). Age- and sex-matched typically developing (TD) control subjects were recruited. The group of CWS consisted of 2 females and 10 males, mean age 50.8 months (range 35–64 months), the TD group consisted of 2 females and 10 males, mean age 51.7 months (range 27–66 months). All children were first language speakers of English and right handed.

TASK

Subjects performed a picture-naming task based on that presented in Levelt et al. (1998). Twenty colored picture stimuli were selected from the colorized Snodgrass and Vanderwart set (Rossion and Pourtois, 2004). Pictures (**Table 1**) were selected on the basis that their name consisted of a single syllable and the age of acquisition of their name was <3 years (Snodgrass and Yuditsky, 1996). A simple picture-naming task was chosen so that the findings of the current study could be compared with those previous seminal magnetoencephalography (MEG) studies of picture-naming in adults (Salmelin et al., 1994, 2000; Levelt et al., 1998) and also because simple, short, repeated vocalization tasks induce very few if any instances of stuttering even in chronic stutterers (Salmelin et al., 2000; Chang et al., 2009).

Table 1 | Pictures used in the naming task.

Word	Age of acquisition (years)
Ear	2.13
Dog	2.23
Hand	2.24
Sun	2.34
House	2.41
Bed	2.42
Sock	2.44
Spoon	2.45
Cat	2.5
Door	2.55
Cup	2.68
Box	2.69
Shoe	2.72
Cake	2.73
Car	2.73
Book	2.79
Fish	2.84
Bird	2.87
Hat	2.9
Duck	2.93

Each subject received one training block to get acquainted with the procedure and to maximize name agreement across items. Subjects lay supine on a plinth in the magnetically shielded room and were presented with the picture-naming stimuli projected via a mirror onto a screen that was situated directly in the participant's line of sight. The experimental presentation was controlled by the Presentation software package (Presentation 14.4, Neurobehavioral Systems, Albany, NY, USA).

Trials began with a white fixation cross appearing in the center of a black background. The duration of the fixation cross was randomly varied between 3000 and 4000 ms after which time, a picture appeared in the center of the screen. The subject was instructed to respond to the picture by naming it as quickly as possible. Vocal responses triggered a voice key connected to a directional microphone positioned on the ceiling of the magnetically shielded room above the subject's head. Timestamps thus collected were used to determine vocal onset reaction times. Trials were terminated as soon as the voice key was triggered. The active response period was limited to 3000 ms. Stimuli were presented in blocks of 20 trials. A single block contained all of the 20 stimuli randomly shuffled prior to the start of the block. Subjects participated in one or two recording sessions.

MAGNETOENCEPHALOGRAPHY

Brain magnetic fields were measured during picture-naming using a custom built pediatric 64-channel whole-head gradiometer MEG system. A detailed description of specifications of this device is available in Johnson et al. (2010).

Before subjects entered the magnetically shielded room for MEG data acquisition, their head shapes were recorded using a digitizing pen (Polhemus Fastrack, Colchester, VT, USA); approximately 200 randomly selected points were recorded for each subject's head surface. The 3D locations of the five head position indicator (HPI) coils attached to a tightly fitting elastic cap, and the locations of three cardinal landmarks (the nasion and bilateral preauricular points) were also digitized. Each subject's head position in the MEG dewar was measured at the start and end of each recording block from the five HPI coils.

Continuous data were acquired at a sampling rate of 1000 Hz and filtered online between 0.03 and 250 Hz. Fieldtrip (Oostenveld et al., 2011) and SPM8 (Litvak et al., 2011) were used for all offline data analyses. Offline, data were filtered (bandpass 1–40 Hz), epoched around the time of stimulus onset (−1000 to 1000 ms), and baseline corrected. Trials containing large amplitude artifacts were removed using the Fieldtrip visual artifact rejection method. Data for each recording block were co-registered with the individual headshape data and then transformed into a common sensor space (the average sensor space across blocks within subjects) using the method described by Knosche (2002) and implemented in Fieldtrip.

SENSOR SPACE ANALYSIS

In order to test whether stuttering status affected the evoked response to picture-naming stimuli, we used topological inference to search the entire sensor space for differences between groups. Based on the random field theory, topological inference for MEG data has been implemented in SPM8 (Litvak et al., 2011) to correct for multiple statistical comparisons across N-dimensional spaces. Briefly, a 2D topographical representation of the evoked field for each sample of the time dimension across the epoch of interest is created. Here, we created a 64×64 pixel image for each of the samples between −1000 and 1000 ms around the stimulus onset. This allowed us to compare differences in both space and time, while correcting for the family wise error (FWE) rate across the multiple comparisons. These images were then taken to the second level of the classical SPM analysis and compared using a two-sample t-test. Significance threshold was set at $p < 0.05$ (FWE-corrected) to determine whether statistically significant differences between groups (CWS vs. TD) existed in the evoked response at the sensor level.

SOURCE ANALYSIS

Source analysis was performed in Matlab (2013b; MathWorks, Inc., Natick, MA, USA) using the SPM8 toolbox for M/EEG. A canonical cortical mesh derived from the MNI template was co-registered and warped, in a non-linear manner, to match the participant's digitized headshape. Leadfields were computed using a single sphere volume conductor model. Source localization was then performed using a group inversion with multiple sparse priors (Friston et al., 2008b; Litvak and Friston, 2008) and the greedy search method (Friston et al., 2008a). This procedure results in a spatial projection of sensor data into (3D) brain space and considers brain activity as comprising a very large number of dipolar sources spread over the cortical sheet, with fixed locations and orientations (Litvak et al., 2011).

In order to minimize the potential for movement and EMG artifacts distorting the source estimation, trials were discarded in which the subject's vocal reaction time was shorter than 700 ms. Based on the approach using MEG to measure language laterality developed by Tanaka et al. (2013), evoked activity for each dipolar source was estimated within a 300 ms Gaussian time window centered on 450 ms after onset of the picture. Given the latency difference for linguistic processing known to exist for young children compared to adults (e.g., Holcomb et al., 1992; Kraus et al., 1993) we chose to shift the window of interest suggested by Tanaka et al. (2013), 50 ms later. According to Levelt et al. (1998), brain activity related to speech planning begins 300 ms after the onset of a picture-naming stimulus.

3D volumetric source maps were smoothed with a full width at half maximum (FWHM) smoothing kernel and passed to a second level SPM analysis. A paired t-test comparing stimulus-locked induced source activation to baseline was performed across the whole sample in order to identify a common network for speech preparation. A two-sample t-test was also conducted between CWS and TD in order to identify any differences in activation between the groups. Resulting SPMs were corrected for FWE. The data were thresholded at the critical FWE t-value and statistically significant difference clusters projected onto a template brain for visualization using xjView[1].

ROI ANALYSIS

In order to test whether there was any effect of group or hemisphere on any of the activations within the ROIs, we performed a multivariate, repeated measures ANOVA on the between subjects factor Group (CWS or TD) and the within subjects factor Hemisphere (left or right) across the three ROIs, which were included as separate variates. This analysis was performed using IBM® SPSS® Statistics version 21.

LATERALITY

In order to assess the degree of lateralization of the speech preparatory process, ROI masks for both hemispheres were constructed using the AAL atlas (Tzourio-Mazoyer et al., 2002) via the wfu_pickatlas toolbox (Maldjian et al., 2003). Following the procedure of Tanaka et al. (2013), we used anatomically defined ROIs that consisted of the supramarginal gyrus (SMG), superior temporal gyrus (STG), and the inferior frontal gyrus (IFG). We chose these areas in line with the core language network presented in Tanaka et al. (2013), that were based on previous language lateralization MEG studies (Bowyer et al., 2005; McDonald et al., 2009). Furthermore, these areas are the key areas in which previous functional imaging studies (e.g., De Nil et al., 2008) have shown there to be laterality anomalies in stuttering subjects. Tanaka et al. (2013) examined the opercular and triangular parts of the IFG separately whereas we chose to create a single ROI that consisted of the triangular, opercular, and orbital parts of the IFG in a single ROI that could be considered to represent Broca's area and its right hemisphere homolog. Volumetric functional images were

[1] http://www.alivelearn.net/xjview

masked using these ROIs and then thresholded at the 25% maximal amplitude across all ROIs. Using the REX toolbox[2], the mean voxel amplitude within these masks was extracted for all subjects. The laterality index (LI) was then calculated using the formula "left − right/left + right." Therefore, LI varies continuously from −1 for pure right hemisphere dominance to +1 for pure left hemisphere dominance.

RESULTS

NUMBER OF TRIALS

The average total number of trials contributing to the analysis was 190 for the PWS and 160 for the TD. There was no significant difference between the two groups in terms of trial numbers ($p = 0.16$). The mean reaction time (mean ± SEM) for CWS was 1239 ± 64 and 1278 ± 72 ms for TD ($p = 0.68$).

SENSOR SPACE ANALYSIS

Following the onset of the picture-naming stimulus, sensor level waveforms were characterized by an m100/200 complex, which was largest over occipital areas – consistent with early visual activation. A later component, peaking around 450 ms, was evident bilaterally in temporal areas and in the left frontal region. This pattern of activation is illustrated in the grand mean sensor plots in **Figure 1**. Sensor space SPMs found no significant between group differences (CWS vs. TD).

SOURCE SPACE ANALYSIS

Compared to baseline, there were six significant activation clusters in the brain during the epoch 300–600 ms after the onset of the naming stimulus (**Figure 2**). Four of these clusters were in the left hemisphere. In total, there were 1049 significantly activated voxels in the left hemisphere and 130 in the right (**Table 2**). In the left hemisphere, the largest cluster was in primary somatosensory and somatosensory association areas. It encompassed part of the posterior frontal lobe intersecting with Brodmann areas 3 and 2 and extended into the anterior-superior and inferior parietal lobe, intersecting with Brodmann areas 7, 5, and 40. The second largest cluster in the left hemisphere was centered on the triangular part of the IFG. This cluster overlaps with the representation of Broca's area (Brodmann areas 45, 46, and 9). Two other small clusters were significantly active, one in the middle temporal gyrus intersecting with Brodmann area 39 and another in the supplementary motor area [SMA (Brodmann area 6)].

In the right hemisphere, there were two significant clusters: the largest was in the SMG intersecting with Brodmann area 40. The other significant cluster was within the SMA Brodmann area 6. There were no significant activation differences between groups.

[2]http://gablab.mit.edu/

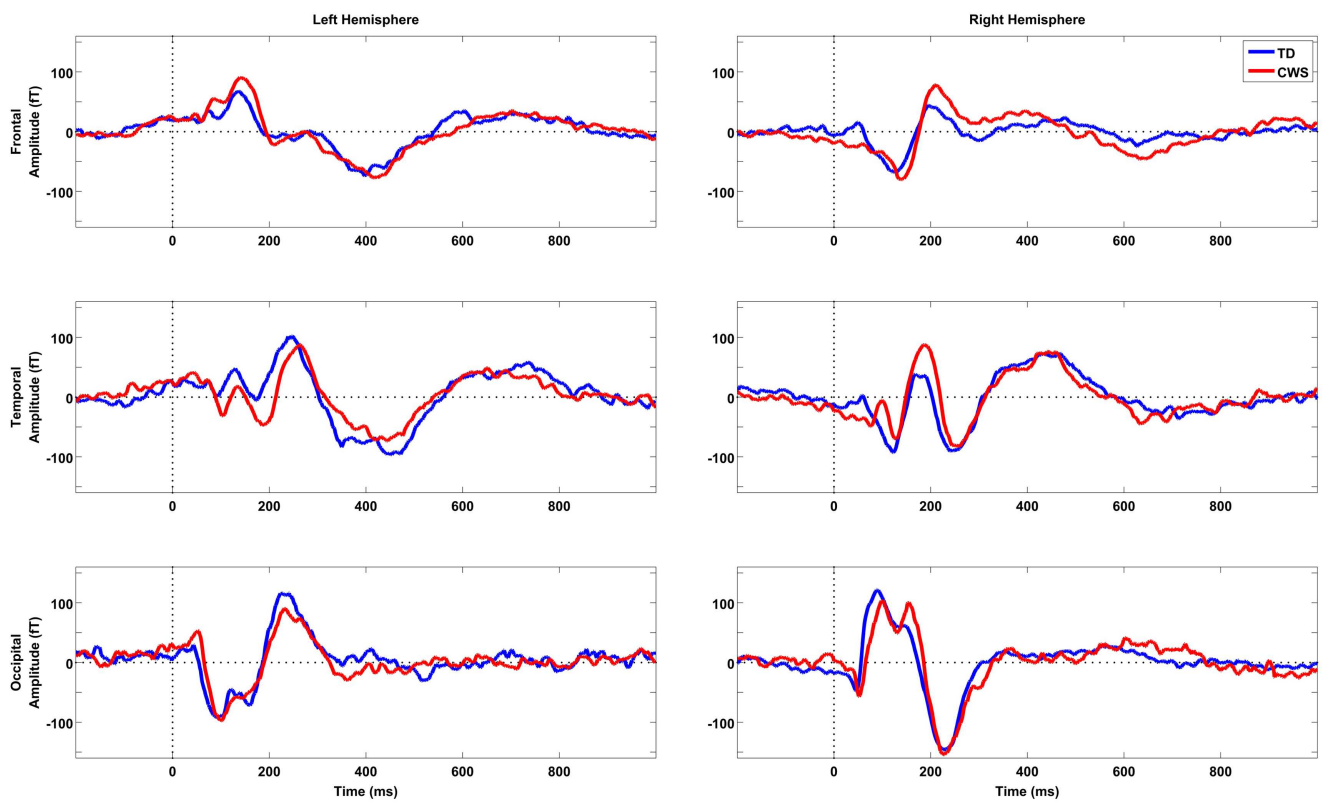

FIGURE 1 | Grand mean sensor space activations for six sample sensors taken from frontal, temporal, and occipital locations in the left and right hemispheres, respectively. TD subjects are depicted in blue ($n = 12$) and CWS in red ($n = 12$). Vertical dotted lines represent picture-naming stimulus onset time.

ROI ANALYSIS

There was a significant main effect of Hemisphere for all ROIs [IFG: $F_{(1,22)} = 32$, $p < 0.001$; SMG: $F_{(1,22)} = 35$, $p < 0.001$; STG: $F_{(1,22)} = 36$, $p < 0.001$] with the level of activation being significantly greater in the left vs. the right hemisphere. There was no significant effect of Group or interaction between Group and Hemisphere.

LATERALIZATION

For all subjects, activity was lateralized to the left for all ROIs (**Table 3**). Lateralization was significantly to the left for all ROIs and there was no significant difference between groups (**Table 4**).

DISCUSSION

The current results are the first functional brain imaging data of overt speech production in preschool-aged CWS. This is an important contribution to a literature based on results from older children and adults, whose brain functions have had many years to develop compensatory strategies.

There is a long history of attributing the cause of stuttering to atypical laterality of speech/language function. The roots of this theory can be traced back to publications in the early twentieth century by Orton (1927) and Travis (1931), hence the lateralization theory of stuttering often being referred to as the Orton–Travis theory. They posited that a failure in development of normal cerebral dominance would lead to cascade of events: competition between the hemispheres, an incoordination of outputs and interruption of fluent speech. Even though the early attempts to test this theory experimentally were inconclusive (Bryngelson, 1935, 1939; Heltman, 1940) and a number of negative findings followed, e.g., Dorman and Porter (1975), interest in the theory has persisted, most likely because of its parsimonious appeal and the persistence of anecdotal evidence suggesting that forced changes in handedness for writing – a common educational practice in the early twentieth century (Kushner, 2012) – gave rise to

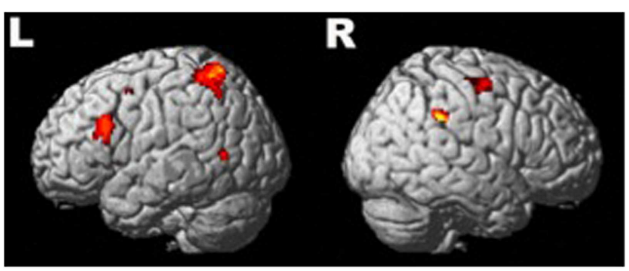

FIGURE 2 | Significant (active > baseline) regions of activation during speech preparation across all subjects ($n = 24$). Four clusters of activation survived correction (FWE) in the left hemisphere and two in the right. Description of the locations is available in **Table 2**.

Table 3 | Laterality indices (LI) for all subjects (CWS and TD) across three ROIs.

Subject	IFG		STG		SMG	
	CWS	TD	CWS	TD	CWS	TD
1	0.16	0.19	0.36	0.23	0.18	0.14
2	0.17	0.20	0.15	0.18	0.01	0.11
3	0.16	0.18	0.14	0.25	0.07	0.22
4	0.19	0.18	0.27	0.38	0.26	0.22
5	0.17	0.20	0.23	0.28	0.22	0.19
6	0.17	0.18	0.55	0.27	0.55	0.28
7	0.17	0.18	0.14	0.30	0.08	0.30
8	0.15	0.19	0.28	0.21	0.11	0.26
9	0.17	0.17	0.20	0.22	0.19	0.13
10	1.00	1.00	0.31	0.60	0.36	0.50
11	0.18	0.20	0.29	0.23	0.09	0.12
12	1.00	0.15	0.35	0.34	0.33	0.29

IFG, inferior frontal gyrus; STG, superior temporal gyrus; SMG, supramarginal gyrus.

Table 4 | Mean (±SEM) laterality indices (LI) for CWS and TD across three ROIs.

ROI	CWS	TD	Two-sample *t*-test	All subjects	One-sample *t*-test
IFG	0.31 ± 0.09	0.25 ± 0.07	$p = 0.63$	0.28 ± 0.06	$p < 0.001$
STG	0.27 ± 0.03	0.29 ± 0.03	$p = 0.68$	0.28 ± 0.02	$p < 0.001$
SMG	0.21 ± 0.04	0.23 ± 0.03	$p = 0.64$	0.22 ± 0.03	$p < 0.001$

IFG, inferior frontal gyrus; STG, superior temporal gyrus; SMG, supramarginal gyrus. Two-sample t-test values refer to tests between controls and stutterers. One-sample t-tests refer to tests of the whole sample's LI against 0 (no laterality). LI varies continuously from −1 for pure right hemisphere dominance to +1 for pure left hemisphere dominance.

Table 2 | MNI coordinates and anatomical labels of FWE-corrected brain sources thresholded at $T > 5.2$ as revealed by task-baseline contrast.

Cluster size (voxels)	Lobe	Area	Hemisphere	Brodmann areas	Peak intensity	MNI coordinates at peak (mm)
718	Parietal	Precuneus, superior parietal lobule, inferior parietal lobule, paracentral lobule Postcentral gyrus	L	7, 5, 40, 3, 2	6.6	−18 −52 58
214	Frontal	Middle frontal gyrus, inferior frontal gyrus	L	9, 46, 45	5.6	−44 22 30
107	Parietal	Inferior parietal lobule, supramarginal gyrus	R	40	6.0	54 −42 36
100	Frontal	Precentral gyrus, middle frontal gyrus	R	6	5.8	34 −10 54
30	Temporal	Middle temporal gyrus	L	39	5.7	−52 −62 6
10	Frontal	Middle frontal gyrus	L	6	5.4	−32 4 50

stuttering or that left handedness conveys a higher risk for stuttering. Indeed, it is still common to find examples such claims as "Most stammering children are left-handed" (du Plessix Gray, 2012) or "In fact, just as human speech – stuttering in particular – is related to cerebral laterality (most stutterers are left-handed)..." (Shell, 2006), in the popular press, despite significant evidence to the contrary (Records et al., 1977; Webster and Poulos, 1987; Ardila et al., 1994; Salihovic and Sinanovic, 2000). While the burgeoning neuroimaging literature on stuttering has conferred some support for the idea that anomalous laterality is the cause of stuttering, such imaging data cannot provide a causal link. Indeed, it has long been contended that right hemispheric overactivations represent reactions to, or compensations for stuttering, rather than being causative agents. For this reason, anatomical or functional demonstrations of normal laterality in young stutterers are powerful evidence against a laterality origin for stuttering and would support a reactive origin for the changes in both functional and structural laterality changes seen in adult stutterers. Our data strongly support the contention that the laterality anomalies of older stutterers reflect compensatory shifting of function rather than an underlying causal dysfunction. This conclusion is supported by a recent neuroanatomical study that reported no differences in right–left asymmetries between 9- and 12-year-old stuttering boys and a matched cohort of controls (Chang et al., 2008).

An important caveat to this conclusion comes from the fact that a significant proportion of those children who begin to stutter will spontaneously recover [up to 80% by some estimations (Yairi and Ambrose, 1992, 1999; Yairi et al., 1993; Kalinowski et al., 2002)]. With this in mind, it is possible that our child participants may be quite different neurologically from children whose stuttering persists into adulthood. That is, while the sample we tested were all current stutterers at the time of our investigation, it must be expected that most of them would not continue to be stutterers into adulthood and therefore a large proportion of our sample consists of stutterers who will recover precisely because they do not have the underlying abnormal laterality that leads to persistent developmental stuttering. This possibility is encapsulated well in the work of Shell (2006) who states, "Particularized lateralization among human children develops ontogenetically at around the time they are learning to speak. Some researchers think this fact may explain why so many children (3–4%) "stumble" in speech and then "outgrow" the problem when lateralization is fully developed. Those children who do not fully lateralize are, according to this view, the children who are the "real" stutterers (about 1%)." Arguing against this possibility, the study by Chang et al. (2008) showed that the brains of recovered stutterers were more like those of current stutterers than control subjects, an observation that suggests that the occurrence of recovery likely reflects initial severity rather than reflecting the existence of a neurologically distinct subgroup. For this reason, we believe our data are still likely to reflect the true status of laterality in the early stages of stuttering, at least in regard to speech production.

The possibility remains though that anomalous laterality of other speech or language-related brain functions might exist in the early stages of stuttering. Indeed, a recent study using near infrared spectroscopy suggests that this may be the case in regard to some aspects of auditory language processing (Sato et al., 2011). Future studies looking to characterize brain activation anomalies in young CWS should include longitudinal following of the subjects so that retrospective analysis of those subjects whose stuttering does not resolve might be carried out. Given a large enough initial cohort, this approach would allow researchers to control for possible heterogeneities within the cohort.

While the interpretation of child MEG data in source space must be considered in light of the inherent uncertainties that govern solutions to the inverse problem, the concordance between the results of the whole-brain analysis presented herein and previous MEG studies of speech in adult subjects suggests that these findings are robust. In the time after early visual processing, and consistent with articulatory planning for speech (Levelt et al., 1998), a strongly left-lateralized brain network was activated. This network consisted of inferior frontal, parietal, and temporal nodes largely consistent with previous MEG studies that have examined speech or speech planning (e.g., Carota et al., 2010). Notably, our results show a distinctly left-lateralized inferior frontal activation, and premotor activity in areas consistent with the SMA activity seen in previous studies (Salmelin et al., 1994, 2000). Furthermore, like the study of Salmelin et al. (2000), the activity we saw in the SMA was right lateralized. We also observed significant parietal lobe activations in our study which, while not consistent with the fMRI literature on overt speech (Indefrey and Levelt, 2004), is consistent with similar MEG studies, which have consistently found activation in both inferior and superior parietal lobes (Salmelin et al., 1994; Levelt et al., 1998; Hulten et al., 2009) including Brodmann area 7 (Carota et al., 2010), which was the most active parietal locus in our findings. Carota et al. (2010) suggest that activation in Brodmann area 7 during speech planning is indicative of the parietal cortex's key role in monitoring motor intention in language.

Our conclusions regarding the lack of laterality differences must be considered within the scope of the limited part of the speech planning process that we have examined. It is important to emphasize that the time window beyond 600 ms was not taken into inversion analysis and, given that the average vocal reaction time was longer than 1000 ms, there remains a significant epoch in which laterality differences might manifest. It is, however, important to note that articulatory mouth movement begins significantly earlier than the onset of overt speech – similar studies to the current one suggest this difference is in the order of 300 ms in adult subjects (Salmelin et al., 2000) hence the speech planning time is not as long as the reaction time as measured by voice key as in the current study. Future development of devices, which allow real-time monitoring of articulatory movements within the MEG environment (e.g., Lau, 2013) should allow for articulatory artifacts to be controlled much more precisely and remove a number of the limitations surrounding the time frame in which brain processing of speech production might be measured.

A number of previous neuroimaging studies using hemodynamic techniques (PET, fMRI) have shown there to be differences between stutterers and non-stutterers in the activation strength

of various cortical and subcortical sources (e.g., Fox et al., 1996, 2000; Braun et al., 1997; De Nil et al., 2000, 2008; Ingham et al., 2000; Neumann et al., 2003; Preibisch et al., 2003; Giraud et al., 2008; Watkins et al., 2008; Chang et al., 2009; Kell et al., 2009; Sakai et al., 2009; Loucks et al., 2011); (for review, see De Nil and Kroll, 2001; Ingham, 2001; Fox, 2003; Brown et al., 2005). However, our study did not find any difference between source activation strength between CWS and TD. This difference may reflect a difference between neuromagnetic approaches to source imaging compared to hemodynamic imaging. Indeed, most previous MEG studies of stuttering have not attempted to analyze differences in source activations, rather utilizing the inherent temporal advantage of MEG to illustrate differences in auditory evoked activations (Salmelin et al., 1998; Beal et al., 2010; Kikuchi et al., 2011b) and temporal dynamics (Salmelin et al., 2000; Biermann-Ruben et al., 2005) or location of discrete dipole sources (Salmelin et al., 2000). Only a single previous study has demonstrated the ability of MEG to characterize cortical activation patterns in stuttering using a distributed sources model, and that was in a single adult subject (Sowman et al., 2012). Our primary aim was to use the other advantages of MEG (passivity, lack of noise, and reduced need for enclosure of the participant) to investigate laterality in children. A previous MEG study using a similar approach has shown that left dominance of parietotemporal coherence in theta band activity is specifically correlated with higher performance of language-related tasks in preschool children (Kikuchi et al., 2011a). The current study also demonstrates the utility and possible sensitivity of MEG-based measures for characterizing laterality in developmental language disorders.

In conclusion, we have demonstrated that in the very early stages of stuttering development, the preparation for speech is not characterized by anomalous lateralization of brain activations. This evidence gives weight to the hypothesis that the right hemispheric biases in chronic stuttering are due to neuroplastic adaptations rather than being an underlying primary source of dysfunction.

ACKNOWLEDGMENTS

This work was funded by the National Health and Medical Research Council (#1003760) and was also supported by the Australian Research Council Centre of Excellence for Cognition and its Disorders (CE110001021) (http://www.ccd.edu.au). Paul F. Sowman was supported by the National Health and Research Council, Australia (#543438) and the Australian Research Council (DE130100868). The authors acknowledge the role of the Kanazawa Institute of Technology in establishing the KIT-Macquarie Brain Research Laboratory.

REFERENCES

Andrews, G., Quinn, P. T., and Sorby, W. A. (1972). Stuttering: an investigation into cerebral dominance for speech. *J. Neurol. Neurosurg. Psychiatr.* 35, 414–418. doi:10.1136/jnnp.35.3.414

Ardila, A., Bateman, J. R., Nino, C. R., Pulido, E., Rivera, D. B., and Vanegas, C. J. (1994). An epidemiologic study of stuttering. *J. Commun. Disord.* 27, 37–48. doi:10.1016/0021-9924(94)90009-4

Beal, D. S., Cheyne, D. O., Gracco, V. L., Quraan, M. A., Taylor, M. J., and De Nil, L. F. (2010). Auditory evoked fields to vocalization during passive listening and active generation in adults who stutter. *Neuroimage* 52, 1645–1653. doi:10.1016/j.neuroimage.2010.04.277

Biermann-Ruben, K., Salmelin, R., and Schnitzler, A. (2005). Right rolandic activation during speech perception in stutterers: a MEG study. *Neuroimage* 25, 793–801. doi:10.1016/j.neuroimage.2004.11.024

Bloodstein, O., and Ratner, N. B. (2008). *A Handbook on Stuttering.* Clifton Park, NY: Delmar Learning.

Bowyer, S. M., Moran, J. E., Weiland, B. J., Mason, K. M., Greenwald, M. L., Smith, B. J., et al. (2005). Language laterality determined by MEG mapping with MR-FOCUSS. *Epilepsy Behav.* 6, 235–241. doi:10.1016/j.yebeh.2004.12.002

Braun, A. R., Varga, M., Stager, S., Schulz, G., Selbie, S., Maisog, J. M., et al. (1997). Altered patterns of cerebral activity during speech and language production in developmental stuttering. An H2(15)O positron emission tomography study. *Brain* 120(Pt 5), 761–784. doi:10.1093/brain/120.5.761

Brown, S., Ingham, R. J., Ingham, J. C., Laird, A. R., and Fox, P. T. (2005). Stuttered and fluent speech production: an ALE meta-analysis of functional neuroimaging studies. *Hum. Brain Mapp.* 25, 105–117. doi:10.1002/hbm.20140

Bryngelson, B. (1935). Sidedness as an etiological factor in stuttering. *Pedagog. Semin. J. Genet. Psychol.* 47, 204–217. doi:10.1080/08856559.1935.9943891

Bryngelson, B. (1939). A study of laterality of stutterers and normal speakers. *J. Speech Hear. Disord.* 4, 231.

Carota, F., Posada, A., Harquel, S., Delpuech, C., Bertrand, O., and Sirigu, A. (2010). Neural dynamics of the intention to speak. *Cereb. Cortex* 20, 1891–1897. doi:10.1093/cercor/bhp255

Chang, S. E., Erickson, K. I., Ambrose, N. G., Hasegawa-Johnson, M. A., and Ludlow, C. L. (2008). Brain anatomy differences in childhood stuttering. *Neuroimage* 39, 1333–1344. doi:10.1016/j.neuroimage.2007.09.067

Chang, S. E., Kenney, M. K., Loucks, T. M., and Ludlow, C. L. (2009). Brain activation abnormalities during speech and non-speech in stuttering speakers. *Neuroimage* 46, 201–212. doi:10.1016/j.neuroimage.2009.01.066

De Nil, L. F., Beal, D. S., Lafaille, S. J., Kroll, R. M., Crawley, A. P., and Gracco, V. L. (2008). The effects of simulated stuttering and prolonged speech on the neural activation patterns of stuttering and nonstuttering adults. *Brain Lang.* 107, 114–123. doi:10.1016/j.bandl.2008.07.003

De Nil, L. F., and Kroll, R. M. (2001). Searching for the neural basis of stuttering treatment outcome: recent neuroimaging studies. *Clin. Linguist. Phon.* 15, 163–168. doi:10.3109/02699200109167650

De Nil, L. F., Kroll, R. M., Kapur, S., and Houle, S. (2000). A positron emission tomography study of silent and oral single word reading in stuttering and nonstuttering adults. *J. Speech Lang. Hear. Res.* 43, 1038–1053. doi:10.1044/jslhr.4304.1038

Dorman, M. F., and Porter, R. J. Jr. (1975). Hemispheric lateralization for speech perception in stutterers. *Cortex* 11, 181–185. doi:10.1016/S0010-9452(75)80042-6

du Plessix Gray, F. (2012). "The paralysis of stuttering [online]," in *The New York Review of Books.* Available at: http://www.nybooks.com/articles/archives/2012/apr/26/paralysis-stuttering/?pagination=false

Fox, P. T. (2003). Brain imaging in stuttering: where next? *J. Fluency Disord.* 28, 265–272. doi:10.1016/j.jfludis.2003.08.001

Fox, P. T., Ingham, R. J., Ingham, J. C., Hirsch, T. B., Downs, J. H., Martin, C., et al. (1996). A PET study of the neural systems of stuttering. *Nature* 382, 158–161. doi:10.1038/382158a0

Fox, P. T., Ingham, R. J., Ingham, J. C., Zamarripa, F., Xiong, J. H., and Lancaster, J. L. (2000). Brain correlates of stuttering and syllable production. A PET performance-correlation analysis. *Brain* 123(Pt 10), 1985–2004. doi:10.1093/brain/123.10.1985

Friston, K., Chu, C., Mourao-Miranda, J., Hulme, O., Rees, G., Penny, W., et al. (2008a). Bayesian decoding of brain images. *Neuroimage* 39, 181–205. doi:10.1016/j.neuroimage.2007.08.013

Friston, K., Harrison, L., Daunizeau, J., Kiebel, S., Phillips, C., Trujillo-Barreto, N., et al. (2008b). Multiple sparse priors for the M/EEG inverse problem. *Neuroimage* 39, 1104–1120. doi:10.1016/j.neuroimage.2007.09.048

Giraud, A. L., Neumann, K., Bachoud-Levi, A. C., Von Gudenberg, A. W., Euler, H. A., Lanfermann, H., et al. (2008). Severity of dysfluency correlates with basal ganglia activity in persistent developmental stuttering. *Brain Lang.* 104, 190–199. doi:10.1016/j.bandl.2007.04.005

Heltman, H. J. (1940). Contradictory evidence in handedness and stuttering. *J. Speech Hear. Disord.* 5, 327.

Holcomb, P. J., Coffey, S. A., and Neville, H. J. (1992). Visual and auditory sentence processing – a developmental analysis using event-related brain potentials. *Dev. Neuropsychol.* 8, 203–241. doi:10.1080/87565649209540525

Hulten, A., Vihla, M., Laine, M., and Salmelin, R. (2009). Accessing newly learned names and meanings in the native language. *Hum. Brain Mapp.* 30, 976–989. doi:10.1002/hbm.20561

Indefrey, P., and Levelt, W. J. (2004). The spatial and temporal signatures of word production components. *Cognition* 92, 101–144. doi:10.1016/j.cognition.2002.06.001

Ingham, R. J. (2001). Brain imaging studies of developmental stuttering. *J. Commun. Disord.* 34, 493–516. doi:10.1016/S0021-9924(01)00061-2

Ingham, R. J., Fox, P. T., Costello Ingham, J., and Zamarripa, F. (2000). Is overt stuttered speech a prerequisite for the neural activations associated with chronic developmental stuttering? *Brain Lang.* 75, 163–194. doi:10.1006/brln.2000.2351

Johnson, B. W., Crain, S., Thornton, R., Tesan, G., and Reid, M. (2010). Measurement of brain function in pre-school children using a custom sized whole-head MEG sensor array. *Clin. Neurophysiol.* 121, 340–349. doi:10.1016/j.clinph.2009.10.017

Kalinowski, J., Dayalu, V. N., and Saltuklaroglu, T. (2002). Cautionary notes on interpreting the efficacy of treatment programs for children who stutter. *Int. J. Lang. Commun. Disord.* 37, 359–361. doi:10.1080/13682820210136250

Kell, C. A., Neumann, K., Von Kriegstein, K., Posenenske, C., Von Gudenberg, A. W., Euler, H., et al. (2009). How the brain repairs stuttering. *Brain* 132, 2747–2760. doi:10.1093/brain/awp185

Kikuchi, M., Shitamichi, K., Yoshimura, Y., Ueno, S., Remijn, G. B., Hirosawa, T., et al. (2011a). Lateralized theta wave connectivity and language performance in 2- to 5-year-old children. *J. Neurosci.* 31, 14984–14988. doi:10.1523/JNEUROSCI.2785-11.2011

Kikuchi, Y., Ogata, K., Umesaki, T., Yoshiura, T., Kenjo, M., Hirano, Y., et al. (2011b). Spatiotemporal signatures of an abnormal auditory system in stuttering. *Neuroimage* 55, 891–899. doi:10.1016/j.neuroimage.2010.12.083

Knosche, T. R. (2002). Transformation of whole-head MEG recordings between different sensor positions. *Biomed. Eng.* 47, 59–62. doi:10.1515/bmte.2002.47.3.59

Kraus, N., McGee, T., Carrell, T., Sharma, A., Micco, A., and Nicol, T. (1993). Speech-evoked cortical potentials in children. *J. Am. Acad. Audiol.* 4, 238–248.

Kushner, H. I. (2012). Retraining left-handers and the aetiology of stuttering: the rise and fall of an intriguing theory. *Laterality* 17, 673–693. doi:10.1080/1357650X.2011.615127

Lau, C. (2013). *Validation of the Magneto-Articulography for the Assessment of Speech Kinematics (MASK) System and Testing for Use in a Clinical Research Setting.* Toronto: Master of Health Science, University of Toronto.

Levelt, W. J., Praamstra, P., Meyer, A. S., Helenius, P., and Salmelin, R. (1998). An MEG study of picture-naming. *J. Cogn. Neurosci.* 10, 553–567. doi:10.1162/089892998562960

Litvak, V., and Friston, K. (2008). Electromagnetic source reconstruction for group studies. *Neuroimage* 42, 1490–1498. doi:10.1016/j.neuroimage.2008.06.022

Litvak, V., Mattout, J., Kiebel, S., Phillips, C., Henson, R., Kilner, J., et al. (2011). EEG and MEG data analysis in SPM8. *Comput. Intell. Neurosci.* 2011, 852961. doi:10.1155/2011/852961

Loucks, T., Kraft, S. J., Choo, A. L., Sharma, H., and Ambrose, N. G. (2011). Functional brain activation differences in stuttering identified with a rapid fMRI sequence. *J. Fluency Disord.* 36, 302–307. doi:10.1016/j.jfludis.2011.04.004

Lu, C., Chen, C., Ning, N., Ding, G., Guo, T., Peng, D., et al. (2010). The neural substrates for atypical planning and execution of word production in stuttering. *Exp. Neurol.* 221, 146–156. doi:10.1016/j.expneurol.2009.10.016

Luessenhop, A. J., Boggs, J. S., Laborwit, L. J., and Walle, E. L. (1973). Cerebral dominance in stutterers determined by Wada testing. *Neurology* 23, 1190–1192. doi:10.1212/WNL.23.11.1190

Maldjian, J. A., Laurienti, P. J., Kraft, R. A., and Burdette, J. H. (2003). An automated method for neuroanatomic and cytoarchitectonic atlas-based interrogation of fMRI data sets. *Neuroimage* 19, 1233–1239. doi:10.1016/S1053-8119(03)00169-1

McDonald, C. R., Thesen, T., Hagler, D. J. Jr., Carlson, C., Devinksy, O., Kuzniecky, R., et al. (2009). Distributed source modeling of language with magnetoencephalography: application to patients with intractable epilepsy. *Epilepsia* 50, 2256–2266. doi:10.1111/j.1528-1167.2009.02172.x

Neumann, K., Euler, H. A., Von Gudenberg, A. W., Giraud, A. L., Lanfermann, H., Gall, V., et al. (2003). The nature and treatment of stuttering as revealed by fMRI A within- and between-group comparison. *J. Fluency Disord.* 28, 381–409. doi:10.1016/j.jfludis.2003.07.003

Oostenveld, R., Fries, P., Maris, E., and Schoffelen, J. M. (2011). FieldTrip: open source software for advanced analysis of MEG, EEG, and invasive electrophysiological data. *Comput. Intell. Neurosci.* 2011, 156869. doi:10.1155/2011/156869

Orton, S. T. (1927). Studies in stuttering. *Arch. Neurol. Psychiatry* 18, 671–672. doi:10.1001/archneurpsyc.1927.02210050003001

Preibisch, C., Neumann, K., Raab, P., Euler, H. A., Von Gudenberg, A. W., Lanfermann, H., et al. (2003). Evidence for compensation for stuttering by the right frontal operculum. *Neuroimage* 20, 1356–1364. doi:10.1016/S1053-8119(03)00376-8

Records, M. A., Heimbuch, R. C., and Kidd, K. K. (1977). Handedness and stuttering: a dead horse? *J. Fluency Disord.* 2, 271–282. doi:10.1016/0094-730X(77)90031-6

Rossion, B., and Pourtois, G. (2004). Revisiting Snodgrass and Vanderwart's object pictorial set: the role of surface detail in basic-level object recognition. *Perception* 33, 217–236. doi:10.1068/p5117

Sakai, N., Masuda, S., Shimotomai, T., and Mori, K. (2009). Brain activation in adults who stutter under delayed auditory feedback: an fMRI study. *Int. J. Speech Lang. Pathol.* 11, 2–11. doi:10.1080/17549500802588161

Salihovic, N., and Sinanovic, O. (2000). Stuttering and left-handedness. *Med. Arh.* 54, 173–175.

Salmelin, R., Hari, R., Lounasmaa, O. V., and Sams, M. (1994). Dynamics of brain activation during picture-naming. *Nature* 368, 463–465. doi:10.1038/368463a0

Salmelin, R., Schnitzler, A., Schmitz, F., and Freund, H. J. (2000). Single word reading in developmental stutterers and fluent speakers. *Brain* 123(Pt 6), 1184–1202. doi:10.1093/brain/123.6.1184

Salmelin, R., Schnitzler, A., Schmitz, F., Jancke, L., Witte, O. W., and Freund, H. J. (1998). Functional organization of the auditory cortex is different in stutterers and fluent speakers. *Neuroreport* 9, 2225–2229. doi:10.1097/00001756-199807130-00014

Sato, Y., Mori, K., Koizumi, T., Minagawa-Kawai, Y., Tanaka, A., Ozawa, E., et al. (2011). Functional lateralization of speech processing in adults and children who stutter. *Front. Psychol.* 2:70. doi:10.3389/fpsyg.2011.00070

Shell, M. (2006). *Stutter.* Cambridge, MA: Harvard University Press.

Snodgrass, J. G., and Yuditsky, T. (1996). Naming times for the Snodgrass and Vanderwart pictures. *Behav. Res. Methods Instrum. Comput.* 28, 516–536. doi:10.3758/BF03200540

Sowman, P. F., Crain, S., Harrison, E., and Johnson, B. W. (2012). Reduced activation of left orbitofrontal cortex precedes blocked vocalization: a magnetoencephalographic study. *J. Fluency Disord.* 37, 359–365. doi:10.1016/j.jfludis.2012.05.001

Tanaka, N., Liu, H., Reinsberger, C., Madsen, J. R., Bourgeois, B. F., Dworetzky, B. A., et al. (2013). Language lateralization represented by spatiotemporal mapping of magnetoencephalography. *Am. J. Neuroradiol.* 34, 558–563. doi:10.3174/ajnr.A3233

Travis, L. E. (1931). *Speech Pathology*. New York, NY: D. Appleton and Co.

Tzourio-Mazoyer, N., Landeau, B., Papathanassiou, D., Crivello, F., Etard, O., Delcroix, N., et al. (2002). Automated anatomical labeling of activations in SPM using a macroscopic anatomical parcellation of the MNI MRI single-subject brain. *Neuroimage* 15, 273–289. doi:10.1006/nimg.2001.0978

Watkins, K. E., Smith, S. M., Davis, S., and Howell, P. (2008). Structural and functional abnormalities of the motor system in developmental stuttering. *Brain* 131, 50–59. doi:10.1093/brain/awm241

Webster, W. G. (1985). Neuropsychological models of stuttering – I. Representation of sequential response mechanisms. *Neuropsychologia* 23, 263–267. doi:10.1016/0028-3932(85)90110-1

Webster, W. G. (1986). Neuropsychological models of stuttering – II. Interhemispheric interference. *Neuropsychologia* 24, 737–741. doi:10.1016/0028-3932(86)90014-X

Webster, W. G. (1997). "Principles of human brain organization related to lateralization of language and speech motor functions in normal speakers and stutterers,"

in *Speech Production: Motor Control, Brain Research and Fluency Disorders: Proceedings of the Third International Conference on Speech Motor Production and Fluency Disorders*, eds W. Hulstijn, H. F. M. Peters, and P. Van Leishout (Amsterdam: Elsevier), 119–139.

Webster, W. G., and Poulos, M. (1987). Handedness distributions among adults who stutter. *Cortex* 23, 705–708. doi:10.1016/S0010-9452(87)80062-X

Weiller, C., Isensee, C., Rijntjes, M., Huber, W., Muller, S., Bier, D., et al. (1995). Recovery from Wernicke's aphasia: a positron emission tomographic study. *Ann. Neurol.* 37, 723–732. doi:10.1002/ana.410370605

Yairi, E., and Ambrose, N. (1992). A longitudinal study of stuttering in children: a preliminary report. *J. Speech Hear. Res.* 35, 755–760.

Yairi, E., and Ambrose, N. G. (1999). Early childhood stuttering I: persistency and recovery rates. *J. Speech Lang. Hear. Res.* 42, 1097–1112.

Yairi, E., Ambrose, N. G., and Niermann, R. (1993). The early months of stuttering: a developmental study. *J. Speech Hear. Res.* 36, 521–528.

Conflict of Interest Statement: The authors declare that the research was conducted in the absence of any commercial or financial relationships that could be construed as a potential conflict of interest.

Received: 01 October 2013; accepted: 09 May 2014; published online: 28 May 2014.
Citation: Sowman PF, Crain S, Harrison E and Johnson BW (2014) Lateralization of brain activation in fluent and non-fluent preschool children: a magnetoencephalographic study of picture-naming. Front. Hum. Neurosci. ***8****:354. doi: 10.3389/fnhum.2014.00354*
This article was submitted to the journal Frontiers in Human Neuroscience.

frontiers in
HUMAN NEUROSCIENCE

METHODS ARTICLE
published: 23 May 2014
doi: 10.3389/fnhum.2014.00338

Encoding cortical dynamics in sparse features

Sheraz Khan[1,2,3]*, Julien Lefèvre[4], Sylvain Baillet[5], Konstantinos P. Michmizos[1,2,3], Santosh Ganesan[1,3], Manfred G. Kitzbichler[1,3,6], Manuel Zetino[1,3], Matti S. Hämäläinen[1], Christos Papadelis[7,8†] and Tal Kenet[1,3†]

[1] *Athinoula A. Martinos Center for Biomedical Imaging, Massachusetts General Hospital/Harvard Medical School/Massachusetts Institute of Technology, Charlestown, MA, USA*
[2] *McGovern Institute, Massachusetts Institute of Technology, Cambridge, MA, USA*
[3] *Department of Neurology, Massachusetts General Hospital, Harvard Medical School, Boston, MA, USA*
[4] *Aix Marseille Université, CNRS, ENSAM, Université de Toulon, LSIS UMR 7296, Marseille, France*
[5] *Montreal Neurological Institute, McGill University, Montreal, QC, Canada*
[6] *Behavioural and Clinical Neuroscience Institute, University of Cambridge, Cambridge, UK*
[7] *BabyMEG Facility, Fetal-Neonatal Neuroimaging and Developmental Science Center, Boston Children's Hospital, Harvard Medical School, Boston, MA, USA*
[8] *Division of Newborn Medicine, Boston Children's Hospital, Harvard Medical School, Boston, MA, USA*

Edited by:
Hubert Preissl, University of Tübingen, Germany

Reviewed by:
Rathinaswamy Bhavanandhan Govindan, Children's National Medical Center, USA
Habib Ammari, École Normale Supérieure, France

****Correspondence:***
Sheraz Khan, Athinoula A. Martinos Center for Biomedical Imaging, Massachusetts General Hospital/Harvard Medical School/Massachusetts Institute of Technology, 1115-Q, 149 13th Street, Charlestown, MA 02129, USA
e-mail: sheraz@nmr.mgh.harvard.edu

† Christos Papadelis and Tal Kenet have contributed equally to this work.

Distributed cortical solutions of magnetoencephalography (MEG) and electroencephalography (EEG) exhibit complex spatial and temporal dynamics. The extraction of patterns of interest and dynamic features from these cortical signals has so far relied on the expertise of investigators. There is a definite need in both clinical and neuroscience research for a method that will extract critical features from high-dimensional neuroimaging data in an automatic fashion. We have previously demonstrated the use of optical flow techniques for evaluating the kinematic properties of motion field projected on non-flat manifolds like in a cortical surface. We have further extended this framework to automatically detect features in the optical flow vector field by using the modified and extended 2-Riemannian Helmholtz–Hodge decomposition (HHD). Here, we applied these mathematical models on simulation and MEG data recorded from a healthy individual during a somatosensory experiment and an epilepsy pediatric patient during sleep. We tested whether our technique can automatically extract salient dynamical features of cortical activity. Simulation results indicated that we can precisely reproduce the simulated cortical dynamics with HHD; encode them in sparse features and represent the propagation of brain activity between distinct cortical areas. Using HHD, we decoded the somatosensory N20 component into two HHD features and represented the dynamics of brain activity as a traveling source between two primary somatosensory regions. In the epilepsy patient, we displayed the propagation of the epileptic activity around the margins of a brain lesion. Our findings indicate that HHD measures computed from cortical dynamics can: (i) quantitatively access the cortical dynamics in both healthy and disease brain in terms of sparse features and dynamic brain activity propagation between distinct cortical areas, and (ii) facilitate a reproducible, automated analysis of experimental and clinical MEG/EEG source imaging data.

Keywords: motion field, optical flow, MEG source imaging, Helmholtz–Hodge decomposition, epilepsy

1. INTRODUCTION

MEG and EEG are the most direct correlates of neural currents measured externally (Baillet et al., 2001). Recent advances in both hardware and software (i.e., increase in number of sensors, faster microprocessors, and more accurate cortical surface reconstructions) have led to significant enhancement in the temporal and spatial resolution of these methods, which can now reach, sub-millisecond and sub-centimeter levels respectively (Murray et al., 2008; Papadelis et al., 2009). MEG and EEG measure the magnetic and electric correlates of intracranial currents respectively. In order to estimate the location and time-course of these neural current generators, we need to solve an ill-posed and non-unique inverse problem. The non-uniqueness of the inverse problem is a result of the non-triviality in the quasi-static Helmholtz equation that links the intra-cranial current sources to the observed extra-cranial fields. Spatiotemporal distributed source solutions, like minimum-norm estimate (MNE), of MEG/EEG have been proposed to overcome this non-triviality (Dale and Sereno, 1993; Hämäläinen and Ilmoniemi, 1994). The resulting current distribution incorporates the anatomical information for each individual brain from the magnetic resonance imaging (MRI), and calculates the time-course of source distributions usually constrained to the cortex. These MNE solvers leads to spatiotemporal linear solutions, and have been extensively used in the neuroimaging community for their relatively accurate source localizations and robustness to the noise levels normally present in MEG/EEG data sets.

This type of analysis leads to a huge amount of high-dimensional data containing large information in both time and

space. Current approaches normally relies on studying cortical current variations at selected short latencies or by subtracting experimental conditions (e.g., standard minus deviant) to find features of interest in both space and time. These approaches allow mapping the local traveling of spatiotemporal cortical current activations on the cortical manifold. This propagation of brain activity via surface connections may represent propagating waves of cortical activity, which can emerge, transverse, or contract on the cortical surface (Ermentrout and Kleinfeld, 2001; Roxin et al., 2005; Gramfort et al., 2011).

The extraction of salient features mapping the spatiotemporal propagation of brain activity across different cortical regions relies so far on the expertise of neuroscience investigators or clinicians, who visually identify and quantify these patterns by using statistical tools. However, this procedure remains problematic since the statistical models are prone to subjective bias of the investigator. There is a definite need for methods that allow the automatic and *a priori* extraction of features of interest in evolving cortical dynamics and mapping in an automatic fashion the propagating activity between different cortical regions.

In this paper, we propose a novel method to overcome these difficulties using mathematical formalism we described previously (Lefèvre and Baillet, 2008; Khan et al., 2011). Our method extracts the spatiotemporal dynamics of EEG/MEG cortical sources using a combination of 2-Riemannian optical flow and Helmholtz–Hodge decomposition (HHD) on a highly-curved cortical manifold. The optical flow is a computer vision technique that represents the apparent motion in the time series of images. The HHD can automatically extract salient features from the optical flow.

Mathematically; HDD decomposes optical flow into:

- a non-rotational component deriving from the gradient of a scalar potential U;
- a non-diverging component deriving from the rotational of a scalar potential A (resp. vectorial potential, in 3D); and
- an harmonic part $\mathbf{H}$, i.e., whose Laplacian vanishes.

In HHD, formalism features of interest are represented as critical points of scalar field U and A. Finding features as critical points in global field potential is much less sensitive to noise in the data and therefore less likely to get false positives (Khan, 2010). In comparison to current density, its spatiotemporal divergent component U yields more focal and compact representation of the cortical activity (Slater et al., 2008; Khan et al., 2011). In order to estimate the spatiotemporal propagation of brain activity, we should initially estimate and extract the features of interest using the diverging component U. Subsequently, HHD's harmonic part $\mathbf{H}$ can infer how the information propagates between cortical areas, by a vector field which is both irrotational and incompressible. This Laplacian vector field can explain causal effects exerted by one brain region onto another. Particularly this vector field is especially applicable in revealing dynamics, which occur briskly in time and over short distances on the cortical manifold.

The detection of features in optical flow motion field using HHD has already been applied in many different imaging fields (Palit et al., 2005; Guo et al., 2006). For instance, it is used in cardiac video analysis, to detect features in cardiac motion fields that reflect pathological activity in the dynamics of cardiac electrical activity. The proposed method is based on previous work done by our group (Lefèvre and Baillet, 2008) where we introduced a variational method to estimate the optical flow on non-flat surfaces using a Riemannian formulation.

This previously proposed technique was used to analyze the global dynamics of cortically-distributed source images obtained from MEG or EEG data with also limited quantification of local dynamics (Lefèvre and Baillet, 2009). It was recently extended by introducing a new formalism to detect local features of the optical flow of cortical dynamics using a modified and extended approach to HHD (Slater et al., 2008; Khan et al., 2011).

This paper is structured as following: the Riemannian framework for optical flow on non-flat surfaces is first briefly introduced. The HHD formalism on 2-Riemannian manifolds will be presented next. Lastly, the application of HHD on simulated and human MEG data will be presented. The methods discussed in this paper are implemented in MatLab and are available for download as plugin to Brainstorm (MEG/EEG data processing software) (Tadel et al., 2011) at http://neuroimage.usc.edu/brainstorm. These methods will also soon be available for MNE–Python framework (Gramfort et al., 2014).

2. MATERIALS AND METHODS

The HHD-based feature detection technique consists of three distinct steps.

- First the optical flow of distributed MEG/EEG MNE estimates is computed on the cortical manifold. In Section 2.1, we will briefly introduce optical flow and its mathematical formulation.
- In the second step, HHD is applied on optical flow computed previously. We will present HHD framework in Section 2.2 and concisely describe its axioms.
- Lastly, detecting the feature of interest in cortical dynamics now becomes the simple problem of identifying critical points in HHD scalar potential U. The traveling cortical dynamics can be tracked by vectors having highest norm in vector field H (see Section 2.3 for details).

2.1. OPTICAL FLOW

We have introduced the concept of optical flow on a 2-Riemannian manifold (Lefèvre and Baillet, 2008), and we shall briefly summarize the approach as follows. Under the seminal hypothesis of the conservation of a scalar field I along streamlines, defined on a surface $\mathcal{M}$, the *optical flow* $\mathbf{V}$ is a vector field that satisfies:

$$\partial_t I + g(\mathbf{V}, \nabla_{\mathcal{M}} I) = 0. \quad (1)$$

Note that the scalar product $g(.,.)$ is modified by the local curvature of $\mathcal{M}$, the domain of interest. The solution to Equation (1) is not unique as long as the components of $\mathbf{V}(p, t)$ orthogonal to $\nabla_{\mathcal{M}} I$ are left unconstrained. This so-called "aperture problem" has been addressed by a large number of methods using e.g., regularization approaches. These latter approaches may be formalized as the minimization problem of an energy functional, which both

includes the regularity of the solution and the agreement to the model:

$$\mathcal{E}(\mathbf{V}) = \int_{\mathcal{M}} \left[\frac{\partial I}{\partial t} + g(\mathbf{V}, \nabla_{\mathcal{M}} I)\right]^2 \mathrm{d}\mu + \lambda \int_{\mathcal{M}} \mathcal{C}(\mathbf{V})\mathrm{d}\mu. \quad (2)$$

Here, we considered a regularity factor operating quadratically on the gradient of the expected vector field:

$$\mathcal{C}(\mathbf{V}) = Tr({}^t\nabla\mathbf{V}.\nabla\mathbf{V}). \quad (3)$$

Note that in order to be an intrinsic tensor, the gradient of a vector field must be defined as the covariant derivative associated to the manifold $\mathcal{M}$. Due to space constraints, we need to refer to essential elements of differential geometry for more information on this notion (Do Carmo, 1993).

2.2. HELMHOLTZ–HODGE DECOMPOSITION ON 2-RIEMANNIAN MANIFOLD

Let us consider $\mathcal{M}$ as a surface (or manifold) parameterized by local charts (x_1, x_2). It is thus possible to obtain a normal vector at each surface point:

$$\mathbf{n}_p = \frac{\partial}{\partial x_1} \wedge \frac{\partial}{\partial x_2}.$$

Note that the normal vector does not depend on the choice of the parameterization (x_1, x_2). We then define the gradient and divergence operators through duality:

$$\mathrm{d}U(\mathbf{V}) = g(\nabla_{\mathcal{M}} U, \mathbf{V}),$$
$$\int_{\mathcal{M}} U \,\mathrm{div}_{\mathcal{M}}\mathbf{H} = -\int_{\mathcal{M}} g(\mathbf{H}, \nabla_{\mathcal{M}} U).$$

Finally, scalar and vectorial curl operators are obtained through:

$$\mathbf{Cu}_{\mathcal{M}} A = \nabla_{\mathcal{M}} A \wedge \mathbf{n},$$
$$\mathrm{cu}_{\mathcal{M}}\mathbf{H} = \mathrm{div}_{\mathcal{M}}(\mathbf{H} \wedge \mathbf{n}).$$

Again, these formulas are intrinsic expressions that do not depend on the parameterization of the surface.

Let us then reformulate results established in Polthier and Preuss (2003) for Riemannian manifolds. Given $\mathbf{V}$, a vector field in $\Gamma^1(\mathcal{M})$, there exists unique functions U and A in $L^2(\mathcal{M})$ and a vector field $\mathbf{H}$ in $\Gamma^1(\mathcal{M})$ such that:

$$\mathbf{V} = \nabla_{\mathcal{M}} U + \mathbf{Cu}_{\mathcal{M}} A + \mathbf{H}, \quad (4)$$

with

$$\mathbf{cu}_{\mathcal{M}}(\nabla_{\mathcal{M}} U) = 0, \qquad \mathrm{div}_{\mathcal{M}}(\mathbf{Cu}_{\mathcal{M}} A) = 0,$$
$$\mathrm{div}_{\mathcal{M}}\mathbf{H} = 0, \qquad \mathbf{cu}_{\mathcal{M}}\mathbf{H} = 0.$$

Following classical constructions, U and A minimize the two following functionals:

$$\int_{\mathcal{M}} ||\mathbf{V} - \nabla_{\mathcal{M}} U||^2, \qquad \int_{\mathcal{M}} ||\mathbf{V} - \mathbf{Cu}_{\mathcal{M}} A||^2,$$

where $||\cdot||$ is the norm associated to the Riemannian metric $g(.,.)$. These two functionals are convex and therefore have a minimum on $L^2(\mathcal{M})$ satisfying:

$$\forall \phi \in L^2(\mathcal{M}), \int_{\mathcal{M}} g(\mathbf{V}, \nabla_{\mathcal{M}}\phi) = \int_{\mathcal{M}} g(\nabla_{\mathcal{M}} U, \nabla_{\mathcal{M}}\phi), \quad (5)$$

$$\forall \phi \in L^2(\mathcal{M}), \int_{\mathcal{M}}, g(\mathbf{V}, \mathbf{Cu}_{\mathcal{M}}\phi) = \int_{\mathcal{M}} g(\mathbf{Cu}_{\mathcal{M}} A, \mathbf{Cu}_{\mathcal{M}}\phi). \quad (6)$$

Through $(\phi_1, \ldots, \phi_n)$ as basis functions, we may write $\mathbf{U} = (U_1, \ldots, U_n)^T$, $\mathbf{A} = (A_1, \ldots, A_n)^T$, and Equations (5) and (6) read, using array notations:

$$\left[\int_{\mathcal{M}} g(\nabla_{\mathcal{M}}\phi_i, \nabla_{\mathcal{M}}\phi_j)\right]_{i,j} \mathbf{U} = \left[\int_{\mathcal{M}} g(\mathbf{V}, \nabla_{\mathcal{M}}\phi_i)\right]_i, \quad (7)$$

$$\left[\int_{\mathcal{M}} g(\mathbf{Cu}_{\mathcal{M}}\phi_i, \mathbf{Cu}_{\mathcal{M}}\phi_j)\right]_{i,j} \mathbf{A} = \left[\int_{\mathcal{M}} g(\mathbf{V}, \mathbf{Cu}_{\mathcal{M}}\phi_i)\right]_i. \quad (8)$$

The harmonic component $\mathbf{H}$ of vector field $\mathbf{V}$ is simply obtained through:

$$\mathbf{H} = \mathbf{V} - \nabla_{\mathcal{M}} U - \mathbf{Cu}_{\mathcal{M}} A. \quad (9)$$

2.3. FEATURE DETECTION AS CRITICAL POINTS OF HHD POTENTIALS

The critical points of a vector field are often classified depending on the eigenvalues of the Jacobian matrix defined locally in a vector field. In our case, however, critical points of the flow can be found as local extrema of the potentials A and U. Finding features as critical points on global potential fields is much less sensitive to noise in the data and therefore is less susceptible to false positives, than with methods using local Jacobian eigenvalues (Tong et al., 2003). Moreover unlike eigenvalues methods, HHD do not pre-specify the number of features.

A sink (resp. a source) corresponds to a local minimum (resp. maximum) of U. Similarly, a counter-clockwise (resp. clockwise) vortex may be detected through a local minimum (resp. maximum) of A. Detection of traveling cortical activity on the surface can be performed by tracking vector $\mathbf{H}$ having largest norm.

3. RESULTS

We will now present the application of HHD on one simulated and two actual MEG datasets. In Section 3.1 under a simulated scenario, HHD is used to track and encode cortical activity as it emerges from the somatosensory cortex, traveling along the central sulcus, and receding in the inferior frontal gyrus. The first MEG dataset presented in Section 3.2 is obtained from a median nerve stimulation paradigm that consists of a train of electrical stimuli applied on the wrist of a healthy adult individual. It is a typical experimental paradigm to elicit activity within the primary somatosensory cortex. The second MEG dataset shown in Section 3.3 is from a pediatric epilepsy patient with tuberous sclerosis complex. In this dataset, we track the propagation of the epileptogenic activity within the irritative zone.

3.1. SIMULATION DATA

The use of HHD to address the quantitative and qualitative evaluation of this technique is illustrated below.

3.1.1. Generation

The brain surface from Freesurfer's FsAverage was selected to demonstrate the applicability of the method on the cortical manifold. This surface consisted of 10,242 vertices and 20,480 triangles. A source on this manifold was generated in the vicinity of the central sulcus, also known as the primary somatosensory area (S1). This source was grown to a patch of 5 cm^2 (geodesic area) in five time steps. Subsequently, a constant vector field was defined in time from the vectorial heat equation. An advection equation (Lefèvre and Baillet, 2008) was used to transverse this patch on the manifold. Finally, this patch was contracted in five time steps in the vicinity of the inferior frontal gyrus. The results of this simulation are presented in **Figure 1**. The three stages of the source evolution are shown as **Figures 1A–C**.

3.1.2. Analysis

We first applied the optical flow on this simulated activity. Optical flow transformed the dynamics of the source's evolution in terms of the motion vector fields that were emerging, traversing, and receding. This optical flow computation was performed in the MNE–Python framework and took 10.75 s to compute. We then applied HHD to the optical flow at each time step, which detects three main features corresponding to the three stages of the simulation. HHD took 30.36 s to decompose optical flow in the discrete feature set. The simulation was performed on a workstation having a Dual Octa Core Xeon CPUs (32 Threads) with 64 GB of RAM.

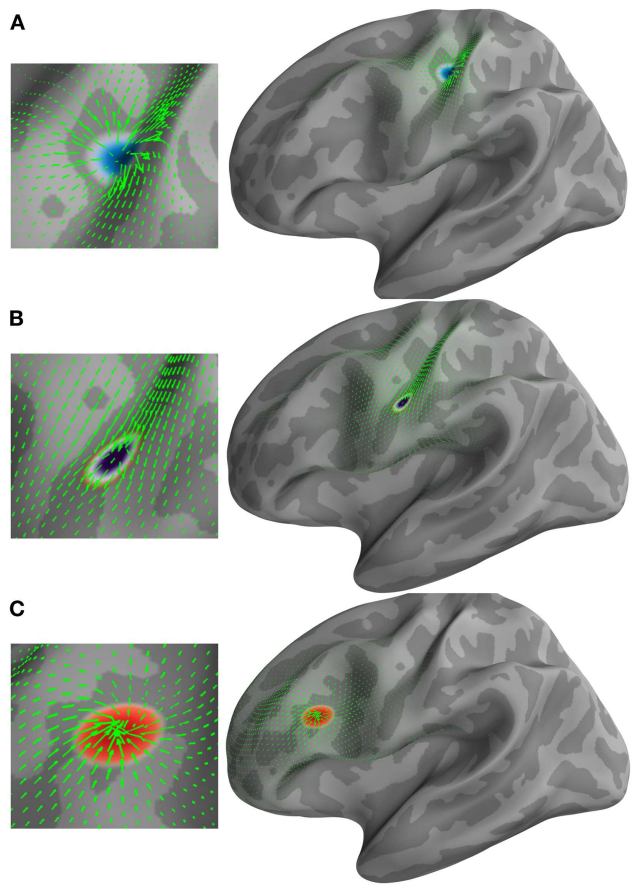

FIGURE 1 | Examples of different types of vector fields (green arrows) and their corresponding *U* and (*H*) HHD components. (A) Emerging source represented by a minima in the scalar potential *U*. **(B)** Traveling source detected by (*H*). **(C)** Receding source represented by a maxima in the scalar potential *U*.

3.1.3. Results

Figure 1 shows the applicability of HHD on the distributed current density maps for three different source configurations: (A) an emerging source; (B) a moving source having constant velocity; and (C) a descending source (sink). HHD automatically detects these three features from optical flow as critical points in U and **H**. A source represented by a minima in the scalar potential U (texture colormap in blue) is shown in **Figure 1A**. The vector field (green arrows) represents optical flow computed earlier. It is indicated in **Figure 1A** that HHD is able to capture the growing dynamics of the cortical activity. In **Figure 1B**, traveling activity is tracked by the highest norm vectors in field **H**. The texture colormap represents the norm of H, where the highest norm is shown with the dark violet texture map. In **Figure 1C**, receding cortical dynamics are captured by a maxima in the scalar potential U. This texture colormap represents U with a maxima shown in red. Again, the vector field is shown with green arrows representing optical flow.

3.2. FEATURE ANALYSIS OF EXPERIMENTAL MEG SOMATOSENSORY DATA

3.2.1. Experiment

MEG data was recorded from a 28-year-old healthy female individual at the MEG laboratory of the Center for Mind/Brain Sciences (CIMeC), University of Trento, Italy. During the experiment, the median nerves of her right and left wrists were electrically stimulated transcutaneously. Approval was obtained from the University of Trento Ethics Committee, Italy, and the subject gave her written informed consent before the experiment. Constant current stimuli with a duration of 0.2 ms, and a pseudo-randomized inter-stimulus interval of 250 ± 50 ms were applied to the subject. Before the start of the experiment, we measured two basic intensity thresholds for each of the subject's wrists. The two parameters were the motor threshold (MTH), defined as the minimal stimulus intensity needed to produce thumb twitching, and the sensory threshold (STH), defined as the minimal stimulus intensity at which the subject was just able to feel a train of stimulus pulses. The stimuli were delivered either to the right or to the left wrist with two intensity levels of $M = MTH + 0.25\,\Delta$ and $S = STH + 0.25\,\Delta$, where $\Delta = MTH - STH$. Here, we used only the data from the right median nerve stimulation and the M intensity level. More details about the experimental design can be found in Papadelis et al. (2012).

Somatosensory evoked fields (SEFs) were recorded at a sampling rate of 5 kHz by using a 306-channel (204 first order planar gradiometers, 102 magnetometers) VectorView MEG system (Elekta-Neuromag Ltd., Helsinki, Finland) placed inside a magnetically shielded room (AK3B, Vacuumschmelze, Hanau, Germany). Hardware filters were adjusted to band-pass the MEG signal in the frequency range of 0.01–1000 Hz. Data from 200 trials were used in this study.

3.2.2. Data analysis

To compensate for head movements during the measurements and suppressing external magnetic disturbances, the signal space separation (SSS) algorithm (Taulu and Simola, 2006), as implemented with the MaxFilter software (Elekta-Neuromag), was performed offline on the raw MEG data. The corrected MEG data were then filtered offline in the band of 0.1–150 Hz and epoched from −50 to 200 ms relative to the stimulus onset. Trials contaminated with artifacts were excluded from further processing. In total, 160 trials survived the rejection criteria. These trials were baseline corrected and then averaged. The subject's MRI was processed using FreeSurfer; cortical and head surfaces were extracted. Cortical surface was downgraded to 50,003 points and elementary current dipoles were positioned at the surface of the cortex of the subject. The multi-sphere forward model was computed and the standard minimum-norm was used to estimate cortical currents. The preprocessing and generation of both the forward and inverse solution was done in Brainstorm (Tadel et al., 2011). The MNE solution was computed at every point within the time window that represents the N20 component (from 15 to 25 ms) (see **Figure 2**, upper panel). The N20 component represents the first cortical response to the electrical stimulation of the median nerve. Optical flow was estimated from the minimum-norm data. HHD was then applied on this optical flow to detect sparse features in cortical dynamics. The computation of optical flow took 50.33 s whereas HHD took 123.73 s on the workstation mentioned in Section 3.1.2. This application was done in the MatLab implementation of the HHD.

3.2.3. Results

Figure 2 shows the applicability of HHD on the distributed source maps of MEG data recorded during the median nerve stimulation experiment. Our method reveals the diverging and contracting cortical mechanisms in the primary somatosensory cortex. Brain responses during N20 were automatically decomposed into two features: a source and a sink.

In **Figure 2**, the upper panel shows the butterfly plot of somatosensory evoked fields (SEFs). Two features identified by HHD are shown in the middle panel of **Figure 2**; an emerging source at 17.3 ms (MNI: −46.74, −30.17, 66.84) and a descending source (sink) at 23.2 ms (MNI: −55.86, −22.26, 51.20). The green arrows represent the motion field of the cortical dynamics as

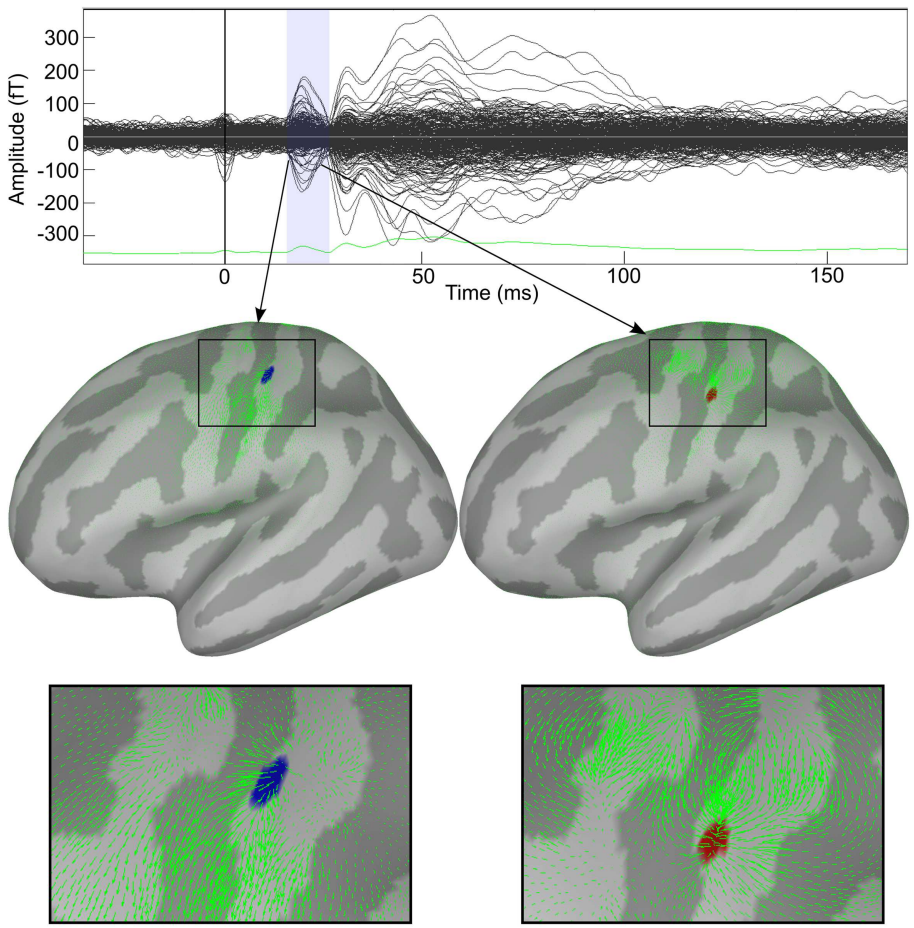

FIGURE 2 | Decomposition of cortical activity in a series of dynamic features. Response to median nerve stimulation of the right wrist. Upper panel shows the butterfly plot of somatosensory evoked fields (SEFs). Two features identified by HHD are shown in the middle panel. Bottom panel shows zoom view of the detected features.

estimated by the optical flow. HHD reveals that the first cortical responses appear at the top of S1 in the central sulcus, travels down the sulcus, and then sinks down at lower edge of the sulcus. The bottom panel presents a zoom up view of these two features. HHD reduces the size of the dataset from $50{,}003 \times 50$ (spatial dimension $\times$ temporal dimension) to two main features. This example presents the concept of our methodology to obtain a compact representation of cortical activity during a cognitive experiment.

3.3. HHD CHARACTERIZATION OF EPILEPTIC ACTIVITY

Our second application of HHD is on MEG data acquired from a subject having clinical history of refractory epilepsy. In this application, we will focus on the property of the U component of HHD, which allows for the detection of activity that changes rapidly in both time and space.

3.3.1. Epileptic data

The data was recorded from a 20-month-old boy, who presented his first seizure at the age of 3 months, with refractory epilepsy as a result of TSC. The patient had multiple subcortical tubers identified on his MRI as patchy areas of T2 prolongation, stable over time (see **Figure 3**). Long-term monitoring revealed 54 seizures in total (46 electroclinical and 8 electrographic seizures) with duration of 10–44 s. The seizure onset was localized at the right posterior quadrant (electrodes P8, O2, P4, T8, and C4). Routine and ambulatory EEG has indicated frequent interictal sharp waves at electrodes C4, Pz, P4, and P8, as well as slowing at the right posterior quadrant.

MEG data were recorded for 45 min during sleep at the BabyMEG facility located at the Radiology Suite of Boston's Children Hospital (Waltham, MA, USA). MEG recordings were performed using a 74-sensor MEG system especially designed for pediatric use ("babySQUID" – Tristan Technologies Inc., San Diego, CA, USA). The babySQUID system is accommodated in a single-layer magnetically shielded room (MSR). MEG data was sampled at 1024 samples per second. The sensor array of MEG was covering the right posterior quadrant. T1-weighted high-resolution magnetization-prepared rapid gradient echo (MPRAGE) structural images were acquired on a 3.0-T Siemens Trio whole body MR scanner (Siemens Medical Systems, Erlangen, Germany) using a 32 channel head coil. Details about the experimental procedure can be found elsewhere (Papadelis et al., 2013). Research MEG and MRI data were acquired and analyzed after explicit parental consent under a protocol approval by the Boston's Children Hospital institutional review board.

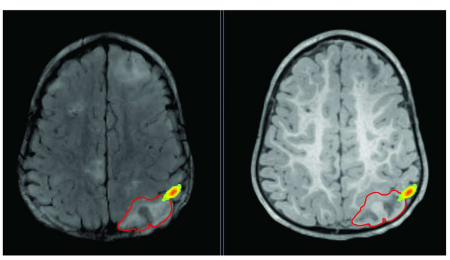

FIGURE 3 | Lesion is shown on T2 (left) and T1 (right) with red outline. Epileptic activity emerging from the edge of the lesion is shown as texture map.

3.3.2. Analysis

A high number of interictal spikes (>20) were identified by a board-certified epileptologist with a consistent spatiotemporal pattern indicating a focal source in the right posterior quadrant. The MEG data was then filtered offline in the band of 0.1–145 Hz. The subject's MRI was processed using brainvisa; cortical and head surfaces were extracted. To compute the forward solution, a boundary-element model (BEM) with a single compartment bounded by the skull's inner surface was assumed (Hämäläinen et al., 1993). The watershed algorithm was used to generate the inner skull surface triangulations from the high-resolution T1 MR images of each participant. The current distribution was estimated using the MNE by fixing the source orientation to be perpendicular to the cortex. The noise covariance matrix used to calculate the inverse operator was estimated from empty-room data. In order to reduce the bias of the MNEs toward superficial currents, we incorporated depth weighting by adjusting the source covariance matrix (Lin et al., 2006). To estimate the epileptic foci for the subject from HHD, a single sharp epileptic spike (**Figure 4A**) was selected. MNE was then computed for this spike in both volume and cortical space. Optical flow was calculated from the MNE estimated cortical currents at each time point during a time window shown in **Figure 4A**. HHD was computed by decomposing this optical flow and extracting the diverging scalar field U. The computation of optical flow and HHD took 34.7 s on the workstation mentioned in Section 3.1.

3.3.3. Results

In **Figure 4B**, MNE activity is presented in the volume at the two arrow points in **Figure 4A**. Average MNE activity on the cortical manifold at these two points is shown in **Figure 4C**. Critical points are then searched in the scalar field. This process results in finding two critical points in this time window, which corresponds to the signature features of this epileptic spike. A source in the posterior occipital region S1, from where the activity emerges, is shown in blue in **Figure 4D**. This activity sinks in the anterior parietal cortex in the vicinity of a subcortical tuber. This sinking activity is shown in red in **Figure 4D**. Finally, the diverging vector field $\nabla_M U$ is computed by taking the gradient of the scalar field U. In **Figure 4D**, the divergence vector field for this epileptic spike is shown with black arrows whereas color texture represents strength of U.

4. DISCUSSION

In this paper, we present the applicability of HHD to high-dimensional neuroimaging data. The HHD-based sparse feature encoding technique works in three steps. First, MNE is computed to estimate cortical current activity. Optical flow is then used to estimate the motion field of distributed cortical dynamics. Finally, the optical flow is decomposed into sparse and compact features using HHD and the neuroimaging feature extraction simplifies to the problem of finding critical points in the scalar potential U and by the highest norm vector of $\mathbf{H}$.

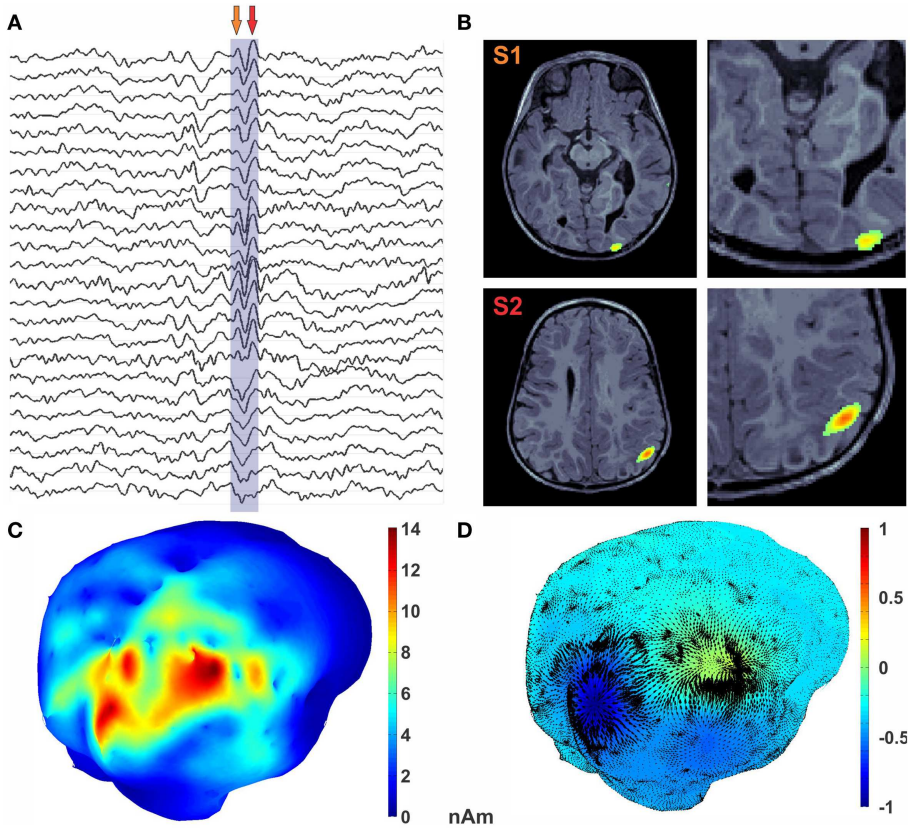

FIGURE 4 | Encoding of epileptic spike in diverging features. (A) MEG traces with epileptic spike marked. **(B)** MRI with MEG activity represented as the color texture. **(C)** Average MEG activity during the spike. **(D)** *U* HHD scalar potential is mapped onto the cortical surface using textured colors. The divergence part of vector flow of MEG sources is represented by green arrows at each vertex location. Critical points in the *U* map (shown with magenta sphere) reveal sources shown in dark blue and sink in red.

The method has been optimized for running in multi-core CPUs in order to decompose high-dimensional MEG/EEG data (~GB) in few seconds on a highly dense (~50,000 vertices) cortical mesh. The method provides a compact representation of the cortical dynamics. The method also allows to track the cortical activity as it appears, disappears, or travels on the cortical manifold. Moreover, HHD can also infer the information flow between cortical regions over short distances and times. Here, we present the application of our method on both simulated and actual MEG data sets.

In the simulated scenario, we generated synthetic cortical activity from the heat vector field and the advection equation. We then applied optical flow and HHD on this simulated data compacting the different stages of these dynamics in three sparse features. These results were in absolute accordance with our generated data. In the cognitive neuroscience application, we encoded spatiotemporal time varying maps of cortical activity during electrical stimulation of the median nerve. We showed that HHD and optical flow can compress cortical dynamics of N20 component in two distinct features; a source and a sink. This is in accordance to recent evidence in the literature of somatosensory processing which demonstrate that the earliest cortical response component (N20) after median nerve stimulation is generated by two generators located within S1 subdivisions and being active following a serial fashion (Inui et al., 2004; Papadelis et al., 2011). The application of our method in neuroscience data may enable the reproducibility of cognitive experiments across different sessions or research centers.

Our method can significantly contribute to epilepsy research, because it is able to detect and map the propagation of interictal spikes across time. MEG and EEG studies have so far shown that these two neuroimaging methods can non-invasively detect the propagation of spikes in epilepsy patients (Sutherling and Barth, 1989; Emerson et al., 1995; Tanaka et al., 2010). We also like to emphasize the importance of initial detection of the spike with a consistent spatiotemporal pattern indicating a focal source by an epileptologist, as the method seeds from it.

The investigation of epileptic spike propagation is important for the understanding of the pathophysiology of epilepsy and for the appropriate clinical decision during the presurgical evaluation of epileptic patients. Spike propagation can reflect neural networks associated with epilepsy (Spencer, 2002), while the propagation pattern of interictal spikes has been shown to be related to the outcome of epilepsy surgery (Hufnagel et al., 2000; Schulz et al.,

2000). In the application of HHD to epilepsy data, we exploited the sensitivity of the divergence component U to fast changes in space and time, such as these during a propagating interictal spike. The epileptic activity at the onset of the interictal spike can be sharp spatio-temporarily, and may easily be detected by HHD. We used HHD in deciphering these complex interictal spike dynamics. Using HHD, we identified where the spike initiated but also tracked its activity as it propagated on the cortical manifold. The application of HHD found two critical points on the cortical manifold, a source and a sink, both located at the abnormally developed tissue surrounding a tuber rather than the tuber itself. The epileptogenic activity was propagating across time along the borders of the tuber, and in any instance was crossing the tuber itself. Our findings are in agreement with previous studies indicating that in TSC patients with epilepsy the epileptogenic tissue is predominately localized in the surroundings of the cortical tubers (Weiner, 2004; Xiao et al., 2006; Major et al., 2009), and a single case study published in this issue (Hunold et al., 2014). The high sensitivity of our method allowed us to map the evolution of the epileptiform activity across time with respect to the location of the tuber. This critical, automatically extracted, spatiotemporal information of interictal spikes may provide more accurate information of spike propagation in epilepsy patients compared to the classical, observer-dependent methods, and thus it may be clinically useful in the presurgical evaluation of epilepsy patients.

5. CONCLUSION

We demonstrate the applicability of our HHD technique on high-dimensional electrophysiological data from neuroscience and clinical research data. Salient features of our technique, which are demonstrated by our results are: (i) sensitivity to spatiotemporal diverging cortical sources rapidly evolving in space and time (within few milliseconds), (ii) consideration of geometry of the cortical manifold on which the neural activity is evolving, (iii) automatic extraction of the spatiotemporal features, (iv) automatic characterization of the cortical activity propagation across different brain regions, (vi) visualization of the salient feature of cortical activity, and (vii) application in both cognitive and clinical neuroscience (i.e., propagation of epileptiform activity). Here, we present some of the possible applications of HHD in the neuroimaging field. We strongly believe that there are much more applications of our method in both neuroscience as well as clinical research. Further improvements of our method include: the discretization to higher-order finite element analysis, statistical analysis of the detected features, and the further reduction of the algorithm computational complexity. HHD is freely available as a plugin for major MEG processing suites (i.e., Brainstorm and MNE–Python) and readers are encouraged to use and extend the proposed method.

ACKNOWLEDGMENTS

This work was supported by the Nancy Lurie Marks Family Foundation (Sheraz Khan, Manfred G. Kitzbichler, Tal Kenet), Simons Foundation (Tal Kenet), NIBIB:5R01EB009048 (Matti S. Hämäläinen), P41RR014075 (Matti S. Hämäläinen), Senior-Scientist Salary Award from the Quebec Fund for Health Research (Sylvain Baillet), NIH 2R01EB009048-05 (Sylvain Baillet) and a Discovery Grant from the Natural Sciences and Engineering Research Council of Canada (Sylvain Baillet).

REFERENCES

Baillet, S., Mosher, J., and Leahy, R. (2001). Electromagnetic brain mapping. *IEEE Signal Process. Mag.* 18, 14–30. doi:10.1109/79.962275

Dale, A. M., and Sereno, M. I. (1993). Improved localization of cortical activity by combining EEG and MEG with MRI cortical surface reconstruction: a linear approach. *J. Cogn. Neurosci.* 5, 162–176. doi:10.1162/jocn.1993.5.2.162

Do Carmo, M. (1993). *Riemannian Geometry*. Boston: Birkhäuser.

Emerson, R. G., Turner, C. A., Pedley, T. A., Walczak, T. S., and Forgione, M. (1995). Propagation patterns of temporal spikes. *Electroencephalogr. Clin. Neurophysiol.* 94, 338–348. doi:10.1016/0013-4694(94)00316-D

Ermentrout, G. B., and Kleinfeld, D. (2001). Traveling electrical waves in cortex: insights from phase dynamics and speculation on a computational role. *Neuron* 29, 33–44. doi:10.1016/S0896-6273(01)00178-7

Gramfort, A., Luessi, M., Larson, E., Engemann, D. A., Strohmeier, D., Brodbeck, C., et al. (2014). MNE software for processing MEG and EEG data. *Neuroimage* 86, 446–460. doi:10.1016/j.neuroimage.2013.10.027

Gramfort, A., Papadopoulo, T., Baillet, S., and Clerc, M. (2011). Tracking cortical activity from M/EEG using graph cuts with spatiotemporal constraints. *Neuroimage* 54, 1930–1941. doi:10.1016/j.neuroimage.2010.09.087

Guo, Q., Mandal, M., Liu, G., and Kavanagh, K. (2006). Cardiac video analysis using Hodge-Helmholtz field decomposition. *Comput. Biol. Med.* 36, 1–20. doi:10.1016/j.compbiomed.2004.06.011

Hämäläinen, M., Hari, R., Ilmoniemi, R., Knuutila, J., and Lounasmaa, O. (1993). Magnetoencephalography: theory, instrumentation, and applications to noninvasive studies of the working human brain. *Rev. Mod. Phys.* 65, 413. doi:10.1103/RevModPhys.65.413

Hämäläinen, M. S., and Ilmoniemi, R. (1994). Interpreting magnetic fields of the brain: minimum norm estimates. *Med. Biol. Eng. Comput.* 32, 35–42. doi:10.1007/BF02512476

Hufnagel, A., Dümpelmann, M., Zentner, J., Schijns, O., and Elger, C. (2000). Clinical relevance of quantified intracranial interictal spike activity in presurgical evaluation of epilepsy. *Epilepsia* 41, 467–478. doi:10.1111/j.1528-1157.2000.tb00191.x

Hunold, A., Haueisen, J., Ahtam, B., Doshi, C., Harini, C., Camposano, S., et al. (2014). Localization of the epileptogenic foci in tuberous sclerosis complex: a pediatric case report. *Front. Hum. Neurosci.* 8:175. doi:10.3389/fnhum.2014.00175

Inui, K., Wang, X., Tamura, Y., Kaneoke, Y., and Kakigi, R. (2004). Serial processing in the human somatosensory system. *Cereb. Cortex* 14, 851–857. doi:10.1093/cercor/bhh043

Khan, S. (2010). *MEG Source Imaging and Dynamic Characterization*. Ph.D. thesis, Paris: Ecole Polytechnique X.

Khan, S., Lefèvre, J., Ammari, H., and Baillet, S. (2011). Feature detection and tracking in optical flow on non-flat manifolds. *Pattern Recognit. Lett.* 32, 2047–2052. doi:10.1016/j.patrec.2011.09.017

Lefèvre, J., and Baillet, S. (2008). Optical flow and advection on 2-Riemannian manifolds: a common framework. *IEEE Trans. Pattern Anal. Mach. Intell.* 30, 1081–1092. doi:10.1109/TPAMI.2008.51

Lefèvre, J., and Baillet, S. (2009). Optical flow approaches to the identification of brain dynamics. *Hum. Brain Mapp.* 30, 1887–1897. doi:10.1002/hbm.20781

Lin, F., Witzel, T., Ahlfors, S., Stufflebeam, S., Belliveau, J., and Hämäläinen, M. (2006). Assessing and improving the spatial accuracy in meg source localization by depth-weighted minimum-norm estimates. *Neuroimage* 31, 160–171. doi:10.1016/j.neuroimage.2005.11.054

Major, P., Rakowski, S., Simon, M. V., Cheng, M. L., Eskandar, E., Baron, J., et al. (2009). Are cortical tubers epileptogenic? Evidence from electrocorticography. *Epilepsia* 50, 147–154. doi:10.1111/j.1528-1167.2008.01814.x

Murray, M. M., Brunet, D., and Michel, C. M. (2008). Topographic ERP analyses: a step-by-step tutorial review. *Brain Topogr.* 20, 249–264. doi:10.1007/s10548-008-0054-5

Palit, B., Basu, A., and Mandal, M. (2005). Applications of the discrete Hodge-Helmholtz decomposition to image and video processing. *Lect. Notes Comput. Sci.* 3776, 497. doi:10.1007/11590316_78

Papadelis, C., Eickhoff, S. B., Zilles, K., and Ioannides, A. A. (2011). Ba3b and ba1 activate in a serial fashion after median nerve stimulation: direct evidence from

combining source analysis of evoked fields and cytoarchitectonic probabilistic maps. *Neuroimage* 54, 60–73. doi:10.1016/j.neuroimage.2010.07.054

Papadelis, C., Harini, C., Ahtam, B., Doshi, C., Grant, E., and Okada, Y. (2013). Current and emerging potential for magnetoencephalography in pediatric epilepsy. *J. Pediatr. Epilepsy* 2, 73–85. doi:10.3233/PEP-13040

Papadelis, C., Leonardelli, E., Staudt, M., and Braun, C. (2012). Can magnetoencephalography track the afferent information flow along white matter thalamocortical fibers? *Neuroimage* 60, 1092–1105. doi:10.1016/j.neuroimage.2012.01.054

Papadelis, C., Poghosyan, V., Fenwick, P. B., and Ioannides, A. A. (2009). Meg's ability to localise accurately weak transient neural sources. *Neurophysiol. Clin.* 120, 1958–1970. doi:10.1016/j.clinph.2009.08.018

Polthier, K., and Preuss, E. (2003). Identifying vector fields singularities using a discrete Hodge decomposition. *Vis. Math.* 3, 113–134. doi:10.1007/978-3-662-05105-4_6

Roxin, A., Brunel, N., and Hansel, D. (2005). Role of delays in shaping spatiotemporal dynamics of neuronal activity in large networks. *Phys. Rev. Lett.* 94, 238103. doi:10.1103/PhysRevLett.94.238103

Schulz, R., Lüders, H., Hoppe, M., Tuxhorn, I., May, T., and Ebner, A. (2000). Interictal EEG and ictal scalp EEG propagation are highly predictive of surgical outcome in mesial temporal lobe epilepsy. *Epilepsia* 41, 564–570. doi:10.1111/j.1528-1157.2000.tb00210.x

Slater, M., Pérez-Marcos, D., Ehrsson, H. H., and Sanchez-Vives, M. V. (2008). Towards a digital body: the virtual arm illusion. *Front. Hum. Neurosci.* 2:6. doi:10.3389/neuro.09.006.2008

Spencer, S. S. (2002). Neural networks in human epilepsy: evidence of and implications for treatment. *Epilepsia* 43, 219–227. doi:10.1046/j.1528-1157.2002.26901.x

Sutherling, W., and Barth, D. (1989). Neocortical propagation in temporal lobe spike foci on magnetoencephalography and electroencephalography. *Ann. Neurol.* 25, 373–381. doi:10.1002/ana.410250409

Tadel, F., Baillet, S., Mosher, J. C., Pantazis, D., and Leahy, R. M. (2011). Brainstorm: a user-friendly application for MEG/EEG analysis. *Comput. Intell. Neurosci.* 2011:879716. doi:10.1155/2011/879716

Tanaka, N., Hämäläinen, M. S., Ahlfors, S. P., Liu, H., Madsen, J. R., Bourgeois, B. F., et al. (2010). Propagation of epileptic spikes reconstructed from spatiotemporal magnetoencephalographic and electroencephalographic source analysis. *Neuroimage* 50, 217–222. doi:10.1016/j.neuroimage.2009.12.033

Taulu, S., and Simola, J. (2006). Spatiotemporal signal space separation method for rejecting nearby interference in MEG measurements. *Phys. Med. Biol.* 51, 1759. doi:10.1088/0031-9155/51/7/008

Tong, Y., Lombeyda, S., Hirani, A., and Desbrun, M. (2003). Discrete multiscale vector field decomposition. *ACM Trans. Graph.* 22, 445–452. doi:10.1145/882262.882290

Weiner, H. L. (2004). Tuberous sclerosis and multiple tubers: localizing the epileptogenic zone. *Epilepsia* 45, 41–42. doi:10.1111/j.0013-9580.2004.04009.x

Xiao, Z., Xiang, J., Holowka, S., Hunjan, A., Sharma, R., Otsubo, H., et al. (2006). Volumetric localization of epileptic activities in tuberous sclerosis using synthetic aperture magnetometry. *Pediatr. Radiol.* 36, 16–21. doi:10.1007/s00247-005-0013-1

Conflict of Interest Statement: The authors declare that the research was conducted in the absence of any commercial or financial relationships that could be construed as a potential conflict of interest.

Received: 10 March 2014; accepted: 05 May 2014; published online: 23 May 2014.
Citation: Khan S, Lefèvre J, Baillet S, Michmizos KP, Ganesan S, Kitzbichler MG, Zetino M, Hämäläinen MS, Papadelis C and Kenet T (2014) Encoding cortical dynamics in sparse features. Front. Hum. Neurosci. ***8****:338. doi: 10.3389/fnhum.2014.00338*
This article was submitted to the journal Frontiers in Human Neuroscience.

frontiers in
HUMAN NEUROSCIENCE

METHODS ARTICLE
published: 24 April 2014
doi: 10.3389/fnhum.2014.00266

Cerebral pressure passivity in newborns with encephalopathy undergoing therapeutic hypothermia

Rathinaswamy Bhavanandhan Govindan[1]*, An N. Massaro[2], Nickie N. Andescavage[2], Taeun Chang[3] and Adré du Plessis[1]

[1] *Division of Fetal and Transitional Medicine, Children's National Medical Center, Washington, DC, USA*
[2] *Division of Neonatology, Children's National Medical Center, Washington, DC, USA*
[3] *Department of Neurology, Children's National Medical Center, Washington, DC, USA*

Edited by:
Hubert Preissl, University of Tübingen, Germany

Reviewed by:
Hari Eswaran, University of Arkansas for Medical Sciences, USA
Srinivasan Vairavan, Philips Research North America, USA

****Correspondence:***
Rathinaswamy Bhavanandhan Govindan, Division of Fetal and Transitional Medicine, Children's National Medical Center, 111 Michigan Avenue North West, Washington, DC 20010, USA
e-mail: rgovinda@childrensnational.org

We extended our recent modification of the power spectral estimation approach to quantify spectral coherence. We tested both the standard and the modified approaches on simulated data, which showed that the modified approach was highly specific and sensitive to the coupling introduced in the simulation while the standard approach lacked these features. We also applied the modified and standard approaches to quantify the pressure passivity in 4 infants receiving therapeutic hypothermia. This was done by measuring the coupling between continuous cerebral hemoglobin differences and mean arterial blood pressure. Our results showed that the modified approach identified a lower pressure passivity index (PPI, percent time the coherence was above a predefined threshold) than the standard approach ($P = 0.0027$).

Keywords: cerebral oximetry, cerebral oxygen extraction, NIRS, spectral analysis, cerebral pressure autoregulation, neonatal encephalopathy, therapeutic hypothermia

1. INTRODUCTION

Cerebral pressure autoregulation buffers the changes in systemic mean arterial pressure (MAP) in order to regulate cerebral blood flow (CBF); in contrast its failure, cerebral pressure passivity (CPP), results in broad changes in CBF that track changes in MAP (Panerai et al., 1995). In normal subjects, CPP operates in a time frame of 5–20 s (0.05–0.25 Hz) and hence the frequency domain approach, namely spectral coherence is used to characterize CPP (Panerai et al., 1995, 1996; Panerai, 1998, 2008; Tsuji et al., 2000; O'Leary et al., 2009). Two continuous physiological signals needed to quantify CPP are MAP and CBF. Studies based on animal models have shown the hemoglobin difference, HbD (oxygenated hemoglobin minus de-oxygenated hemoglobin) acquired using near infrared spectroscopy (NIRS) is a reliable surrogate for CBF (Soul et al., 1998; Tsuji et al., 1998; O'Leary et al., 2009). To date, NIRS is the only device that provides a non-invasive continuous long-term measurement of changes in CBF at the bedside.

Spectral coherence is a technique that allows quantification of the relationship between changes in MAP and changes in CBF (or HbD). However, the spectral coherence approach is highly sensitive to the non-stationarities in the signals. Recently, a modification has been proposed to the power spectral estimation approach to mitigate the effect of non-stationarity in physiological signals. The modified approach taken in Govindan et al. (2013) is directly extended in the current work to quantify the spectral coherence. The performance of the standard coherence approach and the modified approach is discussed using simulated signals. Additionally, these approaches are applied to quantify CPP in newborns receiving hypothermia treatment for neonatal encephalopathy.

2. MATERIALS AND METHODS

2.1. STANDARD COHERENCE ESTIMATION

We used 10 min of HbD and MAP data to quantify CPP using the following steps (Halliday et al., 1995): Step 1: we partitioned the MAP and HbD data into disjointed time windows of 30 s. Step 2: for the data in each window, we calculated periodograms as the square of the magnitude of the Fourier transform of the signals and the cross-spectrum between the signals as the product of the Fourier transform of one signal and the complex conjugate of the Fourier transform of the second signal. Step 3: we averaged the periodograms and the cross-spectra over all the windows to get the estimate of the spectral quantities. We defined coherence as the ratio of the square of the magnitude of the estimate of the cross-spectrum to the product of the estimates of the power spectra of the two signals.

2.2. MODIFIED APPROACH

We modified the coherence estimation approach by dividing the data in 30 s epochs from each signal obtained in step 1 (as in the standard coherence estimation) by their standard deviations. Non-stationarities in the data would cause each epoch to have a different variance; as a result, the spectral estimates for non-stationary epochs would be a poor representation of the corresponding quantities; the normalization by the standard deviation would mitigate this spurious variability caused by the non-stationarity and allow a reasonable estimate of the coherence.

The confidence of the coherence estimate at 100α% is given by $1-(1-\alpha)^{1/(M-1)}$, where M is the number of 30 s epochs involved in the estimation of the coherence. To reliably quantify the coupling between HbD and MAP in the very low-frequency band

(0.05–0.25 Hz), a band that might show spurious coherence due to the contribution from very slow trends such as baseline changes in the signals, we set α to 0.999. For this value of α, the formula yielded a confidence limit of 0.384 for the coherence estimate for a 10 min window. Any value of coherence above this confidence limit was considered statistically significant.

2.3. NUMERICAL SIMULATION TO VALIDATE THE COHERENCE APPROACHES

We generated Gaussian distributed random numbers of the same number of sample size as the 10 min of HbD and MAP signals (6000) to validate the standard and the modified coherence approaches. We denote this time series as $x(t)$. We simulated two different scenarios: one to test the sensitivity and another to test the specificity of the two approaches. Since we expected the coupling between MAP and HbD to occur in the low-frequency band of 0.05–0.25 Hz, we bandpass filtered the noise $[x(t)]$ in the same band using 4th order Butterworth filter with zero-phase distortion. In scenario one, we modified the values of the filtered data at two different time instances as follows: between samples 1001 and 1500, we multiplied the filtered data by a factor of 400. In another instance we multiplied the values of the filtered data between samples 3001 and 4000 by a factor of 200. We denote the modified filtered signal as $y(t)$. We calculated coherence between $x(t)$ and $y(t)$ using the standard and modified approaches to determine which method better captured the coherence between signals.

In scenario 2, we generated an independent random series of 6000 samples. We modified the samples 1001–1500 in this series by multiplying them by a factor of 400. We denote this time series as $z(t)$. This scenario would mimic simultaneous spurious changes in both signals $[y(t)$ and $z(t)]$ not related to physiology. We calculated the coherence between the $z(t)$ and $y(t)$ generated in scenario 1 using both methods to determine which method better identified the spurious change.

We simulated 1000 realizations for each scenario and calculated coherence using the standard and modified approaches. For comparison, we considered the maximum coherence in the frequency band of 0.05–0.25 Hz from both approaches.

2.4. CLINICAL DATA

Continuous recordings of cerebral oximetry (NIRO 200, Hamamatsu Photonics, Hamamatsu, Japan) (HbO_2, Hb, total oxygenation index), blood pressure from an indwelling arterial line (Philips IntelliVue MP70, MA, USA), arterial oximetry (Masimo Corporation, CA, USA) from four newborns were collected in a time-locked manner at a rate of 1 kHz using a custom software developed in LabView (National Instruments, TX, USA). The newborns were receiving therapeutic hypothermia for encephalopathy according to the National Institute of Child Health and Human Development Protocol (Shankaran et al., 2005). Cerebral oximetry was obtained bilaterally, one from the left and another from the right fronto-temporal regions. We calculated HbD as HbO_2–Hb for each hemisphere. We calculated MAP for each cycle of the continuous blood pressure signal using a combination of the lowpass filtering and a peak detection approach. We resampled the MAP into uniformly sampled data using cubic spline at a sample rate of 10 Hz. We also down sampled the HbD signal to 10 Hz. All processing was done off-line using MATLAB (Mathworks, Inc). The study was approved by the Children's National Medical Center Institutional Review Board and informed consent was obtained from the parents of the patients.

2.5. ANALYSIS OF MAP AND HbD

We partitioned the MAP and HbD data into non-overlapping windows of 10 min duration. In each window, we calculated the coherence between MAP and HbD using both the standard and modified approaches. To compare the performance of the each approach, we calculated the pressure passivity index (PPI) as the percent time the data displayed significant coherence during the entire period. We compared the PPI obtained by the modified and standard approaches using the paired t-test. A value of $P < 0.05$ was considered statistically significant.

3. RESULTS

3.1. SIMULATION RESULTS

We displayed the results obtained from the simulation study in **Figure 1**. The standard approach displayed (**Figure 1A**) maximum coherence in the frequency band of 0.05–0.25 Hz only for 14% of the realizations for scenario 1; in contrary, the modified approach showed coherence in the same frequency band for all the realizations (see **Figure 1B**). The standard approach showed coherence in the 0.05–0.25 Hz band for about 52% of the realizations for scenario 2 while the modified approach showed coherence in none of the realizations (see **Figures 1C,D**). Note in scenario 1, we had incorporated coupling in all the realizations whereas in scenario 2 we did not incorporate coupling in any of the realizations.

3.2. CLINICAL RESULTS

We studied four newborns receiving therapeutic hypothermia for neonatal encephalopathy. Study monitoring was initiated within 10–20 h after birth. Infants underwent hypothermia treatment for 72 h, followed by gradual rewarming by 0.5°C/h over 6 h to normothermia. Two infants had favorable outcomes (survived with normal MRI) and the other two had adverse outcomes (death, $n = 1$ or severe deep nuclear gray matter injury on MRI, $n = 1$).

3.3. COHERENCE ANALYSIS OF MAP AND HbD SIGNALS

We displayed the results of coherence analysis of the MAP and HbD signals from two newborns that had favorable outcome in **Figure 2** and from newborns that had adverse outcome in **Figure 3**. We showed the maximum coherence between MAP and HbD in 0.05–0.25 Hz. From both approaches, the two infants that had favorable outcomes showed lower PPI values compared to the infants that had adverse outcomes ($P < 0.001$) (see insets in **Figures 2** and **3**). Further, the modified approach showed lower PPI values compared to the standard approach in most cases. For instance, subjects 2 and 3, had break in the recording between 45.5 and 49 h and 35 and 40 h, respectively. During these instances, the modified coherence did not detect any coupling between HbD and MAP. In contrast, the standard approach falsely detected coupling between HbD and MAP at the edges corresponding to the onset and end of the record breaks where there were no data (see

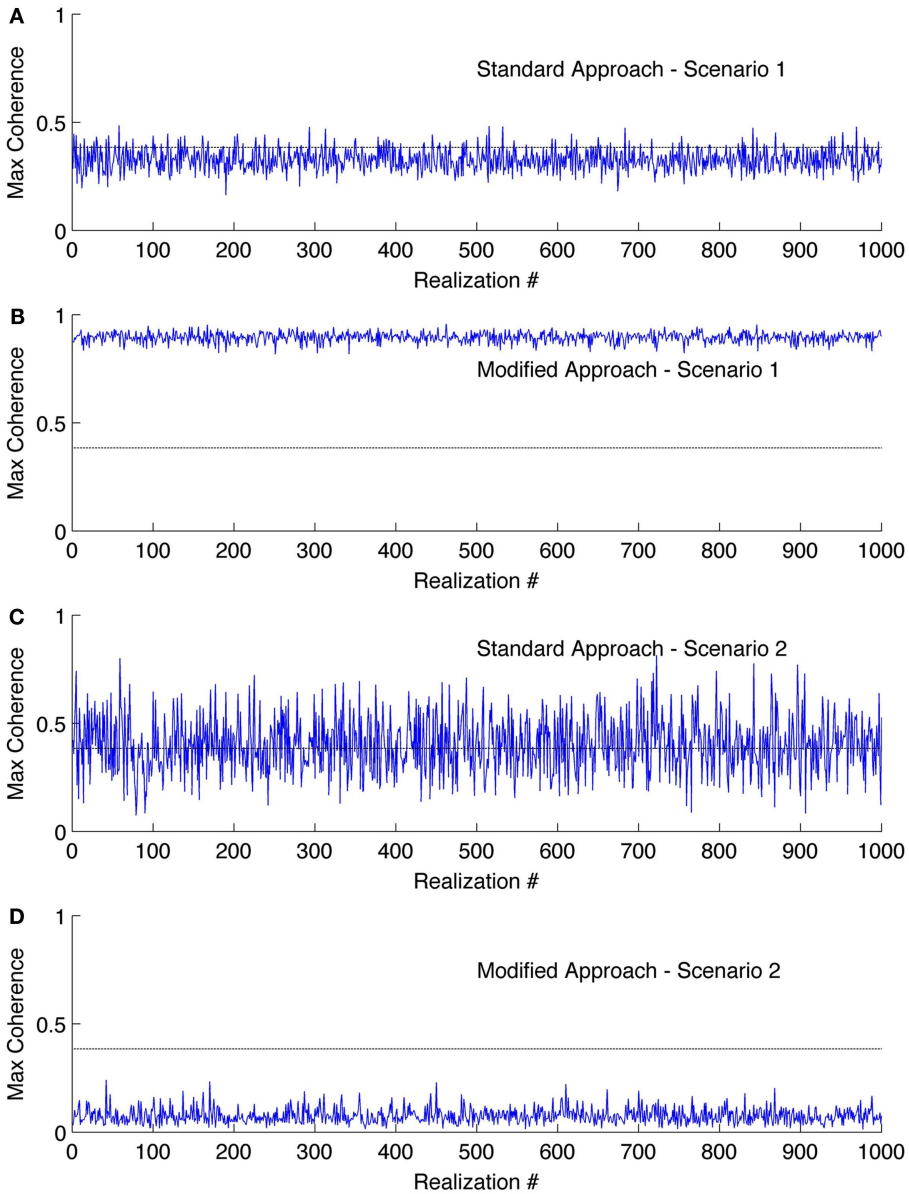

FIGURE 1 | Results of the coherence analysis of simulated data. Maximum coherence obtained in 0.05–0.25 Hz for scenario 1 using **(A)** standard approach and **(B)** the modified approach. Coherence obtained in 0.05–0.25 Hz for scenario 2 using **(C)** standard approach and **(D)** the modified approach. The horizontal line at the coherence value of 0.384 is the confidence limit for coherence estimate.

Figures 2C and **3B**, wherein coherence from both hemispheres exceeded the confidence limits around the break points). For example, in subject 2, the modified approach detected coherence only after the study was restarted at around 49 h, but only in the left hemisphere (see inset in **Figure 2C**) while the standard approach missed to detect this association (see inset in **Figure 2D**). Further, the standard approach detected coherence from both hemispheres when the recording was stopped at 45.5 h (see **Figure 2D**) but the modified approach did not show any coherence at this time point (see **Figure 2C**). We did not have enough number of PPI values to run the t-test independently for each hemisphere and assess the performance of the approaches. Hence, for each approach we combined the PPI values calculated for the left and right hemispheres and compared them using paired t-test. We found a significant difference ($P = 0.0027$) between the results obtained from both approaches with lower PPI values from the modified approach.

4. DISCUSSION

We extend our previous work on the modified spectral estimation approach (Govindan et al., 2013) to coherence estimation. Using numerical simulation we demonstrate that the modified approach has high sensitivity and specificity in characterizing the coherence between two signals. We discuss the application of this approach

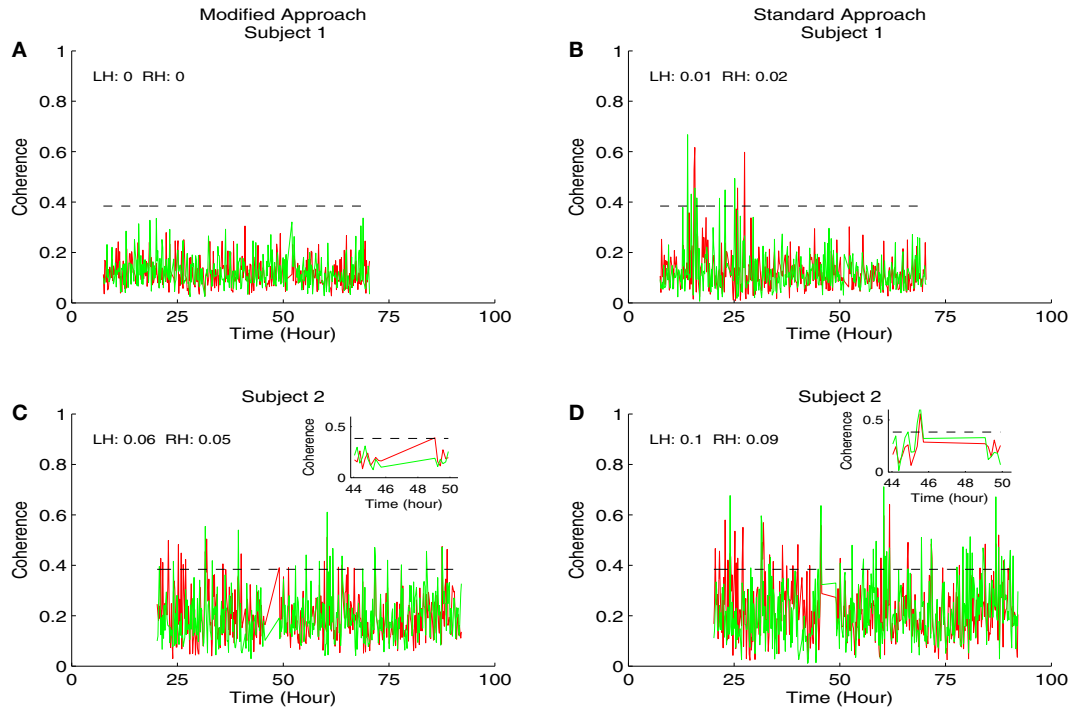

FIGURE 2 | Results of the coherence analysis of MAP and HbD from two newborns from favorable outcome group receiving hypothermia therapy for neonatal encephalopathy. The maximum coherence in 0.05–0.25 Hz was shown in all the plots from time since birth. Results from the modified approach were shown in the left side **(A,C)** and the results from the standard approach were shown in the right side **(B,D)**. Results from subject 1 were shown in **(A,B)** and the results from subject 2 were shown in **(C,D)**. In all the plots, the results from the left hemisphere (LH) were shown in red and the results from the right hemisphere (RH) were shown in green. Also the pressure passivity index (PPI) calculated for LH and RH was given in the inset. The horizontal line at the coherence value of 0.384 is the confidence limit for the coherence estimate. We displayed the insets in **(C,D)** for the portion of the results from the period where the study was stopped at 45.5 h and restarted at 49 h. At the onset of the break, the modified approach showed no significant coherence while the standard approach showed a significant coherence in both hemispheres. Similarly at 49 h after the study was restarted, the modified approach showed coherence only in the left hemisphere while at this point the standard approach showed no significant coherence.

to characterize PPI (a marker of cerebral pressure passivity) as a significant coupling between MAP and HbD.

Scenario 1 in our simulation mimics a surge in the signals that interrupts the detection of coupling between MAP and HbD. On the other hand, scenario 2 mimics a surge in the signals, which falsely characterizes the intact cerebral pressure autoregulation (absence of significant coupling between MAP and HbD) as pressure passivity. The surges introduced in our scenarios are designed to simulate changes in the signals caused by critical care events, for example, endotracheal tube suctioning (Limperopoulos et al., 2008). Such changes may have contributions from physiology, which in turn may affect the ongoing cerebral hemodynamics (cerebral autoregulation). Hence, the methods employed should be robust enough to avoid spurious quantification of CPP. Our numerical simulation results show that the standard approach to estimate coherence lacks sensitivity and specificity in quantifying the association between the two signals during physiologic changes resulting in signal surges. In contrast, the modified approach proposed in this work is highly sensitive and specific in quantifying the association between the signals.

Earlier studies have shown that in critically ill infants, the CPP is not a continuous phenomenon but rather fluctuates in time (Soul et al., 2007; Howlett et al., 2013). Further, infants displaying high PPI values are more likely to have significant cerebrovascular lesions. Thus, it is important to have a reliable method for monitoring CPP in high-risk patients being cared for in the intensive care unit. Perinatal hypoxic ischemic encephalopathy is a major cause of death and disability in children. Our preliminary results show that impaired autoregulation (higher PPI values) can be measured and quantified in HIE newborns who died or had significant MRI injury. In contrast, surviving newborns without MRI injury were observed to have low PPI. Further work is needed, and ongoing, to determine the evolution and importance of CPP in the pathogenesis of perinatal brain injury.

Cerebral pressure passivity identifies the brain unprotected against unstable systemic hemodynamic and oxygenation support. We hypothesize that a sequence of events occurs between the onset of a brain insult and the eventual development of irreversible brain injury. Broadly, this sequence consists of (1) failure of hemodynamic regulation, (2) functional failure (electrocortical dysfunction) followed by (3) failure of the oxygen metabolism as an immediate precursor to permanent structural damage. Failure of hemodynamic regulation is characterized by the PPI analysis. The functional (electrocortical) failure can be studied

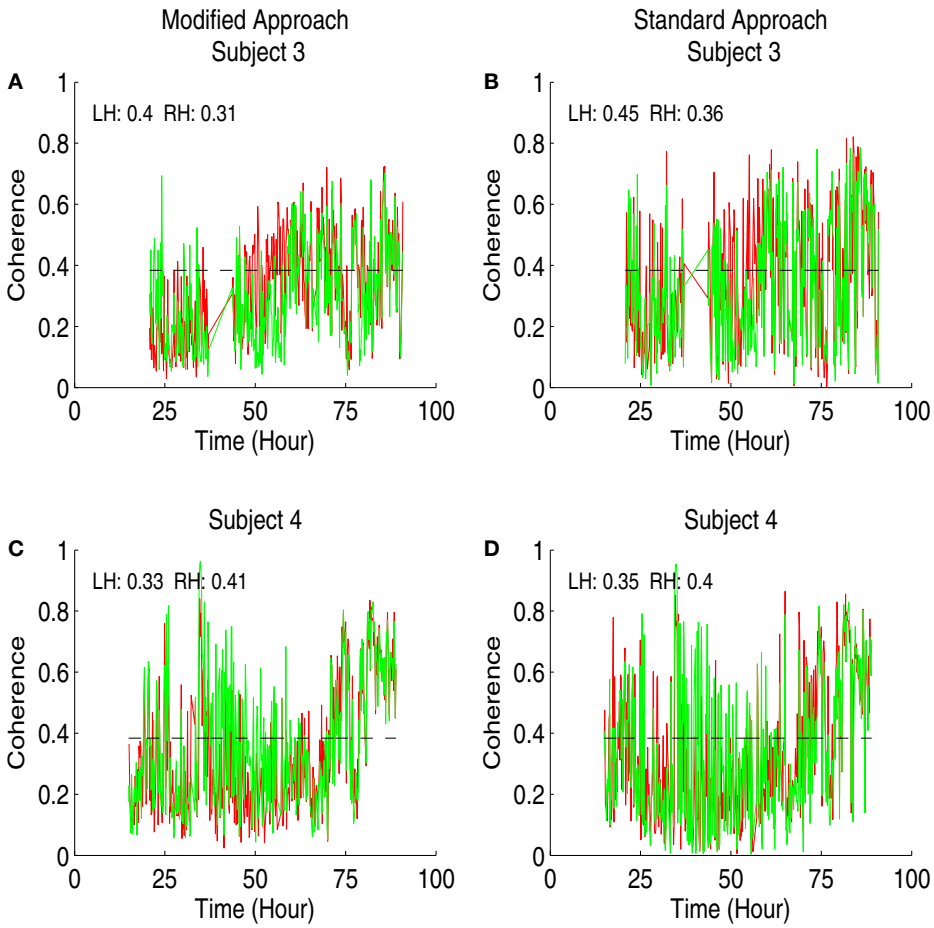

FIGURE 3 | Results of the coherence analysis of MAP and HbD from two newborns from adverse outcome group receiving hypothermia therapy for neonatal encephalopathy. The maximum coherence in 0.05–0.25 Hz was shown in all the plots from time since birth. Results from the modified approach were shown in the left side **(A,C)** and the results from the standard approach were shown in the right side **(B,D)**. Results from subject 3 were shown in **(A,B)** and the results from subject 4 were shown in **(C,D)**. In all the plots, the results from the left hemisphere (LH) were shown in red and the results from the right hemisphere (RH) were shown in green. Also the pressure passivity index (PPI) calculated for LH and RH was given in the inset. The horizontal line at the coherence value of 0.384 is the confidence limit for the coherence estimate.

by measuring the brain activity using SQUID based magnetoencephalographic techniques (Paetau, 2002; Roberts et al., 2014). MEG offers better spatial resolution compared to its electrical homolog electroencephalogram (EEG) (Paetau, 2002). Though both MEG and EEG have submillisecond temporal resolution, MEG has shown to identify deep sources with finer resolution compared to EEG (Paetau, 2002). EEG technology has also evolved over time trending to offer simultaneous dense array measurements from over 100 cortical sites (Welch et al., 2014). Future work would focus on studying simultaneous functional changes of the brain along with NIRS measurements.

5. CONCLUSION

We have demonstrated limitations in the standard coherence approach in quantifying association between two non-stationary signals and propose a modified coherence estimation approach. The modified approach reliably quantifies the association between the signals in the numerical simulations. We will apply the modified coherence estimation approach to a larger patient population to study the relation between PPI and neurologic injury as detected by MRI.

ACKNOWLEDGMENTS

This work was supported by the United States National Institutes of Health under the grants K24 NS057568, UL1RR031988, and KL2 RR031987.

REFERENCES

Govindan, R. B., Massaro, A. N., Niforatos, N., and du Plessis, A. (2013). Mitigating the effect of non-stationarity in spectral analysis – an application to neonate heart rate analysis. *Comput. Biol. Med.* 43, 2001–2006. doi:10.1016/j.compbiomed.2013.09.019

Halliday, D. M., Amjad, A. M., Breeze, P., Conway, B. A., and Farmer, S. F. (1995). A framework for the analysis of mixed time series/point process data theory and application to the study of physiological tremor, single motor unit discharges and electromyograms. *Prog. Biophys. Mol. Biol.* 64, 237–278. doi:10.1016/S0079-6107(96)00009-0

Howlett, J. A., Northington, F. J., Gilmore, M. M., Tekes, A., Huisman, T. A., Parkinson, C., et al. (2013). Cerebrovascular autoregulation and neurologic injury in neonatal hypoxic-ischemic encephalopathy. *Pediatr. Res.* 74, 525–535. doi:10.1038/pr.2013.132

Limperopoulos, C., Gauvreau, K. K., O'leary, H., Basan, H., Eichenwald, E. C., Soul, J. S., et al. (2008). Cerebral hemodynamic changes during intensive care of preterm infants. *Pediatrics* 122, 1006–1013. doi:10.1542/peds.2008-0768

O'Leary, H., Gregas, M. C., Limperopoulos, C., Zaretskaya, I., Bassan, H., Soul, J. S., et al. (2009). Elevated cerebral pressure passivity is associated with prematurity-related intracranial hemorrhage. *Pediatrics* 124, 302–309. doi:10.1542/peds.2008-2004

Paetau, R. (2002). Magnetoencephalography in pediatric neuroimaging. *Dev. Sci.* 5, 361–370. doi:10.1111/1467-7687.00375

Panerai, R., Kelsall, A. W., Rennie, J. M., and Evans, D. H. (1995). Cerebral autoregulation dynamics in premature newborns. *Stroke* 26, 74–80. doi:10.1161/01.STR.26.1.74

Panerai, R., Kelsall, A. W., Rennie, J. M., and Evans, D. H. (1996). Analysis of cerebral blood flow autoregulation in neonates. *IEEE Trans. Biomed. Eng.* 43, 779–788. doi:10.1109/10.508541

Panerai, R. B. (1998). Assessment of cerebral pressure autoregulation in humans – a review of measurement methods. *Physiol. Meas.* 19, 305–338. doi:10.1088/0967-3334/19/3/001

Panerai, R. B. (2008). Cerebral autoregulation: from models to clinical applications. *Cardiovasc. Eng.* 8, 42–59. doi:10.1007/s10558-007-9044-6

Roberts, T. P., Paulson, D. N., Hirschkoff, G., Pratt, K., Mascarenas, A., Miller, P., et al. (2014). Artemis 123: development of a whole-head infant MEG system. *Front. Hum. Neurosci.* 8:99. doi:10.3389/fnhum.2014.00099

Shankaran, S., Laptook, A. R., Ehrenkranz, R. A., Tyson, J. E., McDonand, S. A., Donavan, E. F., et al. (2005). Whole-body hypothermia for neonates with hypoxic-ischemic encephalopathy. *N. Engl. J. Med.* 353, 1574–1584. doi:10.1056/NEJMcps050929

Soul, J., Hammer, P. E., Tsuji, M., Saul, J. P., Bassan, H., Limperopoulos, C., et al. (2007). Fluctuating pressure-passivity is common in the cerebral circulation of sick premature infants. *Pediatr. Res.* 61, 467–473. doi:10.1203/pdr.0b013e31803237f6

Soul, J. S., Wypij, D., Walter, G. L., and du Plessis, A. J. (1998). Cerebral oxygen vasoreactivity in critically ill infants (abstr). *Ann. Neurol.* 44, 535.

Tsuji, M., du Plessis, A., Taylor, G., Crocker, R., and Volpe, J. J. (1998). Near infrared spectroscopy detects cerebral ischemia during hypotension in piglets. *Pediatr. Res.* 44, 591–595. doi:10.1203/00006450-199810000-00020

Tsuji, M., Saul, J. P., du Plessis, A., Eichenwald, E., Sobh, J., Corcker, R., et al. (2000). Cerebral intravascular oxygenation correlates with mean arterial pressure in critically ill premature infants. *Pediatrics* 106, 625–632. doi:10.1542/peds.106.4.625

Welch, M. G., Myers, M. M., Isler, J. R., Fifer, W. P., Sahni, R., Hofer, M. A., et al. (2014). Electroencephalographic activity of preterm infants is increased by family nurture intervention: a randomized controlled trial in the NICU. *Clin. Neurophysiol.* 125, 675–684. doi:10.1016/j.clinph.2013.08.021

Conflict of Interest Statement: The authors declare that the research was conducted in the absence of any commercial or financial relationships that could be construed as a potential conflict of interest.

Received: 13 December 2013; accepted: 10 April 2014; published online: 24 April 2014. Citation: Govindan RB, Massaro AN, Andescavage NN, Chang T and du Plessis A (2014) Cerebral pressure passivity in newborns with encephalopathy undergoing therapeutic hypothermia. Front. Hum. Neurosci. ***8****:266. doi: 10.3389/fnhum.2014.00266*
This article was submitted to the journal Frontiers in Human Neuroscience.

frontiers in
HUMAN NEUROSCIENCE

ORIGINAL RESEARCH ARTICLE
published: 26 March 2014
doi: 10.3389/fnhum.2014.00175

Localization of the epileptogenic foci in tuberous sclerosis complex: a pediatric case report

Alexander Hunold[1], Jens Haueisen[1], Banu Ahtam[2,3], Chiran Doshi[2,4], Chellamani Harini[4], Susana Camposano[4], Simon K. Warfield[5,6], Patricia Ellen Grant[2,3,5], Yoshio Okada[2,4] and Christos Papadelis[2,4]*

[1] *Institute of Biomedical Engineering and Informatics, Ilmenau University of Technology, Ilmenau, Germany*
[2] *Fetal-Neonatal Neuroimaging and Developmental Science Center, Boston Children's Hospital, Harvard Medical School, Boston, MA, USA*
[3] *Department of Newborn Medicine, Boston Children's Hospital, Harvard Medical School, Boston, MA, USA*
[4] *Department of Neurology, Boston Children's Hospital, Harvard Medical School, Boston, MA, USA*
[5] *Department of Radiology, Boston Children's Hospital, Harvard Medical School, Boston, MA, USA*
[6] *Computational Radiology Laboratory, Boston Children's Hospital, Harvard Medical School, Boston, MA, USA*

Edited by:
Hubert Preissl, University of Tübingen, Germany

Reviewed by:
Douglas Owen Cheyne, Hospital for Sick Children, Canada
Pierre Megevand, Hofstra North Shore-LIJ School of Medicine, USA

****Correspondence:***
Christos Papadelis, BabyMEG facility, Boston Children's Hospital, 9 Hope Avenue, Waltham, MA 02453, USA
e-mail: christos.papadelis@childrens.harvard.edu

Tuberous sclerosis complex (TSC) is a rare disorder of tissue growth and differentiation, characterized by benign hamartomas in the brain and other organs. Up to 90% of TSC patients develop epilepsy and 50% become medically intractable requiring resective surgery. The surgical outcome of TSC patients depends on the accurate identification of the epileptogenic zone consisting of tubers and the surrounding epileptogenic tissue. There is conflicting evidence whether the epileptogenic zone is in the tuber itself or in abnormally developed surrounding cortex. Here, we report the localization of the epileptiform activity among the many cortical tubers in a 4-year-old patient with TSC-related refractory epilepsy undergoing magnetoencephalography (MEG), electroencephalography (EEG), and diffusion tensor imaging (DTI). For MEG, we used a prototype system that offers higher spatial resolution and sensitivity compared to the conventional adult systems. The generators of interictal activity were localized using both EEG and MEG with equivalent current dipole (ECD) and minimum norm estimation (MNE) methods according to the current clinical standards. For DTI, we calculated four diffusion scalar parameters for the fibers passing through four ROIs defined: (i) at a large cortical tuber identified at the right quadrant, (ii) at the normal appearing tissue contralateral to the tuber, (iii) at the cluster formed by ECDs fitted at the peak of interictal spikes, and (iv) at the normal appearing tissue contralateral to the cluster. ECDs were consistently clustered at the vicinity of the large calcified cortical tuber. MNE and ECDs indicated epileptiform activity in the same areas. DTI analysis showed differences between the scalar values of the tracks passing through the tuber and the ECD cluster. In this illustrative case, we provide evidence from different neuroimaging modalities, which support the view that epileptiform activity may derive from abnormally developed tissue surrounding the tuber rather than the tuber itself.

Keywords: electroencephalography, epileptogenic zone, equivalent current dipole, magnetoencephalography, pediatric epilepsy, tuberous sclerosis complex

INTRODUCTION

Tuberous sclerosis complex (TSC) is a multi-system, autosomal dominant disorder (Crino et al., 2006) with a prevalence of 7–12/100,000 (O'Callaghan et al., 1998). TSC children present severe neurological symptoms that are mainly related to the cortical tubers, which occur in 80% of these patients (Crino et al., 2006). Approximately 90% of TSC children develop epilepsy; nearly two-thirds of patients have seizure onset within the first year of their life (Curatolo et al., 2002). In these patients, infantile spasms are the most common type of seizures (Chiron et al., 1997) with an onset of as early as 4 months of age. Partial seizures are often seen, whereas generalized seizures are relatively rare (Chiron et al., 1997; Kotagal, 2001).

Approximately 50% of the TSC-related epilepsy cases are refractory to pharmacological therapy (Jansen et al., 2006). Resective epileptic surgery is thus considered for controlling the seizures. Although surgical outcome differs in these patients, many studies report a positive surgical outcome in patients who have undergone surgical resection of the tubers (Bebin et al., 1993; Avellino et al., 1997; Karenfort et al., 2002; Romanelli et al., 2004). A recent systematic review reported that with resective surgery 57% of children achieve seizure freedom and another 18% experience a reduction (>90%) in seizure frequency at 1 year follow-up (Jansen et al., 2007).

The success of resective surgery in TSC patients depends on the accurate identification of the entire epileptogenic tissue (Tran et al., 1997). Multiple potentially epileptogenic tubers are usually present in TSC children and the task is to differentiate those associated with epileptiform activity from the "silent" ones. Another task is to find out whether epileptogenicity derives from

the tubers themselves or the abnormally developed surrounding cortex. Epileptogenic tubers may also occur in eloquent cortex, potentially rendering surgical treatment more difficult. There is conflicting evidence so far regarding these issues. Surgical studies report that the resection of large, calcified tubers is associated with a marked improvement in the seizure profiles of TSC patients (Guerreiro et al., 1998; Koh et al., 2000; Lachhwani et al., 2005). A surgical series using intraoperative electrocorticography (ECoG) indicated that the epileptiform discharges were localized within the cortical tubers (Guerreiro et al., 1998). Other ECoG studies found that the electrographic tubers were silent, and it was the surrounding neural tissue that was epileptogenic (Major et al., 2009).

Currently, the epileptogenic zone is conventionally identified using a combination of invasive and non-invasive imaging modalities. Invasive intracranial recordings serve as gold standard for the localization of the epileptogenic zone; however they are costly, can be difficult due to the cooperation of the child, carry some risk for infection and bleeding (Onal et al., 2003), and neurological damage (Zaccariotti et al., 1999). Intracranial recordings explore limited areas and hence, the success of such studies depends on the hypothesis formed by the results of the non-invasive tests. Scalp ictal EEG can be non-localizing in a significant proportion of children.

Advanced neuroimaging techniques can play a significant role in defining the epileptogenic zone in patients with TSC and multiple lesions (Jacobs et al., 2008; Sugiyama et al., 2009). Usually, data from several imaging modalities, such as electroencephalography (EEG), magnetoencephalography (MEG), diffusion tensor imaging (DTI), single-photon emission computed tomography (SPECT), and positron emission tomography (PET) must be integrated for an accurate presurgical localization. MEG (Kamimura et al., 2006; Xiao et al., 2006; Widjaja et al., 2010) or EEG data (Leal et al., 2008; Ochi et al., 2011; Kargiotis et al., 2013) are frequently reported in the literature. Very few reports present simultaneous MEG and EEG recordings (Iida et al., 2005; Sugiyama et al., 2009) in TSC-related pediatric epilepsy patients. Few other studies report mixed pediatric and adult patient cohorts (Jansen et al., 2006; Wu et al., 2006; Canuet et al., 2008). For source analysis, previous investigations of epileptic foci in TSC patients used various methods for the identification of the epileptic active areas, such as synthetic aperture magnetometry (SAM) (Xiao et al., 2006; Sugiyama et al., 2009), equivalent current dipoles (ECDs) (Iida et al., 2005; Kamimura et al., 2006; Wu et al., 2006; Xiao et al., 2006; Leal et al., 2008; Sugiyama et al., 2009; Widjaja et al., 2010), or multiple signal classification (MUSIC) (Jansen et al., 2006).

Magnetoencephalography is considered as one of the most promising techniques that can help in the non-invasive localization of epileptiform activity in the TSC-related epilepsy population. It provides an excellent localization accuracy of few millimeters for superficial sources (Leahy et al., 1998; Papadelis et al., 2009). Two recent studies presented evidence that MEG is superior compared to other neuroimaging techniques in the identification of the epileptogenic tissue in TSC patients. Wu et al. (2006) showed that MEG was better, in terms of sensitivity, specificity, and accuracy, compared to the ictal video-EEG in the identification of the epileptogenic zone in TSC patients. Jansen et al. (2006) found that epileptiform activity in patients with TSC and epilepsy detected with MEG was closer to a presumed epileptogenic tuber than the epileptiform activity detected with EEG.

DTI is used to detect microstructural changes in cortical development malformations (Widjaja et al., 2010) and to evaluate cortical tubers and normal appearing white matter (NAWM) in TSC patients (Peng et al., 2004; Makki et al., 2007). Previous studies reported increased apparent diffusion coefficient (ADC) and decreased fractional anisotropy (FA) values in the white matter lesions and the perilesional white matter compared to the contralateral NAWM in patients with TSC (Peng et al., 2004; Karadag et al., 2005). TSC patients with epilepsy have also been reported to have white matter abnormalities suggested to be indicative of cortical dysplasia or impaired myelin development due to seizures (Dwyser and Wasterlain, 1982; Jansen et al., 2003; Song et al., 2003; Widjaja et al., 2010), although the radial direction of the white matter abnormalities is more in keeping with dysplasia. Decreased FA (Widjaja et al., 2010) and increased ADC (Jansen et al., 2003) values were found for the cortical tubers within the epileptogenic zone compared to the cortical tubers in the non-epileptogenic zone in TSC patients with epilepsy.

In this case report, we examine a 4-year-old patient with TSC-related epilepsy by using pediatric MEG, EEG, MRI, and DTI. By using MEG and EEG, we aimed to identify whether epileptiform activity in this patient was derived from the tuber itself or its surrounding cortex and quantify the geometric configuration between source localization and tuber margin. For MEG, we used the BabySQUID system that has been especially designed for pediatric use. BabySQUID offers higher spatial resolution (3×) and sensitivity (2×) compared to conventional adult MEG (Okada et al., 2006). By using DTI, we aimed to detect white matter differences between the fibers passing through the calcified tuber, the contralateral NAWM, and the irritative zone as this was indicated by MEG and EEG.

MATERIALS AND METHODS

CLINICAL PRESENTATION

We studied a 4-year-old female patient with refractory epilepsy as a result of TSC. The patient had an uncomplicated perinatal history. Her first seizure (infantile spasms) occurred when she was 4 months old. Cardiac rhabdomyoma, revealed by echocardiography, resulted in the diagnosis of TSC. A *TSC1* mutation was found. MRI revealed multiple tubers in the bilateral frontal, parietal, and occipital lobes. A large calcified tuber was identified in the right parieto-occipital lobe. The following years the patient presented frequent gelastic seizures (smiling for ~5 s) with a daily frequency at maximum.

Previous routine EEG studies at the age of 3 years from this patient reported very frequent right occipital/posterior temporal sharp waves (P8 and O2). Less frequent spikes and sharp waves were identified at the left frontal (F3) as well as right fronto-temporal regions. Intermittent slowing in the left frontal and right posterior quadrant was observed. Ambulatory EEG at the age of 3 years detected five electrographic seizures arising from the right occipital region. Long-term monitoring captured six gelastic seizures with apparent left frontal onset. Very frequent interictal spikes were seen in the right posterior quadrant and left anterior quadrant occurring independently. Although the ictal EEG onset was noted in the left frontal region, source analysis of the ictal onset

revealed a more complex pattern involving both left frontal and right occipito-parietal activity. More specifically, it was noted that there were frequent right posterior temporal interictal spikes that diminish just as frequent low amplitude left frontal spikes were observed, which precede clinical seizure onset. These spikes pause and then left frontal spikes reappear with slightly different spatial and topographic distribution. The source analysis concluded that although the seizures appear to arise from the left frontal source, the right-sided abnormality could serve to facilitate the left frontal seizure source. The alpha-methyl-tryptophan PET scan showed increased uptake over the right parieto-temporo-occipital cortex. It was decided that intracranial EEG was needed to cover both regions. However, patient became seizure free with the introduction of a different antiepileptic medication. Hence, at this time the patient is being followed up closely without a surgical evaluation.

RECORDINGS

Multichannel MEG and EEG signals were simultaneously recorded from the patient for 10 min during sleep when the patient was 4 years old. MEG recordings were performed using BabySQUID (Tristan Technologies Inc., San Diego, USA). The system is equipped with 74 asymmetric axial first-order gradiometers covering the brain partially. A detailed description of BabySQUID can be found in Okada et al. (2006). The system is accommodated in a single-layer magnetically shielded room (MSR) located at the Radiology Suite of Boston Children's Hospital (BCH) at Waltham, MA, USA. EEG recordings were performed using a 32-channel EEG cap specially designed for pediatric use (WaveGuard cap with extended 10–20 layout; ANT b.V., Enschede, Netherlands) with common average reference. Both MEG and EEG data were sampled at 1024 samples per second. Electrocardiography (ECG) data were also recorded simultaneously at the same sampling rate. Clinical data were obtained and research MEG and EEG data were acquired and analyzed after explicit parental consent under a protocol approval by the local institutional review board. **Figure 1** shows the setup of the combined MEG and EEG measurements. During the recordings, the patient's head was placed over the sensor array, which fully covered the right parieto-occipital quadrant where the large classified tuber was located. The patient was sleeping during the entire recording and no movement was observed or recorded during the whole experiment. The co-registration was performed at the beginning and at the end of the recording session, which lasted for 10 min. The observed head movement was <2 mm. The co-registration procedure followed in our lab in epilepsy patients is described in Papadelis et al. (2013).

MRI ACQUISITION

The MRI data were collected at a 3T Siemens Tim Trio MR scanner at BCH when the subject was 4 years old. No sedation or medication was used during the MRI scan. The imaging protocol consisted of structural and diffusion-weighted sequences. The first structural sequence was a T1-weighted high-resolution magnetization-prepared rapid-acquisition gradient-echo (MPRAGE) acquisition, which used volumetric EPI navigators for real time motion correction [voxel size (mm) = 1 × 1 × 1; field of view (FOV) = 19.2 cm; echo time (TE) = 1.74 ms; repetition time (TR) = 2530 ms; flip angle = 7°]. The second structural sequence was a T2-weighted turbo spin-echo FLAIR sequence (TSE-FLAIR) [voxel size (mm) = 0.6250 × 0.6250 × 4.0000; FOV = 25.6 cm; TE = 1.37 ms; TR = 9000 ms; flip angle = 150°]. The diffusion sequence (prescribed axially) used echo-planar (EP) readouts [voxel size (mm) = 1.7 × 1.7 × 2.0; FOV = 22 cm; TE = 78 ms; TR = 8100 ms; flip angle = 90°; 30 gradient diffusion directions at $b = 1000$ s/mm^2; five acquisitions with $b = 0$ s/mm^2].

IDENTIFICATION OF CORTICAL TUBERS

The multifocal tubers were identified by an experienced pediatric neuroradiologist (PEG) and labeled in FreeView (http://surfer.

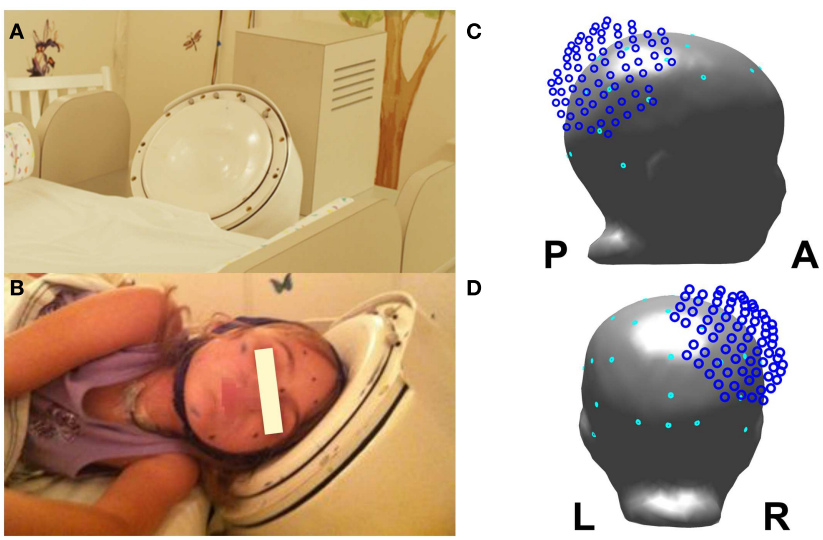

FIGURE 1 | Experimental recordings setup: (A) view of the BabySQUID headrest; (B) the epilepsy patient wearing the pediatric EEG cap and placing her head next to the BabySQUID headrest; (C) lateral view of patient's head model with the relative location of MEG sensors as it was positioned during the recordings (MEG sensors in dark blue and EEG sensor in cyan); (D) posterior view of the head model, the MEG sensors, and EEG electrodes.

nmr.mgh.harvard.edu/). The tuber closest to the ECDs was then manually segmented in FreeView with margins confirmed by an experienced pediatric neuroradiologist (PEG). The tuber margins were used to determine the distance between the ECDs and the tuber (Section MEG and EEG Data Analysis).

MEG AND EEG DATA ANALYSIS

Both EEG and MEG data were band-pass filtered between 1 and 70 Hz with a notch filter applied at 60 Hz. Bad MEG and EEG channels were excluded from further analysis. Interictal spikes were marked independently in EEG and MEG data by a pediatric neurologist (SC). Marked interictal spikes were revisited in order to identify similar spatiotemporal profiles in the time traces of EEG and MEG. A prominent morphology of epileptiform activity was identified in the data of each modality (see MEG and EEG Results for details). This resulted in two groups of interictal spikes, one for EEG and one for MEG signals. The MEG and EEG signals of the interictal spikes in each group were averaged including ± 100 ms around peak latency. For the averaged interictal spikes, we calculated the signal-to-noise ratio (SNR) on the sensor level as 10 times the logarithm of the ratio of the averaged signal power to the averaged noise power. The averaged signal power is the sum of the squared amplitudes of spike activity divided by the duration of the spike activity and the averaged noise power is the averaged squared amplitude of the signal before the spike started. We considered a signal interval of ± 30 ms with respect to the interictal spike peak latency. The noise interval was extracted from -500 to -50 ms with respect to the peak latency. The SNR was calculated for all channels and only the maximum value was reported.

A realistic three compartment boundary element method (BEM) model was constructed based on T1-weighted MRI data, for solving the forward problem. The inner skull boundary, the outer skull boundary, and the skin were automatically segmented and triangulated with 5,120 triangles per surface (Haueisen et al., 1997) using the MNE software (http://martinos.org/mne). For source analysis, we co-registered the EEG and MEG sensor configurations with the BEM model. The MNE software defined a head coordinate system based on left pre-auricular point (LPA), Nasion, and right pre-auricular point (RPA) digitization. The head digitization with Fastrack (Polhemus, Colchester, VT, USA) resulted in a digitization set of points on patient's skin in the head coordinate system including EEG electrode positions. The MRI images and the BEM model were transformed into this head coordinate system. The MEG sensor configuration was defined in the coordinate configuration of the Polaris system (Northern Digital Inc., Waterloo, ON, Canada) used for head digitization in the MSR. Predefined points marked on the patient's skin served as common points in Polhemus and Polaris digitization. Based on these common points, the MEG sensor configuration was transformed onto the BEM model in the head coordinate system.

Since we do not know *a priori* how extended are the epileptiform generators, we analyzed the MEG and EEG data by using two source localization methods: one that assumes a focal underlying generator that explains the observed MEG/EEG signal (i.e., ECD) and one that presumes extended sources [i.e., minimum norm estimates (MNE) (Hämäläinen and Ilmoniemi, 1994)]. MNE software was used for analyzing the MEG and EEG data. The source localization findings of the two methods were finally compared to each other. Our goal was to quantify the distance between the epileptiform source activity and the margin of a distinct calcified tuber. The whole brain volume provided valid source space for the ECD localization and the MNE reconstruction based on the white–gray-matter boundary. The cortical tuber was a valid source space for the ECD analysis, but not for the MNE analysis. Within the tuber volume, it was not feasible to segment a cortical surface. Therefore, the white–gray-matter boundary passed the calcified tuber volume. ECDs were estimated for each interictal spike at the peak latency of each spike, and for the averaged interictal spike from -15 to 0 ms from the peak latency of the averaged spike in increments of 5 ms. This time-interval represented the upslope of the spike from approximately 50% of the peak amplitude to the peak amplitude. For each ECD localized to the averaged interictal spike, we computed the confidence volume using Curry 7 (Compumedics Neuroscan, Charlotte, NC, USA). For the two dipole-clusters formed by ECDs at the individual interictal EEG and MEG spikes, we performed a principal component analysis (PCA) to estimate a representative ellipsoid for the cluster (Ziolkowski et al., 2002). The eigenvalues of the covariance matrix provided the semi axis of the ellipsoid. The ellipsoid was located in the center of the dipole cluster.

MNE solutions at peak time of the averaged interictal spike were also computed with restriction to the boundary between gray and white matter using the MNE software with default parameters, weighted with dynamic statistical parametric mapping (dSPM) (Dale et al., 2000) and thresholded for display. We calculated the distance from each ECD localization to its closest point on the tuber margin. In order to test whether or not the distance between the cluster of dipoles, fitted to each interictal spike, and the tuber margin differs significantly for MEG and EEG, we performed a Wilcoxon rank sum test with a level of significance of 5% for the dipole tuber distance of the two clusters. Further, we computed the distance between each ECD and the maximum point of the MNE solution.

DTI DATA ANALYSIS

Diffusion data were processed with Diffusion Toolkit (http://trackvis.org/dtk/) using HARDI/Q-Ball imaging model and second order Runge Kutta propagation algorithm with an angle threshold of 45° and no FA threshold. A three-dimensional segmentation of the tuber file was transformed to create a mirror image of the tuber and then the transformed tuber was manually edited to match the gyral topography of the left hemisphere using FreeView but preserving the same ROI volume. The dipoles cluster formed by the interictal spikes ECDs was used to define the third ROI (each ECD was considered as a cube with 3 voxels edge). ECDs cloud ROI was also transformed to create a mirror image of itself to be used as another ROI of the same volume on the left hemisphere.

The original and transformed tuber volume files, the ECDs cloud, and the transformed ECDs cloud volume files, as well as the T1 and T2 FLAIR images were co-registered with the b0 image using 3D Slicer software (http://www.slicer.org). The tuber, transformed tuber, ECDs cloud, and the transformed ECDs cloud volumes were imported in TrackVis software (http://trackvis.org)

as ROI files. Fiber tractography was performed with TrackVis software to create fiber tracks that pass through the tuber, the transformed tuber (i.e., contralateral NAWM), the ECDs cloud (i.e., subcortical white matter adjacent to the tuber within epileptogenic zone), and the contralateral ECDs cloud ROIs. We avoid creating a fourth ROI using the MNE results, since the MNE analysis was performed on the boundary between the gray and white matters. Mean scalar measures of FA, ADC, axial diffusivity (AD), and radial diffusivity (RD) were derived for each fiber track.

RESULTS

MEG AND EEG RESULTS

Figure 2 shows all the identified tubers in the patient's brain overlaid on the T1 and T2-weighted structural MRI data. The largest tuber was identified in the right parietal-occipital area with mineralization. Very frequent right posterior temporal/occipital sharp waves (mainly at electrodes P8, P4, and CP6) were observed in EEG signal. These sharp waves always presented the same spatiotemporal profile at the sensor level. Sharp waves and polyspikes were observed from left frontal regions in EEG, but their spatiotemporal map did not consistently present the same topography. For this reason and also due to the presence of predominant epileptic activity in the right posterior quadrant including the occurrence of epileptogenic seizures, we focused our MEG and EEG analysis of simultaneously recorded data on the interictal activity at the right posterior temporal/occipital region.

Within our region of interest in the right parietal-occipital lobe, we identified a total of 304 interictal spikes of which 135 (44% of total spikes) were detected on EEG and MEG within a time frame of ±15 ms between the peak times. These were considered simultaneous spikes. Eighty-five spikes (28% of total spikes) were identified only on MEG, and 84 (28% of total spikes) were uniquely in EEG traces. This resulted in 220 MEG (72% of total) and 219 EEG (72% of total spikes) spikes. An overview of the number of spikes identified in our recordings is given in **Table 1**. **Figure 3** shows 10 s of filtered data from selected MEG and EEG channels. The colored markers indicate the interictal spikes in each modality providing high signal to noise ratio (SNR) at sensor level.

Two groups of interictal spikes were identified independently among the total MEG spikes and the total EEG spikes according to their localization and morphology in the time traces. MEG spikes (blue bars in **Figure 3**) were selected when they presented a polarity reversal between MEG channels 054 and 057. They had a mean duration of ~55 ms. EEG spikes were selected if they had a polarity reversal between EEG channels P8 and O2, and were part of a spike wave complex. Spike duration was ~70 ms; the spike wave complex had a mean duration of ~250 ms. This selection of spikes resulted in 46 spikes in EEG and 57 spikes in MEG, with 17 of them seen in both modalities. Within the group of interictal MEG spikes, we found the SNR on a level of 11.1 ± 2.5 dB and the averaged MEG spike reached a SNR of 21.6 dB. The group of interictal EEG spikes provided a SNR of 11.7 ± 3.1 dB and the averaged EEG spike reached a SNR of 25.6 dB.

Since our MEG system provides partial head coverage, our initial effort was to ensure that the sensor array covered both the minima and maxima of the epileptiform activity. At sensor level, we found lateralized minima on the edge of the sensor array for both MEG and EEG configurations (see **Figure 3**) with respect to the tuber localization, which is in agreement with Ochi et al. (2011). **Figure 4** shows the ECD and MNE localizations for the averaged interictal spikes. Both ECDs and MNE maxima were localized in the immediate vicinity of the calcified tuber.

The cluster formed by the ECDs fitted to the 57 interictal MEG spikes was localized on average in a distance of 4 ± 2 mm laterally with respect to the tuber margin (red dipoles in **Figure 4A**). The equivalent ellipsoid of the dipole cluster circumscribed a volume of 1.9 cm^3 (**Figure 4B**). The analysis of the averaged MEG spike from −15 to 0 ms with respect to peak latency provided a stable magnetic field with respect to its orientation and increased in intensity during the considered time-interval (**Figure 3E**). The dipoles localized to the averaged MEG spike generated a 4.5 mm trace in inferior direction anterior to the calcified tuber (**Figure 3F**). The distance between the ECD localizations and the tuber margin decreased from ~5 to ~3 mm (3.8 ± 0.8 mm). The dipole localized to −15 ms provided a confidence volume of 2.9 cm^3 and the subsequent dipoles provided confidence volumes of 0.4 ± 0.15 cm^3. The ECD fitted to the peak of the averaged interictal MEG spikes was localized ~3 mm anterior lateral to the calcified tuber margin and provided a confidence volume of 0.4 cm^3 (blue dipole on **Figures 4B,C**). The ECDs fitted to the averaged interictal MEG spikes moved across time from −15 to 0 ms staying always at the periphery of the tuber's volume with a superior–inferior direction

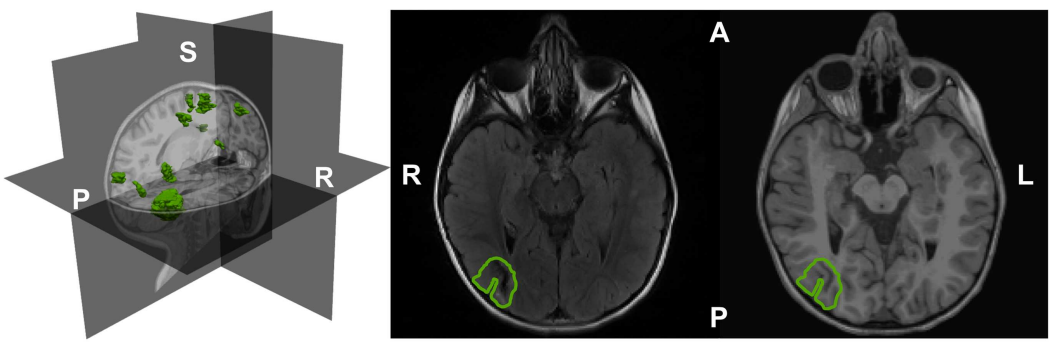

FIGURE 2 | The segmented and rendered tubers (in green) of the epilepsy TSC patient shown in a 3D head representation based on T1-weighted MRI data (left). Tuber outline axial on T2 (center) and T1-weighted MRI images (right). A: anterior; L: left; P: posterior; R: right; S: superior.

by the lateral side of the calcified tuber (**Figure 3F**). The dipole fitted to peak latency reached the maximal goodness of fit (GOF) of 90% with an amplitude of 72.9 nAm. The maximum point of the MNE distribution localized ~4 mm anterior to the calcified tuber margin (**Figures 4B,C**). The distance between the center of the ECD cluster and the ECD localization for the averaged interictal MEG spikes was less than 0.5 mm. The distance between the ECD localization of the averaged interictal MEG spike and the maximum point of the MNE localization was ~11 mm. The difference between the ECD orientation for the averaged interictal MEG spike and the surface normal for the maximum point of the MNE localization was 17.2°. The distance between the ECD cluster center and the MNE localization was ~11 mm, as well.

The ECDs fitted to each of the 46 interictal EEG spikes were localized on average at a distance of 5 ± 2 mm superior to the tuber margin (red dipoles in **Figure 4D**). The equivalent ellipsoid of the dipole cluster circumscribed a volume of 3.8 cm^3 (**Figure 4E**). The analysis of the averaged EEG spike provided a negative pole over the right parietal-occipital region as main feature, which increased in extend and slightly changed its morphology during upslope of the spike from −15 to 0 ms with respect to peak

Table 1 | Number of spikes identified in the data of MEG and EEG channels covering the right parieto-occipital lobe.

	Number	Percentage
Total	304	100
MEG	220	72
EEG	219	72
Common	135	44
Unique MEG	85	19.4
Unique EEG	84	19.1

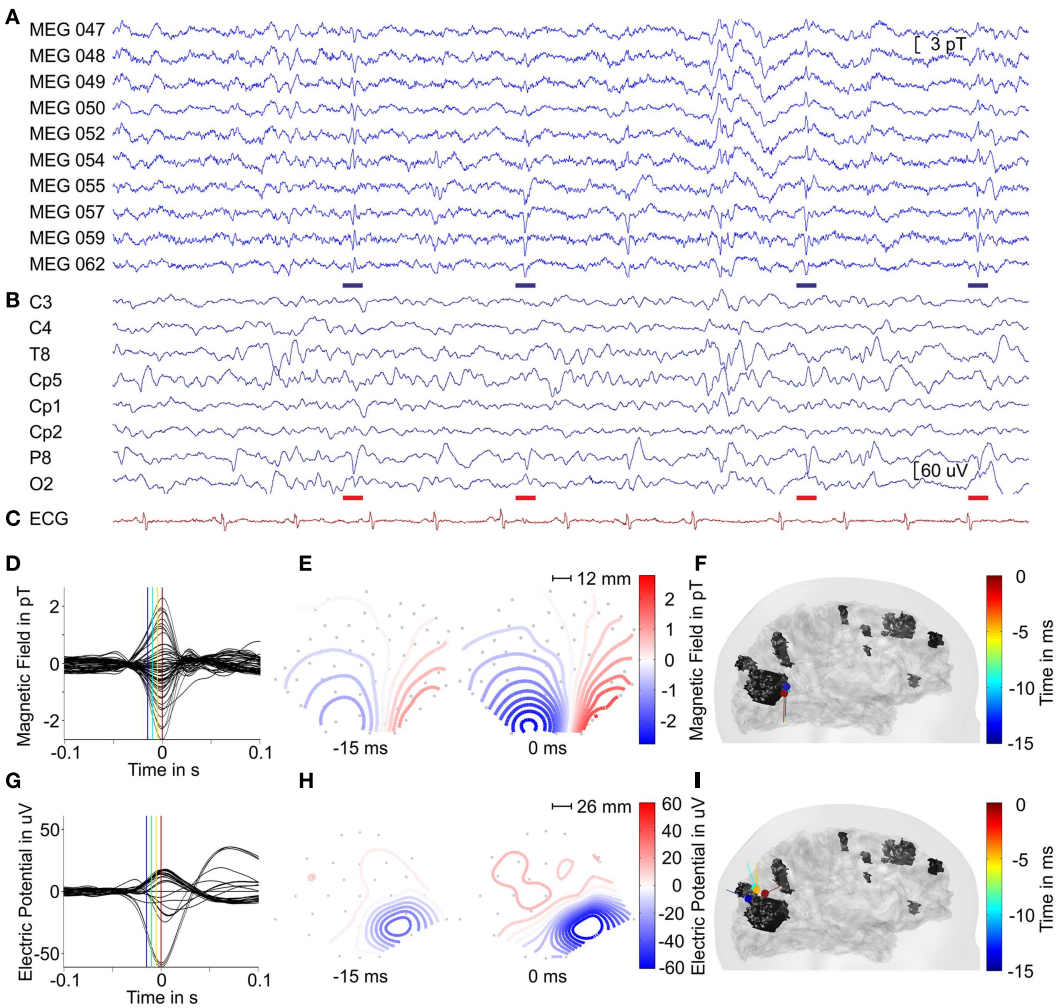

FIGURE 3 | MEG (A) and EEG (B) signals of selected channels and the ECG (C) trace with interictal spikes marked by blue and red bars indicating epileptiform in MEG and EEG in a time-interval of 10 s. Averaged interictal MEG **(D)** and EEG **(G)** spikes. The magnetic field maps **(E)** and electric potential maps **(H)** depicted at labeled time points [blue and red lines in **(D,G)**] of averaged signals. The gray dots indicate sensor positions with a geometrical scale as labeled. For positioning with respect to the head, please compare to **Figure 1**. **(F,I)** Lateral views on the head model with ECD traces of averaged interictal spikes with color coded time information from −15 to 0 ms with respect to peak latency for MEG and EEG, respectively.

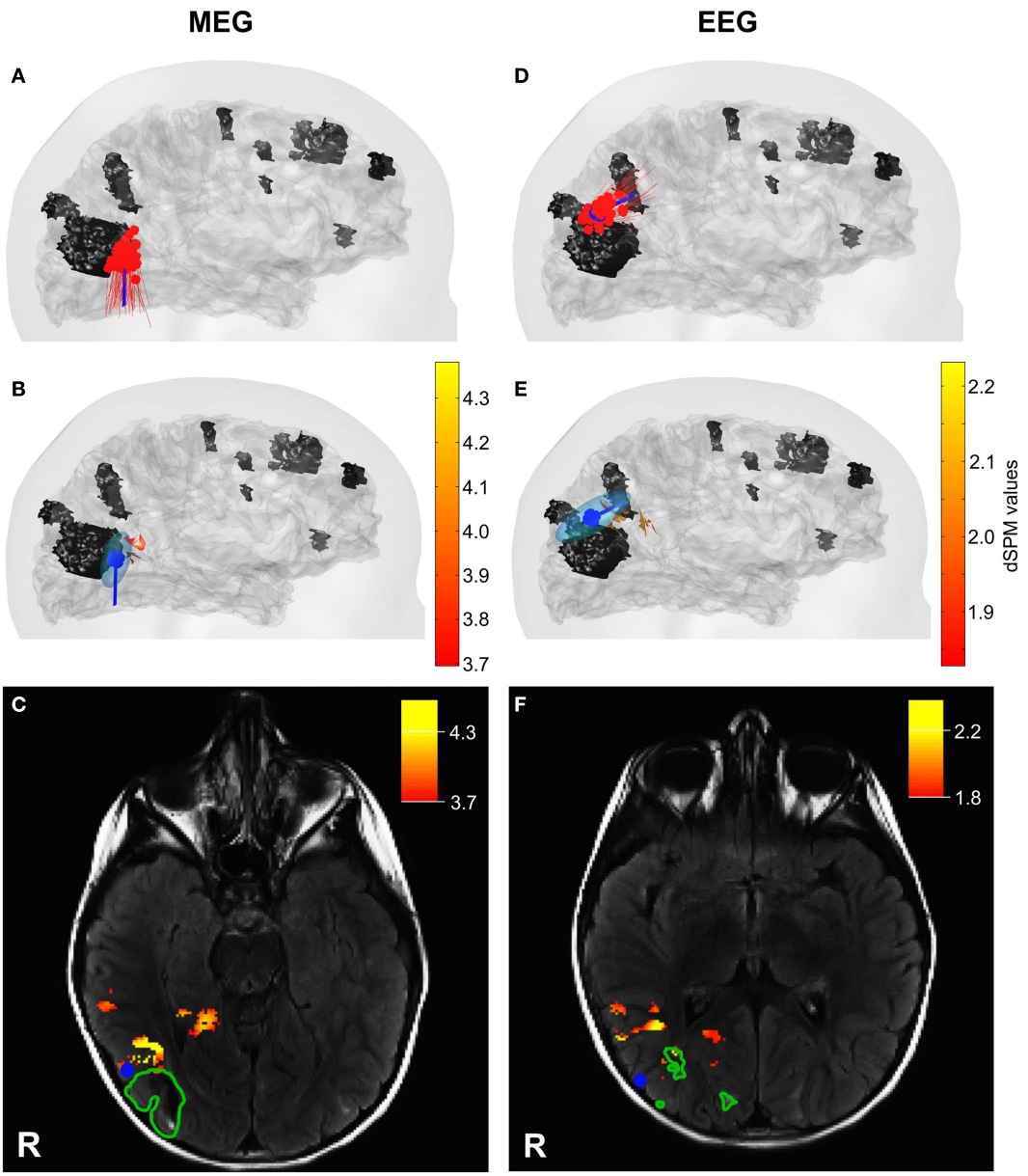

FIGURE 4 | ECD and MNE localizations for interictal MEG (left column) and EEG (right column) spikes. **(A,D)** Lateral views on the head model with ECD localization for each interictal spike (red) and the averaged interictal spikes (blue). **(B,E)** Lateral views on the head model with MNE localizations (red – yellow scale) and ECD for averaged interictal spikes (blue) with ellipsoid representing the dipole-clusters. The tuber volumes are indicated in black. Skin and cortical surface are indicated in gray. **(C,F)** Axial slices of MRI FLAIR images with tuber margins (green), ECD localizations for averaged interictal spike (blue dot), and MNE localizations (red – yellow scale). R: Right.

latency (**Figure 3H**). The dipole trace localized to the averaged EEG spike started superior posterior to the calcified tuber in a distance of ~12 mm to the tuber margin with a dipole orientation in posterior direction. The subsequent dipoles moved ~12 mm anterior and changed orientation to a mainly anterior direction (**Figure 3I**). The distance between the dipole localizations and the tuber margin remained with ~14 and ~12 mm relatively stable (−15 to −5 ms). The dipoles localized to the averaged EEG spikes provided confidence volumes of $11 \pm 6\ cm^3$. The ECD fitted to the averaged interictal EEG spikes was localized at a distance of ~5 mm posterior superior to the calcified tuber margin and provided a confidence volume of $12.6\ cm^3$ (blue dipole in **Figures 4E,F**). The ECDs fitted to the averaged interictal EEG spikes moved slightly across time (from −15 to 0 ms) staying always at the periphery of the tuber's volume in an anterior–posterior direction and turned ~90°(**Figure 3H**). The ECD trace stabilized between 0 and +10 ms. The dipole fitted to peak latency reached the maximal GOF of 70% with an amplitude of 93.6 nAm. The maximum point of the MNE distribution localized ~9 mm away from the margin outside the volume of the calcified tuber (**Figures 4E,F**). The distance between

the center of the ECD cluster and the ECD localization for the averaged interictal EEG spikes was ~2 mm. The distance between the ECD localization of the averaged interictal EEG spike and the maximum point of the MNE localization was ~14 mm. The difference between the ECD orientation for the averaged interictal MEG spike and the surface normal for the maximum point of the MNE localization was 38.7°. The distance between the ECD cluster center and the maximum point of the MNE localization was ~12 mm.

The dipole cluster localized by MEG was significantly closer ($p < 0.05$) to the tuber's margins compared to the one localized by EEG. The distance between the centers of the two ECD clusters for interictal MEG and EEG spikes was ~22 mm. Similarly, the ECDs fitted to the averaged interictal MEG and EEG spikes localized ~22 mm apart. The maximum points of the MNE localizations for the averaged interictal MEG and EEG spikes localized in a distance of ~24 mm to each other.

DTI RESULTS

Figure 5 (upper panel) presents the four ROIs and the corresponding fibers passing through them. **Figure 5** (lower panel) presents the mean for the scalar values of mean FA, ADC, AD, and RD for fiber tracks passing through the four ROIs. The tracks passing through the ECD cluster had the lowest mean FA and the highest mean RD values. The tracks passing through the tuber showed the highest mean FA and highest mean AD values. The mean FA, ADC, and AD values were higher for the tuber tracks than for the ECD cluster tracks with tracks on the contralateral side showing the same pattern. However, the difference between the mean FA, ADC, and AD values for the tuber tracks and the ECD cluster tracks was more pronounced than the difference between the contralateral ROI tracks. Moreover, the increase in the mean RD value observed for the ECD cluster tracks compared with the tuber tracks on the right hemisphere was not observed between the tracks of the left hemisphere. Finally, mean ADC values were higher all together for the tuber tracks and the ECD cluster tracks than the mean ADC values of the contralateral tracks.

DISCUSSION

In this illustrative case, we localized predominant epileptiform brain activity in a 4-year-old child with epilepsy due to TSC by using pediatric MEG, EEG, and DTI. The predominant epileptiform activity, when analyzed by simultaneously recorded MEG and EEG, was consistently localized to the tissue surrounding the tuber rather the tuber itself. DTI results further support the notion that epileptogenicity may come from the surrounding tissue of the tuber, since, they indicate different microstructural features for the white matter tracks passing through the region of electrophysiologic abnormality localized in the vicinity of the tuber compared to the other ROIs. Additional studies are needed to determine if this is a consistent finding in large numbers of TSC patients.

Previous clinical epilepsy studies indicate that epileptiform activity is sometimes visible only in MEG or in EEG (Baumgartner et al., 2000; Yoshinaga et al., 2002; Rodin et al., 2004; Iwasaki et al., 2005). The two techniques provide different sensitivity profiles depending on the orientation and depth of the underlying source (Goldenholz et al., 2009; Ahlfors et al., 2010; Haueisen et al., 2012). For the achievement of a complete picture of the underlying epileptogenic sources, it has been recommended that these two modalities are used simultaneously in epilepsy studies (Nakasato et al., 1994; Stefan et al., 2003). Here, we used both high-resolution MEG and EEG for two reasons: (i) to capture epileptiform activity visible only from a single modality, and (ii) to obtain a complete picture of the entire brain epileptiform activity, since our MEG system has a partial coverage of the head.

In our study, the fraction of the commonly detected interictal spikes in both EEG and MEG was comparable to previous studies [i.e., here 44 vs. 41% in Ramantani et al. (2006) and 51.1% in Park et al. (2004)]. For source localizations to interictal epileptiform activity, it is recommended to perform the analysis during the upslope of the spike since source propagation can already occur during this interval (Alarcon et al., 1994; Lantz et al., 2003; Ray et al., 2007). The ECDs localizations were performed for the averaged interictal MEG and EEG spikes from −15 to 0 ms with respect to the peak latency in intervals of 5 ms. This time-interval represented the upslope of the spike from approximately 50% to the maximum amplitude of the interictal spike. For MEG, the field remained stable with respect to its orientation and increased in intensity during the considered time-interval. The MEG dipole trace remained relatively stable across time during the upslope of the averaged signal. For EEG, the dipole trace presented a slight propagation in anterior direction with an orientation change from posterior to anterior, but the dipoles were always localized outside the calcified tuber in millimeter distances. The dipoles at the peak of the averaged EEG and MEG spikes provided the smallest distance to the tuber margin, and therefore provided the critical configuration for testing our hypothesis. Based on these observations, we performed the localization of single-spikes at the peak time in order to achieve ECDs with relatively high GOF considering the high SNR at this time point.

The ECD localizations of interictal MEG and EEG spikes formed ECD clusters similar to those reported by Iida et al. (2005), Kamimura et al. (2006), Sugiyama et al. (2009), and Widjaja et al. (2010). The generators identified by MEG located closer to the tuber's margins compared to those localized by EEG, which is in line with previous source localization findings in TSC-related epilepsy patients (Jansen et al., 2006; Xiao et al., 2006). ECDs and MNE localization results were in agreement; both were localized to the vicinity of the single calcified tuber (see **Figure 4**). Differences in the localization results of the two source localization methods can be due to the fact that the MNE solutions were constrained to the cortical surface, while ECDs solutions were unconstrained. This hypothesis was supported by the small deviations between the ECD orientations for the averaged interictal spikes and the surface normal for the maximum point of the MNE localizations. The different localization results for MEG and EEG with respect to the calcified tuber may indicate different epileptogenic foci associated to the tuber. These two neuroimaging modalities prefer different source orientation, which can result in the identification and localization of different source aspects. In the present case, the dipole localizations present tangential orientation for interictal MEG spikes and mainly radial orientation for interictal EEG spikes. A direct comparison between the MEG and EEG source localization results cannot be performed, since different number of

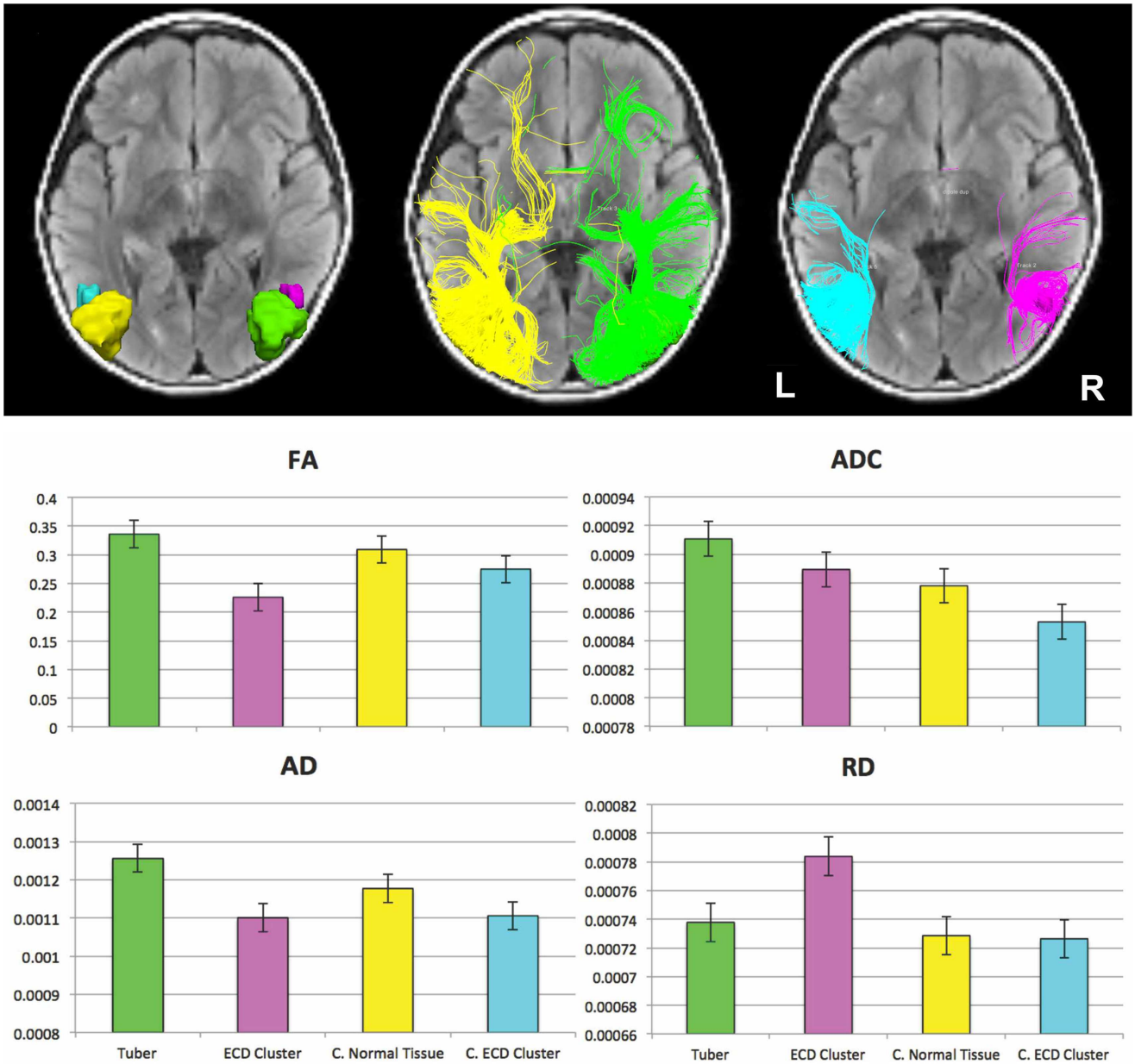

FIGURE 5 | (Upper panel) Fiber tracts passing through the four ROIs. (Left-upper panel) ROIs displayed on an axial FLAIR image: ROI encompassing the cortical and subcortical component of the large right-sided calcified tuber (green), ROI of same volume encompassing normal appearing tissue contralateral to the tuber (yellow) modified to respect gyral folds, ROI encompassing the ECD cluster formed by the MEG dipoles resulting from fitting the interictal spikes (magenta), and ROI of same volume encompassing the normal appearing tissue contralateral to the ECD cluster (cyan). (Middle-upper panel) Fibers passing through the ROIs defined by the tuber (green) and the normal appearing tissue contralateral to the tuber (yellow). (Right-upper panel) Fibers passing through the ECD cluster (magenta) and the normal appearing tissue contralateral to the ECD cluster (cyan). **(Lower panel)** Mean (±SE) for the scalar values of mean FA, ADC, AD, and RD for fiber tracks passing through the large cortical tuber (green), the ECD cluster formed by the dipoles fitted at interictal spikes (magenta), the normal appearing tissue contralateral to the tuber (yellow), and at the normal appearing tissue contralateral to the ECD cluster (cyan).

sensors were used from the two neuroimaging modalities. Indeed, an explanation for the superior localization of the sources for EEG data compared to sources for MEG data could be provided by the fact that our electrode configuration contained very few electrodes below the hairline. In temporal lobe epilepsy, Sperli et al. (2006) indicated a shift of source localizations to dorsal structures when inferior temporal electrodes were not included in the recording setup. Further, the minima of the electric potential and magnetic field maps located on the edge of the sensor arrays and the maxima were incompletely circumscribed. Such an incomplete sampling of

the electric potential and magnetic field could potentially lead to erroneous source localizations (Michel et al., 2004).

However, our findings are in agreement with previous studies indicating that epileptogenic tissue may be predominately localized in the surroundings of cortical tubers (Weiner, 2004; Xiao et al., 2006; Major et al., 2009). The high sensitivity and excellent localization accuracy of our MEG system allowed us to detect and localize accurately the epileptiform activity with respect to the location of the calcified tuber. The localization of single-spikes and averaged spikes were consistent; the two clusters for MEG and EEG were localized in a relatively small region outside tuber's margins. ECD traces across time indicated propagating epileptiform foci localized in the vicinity of a calcified tuber but never passed the tuber's margins going inside the tuber.

The view that epileptiform activity is generated in the surrounding tissue of tubers is supported by both clinical as well as animal studies, which indicate that cortical tubers may not be essential for epileptogenicity. A significant improvement in the seizure profiles of TSC patients has been observed after the resection of these single epileptogenic tubers and their surrounding tissue (Guerreiro et al., 1998; Koh et al., 2000; Lachhwani et al., 2005). Kaufmann et al. (2009) reported a tuberless TSC infant with intractable epilepsy, while cortical synaptic hyperexcitability in the absence of cortical tubers was reported by Wang et al. (2007) in animals.

Our DTI results support the notion that the white matter tracts associated with the region of electrophysiologic abnormality (ECD cluster) have microstructural features that may be distinct from tracts associated with the tuber and tracts generated from a similar ROI in contralateral normal appearing tissue. Decreased FA due to increased RD noted in the ECD cluster may be a sign of disorganized, demyelinated, dysmyelinated, and/or poorly myelinated axons (Beaulieu and Allen, 1994; Gulani et al., 2001; Song et al., 2002, Nair et al., 2005; Song et al., 2005). Similar findings to our ECD cluster were reported in the NAWM surrounding the cortical tubers by Widjaja et al. (2010) who suggested that these abnormal diffusivity values may reflect cortical dysplasia or could be related to ictal and/or interictal activity. These results are also in accordance with animal studies where recurrent seizures are shown to cause impairment in myelin development (Dwyser and Wasterlain, 1982; Song et al., 2003).

The potential etiologies of increased ADC and increased FA in the tuber primarily due to increased AD are less clear. Although prior studies have suggested that reduced axonal density or caliber could increase the extra-axonal space allowing faster water molecule movement parallel to axons (Kumar et al., 2008, 2010; Sun et al., 2008), this explanation is unsatisfying in our case as RD is not increased. Increased ADC values in epileptogenic tubers have been previously reported by Jansen et al. (2003). Here, we provide additional information for tracks passing through the tuber ROI. Prior studies have suggested that increased ADC might be reflective of hypomyelination due to loss of barriers to water motion (Chandra et al., 2006), again the lack of an increase in RD makes this interpretation unsatisfactory.

The present study is an illustrative case of the combined application of MEG and DTI in a single TSC pediatric patient. Our findings support the view that epileptogenicity in TSC patients may be derived from abnormally developed cortex surrounding tubers, but are not conclusive. For MEG, we used an innovative system especially designed for pediatric use that offers better localization accuracy and sensitivity compared to the adult conventional systems for a specific ROI. We provide a detailed and extensive analysis of our data making use of four different neuroimaging modalities (i.e., MEG, EEG, MRI, and DTI). Data from neurophysiological methods, such as MEG and EEG, were combined with data from DTI and MRI to examine how the epileptiform activity is coupled with anatomical changes. Although none of the observations made in this case study is strong enough to completely rule out alternative interpretations, the converging evidence of the independently used neuroimaging modalities makes our hypothesis the most parsimonious explanation and sets the stage for a larger study.

ACKNOWLEDGMENTS

The authors would like to thank Drs. Borjan Gagoski and Benoit Scherrer for their help with MR sequences. This research was supported by the German Federal Ministry of Education and Research (Grant No. 03IPT605A).

REFERENCES

Ahlfors, S. P., Han, J., Belliveau, J., and Hämäläinen, M. S. (2010). Sensitivity of MEG and EEG to source orientation. *Brain Topogr.* 23, 3. doi:10.1007/s10548-010-0154-x

Alarcon, G., Guy, C. N., Binnie, C. D., Walker, S. R., Elwes, R. D., and Polkey, C. E. (1994). Intracerebral propagation of interictal activity in partial epilepsy: implications for source localization. *J. Neurol. Neurosurg. Psychiatry* 57, 4. doi:10.1136/jnnp.57.4.435

Avellino, A. M., Berger, M. S., Rostomily, R. C., Shaw, C. M., and Ojemann, G. A. (1997). Surgical management and seizure outcome in patients with tuberous sclerosis. *J. Neurosurg.* 87, 3. doi:10.3171/jns.1997.87.3.0391

Baumgartner, C., Pataraia, E., Lindinger, G., and Deecke, L. (2000). Neuromagnetic recordings in temporal lobe epilepsy. *J. Clin. Neurophysiol.* 17, 2. doi:10.1097/00004691-200003000-00007

Beaulieu, C., and Allen, P. S. (1994). Determinants of anisotropic water diffusion in nerves. *Magn. Reson. Med.* 31, 4. doi:10.1002/mrm.1910310408

Bebin, E. M., Kelly, P. J., and Gomez, M. R. (1993). Surgical treatment for epilepsy in cerebral tuberous sclerosis. *Epilepsia* 34, 4. doi:10.1111/j.1528-1157.1993.tb00442.x

Canuet, L., Ishii, R., Iwase, M., Kurimoto, R., Ikezawa, K., Azechi, M., et al. (2008). Tuberous sclerosis: localizing the epileptogenic tuber with synthetic aperture magnetometry with excess kurtosis analysis. *J. Clin. Neurosci.* 15, 11. doi:10.1016/j.jocn.2007.03.030

Chandra, P. S., Salamon, N., Huang, J., Wu, J. Y., Koh, S., Vinters, H. V., et al. (2006). FDG-PET/MRI coregistration and diffusion-tensor imaging distinguish epileptogenic tubers and cortex in patients with tuberous sclerosis complex: a preliminary report. *Epilepsia* 47, 9. doi:10.1111/j.1528-1167.2006.00627.x

Chiron, C., Dumas, C., Jambaque, I., Mumford, J., and Dulac, O. (1997). Randomized trial comparing vigabatrin and hydrocortisone in infantile spasms due to tuberous sclerosis. *Epilepsy Res.* 26, 2. doi:10.1016/S0920-1211(96)01006-6

Crino, P. E., Nathanson, K. L., and Henske, E. P. (2006). The tuberous sclerosis complex. *N. Engl. J. Med.* 355, doi:10.1056/NEJMra055323

Curatolo, P., Verdecchia, M., and Bombardieri, R. (2002). Tuberous sclerosis complex: a review of neurological aspects. *Eur. J. Paediatr. Neurol.* 6, doi:10.1053/ejpn.2001.0538

Dale, A., Liu, A., Fischl, B., and Buckner, R. (2000). Dynamic statistical parametric mapping: combining fMRI and MEG for high-resolution imaging of cortical activity. *Neuron* 26, 1. doi:10.1016/S0896-6273(00)81138-1

Dwyser, B. E., and Wasterlain, C. G. (1982). Electroconvulsive seizures in the immature rat adversely affect myelin accumulation. *Exp. Neurol.* 78, 3. doi:10.1016/0014-4886(82)90079-6

Goldenholz, D. M., Ahlfors, S. P., Hämäläinen, M. S., Sharon, D., Ishitobi, M., Vaina, L. M., et al. (2009). Mapping the signal-to-noise-ratios of cortical sources in magnetoencephalography and electroencephalography. *Hum. Brain Mapp.* 30, 4. doi:10.1002/hbm.20571

Guerreiro, M. M., Andermann, F., Andermann, E., Palmini, A., Hwang, P., Hoffman, H. J., et al. (1998). Surgical treatment of epilepsy in tuberous sclerosis strategic and results in 18 patients. *Neurology* 51, 5. doi:10.1212/WNL.51.5.1263

Gulani, V., Webb, A. G., Duncan, I. D., and Lauterbur, P. C. (2001). Apparent diffusion tensor measurements in myelin-deficient rat spinal cords. *Magn. Reson. Med.* 45, doi:10.1002/1522-2594(200102)45:2<191:AID-MRM1025>3.0.CO;2-9

Hämäläinen, M. S., and Ilmoniemi, R. J. (1994). Interpreting magnetic fields of the brain: minimum norm estimates. *Med. Biol. Eng. Comput.* 32, doi:10.1007/2FBF02512476

Haueisen, J., Boettner, A., Funke, M., Brauer, H., and Nowak, H. (1997). The influence of boundary element discretization on the forward and inverse problem in electroencephalography and magnetoencephalography. *Biomed. Eng.* 42, 9. doi:10.1515/bmte.1997.42.9.240

Haueisen, J., Funke, M., Güllmar, D., and Eichardt, R. (2012). Tangential and radial epileptic spike activity: different sensitivity in EEG and MEG. *J. Clin. Neurophysiol.* 29, 4. doi:10.1097/WNP.0b013e3182624491

Iida, K., Otsubo, H., Matsumoto, Y., Ochi, A., Oishi, M., Holowka, S., et al. (2005). Characterizing magnetic spike sources by using magnetoencephalography-guided neuronavigation in epilepsy surgery in pediatric patients. *J. Neurosurg.* 102, 2. doi:10.3171/jns.2005.102.2.0187

Iwasaki, M., Pestana, E., Burgess, R. C., Lüders, H. O., Shamoto, H., and Nakasato, N. (2005). Detection of epileptiform activity by human interpreters: blinded comparison between electroencephalography and magnetoencephalography. *Epilepsia* 46, 1. doi:10.1111/j.0013-9580.2005.21104.x

Jacobs, J., Rohr, A., Moeller, F., Boor, R., Kobayashi, E., LeVan Meng, P., et al. (2008). Evaluation of epileptogenic networks in children with tuberous sclerosis complex using EEG-fMRI. *Epilepsia* 49, 5. doi:10.1111/j.1528-1167.2007.01486.x

Jansen, F. E., Braun, K. P., van Nieuwenhuizen, O., Huiskamp, G., Vincken, K. L., van Huffelen, A. C., et al. (2003). Diffusion-weighted magnetic resonance imaging and identification of the epileptogenic tuber in patients with tuberous sclerosis. *Arch. Neurol.* 60, 11. doi:10.1001/archneur.60.11.1580

Jansen, F. E., Huiskamp, G., van Huffelen, A. C., Bourez-Swart, M., Boere, E., Gebbink, T., et al. (2006). Identification of the epileptogenic tuber in patients with tuberous sclerosis: a comparison of high-resolution EEG and MEG. *Epilepsia* 47, 1. doi:10.1111/j.1528-1167.2006.00373.x

Jansen, F. E., van Huffelen, A. C., Algra, A., and van Nieuwenhuizen, O. (2007). Epilepsy surgery in tuberous sclerosis: a systematic review. *Epilepsia* 48, 8. doi:10.1111/j.1528-1167.2007.01117.x

Kamimura, T., Tohyama, J., Oishi, M., Akasaka, N., Kanazawa, O., Sasagawa, M., et al. (2006). Magnetoencephalography in patients with tuberous sclerosis and localization-related epilepsy. *Epilepsia* 47, 6. doi:10.1111/j.1528-1167.2006.00511.x

Karadag, D., Mentzel, H. J., Güllmar, D., Rating, T., Lobel, U., Brandl, U., et al. (2005). Diffusion tensor imaging in children and adolescents with tuberous sclerosis. *Pediatr. Radiol.* 35, 10. doi:10.1007/s00247-005-1504-9

Karenfort, M., Kruse, B., Freitag, H., Pannek, H., and Tuxhorn, I. (2002). Epilepsy surgery outcome in children with focal epilepsy due to tuberous sclerosis complex. *Neuropediatrics* 33, 5. doi:10.1055/s-2002-36740

Kargiotis, O., Lascano, A. M., Garibotto, V., Spinelli, L., Genetti, M., Wissmeyer, M., et al. (2013). Localization of the epileptogenic tuber with electric source imaging in patients with tuberous sclerosis. *Epilepsy Res.* 108, 2. doi:10.1016/j.eplepsyres.2013.11.003

Kaufmann, R., Kornreich, L., and Goldberg-Stern, H. (2009). Unusual clinical presentation of tuberless tuberous sclerosis complex. *J. Clin. Neurol.* 24, 3. doi:10.1177/0883073808325659

Koh, S., Jayakar, P., Dunoyer, C., Whiting, S. E., Resnick, T. J., Alvarez, L. A., et al. (2000). Epilepsy surgery in children with tuberous sclerosis complex: presurgical evaluation and outcome. *Epilepsia* 41, 9. doi:10.1111/j.1528-1157.2000.tb00327.x

Kotagal, P. (2001). "Epilepsy in the setting of neurocutaneous syndromes," in *The Treatment of Epilepsy: Principles and Practice*, ed. E. Wyllie (Philadelphia: Lippincott Williams & Wilkins), 627–636.

Kumar, R., Macey, P. M., Woo, M. A., Alger, J. R., and Harper, R. M. (2008). Diffusion tensor imaging demonstrates brainstem and cerebellar abnormalities in congenital central hypoventilation syndrome. *Pediatr. Res.* 64, 275–280. doi:10.1203/PDR.0b013e31817da10a

Kumar, R., Macey, P. M., Woo, M. A., and Harper, R. M. (2010). Rostral brain axonal injury in congenital central hypoventilation syndrome. *J. Neurosci. Res.* 88, 10. doi:10.1002/jnr.22385

Lachhwani, D. K., Pestana, E., Gupta, A., Kotagal, P., Bingaman, W., and Wyllie, E. (2005). Identification of candidates for epilepsy surgery in patients with tuberous sclerosis. *Neurology* 64, 9. doi:10.1212/01.WNL.0000160389.93984.53

Lantz, G., Spinelli, L., Seeck, M., de Peralta Menendez, R. G., Sottas, C. C., and Michel, C. M. (2003). Propagation of interictal epileptiform activity can lead to erroneous source localizations: a 128-channel EEG mapping study. *J. Clin. Neurophysiol.* 20, 4. doi:10.1097/00004691-200309000-00003

Leahy, R. M., Mosher, J. C., Spencer, M. E., Huang, M. X., and Lewine, J. D. (1998). A study of dipole localization accuracy for MEG and EEG using a human skull phantom. *Electroencephalogr. Clin. Neurophysiol.* 107, 2.

Leal, A. J., Dias, A. I., Vieira, J. P., Moreira, A., Távora, L., and Calado, E. (2008). Analysis of the dynamics and origin of epileptiform activity in patients with tuberous sclerosis evaluated for surgery of epilepsy. *Clin. Neurophysiol.* 119, 4. doi:10.1016/j.clinph.2007.11.176

Major, P., Rakowski, S., Simon, M. V., Cheng, M. L., Eskandar, E., Baron, J., et al. (2009). Are cortical tubers epileptogenic? Evidence from electrocorticography. *Epilepsia* 50, 1. doi:10.1111/j.1528-1167.2008.01814.x

Makki, M. I., Chugani, D. C., Janisse, J., and Chugani, H. T. (2007). Characteristics of abnormal diffusivity in normal-appearing white matter investigated with diffusion tensor MR imaging in tuberous sclerosis complex. *AJNR Am. J. Neuroradiol.* 28, 9. doi:10.3174/ajnr.A0642

Michel, C. M., Murray, M. M., Lantz, G., Gonzalez, S., Spinelli, L., and Grave de Peralta, R. (2004). EEG source imaging. *Clin. Neurophysiol.* 115, 10. doi:10.1016/j.clinph.2004.06.001

Nair, G., Tanahashi, Y., Low, H. P., Billings-Gagliardi, S., Schwartz, W. J., and Duong, T. Q. (2005). Myelination and long diffusion times alter diffusion-tensor-imaging contrast in myelin-deficient shiverer mice. *Neuroimage* 28, 1. doi:10.1016/j.neuroimage.2005.05.049

Nakasato, N., Levesque, M. F., Barth, D. S., Baumgartner, C., Rogers, R. L., and Sutherling, W. W. (1994). Comparisons of MEG, EEG, and ECoG source localization in neocortical partial epilepsy in humans. *Electroencephalogr. Clin. Neurophysiol.* 91, 3. doi:10.1016/0013-4694(94)90067-1

O'Callaghan, F. J., Shiell, A. W., Osborne, J. P., and Martyn, C. N. (1998). Prevalence of tuberous sclerosis estimated by capture-recapture analysis. *Lancet* 351, 9114. doi:10.1016/2FS0140-6736(05)78872-3

Ochi, A., Hung, R., Weiss, S., Widjaja, E., To, T., Nawa, Y., et al. (2011). Lateralized interictal epileptiform discharges during rapid eye movement sleep correlate with epileptogenic hemisphere in children with intractable epilepsy secondary to tuberous sclerosis complex. *Epilepsia* 52, 11. doi:10.1111/j.1528-1167.2011.03198.x

Okada, Y., Pratt, K., Atwood, C., Mascarenas, A., Reineman, R., Nurminen, J., et al. (2006). BabySQUID: a mobile, high-resolution multichannel magnetoencephalography system for neonatal brain assessment. *Rev. Sci. Instrum.* 77, 2. doi:10.1063/1.2168672

Onal, C., Otsubo, H., Araki, T., Chitoku, S., Ochi, A., Weiss, S., et al. (2003). Complications of invasive subdural grid monitoring in children with epilepsy. *J. Neurosurg.* 98, 5. doi:10.3171/jns.2003.98.5.1017

Papadelis, C., Harini, C., Ahtam, B., Chiran, D., Grant, E., and Okada, Y. (2013). Current and emerging potential for magnetoencephalography in pediatric epilepsy. *J. Pediatr.* Epileplsy 2, 1. doi:10.3233/PEP-13040

Papadelis, C., Poghosyan, V., Fenwick, P. B., and Ioannides, A. A. (2009). MEG's ability to localise accurately weak transient neural sources. *Clin. Neurophysiol.* 120, 11. doi:10.1016/j.clinph.2009.08.018

Park, H. M., Nakasato, N., Iwasaki, M., Shamoto, H., Tominaga, T., and Yoshimoto, T. (2004). Comparison of magnetoencephalographic spikes with and without concurrent electroencephalographic spikes in extratemporal epilepsy. *Tohoku J. Exp. Med.* 203, 3. doi:10.1620/tjem.203.165

Peng, S. S., Lee, W. T., Wang, Y. H., and Huang, K. M. (2004). Cerebral diffusion tensor images in children with tuberous sclerosis: a preliminary report. *Pediatr. Radiol.* 34, 5. doi:10.1007/s00247-004-1162-3

Ramantani, G., Boor, R., Paetau, R., Ille, N., Feneberg, R., Rupp, A., et al. (2006). MEG versus EEG: influence of background activity on interictal spike detection. *J. Clin. Neurophysiol.* 23, 6. doi:10.1097/01.wnp.0000240873.69759.cc

Ray, A., Tao, J. X., Hawes-Ebersole, S. M., and Ebersole, J. S. (2007). Localizing value of scalp EEG spikes: a simultaneous scalp and intracranial study. *Clin. Neurophysiol.* 118, 1. doi:10.1016/j.clinph.2006.09.010

Rodin, E., Funke, M., Berg, P., and Matsuo, F. (2004). Magnetoencephalographic spikes not detected by conventional electroencephalography. *Neurophysiol. Clin.* 115, 9. doi:10.1016/j.clinph.2004.04.002

Romanelli, P., Verdecchia, M., Rodas, R., Seri, S., and Curatolo, P. (2004). Epilepsy surgery for tuberous sclerosis. *Pediatr. Neurol.* 31, 4. doi:10.1016/j.pediatrneurol.2004.05.012

Song, S. K., Sun, S. W., Ju, W. K., Lin, S. J., Cross, A. H., and Neufeld, A. H. (2003). Diffusion tensor imaging detects and differentiates axon and myelin degeneration in mouse optic nerve after retinal ischemia. *Neuroimage* 20, 3. doi:10.1016/j.neuroimage.2003.07.005

Song, S. K., Sun, S. W., Ramsbottom, M. J., Chang, C., Russell, J., and Cross, A. H. (2002). Dysmyelination revealed through MRI as increased radial (but unchanged axial) diffusion of water. *Neuroimage* 17, 3. doi:10.1006/nimg.2002.1267

Song, S. K., Yoshino, J., Le, T. Q., Lin, S. J., Sun, S. W., Cross, A. H., et al. (2005). Demyelination increases radial diffusivity in corpus callosum of mouse brain. *Neuroimage* 26, 1. doi:10.1016/j.neuroimage.2005.01.028

Sperli, F., Spinelli, L., Seeck, M., Kurian, M., Michel, C. M., and Lantz, G. (2006). EEG source imaging in pediatric epilepsy surgery: a new perspective in presurgical workup. *Epilepsia* 47, 6. doi:10.1111/j.1528-1167.2006.00550.x

Stefan, H., Hummel, C., Scheler, G., Genow, A., Druschky, K., Tilz, C., et al. (2003). Magnetic brain source imaging of focal epileptiform activity: a synopsis of 455 cases. *Brain* 126, 11. doi:10.1093/brain/awg239

Sugiyama, I., Imai, K., Yamaguchi, Y., Ochi, A., Akizuki, Y., Go, C., et al. (2009). Localization of epileptic foci in children with intractable epilepsy secondary to multiple cortical tubers by using synthetic aperture magnetometry kurtosis. *J. Neurosurg. Pediatr.* 4, 6. doi:10.3171/2009.7.peds09198

Sun, S. W., Liang, H. F., Cross, A. H., and Song, S. K. (2008). Evolving Wallerian degeneration after transient retinal ischemia in mice characterized by diffusion tensor imaging. *Neuroimage* 40, 1. doi:10.1016/j.neuroimage.2007.11.049

Tran, T. A., Spencer, S. S., Javidan, M., Pacia, S., Marks, D., and Spencer, D. D. (1997). Significance of spikes recorded on intraoperative electrocorticography in patients with brain tumor and epilepsy. *Epilepsia* 38, 10. doi:10.1111/j.1528-1157.1997.tb01203.x

Wang, Y., Greenwood, J. S., Calcagnotto, M. E., Kirsch, H. E., Barbaro, N. M., and Baraban, S. C. (2007). Neocortical hyperexcitability in a human case of tuberous sclerosis complex and mice lacking neuronal expression of TSC1. *Ann. Neurol.* 61, 2. doi:10.1002/ana.21058

Weiner, H. L. (2004). Tuberous sclerosis and multiple tubers: localizing the epileptogenic zone. *Epilepsia* 45(Suppl.4), doi:10.1111/j.0013-9580.2004.04009.x

Widjaja, E., Simao, G., Mahmoodabadi, S. Z., Ochi, A., Snead, O. C., Rutka, J., et al. (2010). Diffusion tensor imaging identifies changes in normal-appearing white matter within the epileptogenic zone in tuberous sclerosis complex. *Epilepsy Res.* 89, 2–3. doi:10.1016/j.eplepsyres.2010.01.008

Wu, J., Sutherling, W., Koh, S., Salamon, N., Jonas, R., Yudovin, S., et al. (2006). Magnetic source imaging localizes epileptogenic zone in children with tuberous sclerosis complex. *Neurology* 66, 8. doi:10.1212/01.wnl.0000208412.59491.9b

Xiao, Z., Xiang, J., Holowka, S., Hunjan, A., Sharma, R., Otsubo, H., et al. (2006). Volumetric localization of epileptic activities in tuberous sclerosis using synthetic aperture magnetometry. *Pediatr. Radiol.* 36, 1. doi:10.1007/s00247-005-0013-1

Yoshinaga, H., Nakahori, T., Ohtsuka, Y., Oka, E., Kitamura, Y., Kiriyama, H., et al. (2002). Benefit of simultaneous recording of EEG and MEG in dipole localization. *Epilepsia* 43, 8. doi:10.1046/j.1528-1157.2002.42901.x

Zaccariotti, V. A., Pannek, H. W., Holthausen, H., and Oppel, F. (1999). Evaluation with subdural plates in children and adolescents. *Neurol. Res.* 21, 463–474.

Ziolkowski, M., Haueisen, J., and Leder, U. (2002). Postprocessing of 3-D current density reconstruction results with equivalent ellipsoids. *IEEE Trans Biomed. Eng.* 49, 11. doi:10.1109/TBME.2002.804580

Conflict of Interest Statement: The authors declare that the research was conducted in the absence of any commercial or financial relationships that could be construed as a potential conflict of interest.

Received: 15 December 2013; accepted: 10 March 2014; published online: 26 March 2014.

Citation: Hunold A, Haueisen J, Ahtam B, Doshi C, Harini C, Camposano S, Warfield SK, Grant PE, Okada Y and Papadelis C (2014) Localization of the epileptogenic foci in tuberous sclerosis complex: a pediatric case report. Front. Hum. Neurosci. ***8****:175. doi: 10.3389/fnhum.2014.00175*

This article was submitted to the journal Frontiers in Human Neuroscience.

frontiers in
HUMAN NEUROSCIENCE

ORIGINAL RESEARCH ARTICLE
published: 24 March 2014
doi: 10.3389/fnhum.2014.00170

Somatosensory evoked field in response to visuotactile stimulation in 3- to 4-year-old children

Gerard B. Remijn[1,2]*, Mitsuru Kikuchi[3], Kiyomi Shitamichi[2], Sanae Ueno[2], Yuko Yoshimura[2,4], Kikuko Nagao[3,4], Tsunehisa Tsubokawa[5], Haruyuki Kojima[6], Haruhiro Higashida[3] and Yoshio Minabe[2]

[1] International Education Center, Kyushu University, Fukuoka, Japan
[2] Department of Psychiatry and Neurobiology, Graduate School of Medical Science, Kanazawa University, Kanazawa, Japan
[3] Research Center for Child Mental Development, Kanazawa University, Kanazawa, Japan
[4] Higher Brain Functions and Autism Research, Department of Child Development, United Graduate School of Child Development, Osaka University, Osaka, Japan
[5] Department of Anesthesiology, Kanazawa University, Kanazawa, Japan
[6] Department of Psychology, Kanazawa University, Kanazawa, Japan

Edited by:
Christos Papadelis, Harvard Medical School, USA

Reviewed by:
Giancarlo Zito, 'S. Giovanni Calibita' Fatebefratelli Hospital, Italy
William C. Gaetz, The Children's Hospital of Philadelphia, USA

***Correspondence:**
Gerard B. Remijn, International Education Center, Faculty of Design, Kyushu University, Minami-ku, Shiobaru 4-9-1, Fukuoka 815-8545, Japan
e-mail: remijn@design.kyushu-u.ac.jp

A child-customized magnetoencephalography system was used to investigate somatosensory evoked field (SEF) in 3- to 4-year-old children. Three stimulus conditions were used in which the children received tactile-only stimulation to their left index finger or visuotactile stimulation. In the two visuotactile conditions, the children received tactile stimulation to their finger while they watched a video of tactile stimulation applied either to someone else's finger (the finger-touch condition) or to someone else's toe (the toe-touch condition). The latencies and source strengths of equivalent current dipoles (ECDs) over contralateral (right) somatosensory cortex were analyzed. In the preschoolers who provided valid ECDs, the stimulus conditions induced an early-latency ECD occurring between 60 and 68 ms mainly with an anterior direction. We further identified a middle-latency ECD between 97 and 104 ms, which predominantly had a posterior direction. Finally, initial evidence was found for a late-latency ECD at about 139–151 ms again more often with an anterior direction. Differences were found in the source strengths of the middle-latency ECDs among the stimulus conditions. For the paired comparisons that could be formed, ECD source strength was more pronounced in the finger-touch condition than in the tactile-only and the toe-touch conditions. Although more research is necessary to expand the data set, this suggests that visual information modulated preschool SEF. The finding that ECD source strength was higher when seen and felt touch occurred to the same body part, as compared to a different body part, might further indicate that connectivity between visual and tactile information is indexed in preschool somatosensory cortical activity, already in a somatotopic way.

Keywords: magnetoencephalography, somatosensory evoked field, somatosensory cortex, preschool child, visuotactile stimulation

INTRODUCTION

Magnetoencephalography (MEG) has become an important tool to investigate cortical activity related to sensory or cognitive processing in children of various ages (e.g., Kimura et al., 2004; Chen et al., 2010; Ciesielski et al., 2010; Gummadavelli et al., 2013). Until recently, pediatric MEG has been predominantly performed with systems designed for adult heads. For young children, such as those of preschool age, the adult MEG helmet is not ideal. Preschoolers have considerably smaller heads than adults, and since magnetic field strength decreases with increasing distance between the expected source location and the MEG sensor array (Marinkovic et al., 2004; Gaetz et al., 2008), MEG measurements can be reliably obtained only if the children are repositioned such that one side of their head is as close to the sensor surface as possible (e.g., Pihko et al., 2009). A further requirement is that the children have to minimize head and bodily movements during testing. Under natural testing conditions this is especially challenging for preschoolers aged 2- to 5-years old, since children in this age group are generally less able to suppress movements and to follow procedural instructions (for a review see Pang, 2011). While substantial MEG research has been performed with sleeping or sedated preschoolers in clinical evaluation settings (e.g., Bercovici et al., 2008; Schwartz et al., 2008; Pihko et al., 2009), few studies so far have accomplished preschool MEG measurements under natural and awake testing conditions in an adult MEG system (Fujioka and Ross, 2008; Gaetz et al., 2010).

In order to facilitate pediatric MEG, a system with a child-customized helmet has recently been developed. This helmet allows a more natural fit around the child's head and has taken away the need for repositioning the head in the dewar (e.g., Gaetz et al., 2008). To date, child-customized MEG has been successfully used with 3- to 6-year-old children to obtain auditory evoked fields to broadband noise (Johnson et al., 2010) and speech (Kikuchi et al., 2011; Ueno et al., 2012; Yoshimura et al., 2012). In

the present study, we employed the system to study preschool cortical activity related to modalities other than hearing. We report a study on preschool somatosensory evoked field (SEF) in response to tactile and (multisensory) visuotactile stimuli.

Our first purpose was to expand the literature on preschool SEF. Preschool SEF in response to tactile stimulation has been reported in relatively few studies, each employing an adult MEG helmet (Gondo et al., 2001; Xiang et al., 2004; Gaetz et al., 2008; Pihko et al., 2009). Pihko et al. (2009) found that, during tactile stimulation to the finger, preschool children (1.6- to 6-years old) show a first prominent deflection in the waveform at around 50 ms (M50 component) over contralateral somatosensory cortex. The same study showed that an earlier component at around 30 ms occurs in toddlers and adults, but seldom in preschoolers. A later deflection at around 100 ms has been observed during stimulation to the thumb of toddlers (Gondo et al., 2001). This deflection, however, has not yet been reported in older preschoolers. Since still only few MEG data on preschool SEF exist, here we further investigate the deflections in the MEG waveform in 3- to 4-year-old children in response to tactile stimulation to the left index finger. The children were in natural, awake resting conditions and positioned in a child-customized MEG system.

Our second purpose was to investigate whether the deflections in the preschool waveform to tactile stimulation would already reflect modulation through visual information. In adults, it has been shown that merely watching stimulation to someone else's body part induces somatosensory activation in the viewer (e.g., Ebisch et al., 2008; Pihko et al., 2010; Meyer et al., 2011; for a review see Keysers et al., 2010). Modulatory effects of visual information containing "touch" to someone else's leg (Keysers et al., 2004), face, neck (Blakemore et al., 2005), and hand (Pihko et al., 2010) have been reported. Modulatory effects of vision have also been reported on SEF in response to tactile stimulation to an observer who watched tactile stimulation to others at the same time (Schaefer et al., 2006).

Some studies with adults have suggested that visuotactile brain responses are somatotopically organized. For example, in a study without direct tactile stimulation to the observer, Blakemore et al. (2005) found that the head area of primary somatosensory cortex was activated when observers watched touch to the face, but not to the neck. Other support for somatotopic organization has been reported in the field of action observation. Both the execution of hand and mouth actions and the mere observation of others' hand and mouth actions evoked activity in the corresponding premotor areas (Gazzola et al., 2006). Also in studies in which an observer watched stimulation to others while receiving direct tactile stimulation to the self, adult somatosensory activity seemed to reflect topographic selectivity. Motor-evoked potentials recorded from a hand region were differently modulated during observation of painful stimuli to the same hand region as compared to the foot (Avenanti et al., 2005). In preschoolers, however, modulation of somatosensory responses through visual information has not yet been explored.

To this end, we studied the effect of vision on preschool SEF with visuotactile stimuli that either concerned the same or a different body part. The stimuli comprised two visuotactile conditions (**Figure 1**). While the children received tactile stimulation to their own left index finger, they either watched mild stimulation of the left index finger (finger-touch condition) or the left toe (toe-touch condition) of someone else on a video. Besides expanding the data set on preschool SEF to unimodal tactile stimulation, i.e., without any visually presented information, we investigated whether already at the preschool age SEF undergoes modulation through vision that is somatotopically selective. If so, the adult data would suggest that SEF source strength differs between stimulation with congruent visuotactile information (finger-touch condition) and incongruent visuotactile information (toe-touch condition).

MATERIALS AND METHODS

ETHICS STATEMENT

The procedures were approved by the Ethics Committee of Kanazawa University Hospital and followed the Declaration of Helsinki. At least one parent/caregiver of each preschool participant provided written, informed consent before participation. Face-scale ratings obtained after the experiment (see below) indicated that none of the preschoolers were uncomfortable with the tactile stimulation seen on video and that felt on the finger.

PARTICIPANTS

Thirty-eight Japanese preschool children (22 females and 16 males), with an average and median age of 4 years ± 1 month, participated in the experiment. All were children from staff members of Kanazawa University Hospital or recruited from nursery schools near the hospital, in Kanazawa city, Japan. The preschoolers were right-handed, as reported by their parent(s)/caregiver(s). All had normal vision and were in normal physical health. Test results from the Japanese adaptation of the Kaufman Assessment Battery for Children (Kaufman et al., 1987) indicated that all were typically developing.

TACTILE STIMULUS AND VISUOTACTILE STIMULI

Tactile stimulation was delivered to the infant's left index finger. A 100-Hz waveform, generated by a sinusoidal oscillator (Uchida Electric, Tokyo, Japan), was used to drive a piezo-electric pulse generator attached to the finger. The repetitive pulse caused a displacement of approximately 0.5 mm of the finger tissue. Each pulse lasted 4 ms and was presented at 2 Hz, with an average time randomization of 50%, for a period of 6 min in total. The intensity of the tactile stimulation was kept constant across participants. The pulse generator and the upper part of the magic tape used to hold the child's finger over the pulse were decorated with a miniature stuffed butterfly made of soft cloth. This was wrapped gently around the participant's index finger.

Two visual stimulus conditions with a duration of 30 s were used (**Figure 1**). In the finger-touch condition, the infant watched a female left hand set against a black background (5.3 cd/m^2). The hand's index finger was alternately and repetitively touched by one of the following six pointy objects: a tine of a metal fork, a tine of a plastic yellow fork, the tip of a black pen, and the tip of a blue pencil, a red pencil, or a yellow pencil. Visual objects were changed as to avoid the theoretical chance of interference from visually evoked magnetic field induced by too much repetition of the same visual stimulus. Movement lasted 5 s for each of the six objects, together constituting a finger-touch stimulus of 30 s. The order of

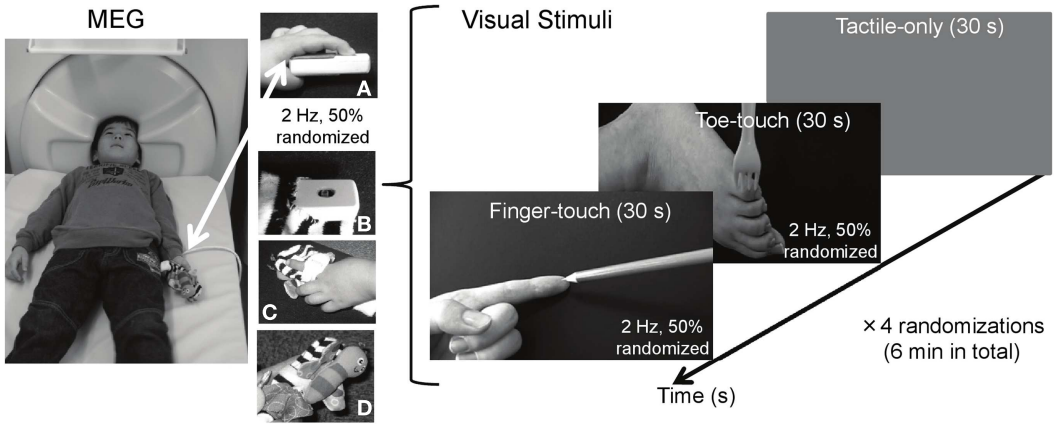

FIGURE 1 | Visuotactile stimulation used during MEG measurements of preschool somatosensory cortex. While tactile stimulation was applied to the left index finger, 3- to 4-year-old children watched tactile stimulation to someone else's left index finger (finger-touch condition) or to someone else's toe (toe-touch condition). The tactile stimulation to the children's left index finger during MEG measurements was applied through a piezo-electric stimulator **(A)**, decorated with a butterfly-like stuffed doll [**(B)** top-view; **(C)** top-view with child's finger; **(D)** side-view].

the objects was randomized for each preschool child. In the toe-touch condition, the participant watched a female left toe against the same black background. In a similar vein as in the finger-touch condition, in six randomized series of 5 s, the outside of the foot just below the little toe was touched by one of the six objects. In both the finger- and the toe-touch conditions, the objects touched the human tissue with a frequency of 2 Hz, with successive touches randomly occurring within 250–750 ms after one another. Since the felt and observed stimulation occurred to the same body part in the finger-touch condition, tactile and seen stimulation were desynchronized in order to avoid the illusion that the observed body part (e.g., the finger in the finger-touch video) was part of the observer' own body. Such a complex percept would be difficult to study reliably with preschoolers and might have been confusing to them. The two visuotactile conditions were presented with a tactile-only condition, in which the infant watched a gray screen ($26.5\,cd/m^2$) with a white fixation cross to rest his/her eyes. The fixation cross subtended 1×1 deg in visual angle ($112.4\,cd/m^2$) and was centered in the middle of the screen.

The finger-touch, toe-touch, and the tactile-only displays were generated and controlled by a personal computer (NEC VersaPro VA9), and back-projected from a display projector (Sharp PG-B10S) through four mirrors onto a 30 cm × 21 cm screen, viewed from supine position through a mirror attached to the MEG dewar. The three stimulus conditions were each repeated four times, with the order randomized for each infant. In total, 240 visual events in the finger-touch and toe-touch conditions were displayed. The total duration of the MEG measurements was 6 min. The infant was instructed to remain in a fixed bodily position and watch the screen.

STIMULI (DIS)COMFORT JUDGMENTS

Before MEG measurement, the infant was asked whether the tactile stimulation to his/her index finger was comfortable or not and told that MEG-recording could be abandoned any time he/she wanted. None of the preschoolers reported dislike or discomfort toward the piezo-electric stimulator and/or the tactile stimulation, which was reported as mild, painless stimulation above sensation threshold. None of the preschoolers opted out of the experiment. After the experiment a face-scale (Wong and Baker, 1988) was used to obtain subjective impressions of the infant's (dis)comfort with the tactile stimulation to the index finger and that seen on video. The face-scale consisted of pictures of cartoon-like faces, showing happiness (smiling) or sadness (in tears) in five intermediate steps (0–4), with "0" representing "no sensation" to "4" representing "uncomfortable sensation." When asked what their score would be if a child were to receive an injection, all preschoolers responded the maximum "4." This indicated they had understood the usage and range of the face-scale. Face-scale ratings were obtained from 35 out of 38 infants. Overall, their ratings showed that the stimuli were not discomforting. In the tactile-only condition, (dis)comfort to the finger stimulation was judged as 1.34 ± 0.26. When watching the finger-touch and the toe-touch video, this was 1.51 ± 0.23 and 1.30 ± 0.21, respectively. One-way analysis of variance (ANOVA) showed no significant difference between conditions [$F(2, 68) = 0.28$, $p = 0.75$].

MEG MEASUREMENTS AND DATA ANALYSIS

Somatosensory evoked field was recorded with a 151-channel SQUID (Super conducting Quantum Interference Device) whole-head coaxial gradiometer MEG system for children (PQ1151R, Yokogawa Electric, Kanazawa, Japan). The pick-up coils of the MEG system were 15.5 mm in diameter, the mean distance between two adjacent coils was 22 mm, and the cool-to-warm (dewar-coil) separation was 20 mm. Recordings were made in a three-layered, magnetically shielded room (Daido Steel, Nagoya, Japan), installed at the MEG-research center of Yokogawa Electric Corporation (Kanazawa, Japan). In an attempt to make the measurement environment less intimidating to the infants, the shielded room was decorated with colorful pictures of cartoon characters, familiar and liked by most Japanese preschoolers. The infant lay in a supine position on a tray-bed (Yokogawa, PQ11TA)

adjusted to the height of the MEG dewar. One staff member (author YY) stayed in the shielded room to comfort the child and to encourage him/her to maintain a steady bodily position.

Magnetoencephalography data were acquired with a sampling rate of 1000 Hz and filtered with a 200-Hz low-pass filter. Time series were segmented into windows of 250 ms (−50 to 200 ms). Around 195–214 segments were averaged for each of the 151 magnetic sensors after baseline correction (−30 to −10 ms). An average of 9.7% of the segments with a noise contamination exceeding ±4 pT was excluded from the data before principal component analysis was performed for general noise reduction. At least 195 tactile events were analyzed for each condition. We determined the position of the head within the MEG dewar by measuring the magnetic fields after passing currents through coils that were attached at three locations of the head surface as the fiduciary points, with respect to the landmarks (nasion and pre-auricular points or mastoid tips). Since magnetic resonance imaging (MRI) anatomical data of the infants were not obtained, a 3-D coordinate system based on fixed MEG sensor locations was applied to calculate the equivalent current dipoles (ECDs) by using a spherical model of the volume conductor. This was fitted to the center of the fixed MEG coordinate system, after confirmation that each infant's head was located in the center of MEG dewar, by measuring the three locations of the head surface mentioned above (also see Yoshimura et al., 2012).

The single ECD model (Sarvas, 1987) was used to estimate the "center of gravity" of the current sources. We analyzed the latencies and the number of major deflection(s) in the waveform in subsequent order, and considered ECDs as valid only when (i) goodness of fit (GOF) was over 80%; (ii) the location of estimated dipoles was stable within ±5 mm of each coordinate during a period of at least 6 ms; and (iii) dipole intensities were less than 80 nA/m. As a consequence of following these criteria, there were cases in which only a single ECD in a multiple-peak waveform was considered for further analyses of source strength. ECDs for each stimulus condition were categorized according to latency with k-means cluster analysis, with the number of clusters set at three, according to the maximum number of observed major deflections in the data. Statistical analyses on the source strength were performed after taking the natural logarithm. Distribution normality was tested with the Shapiro–Wilk test and variance homogeneity was tested with Levene's test. If normality and variance homogeneity were not violated, analysis of variance (ANOVA) with independent samples was used to test the source strength between ECD latency categories within stimulus conditions, and between similar latency categories of different stimulus conditions. Paired t-tests were also performed to test source strengths between similar latency categories of different stimulus conditions, with Bonferroni correction on the alpha-level. Predominance of ECD direction within each latency category (anterior or posterior) was tested with the binomial test.

RESULTS

TACTILE-ONLY CONDITION

Figure 2 shows the three latency categories of the major deflections in the waveforms, with corresponding ECD source strengths, obtained in the tactile-only condition. The latencies of the ECDs that were in accordance with the criteria fell into categories that from here on are referred to as early-, middle-, and late-latency deflections. In the data of 17 infants, an early major deflection occurred on average at 61.65 ± 2.78 ms. In the waveform of four infants, this early peak was the only deflection observed. In eight infants, it was the first of a double-peak waveform, while in five infants, it was the first of a triple-peak waveform. In the waveforms of 11 infants, a middle-latency deflection could be observed on average at 103.82 ± 3.09 ms. In four infants, this middle-latency peak was the only deflection in the waveform. In three infants, it was the second deflection in a double-peak waveform, while in the remaining four, it was the second in a triple-peak waveform. In six infants, a late deflection in the waveform occurred on average at 150.50 ± 6.42 ms. In two infants, it was the late second in a double-peak waveform, whereas in four infants, it was the last in a triple-peak waveform.

In total, only five infants provided waveforms with double-peak deflections both of which obeyed the ECD criteria, whereas only four cases were found in which all three ECDs in a triple-peak waveform were valid. Paired comparisons between ECD source strengths over two or three latency categories would therefore suffer from a lack of power. Instead of repeated-measures ANOVA, one-way ANOVA for independent samples was performed between the source strengths of the ECDs in the three latency categories. Shapiro–Wilk tests showed no evidence for non-normality for the early-latency ($df = 17$, $p = 0.49$), middle-latency ($df = 11$, $p = 0.61$), and the late-latency ECDs ($df = 6$, $p = 0.47$), and homogeneity of variance was met as well (Levene statistic $= 0.63$, $p = 0.54$). The ANOVA showed that source strength did not significantly differ with latency category in the tactile-only condition [$F(2, 33) = 0.12$, $p = 0.89$]. The dipole coordinates and directions of the valid ECDs in the tactile-only condition are depicted in **Figure 3**. The tactile stimulation of the left index finger induced ECDs that were located over contralateral (right) cortex, approximately over somatosensory areas. Because of the young age of the participants, MRI-plots were not performed. Early-latency ECDs predominantly had an anterior dipole direction (14 out of 17 ECDs), rather than a posterior dipole direction. The binomial test showed that this difference was significant (two-sided, $p < 0.05$). Middle-latency ECDs were more often posteriorly directed (8 out of 11 ECDs), while late-latency ECDs were anteriorly directed in two-thirds of the cases (4 out of 6 ECDs). These trends in ECD direction in the middle-latency and late-latency category were not significant.

VISUOTACTILE CONDITIONS

The finger-touch condition induced major deflections with latency clusters that were similar as those observed in the tactile-only condition. In the finger-touch condition, an early-latency deflection occurred at 67.44 ± 1.60 ms ($n = 16$). In five children, this was the only major deflection in the waveform. In five children, it was the first of a double-peak waveform, and in six children, it was the first of a triple-peak waveform. A middle-latency deflection occurred at 101.50 ± 2.45 ms ($n = 16$). In four children, this was the only deflection in the waveform, in seven children, it was the second in a double-peak waveform, and in five children, it was the second in a triple-peak waveform. A late-latency deflection in the

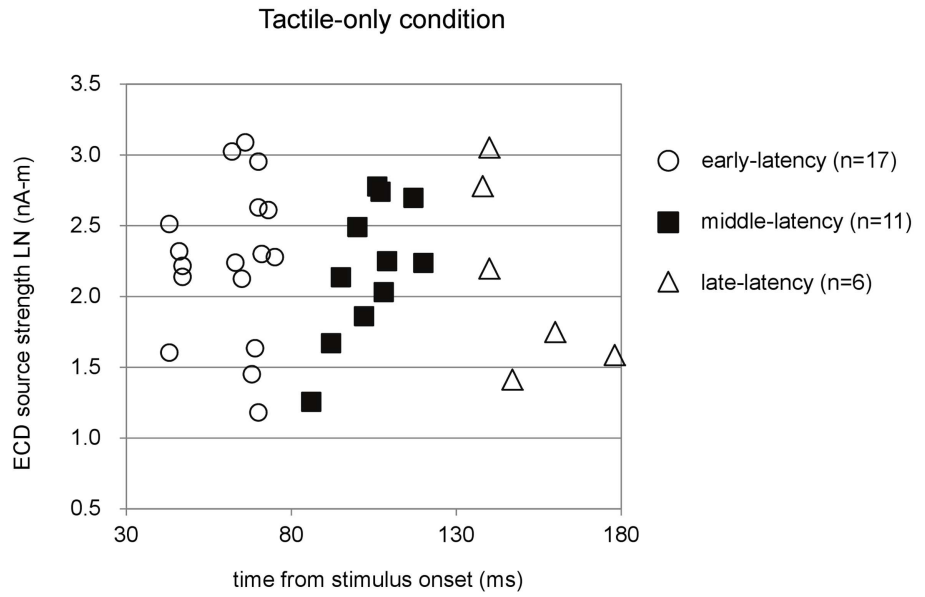

FIGURE 2 | Preschool ECD latencies and source strengths in the tactile-only condition. ECDs were obtained during piezo-electric stimulation to the left index finger of 3- to 4-year-old children. Note that the same participant could have provided data for more than one latency category, i.e., showed double-peak or triple-peak deflections in the MEG waveform that obeyed the ECD criteria. LN, natural logarithm; nA-m, nano-Ampere per meter; ms, milliseconds.

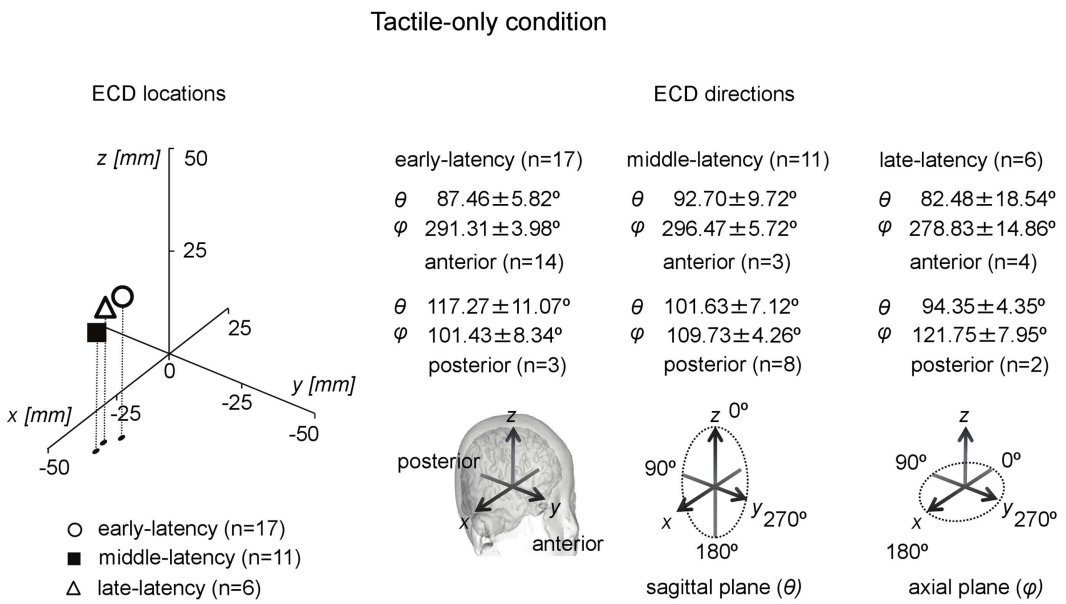

FIGURE 3 | Preschool ECD locations and directions in the tactile-only condition. ECDs were obtained during tactile stimulation to the left index finger, resulting in ECD locations in contralateral right hemisphere. Early-latency ECDs predominantly had an anterior direction. No significantly dominant direction pattern was observed for middle-latency and late-latency ECDs. Note that the same participant could have provided data for more than one category, i.e., showed double-peak or triple-peak deflections in the MEG waveform that obeyed the ECD criteria.

finger-touch condition occurred on average at 139.70 ± 3.38 ms ($n = 10$). It was the only deflection in the waveform of two children, the late second in the waveform of three children, and the third in the triple-peak waveform of five children. Only six children provided valid ECDs for both the early- and middle-latency categories, whereas only four children provided waveforms in which all ECDs in a triple-peak waveform were valid. One-way ANOVA for independent samples was therefore performed also

for the finger-touch data. Shapiro–Wilk tests showed no normality violations for the early-latency (df = 16, $p = 0.26$), middle-latency (df = 16, $p = 0.06$), and the late-latency ECD groups (df = 10, $p = 0.91$). The variances among the three groups also did not differ significantly (Levene statistic = 0.42, $p = 0.66$). One-way ANOVA showed no significant difference in source strength between the latency categories in the finger-touch condition [$F(2, 41) = 0.24$, $p = 0.79$].

In the toe-touch condition an early-latency deflection occurred at 60.82 ± 2.53 ms ($n = 22$). This deflection was the only peak in the waveform of six children, the first in a double-peak waveform observed in 12 children, and the first in a triple-peak waveform of four children. A middle-latency deflection occurred on average at 97.75 ± 2.75 ms ($n = 12$). This was a single deflection in the waveform of seven children, the second in a double-peak waveform in two children, and the second in a triple-peak waveform in three children. A late-latency deflection in the toe-touch condition appeared at 139.27 ± 3.88 ms ($n = 15$). For two children, this was the only valid major deflection. For eight children, it was the second deflection in a double-peak waveform, and for five children, it was the third in a triple-peak waveform. Four children provided valid ECDs for both the early- and middle-latency categories, and only three preschoolers provided waveforms in which all ECDs in a triple-peak waveform were valid. Shapiro–Wilk tests showed no normality violations for the early-latency (df = 22, $p = 0.09$), middle-latency (df = 12, $p = 0.53$), and the late-latency ECD groups (df = 15, $p = 0.21$). The variances among the three groups also did not differ significantly (Levene statistic = 0.48, $p = 0.62$). One-way ANOVA for independent samples showed that source strength differed significantly between latency categories in the toe-touch condition [$F(2, 48) = 3.59$, $p = 0.036$]. *Post hoc* Bonferroni tests showed that for the toe-touch condition the source strength in the early-latency category was higher than that in the middle-latency category ($p = 0.034$).

The ECDs in all three latency categories in both visuotactile conditions were located at the contralateral hemisphere. Analysis of ECD directions showed that ECDs in the early-latency category had a predominantly anterior direction. In the finger-touch condition 16 out of 17 ECDs were anteriorly directed. The binomial test showed that this difference was significant (two-sided, $p < 0.01$). In the toe-touch condition, 18 out of 22 ECDs with an early-latency had an anterior direction, which was significant as well (two-sided, $p < 0.01$). ECDs in the middle-latency category were significantly more posteriorly than anteriorly directed. In the finger-touch condition, 14 out of 16 ECDs (two-sided, $p < 0.01$), and in the toe-touch condition, 10 out of 12 (two-sided, $p < 0.05$) were posteriorly located. Late-latency ECDs again were significantly more anteriorly directed. Nine out of 10 ECDs in the finger-touch condition and 12 out of 15 ECDs in the toe-touch condition had an anterior direction (two-sided, $p < 0.05$ in both cases).

COMPARISONS BETWEEN ECD SOURCE STRENGTHS IN THE TACTILE-ONLY AND THE VISUOTACTILE CONDITIONS

For each latency category, ECD source strength between the three stimulus conditions was first compared with ANOVA for independent samples. ANOVA was performed after Levene's tests showed no deviance from distribution normality in the early-latency (Levene's statistic = 0.63, $p = 0.53$), the middle-latency (Levene's statistic = 1.38, $p = 0.37$), and the late-latency (Levene's statistic = 1.16, $p = 0.33$) ECD source strengths between stimulus conditions. In the case of unpaired comparisons, source strength between the tactile-only, the finger-touch, and the toe-touch condition did not differ for the early-latency [$F(2, 54) = 0.12$, $p = 0.89$], the middle-latency [$F(2, 38) = 1.35$, $p = 0.27$], and the late-latency [$F(2, 30) = 0.18$, $p = 0.83$] categories.

Paired comparisons between ECD source strengths in similar latency categories could be made with a limited number of cases. Because few children provided data for all three latency categories in all three stimulus conditions, repeated-measures ANOVA was not performed. Instead, where possible, we performed *t*-tests between pairs of stimulus conditions and applied Bonferroni correction on the alpha-level. The main results are depicted in **Figures 4–6**. Paired comparisons between the tactile-only and the finger-touch condition were made for the early-latency and the middle-latency category (**Figure 4**). The late-latency category provided only four pairs and thus was not tested. Six children provided valid pairs of early-latency ECD source strengths. Shapiro–Wilk tests showed no violations of distribution normality for the early-latency tactile-only (df = 6, $p = 0.11$) and the finger-touch condition (df = 6, $p = 0.06$). Under similar variances (Levene's statistic = 0.05, $p = 0.83$), ECD source strength did not differ between the two stimulus conditions ($t = -0.52$, df = 5, $p = 0.63$). Eight children provided valid ECDs in the middle-latency category. Both the data in the tactile-only (df = 8, $p = 0.89$) and the finger-touch conditions (df = 8, $p = 0.40$) were normally distributed and showed similar variances (Levene's statistic = 0.43, $p = 0.53$). In the middle-latency category, ECD source strength in the finger-touch condition was significantly higher than in the tactile-only condition with a Bonferroni-corrected alpha-level of 0.017 for multiple paired comparisons ($t = -3.66$, df = 7, $p < 0.01$).

Paired comparisons between the tactile-only and the toe-touch conditions were also made just for the early-latency and the middle-latency category, since late-latency data were provided by only five children (**Figure 5**). Thirteen children provided valid pairs of early-latency ECD source strengths, which were normally distributed in the tactile-only condition (df = 13, $p = 0.46$) and the toe-touch condition (df = 13, $p = 0.06$). Under similar variances (Levene's statistic = 0.34, $p = 0.57$), no significant difference was found between early-latency source strengths ($t = -0.80$, df = 12, $p = 0.44$). Seven pairs could be formed with valid middle-latency ECD data. These were normally distributed in both the tactile-only condition (df = 7, $p = 0.93$) and the toe-touch condition (df = 7, $p = 0.53$) and showed no unequal variances (Levene's statistic = 2.92, $p = 0.11$). In the middle-latency category, ECD source strength in the tactile-only condition was higher than that in the toe-touch condition ($t = 3.23$, df = 6, $p = 0.018$). With the Bonferroni-corrected alpha-level ($p = 0.017$), however, this difference would strictly be not significant.

Paired comparisons between the two visuotactile conditions could be made for all three latency categories (**Figure 6**). In the early-latency category 11 paired comparisons could be made. Shapiro–Wilk tests showed no violation of source strength normality in the early-latency finger-touch (df = 11, $p = 0.34$) and

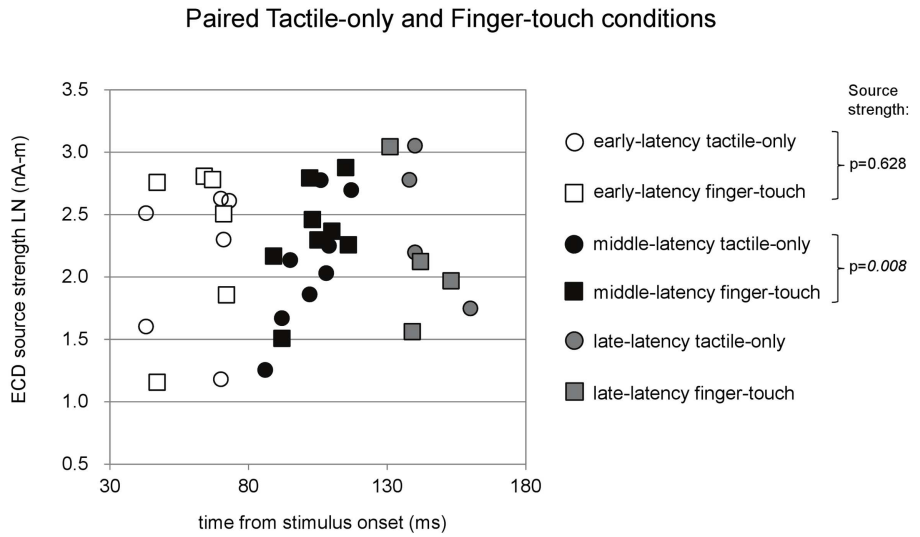

FIGURE 4 | Preschool ECD latencies and source strengths in paired tactile-only and finger-touch conditions. Circles show the tactile-only data and squares show the finger-touch data. White symbols show early-latency pairs ($n = 6$), black symbols show middle-latency pairs ($n = 8$), and gray symbols show late-latency pairs ($n = 4$). In the middle-latency category, ECD source strength was significantly higher in the finger-touch (filled black squares) than in the tactile-only condition (filled black circles). LN, natural logarithm; nA-m, nano-Ampere per meter; ms, millisecond.

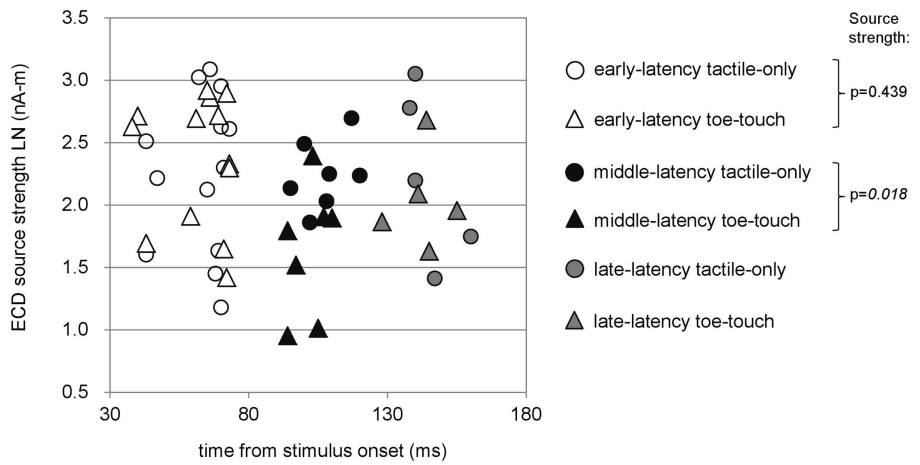

FIGURE 5 | Preschool ECD latencies and source strengths in paired tactile-only and toe-touch conditions. Circles show the tactile-only data and triangles show the toe-touch data. White symbols show early-latency pairs ($n = 13$), black symbols show middle-latency pairs ($n = 7$), and gray symbols show late-latency pairs ($n = 5$). In the middle-latency category, ECD source strength was higher in the tactile-only (filled black circles) than in the toe-touch condition (filled black triangles), but the difference strictly did not reach significance with Bonferroni correction of the alpha-level. LN, natural logarithm; nA-m, nano-Ampere per meter; ms, millisecond.

toe-touch condition ($df = 11$, $p = 0.48$). The variances in the source strengths also did not differ significantly (Levene statistic $= 0.30$, $p = 0.59$), and neither did the source strengths themselves ($t = 1.89$, $df = 10$, $p = 0.09$). For seven pairs in the late-latency category, source strength normality in the finger-touch ($df = 7$, 0.34) and the toe-touch ($df = 7$, 0.25) condition was not violated. Under homogeneity of variances (Levene's statistic $= 0.06$, $p = 0.81$), source strength in the late-latency categories did not significantly differ between the finger-touch and the toe-touch conditions ($t = 0.17$, $df = 6$, $p = 0.87$). Also for the middle-latency category seven pairs could be made. Both the source strength in the finger-touch ($df = 7$, $p = 0.24$) and toe-touch conditions ($df = 7$, $p = 0.55$) was normally distributed and variances were homogeneous (Levene's statistic $= 0.33$,

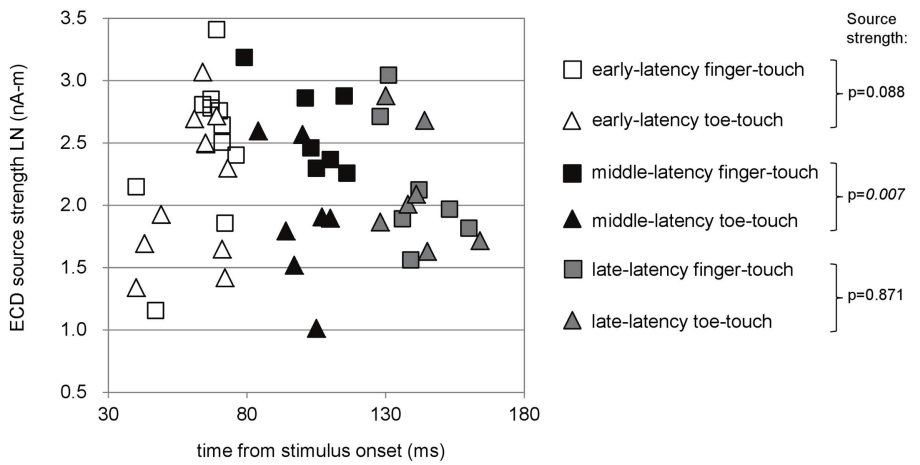

FIGURE 6 | Preschool ECD latencies and source strengths in paired finger-touch and toe-touch conditions. Squares show the finger-touch data and triangles show the toe-touch data. White symbols show early-latency pairs ($n = 11$), black symbols show middle-latency pairs ($n = 7$), and gray symbols show late-latency pairs ($n = 7$). In the middle-latency category, ECD source strength was significantly higher in the finger-touch (filled black squares) than in the toe-touch condition (filled black triangles). LN, natural logarithm; nA-m, nano-Ampere per meter; ms, millisecond.

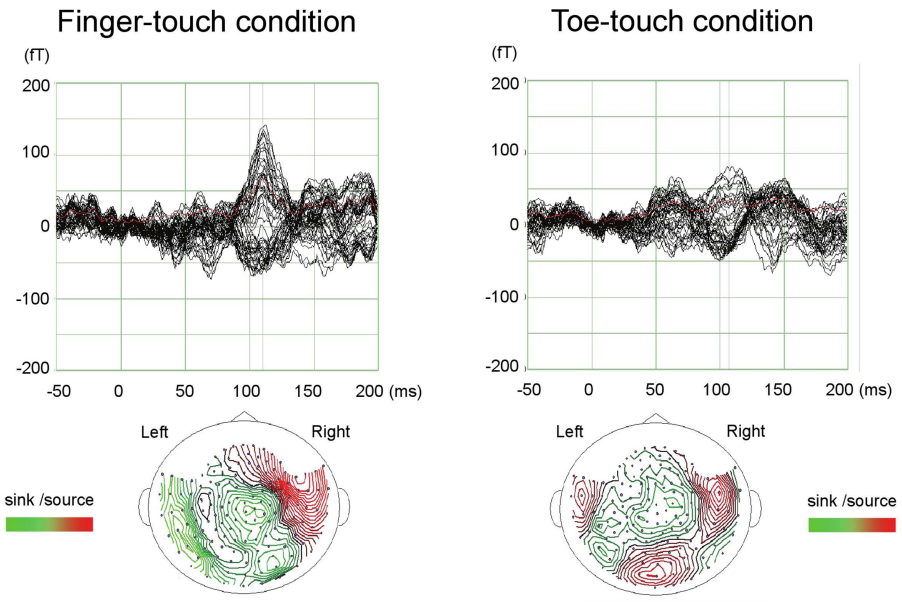

FIGURE 7 | An example of preschool SEF waveforms in the visuotactile finger-touch condition (left) and the toe-touch condition (right). The waveforms (top) and estimated ECDs (bottom) are shown for a 36-month-old girl. fT, femto-Tesla.

$p = 0.57$). The middle-latency source strength observed in the finger-touch condition was significantly higher than that in the toe-touch condition ($t = 3.97$, $df = 6$, $p < 0.01$). An example of the difference in the waveforms induced by the finger-touch and toe-touch conditions is depicted in **Figure 7**. ECD locations and directions of the paired finger- and toe-touch conditions are shown in **Figure 8**.

In summary, comparisons between ECD source strengths observed in the middle-latency categories of the three stimulus conditions showed that source strength was higher in the tactile-only condition than in the toe-touch condition. With a decreased alpha-level of 0.017 to correct for multiple comparisons, however, this difference was not significant. Even with alpha-level correction, however, middle-latency ECD source strength in

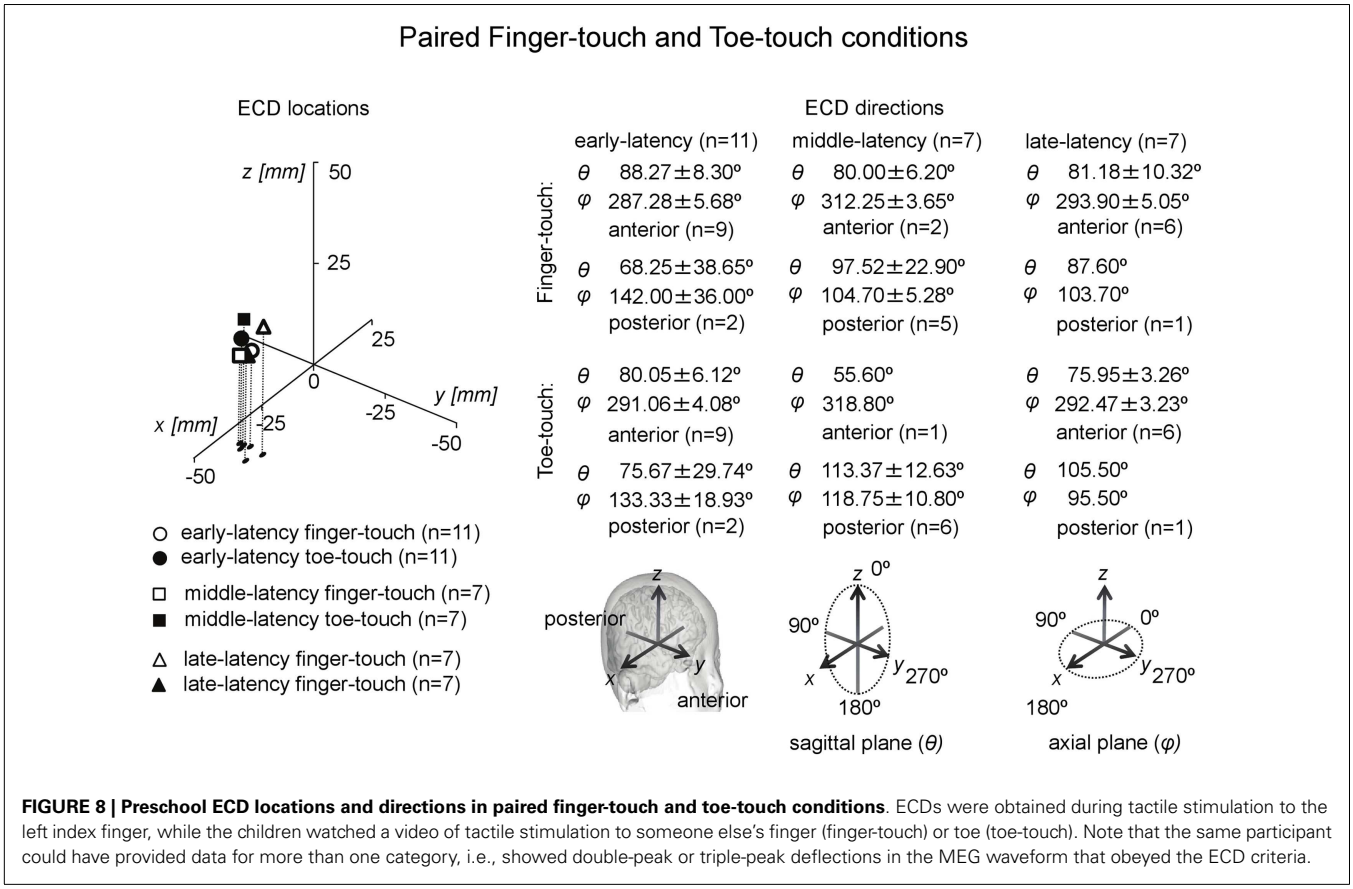

FIGURE 8 | Preschool ECD locations and directions in paired finger-touch and toe-touch conditions. ECDs were obtained during tactile stimulation to the left index finger, while the children watched a video of tactile stimulation to someone else's finger (finger-touch) or toe (toe-touch). Note that the same participant could have provided data for more than one category, i.e., showed double-peak or triple-peak deflections in the MEG waveform that obeyed the ECD criteria.

the finger-touch condition was significantly higher than in the toe-touch and the tactile-only conditions.

DISCUSSION

The present study is the first to use a child-customized MEG system to study somatosensory responses in preschool children. Besides a tactile-only condition, in which the left index finger of the preschoolers was stimulated, two visuotactile conditions were used. In one condition, the child received tactile stimulation to the index finger and at the same time watched a video of someone else being touched at the index finger. In another condition, the child received the tactile stimulation to the finger while watching a video of someone else being touched on the toe. ECD analysis showed that all three conditions induced contralateral (right-hemispheric) activity, which enabled valid dipole estimation in about 60% of the children. For all three stimulus conditions, a first valid ECD could be identified with a latency between 60 and 68 ms. This early-latency ECD had a predominantly anterior direction. The early-latency ECD strongly resembles that reported by Pihko et al. (2009), who analyzed preschool SEF with an adult MEG system. They too found a major deflection in the preschool waveform associated with an anteriorly directed dipole occurring around 60 ms (M60), but mainly in toddlers around 1 year of age in combination with an earlier component around 30 ms (M30). According to the authors, few preschoolers in the age of 1.6- to 6-years of age showed the M30, which is in accordance with the present study, but the preschoolers in the study of Pihko et al. (2009) did show a relatively prominent adult-like M50 with a posterior dipole direction. In the present study, over all conditions combined and including the cases that could not be considered in the paired comparisons, only eight preschoolers showed a posterior early-latency ECD. The average latency of this ECD was 50 ± 3.86 ms and thus indeed an M50. The vast majority (48) of the combined early-latency ECDs, however, had an anterior location with a longer latency between 60 and 68 ms. In the present study, most preschoolers thus still showed an M60. The source strengths of these early-latency ECDs did not differ between stimulus conditions. In the toe-touch condition, the early-latency ECD had a significantly more pronounced source strength than the following, middle-latency ECD.

The second, middle-latency ECD occurred on average between 97 and 104 ms in all three stimulus conditions. This latency seems to correspond with the data of Gondo et al. (2001), who reported a deflection with a latency of about 100 ms in the SEF of toddlers in response to tactile stimulation to the thumb. In the present data, the middle-latency deflection was posteriorly directed in 32 out of 39 ECDs combined over the three stimulus conditions. We further found that the source strength of the middle-latency ECD was subject to visual modulation. Although not significant with unpaired comparisons, the middle-latency ECD source strength in the finger-touch condition was significantly higher than that in the toe-touch condition in the case of paired comparisons ($n = 7$). Although paired comparisons between the source

strengths observed in the visuotactile and tactile-only conditions might be inappropriate, since the tactile-only condition was a condition in which the participants could rest their eyes on the screen and arguably made less eye movements, we further found that the finger-touch condition induced a significantly higher middle-latency source strength than the tactile-only condition for $n = 8$. ECD source strength, by contrast, was higher in the tactile-only than in the toe-touch condition in the middle-latency category. With Bonferroni correction on the alpha-level, however, this difference was not significant.

The differences in middle-latency source strength between stimulus conditions suggest that visual information modulates preschool SEF. The difference between congruent (finger-touch) and incongruent (toe-touch) visuotactile stimulation might further suggest that somatotopic linkage for seen and felt touch already develops in early childhood. Out of behavioral necessity, children must learn to recognize congruent visual and tactile information that is behaviorally relevant to them as soon as possible. For example, they must quickly learn to recognize whether an object can cause comfort or pain – often by visuotactile inspection. The sparse literature related to somatotopy in child cortex concerns studies on phantom limb experiences in persons with congenitally absent limbs. In spite of being limb-deficient from birth, some of these persons experienced phantom limbs since early childhood (Poeck, 1964). The representations are likely built up through visuotactile input (Hunter et al., 2003), for example, from observation and feeling the intact limb of the self and others. Further research is necessary, though, to gain more evidence for somatotopy in the preschool brain and to clarify the mechanisms that mediate it. In the present experiment, factors such as attentional engagement toward the stimuli may have contributed to the source strength difference in the paired middle-latency ECDs obtained in the visuotactile conditions. Some MEG studies with visuotactile stimuli have implicated or specifically investigated the role of attentional engagement to the stimuli (Mima et al., 1998; Iguchi et al., 2002, 2005; Hesse et al., 2010). We can speculate, for example, that while watching the finger-touch video the children increased their attention to the stimulation to their own finger. When watching the toe-touch video, however, the children might have "ignored" the stimulation to their finger by concentrating more on their toe. This could have caused a contrast in the response strength between the toe-touch and the finger-touch conditions, assuming that the videos of stimulation to someone else's body part indeed could manipulate attentional focus of the preschooler to his/her own body part. Future research might attempt to further investigate this by quantifying the viewers' looking behavior to the video by using an eye-tracking device. Inquiries about attentional engagement to the videos and their own body part might be performed with an interview, although preschoolers might not always provide accurate and reliable answers.

Besides the early- and middle-latency ECDs, a valid ECD with a late-latency could be observed in all the stimulus conditions. The late-latency ECD occurred between 139 and 151 ms and, to our knowledge, has not been reported in preschoolers before. In the tactile-only condition, the dipole direction was anterior in four out of six children. In the two visuotactile conditions this trend was stronger: in 21 out of 25 combined ECDs the dipole direction was anteriorly directed. Significant source strength differences in the late-latency ECDs were not found between stimulus conditions.

In summary, the present study with the child-customized MEG system confirmed the occurrence of an early-latency ECD connected with tactile stimulation to the finger with a latency of about 65 ms and a predominantly anterior direction. Middle-latency ECDs were observed at around 100 ms with a predominantly posterior dipole direction. Source strength differences between paired middle-latency ECDs suggest SEF modulation through visual information in general, with congruent visuotactile information (finger-touch condition) inducing a significantly larger source strength than incongruent visuotactile information (toe-touch condition). This might reflect the development of brain functional connectivity between visual and somatosensory areas, presumably in a somatotopic way. The present preschool data further indicate the occurrence of a late-latency ECD (around 145 ms), which tended to have an anterior direction. Further research on somatosensory activity in preschool cortex is necessary to test the existence and development of (somatotopic) modulation by visual information and to expand the data in general. Also with the child-customized MEG system used here, data contamination due to motion and concentration artifacts limited the quality of the data and, hence, the number of valid ECDs that could be used for statistical comparisons.

ACKNOWLEDGMENTS

This study was supported by the Strategic Research Program for Brain Sciences of MEXT and grant 22591276 from the Japan Society for the Promotion of Science (JSPS) to Gerard B. Remijn and Mitsuru Kikuchi. The authors would like to thank everyone at Yokogawa Electric Inc., Kanazawa, Japan for technical assistance, all the participants, and the parents/caregivers of the participants. We thank Dr. Elena Pihko for informal comments on the experiment and the two reviewers for their comments on the manuscript.

REFERENCES

Avenanti, A., Bueti, D., Galati, G., and Aglioti, S. M. (2005). Transcranial magnetic stimulation highlights the sensorimotor side of empathy for pain. *Nat. Neurosci.* 8, 955–960. doi:10.1038/nn1481

Bercovici, E., Pang, E. W., Sharma, R., Mohamed, I. S., Imai, K., Fujimoto, A., et al. (2008). Somatosensory-evoked fields on magnetoencephalography for epilepsy infants younger than 4 years with total intravenous anesthesia. *Clin. Neurophysiol.* 119, 1328–1334. doi:10.1016/j.clinph.2008.02.018

Blakemore, S.-J., Bristow, D., Bird, G., Frith, C., and Ward, J. (2005). Somatosensory activations during the observation of touch and a case of vision-touch synaesthesia. *Brain* 128, 1571–1583. doi:10.1093/brain/awh500

Chen, Y., Xiang, J., Kirtman, E. G., Wang, Y., Kotecha, R., and Liu, Y. (2010). Neuromagnetic biomarkers of visuocortical development in healthy children. *Clin. Neurophysiol.* 121, 1555–1562. doi:10.1016/j.clinph.2010.03.029

Ciesielski, K. T., Ahlfors, S. P., Bedrick, E. J., Kerwin, A. A., and Hämäläinen, M. S. (2010). Top-down control of MEG alpha-band activity in children performing Categorical N-Back Task. *Neuropsychologia* 48, 3573–3579. doi:10.1016/j.neuropsychologia.2010.08.006

Ebisch, S. J., Perrucci, M. G., Ferretti, A., Del Gratta, C., Romani, G. L., and Gallese, V. (2008). The sense of touch: embodied simulation in a visuotactile mirroring mechanism for observed animate and inanimate touch. *J. Cogn. Neurosci.* 20, 1611–1623. doi:10.1162/jocn.2008.20111

Fujioka, T., and Ross, B. (2008). Auditory processing indexed by stimulus-induced alpha desynchronization in children. *Int. J. Psychophysiol.* 2, 130–140. doi:10.1016/j.ijpsycho.2007.12.004

Gaetz, W., MacDonald, M., Cheyne, D., and Snead, O. C. (2010). Neuromagnetic imaging of movement-related cortical oscillations in children and adults: age predicts post-movement beta rebound. *Neuroimage* 51, 792–807. doi:10.1016/j.neuroimage.2010.01.077

Gaetz, W., Otsubo, H., and Pang, E. W. (2008). Magnetoencephalography for clinical pediatrics: the effect of head positioning on measurement of somatosensory evoked fields. *Clin. Neurophysiol.* 119, 1923–1933. doi:10.1016/j.clinph.2008.04.291

Gazzola, V., Aziz-Zadeh, L., and Keysers, C. (2006). Empathy and the somatotopic auditory mirror system in humans. *Curr. Biol.* 16, 1824–1829. doi:10.1016/j.cub.2006.07.072

Gondo, K., Tobimatsu, S., Kira, R., Tokunaga, Y., Yamamoto, T., and Hara, T. (2001). A magentoencephalographic study on development of the somatosensory cortex in infants. *Neuroreport* 12, 3227–3231. doi:10.1097/00001756-200110290-00017

Gummadavelli, A., Wang, Y., Guo, X., Pardos, M., Chu, H., Liu, Y., et al. (2013). Spatiotemporal and frequency signatures of word recognition in the developing brain: a magnetoencephalography study. *Brain Res.* 1498, 20–32. doi:10.1016/j.brainres.2013.01.001

Hesse, M. D., Nishitani, N., Fink, G. R., Jousmäki, V., and Hari, R. (2010). Attenuation of somatosensory responses to self-produced tactile stimulation. *Cereb. Cortex* 20, 425–432. doi:10.1093/cercor/bhp110

Hunter, J. P., Katz, J., and Davis, K. D. (2003). The effect of tactile and visual sensory inputs on phantom limb awareness. *Brain* 126, 579–589. doi:10.1093/brain/awg054

Iguchi, Y., Hoshi, Y., Tanosaki, M., Taira, M., and Hashimoto, I. (2002). Selective attention regulates spatial and intensity information processing in the human primary somatosensory cortex. *Neuroreport* 13, 2335–2339. doi:10.1097/00001756-200212030-00033

Iguchi, Y., Hoshi, Y., Tanosaki, M., Taira, M., and Hashimoto, I. (2005). Attention induces reciprocal activity in the human somatosensory cortex enhancing relevant- and suppressing irrelevant inputs from fingers. *Clin. Neurophysiol.* 116, 1077–1087. doi:10.1016/j.clinph.2004.12.005

Johnson, B. W., Crain, S., Thornton, R., Tesan, G., and Read, M. (2010). Measurement of brain function in pre-school children using a custom sized whole-head MEG sensor array. *Clin. Neurophysiol.* 121, 340–349. doi:10.1016/j.clinph.2009.10.017

Kaufman, A. S., O'Neal, M. R., Avant, A. H., and Long, S. W. (1987). Introduction to the Kaufman Assessment Battery for Children (K-ABC) for pediatric neuroclinicians. *J. Child Neurol.* 2, 3–16. doi:10.1177/088307388700200102

Keysers, C., Kaas, J. H., and Gazzola, V. (2010). Somatosensation in social perception. *Nat. Rev. Neurosci.* 11, 417–428. doi:10.1038/nrn2919

Keysers, C., Wicker, B., Gazzola, V., Anton, J. L., Fogassi, L., and Gallese, V. (2004). A touching sight: SII/PV activation during the observation and experience of touch. *Neuron* 42, 335–346. doi:10.1016/S0896-6273(04)00156-4

Kikuchi, M., Shitamichi, K., Yoshimura, Y., Ueno, S., Remijn, G. B., Hirosawa, T., et al. (2011). Lateralized theta wave connectivity and language performance in 2- to 5-year-old children. *J. Neurosci.* 31, 14984–14988. doi:10.1523/JNEUROSCI.2785-11.2011

Kimura, I., Kubot, M., Hirose, H., Yumoto, M., and Sakakihara, Y. (2004). Children are sensitive to averted eyes at the earliest stage of gaze processing. *Neuroreport* 15, 1345–1348. doi:10.1097/01.wnr.0000129574.43925.59

Marinkovic, K., Cox, B., Reid, K., and Halgren, E. (2004). Head position in the MEG helmet affects the sensitivity to anterior sources. *Neurol. Clin. Neurophysiol.* 2004:30.

Meyer, K., Kaplan, J. T., Essex, R., Damasio, H., and Damasio, A. (2011). Seeing touch is correlated with content-specific activity in primary somatosensory cortex. *Cereb. Cortex* 21, 2113–2121. doi:10.1093/cercor/bhq289

Mima, T., Nagamine, T., Nakamura, K., and Shibasaki, H. (1998). Attention modulates both primary and second somatosensory cortical activities in humans: a magnetoencephalographic study. *J. Neurophysiol.* 80, 2215–2221.

Pang, E. W. (2011). Practical aspects of running developmental studies in the MEG. *Brain Topogr.* 24, 253–260. doi:10.1007/s10548-011-0175-0

Pihko, E., Nangini, C., Jousmäki, V., and Hari, R. (2010). Observing touch activates human primary somatosensory cortex. *Eur. J. Neurosci.* 31, 1836–1843. doi:10.1111/j.1460-9568.2010.07192.x

Pihko, E., Nevalainen, P., Stephen, J., Okada, Y., and Lauronen, L. (2009). Maturation of somatosensory cortical processing from birth to adulthood revealed by magnetoencephalograph. *Clin. Neurophysiol.* 120, 1552–1561. doi:10.1016/j.clinph.2009.05.028

Poeck, K. (1964). Phantoms following amputation in early childhood and in congenital absence of limbs. *Cortex* 1, 269–275. doi:10.1016/S0010-9452(64)80002-2

Sarvas, J. (1987). Basic mathematical and electromagnetic concepts of the biomagnetic inverse problem. *Phys. Med. Biol.* 32, 11–22. doi:10.1088/0031-9155/32/1/004

Schaefer, M., Flor, H., Heinze, H.-J., and Rotte, M. (2006). Dynamic modulation of the primary somatosensory cortex during seeing and feeling a touched hand. *Neuroimage* 29, 587–592. doi:10.1016/j.neuroimage.2005.07.016

Schwartz, E. S., Dlugos, D. J., Storm, P. B., Dell, J., Magee, R., Flynn, T. P., et al. (2008). Magnetoencephalography for pediatric epilepsy: how we do it. *AJNR Am. J. Neuroradiol.* 29, 832–837. doi:10.3174/ajnr.A1029

Ueno, S., Okumura, E., Remijn, G. B., Yoshimura, Y., Kikuchi, M., Shitamichi, K., et al. (2012). Spatiotemporal frequency characteristics of cerebral oscillations during the perception of fundamental frequency contour changes in one-syllable intonation. *Neurosci. Lett.* 515, 141–146. doi:10.1016/j.neulet.2012.03.031

Wong, D., and Baker, C. (1988). Pain in children: comparison of assessment scales. *Pediatr. Nurs.* 14, 9–17.

Xiang, J., Holowka, S., Qiao, H., Sun, B., and Chuang, S. (2004). Volumetric estimation of functional brain regions in small children using spatially filtered magnetoencephalography: differentiating thumb from middle finger. *Neurol. Clin. Neurophysiol.* 2004:110.

Yoshimura, Y., Kikuchi, M., Shitamichi, K., Ueno, S., Remijn, G. B., Haruta, Y., et al. (2012). Language performance and auditory evoked fields in 2- to 5-year-old children. *Eur. J. Neurosci.* 35, 644–650. doi:10.1111/j.1460-9568.2012.07998.x

Conflict of Interest Statement: The authors declare that the research was conducted in the absence of any commercial or financial relationships that could be construed as a potential conflict of interest.

Received: 05 November 2013; accepted: 07 March 2014; published online: 24 March 2014.

Citation: Remijn GB, Kikuchi M, Shitamichi K, Ueno S, Yoshimura Y, Nagao K, Tsubokawa T, Kojima H, Higashida H and Minabe Y (2014) Somatosensory evoked field in response to visuotactile stimulation in 3- to 4-year-old children. Front. Hum. Neurosci. ***8****:170. doi: 10.3389/fnhum.2014.00170*

This article was submitted to the journal Frontiers in Human Neuroscience.

frontiers in
HUMAN NEUROSCIENCE

REVIEW ARTICLE
published: 17 March 2014
doi: 10.3389/fnhum.2014.00158

Development of human somatosensory cortical functions – what have we learned from magnetoencephalography: a review

Päivi Nevalainen[1,2]*, Leena Lauronen[1,2] and Elina Pihko[3]

[1] *BioMag Laboratory, Hospital District of Helsinki and Uusimaa, HUS Medical Imaging Center, Helsinki University Central Hospital, University of Helsinki, Helsinki, Finland*

[2] *Department of Clinical Neurophysiology, Children's Hospital, HUS Medical Imaging Center, Helsinki University Central Hospital, University of Helsinki, Helsinki, Finland*

[3] *Brain Research Unit, O.V. Lounasmaa Laboratory, Aalto University School of Science, Espoo, Finland*

Edited by:
Hubert Preissl, University of Tübingen, Germany

Reviewed by:
Douglas Owen Cheyne, The Hospital for Sick Children, Canada
Margot J. Taylor, The Hospital for Sick Children, Canada

Correspondence:
Päivi Nevalainen, BioMag Laboratory, Hospital District of Helsinki and Uusimaa, HUS Medical Imaging Center, Helsinki University Central Hospital, P.O. Box 340, Helsinki FIN-00029 HUS , Finland
e-mail: paivi.nevalainen@helsinki.fi

The mysteries of early development of cortical processing in humans have started to unravel with the help of new non-invasive brain research tools like multichannel magnetoencephalography (MEG). In this review, we evaluate, within a wider neuroscientific and clinical context, the value of MEG in studying normal and disturbed functional development of the human somatosensory system. The combination of excellent temporal resolution and good localization accuracy provided by MEG has, in the case of somatosensory studies, enabled the differentiation of activation patterns from the newborn's primary (SI) and secondary somatosensory (SII) areas. Furthermore, MEG has shown that the functioning of both SI and SII in newborns has particular immature features in comparison with adults. In extremely preterm infants, the neonatal MEG response from SII also seems to potentially predict developmental outcome: those lacking SII responses at term show worse motor performance at age 2 years than those with normal SII responses at term. In older children with unilateral early brain lesions, bilateral alterations in somatosensory cortical activation detected in MEG imply that the impact of a localized insult may have an unexpectedly wide effect on cortical somatosensory networks. The achievements over the last decade show that MEG provides a unique approach for studying the development of the somatosensory system and its disturbances in childhood. MEG well complements other neuroimaging methods in studies of cortical processes in the developing brain.

Keywords: magnetoencephalography, newborn, brain development, somatosensory system, preterm infant, cerebral palsy

INTRODUCTION

Around the time of full-term birth, the central nervous system (CNS) of a human newborn is developing dramatically (**Figure 1**). Transient fetal brain structures, such as the subplate zone, are resolving (Kostovic and Rakic, 1990; De Graaf-Peters and Hadders-Algra, 2006) and neurotransmitter systems are undergoing marked changes (Ben-Ari et al., 2004; Herlenius and Lagercrantz, 2004; Dzhala et al., 2005). The active phase in dendritic development and synaptogenesis continues for months to years after birth (Huttenlocher and Dabholkar, 1997), whereas myelination, axonal withdrawal, and synapse elimination may continue up to the third decade of life (Huttenlocher and Dabholkar, 1997). (For a review on the ontogeny of the human CNS, see De Graaf-Peters and Hadders-Algra, 2006.) Considering all of these ongoing changes, early infancy is a very exiting period to investigate the building of neural networks and their functional development.

In recent years, several non-invasive brain research methods have been introduced for *in vivo* studies of the developing CNS. Advanced magnetic resonance imaging (MRI) techniques [such as voxel-based morphometry and diffusion tensor imaging (DTI)] allow not only the visualization but also the quantification of gray and white matter structures (e.g., Mathur et al., 2010). Furthermore, functional MRI (fMRI) detects hemodynamic changes related to neural activation providing spatially accurate information about brain activation in response to a stimulus (for a review, see e.g., Seghier and Hüppi, 2010) or about the so called resting-state networks (for a review, see e.g., Smyser et al., 2011). Of the available neurophysiological methods, electroencephalography (EEG) and evoked potentials have a long history in studies of all age groups. Magnetoencephalography (MEG), on the other hand, has been used in studies of newborns and infants only relatively recently (for a review, see e.g., Huotilainen, 2006; Lauronen et al., 2011). All of these brain research methodologies have their pros and cons, and combining the results obtained with different methods provides a comprehensive picture of brain development. This review discusses the discoveries made with MEG concerning normal and abnormal development of the human somatosensory system in infancy and childhood.

Magnetoencephalography detects the weak extracranial magnetic fields produced by synchronous activity of tens of thousands of cortical pyramidal neurons. More specifically, the MEG

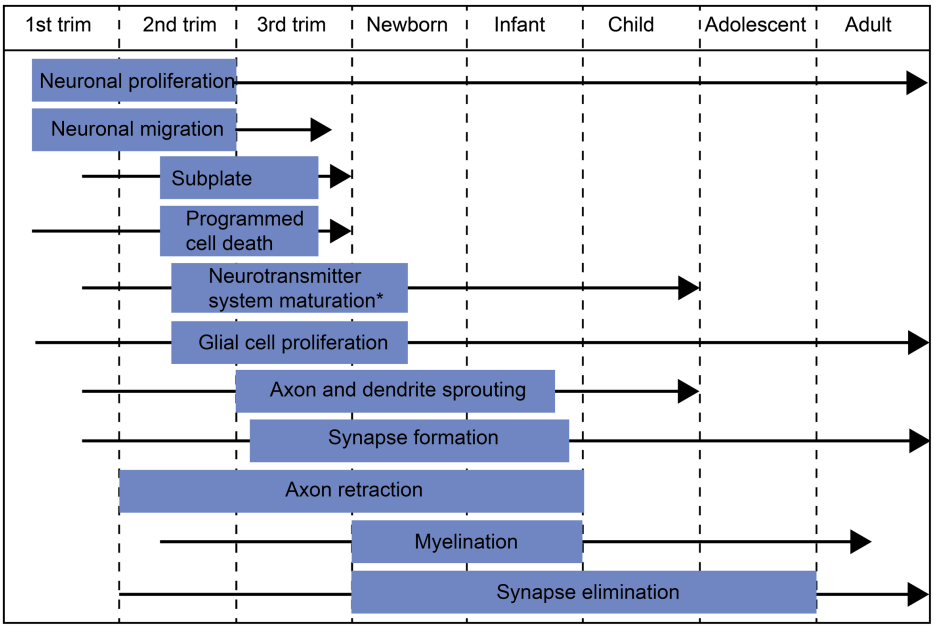

FIGURE 1 | Schematic diagram of major developmental events during embryonic/fetal life and infancy/early childhood. The blue box indicates the most active period of each developmental process and the black arrow the period when the process continues at a slower pace. *The most active period in neurotransmitter system maturation in general. The exact timescales of maturation for different neurotransmitter systems may differ from the indicated period.

signal is thought to reflect synaptically induced intracellular currents flowing in the apical dendrites of cortical pyramidal cells (Hämäläinen et al., 1993). Thus, similar to EEG, the temporal resolution of MEG is in the millisecond range. In the spatial domain, source localization is simpler for MEG than EEG data due to the inherently different properties of the two methods: MEG is less sensitive to conductivity differences between the measuring device and the active brain source, and MEG preferentially detects sources oriented tangentially to the skull surface, whereas EEG detects both radial and tangential sources (Hämäläinen et al., 1993). Consequently, with MEG, brain processes can be studied relatively accurately both in time and space.

Somatosensory responses can be evoked by electrical stimulation of a peripheral nerve (e.g., median nerve) or by tactile stimulation of the skin (e.g., on the digits). Stimulation of the median nerve at the wrist activates a mixture of afferent and efferent fibers, including those innervating many types of cutaneous receptors in about two thirds of the palmar side of the hand. In most of the experiments reviewed here, the tactile stimulation was provided with an inflatable plastic diaphragm driven with pulses of compressed air. Such a stimulus feels like a gentle tap on the fingertip and activates mainly slowly adapting mechanoreceptors in a relatively localized skin area. Compared with median nerve stimulation, the early somatosensory evoked field (SEF) deflections to tactile stimulation have usually lower response amplitudes, and slightly longer latencies (**Figure 2**), partly due to the more distal stimulation site (e.g., wrist vs. fingertip). Nevertheless, in adults, the early cortical SEFs to both median nerve (SEF_{MN}) and tactile stimulation (SEF_T) consist of an initial deflection with an underlying current source pointing anteriorly (though this deflection is often minute after tactile stimulation, **Figure 2**, $SEF_{MN}20$ and SEF_T30[1]), and a subsequent deflection with current pointing posteriorly (**Figure 2**, $SEF_{MN}35$ and SEF_T50). The following sections discuss how and when such somatosensory response patterns are attained in infancy and what kind of underlying processes this development might reflect.

NORMAL DEVELOPMENT OF THE SOMATOSENSORY SYSTEM

In the following sections, we first review different aspects of somatosensory development and then discuss the relevant findings of developmental somatosensory MEG studies.

FROM THE PERIPHERY TO THE PRIMARY SOMATOSENSORY AREAS

Postmortem studies in human infants have shown that in the primary somatosensory areas, thalamic axons grow through

[1]The nomenclature used in the SEF and SEP literature for the different response components is variable and easily confusing. It is based on a long tradition of SEP studies, where the components are named according to their latency and the direction of the potential difference in an electrode, e.g., N20 for a deflection at 20 ms with a negative value with respect to a reference electrode. SEFs are often named accordingly, e.g., N20m, with the *m* referring to "magnetic." The nomenclature gets even more confusing with different stimulation methods and in recordings of infants/children, where latencies (and hence nomenclature) deviate from those of adults. For clarity, in this review, we will use SEF/SEP_{MN} and SEF/SEP_T for adult responses to median nerve and tactile stimuli, respectively, and sef/sep_{MN} and sef/sep_T for the respective responses of children. The number following the abbreviation of a response component refers to the latency of each response; e.g., $SEF_{MN}20$ indicates adult SEF to median nerve stimulation peaking at 20 ms.

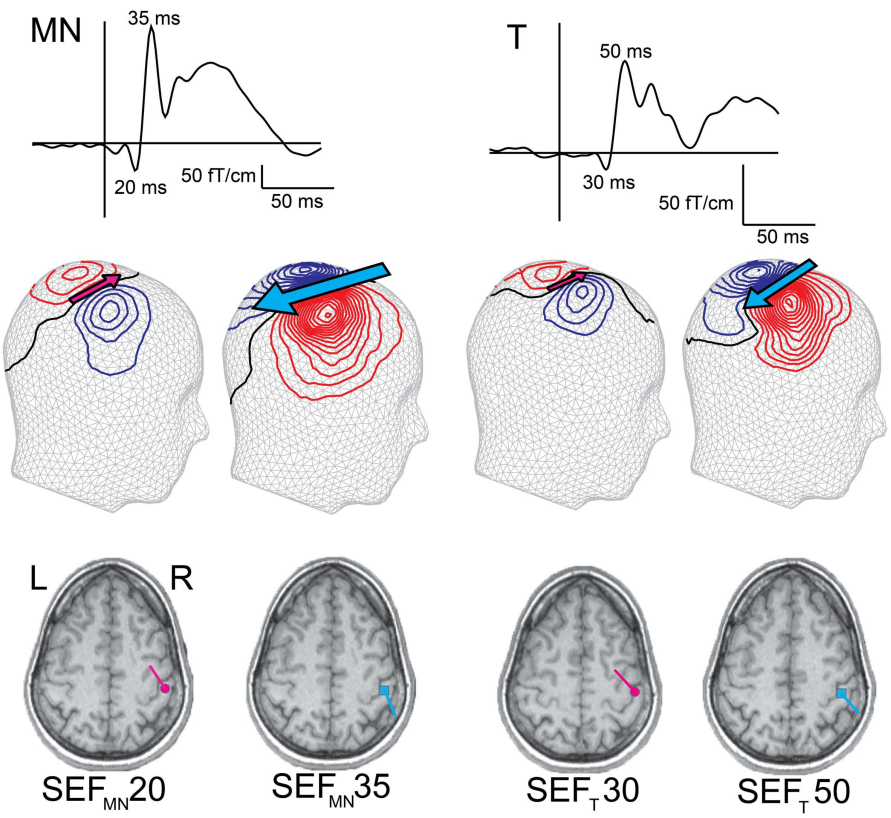

FIGURE 2 | Early adult SEFs to median nerve (SEF$_{MN}$) and tactile (SEF$_T$) stimulation. The SEF waveform from one gradiometer channel shows SEF$_{MN}$20/SEF$_T$30 and SEF$_{MN}$35/SEF$_T$50 deflections, and the magnetic contours – reflected on a head surface – reveal the different current orientations (indicated by the pink and blue arrows). Compared with SEF$_{MN}$, the SEF$_T$ latencies are slightly longer and amplitudes lower (note the different amplitude scales). Both stimulation methods, however, elicit an initial anteriorly pointing dipolar source, SEF$_{MN}$20/SEF$_T$30 (though in some subjects this deflection is minute to tactile stimulation), followed by a posteriorly pointing dipolar source, SEF$_{MN}$35/SEF$_T$50. The dipoles are superimposed on individual MRIs and both sources are localized in SI.

the subplate, a transient fetal structure underneath the cortical plate, between the 17 and 26th gestational weeks (GW[2]) (Kostovic and Rakic, 1990; Kostovic et al., 1995). During the early preterm period (26th–34th GW), these axons grow to the cortical plate and form the first thalamo-cortical connections, constituting the anatomical pathway for sensory impulses from the periphery to the cortex. Myelination starts in the human telencephalon around the 14th GW (Zecevic et al., 1998). In the pre- and post-central gyri, myelin is detectable around the 35th GW (Iai et al., 1997). Myelination then proceeds actively during the first postnatal year (Brody et al., 1987) and continues at a slower pace thereafter. In accordance with changes caused by pre-myelination and myelination, *in vivo* DTI data show a basic pattern of white matter maturation both before and after term-age. As a function of gestational age, mean diffusivity decreases and fractional anisotropy (a measure of relative degree of directionality of diffusion in a voxel) increases in a posterior-to-anterior and a central-to-peripheral order (Hüppi et al., 1998a; Berman et al., 2005; Yoshida et al., 2013).

In human infants, the functionality of the early connections from the periphery through thalamus to the primary somatosensory cortex (SI) can be explored *in vivo* with somatosensory evoked potentials (SEPs) recorded on the scalp, or with SEFs recorded extracranially with MEG. In preterm infants, median nerve SEPs are recordable on the scalp already by the 25th GW (Hrbek et al., 1973). In the youngest preterm infants (<30 GW), the most striking feature of the scalp SEP is a large negative wave with a mean duration of 1500 ms (Hrbek et al., 1973; Vanhatalo et al., 2009). This slow wave can be detected without averaging when a tactile stimulus is given between bursts of the *tracé discontinue* EEG pattern of preterm infants (Milh et al., 2007; Vanhatalo et al., 2009). A concerted action of the subplate and cortex may be required for generation of this component (Kanold, 2009; Vanhatalo et al., 2009). With increasing gestational age, the amplitude of this slow wave gradually decreases and an earlier component, usually referred to as N1 in the literature, becomes detectable with a latency of approximately 90 ms somewhere between the 27th

[2]Gestational weeks (GW), used in clinical practice to describe the length of pregnancy and fetus age, are traditionally calculated from the first day of the last menstruation (approximately 2 weeks before conception), but presently determined by ultrasound scans during pregnancy. For uniformity, we will use gestational weeks (rather than conceptional weeks calculated from the day of conception) throughout this review.

(Taylor et al., 1996) and 29th GW (Hrbek et al., 1973). Toward term-age, the N1 latency rapidly decreases (Hrbek et al., 1973; Klimach and Cooke, 1988a; Karniski et al., 1992; Taylor et al., 1996; Smit et al., 2000), reaching approximately 30 ms at term-age ($sep_{MN}30$), though with considerable inter-individual variability (Desmedt and Manil, 1970; Hrbek et al., 1973; Laget et al., 1976; Zhu et al., 1987; Laureau et al., 1988; Laureau and Marlot, 1990; George and Taylor, 1991; Gibson et al., 1992; Karniski, 1992).

In term-age infants, primary somatosensory responses have also been studied with MEG. In accordance with the neonatal $sep_{MN}30$, the initial SEF to median nerve stimulation in full-term newborns peaks at around 30 ms ($sef_{MN}30$). The MEG data together with earlier EEG findings suggest that this earliest cortical response in newborns reflects activation of a similar cortical ensemble as the earliest SEF_{MN} response in adults ($SEF_{MN}20$ peaking at 20 ms) (Lauronen et al., 2006) – that is, summated intracellular currents in cortical pyramidal cells in SI, specifically area 3b in the anterior wall of postcentral gyrus (Allison et al., 1989a). Since the current direction in SI pyramidal cells during this early response is oriented from deeper to more superficial cortical layers, MEG source modeling yields an anteriorly pointing current dipole, which in SEP is recorded as a posterior negativity ($SEP_{MN}20$ in adults and $sep_{MN}30$ in infants).

The development of this early response during childhood is primarily reflected in its latency (**Figure 3**). Although the absolute latencies differ between studies (due to, e.g., different stimulation method, filter settings, vigilance state/anesthesia), the general rule is that until the age of approximately 3–5 years, the $sep_{MN}30$ and sef_T30 latency decreases and slightly increases thereafter (e.g., Laget et al., 1976; Lauronen et al., 1997; Boor and Goebel, 2000; Gondo et al., 2001; Bercovici et al., 2008; Doria-Lamba et al., 2009; Pihko et al., 2009). These latency changes reflect the increasing neural conduction velocities following myelination and maturation opposed by physical growth of the body and limbs (Müller et al., 1994; Boor and Goebel, 2000; García et al., 2000).

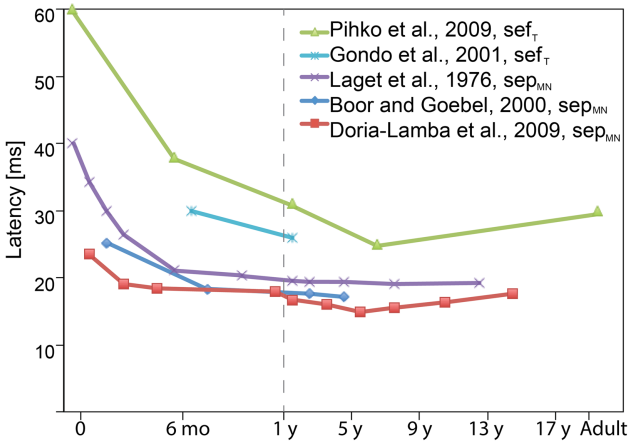

FIGURE 3 | Schematic diagram showing the latency evolution of the earliest cortical $sep_{MN}30$ and sef_T30 components with age as reported in various studies. The general rule is that the $sep_{MN}30$ and sef_T30 latency decreases until the age of approximately 3–5 years, and slightly increases thereafter. The absolute latencies vary between studies due to differences in, e.g., stimulation methods and filter settings. Many of the studies also grouped subjects of different ages together in which case the figure displays the midpoint of the reported age range (when the average age was not reported). (Note the different age scales before and after 1 year.)

DEVELOPMENT OF LOCAL CORTICAL CIRCUITS AND INTRACORTICAL PROCESSING

Besides the wiring of thalamo-cortical connections, major developmental changes also occur within the cortex during the second and third trimester as well as postnatally (Marin-Padilla, 1970). Between the 28 and 40th GW, the brain volume more than doubles and cortical gray matter volume extends fourfold (Hüppi et al., 1998b). Postmortem data of human infants show that development of dendrites of cortical pyramidal cells begins during the second trimester from the deeper cortical layers, followed by more superficial layers (Mrzljak et al., 1992). The number of basal dendrites stabilizes around the 27th GW, but their growth in length accelerates during the third trimester and continues postnatally (Mrzljak et al., 1992). Along with dendritic development, the number of synaptic connections increases, starting in the primary sensory areas during the second trimester and proceeding toward higher-order areas. The "boom time" for cortical synaptogenesis in the primary sensory areas extends over the third trimester and the first three postnatal months, resulting in a sixfold increase in synaptic density (Huttenlocher and Dabholkar, 1997). Of intracortical connections in the visual cortex, the first to form are the vertical intracolumnar connections around the 26–29th GW. Horizontal connections follow with intercolumnar projections within layers IVB/V forming around 37th GW and long-range horizontal connections within layer II/III only after 16 postnatal weeks (Burkhalter et al., 1993). These changes in cortical neural structures are also observable *in vivo* with DTI of the gray matter, where both the mean diffusivity (reflecting an increase in neurite number, cellular complexity, and synapse formation), and fractional anisotropy decline (reflecting an increase in dendritic elongation and branching orthogonal to cortical columns) (Ball et al., 2013). After the third postnatal month, the synaptic density in primary sensory areas decreases gradually, reaching adult levels around puberty (Huttenlocher and Dabholkar, 1997). Some studies on monkeys suggest that the most rapid phase of synapse elimination may occur as late as puberty (Bourgeois and Rakic, 1993).

Marked changes in several neurotransmitter systems also take place around term. One example is the effect of gamma-aminobutyric acid (GABA) on the post-synaptic neuron. In the adult brain, GABA is an inhibitory neurotransmitter. At early stages of development, however, $GABA_A$ receptor activation leads to depolarization (i.e., synaptic excitation) of the post-synaptic neuron due to high intracellular Cl^- concentration (Ben-Ari et al., 2004). The change from GABAergic excitation to inhibition in humans likely takes place around or shortly after term (Dzhala et al., 2005).

Evaluating the effects of these changes in the intracortical wiring and "chemistry" of cortical neural processing *in vivo* is not straight forward, but some inferences can be made from careful examination of neurophysiological data. The deflections following the adult $SEF_{MN}20/SEP_{MN}20$ or neonatal $sef_{MN}30/sep_{MN}30$ are considered to represent a "higher" level of information processing

either within local neural circuits of the primary cortical area or in higher-order cortical areas. In a developmental SEP study, Laget and coworkers (Laget et al., 1976) describe substantial changes in the early sep_{MN} sequence as a function of age. In awake term-age newborns, the early cortical sep_{MN} usually consisted of a wide initial surface negative potential in the parietal area, peaking at around 40 ms and lasting up to 100 ms. Already during the first postnatal month, a notch directed toward the baseline divided this wide neonatal response into two distinct peaks, the first of which peaked at 30 ms. The notch then grew in amplitude with increasing age and crossed the baseline at around 3–4 months of age. The overall sep_{MN} morphology attained an adult-like form by age 3 years (Laget et al., 1976). However, as only four recording electrodes were used and, consequently, no source modeling was applicable, it is difficult to infer whether the described changes represent the development of local or larger-scale processing.

Modeling the neural sources underlying the early cortical somatosensory responses in MEG has revealed fundamental, qualitative differences in the cortical activity pattern of neonates compared with school-age children or adults. In adults, regardless of the method of somatosensory stimulation, the hallmark of the early SEF in central contralateral areas is a quick transition from the initial, anteriorly pointing dipolar source (i.e., $SEF_{MN}20/SEF_T30$, **Figure 2**) to a more prominent posteriorly pointing source (i.e., $SEF_{MN}35/SEF_T50$, **Figure 2**). In neonates, no such posteriorly pointing source has been detected at all. Instead, in newborns, the activity of the initial anteriorly pointing source continues over the first 100 ms after both median nerve and tactile stimulation. This difference between adults and newborns holds with different interstimulus intervals (ISI) as well as different vigilance states (particularly also when adults are examined during sleep) (Nevalainen et al., 2008; Pihko et al., 2009). Thus, the neural populations generating the posteriorly pointing neural current source in adult SI are not similarly activated in neonates.

Some previous neonatal SEP studies seemingly disagree with the MEG data by reporting an "adult-like" initial parietal negativity followed by a positivity in the same area with only slightly prolonged latencies (Willis et al., 1984; Laureau et al., 1988; George and Taylor, 1991). This may, however, be an artificial effect of the highpass filter setting applied in these studies (see Pihko and Lauronen, 2004). Others using a lower highpass cutoff value showed a clearly distinct morphology of early neonatal SEPs compared with those of adults (Desmedt and Manil, 1970; Hrbek et al., 1973; Laget et al., 1976; Karniski, 1992; Karniski et al., 1992). Part of the differences between the SEF and SEP data also naturally arises from the different sources preferentially detected by the two methods: tangential in MEG and both tangential and radial in EEG/SEP.

The exact reason for the lack of a posteriorly pointing SI SEF component in newborns can only be speculated, since no general agreement exists on the cellular-level generation mechanism, even in adults (see, e.g., Huttunen, 1997). Whereas the earliest cortical response ($SEF_{MN}20/SEF_T30$ and $SEP_{MN}20$) is generally agreed to represent thalamo-cortical excitation of pyramidal cells in area 3b of SI (Allison et al., 1989a), the mechanism underlying $SEF_{MN}35/SEF_T50$ is not as straight forward. During the $SEF_{MN}35/SEF_T50$, the intracellular current flow is directed from superficial to deeper cortical layers (i.e., opposite to that of $SEF_{MN}20/SEF_T30$). Such intracellular current could be generated by either inhibition in deeper cortical layers (Huttunen and Hömberg, 1991; Wikström et al., 1996; Restuccia et al., 2002; Huttunen et al., 2008), or by excitation of the pyramidal cell apical dendrites in layers I/II (Allison et al., 1989a). In area 1 of monkeys, both mechanisms seem important in the generation of a similar "superficial-to-deep" intracellular current dipole following the initial "deep-to-superficial" dipole (Gardner and Costanzo, 1980; Gardner et al., 1984; Kulics and Cauller, 1986; Cauller and Kulics, 1991; Nicholson Peterson et al., 1995). In newborns, the absence of a posteriorly pointing source could reflect a lack of functional cortico-cortical connectivity necessary for mediating the response, since many of these connections are established postnatally (Burkhalter et al., 1993; Kostovic and Jovanov-Miloševic, 2006). Alternatively, the possibly still immature GABAergic inhibition could result in absence of the posteriorly pointing SI SEF, since such response is also absent in patients with Angelman syndrome, a disorder caused by a deletion in the $GABA_A$ receptor subunit gene (Egawa et al., 2008). Furthermore, the long-duration of the initial neonatal response might reflect prolonged excitation in the proximal parts of apical dendrites of the pyramidal cells in area 3b, due to, e.g., slow kinetics of intrinsic membrane conductances (Kim et al., 1995; Moody and Bosma, 2005) and immature neurotransmitter receptors.

Though the exact mechanism for the lack of a posteriorly pointing SI SEF component in newborns remains unclear, it clearly reflects immaturity of somatosensory cortical processing. Consequently, emergence of the posteriorly pointing SI SEF likely reflects maturation of the functional somatosensory network. The transition from the neonatal SI response to the adult-like response occurs gradually during the first couple of years of life (**Figure 4**, Pihko et al., 2009). By 6 months of age, the originally wide U-shaped neonatal tactile SEF-response has turned into a W-shaped response with an emerging notch (Gondo et al., 2001; Pihko et al., 2009). This notch gradually grows in amplitude and crosses the baseline at around age 2 years, when the field pattern, location and direction of the underling currents begin to resemble those of the adult $SEF_{MN}35/SEF_T50$. After 2 years of age, the morphology of the responses gradually turns into the mature form with the posteriorly pointing source becoming more and the anteriorly pointing less prominent (**Figure 4**, Pihko et al., 2009). In school-age children and adolescents, the SEF-response sequence (i.e., anteriorly pointing dipolar source followed by a prominent posteriorly pointing source), is very similar to that of adults (Lauronen et al., 1997; Lauronen, 2001; Xiang et al., 2003; Bast et al., 2007; Nevalainen et al., 2012a). In general, the developmental pattern observed with MEG has a lot in common with the SEP morphology development described by Laget et al. (1976). However, the developmental changes occur at a younger age in SEPs than SEFs, for which there are several possible explanations. First, the SEP study used median nerve stimulation, whereas the developmental SEF study applied tactile stimulation of the index finger. Second, the SEP recordings were performed in awake infants and children, whereas SEFs were recorded during sleep. Third, neural activity in gyri may have a greater contribution to the change in SEPs, whereas MEG mainly reflects activity within sulci. For example, the notch in Laget et al.'s (1976) data may represent activity in

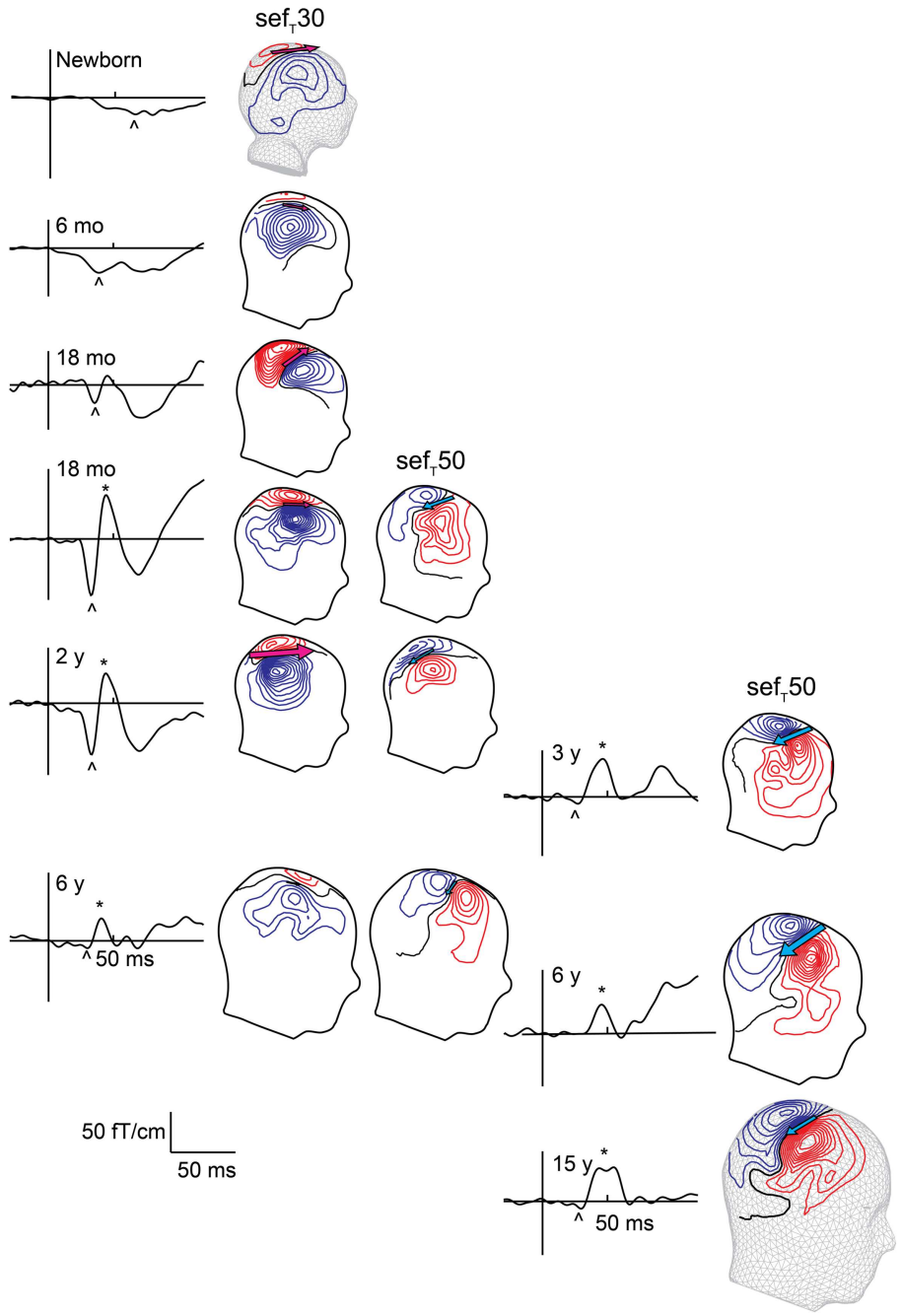

FIGURE 4 | Evolution of early sef$_T$ responses with age. Left column shows responses measured during sleep, and right column shows responses in awake subjects. The SEF waveform from one gradiometer channel shows the responses at different ages. The sef$_T$30 is marked with an arrowhead and sef$_T$50 with an asterisk. sef$_T$50 appears around 1–2 years with inter-individual variation in timing and prominence. With age the amplitude of sef$_T$30 decreases while that of the sef$_T$50 increases. The magnetic contours – reflected on a head surface – reveal the different current orientations (indicated by the pink and blue arrows) underlying the sef$_T$30 and sef$_T$50: during the sef$_T$30 the underlying current points anteriorly, and during the sef$_T$50 posteriorly.

the crown of the postcentral gyrus (area 1), which could go unnoticed in MEG. A combined multielectrode EEG–MEG study would clearly provide invaluable information about the differences and similarities in SEP and SEF development and clarify the underlying developmental phenomena.

INTEGRATION OF SOMATOSENSORY INFORMATION IN LARGE-SCALE CORTICAL NETWORKS

Relatively little is known about the development of long cortico-cortical connections and the functionality of large-scale neural networks in the prenatal and neonatal period. In humans, callosal

unmyelinated fibers are detectable in DTI around the 28th GW (Hüppi et al., 1998a). Postmortem anatomical studies show that after the 35th GW, the long cortico-corticals (e.g., callosal fibers) grow into the cortical plate (Kostovic and Jovanov-Miloševic, 2006). In mice, the region- and layer-specific targeting of callosal projections in the contralateral SI is dependent on electrical excitation and synaptic output of the callosal neurons (Wang et al., 2007). Furthermore, in rhesus monkeys, callosal axons are first overproduced, being three to four times more numerous in newborn than adult monkeys, and their refinement takes place postnatally through callosal axon elimination (LaMantia and Rakic, 1990). Maturation of the callosal connections in humans continues years after birth, as indicated by DTI anisotropy of the corpus callosum, which increases between childhood (7–11 years) and adolescence (15–17 years) (Koerte et al., 2009). Specific knowledge about the development of non-callosal, long cortico-cortical connections is sparse. In general, cortical projection neurons initially have relatively widespread distributions, which become more restricted during development through elimination of functionally inappropriate axon segments and branches (O'Leary et al., 2007).

Recent fMRI data suggest that several resting-state functional networks, including a network encompassing bilateral sensorimotor regions, are present at term-equivalent age (Fransson et al., 2007, 2009; Lin et al., 2008). The neonatal resting-state networks are, however, relatively restricted to homotopic counterparts in the two hemispheres with strong interhemispheric but limited intrahemispheric connectivity, whereas in adults, highly integrated interhemispheric and intrahemispheric connections between disparate regions exist (e.g., Biswal et al., 2010). In general, an increase in strength, complexity, and regional variability of networks are the hallmarks of resting-state fMRI across all periods of development that have been investigated (Lin et al., 2008; Fair et al., 2009; Gao et al., 2009; Supekar et al., 2009; Smyser et al., 2010). Accordingly, the interhemispheric connectivity between the left and right sensorimotor cortices increases both during the preterm period (Doria et al., 2010; Smyser et al., 2010) as well as between birth and age 2 years (Lin et al., 2008; however, see also Liu et al., 2008). Differences in the architecture of the resting-state networks between newborns and adults have also been demonstrated with a graph-theoretical analysis approach to fMRI data. In the adult brain, cortical hubs (brain areas with a disproportionately high degree of functional connectivity, suggesting an important role in the control of information flow) and their related cortical networks are mainly located in higher-order association areas such as posterior cingulate, lateral temporal, lateral parietal, and medial/lateral prefrontal cortices (Achard et al., 2006; Buckner et al., 2009). In contrast, in newborns, cortical hubs and their associated cortical networks are mainly found in primary sensory and motor brain regions (Fransson et al., 2011). However, the resting-state (or background) neural activity during early development and adulthood are different both in terms of generative mechanisms and function. Consequently, the results of developmental resting-state studies using indirect measures of neural activity (such as hemodynamic changes in fMRI) should be interpreted conservatively (Colonnese and Khazipov, 2012). In adults resting-state fMRI activity is thought to reflect the slow modulation of ongoing oscillatory activity generated by dense cortico-cortical networks. During early development (particularly during prematurity), however, the source of the slow fluctuations in resting-state fMRI may reflect alternating periods of electrical silence and bursts generated in sensory networks, driven by spontaneous activity in the periphery that interacts with the thalamo-cortical networks (Colonnese and Khazipov, 2012).

Altogether, studies of resting-state networks and brain anatomy suggest that at the time of full-term birth, the large-scale brain networks are immature and their connectivity patterns restricted. However, both fMRI and MEG studies in newborns have demonstrated ipsilateral SI responses, and MEG studies have revealed bilateral SII responses at term-age.

In fMRI, unilateral passive finger extension–flexion movements elicited BOLD (blood-oxygen-level dependent) responses in contra- and ipsilateral SI without significant differences between the hemispheres. This was interpreted as immature lateralization of somatosensory processing in newborns (Erberich et al., 2006; Heep et al., 2009). MEG responses from ipsilateral SI are detectable only in a minority of healthy newborns, however, and have longer latencies (approximately 20-100 ms) than the contralateral responses (Nevalainen et al., 2008). This suggests that the ipsilateral SEFs are unlikely to represent cortical activation via direct thalamo-cortical pathways, but could be generated through callosal connections that can be relatively abundant at term-age (LaMantia and Rakic, 1990). The millisecond scale latency difference between the contra- and ipsilateral MEG SI activations in neonates would go unnoticed in fMRI, likely explaining the lack of difference between signals at contra- and ipsilateral SI reported by Erberich et al. (2006). Interestingly, at 3 months of age follow-up, the BOLD fMRI signal changes already exhibit an adult-like contralateral SI activation, which persisted at 6 and 9 months (Erberich et al., 2006; Heep et al., 2009). No MEG or EEG reports exist on ipsilateral SI response development in early childhood after the neonatal period.

In adults, unilateral tactile stimulation elicits ipsilateral positive BOLD signals in the posterior parts of SI, probably area 2, in agreement with the bilateral representation of digits in area 2 in monkeys (Fabri et al., 1999; Polonara et al., 1999; Iwamura et al., 2002). With MEG, activation of ipsilateral SI in adult subjects has been detected in some studies (Korvenoja et al., 1995; Kanno et al., 2003; Hadoush et al., 2010; Pihko et al., 2010). Intracranial recordings confirm the presence of ipsilateral SEPs in some epilepsy and tumor patients. In contrast to contralateral responses, they originate only from Brodmann areas 1 and 2, have longer latencies, smaller amplitudes, and no initial surface negativity or phase reversal across the central sulcus (Allison et al., 1989b; Noachtar et al., 1997). The difference in sensitivity to the direction of underlying currents (mostly radial from area 1) and synchronization of activity could explain why ipsilateral responses from areas 1 and 2 are detected better with fMRI than MEG. Another explanation for the rarely reported ipsilateral SI responses in adults may involve transcallosal inhibition of ipsilateral area 3b after unilateral somatosensory stimulation (Hlushchuk and Hari, 2006). In the motor system, transcallosal inhibition is absent in infancy and early childhood (Müller et al., 1997; Heinen et al., 1998). The presence of ipsilateral SI responses

could reflect lack of transcallosal inhibition in the somatosensory system in early childhood.

Knowledge of somatosensory processing beyond SI was limited before the era of MEG and modern neuroimaging. Since then, these methods have shown that, in the mature somatosensory system, information processing takes place in a wide network, including at least frontoparietal operculum (e.g., the bilateral SII), posterior parietal cortex, and mesial paracentral lobule (see, e.g., Hari and Forss, 1999 for MEG and Disbrow et al., 2000 for fMRI).

Neonatal MEG studies have demonstrated that, after tactile and median nerve stimulation, a prominent deflection in the contralateral hemisphere peaks at about 230 ms ($sef_{MN}230/sef_T230$; **Figure 5**). The generator source underlying this deflection has been localized to the parietal operculum and thus sef_T230 most likely represents activity in SII (Pihko et al., 2005; Nevalainen et al., 2008, 2012b). This indicates that the connections to and the neurons in SII are sufficiently developed to produce a detectable SEF response at full-term-age, although with a longer peak latency (approximately 230 ms) than in adulthood (approximately 100 ms; e.g., Hari and Forss, 1999). The neonatal SII response does have some similar characteristics with the mature SII response: it is often detectable not only contralaterally but also ipsilaterally and is diminished with the shortening of the ISI (Nevalainen et al., 2008). Interestingly though, the neonatal SII response is particularly prominent in quiet sleep (Pihko et al., 2004; Nevalainen et al., 2008), whereas in adults it is diminished or even vanishes in non-REM sleep (Kitamura et al., 1996; Kakigi et al., 2003; our own unpublished observation). Thus, from an ontogenetic point of view, SII activation in quiet sleep in newborns may have a function in the maturation of the somatosensory neural network. No reports exist about the development of SII responses in early childhood after the neonatal period.

In neonatal SEP studies, several investigators consistently detected a peak at a latency of around 230 ms (Desmedt and Manil, 1970; Hrbek et al., 1973; Laget et al., 1976; Karniski, 1992; Pihko and Lauronen, 2004; Pihko et al., 2004), with a positivity at the vertex (Desmedt and Manil, 1970; Pihko and Lauronen, 2004; Pihko et al., 2004). Although this SEP response was usually recorded with only a few electrodes, and hence no source modeling was applicable, in retrospect with knowledge from MEG studies, it can be interpreted to represent activity from SII. SEP studies on the evolution of this response with age are also lacking.

EARLY BRAIN INSULTS AND SOMATOSENSORY SYSTEM DEVELOPMENT

The "age-specific" nervous system of children affects the way in which neural dysfunction presents itself in childhood. First, the lesion types themselves depend on age, since periods of specific neurodevelopmental events are also periods of specific vulnerability. For example, asphyxia in preterm infants preferentially affects periventricular regions, whereas in term infants, cortical regions, thalamus, basal ganglia, and brainstem are more often affected. Second, whereas in adults neurological dysfunction causes specific and localized signs (e.g., hemiplegia in case of stroke in the medial cerebral artery area), in young infants it may present as generalized and non-specific symptoms (e.g., a preterm infant with a unilateral intraventricular hemorrhage (IVH) may present with generalized hypotonia or hypertonia, hypokinesia, or hyperexcitability) (Hadders-Algra, 2004). Furthermore, due to ongoing brain development, the long-term outcome after brain insults occurring prenatally or in early infancy is very different from outcome after an insult occurring in adulthood. The capacity for plastic reorganization after insults is much greater in the developing, immature brain. On the other hand, the mature patterns for information processing that need to be regained after the insult never existed in the immature brain in the first place, and the insult may instead compromise normal developmental processes (Kolb, 1999). The outcome after an early insult is also difficult to predict, since neurodevelopmental changes can induce a disappearance of observed symptoms present at an earlier age. Alternatively, functional deficits may only be recognized with increasing age because of the age-related increase in the complexity of neural functions (Hadders-Algra, 2002). The pathogenic mechanisms leading to the variable neurological deficits after early brain insults are also poorly understood, as *in vivo* studies of the functional development of the human brain have only been enabled recently

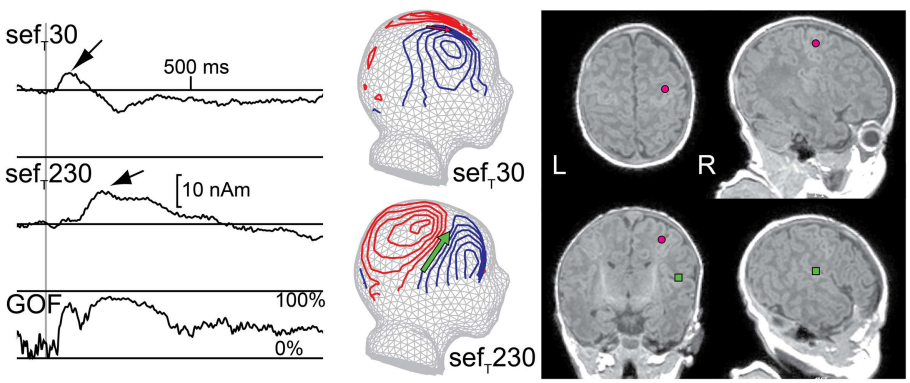

FIGURE 5 | Responses from primary (SI) and secondary (SII) somatosensory areas in a newborn. Left: multidipole model showing SI and SII source waveforms for the right hemisphere of one newborn. Middle: magnetic field patterns during M60 (SI) and M200 (SII) peaks reflected on a spherical surface and projected onto a schematic newborn head. Right: SI (pink circle) and SII (green square) ECD locations on the newborn's axial, coronal, and sagittal magnetic resonance images (MRIs). (GOF = goodness of fit)

by non-invasive investigation methods. In pediatric patient populations, MEG studies may, thus, be aimed at resolving questions concerning pathophysiological processes or to find neurophysiological biomarkers for predicting outcome in risk groups. Examples of both approaches are provided in the following sections.

SEFs IN PREDICTING NEURODEVELOPMENTAL OUTCOME IN PRETERM INFANTS

Although the survival of very preterm infants has increased significantly during recent decades (Vohr et al., 2005), many of these infants still develop with neurological impairments. Neonatal neurological examination is challenged by the non-specificity of signs of neural dysfunction (discussed above) and, consequently, complementary biomarkers for adverse outcome have been sought from neuroimaging and neurophysiology. As the period of active dendritic development and synapse formation is likely to offer better possibilities for rehabilitation than later periods (Kolb, 1999), interventions need to be started at an early age (note, however, the suggested reasons for restricting interventions before term-age: De Graaf-Peters and Hadders-Algra, 2006). Consequently, early prediction of outcome is essential for rehabilitation resources to be offered to those most in need.

Classical risk factors for adverse neurological outcome, including cystic periventricular leukomalacia (PVL) and grade III–IV IVH picked up by cranial ultrasound (Neil and Inder, 2004), are seen ever more rarely, and preterm infants with normal cranial ultrasound may have adverse outcomes (Laptook et al., 2005). At present, the type of pathology suggested to account for most of the neurological problems of preterm infants is diffuse white matter injury (WMI) (Khwaja and Volpe, 2008). WMI is further associated with impaired cerebral cortical development (Inder et al., 1999) and is also likely to lead to impaired development of cortico-cortical connectivity (Mathur and Inder, 2009). In preterm infants, moderate to severe white matter abnormalities in MRI at term-age are associated with severe cognitive and motor dysfunction at 2 years of age (Woodward et al., 2006) and cognitive, language and executive function impairment at 4 and 6 years of age (Woodward et al., 2012).

Furthermore, defects in the microstructural development of the cortex, reflected in DTI as higher mean diffusivity and fractional anisotropy in gray matter in preterm vs. term infants at term-equivalent age, may underlie adverse neurodevelopmental outcome. A slower decline in mean diffusivity during the preterm period was associated with lower overall developmental scores in Griffiths Mental Development Scales at 2 years corrected age (Ball et al., 2013). Moreover, at term-equivalent age, fMRI data have demonstrated significant differences between the resting-state networks of preterm infants and term-born controls. Specifically, functional connectivity between thalamus and sensorimotor cortex was weaker in the preterm infants than in the full-term infants (Smyser et al., 2010).

Possible injury to the thalamo-cortical connections due to periventricular pathology has also motivated a wealth of SEP studies in preterm infants to assess the predictive value of abnormal (absent or delayed depending on the study) median nerve $sep_{MN}30$ (usually referred to as N1 in the literature; Klimach and Cooke, 1988b; Willis et al., 1989; de Vries et al., 1992; Pierrat et al., 1997) and the earliest posterior tibial nerve SEP (referred to as P1) from SI for future cerebral palsy (CP) (White and Cooke, 1994; Pierrat et al., 1997; Pike and Marlow, 2000). Results have been, however, somewhat contradictory, with specificity, sensitivity, and positive and negative predictive values varying markedly between studies. At least part of this variation is probably explained by differences in patient inclusion criteria, methods of SEP assessment, and outcome measure as well as technical difficulties in reliably recording the responses, particularly in the youngest infants (Smit et al., 2000).

A recent MEG study has expanded the somatosensory response evaluation from SI to SII, thus including cortico-cortical processing assessment. SEFs were recorded at term-age from 39 extremely preterm infants (born <28 GW) whose neurodevelopmental outcome was assessed at 2 years corrected age (Rahkonen et al., 2013). MEG data showed that, while SI responses were present in all the preterm infants, the SII response was absent uni- or bilaterally in a third of them. At follow-up, those infants with SII responses missing at term had worse neuromotor and overall developmental scores in the Griffiths Mental Developmental Scales assessment than the preterm infants with normal SII response present at term (Rahkonen et al., 2013). On the contrary, in this study, mild white matter abnormalities in MRI at term-age were not associated with adverse neurodevelopment (the study group did not include infants with moderate/severe WMI) (Rahkonen et al., 2013). It was speculated that the absence of SII responses may reflect not only damage to the connections within the sensorimotor networks but also more widespread disturbances in the development of cortico-cortical connectivity. Behaviorally, SII areas are considered to be involved in the integration of somatic inputs across large portions of the hand, sensorimotor integration, and bimanual coordination (see, e.g., Disbrow et al., 2000 for a discussion), motivating further SII response studies in preterm infants. Many such infants develop with minor neuromotor dysfunction and poor coordination (Hadders-Algra, 2002; Saigal and Doyle, 2008).

MEG INVESTIGATIONS OF SENSORIMOTOR SYSTEM REORGANIZATION AFTER LESIONS TO THE DEVELOPING BRAIN – CP PATIENTS

Cerebral palsy, caused by an early lesion to the developing brain, is a persistent disorder of movement and posture often accompanied by various sensory deficits. When the early lesion is unilateral and severe enough, in some individuals the sensorimotor networks may develop into an unusual configuration. During normal development, the originally bilateral cortico-spinal motor innervation (Eyre et al., 2001; Eyre, 2003) is reduced to mainly contralateral connections during the first two postnatal years through elimination of most ipsilateral projections. However, after an early unilateral brain insult, the ipsilateral cortico-spinal projections can be, to a great extent, maintained. In such cases of hemiplegic CP, instead of the normal contralateral motor representation, transcranial magnetic stimulation (TMS) may demonstrate bilateral or completely ipsilateral motor representation of the plegic extremity depending on the timing, location, and extent of the lesion (Staudt et al., 2002, 2004, 2006; Eyre, 2007). The mechanisms for preservation of the ipsilateral cortico-spinal projections are thought to involve activity-dependent competition for spinal synaptic space (Eyre, 2007).

Contrary to the motor system, after both subcortical and cortico-subcortical early brain lesions, primary somatosensory representation of the affected hand generally remains in the contralateral (i.e., ipsilesional) hemisphere as demonstrated by MEG (Gerloff et al., 2006; Staudt et al., 2006; Wilke et al., 2009; Nevalainen et al., 2012a; Pihko et al., 2014), SEPs (Guzzetta et al., 2007), and fMRI (Wilke et al., 2009). Consequently, contralesionally organized motor representation results in the dissociation of somatosensory and motor cortical representations (Staudt et al., 2006; Guzzetta et al., 2007; Wilke et al., 2009). With limited interhemispheric and intrahemispheric reorganization capability, the somatosensory system seems to be particularly vulnerable to lesions extending to the neocortex (Wilke et al., 2009), especially those including areas SI, SII, and/or inferior parietal cortex (Juenger et al., 2011). When the cortex is spared, ascending thalamo-cortical tracts are able to bypass subcortical periventricular white matter lesions, as shown by DTI, and connect to their normal destinations in SI, even in patients with extensive subcortical lesions and ipsilateral motor representation (Staudt et al., 2006). Clinically, somatosensory abilities in such patients are relatively well preserved (Wilke et al., 2009), despite the fact that the fiber count in the thalamo-cortical somatosensory tract may be reduced (Thomas et al., 2005).

In CP patients with unilateral subcortical lesions and contralateral somatosensory representation, somatosensory MEG data reveal alterations in cortical somatosensory processing in both hemispheres (Nevalainen et al., 2012a). First, after median nerve stimulation, the normal activation sequence of SI ($SEF_{MN}20$–$SEF_{MN}35$) was disrupted in both hemispheres by an additional peak, $SEF_{MN}25$, with posterior current orientation, preceding a delayed $SEF_{MN}35$. Second, within SI, the cortical representations of contralateral digits II and V were located abnormally close to each other in both hemispheres. Unilateral spatial alterations in the hand representation area have been detected by fMRI, where the area activated by passive hand movement showed larger inter-individual spatial variability in the affected than unaffected hemisphere in patients with CP (Wilke et al., 2009). Third, compared with typically developing adolescents, in the CP patients, SEFs from ipsilateral SI in response to stimulation of the normal hand were more frequent. Thus, the ipsilateral responses in the CP patients do not suggest contralesional (i.e., ipsilateral) reorganization of the somatosensory representation from the affected hand (Nevalainen et al., 2012a). They may, however, reflect another form of unusual organization of the sensorimotor networks and/or lack of the usual ipsilateral area 3b inhibition (Hlushchuk and Hari, 2006). Deficient transcallosal inhibition between the motor cortices has been demonstrated with TMS in some (Heinen et al., 1999), though not all, diplegic CP patients (Koerte et al., 2011).

The dissociation of primary motor and somatosensory representations into different hemispheres in some individuals with CP offers a unique opportunity to study reactivity of sensorimotor oscillations separately from SI and the primary motor area (MI). (Usually, SI and MI locations in the post- and precentral gyri are in such close proximity to each other that separating sources originating from the two areas with certainty in MEG is difficult.) In three CP patients, Gerloff et al. (2006) observed using MEG the corticomuscular coherence to voluntary, paretic hand isometric contraction in the ipsilateral precentral gyrus at a location similar to where TMS evoked responses in the paretic hand muscles. This result suggests that the cortical signal coherent with electromyography during isometric contraction represents the driving volley from MI, and not sensory feedback processing within SI. In another study, in two CP patients with dissociation of motor and somatosensory representations, stimulation of the median nerve of the affected hand did not modulate the sensorimotor beta-band oscillations in either hemisphere, even though oscillations in alpha-band were modulated in both hemispheres (Pihko et al., 2014). These data suggest that the somatosensory afferent flow to the contralateral cortex was unable to influence the excitability of the motor cortex in the ipsilateral hemisphere controlling the affected hand.

Discoveries of the large-scale alterations in the wiring of the sensorimotor brain networks in people with CP clearly demonstrate the power of multimodal functional investigation of the developing brain. MEG is an essential tool in the brain development investigation toolbox, particularly when used in combination with other non-invasive methods, such as DTI, fMRI, and TMS. The puzzle of brain network organization after early insults of different scale, timing, and etiology, however, still remains only partly solved. The heterogeneity in this patient population calls for large multi-methodological studies to reveal the principles of vulnerability vs. plastic potential in brain organization after early brain insults.

LIMITATIONS OF MEG IN DEVELOPMENTAL SOMATOSENSORY STUDIES

Studying children – infants in particular – with MEG or most of the other new non-invasive brain research methods is not and will never become as straightforward as studying adults. First, up to a certain age, only passive paradigms are applicable. Moreover, as most of the new research methods require staying either relatively (e.g., MEG) or completely (e.g., fMRI) still, the youngest subjects can only be studied during sleep (or anesthesia), which requires a lot of time and patience and may alter the results. Furthermore, when studying brain function during sleep, the sleep stage needs to be carefully monitored since the background neural activity changes dramatically between different sleep stages, thus the possible effect of sleep stage on the phenomena of interest cannot be ignored (in fact, it would be rather surprising if sleep stage had no effect). To compare groups, the recordings need to be done at the same vigilance and/or sleep stage, which usually lengthens the recording times. In our experience, most of the failures in infant MEG measurements result from the infant not falling asleep within the reserved time slot.

In addition, we have faced challenges in head position measurement more often in measurements of infants than adults or older children. These problems are likely to arise from the disproportionately large size of the adult sensor helmet compared with the newborn's head, resulting in a longer distance between some of the position indicator coils and the MEG sensors and, consequently, worse signal-to-noise ratio for the head position measurement. For reliable SEF recordings, the head of a newborn/infant needs to be close to the surface of the measuring helmet (Gaetz et al., 2008). With an adult-sized sensor array, this is possible only for

FIGURE 6 | Positioning infants and children in the MEG sensor array for somatosensory recordings. Left: the head of a newborn can be positioned sideways in an adult-size MEG helmet so that one hemisphere is close to the sensors (occipital part of the helmet) and activity from that hemisphere can be recorded. Right: 6-year-old child sleeping with his head in an adult-size helmet. The head is positioned close to the right side of the helmet, the left hemisphere is further away from the sensors, and a small pillow fills the gap, restricting head movements.

one hemisphere at a time (**Figure 6**). The babySQUID, a special MEG instrument with infant-size but open headrest covering only part of one hemisphere, has the same problem (Okada et al., 2006; Papadelis et al., 2013). Thus, the number of possible paradigms in infants is reduced as, e.g., recording from both hemispheres simultaneously is not feasible. This doubles the measurement time when both ipsilateral and contralateral activity is of interest and largely prevents studies of interhemispheric interactions. Recently developed pediatric-sized measuring helmets have already proven successful in studying pre-school-age children (Johnson et al., 2010; Tesan et al., 2010) and are likely to considerably enhance the variability of possible paradigms for future MEG studies in the smallest subjects once still smaller helmets become commercially available (Edgar et al., 2012; see also Roberts et al., 2014 in this Research Topic).

Possible head movements during the measurement constitute another important issue in developmental MEG studies. Conducting recordings during sleep in the smallest subjects compensates for most of the movements, and continuous head position measurement likely deals with twitches during sleep (Taulu et al., 2004; Wehner et al., 2008). However, experience in applying continuous head position measurement in infants is at the moment sparse (Imada et al., 2006; Bosseler et al., 2013). In addition, artifacts in MEG produced by the electrical MN stimulation are greater in newborns, due to the proximity of the stimulation electrodes to the sensors. Therefore, non-electric tactile stimuli for somatosensory studies have turned out to be a good alternative in studies of infants.

As a clinical tool in our hospital, MEG is only used in a very limited number of patients, mainly those considered for epilepsy surgery to localize epileptic foci (e.g., Wilenius et al., 2013). MEG can also be used to localize the SI as part of pre-surgical functional mapping (e.g., Ochi and Otsubo, 2008; Tovar-Spinoza et al., 2008). In order for MEG to become a valuable tool for other purposes in the field of clinical neonatology or pediatrics, major developments in both machinery and analysis methods are still required. The devices should be mobile or located closer to neonatal units to allow studies of sick infants, and – in an optimal future scenario – the measurement helmet would be adjustable to the child's head size. Furthermore, more automated analysis pipelines would greatly facilitate the possibility of using MEG as a tool to detect abnormality in neonatal brain activity.

CONCLUSION AND FUTURE PROSPECTS

In the last decade, MEG has provided a wealth of new information about normal and abnormal development of somatosensory cortical processing in early infancy, which would have been very hard to infer using other methods. Thus, a solid ground has been established to investigate the developing brain using MEG. With the somatosensory system, new information related to SII responses provides opportunities for studying higher cortical processing in neonates at risk for adverse outcome. Since neonatal care has significantly improved in the last decades, there is a growing need to detect the subtle disturbances that possibly cause problems in higher cortical functions but are evident clinically only later in life, e.g., during school years. MEG as a technique offers great possibilities for studying the pathophysiologic mechanisms underlying such subtle disturbances from a neuroscientific perspective.

AUTHOR CONTRIBUTIONS

Päivi Nevalainen had the main responsibility of writing the manuscript and preparing the figures. Leena Lauronen and Elina Pihko helped to design the outline and content of the manuscript and edited the manuscript and figures. Elina Pihko also prepared **Figures 4** and **6**.

ACKNOWLEDGMENTS

We thank Professors Helena Pihko and Riitta Hari for useful comments on the manuscript, Dr Cathy Nangini for language

editing, and Professor Lauri Parkkonen for the baby mesh. The study was financially supported by the aivoAALTO project of Aalto University.

REFERENCES

Achard, S., Salvador, R., Whitcher, B., Suckling, J., and Bullmore, E. (2006). A resilient, low-frequency, small-world human brain functional network with highly connected association cortical hubs. *J. Neurosci.* 26, 63–72. doi:10.1523/JNEUROSCI.3874-05.2006

Allison, T., McCarthy, G., Wood, C. C., Darcey, T. M., Spencer, D. D., and Williamson, P. D. (1989a). Human cortical potentials evoked by stimulation of the median nerve. I. Cytoarchitectonic areas generating short-latency activity. *J. Neurophysiol.* 62, 694–710.

Allison, T., McCarthy, G., Wood, C. C., Darcey, T. M., Spencer, D. D., and Williamson, P. D. (1989b). Human cortical potentials evoked by stimulation of the median nerve. II. Cytoarchitectonic areas generating long-latency activity. *J. Neurophysiol.* 62, 711–722.

Ball, G., Srinivasan, L., Aljabar, P., Counsell, S. J., Durighel, G., Hajnal, J. V., et al. (2013). Development of cortical microstructure in the preterm human brain. *Proc. Natl. Acad. Sci. U.S.A.* 110, 9541–9546. doi:10.1073/pnas.1301652110

Bast, T., Wright, T., Boor, R., Harting, I., Feneberg, R., Rupp, A., et al. (2007). Combined EEG and MEG analysis of early somatosensory evoked activity in children and adolescents with focal epilepsies. *Clin. Neurophysiol.* 118, 1721–1735. doi:10.1016/j.clinph.2007.03.037

Ben-Ari, Y., Khalilov, I., Represa, A., and Gozlan, H. (2004). Interneurons set the tune of developing networks. *Trends Neurosci.* 27, 422–427. doi:10.1016/j.tins.2004.05.002

Bercovici, E., Pang, E. W., Sharma, R., Mohamed, I. S., Imai, K., Fujimoto, A., et al. (2008). Somatosensory-evoked fields on magnetoencephalography for epilepsy infants younger than 4 years with total intravenous anesthesia. *Clin. Neurophysiol.* 119, 1328–1334. doi:10.1016/j.clinph.2008.02.018

Berman, J. I., Mukherjee, P., Partridge, S. C., Miller, S. P., Ferriero, D. M., Barkovich, A. J., et al. (2005). Quantitative diffusion tensor MRI fiber tractography of sensorimotor white matter development in premature infants. *Neuroimage* 27, 862–871. doi:10.1016/j.neuroimage.2005.05.018

Biswal, B. B., Mennes, M., Zuo, X.-N., Gohel, S., Kelly, C., Smith, S. M., et al. (2010). Toward discovery science of human brain function. *Proc. Natl. Acad. Sci. U.S.A.* 107, 4734–4739. doi:10.1073/pnas.0911855107

Boor, R., and Goebel, B. (2000). Maturation of near-field and far-field somatosensory evoked potentials after median nerve stimulation in children under 4 years of age. *Clin. Neurophysiol.* 111, 1070–1081. doi:10.1016/S1388-2457(00)00262-5

Bosseler, A. N., Taulu, S., Pihko, E., Mäkelä, J. P., Imada, T., Ahonen, A., et al. (2013). Theta brain rhythms index perceptual narrowing in infant speech perception. *Front. Psychol.* 4:690. doi:10.3389/fpsyg.2013.00690

Bourgeois, J., and Rakic, P. (1993). Changes of synaptic density in the primary visual cortex of the macaque monkey from fetal to adult stage. *J. Neurosci.* 13, 2801–2820.

Brody, B. A., Kinney, H. C., Kloman, A. S., and Gilles, F. H. (1987). Sequence of central nervous system myelination in human infancy. I. An autopsy study of myelination. *J. Neuropathol. Exp. Neurol.* 46, 283–301. doi:10.1097/00005072-198705000-00005

Buckner, R. L., Sepulcre, J., Talukdar, T., Krienen, F. M., Liu, H., Hedden, T., et al. (2009). Cortical hubs revealed by intrinsic functional connectivity: mapping, assessment of stability, and relation to Alzheimer's disease. *J. Neurosci.* 29, 1860–1873. doi:10.1523/JNEUROSCI.5062-08.2009

Burkhalter, A., Bernardo, K. L., and Charles, V. (1993). Development of local circuits in human visual cortex. *J. Neurosci.* 13, 1916–1931.

Cauller, L. J., and Kulics, A. T. (1991). The neural basis of the behaviorally relevant N1 component of the somatosensory-evoked potential in SI cortex of awake monkeys: evidence that backward cortical projections signal conscious touch sensation. *Exp. Brain Res.* 84, 607–619. doi:10.1007/BF00230973

Colonnese, M., and Khazipov, R. (2012). Spontaneous activity in developing sensory circuits: implications for resting state fMRI. *Neuroimage* 62, 2212–2221. doi:10.1016/j.neuroimage.2012.02.046

De Graaf-Peters, V. B., and Hadders-Algra, M. (2006). Ontogeny of the human central nervous system: what is happening when? *Early Hum. Dev.* 82, 257–266. doi:10.1016/j.earlhumdev.2005.10.013

de Vries, L. S., Eken, P., Pierrat, V., Daniels, H., and Casaer, P. (1992). Prediction of neurodevelopmental outcome in the preterm infant: short latency cortical somatosensory evoked potentials compared with cranial ultrasound. *Arch. Dis. Child.* 67, 1177–1181. doi:10.1136/adc.67.10_Spec_No.1177

Desmedt, J. E., and Manil, J. (1970). Somatosensory evoked potentials of the normal human neonate in REM sleep, in slow wave sleep and in waking. *Electroencephalogr. Clin. Neurophysiol.* 29, 113–126. doi:10.1016/0013-4694(70)90114-8

Disbrow, E., Roberts, T. I. M., and Krubitzer, L. (2000). Somatotopic organization of cortical fields in the lateral sulcus of *Homo sapiens*: evidence for SII and PV. *J. Comp. Neurol.* 418, 1–21. doi:10.1002/(SICI)1096-9861(20000228)418:1<1::AID-CNE1>3.0.CO;2-P

Doria, V., Beckmann, C. F., Arichi, T., Merchant, N., Groppo, M., Turkheimer, F. E., et al. (2010). Emergence of resting state networks in the preterm human brain. *Proc. Natl. Acad. Sci. U.S.A.* 107, 20015–20020. doi:10.1073/pnas.1007921107

Doria-Lamba, L., Montaldi, L., Grosso, P., Veneselli, E., and Giribaldi, G. (2009). Short latency evoked somatosensory potentials after stimulation of the median nerve in children: normative data. *J. Clin. Neurophysiol.* 26, 176–182. doi:10.1097/WNP.0b013e3181a76a56

Dzhala, V. I., Talos, D. M., Sdrulla, D. A., Brumback, A. C., Mathews, G. C., Benke, T. A., et al. (2005). NKCC1 transporter facilitates seizures in the developing brain. *Nat. Med.* 11, 1205–1213. doi:10.1038/nm1301

Edgar, J., Paulson, P., Hirschkoff, E., Pratt, K., Mascarenas, A., Miller, P., et al. (2012). "Artemis 123: development of a whole-head infant MEG system," in *18th International Conference on Biomagnetism*, Paris.

Egawa, K., Asahina, N., Shiraishi, H., Kamada, K., Takeuchi, F., Nakane, S., et al. (2008). Aberrant somatosensory-evoked responses imply GABAergic dysfunction in Angelman syndrome. *Neuroimage* 39, 593–599. doi:10.1016/j.neuroimage.2007.09.006

Erberich, S. G., Panigrahy, A., Friedlich, P., Seri, I., Nelson, M. D., and Gilles, F. (2006). Somatosensory lateralization in the newborn brain. *Neuroimage* 29, 155–161. doi:10.1016/j.neuroimage.2005.07.024

Eyre, J. A. (2003). Development and plasticity of the corticospinal system in man. *Neural Plast.* 10, 93–106. doi:10.1155/NP.2003.93

Eyre, J. A. (2007). Corticospinal tract development and its plasticity after perinatal injury. *Neurosci. Biobehav. Rev.* 31, 1136–1149. doi:10.1016/j.neubiorev.2007.05.011

Eyre, J. A., Taylor, J. P., Villagra, F., Smith, M., and Miller, S. (2001). Evidence of activity-dependent withdrawal of corticospinal projections during human development. *Neurology* 57, 1543–1554. doi:10.1212/WNL.57.9.1543

Fabri, M., Polonara, G., Quattrini, A., Salvolini, U., Del Pesce, M., and Manzoni, T. (1999). Role of the corpus callosum in the somatosensory activation of the ipsilateral cerebral cortex: an fMRI study of callosotomized patients. *Eur. J. Neurosci.* 11, 3983–3994. doi:10.1046/j.1460-9568.1999.00829.x

Fair, D. A., Cohen, A. L., Power, J. D., Dosenbach, N. U. F., Church, J. A., Miezin, F. M., et al. (2009). Functional brain networks develop from a "local to distributed" organization. *PLoS Comput. Biol.* 5:e1000381. doi:10.1371/journal.pcbi.1000381

Fransson, P., Åden, U., Blennow, M., and Lagercrantz, H. (2011). The functional architecture of the infant brain as revealed by resting-state fMRI. *Cereb. Cortex* 21, 145–154. doi:10.1093/cercor/bhq071

Fransson, P., Skiöld, B., Engström, M., Hallberg, B., Mosskin, M., Åden, U., et al. (2009). Spontaneous brain activity in the newborn brain during natural sleep – an fMRI study in infants born at full term. *Pediatr. Res.* 66, 301–305. doi:10.1203/PDR.0b013e3181b1bd84

Fransson, P., Skiöld, B., Horsch, S., Nordell, A., Blennow, M., Lagercrantz, H., et al. (2007). Resting-state networks in the infant brain. *Proc. Natl. Acad. Sci. U.S.A.* 104, 15531–15536. doi:10.1073/pnas.0704380104

Gaetz, W., Otsubo, H., and Pang, E. W. (2008). Magnetoencephalography for clinical pediatrics: the effect of head positioning on measurement of somatosensory-evoked fields. *Clin. Neurophysiol.* 119, 1923–1933. doi:10.1016/j.clinph.2008.04.291

Gao, W., Zhu, H., Giovanello, K. S., Smith, J. K., Shen, D., Gilmore, J. H., et al. (2009). Evidence on the emergence of the brain's default network from 2-week-old to 2-year-old healthy pediatric subjects. *Proc. Natl. Acad. Sci. U.S.A.* 106, 6790–6795. doi:10.1073/pnas.0811221106

García, A., Calleja, J., Antolín, F. M., and Berciano, J. (2000). Peripheral motor and sensory nerve conduction studies in normal infants and children. *Clin. Neurophysiol.* 111, 513–520. doi:10.1016/S1388-2457(99)00279-5

Gardner, E. P., and Costanzo, R. M. (1980). Temporal integration of multiple-point stimuli in primary somatosensory cortical receptive fields of alert monkeys. *J. Neurophysiol.* 43, 444–468.

Gardner, E. P., Hämäläinen, H. A., Warren, S., Davis, J., and Young, W. (1984). Somatosensory evoked potentials (SEPs) and cortical single unit responses

elicited by mechanical tactile stimuli in awake monkeys. *Electroencephalogr. Clin. Neurophysiol.* 58, 537–552. doi:10.1016/0013-4694(84)90044-0

George, S., and Taylor, M. J. (1991). Somatosensory evoked potentials in neonates and infants: developmental and normative data. *Electroencephalogr. Clin. Neurophysiol.* 80, 94–102. doi:10.1016/0168-5597(91)90146-O

Gerloff, C., Braun, C., Staudt, M., Hegner, Y. L., Dichgans, J., and Krägeloh-Mann, I. (2006). Coherent corticomuscular oscillations originate from primary motor cortex: evidence from patients with early brain lesions. *Hum. Brain Mapp.* 27, 789–798. doi:10.1002/hbm.20220

Gibson, N., Brezinova, V., and Levene, M. (1992). Somatosensory evoked potentials in the term newborn. *Electroencephalogr. Clin. Neurophysiol.* 84, 26–31. doi:10.1016/0168-5597(92)90065-J

Gondo, K., Tobimatsu, S., Kira, R., Tokunaga, Y., Yamamoto, T., and Hara, T. (2001). A magnetoencephalographic study on development of the somatosensory cortex in infants. *Neuroreport* 12, 3227–3231. doi:10.1097/00001756-200110290-00017

Guzzetta, A., Bonanni, P., Biagi, L., Tosetti, M., Montanaro, D., Guerrini, R., et al. (2007). Reorganisation of the somatosensory system after early brain damage. *Clin. Neurophysiol.* 118, 1110–1121. doi:10.1016/j.clinph.2007.02.014

Hadders-Algra, M. (2002). Two distinct forms of minor neurological dysfunction: perspectives emerging from a review of data of the Groningen Perinatal Project. *Dev. Med. Child Neurol.* 44, 561–571. doi:10.1111/j.1469-8749.2002.tb00330.x

Hadders-Algra, M. (2004). General movements: a window for early identification of children at high risk for developmental disorders. *J. Pediatr.* 145, S12–S18. doi:10.1016/j.jpeds.2004.05.017

Hadoush, H., Inoue, K., Nakanishi, K., Kurumadani, H., Sunagawa, T., and Ochi, M. (2010). Ipsilateral primary sensorimotor cortical response to mechanical tactile stimuli. *Neuroreport* 21, 108–113. doi:10.1097/WNR.0b013e3283349a17

Hämäläinen, M., Hari, R., Ilmoniemi, R., Knuutila, J., and Lounasmaa, O. (1993). Magnetoencephalography – theory, instrumentation, and applications to noninvasive studies of the working human brain. *Rev. Mod. Phys.* 65, 413–497. doi:10.1103/RevModPhys.65.413

Hari, R., and Forss, N. (1999). Magnetoencephalography in the study of human somatosensory cortical processing. *Philos. Trans. R. Soc. Lond. B Biol. Sci.* 354, 1145–1154. doi:10.1098/rstb.1999.0470

Heep, A., Scheef, L., Jankowski, J., Born, M., Zimmermann, N., Sival, D., et al. (2009). Functional magnetic resonance imaging of the sensorimotor system in preterm infants. *Pediatr.* 123, 294–300. doi:10.1542/peds.2007-3475

Heinen, F., Glocker, F.-X., Fietzek, U., Meyer, B., Lücking, C., and Korinthenberg, R. (1998). Absence of transcallosal inhibition following focal magnetic stimulation in preschool children. *Ann. Neurol.* 43, 608–612. doi:10.1002/ana.410430508

Heinen, F., Kirschner, J., Fietzek, U., Glocker, F. X., Mall, V., and Korinthenberg, R. (1999). Absence of transcallosal inhibition in adolescents with diplegic cerebral palsy. *Muscle Nerve* 22, 255–257. doi:10.1002/(SICI)1097-4598(199902)22:2<255::AID-MUS14>3.0.CO;2-7

Herlenius, E., and Lagercrantz, H. (2004). Development of neurotransmitter systems during critical periods. *Exp. Neurol.* 190(Suppl.), S8–S21. doi:10.1016/j.expneurol.2004.03.027

Hlushchuk, Y., and Hari, R. (2006). Transient suppression of ipsilateral primary somatosensory cortex during tactile finger stimulation. *J. Neurosci.* 26, 5819–5824. doi:10.1523/JNEUROSCI.5536-05.2006

Hrbek, A., Karlberg, P., and Olsson, T. (1973). Development of visual and somatosensory evoked responses in pre-term newborn infants. *Electroencephalogr. Clin. Neurophysiol.* 34, 225–232. doi:10.1016/0013-4694(73)90249-6

Huotilainen, M. (2006). Magnetoencephalography of the newborn brain. *Semin. Fetal Neonatal Med.* 11, 437–443. doi:10.1016/j.siny.2006.07.003

Hüppi, P. S., Maier, S. E., Peled, S., Zientara, G. P., Barnes, P. D., Jolesz, F. A., et al. (1998a). Microstructural development of human newborn cerebral white matter assessed in vivo by diffusion tensor magnetic resonance imaging. *Pediatr. Res.* 44, 584–590. doi:10.1203/00006450-199810000-00019

Hüppi, P. S., Warfield, S., Kikinis, R., Barnes, P. D., Zientara, G. P., Jolesz, F. A., et al. (1998b). Quantitative magnetic resonance imaging of brain development in premature and mature newborns. *Ann. Neurol.* 43, 224–235. doi:10.1002/ana.410430213

Huttenlocher, P. R., and Dabholkar, A. S. (1997). Regional differences in synaptogenesis in human cerebral cortex. *J. Comp. Neurol.* 387, 167–178. doi:10.1002/(SICI)1096-9861(19971020)387:23.0.CO;2-Z

Huttunen, J. (1997). Does the P35m SEF deflection really come from the motor cortex? *Electroencephalogr. Clin. Neurophysiol.* 104, 101–102.

Huttunen, J., and Hömberg, V. (1991). Influence of stimulus repetition rate on cortical somatosensory potentials evoked by median nerve stimulation: implications for generation mechanisms. *J. Neurol. Sci.* 105, 37–43. doi:10.1016/0022-510X(91)90115-N

Huttunen, J., Pekkonen, E., Kivisaari, R., Autti, T., and Kähkönen, S. (2008). Modulation of somatosensory evoked fields from SI and SII by acute GABA A-agonism and paired-pulse stimulation. *Neuroimage* 40, 427–434. doi:10.1016/j.neuroimage.2007.12.024

Iai, M., Yamamura, T., and Takashima, S. (1997). Early expression of proteolipid protein in human fetal and infantile cerebri. *Pediatr. Neurol.* 8994, 235–239. doi:10.1016/S0887-8994(97)00099-4

Imada, T., Zhang, Y., Cheour, M., Taulu, S., Ahonen, A., and Kuhl, P. K. (2006). Infant speech perception activates Broca's area: a developmental magnetoencephalography study. *Neuroreport* 17, 957–962. doi:10.1097/01.wnr.0000223387.51704.89

Inder, T. E., Hüppi, P. S., Warfield, S., Kikinis, R., Zientara, G. P., Barnes, P. D., et al. (1999). Periventricular white matter injury in the premature infant is followed by reduced cerebral cortical gray matter volume at term. *Ann. Neurol.* 46, 755–760. doi:10.1002/1531-8249(199911)46:53.0.CO;2-0

Iwamura, Y., Tanaka, M., Iriki, A., Taoka, M., and Toda, T. (2002). Processing of tactile and kinesthetic signals from bilateral sides of the body in the postcentral gyrus of awake monkeys. *Behav. Brain Res.* 135, 185–190. doi:10.1016/S0166-4328(02)00164-X

Johnson, B. W., Crain, S., Thornton, R., Tesan, G., and Reid, M. (2010). Measurement of brain function in pre-school children using a custom sized whole-head MEG sensor array. *Clin. Neurophysiol.* 121, 340–349. doi:10.1016/j.clinph.2009.10.017

Juenger, H., de Haan, B., Krägeloh-Mann, I., Staudt, M., and Karnath, H.-O. (2011). Early determination of somatosensory cortex in the human brain. *Cereb. Cortex* 21, 1827–1831. doi:10.1093/cercor/bhq258

Kakigi, R., Naka, D., Okusa, T., Wang, X., Inui, K., Qiu, Y., et al. (2003). Sensory perception during sleep in humans: a magnetoencephalograhic study. *Sleep Med.* 4, 493–507. doi:10.1016/S1389-9457(03)00169-2

Kanno, A., Nakasato, N., Hatanaka, K., and Yoshimoto, T. (2003). Ipsilateral area 3b responses to median nerve somatosensory stimulation. *Neuroimage* 18, 169–177. doi:10.1006/nimg.2002.1283

Kanold, P. O. (2009). Subplate neurons: crucial regulators of cortical development and plasticity. *Front. Neuroanat.* 3:16. doi:10.3389/neuro.05.016.2009

Karniski, W. (1992). The late somatosensory evoked potential in premature and term infants. I. Principal component topography. *Electroencephalogr. Clin. Neurophysiol.* 84, 32–43. doi:10.1016/0168-5597(92)90066-K

Karniski, W., Wyble, L., Lease, L., and Blair, R. (1992). The late somatosensory evoked potential in premature and term infants. II. Topography and latency development. *Electroencephalogr. Clin. Neurophysiol.* 84, 44–54. doi:10.1016/0168-5597(92)90066-K

Khwaja, O., and Volpe, J. J. (2008). Pathogenesis of cerebral white matter injury of prematurity. *Arch. Dis. Child. Fetal Neonatal Ed.* 93, 1–20. doi:10.1136/adc.2006.108837

Kim, H., Fox, K., and Connors, B. (1995). Properties of excitatory synaptic events in neurons of primary somatosensory cortex of neonatal rats. *Cereb. Cortex* 5, 148–157. doi:10.1093/cercor/5.2.148

Kitamura, Y., Kakigi, R., Hoshiyama, M., Koyama, S., and Nakamura, A. (1996). Effects of sleep on somatosensory evoked responses in human: a magnetoencephalographic study. *Brain Res. Cogn. Brain Res.* 4, 275–279. doi:10.1016/S0926-6410(96)00066-3

Klimach, V. J., and Cooke, R. W. (1988a). Maturation of the neonatal somatosensory evoked response in preterm infants. *Dev. Med. Child Neurol.* 30, 208–214. doi:10.1111/j.1469-8749.1988.tb04752.x

Klimach, V. J., and Cooke, R. W. (1988b). Short-latency cortical somatosensory evoked responses of preterm infants with ultrasound abnormality of the brain. *Dev. Med. Child Neurol.* 30, 215–221. doi:10.1111/j.1469-8749.1988.tb04753.x

Koerte, I., Heinen, F., Fuchs, T., Laubender, R. P., Pomschar, A., Stahl, R., et al. (2009). Anisotropy of callosal motor fibers in combination with transcranial magnetic stimulation in the course of motor development. *Invest. Radiol.* 44, 279–284. doi:10.1097/RLI.0b013e31819e9362

Koerte, I., Pelavin, P., Kirmess, B., Fuchs, T., Berweck, S., Laubender, R. P., et al. (2011). Anisotropy of transcallosal motor fibres indicates functional impairment in children with periventricular leukomalacia. *Dev. Med. Child Neurol.* 53, 179–186. doi:10.1111/j.1469-8749.2010.03840.x

Kolb, B. (1999). Synaptic plasticity and the organization of behaviour after early and late brain injury. *Can. J. Exp. Psychol.* 53, 62–75. doi:10.1037/h0087300

Korvenoja, A., Wikström, H., Huttunen, J., Virtanan, J., Laine, P., Aronen, H. J., et al. (1995). Activation of ipsilateral primary sensorimotor cortex by median nerve stimulation. *Neuroreport* 6, 2589–2593. doi:10.1097/00001756-199512150-00033

Kostovic, I., and Jovanov-Miloševic, N. (2006). The development of cerebral connections during the first 20–45 weeks' gestation. *Semin. Fetal Neonatal Med.* 11, 415–422. doi:10.1016/j.siny.2006.07.001

Kostovic, I., Judas, M., Petanjek, Z., and Simic, G. (1995). Ontogenesis of goal-directed behavior: anatomo-functional considerations. *Int. J. Psychophysiol.* 19, 85–102. doi:10.1016/0167-8760(94)00081-O

Kostovic, I., and Rakic, P. (1990). Developmental history of the transient subplate zone in the visual and somatosensory cortex of the macaque monkey and human brain. *J. Comp. Neurol.* 297, 441–470. doi:10.1002/cne.902970309

Kulics, A. T., and Cauller, L. J. (1986). Cerebral cortical somatosensory evoked responses, multiple unit activity and current source-densities: their interrelationships and significance to somatic sensation as revealed by stimulation of the awake monkey's hand. *Exp. Brain Res.* 62, 46–60. doi:10.1007/BF00237402

Laget, P., Raimbault, J., D'Allest, A. M., Flores-Guevara, R., Mariani, J., and Thieriot-Prevost, G. (1976). Maturation of somesthetic evoked potentials in man. *Electroencephalogr. Clin. Neurophysiol.* 40, 499–515. doi:10.1016/0013-4694(76)90080-8

LaMantia, A., and Rakic, P. (1990). Axon overproduction and elimination developing rhesus monkey in the corpus callosum of the rhesus monkey. *J. Neurosci.* 10, 2156–2175.

Laptook, A. R., O'Shea, T. M., Shankaran, S., and Bhaskar, B. (2005). Adverse neurodevelopmental outcomes among extremely low birth weight infants with a normal head ultrasound: prevalence and antecedents. *Pediatrics* 115, 673–680. doi:10.1542/peds.2004-0667

Laureau, E., Majnemer, A., Rosenblatt, B., and Riley, P. (1988). A longitudinal study of short latency somatosensory evoked responses in healthy newborns and infants. *Electroencephalogr. Clin. Neurophysiol.* 71, 100–108. doi:10.1016/0168-5597(88)90011-1

Laureau, E., and Marlot, D. (1990). Somatosensory evoked potentials after median and tibial nerve stimulation in healthy newborns. *Electroencephalogr. Clin. Neurophysiol.* 76, 453–458. doi:10.1016/0013-4694(90)90098-5

Lauronen, L. (2001). *Neuromagnetic Studies on Somatosensory Functions in CLN3, CLN5 and CLN8 forms of Neuronal Ceroid Lipofuscinoses.* Academic Dissertation, University of Helsinki, Helsinki, 35–36.

Lauronen, L., Heikkilä, E., Autti, T., Sainio, K., Huttunen, J., Aronen, H. J., et al. (1997). Somatosensory evoked magnetic fields from primary sensorimotor cortex in juvenile neuronal ceroid lipofuscinosis. *J. Child Neurol.* 12, 355–360. doi:10.1177/088307389701200603

Lauronen, L., Nevalainen, P., and Pihko, E. (2011). Magnetoencephalography in neonatology. *Neurophysiol. Clin.* 42, 27–34. doi:10.1016/j.neucli.2011.08.006

Lauronen, L., Nevalainen, P., Wikström, H., Parkkonen, L., Okada, Y., and Pihko, E. (2006). Immaturity of somatosensory cortical processing in human newborns. *Neuroimage* 33, 195–203. doi:10.1016/j.neuroimage.2006.06.041

Lin, W., Zhu, Q., Gao, W., Chen, Y., Toh, C., Gerig, G., et al. (2008). Functional connectivity MR imaging reveals cortical functional connectivity in the developing brain. *AJNR Am. J. Neuroradiol.* 29, 1883–1889. doi:10.3174/ajnr.A1256

Liu, W., Flax, J. F., Guise, K. G., Sukul, V., and Benasich, A. A. (2008). Functional connectivity of the sensorimotor area in naturally sleeping infants. *Brain Res.* 1223, 42–49. doi:10.1016/j.brainres.2008.05.054

Marin-Padilla, M. (1970). Prenatal and early postnatal ontogenesis of the human motor cortex: a Golgi study. I. The sequential development of the cortical layers. *Brain Res.* 23, 167–183. doi:10.1016/0006-8993(70)90038-7

Mathur, A., and Inder, T. E. (2009). Magnetic resonance imaging – insights into brain injury and outcomes in premature infants. *J. Commun. Disord.* 42, 248–255. doi:10.1016/j.jcomdis.2009.03.007

Mathur, A., Neil, J. J., and Inder, T. E. (2010). Understanding brain injury and neurodevelopmental disabilities in the preterm infant: the evolving role of advanced MRI. *Semin. Perinatol.* 34, 57–66. doi:10.1053/j.semperi.2009.10.006

Milh, M., Kaminska, A., Huon, C., Lapillonne, A., Ben-Ari, Y., and Khazipov, R. (2007). Rapid cortical oscillations and early motor activity in premature human neonate. *Cereb. Cortex* 17, 1582–1594. doi:10.1093/cercor/bhl069

Moody, W. J., and Bosma, M. M. (2005). Ion channel development, spontaneous activity, and activity-dependent development in nerve and muscle cells. *Physiol. Rev.* 85, 883–941. doi:10.1152/physrev.00017.2004

Mrzljak, L., Uylings, H., Kostovic, I., and van Eden, C. (1992). Prenatal development of neurons in the human prefrontal cortex. II. A quantitative Golgi study. *J. Comp. Neurol.* 316, 485–496. doi:10.1002/cne.903160408

Müller, K., Ebner, B., and Hömberg, V. (1994). Maturation of fastest afferent and efferent central and peripheral pathways: no evidence for a constancy of central conduction delays. *Neurosci. Lett.* 166, 9–12. doi:10.1016/0304-3940(94)90828-1

Müller, K., Kass-Iliyya, F., and Reitz, M. (1997). Ontogeny of ipsilateral corticospinal projections: a developmental study with transcranial magnetic stimulation. *Ann. Neurol.* 42, 705–711. doi:10.1002/ana.410420506

Neil, J. J., and Inder, T. E. (2004). Imaging perinatal brain injury in premature infants. *Semin. Perinatol.* 28, 433–443. doi:10.1053/j.semperi.2004.10.004

Nevalainen, P., Lauronen, L., Sambeth, A., Wikström, H., Okada, Y., and Pihko, E. (2008). Somatosensory evoked magnetic fields from the primary and secondary somatosensory cortices in healthy newborns. *Neuroimage* 40, 738–745. doi:10.1016/j.neuroimage.2007.09.075

Nevalainen, P., Pihko, E., Mäenpää, H., Valanne, L., Nummenmaa, L., and Lauronen, L. (2012a). Bilateral alterations in somatosensory cortical processing in hemiplegic cerebral palsy. *Dev. Med. Child Neurol.* 54, 361–367. doi:10.1111/j.1469-8749.2011.04165.x

Nevalainen, P., Pihko, E., Metsäranta, M., Sambeth, A., Wikström, H., Okada, Y., et al. (2012b). Evoked magnetic fields from primary and secondary somatosensory cortices: a reliable tool for assessment of cortical processing in the neonatal period. *Clin. Neurophysiol.* 123, 2377–2383. doi:10.1016/j.clinph.2012.05.021

Nicholson Peterson, N., Schroeder, C. E., and Arezzo, J. C. (1995). Neural generators of early cortical somatosensory evoked potentials in the awake monkey. *Electroencephalogr. Clin. Neurophysiol.* 96, 599–611.

Noachtar, S., Lüders, H. O., Dinner, D. S., and Klem, G. (1997). Ipsilateral median somatosensory evoked potentials recorded from human somatosensory cortex. *Electroencephalogr. Clin. Neurophysiol.* 104, 189–198. doi:10.1016/S0168-5597(97)00013-0

Ochi, A., and Otsubo, H. (2008). Magnetoencephalography-guided epilepsy surgery for children with intractable focal epilepsy: SickKids experience. *Int. J. Psychophysiol.* 68, 104–110. doi:10.1016/j.ijpsycho.2007.12.008

Okada, Y., Pratt, K., Atwood, C., Mascarenas, A., Reineman, R., Nurminen, J., et al. (2006). BabySQUID: a mobile, high-resolution multichannel magnetoencephalography system for neonatal brain assessment. *Rev. Sci. Instrum.* 77, 024301. doi:10.1063/1.2168672

O'Leary, D. D. M., Chou, S.-J., and Sahara, S. (2007). Area patterning of the mammalian cortex. *Neuron* 56, 252–269. doi:10.1016/j.neuron.2007.10.010

Papadelis, C., Harini, C., Ahtam, B., Doshi, C., Grant, E., and Okada, Y. (2013). Current and emerging potential for magnetoencephalography in pediatric epilepsy. *J. Pediatr. Epilepsy* 2, 73–85. doi:10.3233/PEP-13040

Pierrat, V., Eken, P., and de Vries, L. (1997). The predictive value of cranial ultrasound and of somatosensory evoked potentials after nerve stimulation for adverse neurological outcome in preterm infants. *Dev. Med. Child Neurol.* 39, 398–403. doi:10.1111/j.1469-8749.1997.tb07453.x

Pihko, E., and Lauronen, L. (2004). Somatosensory processing in healthy newborns. *Exp. Neurol.* 190(Suppl. 1), S2–S7. doi:10.1016/j.expneurol.2004.01.024

Pihko, E., Lauronen, L., Wikström, H., Parkkonen, L., and Okada, Y. (2005). Somatosensory evoked magnetic fields to median nerve stimulation in newborns. *Int. Congr. Ser.* 1278, 211–214. doi:10.1016/j.ics.2004.11.002

Pihko, E., Lauronen, L., Wikström, H., Taulu, S., Nurminen, J., Kivitie-Kallio, S., et al. (2004). Somatosensory evoked potentials and magnetic fields elicited by tactile stimulation of the hand during active and quiet sleep in newborns. *Clin. Neurophysiol.* 115, 448–455. doi:10.1016/S1388-2457(03)00349-3

Pihko, E., Nangini, C., Jousmäki, V., and Hari, R. (2010). Observing touch activates human primary somatosensory cortex. *Eur. J. Neurosci.* 31, 1836–1843. doi:10.1111/j.1460-9568.2010.07192.x

Pihko, E., Nevalainen, P., Stephen, J., Okada, Y., and Lauronen, L. (2009). Maturation of somatosensory cortical processing from birth to adulthood revealed by magnetoencephalography. *Clin. Neurophysiol.* 120, 1552–1561. doi:10.1016/j.clinph.2009.05.028

Pihko, E., Nevalainen, P., Vaalto, S., Laaksonen, K., Mäenpää, H., Valanne, L., et al. (2014). Reactivity of sensorimotor oscillations is altered in children with hemiplegic cerebral palsy: a magnetoencephalographic study. *Hum. Brain Mapp.* doi:10.1002/hbm.22462

Pike, A., and Marlow, N. (2000). The role of cortical evoked responses in predicting neuromotor outcome in very preterm infants. *Early Hum. Dev.* 57, 123–135. doi:10.1016/S0378-3782(99)00061-4

Polonara, G., Fabri, M., Manzoni, T., and Salvolini, U. (1999). Localization of the first and second somatosensory areas in the human cerebral cortex with functional MR imaging. *AJNR Am. J. Neuroradiol.* 20, 199–205.

Rahkonen, P., Nevalainen, P., Lauronen, L., Pihko, E., Lano, A., Vanhatalo, S., et al. (2013). Cortical somatosensory processing measured by magnetoencephalography predicts neurodevelopment in extremely low-gestational-age infants. *Pediatr. Res.* 73, 763–771. doi:10.1038/pr.2013.46

Restuccia, D., Valeriani, M., Grassi, E., Gentili, G., Mazza, S., Tonali, P., et al. (2002). Contribution of GABAergic cortical circuitry in shaping somatosensory evoked scalp responses: specific changes after single-dose administration of tiagabine. *Clin. Neurophysiol.* 113, 656–671. doi:10.1016/S1388-2457(02)00034-2

Roberts, T. P. L., Paulson, D. N., Hirschkoff, E., Pratt, K., Mascarenas, A., Miller, P., et al. (2014). Artemis 123: development of a whole-head infant and young child MEG system. *Front. Hum. Neurosci.* 8:99. doi:10.3389/fnhum.2014.00099

Saigal, S., and Doyle, L. W. (2008). An overview of mortality and sequelae of preterm birth from infancy to adulthood. *Lancet* 371, 261–269. doi:10.1016/S0140-6736(08)60136-1

Seghier, M. L., and Hüppi, P. S. (2010). The role of functional magnetic resonance imaging in the study of brain development, injury, and recovery in the newborn. *Semin. Perinatol.* 34, 79–86. doi:10.1053/j.semperi.2009.10.008

Smit, B. J., Ongerboer de Visser, B. W., de Vries, L. S., Dekker, F. W., and Kok, J. H. (2000). Somatosensory evoked potentials in very preterm infants. *Clin. Neurophysiol.* 111, 901–908. doi:10.1016/S1388-2457(00)00245-5

Smyser, C. D., Inder, T. E., Shimony, J. S., Hill, J. E., Degnan, A. J., Snyder, A. Z., et al. (2010). Longitudinal analysis of neural network development in preterm infants. *Cereb. Cortex* 20, 2852–2862. doi:10.1093/cercor/bhq035

Smyser, C. D., Snyder, A. Z., and Neil, J. J. (2011). Functional connectivity MRI in infants: exploration of the functional organization of the developing brain. *Neuroimage* 56, 1437–1452. doi:10.1016/j.neuroimage.2011.02.073

Staudt, M., Braun, C., Gerloff, C., Erb, M., Grodd, W., and Krägeloh-Mann, I. (2006). Developing somatosensory projections bypass periventricular brain lesions. *Neurology* 67, 522–525. doi:10.1212/01.wnl.0000227937.49151.fd

Staudt, M., Gerloff, C., Grodd, W., Holthausen, H., Niemann, G., and Krägeloh-Mann, I. (2004). Reorganization in congenital hemiparesis acquired at different gestational ages. *Ann. Neurol.* 56, 854–863. doi:10.1002/ana.20297

Staudt, M., Grodd, W., Gerloff, C., Erb, M., Stitz, J., and Krägeloh-Mann, I. (2002). Two types of ipsilateral reorganization in congenital hemiparesis: a TMS and fMRI study. *Brain* 125, 2222–2237. doi:10.1093/brain/awf227

Supekar, K., Musen, M., and Menon, V. (2009). Development of large-scale functional brain networks in children. *PLoS Biol.* 7:e1000157. doi:10.1371/journal.pbio.1000157

Taulu, S., Simola, J., and Kajola, M. (2004). MEG recordings of DC fields using the signal space separation method (SSS). *Neurol. Clin. Neurophysiol.* 2004, 35.

Taylor, M. J., Boor, R., and Ekert, P. G. (1996). Preterm maturation of the somatosensory evoked potential. *Electroencephalogr. Clin. Neurophysiol.* 100, 448–452. doi:10.1016/S0921-884X(96)95218-2

Tesan, G., Johnson, B. W., Reid, M., Thornton, R., and Crain, S. (2010). Measurement of neuromagnetic brain function in pre-school children with custom sized MEG. *J. Vis. Exp.* 36, 1–4. doi:10.3791/1693

Thomas, B., Eyssen, M., Peeters, R., Molenaers, G., Van Hecke, P., De Cock, P., et al. (2005). Quantitative diffusion tensor imaging in cerebral palsy due to periventricular white matter injury. *Brain* 128, 2562–2577. doi:10.1093/brain/awh600

Tovar-Spinoza, Z. S., Ochi, A., Rutka, J. T., Go, C., and Otsubo, H. (2008). The role of magnetoencephalography in epilepsy surgery. *Neurosurg. Focus* 25, E16. doi:10.3171/FOC/2008/25/9/E16

Vanhatalo, S., Jousmäki, V., Andersson, S., and Metsäranta, M. (2009). An easy and practical method for routine, bedside testing of somatosensory systems in extremely low birth weight infants. *Pediatr. Res.* 66, 710–713. doi:10.1203/PDR.0b013e3181be9d66

Vohr, B. R., Wright, L. L., Poole, W. K., and McDonald, S. A. (2005). Neurodevelopmental outcomes of extremely low birth weight infants <32 weeks' gestation between 1993 and 1998. *Pediatrics* 116, 635–643. doi:10.1542/peds.2004-2247

Wang, C.-L., Zhang, L., Zhou, Y., Zhou, J., Yang, X.-J., Duan, S., et al. (2007). Activity-dependent development of callosal projections in the somatosensory cortex. *J. Neurosci.* 27, 11334–11342. doi:10.1523/JNEUROSCI.3380-07.2007

Wehner, D. T., Hämäläinen, M. S., Mody, M., and Ahlfors, S. P. (2008). Head movements of children in MEG: quantification, effects on source estimation, and compensation. *Neuroimage* 40, 541–550. doi:10.1016/j.neuroimage.2007.12.026

White, C., and Cooke, R. W. (1994). Somatosensory evoked potentials following posterior tibial nerve stimulation predict later motor outcome. *Dev. Med. Child Neurol.* 36, 34–40.

Wikström, H., Huttunen, J., Korvenoja, A., Virtanen, J., Salonen, O., Aronen, H., et al. (1996). Effects of interstimulus interval on somatosensory evoked magnetic fields (SEFs): a hypothesis concerning SEF generation at the primary sensorimotor cortex. *Electroencephalogr. Clin. Neurophysiol.* 100, 479–487. doi:10.1016/S0921-884X(96)95688-X

Wilenius, J., Medvedovsky, M., Gaily, E., Metsähonkala, L., Mäkelä, J. P., Paetau, A., et al. (2013). Interictal MEG reveals focal cortical dysplasias: special focus on patients with no visible MRI lesions. *Epilepsy Res.* 105, 337–348. doi:10.1016/j.eplepsyres.2013.02.023

Wilke, M., Staudt, M., Juenger, H., Grodd, W., Braun, C., and Krägeloh-Mann, I. (2009). Somatosensory system in two types of motor reorganization in congenital hemiparesis: topography and function. *Hum. Brain Mapp.* 30, 776–788. doi:10.1002/hbm.20545

Willis, J., Duncan, M. C., Bell, R., Pappas, F., and Moniz, M. (1989). Somatosensory evoked potentials predict neuromotor outcome after periventricular hemorrhage. *Dev. Med. Child Neurol.* 31, 435–439. doi:10.1111/j.1469-8749.1989.tb04021.x

Willis, J., Seales, D., and Frazier, E. (1984). Short latency somatosensory evoked potentials in infants. *Electroencephalogr. Clin. Neurophysiol.* 59, 366–373. doi:10.1016/0168-5597(84)90038-8

Woodward, L. J., Anderson, P. J., Austin, N. C., Howard, K., and Inder, T. E. (2006). Neonatal MRI to predict neurodevelopmental outcomes in preterm infants. *N. Engl. J. Med.* 355, 685–694. doi:10.1056/NEJMoa053792

Woodward, L. J., Clark, C. A. C., Bora, S., and Inder, T. E. (2012). Neonatal white matter abnormalities an important predictor of neurocognitive outcome for very preterm children. *PLoS ONE* 7:e51879. doi:10.1371/journal.pone.0051879

Xiang, J., Holowka, S., Sharma, R., Hunjan, A., Otsubo, H., and Chuang, S. (2003). Volumetric localization of somatosensory cortex in children using synthetic aperture magnetometry. *Pediatr. Radiol.* 33, 321–327. doi:10.1007/s00247-003-0883-z

Yoshida, S., Oishi, K., Faria, A. V., and Mori, S. (2013). Diffusion tensor imaging of normal brain development. *Pediatr. Radiol.* 43, 15–27. doi:10.1007/s00247-012-2496-x

Zecevic, N., Andjelkovic, A., Matthieu, J., and Tosic, M. (1998). Myelin basic protein immunoreactivity in the human embryonic CNS. *Brain Res. Dev. Brain Res.* 105, 97–108. doi:10.1016/S0165-3806(97)00176-4

Zhu, Y., Georgesco, M., and Cadilhac, J. (1987). Normal latency values of early cortical somatosensory evoked potentials in children. *Electroencephalogr. Clin. Neurophysiol.* 68, 471–474. doi:10.1016/0168-5597(87)90058-X

Conflict of Interest Statement: The authors declare that the research was conducted in the absence of any commercial or financial relationships that could be construed as a potential conflict of interest.

Received: 30 November 2013; accepted: 03 March 2014; published online: 17 March 2014.

Citation: Nevalainen P, Lauronen L and Pihko E (2014) Development of human somatosensory cortical functions – what have we learned from magnetoencephalography: a review. Front. Hum. Neurosci. ***8****:158. doi: 10.3389/fnhum.2014.00158*

This article was submitted to the journal Frontiers in Human Neuroscience.

frontiers in
HUMAN NEUROSCIENCE

PERSPECTIVE ARTICLE
published: 13 March 2014
doi: 10.3389/fnhum.2014.00151

Potential use of MEG to understand abnormalities in auditory function in clinical populations

Eric Larson*[1] *and Adrian K. C. Lee*[1,2]

[1] *Institute for Learning and Brain Sciences, University of Washington, Seattle, WA, USA*
[2] *Department of Speech and Hearing Sciences, University of Washington, Seattle, WA, USA*

Edited by:
Christos Papadelis, Harvard Medical School, USA

Reviewed by:
Sheraz Khan, Massachusetts General Hospital, USA
David R. Moore, University of Cincinnati College of Medicine, USA

****Correspondence:***
Adrian K. C. Lee, University of Washington, Portage Bay Building Box 357988, 1715 NE Columbia Road, Seattle, WA 98195, USA
e-mail: akclee@uw.edu

Magnetoencephalography (MEG) provides a direct, non-invasive view of neural activity with millisecond temporal precision. Recent developments in MEG analysis allow for improved source localization and mapping of connectivity between brain regions, expanding the possibilities for using MEG as a diagnostic tool. In this paper, we first describe inverse imaging methods (e.g., minimum-norm estimation) and functional connectivity measures, and how they can provide insights into cortical processing. We then offer a perspective on how these techniques could be used to understand and evaluate auditory pathologies that often manifest during development. Here we focus specifically on how MEG inverse imaging, by providing anatomically based interpretation of neural activity, may allow us to test which aspects of cortical processing play a role in (central) auditory processing disorder [(C)APD]. Appropriately combining auditory paradigms with MEG analysis could eventually prove useful for a hypothesis-driven understanding and diagnosis of (C)APD or other disorders, as well as the evaluation of the effectiveness of intervention strategies.

Keywords: magnetoencephalography, minimum-norm estimates, audition, clinical practice, central auditory processing disorder

INTRODUCTION

Magnetoencephalography (MEG) is a non-invasive human physiology technique that records magnetic field patterns from hundreds of sensors simultaneously with millisecond precision. Like electroencephalography (EEG), MEG principally measures neural activity from large populations of (>50,000) cortical pyramidal neurons firing with close temporal and spatial alignment (Okada, 1983; Hämäläinen et al., 1993), but measures the magnetic field surrounding the head as opposed to the electric potential at the scalp. This leads to less distortion of MEG signals due to the propagation of signals through the scull and scalp, and gives MEG a complementary sensitivity profile to neural sources (Goldenholz et al., 2008) and finer spatial resolution (e.g., Sharon et al., 2007), allowing for potentially more accurate mapping of sensor measurements onto neural structures. Combining MEG and EEG for imaging cortical sources has also been shown to sharpen localization compared to using either measurement alone (Sharon et al., 2007), indicating that MEG and EEG provide complementary methods for measuring neural activity.

Magnetoencephalography has been used for over 30 years to better understand auditory processing. About a decade after the first reported MEG recording of human brain activity (Cohen, 1968), researchers used MEG recordings to disambiguate the location of neural generators of the auditory N100 response to stimuli, showing they emerge from bilateral auditory cortices instead of frontal regions (Hari et al., 1980). Since then MEG has seen widespread use in basic science research in audition as well as other domains, accompanied by expansions into sophisticated analysis methods. The high temporal resolution of MEG as an electrophysiological measure positions it to be especially appropriate for use in analyzing auditory processing, where stimuli are necessarily characterized in terms of their fluctuations in time (e.g., see Shamma et al., 2011). Although multiple authors have covered standard practices for conducting MEG studies (Barkley, 2004; Liu et al., 2010; Lee et al., 2012) and reporting the methods and results (Gross et al., 2013) from MEG experiments, adoption of MEG as a tool to facilitate diagnosis has remained limited.

Here we will provide a perspective on potential ways in which MEG could, with additional time, effort, and validation, influence clinical practice for developmental pathology. In terms of methodology, we will specifically focus here on inverse imaging methods because they provide an accurate mapping from sensor readings onto underlying neural anatomical structures. Additionally, connectivity measures derived from these inverse imaging methods can also be informative in identifying interactions between nodes of brain networks. In terms of application, we will focus on how MEG could come to influence practice surrounding (central) auditory processing disorder [(C)APD], which often manifests during childhood as difficulty hearing in noisy environments (e.g., classrooms) despite normal audiometric measurements (i.e., often interpreted as typical peripheral sensitivity). We speculate about how MEG, auditory paradigms, and specific analysis methods could be combined to diagnose or help guide treatment of (C)APD, or, by extension, other disorders that manifest during development.

MEG ANALYSIS METHODS

A common method of MEG analysis is to examine trial-averaged signals directly at the sensor-level, commonly known as event-related fields or potentials (ERF/Ps), which could prove useful for

multiple clinical purposes (Reite et al., 1999). Recent reviews have also covered how ERF/Ps can be used to highlight different stages of auditory processing (Alain and Tremblay, 2007; Näätänen et al., 2007) and thus could eventually be used for clinical assessment and therapy (Näätänen, 2003; Duncan et al., 2009). In some situations, however, analyzing MEG or EEG signals in sensor-space can make it difficult to infer which neural structures underlie observed changes, as there may not always be a simple relationship between a particular sensor time series and neuroanatomical function. To link sensor readings to neurophysiology, clinical MEG use up to the present day has primarily relied upon equivalent current dipole (ECD) models (Stufflebeam et al., 2009; Zhu et al., 2012). ECD models estimate the time-varying locations, orientations, and amplitudes of a small number of (i.e., generally fewer than 10) dipole sources in the brain in order to account for the variance observed in the MEG sensors.

Although ECD modeling helps map sensor activity onto brain structures, it has a limited ability to localize multiple distributed or extended sources, such as those likely recruited in complex cognitive tasks. However, other localization methods have been developed for analyzing MEG data to address some of these limitations. Since time-series analysis of ERF/Ps and ECDs has predominantly received focus in previous work, we will focus here on describing some of these methodological developments in MEG inverse imaging and analysis beyond sensor-space (ERF/P) or ECD modeling of time series, and discuss the potential advantages these methods could confer for clinical use.

Localizing the neural generators in the brain underlying MEG (and/or EEG) measurements is a mathematically underconstrained problem, as there are infinite solutions that could give rise to the observed electro-magnetic patterns (an observation made as early as Helmholtz, 1853). Therefore, any analysis method – including analyzing signals directly from individual sensors or ECD fitting – relies on some set of assumptions to interpret MEG data. Accurately projecting these data onto neural sources in the brain is known as the "inverse problem." The classic ECD approach, for example, solves this problem by assuming that measurements should be explained as fully as possible by a handful of predefined focal brain sources. By contrast, inverse imaging approaches use a large, fixed set (often thousands) of dipole-like brain sources constructed *a priori* to form what is known as a *source space*, and the time-varying amplitude of each source is estimated to account for the observed sensor data (see Baillet, 2010 for an in-depth discussion). These brain sources are often constrained (assumed) to be approximately normal to the cortical surface using accurate individualized structural MRI information (Dale and Sereno, 1993; Lin et al., 2006), reflecting the sensitivity of MEG predominantly to cortical sources (Hämäläinen et al., 1993). Thus, inverse imaging provides a view into brain activation across all of neocortex, which critically allows for interpretation of the observed activations in terms of underlying brain function. This shift in analysis and interpretation in turn facilitates immediate comparison to and integration with other neuroimaging techniques that image neural activation in the brain (e.g., fMRI or PET) as well as animal models by way of homologous or analogous regions. It also allows us to more readily formulate and test hypotheses regarding the mapping between brain anatomy and cortical (dys)function.

The end result of MEG inverse imaging computations is a set of time-varying estimates of neural activity mapped onto the brain. However, different inverse solutions can be employed based on the task and neural activity under investigation. The minimum-norm estimate (MNE) approach is perhaps the most prominent distributed inverse imaging method (Hämäläinen and Ilmoniemi, 1994). In MNE, neural currents in the brain are assumed to be low-amplitude and distributed broadly, which can be mathematically expressed as minimizing the L2-norm (also known as a Euclidean norm, i.e., the sum of squared values) of currents in the brain. For complex cognitive tasks that are likely to recruit multiple brain regions, MNE is often a good choice because it is designed to localize distributed sources of neural activity. For example, MNE analysis would likely be useful for studying the neural activation during complex auditory or audio-visual attention tasks, since such tasks have been shown to engage broad, distributed cortical networks (e.g., Corbetta et al., 2008). Despite the fact that MNE by definition will create point spread even for focal activations, MNE has been shown to localize focal activity well enough for potential use in clinical applications (Shiraishi et al., 2013). Other inverse methods (e.g., minimum-current or mixed "L1–L2" norm estimates; Matsuura and Okabe, 1995; Uutela et al., 1999; Ou et al., 2009; Gramfort et al., 2012) have been designed specifically for tasks where a limited number of focal activations are expected *a priori* (e.g., N100 localizations that are restricted to primary sensory areas). However, we suggest here that MNE is the best all-around choice for exploring the cortical dynamics in auditory tasks, where potentially extensive cortical networks could be involved (e.g., Larson and Lee, 2013, 2014).

With these time-varying neural activations obtained using inverse imaging, it can be informative to use time-series analyses to identify peak locations (spatio-temporal) regions of significant activation, or latency differences between areas or conditions. Although such time-series analyses have received the largest focus in past studies, a rapidly growing area of research in neuroimaging is in connectivity analysis, which seeks to determine the relationships between two or more neural populations (Friston and Frith, 1995; Banerjee et al., 2012). One advantage of connectivity analysis using MEG is that the fine time resolution allows for analysis of rapidly varying neural activity, compared to fMRI-based connectivity measures, which must operate on the time scale of seconds due to acquisition and physiological constraints (Fox and Raichle, 2007). However, calculating functional connectivity using MEG often requires careful treatment due to signal mixing, point spread, and potentially ambiguous localization. Multiple connectivity measures have thus been recently devised to help compensate for these potential confounds (Vinck et al., 2011), including some that estimate the time-delay in information propagation between sources (Nolte et al., 2008). These types of methods can give us additional insight into how neural structures communicate at the systems-level in order to accomplish different tasks.

POTENTIAL APPLICATIONS FOR (C)APD (AND BEYOND)

We propose that using these MEG analysis methods in concert with targeted behavioral experiments could have a potential impact on

the evaluation of pathologies that often manifest during development. Although many such potential applications exist, here we focus on how recently developed MEG methods could be used for diagnosis or therapeutic intervention in (C)APD. Note that although (C)APD is most often diagnosed in children, most of the ideas presented here apply equally well to experiments that involved adults or children with (C)APD.

Listeners with (C)APD often experience difficulties understanding speech in noisy acoustic environments despite having normal audiological pure-tone thresholds. Around 5% of children referred to audiological clinics for listening problems have normal-hearing thresholds, leading to (C)APD diagnoses (Chermak and Musiek, 1997; Moore et al., 2010). Nonetheless, the precise definition of (C)APD is a source of some debate. For example, the American Speech-Language-Hearing Association (ASHA) Technical Report (ASHA Working Group on Auditory Processing Disorders, 2005) describes (C)APD as a deficit in neural processing of auditory stimuli that is not due to higher order language, cognitive, or related factors. However, (central) auditory processing can be defined as broadly as the efficiency and effectiveness by which the central nervous system (CNS) utilizes auditory information, or as narrowly as the perceptual processing of auditory information in the CNS insofar as the neurobiological activity gives rise to electrophysiological auditory potentials.

Many clinicians prefer a related but more functional definition provided by ASHA. In this definition, diagnosis of (C)APD is based on observed difficulties in the perceptual processing of auditory information, as demonstrated by a patient having poor performance in one or more of the following skills: sound localization and lateralization; auditory discrimination; auditory pattern recognition; temporal aspects of audition; or performance with competing acoustic signals and with degraded acoustic signals (ASHA Working Group on Auditory Processing Disorders, 2005). It is further argued that the only tests that can be validly used to diagnose (C)APD are those that can be used to infer a physical lesion in a particular part of the brain (e.g., AAA, 2010). Theoretical models, such as the Buffalo model (Katz, 1992) and the Bellis/Ferre model (Ferre, 1997; Bellis, 2003), have emerged to guide clinicians in their interventions with (C)APD patients by linking some of these behavioral test results with potential dysfunction and/or lesions in the CNS (Jutras et al., 2007). For example, the Buffalo model proposes four (C)APD subcategories, one of which links the ability to understand speech in noise and auditory short-term, working memory, and attention. This is referred to as the "tolerance-fading memory category" implicating a dysfunction in the frontal or anterior-temporal cortex. Similarly, another category ("integration category") links difficulties integrating auditory and other types of information, such as that from visual stimuli (Stecker, 1998) to expected lesions in the corpus callosum or the angular gyrus (Katz, 1992).

These sorts of theoretical models and their associated lesion studies (Musiek and Sachs, 1980; Bamiou et al., 2007; Boscariol et al., 2010) take important steps in forming a basis for our understanding the role of the CNS in (central) auditory processing. However, requiring or presupposing links between the observed dysfunctions in behavior specifically to brain lesions may be less informative than links to a broader class of neural dysfunction. Here, we believe that modern neuroimaging studies could be used to shed light on these phenomena to identify pathological neural processing during behavior. Moreover, these techniques allow us to carry out hypothesis-driven experiments rooted in theories of cognitive neuroscience to help constrain and test for the neural basis of APD. For example, over the past few decades there has been a growing appreciation that the attentional network in the cortex may be supramodal – that is, auditory and visual attention may utilize shared resources at the cortical level (see Lee et al., 2014 for a review). Neuroimaging can thus help us understand the extent to which supramodal versus auditory-specific attention mechanisms are engaged during complex listening tasks. This positions us in turn to test how neurobiological activity in the cortex is involved in (dys)functional auditory processing. The spatial and temporal resolution of inverse-imaging MEG methods are particularly appropriate for identifying the neural substrates underlying (C)APD. Such a neuroimaging approach could prove useful for (at least) the following four reasons: (1) it would give us insight into the cortical neural mechanisms underlying (C)APD and compensation strategies employed by subjects (thereby complementing ABR analyses that measure sub-cortical mechanisms), (2) it would enable us to link patient's performance in clinical behavioral tests to these underlying neural structures, (3) it could lead to the development of novel intervention strategies based on the identified neural pathologies, and (4) it would allow for determining the extent to which intervention strategies managed to restore typical neural function or promote compensation strategies.

Recently, a large-scale pediatric study showed that variability in subject responses (as opposed to overall performance levels) during an auditory task better accounted for individual listening ability (Moore et al., 2010). In another study, behavioral tests designed to tax top-down auditory attention were able to account for some of the variability in listening performance in complex settings for normal-hearing adult listeners (e.g., Zhang et al., 2012). These types of results suggest that cognitive factors such as the ability to consciously direct attention to stimuli (or tasks) of interest play an important role in hearing in complex settings. However, the neural underpinnings of such function are only partially understood. For example, we recently found a correlation between how well subjects can voluntarily switch auditory spatial attention and activity in the right temporoparietal junction (Larson and Lee, 2013, 2014), suggesting that an area understood to be involved in visuo-spatial attention (Corbetta et al., 2008) mediates effective control of auditory attention. Whole-brain inverse imaging should help accurately capture and characterize the dynamics of the distributed cortical networks that participate in these tasks, and allow us to form and test hypotheses regarding how attention network dysfunction could manifest in (C)APD.

Further integration of such tasks with MEG recording could allow for informative brain–behavior correlations that lead identification of neural pathologies and/or potential diagnostic strategies for (C)APD. To our knowledge, MEG has not been used to examine the cortical processing involved in (C)APD, perhaps in part because focus has been predominantly on sub-cortical processing in (C)APD. MEG may thus serve as a complement to auditory brainstem response measurements, which have previously been suggested as a potential diagnostic tool (Catts et al.,

1996; Chermak and Musiek, 1997), by isolating dynamics at the cortical level that are useful in understanding the relationship between neural processing and behavior in order to aid effective diagnosis via behavioral tests. For example, having subjects with (C)APD perform attention-demanding tasks using auditory and visual stimuli may reveal irregularities in processing or connectivity between the primary sensory areas (i.e., auditory and/or visual cortices) and the cortical attention network. These tasks could thus address the extent to which APD is related to disruptions in modality-specific versus supra-modal network components. In this way, MEG (or even better, combined M/EEG) could be used to extend the findings of previous studies showing differences in cortical processing using EEG (e.g., Kraus et al., 1993; Gavin et al., 2011) by enabling connectivity-based analyses, mapping activity onto neural structures to formulate and test hypotheses regarding the nature of disrupted function, and by providing a complementary view of cortical neural activity that may be involved in (C)APD.

As the co-morbidity of (C)APD with other disorders (such as attention deficit hyperactivity disorder or autism spectrum disorder) may complicate behavioral diagnosis of (C)APD, MEG may prove useful as a tool to help isolate the extent to which different neural structures are involved in each of these pathologies. Other measurements such as ABR would also serve as a useful complement to MEG by measuring the function of midbrain and earlier auditory structures. This would provide a more complete perspective on how the brain may influence subject behavior (e.g., Kraus, 2012), especially in terms of top-down influences from cortical areas (Lehmann and Schönwiesner, 2014). Once MEG is used to isolate specific cortical structures involved in (C)APD, understanding the geometry of the anatomical region involved could facilitate development of an EEG protocol to provide a simpler, easier, and cheaper method to deploy in the clinic. These ideas regarding how MEG could shed light on (C)APD could readily be extended to other pathologies that manifest during development with auditory dysfunction, or to help tease apart the extent to which normal auditory neural function has been disrupted.

CONCLUSION

There are multiple strengths of MEG as a neurophysiological measure that have yet to be fully leveraged for evaluating pathologies that manifest during development. Combining improved source localization and connectivity measures with auditory paradigms have increased our capability to identify how neural activity relates to behavior. Given the ability of MEG to track the rapid dynamics that may underlie many forms of normal and abnormal auditory processing, researchers may be able to use MEG as a tool to help understand and diagnose (C)APD, and eventually evaluate the neural outcomes of various treatments.

ACKNOWLEDGMENTS

Thanks to Ross K. Maddox for helpful comments. This work was supported by National Institutes of Health (NIH) grants R00DC010196; R01DC013260 (Adrian K. C. Lee), training grant T32DC000018 (Eric Larson), fellowship F32DC012456 (Eric Larson), and an NIH LRP fellowship (Eric Larson).

REFERENCES

AAA. (2010). *American Academy of Audiology Clinical Practice Guidelines: Diagnosis, Treatment and Management of Children and Adults with Central Auditory Processing Disorder*. Available at: http://www.audiology.org/resources/documentlibrary/Documents/CAPD%20Guidelines%208-2010.pdf

Alain, C., and Tremblay, K. (2007). The role of event-related brain potentials in assessing central auditory processing. *J. Am. Acad. Audiol.* 18, 573–589. doi:10.3766/jaaa.18.7.5

ASHA Working Group on Auditory Processing Disorders. (2005). *(Central) Auditory Processing Disorders*. Rockville, MD: American Speech-Language-Hearing Association.

Baillet, S. (2010). "The dowser in the fields: searching for MEG sources," in *MEG: An Introduction to Methods*, eds P. C. Hansen, M. Kringelbach, and R. Salmelin (New York: Oxford University Press), 83–123.

Bamiou, D.-E., Free, S. L., Sisodiya, S. M., Chong, W. K., Musiek, F., Williamson, K. A., et al. (2007). Auditory interhemispheric transfer deficits, hearing difficulties, and brain magnetic resonance imaging abnormalities in children with congenital aniridia due to PAX6 mutations. *Arch. Pediatr. Adolesc. Med.* 161, 463–469. doi:10.1001/archpedi.161.5.463

Banerjee, A., Pillai, A. S., and Horwitz, B. (2012). Using large-scale neural models to interpret connectivity measures of cortico-cortical dynamics at millisecond temporal resolution. *Front. Syst. Neurosci.* 5:102. doi:10.3389/fnsys.2011.00102

Barkley, G. L. (2004). Controversies in neurophysiology. MEG is superior to EEG in localization of interictal epileptiform activity: pro. *Clin. Neurophysiol.* 115, 1001–1009. doi:10.1016/j.clinph.2003.12.011

Bellis, T. J. (2003). *Assessment and Management of Central Auditory Processing Disorders in the Educational Setting: From Science to Practice*. Clifton Park, NY: Delmar Learning.

Boscariol, M., Garcia, V. L., Guimarães, C. A., Montenegro, M. A., Hage, S. R. V., Cendes, F., et al. (2010). Auditory processing disorder in perisylvian syndrome. *Brain Dev.* 32, 299–304. doi:10.1016/j.braindev.2009.04.002

Catts, H., Chermak, G., Craig, C., Johnston, J., Keith, R., Musiek, F., et al. (1996). *Central Auditory Processing: Current Status of Research and Implications for Clinical Practice*. Available at: http://dx.doi.org/10.1044/policy.TR1996-00241

Chermak, G. D., and Musiek, F. E. (1997). *Central Auditory Processing: New Perspectives*, 1st Edn. San Diego, CA: Singular Publishing Group Inc.

Cohen, D. (1968). Magnetoencephalography: evidence of magnetic fields produced by alpha-rhythm currents. *Science* 161, 784–786. doi:10.1126/science.161.3843.784

Corbetta, M., Patel, G., and Shulman, G. L. (2008). The reorienting system of the human brain: from environment to theory of mind. *Neuron* 58, 306–324. doi:10.1016/j.neuron.2008.04.017

Dale, A. M., and Sereno, M. I. (1993). Improved localization of cortical activity by combining EEG and MEG with MRI cortical surface reconstruction: a linear approach. *J. Cogn. Neurosci.* 5, 162–176. doi:10.1162/jocn.1993.5.2.162

Duncan, C. C., Barry, R. J., Connolly, J. F., Fischer, C., Michie, P. T., Näätänen, R., et al. (2009). Event-related potentials in clinical research: guidelines for eliciting, recording, and quantifying mismatch negativity, P300, and N400. *Clin. Neurophysiol.* 120, 1883–1908. doi:10.1016/j.clinph.2009.07.045

Ferre, J. M. (1997). *Processing Power: A Guide to CAPD Assessment and Management*, 2nd Edn. San Antonio, TX: Communication Skill Builders.

Fox, M. D., and Raichle, M. E. (2007). Spontaneous fluctuations in brain activity observed with functional magnetic resonance imaging. *Nat. Rev. Neurosci.* 8, 700–711. doi:10.1038/nrn2201

Friston, K. J., and Frith, C. D. (1995). Schizophrenia: a disconnection syndrome? *Clin. Neurosci.* 3, 89–97.

Gavin, W. J., Dotseth, A., Roush, K. K., Smith, C. A., Spain, H. D., and Davies, P. L. (2011). Electroencephalography in children with and without sensory processing disorders during auditory perception. *Am. J. Occup. Ther.* 65, 370–377. doi:10.5014/ajot.2011.002055

Goldenholz, D., Ahlfors, S., Hämäläinen, M., Sharon, D., Ishitobi, M., Vaina, L., et al. (2008). Mapping the signal-to-noise-ratios of cortical sources in magnetoencephalography and electroencephalography. *Hum. Brain Mapp.* Available at: http://www3.interscience.wiley.com/journal/119054055/abstract?CRETRY=1&SRETRY=0

Gramfort, A., Kowalski, M., and Hämäläinen, M. (2012). Mixed-norm estimates for the M/EEG inverse problem using accelerated gradient methods. *Phys. Med. Biol.* 57, 1937–1961. doi:10.1088/0031-9155/57/7/1937

Gross, J., Baillet, S., Barnes, G. R., Henson, R. N., Hillebrand, A., Jensen, O., et al. (2013). Good practice for conducting and reporting MEG research. *Neuroimage* 65, 349–363. doi:10.1016/j.neuroimage.2012.10.001

Hämäläinen, M., Hari, R., Ilmoniemi, R. J., Knuutila, J., and Lounasmaa, O. V. (1993). Magnetoencephalography – theory, instrumentation, and applications to noninvasive studies of the working human brain. *Rev. Mod. Phys.* 65, 413–497. doi:10.1103/RevModPhys.65.413

Hämäläinen, M. S., and Ilmoniemi, R. J. (1994). Interpreting magnetic fields of the brain: minimum norm estimates. *Med. Biol. Eng. Comput.* 32, 35–42. doi:10.1007/BF02512476

Hari, R., Aittoniemi, K., Järvinen, M.-L., Katila, T., and Varpula, T. (1980). Auditory evoked transient and sustained magnetic fields of the human brain localization of neural generators. *Exp. Brain Res.* 40. Available at: http://www.springerlink.com.offcampus.lib.washington.edu/content/k621374617717752/ doi:10.1007/BF00237543

Helmholtz, H. (1853). Ueber einige gesetze der vertheilung elektrischer ströme in körperlichen leitern mit anwendung auf die thierisch-elektrischen versuche. *Ann. Phys.* 165, 211–233. doi:10.1002/andp.18531650702

Jutras, B., Loubert, M., Dupuis, J.-L., Marcoux, C., Dumont, V., and Baril, M. (2007). Applicability of central auditory processing disorder models. *Am. J. Audiol.* 16, 100–106. doi:10.1044/1059-0889(2007/014)

Katz, J. (1992). "Classification of auditory processing disorders," in *Central Auditory Processing: A Transdisciplinary View*, eds N. A. Stecker, D. Henderson, and J. Katz (St. Louis: Mosby Year Book), 81–91.

Kraus, N. (2012). Atypical brain oscillations: a biological basis for dyslexia? *Trends Cogn. Sci.* 16, 12–13. doi:10.1016/j.tics.2011.12.001

Kraus, N., McGee, T., Ferre, J., Hoeppner, J. A., Carrell, T., Sharma, A., et al. (1993). Mismatch negativity in the neurophysiologic/behavioral evaluation of auditory processing deficits: a case study. *Ear Hear.* 14, 223–234. doi:10.1097/00003446-199308000-00001

Larson, E., and Lee, A. K. C. (2013). The cortical dynamics underlying effective switching of auditory spatial attention. *Neuroimage* 64, 365–370. doi:10.1016/j.neuroimage.2012.09.006

Larson, E., and Lee, A. K. C. (2014). Switching auditory attention using spatial and non-spatial features recruits different cortical networks. *Neuroimage* 84, 681–687. doi:10.1016/j.neuroimage.2013.09.061

Lee, A. K., Larson, E., and Maddox, R. K. (2012). Mapping cortical dynamics using simultaneous MEG/EEG and anatomically-constrained minimum-norm estimates: an auditory attention example. *J. Vis. Exp.* e4262. doi:10.3791/4262

Lee, A. K. C., Larson, E., Maddox, R. K., and Shinn-Cunningham, B. G. (2014). Using neuroimaging to understand the cortical mechanisms of auditory selective attention. *Hear. Res.* 307, 111–120. doi:10.1016/j.heares.2013.06.010

Lehmann, A., and Schönwiesner, M. (2014). Selective attention modulates human auditory brainstem responses: relative contributions of frequency and spatial cues. *PLoS ONE* 9:e85442. doi:10.1371/journal.pone.0085442

Lin, F.-H., Belliveau, J. W., Dale, A. M., and Hämäläinen, M. S. (2006). Distributed current estimates using cortical orientation constraints. *Hum. Brain Mapp.* 27, 1–13. doi:10.1002/hbm.20155

Liu, H., Tanaka, N., Stufflebeam, S., Ahlfors, S., and Hämäläinen, M. (2010). Functional mapping with simultaneous MEG and EEG. *J. Vis. Exp.* Available at: http://www.jove.com/video/1668/functional-mapping-with-simultaneous-meg-and-eeg doi:10.3791/1668

Matsuura, K., and Okabe, Y. (1995). Selective minimum-norm solution of the biomagnetic inverse problem. *IEEE Trans. Biomed. Eng.* 42, 608–615. doi:10.1109/10.387200

Moore, D. R., Ferguson, M. A., Edmondson-Jones, A. M., Ratib, S., and Riley, A. (2010). Nature of auditory processing disorder in children. *Pediatrics* 126, e382–e390. doi:10.1542/peds.2009-2826

Musiek, F. E., and Sachs, E. Jr. (1980). Reversible neuroaudiologic findings in a case of right frontal lobe abscess with recovery. *Arch. Otolaryngol.* 106, 280–283. doi:10.1001/archotol.1980.00790290032011

Näätänen, R. (2003). Mismatch negativity: clinical research and possible applications. *Int. J. Psychophysiol.* 48, 179–188. doi:10.1016/S0167-8760(03)00053-9

Näätänen, R., Paavilainen, P., Rinne, T., and Alho, K. (2007). The mismatch negativity (MMN) in basic research of central auditory processing: a review. *Clin. Neurophysiol.* 118, 2544–2590. doi:10.1016/j.clinph.2007.04.026

Nolte, G., Ziehe, A., Nikulin, V. V., Schlögl, A., Krämer, N., Brismar, T., et al. (2008). Robustly estimating the flow direction of information in complex physical systems. *Phys. Rev. Lett.* 100, 234101. doi:10.1103/PhysRevLett.100.234101

Okada, Y. (1983). "Neurogenesis of evoked magnetic fields," in *Biomagnetism. An Interdisciplinary Approach*, eds S. H. Williamson, G. L. Romani, L. Kaufman, and I. Modena (New York, NY: Springer), 399–408.

Ou, W., Hämäläinen, M. S., and Golland, P. (2009). A distributed spatio-temporal EEG/MEG inverse solver. *Neuroimage* 44, 932–946. doi:10.1016/j.neuroimage.2008.05.063

Reite, M., Teale, P., and Rojas, D. C. (1999). Magnetoencephalography: applications in psychiatry. *Biol. Psychiatry* 45, 1553–1563. doi:10.1016/S0006-3223(99)00062-1

Shamma, S. A., Elhilali, M., and Micheyl, C. (2011). Temporal coherence and attention in auditory scene analysis. *Trends Neurosci.* 34, 114–123. doi:10.1016/j.tins.2010.11.002

Sharon, D., Hämäläinen, M. S., Tootell, R. B. H., Halgren, E., and Belliveau, J. W. (2007). The advantage of combining MEG and EEG: comparison to fMRI in focally stimulated visual cortex. *Neuroimage* 36, 1225–1235. doi:10.1016/j.neuroimage.2007.03.066

Shiraishi, H., Haginoya, K., Nakagawa, E., Saitoh, S., Kaneko, Y., Nakasato, N., et al. (2013). Magnetoencephalography localizing spike sources of atypical benign partial epilepsy. *Brain Dev.* 36, 21–27. doi:10.1016/j.braindev.2012.12.011

Stecker, N. A. (1998). "Overview and update of central auditory processing disorders," in *Central Auditory Processing Disorders: Mostly Management*, eds M. G. Masters, N. A. Stecker, and J. Katz (Boston, MA: Allyn and Bacon), 1–32.

Stufflebeam, S. M., Tanaka, N., and Ahlfors, S. P. (2009). Clinical applications of magnetoencephalography. *Hum. Brain Mapp.* 30, 1813–1823. doi:10.1002/hbm.20792

Uutela, K., Hämäläinen, M., and Somersalo, E. (1999). Visualization of magnetoencephalographic data using minimum current estimates. *Neuroimage* 10, 173–180. doi:10.1006/nimg.1999.0454

Vinck, M., Oostenveld, R., van Wingerden, M., Battaglia, F., and Pennartz, C. M. A. (2011). An improved index of phase-synchronization for electrophysiological data in the presence of volume-conduction, noise and sample-size bias. *Neuroimage* 55, 1548–1565. doi:10.1016/j.neuroimage.2011.01.055

Zhang, Y.-X., Barry, J. G., Moore, D. R., and Amitay, S. (2012). A new test of attention in listening (TAIL) predicts auditory performance. *PLoS ONE* 7:e53502. doi:10.1371/journal.pone.0053502

Zhu, M., Zhang, W., Dickens, D., and Ding, L. (2012). "Evaluations of sparse source imaging and minimum norm estimate methods in both simulation and clinical MEG data," in *2012 Annual International Conference of the IEEE Engineering in Medicine and Biology Society (EMBC)*, San Diego, CA: IEEE. 6744–6747.

Conflict of Interest Statement: The authors declare that the research was conducted in the absence of any commercial or financial relationships that could be construed as a potential conflict of interest.

Received: 01 October 2013; accepted: 27 February 2014; published online: 13 March 2014.

*Citation: Larson E and Lee AKC (2014) Potential use of MEG to understand abnormalities in auditory function in clinical populations. Front. Hum. Neurosci. **8**:151. doi: 10.3389/fnhum.2014.00151*

This article was submitted to the journal Frontiers in Human Neuroscience.

frontiers in
HUMAN NEUROSCIENCE

TECHNOLOGY REPORT ARTICLE
published: 03 March 2014
doi: 10.3389/fnhum.2014.00099

Artemis 123: development of a whole-head infant and young child MEG system

Timothy P. L. Roberts[1]*, Douglas N. Paulson[2], Eugene Hirschkoff[2], Kevin Pratt[2], Anthony Mascarenas[2], Paul Miller[2], Mengali Han[2], Jason Caffrey[2], Chuck Kincade[2], Bill Power[2], Rebecca Murray[1], Vivian Chow[1], Charlie Fisk[1], Matthew Ku[1], Darina Chudnovskaya[1], John Dell[1], Rachel Golembski[1], Peter Lam[1], Lisa Blaskey[1], Emily Kuschner[1], Luke Bloy[1], William Gaetz[1] and J. Christopher Edgar[1]

[1] *Department of Radiology, Lurie Family Foundations MEG Imaging Center, The Children's Hospital of Philadelphia, Philadelphia, PA, USA*
[2] *Tristan Technologies, Inc., San Diego, CA, USA*

Edited by:
Christos Papadelis, Boston Children's Hospital, Harvard Medical School, USA

Reviewed by:
Douglas Owen Cheyne, Hospital for Sick Children, Canada
Blake Warren Johnson, Macquarie University, Australia

***Correspondence:**
Timothy P. L. Roberts, Department of Radiology, Lurie Family Foundations MEG Imaging Center, The Children's Hospital of Philadelphia, 34th and Civic Center Boulevard, Wood Building, Suite 2115, Philadelphia, PA 10104, USA
e-mail: robertstim@email.chop.edu

Background: A major motivation in designing the new infant and child magnetoencephalography (MEG) system described in this manuscript is the premise that electrophysiological signatures (resting activity and evoked responses) may serve as biomarkers of neurodevelopmental disorders, with neuronal abnormalities in conditions such as autism spectrum disorder (ASD) potentially detectable early in development. Whole-head MEG systems are generally optimized/sized for adults. Since magnetic field produced by neuronal currents decreases as a function of distance^{2}and infants and young children have smaller head sizes (and thus increased brain-to-sensor distance), whole-head adult MEG systems do not provide optimal signal-to-noise in younger individuals. This spurred development of a whole-head infant and young child MEG system – Artemis 123.

Methods: In addition to describing the design of the Artemis 123, the focus of this manuscript is the use of Artemis 123 to obtain auditory evoked neuromagnetic recordings and resting-state data in young children. Data were collected from a 14-month-old female, an 18-month-old female, and a 48-month-old male. Phantom data are also provided to show localization accuracy.

Results: Examination of Artemis 123 auditory data showed generalizability and reproducibility, with auditory responses observed in all participants. The auditory MEG measures were also found to be manipulable, exhibiting sensitivity to tone frequency. Furthermore, there appeared to be a predictable sensitivity of evoked components to development, with latencies decreasing with age. Examination of resting-state data showed characteristic oscillatory activity. Finally, phantom data showed that dipole sources could be localized with an error less than 0.5 cm.

Conclusions: Artemis 123 allows efficient recording of high-quality whole-head MEG in infants four years and younger. Future work will involve examining the feasibility of obtaining somatosensory and visual recordings in similar-age children as well as obtaining recordings from younger infants. Thus, the Artemis 123 offers the promise of detecting earlier diagnostic signatures in such neurodevelopmental disorders.

Keywords: infant, young child, magnetoencephalography, resting-state, auditory

INTRODUCTION

A major motivation in the design of the new infant and child magnetoencephalography (MEG) system described in this manuscript is the premise that electrophysiological signatures (resting activity and evoked responses) may serve as biomarkers of neurodevelopmental disorders, with neuronal abnormalities in conditions such as autism spectrum disorder (ASD) potentially detectable very early in development. Opportunity for very early therapeutic interventions (behavioral and pharmacological) could be achieved via the use of diagnostic, stratification and neurobiological biomarkers, derived from resting, evoked and oscillatory neuronal measures.

Whereas adult whole-head MEG systems have been instrumental in the investigation of neural activity during development, adult MEG systems do not provide optimal, or in some cases even adequate, signal-to-noise ratio (SNR) in younger individuals (e.g., Gaetz et al., 2008). Specifically, the smaller head size of infants and young children leads to an increased distance between the sites of neuronal activity (brain) and MEG sensors. Further, conventional systems have an additional relatively large displacement of MEG sensor inside the helmet (∼1.5–2 cm) and thus an additional head-surface to detection-coil distance. Ultimately, the distance between brain-source and MEG detection-coil (including brain-to-helmet and helmet-to-coil distances), coupled with the

fact that the magnetic field strength produced by neuronal currents decreases as a function of the square of the distance, leads to smaller measurable signal amplitudes with conventional MEG detection hardware. The above factors greatly hinder the accurate detection, characterization, and localization of neuronal activity in young children.

Although the generators of neural activity can, in principle, be recorded from the scalp using electroencephalography (EEG) at least after the complete closure of the fontanelles (secondary to skull ossification) by approximately 18-months-old, the need to obtain accurate measures of left versus right hemisphere activity makes MEG a more attractive method, especially for auditory studies (e.g., see Edgar et al., 2003). Another advantage of MEG over EEG is decreased contamination from non-brain high frequency signals (e.g., microsaccades, muscle), especially when examining beta (12–30 Hz) and gamma (>30 Hz) activity (Muthukumaraswamy, 2013).

The 76-channel babySQUID®, developed in 2005, showed the advantage of placing the head closer to the MEG sensors in infants and children (Okada et al., 2006). In 2009, a whole-head MEG system was developed for infants and children (Johnson et al., 2009). This system, with a 53.4 cm circumference helmet accommodating >90% of 5-year-old US Caucasian boys, provided excellent recordings of left and right auditory responses in four-year-old subjects. As Johnson et al. note, the smaller MEG helmet allowed placement of the MEG sensors closer to the head-surface as well as a more symmetric placement of the head with respect to the MEG sensors, thus providing similar left and right hemisphere SNR (in larger adult-sized helmets the child's head is able to move and thus is more likely to be asymmetrically placed with respect to the helmet sides). Several recent studies have reported findings from this 64-channel whole-head young child MEG system, now modified to 151-channels (PQ 1151R; Yokogawa/KIT, Kanazawa, Japan). Kikuchi et al. (2011) used this system to examine language lateralization in children aged 2- to 5-years-old, and Yoshimura et al. (2012) examined the development of 50 and 100 ms auditory responses in children aged 2- to 5-years-old. This same laboratory has recently begun to use this system to examine auditory processes in children with ASD (Kikuchi et al., 2013; Yoshimura et al., 2013). Findings from the above studies indicate that this is a fruitful area of research and emphasize the importance of whole-head (as opposed to unilateral, or partial coverage) MEG recordings in the investigation of bilateral responses as well as the study of hemispheric lateralization.

The above considerations spurred development of a novel whole-head infant and young child MEG system – the Artemis 123. This system, optimized for children 3 years and younger, was designed around a 50 cm helmet, where 50 cm represents the median head circumference of a 3-year-old child in the USA (Centre for Disease Control), thus allowing closer placement of the helmet to the underlying neuronal sources. The Artemis 123® hardware also incorporates a coil-in-vacuum sensor configuration as opposed to having the sensor geometry immersed in liquid helium. Sensors immersed in liquid helium require an insulated dewar helmet with the detection-coils necessarily located at a distance, typically greater than 1.5–2 cm, from the head-surface. The coil-in-vacuum configuration allows placement of the detection-coils (sensors) as close as 6 mm from the scalp, thereby mitigating the second source of source-sensor displacement (sensor to helmet surface distance), and providing a substantial increase in brain signal amplitude compared to a MEG system with the same sensor geometry immersed in liquid helium. Furthermore, a proprietary method for minimizing dimensional changes on cooling has an added benefit of greatly reducing the sensor's susceptibility to vibration, such as that induced by patient motion while in the helmet.

As introduced above, a major motivation in the design of this new infant and child MEG system is the premise that electrophysiological signatures during brain development may serve as biomarkers of disease/disorder, with neuronal abnormalities potentially detectable very early in development. Specifically, growing evidence in school-aged children indicates that MEG-detected auditory cortex responses to simple tone (e.g., Gage et al., 2003; Roberts et al., 2010) and changing vowel stimuli (e.g., Roberts et al., 2011) may delineate children with disorders such as ASD from typically developing peers (for review see Kujala et al., 2013) and potentially serve as biomarkers for stratification in clinical trials. In addition to evoked response latency and amplitude measures, assessment of left and right superior temporal gyrus neural oscillatory activity in ASD [e.g., total power and inter-trial coherence (ITC)] also suggests ASD biomarkers (Wilson et al., 2007; Rojas et al., 2008; Edgar et al., 2013). The use of such auditory neural signatures as "early detection" biomarkers is predicated on the ability to measure these signals in pre-diagnostic groups. As autism is typically diagnosed by clinical presentation in young childhood, *earlier* diagnosis would require sensitivity to atypical brain activity in the young infant (<2–3 years of age). Hence the design of the Artemis 123 is optimized to detect brain activity from children ∼6- to ∼36-months-old.

Given this clinically motivated backdrop of sensitivity to left and right auditory evoked-field morphology in infancy and early childhood, the focus of this manuscript is on the use of Artemis 123 to obtain neuromagnetic auditory recording in children 14 to 48 months. Additionally, given findings that show resting-state oscillatory abnormalities in ASD (Cornew et al., 2012), resting-state data is also obtained to examine the feasibility of examining endogeneous brain rhythms (e.g., 8–12 Hz alpha rhythms). Finally, phantom data are provided to show the localization accuracy of the system.

MATERIALS AND METHODS

ARTEMIS123 HARDWARE AND SOFTWARE

The Artemis 123 biomagnetometer is a member of the babySQUID® product family, used to non-invasively measure the weak magnetic fields produced by electrical brain activity. A CAD drawing of the system is shown in **Figure 1A**. The sensors (**Figure 1B**), an array of superconducting detection-coils, are housed within a realistically shaped helmet, with whole-head coverage optimized for the median three-year-old (i.e., 50 cm circumference). The Artemis 123 sensor system is comprised of 135 channels of magnetic field pick-up coils, each connected to a low temperature SQUID (Superconducting QUantum Interference Device). The Artemis 123 is located inside a magnetic shielded

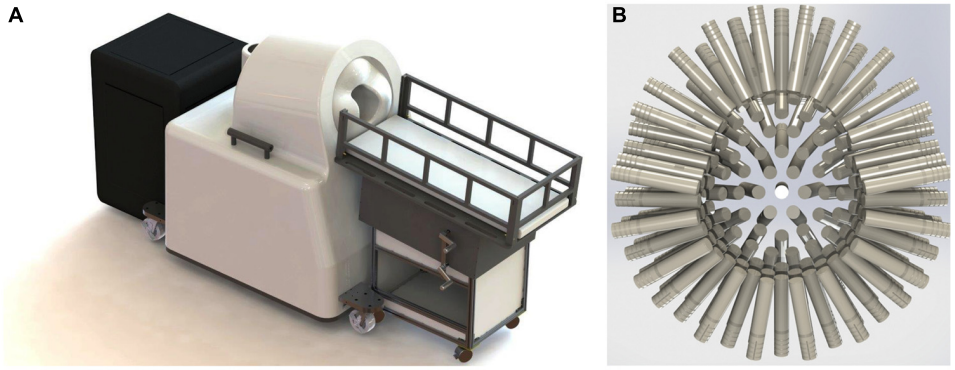

FIGURE 1 | (A) The Tristan Technologies Inc. Artemis 123 biomagnetometer is a member of the babySQUID® product family (CAD drawing). Shown are the mobile bed, the sensor unit, and cart containing SQUID electronics, all located within the MSR. **(B)** View of the helmet and sensor array (frontal sensors on top): 123 first-order gradiometers (15 mm coil diameter and 60 mm baseline) are housed within a realistic head-shaped helmet, with whole-head coverage optimized for the median three-year-old (50 cm circumference).

room (MSR) manufactured by Vacuumschmelze (GmbH & Co. KG).

Of the 135 channels, 123 are first order axial gradiometers (number of turns in the gradiometer are +5 and −5) with a 15 mm coil diameter and 60 mm baseline. Using a coil-in-vacuum configuration, the distance from these 123 sensors to outer surface is as little as 6 mm and less than 9 mm throughout, with noise performance better than 10 fT/$\sqrt{}$Hz. The Artemis 123 also includes twelve reference channels: two sets of 3-axis magnetometers and two pairs of three reference gradiometers. Reference channels measure environmental and extraneous brain magnetic signals so that this "noise" can be removed from the brain signals of interest detected in the axial gradiometer channels.

For the Artemis 123 SQUID electronics, Tristan Technologies Inc.'s 400 series iMAG® electronics are used. These are conventional transformer-coupled SQUID electronics following a flux modulation scheme. Circuit boards are grouped in units of four channels with a local microprocessor. This architecture provides a number of important features. First, the flux modulation scheme gives the SQUIDs a flat frequency response from below 0.5 Hz to in excess of 40 kHz. Second, transformer coupling of the SQUID voltage allows the use of high-resistivity cabling in the dewar, allowing many SQUIDs to be run inside the dewar vacuum space with minimal impact on liquid helium consumption. Finally, this method allows for unshielded operation with linearity on the order of a part per million. The system sensitivity in Tesla (least-significant bit) is 0.6 fT/bit on gain 100, and the dynamic range in Tesla (least-significant bit) is +/− 250 nT on gain 1. The optimal tuning parameters for each SQUID sensor are stored in EEPROM. Although re-tuning is possible, in our experience daily tuning is generally not required as the system does not trap flux during normal operation. In addition, the Artemis 123 has no problem maintaining lock. For example, at the manufacturing facility (Tristan Technologies Inc.), it was observed that the system held lock in a completely unshielded environment, despite adjacency to a large running vacuum pump station.

The Artemis 123 data acquisition system (**Figure 2**) utilizes a fiber optic linked expandable PXI architecture, enabling the acquisition chassis to reside just outside the MSR in an RF-shielded cabinet. The fiber optic link that connects the PXI chassis to the host PC running the operating software provides galvanic isolation from the electrical circuits outside the MSR while enabling

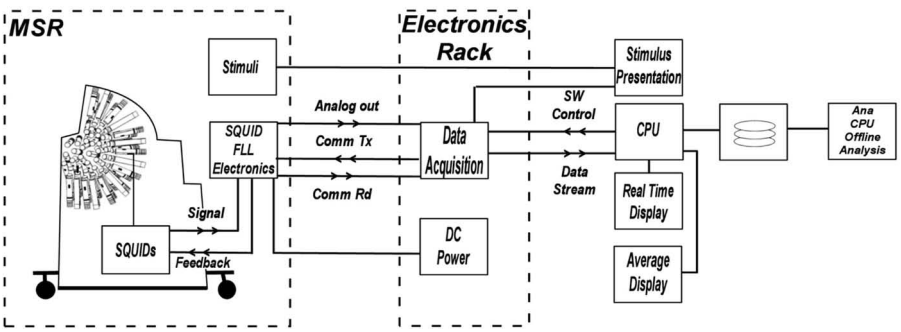

FIGURE 2 | Block diagram of electronics system functions. The architecture provides control and real-time processing for MEG, EEG, and A/D input channels as well as fast off-line processing. The acquisition hardware consists of up to 160 simultaneously sampled 24-bit channels with built-in anti-alias filtering, plus up to an additional 96 16-bit auxiliary channels.

data transport bandwidth of up to 80 MB/s. The acquisition hardware consists of up to 160 simultaneously sampled 24-bit channels with built-in anti-alias filtering, plus up to an additional 96 16-bit auxiliary channels. Thus, simultaneous EEG, EMG or other continuous electrical recordings are achievable. The external electronics cabinet also contains an isolation transformer and DC power supplies for the SQUID electronics in the room, and power from the supplies enter the MSR through EMI filters.

The control software for the Artemis 123 biomagnetometer runs on a PC workstation, and Windows OS. The Artemis 123 operating system is written in LabView® for rapid development and to simplify communications with National Instruments data acquisition boards. The software features simultaneous displays in a split-screen configuration (e.g., continuous data on the left and averaged data on the right). The control software is capable of graphing all channels on a strip chart display, detecting and processing event-related averages, continuously refreshing the averaged data graph, applying filters, and recording the data to disk, all at a sustained 5 kHz sample rate. The available filtering options in various points throughout the data stream, coupled with the ability to "play back" a saved data file, enables the Artemis 123 acquisition software to also be used as a post-processing tool.

Examining recordings obtained in the empty MSR, **Figure 3** shows two spectra, one of the raw primary sensor outputs (**Figure 3A**) and one with weights generated from the reference magnetometers applied to all sensors (**Figure 3B**) as a spatial filter to reduce external noise sources. The spectrum for each channel is the grand average of 36 averages of 8192-point FFTs (1.62 s epochs), with the figure showing the average across all sensor channels. For **Figure 3B**, prior to generation of weights, the data were band-passed from 5 to 200 Hz and then notch filters applied at the line frequency and all harmonics (i.e., 60, 120, 180, 240, and 300 Hz). Weights were obtained by calculating the covariance between signal and reference channels across the selected frequency bands. These weights were then applied to the raw data with no temporal filtering.

The **Figure 3A** power spectrum shows several large peaks below 100 Hz. These include the 60 Hz powerline peak as well as a peak at ∼24 Hz which reflects noise from the local mass transport/train system. **Figure 3B** shows that via spatial filtering the reference channels can be used to remove most of the noise activity below 100 Hz. Of note, the 60 Hz peak observed in **Figure 3** is of comparable, or even smaller, amplitude than the 60 Hz peak observed in the CTF 275 system located in the same room when the CTF 3rd order noise reduction option is turned off.

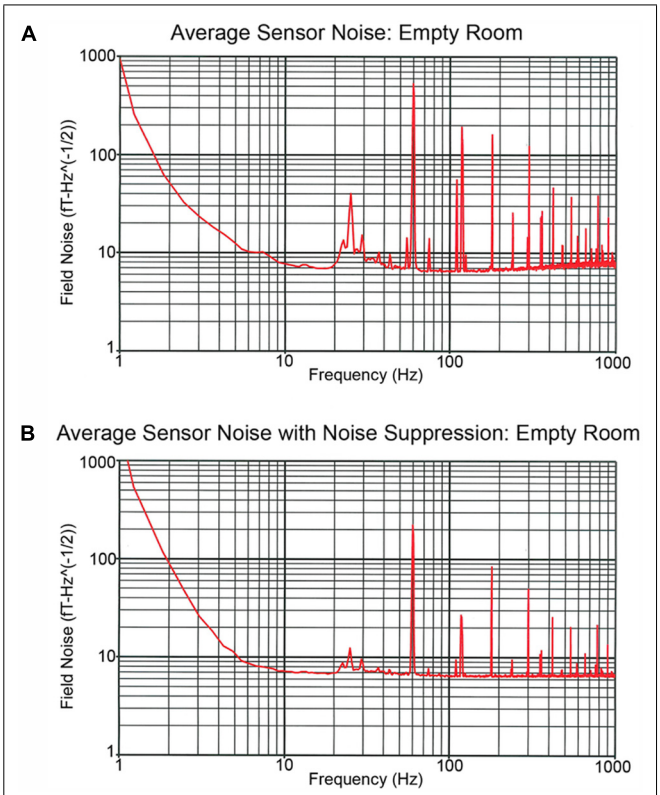

FIGURE 3 | Recordings obtained in the empty MSR. (A,B) show the spectra averaged across all sensor channels. The **(A)** power spectrum shows several large peaks below 100 Hz. These include the 60 Hz powerline peak as well as a peak at ∼24 Hz which reflects noise from the local mass transport/train system. In **(B)**, the reference channels were used to remove external noise, the weights obtained by calculating the covariance between signal and reference channels and then the weights applied to the raw data with no temporal filtering. **(B)** shows that via spatial filtering most of the noise activity below 100 Hz is removed.

PHANTOM RECORDINGS

A custom made Artemis 123 compatible spherical saline-filled electrolyte phantom was constructed (12.7 cm diameter; 40 cm circumference, see **Figure 4A**). Two current dipoles were each constructed as a pair of gold spheres of approximately 2 mm diameter with 9 mm between anode and cathode. The two current dipoles were positioned at (1.8, 0, 4.0) cm or (−1.8, 0, 2.0) cm, relative to the center of the sphere.

Dipoles were driven by a 40 Hz sinusoidal current source at each of two different driving voltages, 1 and 0.5 V. Three head position indicator coils (HPIs) were affixed to the phantom at (6.35, 0, 0) cm, (0, −6.35, 0) cm, and (0, 6.35, 0) cm to identify the phantom location within the sensor array (approximating the nasion and pre-auricular points that might be used as anatomic fiducial landmarks). The HPI coils were driven by 0.1 V sinusoidal current sources each with a unique non-harmonic frequency, 700, 750, and 800 Hz. Ten seconds of data (40 trials of 0.250 s duration) were acquired for each dipole activation and each driving voltage strength using a sample rate of 5 kHz. HPI localization was achieved by first demodulating each of the HPI signals from the sensor waveforms. Demodulated signals were then low-pass filtered (8 Hz) and averaged, yielding a single topography for each of the HPI sources. Magnetic dipoles were fit, using a combination of grid search and gradient descent algorithms, to the observed topographies, thereby identifying the locations of each of the HPIs.

For each data acquisition, a single sphere head model (radius 6.7 cm) was determined from the HPI locations. The MEG waveforms were down-sampled to 500 Hz and filtered with a 10–50 Hz band-pass. Sensor waveforms were then averaged across trials and localized by single equivalent current dipole fitting.

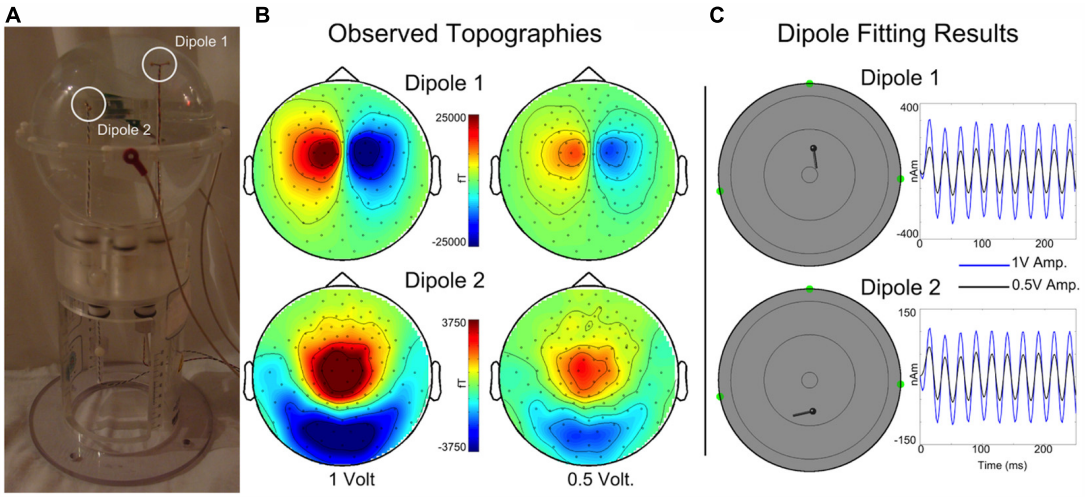

FIGURE 4 | (A) A custom spherical saline-filled phantom with two dipole locations indicated with white circles. **(B)** Observed topographies for activated Dipoles 1 and 2 are shown for a 40 Hz sinusoidal current source at 1 and 0.5 driving voltages. **(C)** The corresponding dipole model locations and moment traces for each voltage. Estimated source localization error is less than 0.5 cm. (Of note, the Artemis 123 phantom is a scaled-down version of the CTF/MISL phantom, designed to fit into the existing CTF/MISL stand (visible in **Figure 3A**). In addition, the electrodes provided by CTF/MISL are the same as those used in the Artemis 123 phantom.).

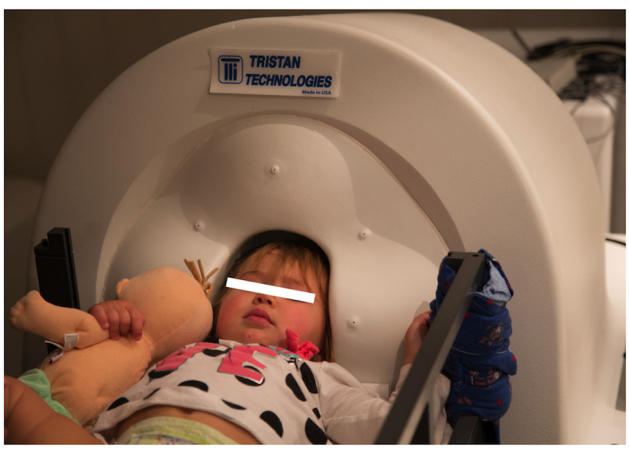

FIGURE 5 | A 14-month-old participant undergoing MEG recording.

HUMAN RECORDINGS

MEG data was collected at 5 kHz per channel. Resting-state and auditory evoked data were collected from a 14-month-old female, an 18-month-old female, and a 48-month-old male, with data obtained from all participants in a supine position (**Figure 5**). Data were obtained in the 14-month-old female while asleep, and from the two other participants while they watched a silent video projected onto the ceiling. All recordings were performed in the afternoon. All subjects were typically developing.

Resting-state

Resting-state data were obtained over periods of up to 60 s with minimal observed head motion. In the two awake cases, data was acquired in the eyes-open state (except for occasional blinks).

Auditory stimulation

500 and 1000 Hz sinusoidal tone stimuli were presented at a comfortable hearing level using a 60cm × 60cm plane-wave electrostatic directional flat-panel speaker (Panphonics Sound-Shower SSHP60x60, Tampere, Finland). Stimuli were of 300 ms duration (10 ms linear onset ramps) and presented with a 2 s inter-stimulus interval (± 0.3 s). 500 and 1000 Hz tones were presented in separate non-interleaved blocks. Stimuli were presented until at least 100 trials per condition were collected.

Auditory data were analyzed using BESA^{TM} 6.0 (BESA Gmbh, Graefelfing, Germany). Data periods exhibiting artifacts (e.g., muscle) were manually identified and removed. Artifact-free epochs were then averaged according to stimulus type and filtered using a 3 Hz (12 dB/octave, zero-phase) to 40 Hz (48 dB/octave, zero-phase) band-pass. Auditory responses were averaged over a 600 ms epoch, including a 200 ms pre-stimulus interval. The presence or absence of middle latency (∼M50) and long latency (∼M100) responses in the left and right hemisphere was determined by the magnetic field topography. In particular, presence of M50- and M100-like evoked response components was determined based on left and right hemisphere ingoing and outgoing flux topography (e.g., for "M100" left hemisphere ingoing anterior, outgoing posterior, and vice-versa for the right hemisphere). In view of the potential application of infant auditory MEG to detection of early signs of ASD, particular focus was placed on determining the latency of evoked responses. While latency can be determined at the sensor-level, a level of noise reduction can be obtained by principal component analysis (PCA) to more clearly delineate evoked response components. An additional SNR advantage can be achieved by estimating the neural timecourse in source space, through single equivalent dipole fitting, beam-forming, or other localization techniques. In this manuscript, a simple standard brain regional source and lead field approach

(with empirically optimized source orientation) to source space estimation is presented, which nonetheless confers some SNR advantage over sensor-level estimates.

Additionally, again following previous results in older children, time frequency analysis was demonstrated – using complex demodulation methods as described in Edgar et al. (2013) and implemented in BESA to yield spectrotemporal profiles of total power, evoked power and ITC from left and right hemisphere auditory sources.

RESULTS

PHANTOM DATA

Topographies are shown in **Figure 4B** for each dipole and drive voltage; note that for visualization purposes topologies for each dipole are scaled separately. Current dipoles were fit using the Fieldtrip software package (Oostenveld et al., 2011) to the averaged dataset, yielding locations and time courses for each dipole and drive voltage (**Figure 4C**). The mean dipole locations (each dipole was localized for 1 and 0.5 V drive amplitudes) were as follows: Dipole 1 – (1.95, −0.28, 3.93) cm, Dipole 2 – (−2.28, −0.23, 2.02) cm with standard deviations (0.03, 0.00, 0.01) cm and (0.08, 0.06, 0.16) cm. Estimated root mean square source localization error was less than 0.5 cm.

Resting-state

Resting-state data were obtained from all three subjects. **Figure 6** shows resting-state activity from a typical subject.

The raw recordings in the left panel show "alpha" activity (8 Hz), with the top-view inset showing the topography distinctive to resting-state alpha with alpha activity larger in occipital than frontal sensors. The panel to the right shows heartbeat in many of the channels, characteristic of clinical MEG recordings and illustrating a potential confounding artifact (note, the physical distance from heart to helmet is closer in infants than in older children or adults). Multiple "cardiac artifact" elimination schemes have been proposed (e.g., Breuer et al., 2013).

AUDITORY DATA

Figure 7 illustrates a sensor-level view of MEG auditory evoked waveforms along with left- and right-hemisphere "M50" magnetic field instantaneous topographic overlays for a 14-month-old participant undergoing stimulation with a 500 Hz sinusoidal tone. Clear bilateral evoked responses are resolved, along with dipolar magnetic field topographies amenable to single equivalent current dipole modeling. Note that the lateral temporal sensors exhibit greater evoked response amplitudes than frontal or occipital sensors, indicating the spatial discrimination of the device.

Figure 8 illustrates post-processing of the averaged evoked sensor-level response for the 14-month-old participant, showing source space estimation of the time course of the right superior temporal gyrus auditory response, revealing resolvable component events, characterizable in terms of amplitude and latency. **Figure 8D** extends the analysis to the spectrotemporal domain, allowing resolution of stimulus-related inter-trial coherence in lower (<20 Hz) domains.

Figure 9 represents the ability of auditory evoked recordings to assess neuronal encoding of stimulus features such as frequency

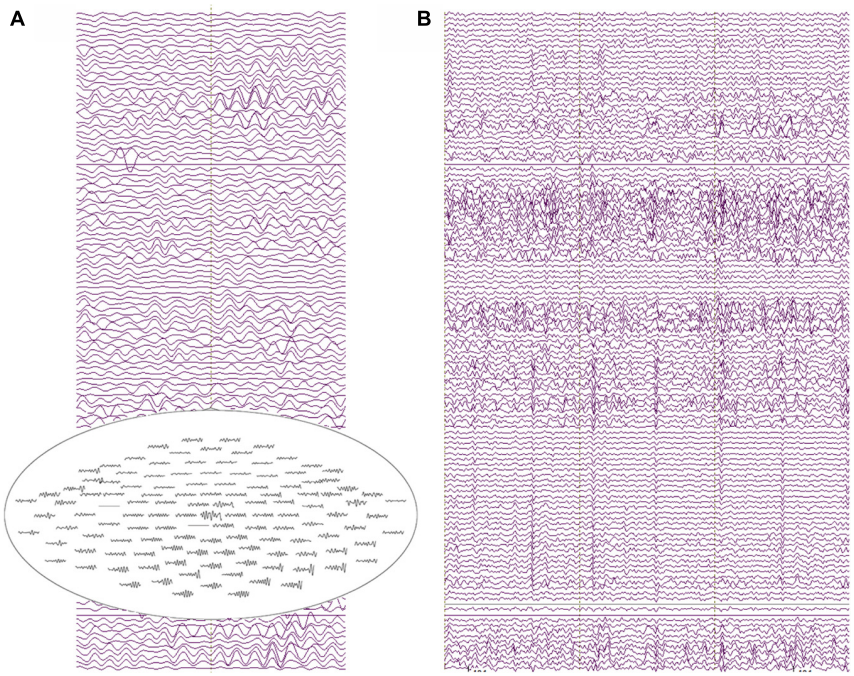

FIGURE 6 | (A) Two seconds of resting-state recordings from an 18-month-old participant. Several channels exhibit resolvable alpha activity in the resting MEG data with increased amplitude from posterior sensor locations (see the top-view sensor inset). **(B)** 3 s of resting-state data showing heart-beat activity in most MEG channels for the same participant (approximately two heartbeats per second).

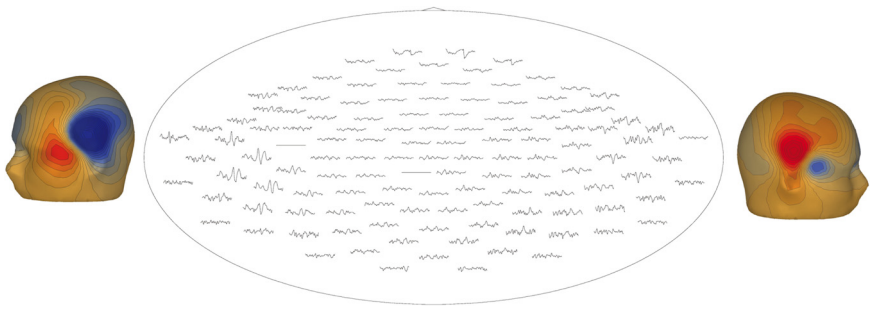

FIGURE 7 | Top-down view of MEG auditory evoked waveforms and left- and right-hemisphere "M50" magnetic field topographies for an 18-month-old participant (500 Hz tone). In the top-down view frontal sensors are shown at the top and occipital-parietal sensors at the bottom.

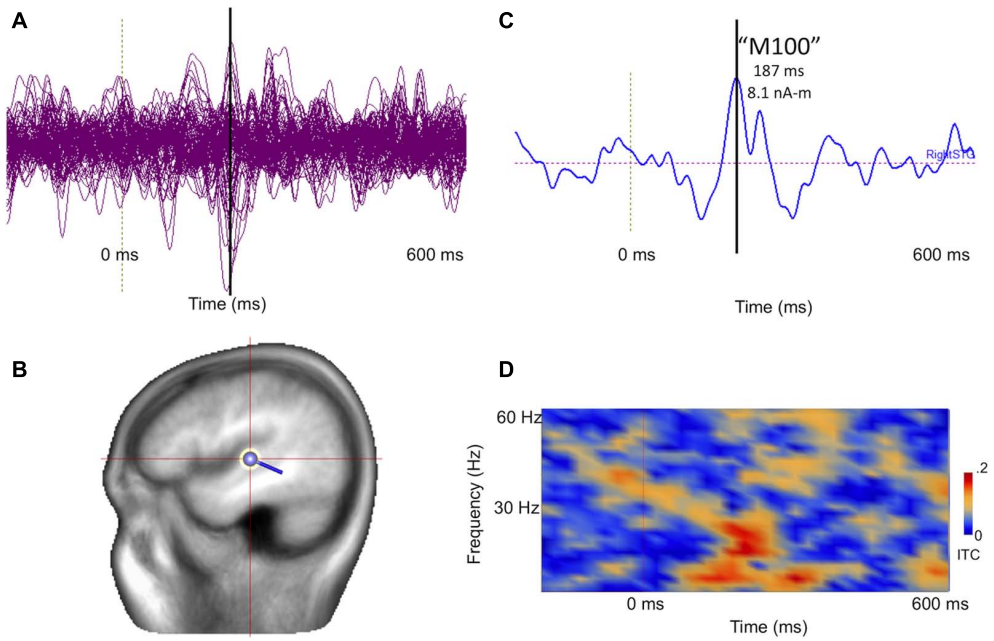

FIGURE 8 | (A) Collapsed ("butterfly") plot of MEG auditory evoked sensor waveforms for a 14-month-old participant experiencing stimulation with a 1000 Hz tone, showing data from all MEG channels with stimulus locked averaging from −200 to 600 ms with respect to tone onset (filtered 3–40 Hz). **(B)** A dipolar regional source is shown for the right superior temporal gyrus in a standard head model. **(C)** Source time course of the right superior temporal gyrus waveform, indicating a clear deflection at approximately 180 ms (vertical line). **(D)** Time-frequency transformation of the single–trial data allows estimation of inter-trial coherence (ITC), or phase-locking, for the source (time on x axis and frequency on y axis). Bright red regions post-stimulus indicate increased superior temporal gyrus phase-locking to the 1000 Hz tone, particularly at lower frequencies.

in young children. In this example, an 18-month-old participant underwent stimulation with 500 and 1000 Hz sinusoidal tones. Sensor-level waveforms were averaged and decomposed using PCA, and the PCA waveforms for each stimulus overlaid to illustrate a stimulus-frequency-dependent latency shift of the M50 evoked response (analogous to that described by Roberts and Poeppel, 1996). Sensor-level findings are recapitulated in source space using regional source modeling, with a similar auditory latency shift observed.

Middle latency responses (analogous to the M50 described in older children and adults) also appear to exhibit a developmental time course. The preliminary data examined in this study were consistent with a maturational shortening of the "M50" latency from 180 ms at 14 months through 156 ms at 18 months to 147 ms at 48 months (500 Hz tone stimulation) as described by Paetau et al. (1995) and Roberts et al. (2013). Of note, data from the youngest participant was acquired during sleep. Sleep may additionally modulate (prolong) evoked response latency.

DISCUSSION

Present findings show that the Artemis 123 provides high-quality recordings from individuals aged 14 to 48 months. In particular, examination of Artemis 123 auditory data showed generalizability, with auditory responses observed in all three participants. The auditory MEG measures were also found to be manipulable

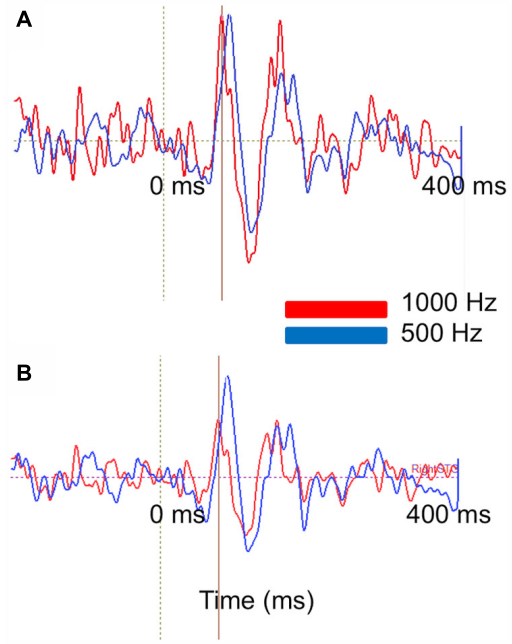

FIGURE 9 | Stimulus attribute (frequency) encoding is reflected at both the sensor and source levels. (A) PCA on MEG auditory evoked sensor waveforms comparing a 1000 Hz (red) and 500 Hz (blue) auditory response in an 18-month-old-subject. Waveforms are shown from −200 to 400 ms. **(B)** Right superior temporal gyrus source waveforms in the same subject. Time courses are shown from −200 to 400 ms. At sensor and source level a slight latency shift is resolvable (with the higher frequency stimulus eliciting a shorter latency response).

(**Figure 9**), exhibiting sensitivity to tone frequency. Furthermore, there appeared to be a predictable sensitivity of evoked response components to development, with latencies decreasing with age. Given the atypical developmental trajectory of M50 latency in disorders such as ASD (e.g., Roberts et al., 2013), this offers exciting potential for assessment of auditory system development as well as early detection of atypical auditory processing. Examination of resting-state rhythms also showed characteristic resting-state oscillatory activity (posterior resting-state alpha, heartbeat activity), indicating that the Artemis 123 provides quality recordings of resting-state rhythms in young children, with potential for analyses of resting-state functional networks and connectivity. Future work will involve examining the feasibility of obtaining somatosensory and visual recordings in similar-age children as well as obtaining recordings from infants. Finally, phantom data showed that dipole sources could be localized with an error less than 0.5 cm.

Given that in many studies it will not be possible to obtain magnetic resonance imaging (MRI) data from infants and young children, for some studies it will be necessary to apply techniques (some already developed) to align MEG data to template MRIs. As an example, this could accomplished via affine point based registration techniques to align individualized headshape models (derived from head-surface points) to the scalp of age-matched MRI templates. The transformed age-matched MRI template could then be used for visualization and additional head modeling required for source localization. Once developed, in future studies it will also be possible to use the HPI data to determine the location of the child's head with respect to the MEG sensors and then co-register the MEG and MRI data for source localization. Unlike EEG electrical fields, as MEG magnetic fields are insensitive to changes in conductivity profiles (e.g., between tissue, CSF, skull, skin) a single-shell head model can be used for source localization (Lewine and Orrison, 1995).

There are several unresolved technical challenges. First, given that it is difficult to obtain recordings in young children and infants over an extended period of time, developing paradigms that quickly provide multiple measures is of interest. For example, a paradigm that simultaneously presents auditory, visual, and somatosensory stimuli would allow assessment of the integrity of multiple primary sensory areas in less than five minutes. Second, for longer paradigms and tasks, it will be important to develop procedures to correct for head movement. With the ability to collect MEG data with the HPI coils active throughout the recording, at a minimum this could involve using the HPI information to remove MEG data where the participant's head moves beyond a threshold. Given the acquisition of continuous HPI data, however, procedures can be developed to compensate for head motion (Stolk et al., 2013). Finally, in some infants (as exemplified in the youngest participant described in this manuscript) it might be necessary to obtain data during sleep (i.e., recordings during naptime or in the evening). For such studies it will be important to determine the effect of sleep on primary sensory (as well as non-task "resting") activity, motivating detailed comparative studies in awake and sleeping states.

As previously noted, examination of the continuous recordings showed that the Artemis 123 provided quality recordings of resting brain activity as well as common non-brain artifacts (**Figure 6**). Using adult MEG systems, clinical MEG recordings are obtained in individuals with epilepsy to localize the generator(s) of epileptiform activity and also in individuals with lesions to localize eloquent cortex (Roberts et al., 1995, 2000; Roberts and Rowley, 1997; Gaetz et al., 2009). Although clinical MEG studies are performed in infants, a limitation of these studies is that in very young children the MEG sensors are far from the infant's brain. Clinical MEG infant and young child studies using the Artemis 123 would provide measures of epileptiform activity with significantly higher sensitivity than adult MEG system, thus potentially providing more accurate estimates of the location of brain pathology in clinical infant groups. It remains to be established whether this sensitivity translates straightforwardly to increased signal to noise ratio, given the expected increase in sensitivity to other coincident brain activity.

Although present findings show that quality recordings can be obtained in infants and young children, there are several limitations to consider. First, although the helmet was sized so that sensors can be placed as close as possible to a typical three-year-old's head, examination of normative head circumference charts shows that two-year-olds with head circumferences above the 90th percentile and three-year-olds with head circumferences above the 95th percentile will not fit into the helmet (see normative charts in Roche et al., 1987; given slightly smaller head

circumferences in females than males, more two- and three-year-old girls than boys will fit into the helmet). As such, although the Artemis 123 will accommodate the majority of children three and under, many children four years and older will not fit into the Artemis123 helmet, thus placing limits on the age-range that can be examined in Artemis 123 studies. Although a limitation, reducing helmet size was a major consideration in achieving improved sensitivity to infant and young child brain activity, and with our ongoing interest in early signs of ASD as well as language acquisition during the 12–30 month period, the Artemis 123 helmet size was selected to be optimal for this period of development.

For MEG studies examining brain function in children across a broad age-range, it would be possible to obtain data in the youngest children using the Artemis 123 and in older children using an adult MEG system. Although such studies are clearly of interest, in these studies it will be necessary to determine equivalence in the dependent variables of interest between the infant/young child and adult MEG systems. For example, although latency measures are likely similar between infant and adult MEG systems it remains to be determined if the infant MEG system amplitude measures need to be scaled to be comparable to an adult MEG system. Studies examining children (e.g., a four-year-old) in the Artemis 123 and an adult system are needed. In our laboratory, the Artemis 123 is sited next to an adult CTF 275 system (VSM), making such comparisons possible.

Another limitation worth noting is that, at present it is not possible to correct for head motion and thus it is necessary for the participant to remain still throughout the recording. This is, however, a temporary limitation - the Artemis 123 provides the ability to continuously record head movement via the head coils and, as such, algorithms to correct for head motion can be developed. Finally, although the Artemis 123 has reference channels, these reference channels were not used to remove external noise in the present human data recordings [in the Methods it was shown that a spatial filter can be used to remove external noise from empty room data (e.g., train and 60 Hz power-line noise)]. Although noise-cancellation procedures using the reference channels will be developed, it is of note that quality human recordings were obtained without the use of the reference channels.

To conclude, this manuscript describes the design and implementation of a whole-head biomagnetometer optimized for infants and small children. Phantom studies confirm signal detection and source localization ability. Preliminary infant studies demonstrate recordings at rest and during stimulus presentation and illustrate the generalizability of recordings. Furthermore, auditory evoked response component latencies illustrate sensitivity to stimulus features and potentially representing the neural processes underlying feature encoding and representation in the brain. Finally, latencies appear to mature (shorten) with increasing age, potentially indexing development of primary and secondary auditory areas. These latter two attributes (representation and development) have been observed as atypical in certain disease populations (including ASD). The Artemis 123 offers promise as a means of detecting earlier diagnostic signatures in such neurodevelopmental disorders.

ACKNOWLEDGMENTS

This research was supported by grants from the Nancy Lurie Marks Family Foundations, the Lurie Family Foundations, NIH-R01DC008871, NIH-P30HD026979 and a grant from HRSA. Dr. Roberts gratefully acknowledges the Oberkircher family for the Oberkircher Family Chair in Pediatric Radiology at CHOP.

REFERENCES

Breuer, L., Cammers, J., Roberts, T. P., and Shah, N. (2013). A constrained ICA approach for real-time cardiac artifact rejection in magnetoencephalography. *IEEE Trans. Biomed. Eng.* [Epub ahead of print].

Cornew, L., Roberts, T. P., Blaskey, L., and Edgar, J. C. (2012). Resting-state oscillatory activity in autism spectrum disorders. *J. Autism Dev. Disord.* 42, 1884–1894. doi: 10.1007/s10803-011-1431-6

Edgar, J. C., Huang, M. X., Weisend, M. P., Sherwood, A., Miller, G. A., Adler, L. E., et al. (2003) Interpreting abnormality: an EEG and MEG study of P50 and the auditory paired-stimulus paradigm. *Biol. Psychol.* 65, 1–20. doi: 10.1016/S0301-0511(03)00094-2

Edgar, J. C., Khan, S. Y., Blaskey, L., Chow, V. Y., Rey, M., Gaetz, W., et al. (2013). Neuromagnetic oscillations predict evoked-response latency delays and core language deficits in autism spectrum disorders. *J. Autism Dev. Disord.* doi: 10.1007/s10803-013-1904-x [Epub ahead of print].

Gaetz, W., Cheyne, D., Rutka, J. T., Drake, J., Benifla, M., Strantzas, S., et al. (2009). Presurgical localization of primary motor cortex in pediatric patients with brain lesions by the use of spatially filtered magnetoencephalography. *Neurosurgery* 64(3 Suppl.):ons177–185; discussion ons186. doi: 10.1227/01.NEU.0000316433.10913.32

Gaetz, W., Otsubo, H., and Pang, E. W (2008). Magnetoencephalography for clinical pediatrics: the effect of head positioning on measurement of somatosensory-evoked fields. *Clin. Neurophysiol.* 119, 1923–1933. doi: 10.1016/j.clinph.2008.04.291

Gage, N. M., Siegel, B., and Roberts, T. P. (2003). Cortical auditory system maturational abnormalities in children with autism disorder: an MEG investigation. *Brain Res. Dev. Brain Res.* 144, 201–209. doi: 10.1016/S0165-3806(03)00172-X

Johnson, B. W., Crain, S., Thornton, R., Tesan, G., and Reid, M. (2009). Measurement of brain function in pre-school children using a custom sized whole-head MEG sensor array. *Clin. Neurophysiol.* 121, 340–349. doi: 10.1016/j.clinph.2009.10.017

Kikuchi, M., Shitamichi, K., Yoshimura, Y., Ueno, S., Remijn, G. B., Hirosawa, T., et al. (2011). Lateralized theta wave connectivity and language performance in 2- to 5-year-old children. *J. Neurosci.* 31, 14984–14988. doi: 10.1523/JNEUROSCI.2785-11.2011

Kikuchi, M., Yoshimura, Y., Shitamichi, K., Ueno, S., Hirosawa, T., Munesue, T., et al. (2013). A custom magnetoencephalography device reveals brain connectivity and high reading/decoding ability in children with autism. *Sci. Rep.* 3:1139. doi: 10.1038/srep01139

Kujala, T., Lepistö, T., and Näätänen, R. (2013). The neural basis of aberrant speech and audition in autism spectrum disorders. *Neurosci. Biobehav. Rev.* 37, 697–704. doi: 10.1016/j.neubiorev.2013.01.006

Lewine, J. D., and Orrison, W. W. Jr. (1995). Magnetic source imaging: basic principles and applications in neuroradiology. *Acad. Radiol.* 2, 436–440. doi: 10.1016/S1076-6332(05)80351-4

Muthukumaraswamy, S. D. (2013). High-frequency brain activity and muscle artifacts in MEG/EEG: a review and recommendations. *Front. Hum. Neurosci.* 7:138. doi: 10.3389/fnhum.2013.00138

Okada, Y., Pratt, K., Atwood, C., Mascarenas, A., Reineman, R., Nurminen, J., et al. (2006). BabySQUID: a mobile, high-resolution multichannel magnetoencephalography system for neonatal brain assessment. *Rev. Sci. Instrum.* 77, 24–31.

Oostenveld, R., Fries, P., Maris, E., and Schoffelen, J. M. (2011). FieldTrip: open source software for advanced analysis of MEG, EEG, and invasive electrophysiological data. *Comput. Intell. Neurosci.* 2011:156869. doi: 10.1155/2011/156869

Paetau, R., Ahonen, A., Salonen, O., and Sams, M. (1995). Auditory evoked magnetic fields to tones and pseudowords in healthy children and adults. *J. Clin. Neurophysiol.* 12, 177–185. doi: 10.1097/00004691-199503000-00008

Roberts, T. P., Cannon, K. M., Tavabi, K., Blaskey, L., Khan, S. Y., Monroe, J. F., et al. (2011). Auditory magnetic mismatch field latency: a biomarker for language impairment in autism. *Biol. Psychiatry* 70, 263–269. doi: 10.1016/j.biopsych.2011.01.015

Roberts, T. P., Ferrari, P., Perry, D., Rowley, H. A., and Berger, M. S. (2000). Presurgical mapping with magnetic source imaging: comparisons with intraoperative findings. *Brain Tumor Pathol.* 17, 57–64. doi: 10.1007/BF02482736

Roberts, T. P., Khan, S. Y., Rey, M., Monroe, J. F., Cannon, K., Blaskey, L., et al. (2010). MEG detection of delayed auditory evoked responses in autism spectrum disorders: towards an imaging biomarker for autism. *Autism Res.* 3, 8–18. doi: 10.1002/aur.111

Roberts, T. P., Lanza, M. R., Dell, J., Qasmieh, S., Hines, K., Blaskey, L., et al. (2013). Maturational differences in thalamocortical white matter microstructure and auditory evoked response latencies in autism spectrum disorders. *Brain Res.* 1537, 79–85. doi: 10.1016/j.brainres.2013.09.011

Roberts, T. P., and Poeppel, D. (1996). Latency of auditory evoked M100 as a function of tone frequency. *Neuroreport* 26, 1138–1140. doi: 10.1097/00001756-199604260-00007

Roberts, T. P., and Rowley, H. A. (1997). Magnetic source imaging as a tool for presurgical functional brain mapping. *Neurosurg. Clin. N. Am.* 8, 421–438.

Roberts, T., Rowley, H., and Kucharczyk, J. (1995). Applications of magnetic source imaging to presurgical brain mapping. *Neuroimaging Clin. N. Am.* 5, 251–266.

Roche, A. F., Mukherjee, D., Guo, S., and Moore, W. M. (1987). Head circumference reference data: birth to 18 years. *Pediatrics* 79, 706–712.

Rojas, D. C., Maharajh, K., Teale, P., and Rogers, S. J. (2008). Reduced neural synchronization of gamma-band MEG oscillations in first-degree relatives of children with autism. *BMC Psychiatry* 8:66. doi: 10.1186/1471-244X-8-66

Stolk, A., Todorovic, A., Schoffelen, J. M., Oostenveld, R. (2013). Online and offline tools for head movement compensation in MEG. *Neuroimage* 68, 39–48. doi: 10.1016/j.neuroimage.2012.11.047

Wilson, T. W., Rojas, D. C., Reite, M. L., Teale, P. D., Rogers, S. J. (2007). Children and adolescents with autism exhibit reduced MEG steady-state gamma responses. *Biol. Psychiatry* 62, 192–197. doi: 10.1016/j.biopsych.2006.07.002

Yoshimura, Y., Kikuchi, M., Shitamichi, K., Ueno, S., Remijn, G. B., Haruta, Y., et al. (2012). Language performance and auditory evoked fields in 2- to 5-year-old children. *Eur. J. Neurosci.* 35, 644–650. doi: 10.1111/j.1460-9568.2012.07998.x

Yoshimura, Y., Kikuchi, M., Ueno, S., Okumura, E., Hiraishi, H., Hasegawa, C., et al. (2013). The brain's response to the human voice depends on the incidence of autistic traits in the general population. *PLoS ONE* 8:e80126. doi: 10.1371/journal.pone.0080126

Conflict of Interest Statement: Several of the authors (Mascarenas, Miller, Han, Caffrey, Kincade, and Power) are employees of Tristan Technologies Inc.. Drs Paulson and Pratt have ownership interests in Tristan Technologies Inc. Dr Hirschkoff is a board member and consultant for Tristan Technologies Inc. Dr. Roberts has served as a paid speaker on behalf of Elekta Oy and Siemens Medical Solutions. Additionally Dr. Roberts holds stock options in Prism Medical Imaging in return for consulting services. Other authors have no conflicts of interest to report.

Received: 10 December 2013; accepted: 09 February 2014; published online: 03 March 2014.

Citation: Roberts TPL, Paulson DN, Hirschkoff E, Pratt K, Mascarenas A, Miller P, Han M, Caffrey J, Kincade C, Power B, Murray R, Chow V, Fisk C, Ku M, Chudnovskaya D, Dell J, Golembski R, Lam P, Blaskey L, Kuschner E, Bloy L, Gaetz W and Edgar JC (2014) Artemis 123: development of a whole-head infant and young child MEG system. Front. Hum. Neurosci. ***8****:99. doi: 10.3389/fnhum.2014.00099*

This article was submitted to the journal Frontiers in Human Neuroscience.

frontiers in
HUMAN NEUROSCIENCE

ORIGINAL RESEARCH ARTICLE
published: 14 February 2014
doi: 10.3389/fnhum.2014.00082

Atypical right hemisphere specialization for object representations in an adolescent with specific language impairment

Timothy T. Brown[1,2,3]*, Matthew Erhart[1,4], Daniel Avesar[5], Anders M. Dale[1,2,4], Eric Halgren[1,2,4] and Julia L. Evans[6,7]

[1] Multimodal Imaging Laboratory, University of California San Diego, La Jolla, CA, USA
[2] Department of Neurosciences, School of Medicine, University of California San Diego, La Jolla, CA, USA
[3] Center for Human Development, University of California San Diego, La Jolla, CA, USA
[4] Department of Radiology, School of Medicine, University of California San Diego, La Jolla, CA, USA
[5] Program in Experimental and Molecular Medicine, Dartmouth Medical School, Hanover, NH, USA
[6] Center for Research in Language, University of California San Diego, La Jolla, CA, USA
[7] School of Behavioral and Brain Sciences, University of Texas Dallas, Dallas, TX, USA

Edited by:
Christos Papadelis, Harvard Medical School, USA

Reviewed by:
Charline Urbain, The Hospital for Sick Children, Canada
Gerard Bastiaan Remijn, Kyushu University, Japan

***Correspondence:**
Timothy T. Brown, Department of Neurosciences, UCSD School of Medicine, 8950 Villa La Jolla Drive, Suite C-101, La Jolla, CA 92037, USA
e-mail: ttbrown@ucsd.edu

Individuals with a diagnosis of specific language impairment (SLI) show abnormal spoken language occurring alongside normal non-verbal abilities. Behaviorally, people with SLI exhibit diverse profiles of impairment involving phonological, grammatical, syntactic, and semantic aspects of language. In this study, we used a multimodal neuroimaging technique called anatomically constrained magnetoencephalography (aMEG) to measure the dynamic functional brain organization of an adolescent with SLI. Using single-subject statistical maps of cortical activity, we compared this patient to a sibling and to a cohort of typically developing subjects during the performance of tasks designed to evoke semantic representations of concrete objects. Localized patterns of brain activity within the language impaired patient showed marked differences from the typical functional organization, with significant engagement of right hemisphere heteromodal cortical regions generally homotopic to the left hemisphere areas that usually show the greatest activity for such tasks. Functional neuroanatomical differences were evident at early sensoriperceptual processing stages and continued through later cognitive stages, observed specifically at latencies typically associated with semantic encoding operations. Our findings show with real-time temporal specificity evidence for an atypical right hemisphere specialization for the representation of concrete entities, independent of verbal motor demands. More broadly, our results demonstrate the feasibility and potential utility of using aMEG to characterize individual patient differences in the dynamic functional organization of the brain.

Keywords: magnetoencephalography, specific language impairment, object concepts, semantic representations, hemispheric specialization, cerebral dominance

INTRODUCTION

Children with receptive or expressive language impairments who have normal hearing, an ordinary environment and rearing experiences, and show no other signs of developmental or neurological disorder are diagnosed with specific language impairment (SLI). Previously referred to as developmental aphasia or dysphasia, SLI is commonly encountered by speech-language clinicians and is found in disproportionate numbers of programs for children and adolescents with academic and behavioral dysfunction (Stark et al., 1988). The psycholinguistic manifestation of SLI can be highly variable across individuals, with primary impairments often evident within multiple aspects of language involving phonology, grammar, syntax, and semantics (Bishop, 2006).

Neurological and cognitive neuroscientific studies of functional brain organization demonstrate a prominent role of the left cerebral hemisphere generally in receptive and expressive language as well as specifically for the representation of semantic information, including word meanings and object concepts (Vigneau et al., 2006). A large body of research demonstrates that semantic knowledge about concrete entities is represented by distributed networks of discrete cortical regions most prominently involving large portions of the left temporal lobe and left ventral prefrontal cortex, as well as parietal and occipital areas (Martin and Chao, 2001; Binder and Desai, 2011), with these regions playing dissociable roles in relatively more perceptual versus conceptual processing. Despite undergoing significant developmental changes (Schlaggar et al., 2002; Brown et al., 2005; Szaflarski et al., 2006) and commonly involving regions of the right hemisphere as well (Martin and Chao, 2001; Binder and Desai, 2011; Donnelly et al., 2011), the typically developing cerebral functional organization for encoding word and object meanings shows a left hemisphere prominence (Martin, 1999) that is present even during infancy (Travis et al., 2011).

Atypical hemispheric specialization in SLI has been suggested in the scientific literature since the early twentieth century (Orton, 1925), but evidence has been inconsistent, particularly within functional neuroimaging experiments (Whitehouse and Bishop, 2008). Volumetric postmortem and structural imaging studies generally have found right-greater-than-left asymmetries in temporal and inferior prefrontal regions in SLI (Jernigan et al., 1991; Plante et al., 1991; Gauger et al., 1997; De Fossé et al., 2004) and greater overall "right-heavy" asymmetry in higher-order association cortex in children with developmental language disorder as compared to the "left-heavy" profile typically shown by control children (Herbert et al., 2005). Pars triangularis (Broca's area) and perisylvian regions have been implicated specifically, found to be significantly smaller in SLI on the left or to show significantly greater rightward asymmetry (Gauger et al., 1997). At least one structural imaging study found no discernable differences between language impaired and typically developing children in unilateral measurements or bilateral left–right asymmetry of posterior intrasylvian anatomy (Preis et al., 1998).

Functional neuroimaging studies of language impairment have found evidence strongly suggestive of abnormal lateralization patterns in brain activity, but common methodological caveats have often limited a strong interpretation of the results. For example, Whitehouse and Bishop used functional transcranial Doppler ultrasonography (fTCD) to measure cerebral blood flow in 11 young adults with SLI during performance of a letter fluency task (Whitehouse and Bishop, 2008). Interestingly, they compared these subjects with young adults who had a childhood history of SLI but no longer met diagnostic criteria, as well as with adults with a diagnosis of autism and a control group. While silently generating words to a given letter, all of the participants in the SLI-history group and the majority of both the autistic and control subjects showed greater activation in the left compared to the right middle cerebral artery, interpreted by the authors as indicating left hemisphere dominance. In contrast, the majority of individuals with SLI showed brain activity that was deemed either strongly right-lateralized (54.5%) or bilaterally prominent (27.3%).

Atypical hemispheric specialization in SLI has also been suggested in the limited number of functional magnetic resonance imaging (fMRI) studies conducted to date (Hugdahl et al., 2004; Ellis Weismer et al., 2005; Dibbets et al., 2006; Badcock et al., 2012). For example, Badcock et al. compared structural and functional MRI measures during a language task in a group of eight individuals with SLI, their unaffected siblings, and typically developing controls. Anatomically, language impaired participants showed significantly more gray matter than controls in the left inferior frontal gyrus (IFG) and significantly less gray matter in bilateral superior temporal sulcus (STS) and in the right caudate nucleus. Physiologically, when activity during the performance of a covert naming task was contrasted with a silent baseline or passive listening to reversed speech, individuals with SLI showed reduced activity in comparison with the sibling and typical groups. Interestingly, these decrements in brain activity were localized to the same areas implicated in the structural morphological analysis. Furthermore, they observed "clearly left" lateralization of brain activity within the sibling and typical groups, but this was subjectively reduced in SLI. Brain-wide, there were no regions found that showed greater activation in SLI than the other groups. Had this been found, the authors state that it "might have been interpreted as evidence for different functional organization for language or compensatory or maladaptive reorganization." Badcock et al. also reported that patterns of brain activity in the SLI group were found to show more variability than the unaffected siblings and control group, as measured by laterality indices.

Despite the highly suggestive findings from these fTCD and fMRI studies, covert language tasks were used in these experiments, so no objective measures of subject task compliance and level of performance could be collected during scanning. Therefore, the greater heterogeneity in brain activity and overall under-activation by SLI could be explained simply by worse task performance within the clinical group (Murphy and Garavan, 2004), which would be expected for such tasks based on their diagnosis. Because of this, even for the sibling and control groups used for comparison, there is no way to be reasonably sure that the observed brain activity maps reflect physiological responses that were constrained to the cognitive processes of interest. This issue is common in developmental functional neuroimaging studies and limits the degree to which the desired conclusions can be drawn about the observed differences in functional brain organization (Brown et al., 2003, 2006; Palmer et al., 2004; Poldrack, 2010).

As many of the studies reviewed above point out, atypical cerebral dominance is not evident in all cases of poor language development, nor in all individuals with a diagnosis of SLI. Such patient heterogeneity in functional brain organization can contribute to equivocal results when comparisons are made between a clinical group and control group. Notably, group-averaged brain activity maps reveal only those functional neuroanatomical components that are most similar across subjects and will obscure individual differences. In groups that have especially high inter-individual variability, averaged activity patterns may not be particularly representative of any individual. So, in order to achieve a clearer understanding of the relationships between cognitive functioning and functional brain organization, it may be useful to look more closely at individual patients, particularly with clinical groups such as SLI, which already have been shown to be cognitively and neurologically heterogeneous.

In addition, the majority of functional neuroimaging studies of SLI to date have used fMRI. Despite excellent spatial resolution, fMRI measures neural activity only indirectly, relying on a sluggish vascular response with poor temporal resolution. This inability to separate brain responses in time makes it considerably more difficult to isolate and identify specific cognitive functions that may be driving language task performance, such as sensory, perceptual, semantic, and motor processes (Posner, 1978, 2005; Cohen, 2011).

The purpose of the current study was to use a multimodal neuroimaging technique called anatomically constrained magnetoencephalography (aMEG) to localize with millisecond temporal sensitivity potentially atypical components of the functional brain organization within an individual patient. Here, we used a task paradigm designed specifically to engage cortical systems involved in the semantic representation of concrete objects in an individual with a diagnosis of SLI, comparing him to a group of typically developing individuals with no history of language problems. For comparison, we also applied identical methods to measure the

dynamic functional brain organization of this patient's younger sister, who shows normal language abilities. Although differing by sex and age, she provides a useful comparison of the single-subject analysis methods.

For several reasons, we believed aMEG methods would provide a fruitful approach to the study of one patient. In addition to its sub-millisecond temporal resolution, aMEG provides excellent signal-to-noise properties and enhanced localization of brain activity through the use of noise-normalized source estimates constrained to the cortical reconstruction of each individual subject and aligned using sulcal and gyral surface-based registration (Dale et al., 2000; Dale and Halgren, 2001). Unlike single-dipole fitting MEG methods, the aMEG technique assumes multiple, distributed, and simultaneous cortical generators, which functional neuroimaging and recording methods overwhelmingly show is an appropriate assumption for cognitive tasks.

The primary questions posed in our experiment were: (1) does the dynamic functional brain organization for the semantic processing of concrete objects within an individual with a diagnosis and developmental history of SLI differ from that of a sample of typically developing individuals? (2) If so, how does the functional organization differ, topographically and temporally? (3) Specifically, does this individual show atypical aspects of the functional organization only during latencies that are associated with semantic encoding processes, or does he differ across all latencies measured? (4) Using the same conceptual and methodological approach, does the dynamic functional brain organization of an adolescent sibling with no history of language learning disorder mirror any of the differences found in the individual with SLI, or, instead, appear normal according to these methods? And more generally, (5) do aMEG techniques show feasibility and utility for mapping brain activity within individual patients, using activity distributions from a group of control subjects for direct comparison? In attempting to answer these questions, we hoped to assess both practical and substantive aspects of using aMEG to study individual differences in the dynamic functional organization of the brain.

MATERIALS AND METHODS

SUBJECTS

One left-handed adolescent male diagnosed with specific language impairment (SLI-1; aged 17.8 years), 1 right-handed female sibling (Sib-1; aged 16.1 years), and a group of 12 typically developing right-handed individuals (mean age = 20.9 years, SD = 1.7, range = 18.2–23.5; five female) performed semantic processing tasks during MEG recording. The two individuals who were minors gave assent to participate with parental informed consent, and all control subjects gave informed consent using protocols approved by the UCSD Human Research Protections Program.

The primary characteristic of SLI is the failure to master spoken and written language expression and comprehension despite normal non-verbal intelligence, normal hearing acuity, and no overt physical causes, recognized syndromes, or mitigating medical factors known to cause language disorders in children. SLI-1 was diagnosed at age 4 years with expressive and receptive language delay, meeting criteria for SLI. He had no hearing or other sensory impairments and no history of serious medical problems. He has been followed clinically continuously since that time and received services during school age for language and auditory processing deficits – the only member of his family to qualify for such services. He was never diagnosed with a speech articulation disorder and so did not receive any speech-motor therapy, nor any other special services related to learning and development.

In late adolescence, SLI-1 continues to meet criteria for language impairment. Standard scores (population mean = 100, SD = 15) showed a squarely average non-verbal IQ (102, Leiter-R; Roid and Miller, 1997) but below average performance on a language battery emphasizing grammar and semantics (82; Comprehensive Receptive and Expressive Vocabulary Test, Second Edition – CREVT-2; Wallace and Hammill, 2002). His receptive language score was 82 and expressive language score was 73. Measures of comprehension of non-literal language, deriving meaning from context, and composite language knowledge ranged from about 2 to 2.5 SD below average (72, 60, and 62, respectively; Comprehensive Assessment of Spoken Language – CASL; Carrow-Woolfolk, 1999). On the Clinical Evaluation of Language Fundamentals (CELF-4; Semel et al., 2003), SLI-1 also scored within the clinical range on tests of formulating sentences and recalling sentences (five and six, respectively; mean/SD = 10/3) but scored in the low average range on word classes (eight). On a measure of hand preference based on the Edinburgh questionnaire (Oldfield, 1971), SLI-1 reported being strongly left-handed.

On the same battery of measures, Sib-1 showed above-average non-verbal IQ (127) and above-average performance on a comprehensive language battery emphasizing semantics and grammar (120; CREVT-2). Her receptive language was 1 SD above average (115), and expressive language was within the average range (108). On standardized measures of the comprehension of non-literal meaning, deriving meaning from context, and composite language knowledge, Sib-1 scored within the average range (105, 93, and 99, respectively; CASL). On the CELF-4, she scored within the average to above-average range on tests of formulating sentences, recalling sentences, and word classes (13, 11, and 14, respectively). She reported being strongly right-handed.

Typically developing control subjects were screened by interview and questionnaire to rule out history of developmental learning disorder, head injury, neurological or psychiatric disorder, or other major medical problems. Of the 12 control participants, 8 were undergraduate college or junior college students, and 4 were working full time. All were strongly right-handed. All denied currently taking psychotropic medication. All participants were screened for MRI and MEG safety by self-report and metal detector.

MEG DATA ACQUISITION AND TASK PARADIGM

Event-related fields were measured using a 306-channel whole-head Elekta NEUROMAG system inside a six-layer combination active–passive shielded room (IMEDCO-AG, Switzerland). The tasks, based on previously published studies of semantic processing (Dale et al., 2000; Marinkovic et al., 2003) were pilot-tested and modified to be more easily performed by children and adolescents and involved the presentation of two types of visual stimuli: printed words (high frequency, early acquired, highly imaginable concrete nouns; e.g., bed, mouse, door, whale, bug,

house, leaf) and simple line drawings of lexically equivalent common, nameable objects. Picture and word stimuli were presented as white lines or letters against a black background. Subjects were instructed to respond to each item with laser-detected index finger lifts (one with the left hand, one with the right), indicating whether or not the object conveyed by word or image was small enough in size to fit into a shoebox. Stimuli were balanced with regard to the number of large versus small objects. Onscreen stimulus duration for words and pictures was 300 ms, delivered with interstimulus intervals jittered between 3 and 5 s. Words and pictures were presented roughly equal in size, subtending approximately 4° of visual angle in their largest dimension. Picture and word stimuli were delivered in eight separate, alternating task runs (four picture runs, four word runs), each presenting 40 items and lasting about 4 min.

MRI DATA ACQUISITION

High-resolution T1-weighted structural MRI scans optimized for gray/white matter contrast were acquired at 1.5 T for all subjects [time to echo (TE) = 3.8 ms, time to repetition (TR) = 10.7 ms, time to inversion (TI) = 1000 ms, flip angle = 8°, trigger delay (TD) = 750 ms, bandwidth = 31.25 Hz/pixel, field of view (FOV) = 24 cm, matrix = 192 × 192, slice thickness = 1.2 mm]. Real-time head motion tracking and correction was performed using PROMO, as described previously for prospective motion correction in spiral-navigated 3D pulse sequences (White et al., 2010). PROMO has been shown qualitatively and quantitatively to significantly improve image quality and reduce distortions caused by head motion and related artifacts, to increase the reliability of MR-derived brain measures (e.g., volume, thickness), and to improve the clinical diagnostic utility of structural MRI data when acquired in difficult-to-scan groups such as children (Brown et al., 2010; Kuperman et al., 2011).

MULTIMODAL IMAGE PROCESSING AND ANALYSIS

Multimodal brain activity maps were produced by generating a three-dimensional reconstruction of the cortical surface for each individual using MRI data (Fischl et al., 1998, 1999a,b; Dale et al., 1999) and spatially constraining the source estimations of MEG-derived noise-normalized dipole strength to its geometry (Dale et al., 2000; Dale and Halgren, 2001). Dynamic statistical parametric maps (dSPMs) of cortical activity were computed for the two individuals and for the average of the typically developing group, spanning seven time windows based on previous aMEG studies of visual lexical semantic processing (Dale et al., 2000; Marinkovic et al., 2003; Leonard et al., 2010, 2011). Time windows were chosen to display separable brain activity events occurring across sensory, perceptual, and cognitive-semantic processing stages. At early latencies, beginning at 120 ms, windows 50 ms wide were used to reveal brief, localized visual activity that has been observed in previous aMEG studies using visual semantic paradigms with similarly timed events (Dale et al., 2000; Marinkovic et al., 2003; Leonard et al., 2010, 2011). Rather than choosing single dSPM frames at several discrete latencies (that is, show maps restricted to exactly one selected time point, such as 120, 158, or 400 ms), data were averaged within these time window blocks and displayed as such to provide a more complete representation of total brain activity over time, and one less prone to frame selection biases. dSPMs were produced using only trials with correct task responses, reflecting cortical activity only during the successful evocation of semantic representations in every participant.

In order to more directly reveal how the dynamic patterns of cortical activity in SLI-1 and Sib-1 probabilistically compare with that of control subjects, and to avoid relying solely on qualitative evaluations of thresholded dSPM images, we also computed *z*-statistic maps showing the degree of similarity and dissimilarity in activity amplitude estimates at all cortical locations and all time points for both SLI-1 and Sib-1 in relation to the distribution of cortical activity for the comparison group, expressed in standard deviation (SD) units.

RESULTS

BEHAVIOR

During MEG recording, behavioral task accuracies were similar between the two siblings for both word (SLI-1 = 68%; Sib-1 = 69%) and picture stimuli (SLI-1 = 83%; Sib-1 = 80%). Out of 160 total words, SLI-1 responded accurately to 109 items, and SIB-1 110. For pictures, SLI-1 responded correctly to 133 stimuli, and SIB-1 128 items. Response times (RTs) were somewhat slower for SLI-1 for both words [SLI-1 = 1044 ms (mean)/438 (SD); Sib-1 = 915/548] and pictures (SLI-1 = 877/269; Sib-1 = 766/302).

On average, typically developing subjects performed more accurately and faster than the siblings for both words (89/6%, range = 77–96; RT = 820/146, range = 590–1063) and pictures (87/7%, range = 75–96; RT = 757/125, range = 582–957). Out of 160 words total, the control group responded correctly on average to 142 items and ranged across individuals from 123 items correct to 154. For picture stimuli, the mean number of items correct for the control group was 139 out of 160, with a range from 120 correct trials to 154. Therefore, for word stimuli, both of the siblings performed with lower accuracy than the lowest performing control subject. For pictures, however, they both outperformed the lowest scoring control participant. As indicated by the RT ranges, both SLI-1 and Sib-1 responded, on average, faster for both words and pictures than the slowest typically developing control subject.

IMAGING

Noise-normalized dSPMs for the typically developing control group were strongly consistent with the results of previous aMEG and fMRI studies of the semantic processing of words and pictures (Dale et al., 2000; Dale and Halgren, 2001; Martin and Chao, 2001; Marinkovic et al., 2003; Vigneau et al., 2006; Leonard et al., 2010, 2011; Binder and Desai, 2011). During the processing of words, early lateral visual responses occurred between 120 and 170 ms in bilateral occipitotemporal regions and were stronger on the left (**Figure 1**). Within 50 ms, activity spread across multiple regions bilaterally, including intraparietal and transverse occipital sulci, lateral occipitotemporal and temporal cortex, and anteriorly along perisylvian regions. By 300 ms, cortical activity became more strongly left lateralized and included left frontal operculum after about 400 ms. Qualitatively, Sib-1 showed a dynamic functional brain organization for processing words that was similar to the typically developing group. Her earliest lateral visual response occurred during 120–170 ms and was located in left

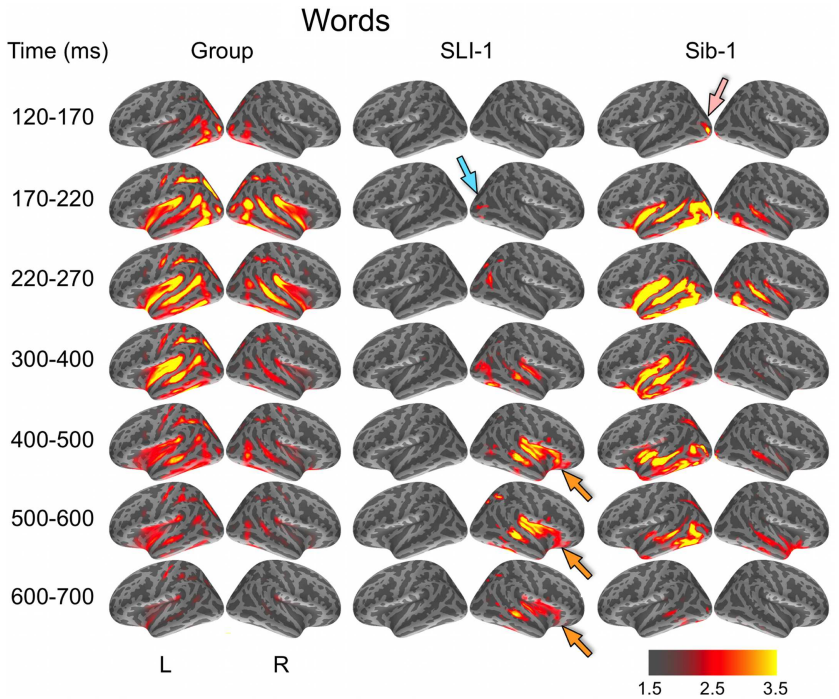

FIGURE 1 | Group and single-subject dSPMs of mean cortical activity during the semantic processing of words. In comparison to the functional organization of both the control group and sibling, SLI-1 showed strongly right-lateralized activity, from early sensoriperceptual to later cognitive stages. His early lateral occipital response was on the opposite side and somewhat delayed in time (blue arrow) in relation to his sister (pink arrow). During latencies typically associated with semantic encoding, he showed sustained activity within right temporal, perisylvian, and frontal opercular regions (orange arrows). Color scale represents square root of *F* values, which are a measure of signal-to-noise.

middle occipital sulcus (pink arrow). Activity then spread bilaterally and anteriorly along occipitotemporal and perisylvian regions and, similar to the group, became more strongly left lateralized at 300 ms. Sustained left lateralized activity was apparent through 600 ms and at 500 ms included bilateral anterior insula and temporal poles.

In striking contrast to both the comparison group and to his younger sister, SLI-1 showed no cortical activity within the left hemisphere that surpassed the same threshold during the semantic processing of words. In general, his functional neuroanatomy was notable for being strongly right-lateralized, less distributed, and somewhat delayed in time. In contrast to the other subjects, the first discernable lateral visual response for SLI-1 occurred at 170–220 ms and was located within the right hemisphere (blue arrow). Activity then spread anteriorly more slowly and only on the right, engaging middle temporal, and right perisylvian regions only by about 300 ms. From 400 to 700 ms, SLI-1 showed sustained activity within right middle temporal, perisylvian, and frontal opercular areas (orange arrows).

During the evocation of semantic representations by picture stimuli, typically developing subjects showed spatiotemporal activity patterns that varied from word stimuli in ways consistent with previous aMEG studies. In general, neural activity was less strongly left lateralized, including early lateral visual responses within posterior occipitotemporal regions as well as later, from 300 to 600 ms (**Figure 2**). As with word processing, the dynamic functional organization shown by Sib-1 for pictures was similar to that of the comparison group, although qualitatively more strongly left lateralized. Her earliest lateral visual response was likewise apparent within the 120- to 170-ms time window, but only within middle and inferior occipital sulci on the left (pink arrow). Activity then spread anteriorly along left occipitotemporal and perisylvian regions and was weaker on the right than for the typically developing controls. From 300 to 500 ms, activity for Sib-1 was somewhat more bilaterally evident for pictures than it was for words. Overall, her engagement of cortical areas during the presentation of pictures declined earlier than for words, especially within left anterior temporal and insular regions.

Just as for word stimuli, SLI-1 showed a functional neuroanatomy during the evocation of object concepts by pictures that were very different from both his sister and the comparison group. Again, his spatiotemporal patterns of activity were most notable for being strongly right-lateralized and somewhat delayed in time. Similar to words, picture stimuli evoked an early lateral visual response at 170–220 ms within right anterior occipital sulcus (blue arrow). Activity then spread first throughout proximal right occipital areas then involved right posterior perisylvian regions weakly. From 400 to 600 ms, SLI-1 showed sustained activity within right perisylvian and frontal opercular regions similar to (but weaker than) that observed during his semantic processing of words (orange arrows).

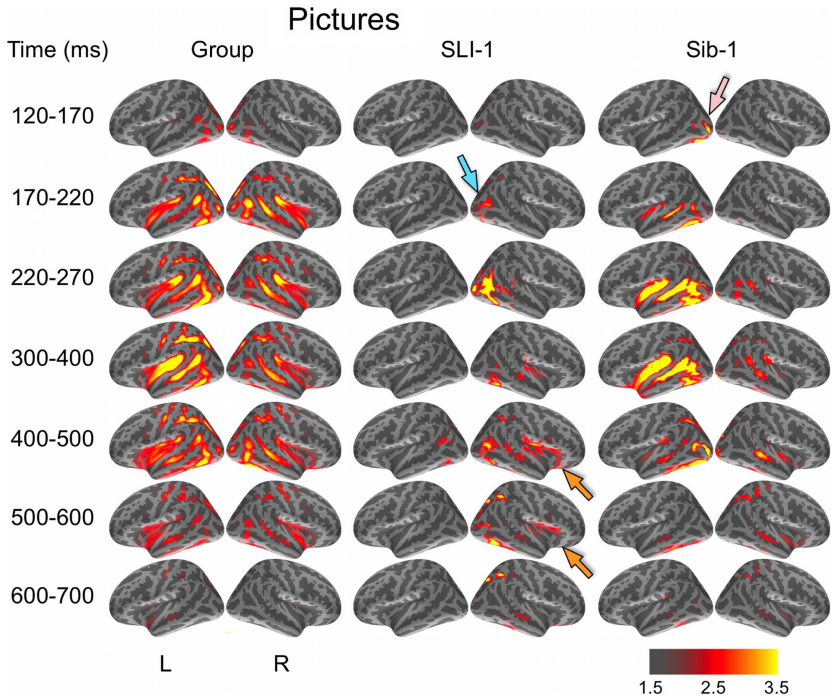

FIGURE 2 | Group and single-subject dSPMs of mean cortical activity during the semantic processing of pictures. In comparison to the functional organization of both the control group and sibling, SLI-1 showed strongly right-lateralized activity, from early sensoriperceptual to later cognitive stages. Similar to word processing, his early lateral occipital response was on the opposite side and somewhat delayed in time (blue arrow) in relation to his sister (pink arrow). During latencies typically associated with semantic encoding, he showed activity within right temporal, perisylvian, and frontal opercular regions (orange arrows), although weaker than for words. Color scale represents square root of *F* values, which are a measure of signal-to-noise.

In a direct, vertex-wise comparison to the distribution of neural activity at all cortical locations and time points within the typically developing group using *z*-scores, SLI-1 showed differences from the typical dynamic functional organization that agreed with qualitative comparisons of the dSPMs. During the semantic processing of words, SLI-1 showed relative under-recruitment of many cortical regions bilaterally at early latencies, including perisylvian, anterior temporal, opercular, and lateral and superior frontal cortex (**Figure 3**). Beginning at 220 ms, he showed the strongest areas of relative under-engagement within left frontal opercular and anterior temporal regions, continuing to 400 ms. At the same time, he began to show notable relative over-recruitment of regions within the right occipital cortex (green arrow), which also extended to 400 ms. At 400 ms, SLI-1 showed greater activity than typically developing controls in several right hemisphere perisylvian cortical areas extending from subcentral sulcus to right frontal operculum. These regions showed sustained relative over-activity that continued from 500 to 700 ms (yellow arrows), where additional right hemisphere temporal and parietal over-activity also became apparent. When picture stimuli were used to evoke object representations, SLI-1 showed only relative under-activation within the left hemisphere and over-activation only within the right hemisphere. Just as for words, he showed early over-recruitment of right middle and inferior occipital regions beginning at 220 ms (green arrows). From 500 to 700 ms, he showed late over-recruitment of right frontal regions similar to those for words (yellow arrows) and also over-recruitment of parietal, occipital, and temporal areas.

At the earliest latencies, the *z*-maps for Sib-1 revealed relative under-engagement of many bilateral anterior regions during word and picture processing that was similar to her brother. Interestingly, however, she showed notable relative over-recruitment of the left temporal pole in relation to the control group, which was consistently at 300–400 ms for both stimulus types (violet arrows). At late semantic processing stages, several cortical regions within right frontal and parietal, bilateral temporal, and left occipitotemporal cortex, showed greater levels of activity than the comparison group for pictures and words.

DISCUSSION

The primary purpose of our study was to test the feasibility and usefulness of anatomically constrained MEG for making direct comparisons between individual patients and typically developing control subjects in the dynamic functional organization of the brain. Using this multimodal functional neuroimaging technique, which provides the uncommon ability to localize cortical activity with millisecond temporal resolution, our findings revealed in an individual patient with a history of developmental language disorder an atypical right hemisphere specialization for the semantic representation of concrete entities.

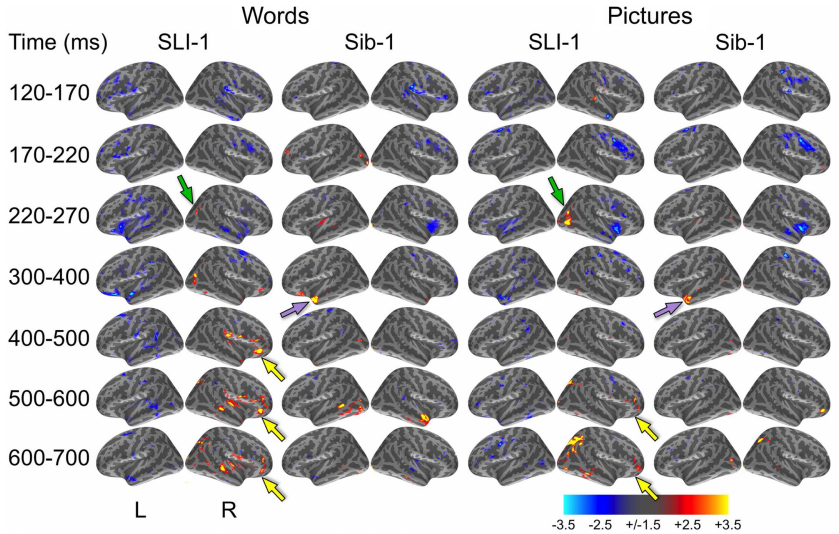

FIGURE 3 | *z*-Statistic maps of single-subject cortical activity in relation to the typically developing control group during the semantic processing of words and pictures. In direct comparison to the control group, SLI-1 showed relative under-activation of many left hemisphere regions and over-activation of only right hemisphere regions. This included early over-recruitment of right lateral occipital cortex for both words and pictures (green arrows), as well as later over-recruitment of right frontal opercular regions during semantic latencies (yellow arrows). Compared to controls, Sib-1 showed early under-engagement of right anterior regions for words and pictures, consistent over-engagement of left temporal pole 300–400 ms (violet arrows), and over-recruitment of several left and right areas at the latest time windows. Color scale represents *z*-statistics (standard deviation units).

Several aspects of our study support this interpretation. Using single-subject statistical maps, this patient showed strongly right-lateralized brain responses during the successful performance of a task that requires the evocation of semantic representations of visual objects when no spoken verbal response was required. Strong engagement of right hemisphere perisylvian regions was observed even during middle and late latencies typically associated with semantic encoding processes. His marked right hemisphere predominance was evident from early sensoriperceptual through later cognitive processing stages and was utilized for the semantic processing of both word and picture stimuli. During performance of the same tasks, typically developing control subjects, in contrast, showed bilateral involvement at early latencies followed by activity predominantly within the left hemisphere, especially during the processing of words. This is strongly consistent with the topography and timing from previous aMEG and fMRI studies of the semantic processing of pictures and words. As an additional control comparison for our single-subject analysis methods, the dynamic functional brain organization of a younger sibling with normal language development was found to be largely similar to the control group. Vertex-wise direct comparison of the patient and sibling to the distribution of cortical activity at every location and time point shown by the control group verified differences revealed by the comparison of independent brain activity maps.

Altogether, the functional neuroanatomical differences for this individual suggest a supramodal neural system for object concepts that appears similar to the left lateralized organization previously observed within association cortex in typically developing adults (Marinkovic et al., 2003), except that it is supported by the right hemisphere and appears to be engaged somewhat later in time. In bypassing reliance on auditory input, avoiding speech-motor demands, recording overt behavioral responses, mapping only successful trials, and localizing brain activity with millisecond temporal resolution, our interpretation of the functional organization can be more convincingly constrained to operations that involve semantic encoding and object representations. In contrast with traditional approaches testing cerebral functional specialization using naming, our findings were obtained without requiring speech-motor production components of language processing.

Language is made possible by a complex set of processing operations involving distributed mechanisms within the brain. Perhaps because of this, its development is surprisingly robust in the face of adverse neurological circumstances, such as early stroke, head trauma, and even hemispherectomy (Muller et al., 1998; Vicari et al., 2000; Bates et al., 2001; Fair et al., 2006; Liegeois et al., 2008; Trauner et al., 2013). This strongly suggests that there are multiple pathways to effective language learning and that the brain finds a detour when one pathway is blocked. Children who receive a clinical diagnosis of SLI, however, tend not to have a single problem cognitive area and instead display multiple underlying deficits (Bishop, 2006). By selectively probing object representations within only one patient, we hoped to learn something about the functional brain organization that might not be apparent from a group-averaged imaging study where patient heterogeneity in functional organization might produce equivocal results. Interestingly, we found strongly right-lateralized cortical responses within the very first individual with SLI we have tested.

Although these results strongly suggest an atypical functional brain organization for semantic processing, our study is limited

in providing leverage to make inferences about several important etiological factors. Theories of abnormal right hemisphere involvement in developmental language disorders have existed for decades and emphasize atypical cerebral dominance for the motor control of speech and limb praxis (Zangwill, 1960; Satz, 1972; Geschwind and Galaburda, 1985). So, tasks used to test language lateralization typically employ an overt verbal production component such as spoken naming. However, even among left-handers such as SLI-1, who represent only about 10% of the world's population (Hardyck and Petrinovich, 1977), estimates of right hemisphere language dominance are thought to be relatively rare, ranging between about 7 and 27% even when mixed/bilateral dominance is included (Rasmussen and Milner, 1977; Knecht et al., 2000; Drane et al., 2012). This means that only somewhere between 0.7 and 2.7% of the general population would be estimated to show right hemisphere or bilateral language dominance for spoken naming, the task commonly used in these studies. The fact that the large majority of left-handed individuals still seem to have left-dominant language representation suggests that it is common for dominant limb motor control to be decoupled from (i.e., contralateral to) dominant language representation.

The implications for the lateralization of the motor control of speech specifically, which is thought to follow lateralization for handedness, are unclear from available evidence. When language lateralization is probed using hemispheric anesthetization (i.e., the Wada procedure), are object concepts consistently represented within the hemisphere predominantly responsible for verbal motor control and speech production? Put another way, is a patient's inability to name objects in these experiments driven solely by arrest of the verbal articulators, by an inability to access the semantic representations required for naming, or by both? By disentangling these functions within an individual patient with a language learning disorder, we hoped to identify specifically whether object concepts themselves might be functionally organized in an atypical fashion, independent of verbal production demands. Perhaps some forms of developmental language learning disorder are caused by a mismatch between which hemisphere is dominant for speech-motor control and which specializes for the semantic encoding of object concepts and word meanings, causing access difficulties during language production. Although SLI-1 is strongly left-handed, this could be the case for his verbal praxis and will need to be tested further.

Our findings with SLI-1 are consistent with a number of cognitive developmental interpretations and models of hemispheric specialization, including possibly "weaker" semantic representations and the coarse encoding hypothesis (Beeman et al., 1994; Borovsky et al., 2013). His spontaneous task performance level, which provides one objective measure of the strength or accessibility of these semantic representations, might suggest that SLI-1's representations are no weaker than those of his sister, who performed similarly and nevertheless did not show strongly right-lateralized activity. Within the context of his clinical profile and developmental history, however, the present findings certainly suggest that his atypical functional brain organization is a contributor to and/or a product of his difficulties with language learning.

Interestingly, both SLI-1 and Sib-1 showed regions of sustained relative underactivity as compared to the control group during the processing of both words and pictures. This under-recruitment was most prominent at early latencies, from stimulus onset until about 270 ms, and included perisylvian regions, particularly on the right for Sib-1. These effects may relate to speed of processing differences between these two individuals and the control group. Although both SLI-1 and Sib-1 responded, on average, faster for both words and pictures than the slowest typically developing control subject, their behavioral RTs were nevertheless slower than the average of the comparison group. SLI-1 responded on average 224 ms slower than the average of controls while processing words and 120 ms slower for pictures. Sib-1's average behavioral response was 95 ms slower than the control average for words but only 9 ms slower than that for control participants for pictures, suggesting that these early decrements in activity within the right hemisphere cannot be solely accounted for by slower task performance.

Several additional substantive issues and limitations with our study warrant further discussion. First, our group of control participants differed from one or both of the other individuals along two relevant characteristics: age and handedness. Because of this, we do not attempt to make any strong inferences about either the specific role of handedness in our findings or about the developmental state or phase of the individual subjects. Since this experiment employed a relatively untested collection of techniques as applied to single patients, we began by comparing SLI-1 to a group representative of typically developing adolescents and young adults comprised of right-handed individuals. Indeed, it would be interesting and informative to compare SLI-1 in the same way to an individual or group showing otherwise cognitively normal left-handedness. Such a comparison would be required to make inferences about the specific role of handedness in SLI-1's functional neuroanatomical differences. However, the scientific evidence would suggest, assuming a representative subject or sample of left-handed participants was obtained, that a direct comparison of SLI-1 with them might yield results similar to what we found in right-handers. Nevertheless, this is an empirical question that will require future experiments. The present study is only able to address the first-order question of how the dynamic functional brain organization for semantic processing in an individual with SLI differs from typically developing, right-handed controls.

Secondly, the range of ages for the control group was not ideal for making inferences about the two siblings in relation to age-matched peers, since the control group was somewhat older. The individual with SLI was 3.1 years younger than the control group average and 0.4 years younger than the youngest control subject. His sister (Sib-1) was 4.8 years younger than the control group average and 2.1 years younger than the youngest control subject. So, we attempt to make no inferences about either of these individuals in relation to the ages or developmental phase of the control group. Instead, we have characterized brain activity in each participant both independently of the other participants and in direct relation to the distribution of brain activity from the same control group. So, their z-stat maps show levels of activity relative to the same distribution, making them a useful comparison with one another despite their age difference. Additionally, since SLI-1 is older than Sib-1, this comparison provides evidence that SLI-1's atypical functional organization cannot be solely attributed to

being somewhat younger than the control sample. If this were true, his even younger sibling should show the same pattern.

That being said, available evidence from large-scale functional neuroimaging studies suggests that data from one 16- or 17-year-old participant would not be developmentally detectably different from that of individuals 18- to 23-years-old, because the developmental signal at these ages will be overpowered by the vast range of differences across individuals, even of the same age. From early school age into young adulthood, the range of individual differences variability in brain activity measures at a given age far exceeds the range of developmental changes that occur on average across even several years of development (Brown et al., 2005; Dosenbach et al., 2010). These studies, as well as positron emission tomography (PET) measurements of cerebral glucose metabolic rates (Chugani et al., 1987; Chugani and Phelps, 1991), also show that the slope of annualized developmental changes in activity decreases from late grade school age into adolescence and young adulthood, asymptoting during the ages studied here. This has been shown to be similar for many anatomical brain features as well, including morphological, diffusion, and signal intensity measures (Giedd et al., 1999; Sowell et al., 2003; Brown et al., 2012). Our data collected from Sib-1 demonstrate this point. Despite being about 2 years younger than the youngest control subject and about 5 years younger than the average age of the control group, the cortical regions that she engages during semantic processing show activity levels that fall predominantly within a similar dynamic range. Nevertheless, the specific ages of the control comparison group will become eminently more consequential when one seeks to make specific *maturational* or *developmental* inferences about the brain activity measures of one individual.

In light of our atypical findings for SLI-1, the data from the younger sibling become an especially useful comparison. Using methods identical to those applied with the language impaired adolescent, including use of the same statistical thresholds, both kinds of maps computed for Sib-1 (i.e., independent thresholded dSPMs and z-maps relative to the distributions of brain activity from the control group) revealed a functional brain organization that is largely similar to the control group. This provides evidence that the anomalous nature of the results found with SLI-1 cannot be explained simply by the single-subject analytic approach. The patterns of brain activity in a younger, language-typical individual – even from the same family – show a more typical functional organization for the same tasks.

Fortuitously, the siblings performed similarly on both types of cognitive tasks during MEG recording. This strengthens the confidence with which we can fairly compare their observed cortical functional organizations. Specifically, it further suggests that SLI-1's strongly rightward organization is not due solely to the fact that he was performing more poorly than the control group on average. If this were the case, Sib-1 would have shown similar right-lateralized activity. This point is important in light of recent MEG studies that have shown that right hemisphere participation in semantic decision tasks may increase with greater task difficulty in adults (Donnelly et al., 2011) or with objects that are never-before-seen and for which the names are newly encoded in children (Urbain et al., 2013). Interestingly, a very similar experimental paradigm using novel objects and names with adults showed instead that learning the names of new objects utilizes a cortical network very similar to the set of regions used for naming familiar items (Cornelissen et al., 2004). Important to note for all of these studies, left hemisphere activity was prominent despite relative increases in right hemisphere involvement. This progression from strong bilateral to reduced right hemisphere involvement during word learning is consistent with findings from studies of normal developmental changes in lexical semantic processing using both fMRI (Schlaggar et al., 2002; Brown et al., 2005; Szaflarski et al., 2006) and MEG (Ressel et al., 2008), as well as for second-language word learning in bilingual adults (Leonard et al., 2010, 2011).

More broadly, our results demonstrate the feasibility and potential utility of using aMEG to characterize individual differences in the cortical activity dynamics associated with specific cognitive functions. Scientifically and clinically, there are many reasons for developing improved functional neuroimaging methods to characterize single patients, not the least of which is to inform diagnostic assessment and individualized treatment planning. However, there have been technical, methodological, and conceptual barriers commonly encountered, such as weak signal-to-noise characteristics of the brain activity measures taken from only one patient, as well as the limited statistical approaches that can be adopted for making probabilistic comparisons and hypothesis tests based on data from a single-subject. Here, we used a whole-brain z-statistic technique that has been employed previously in case studies with fMRI data (Turkeltaub et al., 2004; Fair et al., 2006), which has the benefit of being conceptually straightforward but remains statistically descriptive.

Further development of multimodal functional neuroimaging approaches for single patients, such as with aMEG, will be crucial for providing a better understanding of the specific subcomponents underlying atypical brain-cognition-behavior linkages. Future aMEG experiments with both healthy and clinical subjects should focus on a more nuanced relation of the temporal dynamics of the functional brain organization to specific information processing operations, moving away from simple dichotomies involving broad psychological constructs such as left versus right "language dominance." Further, much work is needed in characterizing how this dynamic functional mosaic changes across different ages. We believe that more research into these kinds of distinctions will help refine our understanding of the role of hemispheric specialization in developmental language disorders and how sensoriperceptual processes, motor control, and semantic representations come together to support human language. This will undoubtedly aid in the early detection of developmental cognitive disorders, biologically inform our clinical diagnostic schemes, and improve our ability to individually tailor treatments.

AUTHOR CONTRIBUTIONS

Timothy T. Brown and Eric Halgren designed the experiment. Eric Halgren and Anders M. Dale developed the multimodal imaging methods. Timothy T. Brown, Matthew Erhart, and Daniel Avesar collected the MEG and MRI data, and Julia L. Evans collected and interpreted the behavioral data and performed the clinical diagnosis. Timothy T. Brown, Matthew Erhart, and Daniel Avesar

processed and analyzed the imaging data. Timothy T. Brown wrote and edited the manuscript with input from the other authors.

ACKNOWLEDGMENTS

The authors gratefully thank the volunteer research subjects and parents who participated in this study. This study was funded in part by support from an Innovative Research Award from the Kavli Institute for Brain and Mind (Timothy T. Brown, Eric Halgren), by the National Institute of Neurological Disorders and Stroke (P50 NS022343; Timothy T. Brown, Eric Halgren, Anders M. Dale), and by the National Institute On Deafness and Other Communication Disorders (R01 DC005650; Julia L. Evans).

REFERENCES

Badcock, N. A., Bishop, D. V., Hardiman, M. J., Barry, J. G., and Watkins, K. E. (2012). Co-localisation of abnormal brain structure and function in specific language impairment. *Brain Lang.* 120, 310–320. doi:10.1016/j.bandl.2011.10.006

Bates, E., Reilly, J., Wulfeck, B., Dronkers, N., and Opie, M. (2001). Differential effects of unilateral lesions on language production in children and adults. *Brain Lang.* 79, 223–265. doi:10.1006/brln.2001.2482

Beeman, M., Friedman, R. B., Grafman, J., Perez, E., Diamond, S., and Lindsay, M. B. (1994). Summation priming and coarse semantic coding in the right hemisphere. *J. Cogn. Neurosci.* 6, 26–45. doi:10.1162/jocn.1994.6.1.26

Binder, J. R., and Desai, R. H. (2011). The neurobiology of semantic memory. *Trends Cogn. Sci. (Regul. Ed.)* 15, 527–536. doi:10.1016/j.tics.2011.10.001

Bishop, D. V. (2006). What causes specific language impairment in children? *Curr. Dir. Psychol. Sci.* 15, 217–221. doi:10.1111/j.1467-8721.2006.00439.x

Borovsky, A., Kutas, M., and Elman, J. L. (2013). Getting it right: word learning across the hemispheres. *Neuropsychologia* 51, 825–837. doi:10.1016/j.neuropsychologia.2013.01.027

Brown, T. T., Kuperman, J. M., Chung, Y., Erhart, M., McCabe, C., Hagler, D. J. Jr., et al. (2012). Neuroanatomical assessment of biological maturity. *Curr. Biol.* 22, 1–6. doi:10.1016/j.cub.2012.07.002

Brown, T. T., Kuperman, J. M., Erhart, M., White, N. S., Roddey, J. C., Shankaranarayanan, A., et al. (2010). Prospective motion correction of high-resolution magnetic resonance imaging data in children. *Neuroimage* 53, 139–145. doi:10.1016/j.neuroimage.2010.06.017

Brown, T. T., Lugar, H. M., Coalson, R. S., Miezin, F. M., Petersen, S. E., and Schlaggar, B. L. (2005). Developmental changes in human cerebral functional organization for word generation. *Cereb. Cortex* 15, 275–290. doi:10.1093/cercor/bhh129

Brown, T. T., Petersen, S. E., and Schlaggar, B. L. (2003). Functional neuroimaging approaches to the study of human brain development. *Perspect. Neurophysiol. Neurogenic Speech Lang. Disord.* 13, 3–10. doi:10.1044/nnsld13.2.3

Brown, T. T., Petersen, S. E., and Schlaggar, B. L. (2006). Does human functional brain organization shift from diffuse to focal with development? *Dev. Sci.* 9, 9–11. doi:10.1111/j.1467-7687.2005.00455.x

Carrow-Woolfolk, E. (1999). *Comprehensive Assessment of Spoken Language.* Circle Pines, MN: American Guidance Services.

Chugani, H. T., and Phelps, M. E. (1991). Imaging human brain development with positron emission tomography. *J. Nucl. Med.* 32, 23–26.

Chugani, H. T., Phelps, M. E., and Mazziotta, J. C. (1987). Positron emission tomography study of human brain functional development. *Ann. Neurol.* 22, 487–497. doi:10.1002/ana.410220408

Cohen, M. X. (2011). It's about time. *Front. Hum. Neurosci.* 5:2. doi:10.3389/fnhum.2011.00002

Cornelissen, K., Laine, M., Renvall, K., Saarinen, T., Martin, N., and Salmelin, R. (2004). Learning new names for new objects: cortical effects as measured by magnetoencephalography. *Brain Lang.* 89, 617–622. doi:10.1016/j.bandl.2003.12.007

Dale, A. M., Fischl, B., and Sereno, M. I. (1999). Cortical surface-based analysis. I. Segmentation and surface reconstruction. *Neuroimage* 9, 179–194. doi:10.1006/nimg.1998.0395

Dale, A. M., and Halgren, E. (2001). Spatiotemporal mapping of brain activity by integration of multiple imaging modalities. *Curr. Opin. Neurobiol.* 11, 202–208. doi:10.1016/S0959-4388(00)00197-5

Dale, A. M., Liu, A. K., Fischl, B. R., Buckner, R. L., Belliveau, J. W., Lewine, J. D., et al. (2000). Dynamic statistical parametric mapping: combining fMRI and MEG for high-resolution imaging of cortical activity. *Neuron* 26, 55–67. doi:10.1016/S0896-6273(00)81138-1

De Fossé, L., Hodge, S. M., Makris, N., Kennedy, D. N., Caviness, V. S. Jr., McGrath, L., et al. (2004). Language-association cortex asymmetry in autism and specific language impairment. *Ann. Neurol.* 56, 757–766. doi:10.1002/ana.20275

Dibbets, P., Bakker, K., and Jolles, J. (2006). Functional MRI of task switching in children with specific language impairment (SLI). *Neurocase* 12, 71–79. doi:10.1080/13554790500507032

Donnelly, K. M., Allendorfer, J. B., and Szaflarski, J. P. (2011). Right hemispheric participation in semantic decision improves performance. *Brain Res.* 1419, 105–116. doi:10.1016/j.brainres.2011.08.065

Dosenbach, N. U., Nardos, B., Cohen, A. L., Fair, D. A., Power, J. D., Church, J. A., et al. (2010). Prediction of individual brain maturity using fMRI. *Science* 329, 1358–1361. doi:10.1126/science.1194144

Drane, D. L., Roraback-Carson, J., Hebb, A. O., Hersonskey, T., Lucas, T., Ojemann, G. A., et al. (2012). Cortical stimulation mapping and Wada results demonstrate a normal variant of right hemisphere language organization. *Epilepsia* 53, 1790–1798. doi:10.1111/j.1528-1167.2012.03573.x

Ellis Weismer, S., Plante, E., Jones, M., and Tomblin, J. B. (2005). A functional magnetic resonance imaging investigation of verbal working memory in adolescents with specific language impairment. *J. Speech Lang. Hear. Res.* 48, 405–425. doi:10.1044/1092-4388(2005/028)

Fair, D. A., Brown, T. T., Petersen, S. E., and Schlaggar, B. L. (2006). fMRI reveals novel functional neuroanatomy in a child with perinatal stroke. *Neurology* 67, 2246–2249. doi:10.1212/01.wnl.0000249348.84045.0e

Fischl, B., Dale, A. M., Sereno, M. I., Tootell, R. B., and Rosen, B. R. (1998). A coordinate system for the cortical surface. *Neuroimage* 7, S740.

Fischl, B., Sereno, M. I., and Dale, A. (1999a). Cortical surface-based analysis. II: inflation, flattening, and a surface-based coordinate system. *Neuroimage* 9, 195–207. doi:10.1006/nimg.1998.0396

Fischl, B., Sereno, M. I., Tootell, R. B., and Dale, A. M. (1999b). High-resolution intersubject averaging and a coordinate system for the cortical surface. *Hum. Brain Mapp.* 8, 272–284. doi:10.1002/(SICI)1097-0193(1999)8:4<272::AID-HBM10>3.0.CO;2-4

Gauger, L. M., Lombardino, L. J., and Leonard, C. M. (1997). Brain morphology in children with specific language impairment. *J. Speech Lang. Hear. Res.* 40, 1272–1284.

Geschwind, N., and Galaburda, A. M. (1985). Cerebral lateralization. Biological mechanisms, associations, and pathology: III. A hypothesis and a program for research. *Arch. Neurol.* 42, 634–654. doi:10.1001/archneur.1985.04060060019009

Giedd, J. N., Blumenthal, J., Jeffries, N. O., Castellanos, F. X., Liu, H., Zijdenbos, A., et al. (1999). Brain development during childhood and adolescence: a longitudinal MRI study. *Nat. Neurosci.* 2, 861–863. doi:10.1038/13158

Hardyck, C., and Petrinovich, L. F. (1977). Left-handedness. *Psychol. Bull.* 84, 385–404. doi:10.1037/0033-2909.84.3.385

Herbert, M. R., Ziegler, D. A., Deutsch, C. K., O'Brien, L. M., Kennedy, D. N., Filipek, P. A., et al. (2005). Brain asymmetries in autism and developmental language disorder: a nested whole-brain analysis. *Brain* 128, 213–226. doi:10.1093/brain/awh330

Hugdahl, K., Gundersen, H., Brekke, C., Thomsen, T., Rimol, L. M., Ersland, L., et al. (2004). FMRI brain activation in a Finnish family with specific language impairment compared with a normal control group. *J. Speech Lang. Hear. Res.* 47, 162–172. doi:10.1044/1092-4388(2004/014)

Jernigan, T. L., Hesselink, J. R., Sowell, E., and Tallal, P. A. (1991). Cerebral structure on magnetic resonance imaging in language- and learning-impaired children. *Arch. Neurol.* 48, 539–545. doi:10.1001/archneur.1991.00530170103028

Knecht, S., Drager, B., Deppe, M., Bobe, L., Lohmann, H., Floel, A., et al. (2000). Handedness and hemispheric language dominance in healthy humans. *Brain* 123, 2512–2518. doi:10.1093/brain/123.12.2512

Kuperman, J. M., Brown, T. T., Ahmadi, M. E., Erhart, M. J., White, N. S., Roddey, J. C., et al. (2011). Prospective motion correction improves diagnostic utility of pediatric MRI scans. *Pediatr. Radiol.* 41, 1578–1582. doi:10.1007/s00247-011-2205-1

Leonard, M. K., Brown, T. T., Travis, K. E., Gharapetian, L., Hagler, D. J. Jr., Dale, A. M., et al. (2010). Spatiotemporal dynamics of bilingual word processing. *Neuroimage* 49, 3286–3294. doi:10.1016/j.neuroimage.2009.12.009

Leonard, M. K., Torres, C., Travis, K. E., Brown, T. T., Hagler, D. J. Jr., Dale, A. M., et al. (2011). Language proficiency modulates the recruitment of non-classical

language areas in bilinguals. *PLoS ONE* 6:e18240. doi:10.1371/journal.pone.0018240

Liegeois, F., Connelly, A., Baldeweg, T., and Vargha-Khadem, F. (2008). Speaking with a single cerebral hemisphere: fMRI language organization after hemispherectomy in childhood. *Brain Lang.* 106, 195–203. doi:10.1016/j.bandl.2008.01.010

Marinkovic, K., Dhond, R. P., Dale, A. M., Glessner, M., Carr, V., and Halgren, E. (2003). Spatiotemporal dynamics of modality-specific and supramodal word processing. *Neuron* 38, 487–497. doi:10.1016/S0896-6273(03)00197-1

Martin, A. (1999). Automatic activation of the medial temporal lobe during encoding: lateralized influences of meaning and novelty. *Hippocampus* 9, 62–70. doi:10.1002/(SICI)1098-1063(1999)9:1<62::AID-HIPO7>3.0.CO;2-K

Martin, A., and Chao, L. L. (2001). Semantic memory and the brain: structure and processes. *Curr. Opin. Neurobiol.* 11, 194–201. doi:10.1016/S0959-4388(00)00196-3

Muller, R. A., Chugani, H. T., Muzik, O., and Mangner, T. J. (1998). Brain organization of motor and language functions following hemispherectomy: a [(15)O]-water positron emission tomography study. *J. Child Neurol.* 13, 16–22. doi:10.1177/088307389801300103

Murphy, K., and Garavan, H. (2004). Artifactual fMRI group and condition differences driven by performance confounds. *Neuroimage* 21, 219–228. doi:10.1016/j.neuroimage.2003.09.016

Oldfield, R. C. (1971). The assessment and analysis of handedness: the Edinburgh inventory. *Neuropsychologia* 9, 97–113. doi:10.1016/0028-3932(71)90067-4

Orton, S. T. (1925). "Word blindness" in school children. *Arch. Neurol. Psychiatry* 14, 581–615. doi:10.1001/archneurpsyc.1925.02200170002001

Palmer, E. D., Brown, T. T., Petersen, S. E., and Schlaggar, B. L. (2004). Investigation of the functional neuroanatomy of single word reading and its development. *Sci. Stud. Read.* 8, 203–223. doi:10.1207/s1532799xssr0803_2

Plante, E., Swisher, L., Vance, R., and Rapcsak, S. (1991). MRI findings in boys with specific language impairment. *Brain Lang.* 41, 52–66. doi:10.1016/0093-934X(91)90111-D

Poldrack, R. A. (2010). Interpreting developmental changes in neuroimaging signals. *Hum. Brain Mapp.* 31, 872–878. doi:10.1002/hbm.21039

Posner, M. I. (1978). *Chronometric Explorations of Mind.* Hillsdale, NJ: Erlbaum.

Posner, M. I. (2005). Timing the brain: mental chronometry as a tool in neuroscience. *PLoS Biol.* 3:e51. doi:10.1371/journal.pbio.0030051

Preis, S., Jancke, L., Schittler, P., Huang, Y., and Steinmetz, H. (1998). Normal intrasylvian anatomical asymmetry in children with developmental language disorder. *Neuropsychologia* 36, 849–855. doi:10.1016/S0028-3932(98)00033-5

Rasmussen, T., and Milner, B. (1977). The role of early left-brain injury in determining lateralization of cerebral speech functions. *Ann. N. Y. Acad. Sci.* 299, 355–369. doi:10.1111/j.1749-6632.1977.tb41921.x

Ressel, V., Wilke, M., Lidzba, K., Lutzenberger, W., and Krageloh-Mann, I. (2008). Increases in language lateralization in normal children as observed using magnetoencephalography. *Brain Lang.* 106, 167–176. doi:10.1016/j.bandl.2008.01.004

Roid, G. H., and Miller, L. J. (1997). *Leiter International Performance Scale-Revised.* Wood Dale, IL: Stoelting Co.

Satz, P. (1972). Pathological left-handedness: an explanatory model. *Cortex* 8, 121–135. doi:10.1016/S0010-9452(72)80013-3

Schlaggar, B. L., Brown, T. T., Lugar, H. M., Visscher, K. M., Miezin, F. M., and Petersen, S. E. (2002). Functional neuroanatomical differences between adults and school-age children in the processing of single words. *Science* 296, 1476–1479. doi:10.1126/science.1069464

Semel, E., Wiig, E. H., and Secord, W. A. (2003). *Clinical Evaluation of Language Fundamentals*, 4th Edn. San Antonio, TX: The Psychological Corporation.

Sowell, E. R., Peterson, B. S., Thompson, P. M., Welcome, S. E., Henkenius, A. L., and Toga, A. W. (2003). Mapping cortical change across the human life span. *Nat. Neurosci.* 6, 309–315. doi:10.1038/nn1008

Stark, R. E., Tallal, P., and McCauley, R. J. (1988). *Language, Speech and Reading Disorders in Children: Neuropsychological Studies.* Austin, TX: Pro-Ed.

Szaflarski, J. P., Schmithorst, V. J., Altaye, M., Byars, A. W., Ret, J., Plante, E., et al. (2006). A longitudinal functional magnetic resonance imaging study of language development in children 5 to 11 years old. *Ann. Neurol.* 59, 796–807. doi:10.1002/ana.20817

Trauner, D. A., Eshagh, K., Ballantyne, A. O., and Bates, E. (2013). Early language development after peri-natal stroke. *Brain Lang.* 127, 399–403. doi:10.1016/j.bandl.2013.04.006

Travis, K. E., Leonard, M. K., Brown, T. T., Hagler, D. J. Jr., Curran, M., Dale, A. M., et al. (2011). Spatiotemporal neural dynamics of word understanding in 12- to 18-month-old-infants. *Cereb. Cortex* 21, 1832–1839. doi:10.1093/cercor/bhq259

Turkeltaub, P. E., Flowers, D. L., Verbalis, A., Miranda, M., Gareau, L., and Eden, G. F. (2004). The neural basis of hyperlexic reading. An FMRI case study. *Neuron* 41, 11–25. doi:10.1016/S0896-6273(03)00803-1

Urbain, C., Bourguignon, M., Op de Beeck, M., Schmitz, R., Galer, S., Wens, V., et al. (2013). MEG correlates of learning novel objects properties in children. *PLoS ONE* 8:e69696. doi:10.1371/journal.pone.0069696

Vicari, S., Albertoni, A., Chilosi, A. M., Cipriani, P., Cioni, G., and Bates, E. (2000). Plasticity and reorganization during language development in children with early brain injury. *Cortex* 36, 31–46. doi:10.1016/S0010-9452(08)70834-7

Vigneau, M., Beaucousin, V., Herve, P. Y., Duffau, H., Crivello, F., Houde, O., et al. (2006). Meta-analyzing left hemisphere language areas: phonology, semantics, and sentence processing. *Neuroimage* 30, 1414–1432. doi:10.1016/j.neuroimage.2005.11.002

Wallace, G., and Hammill, D. D. (2002). *Comprehensive Receptive and Expressive Vocabulary Test*, 2nd Edn. Austin, TX: Pro-Ed.

White, N., Roddey, C., Shankaranarayanan, A., Han, E., Rettmann, D., Santos, J., et al. (2010). PROMO: real-time prospective motion correction in MRI using image-based tracking. *Magn. Reson. Med.* 63, 91–105. doi:10.1002/mrm.22176

Whitehouse, A. J., and Bishop, D. V. (2008). Cerebral dominance for language function in adults with specific language impairment or autism. *Brain* 131, 3193–3200. doi:10.1093/brain/awn266

Zangwill, O. L. (1960). *Cerebral Dominance and Its Relation to Psychological Function.* Springfield, IL: C. C. Thomas.

Conflict of Interest Statement: Anders M. Dale and Eric Halgren are founders of and hold equity interest in Cortechs Labs, La Jolla, CA, USA and serve on its scientific advisory board. The terms of this arrangement have been reviewed and approved by UCSD in accordance with its conflict of interest policies. The other co-authors declare that the research was conducted in the absence of any commercial or financial relationships that could be construed as a potential conflict of interest.

Received: 02 October 2013; accepted: 03 February 2014; published online: 14 February 2014.

Citation: Brown TT, Erhart M, Avesar D, Dale AM, Halgren E and Evans JL (2014) Atypical right hemisphere specialization for object representations in an adolescent with specific language impairment. Front. Hum. Neurosci. ***8****:82. doi: 10.3389/fnhum.2014.00082*

This article was submitted to the journal Frontiers in Human Neuroscience.

frontiers in
HUMAN NEUROSCIENCE

HYPOTHESIS AND THEORY ARTICLE
published: 10 February 2014
doi: 10.3389/fnhum.2014.00062

Clinical application of spatiotemporal distributed source analysis in presurgical evaluation of epilepsy

Naoaki Tanaka* and Steven M. Stufflebeam

Athinoula A. Martinos Center for Biomedical Imaging, Massachusetts General Hospital, Charlestown, MA, USA

Edited by:
Christos Papadelis, Harvard Medical School, USA

Reviewed by:
Mohamad Zakaria Koubeissi, George Washington University, USA
Yosuke Kakisaka, Tohoku University, Japan

****Correspondence:***
Naoaki Tanaka, Athinoula A. Martinos Center for Biomedical Imaging, Massachusetts General Hospital, 149 Thirteenth Street, Suite 2301, Charlestown, MA 02129, USA
e-mail: naoro@nmr.mgh.harvard.edu

Magnetoencephalography (MEG), which acquires neuromagnetic fields in the brain, is a useful diagnostic tool in presurgical evaluation of epilepsy. Previous studies have shown that MEG affects the planning intracranial electroencephalography placement and correlates with surgical outcomes by using a single dipole model. Spatiotemporal source analysis using distributed source models is an advanced method for analyzing MEG, and has been recently introduced for analyzing epileptic spikes. It has advantages over the conventional single dipole analysis for obtaining accurate sources and understanding the propagation of epileptic spikes. In this article, we review the source analysis methods, describe the techniques of the distributed source analysis, interpretation of source distribution maps, and discuss the benefits and feasibility of this method in evaluation of epilepsy.

Keywords: magnetoencephalography, epilepsy, distributed source analysis, spike propagation, minimum norm estimate, epilepsy surgery

INTRODUCTION

Magnetoencephalography (MEG) is an important, non-invasive diagnostic tool, which acquires neuromagnetic fields generated in the brain with high spatial and temporal resolution. Clinical usefulness of MEG, especially in presurgical evaluation of epilepsy, is well documented in recent reviews (Stufflebeam et al., 2009; Stufflebeam, 2011). Currently, clinical applications of MEG are divided into two categories: (1) spontaneous brain activity analysis, including epileptic spike mapping, most often for determining an irritative zone, (2) mapping of eloquent cortex, such as primary motor cortex and language area for avoiding postsurgical functional deficits (Stufflebeam et al., 2009; Stufflebeam, 2011).

Source localization of MEG spikes is frequently performed in clinical practice for identifying an irritative zone (Otsubo and Snead, 2001; Chuang et al., 2006; Stufflebeam, 2011), providing spatial information of spike activities at the sensor level. Source analysis of MEG typically incorporates anatomical information derived from each individual's magnetic resonance imaging (MRI), and calculates the sources of neural activities by applying a certain mathematical model to the measured magnetic fields. These cortical and subcortical sources are visualized on the MRI or MRI-based anatomical atlas, and provide current dipole distribution maps.

Calculating intracranial sources from MEG obtained outside the brain, an example of the inverse problem, is mathematically non-unique and ill-posed. Certain assumptions are necessary for providing the proper source modeling. Thus, many procedures of source analysis have been proposed, such as single dipole, multi-dipole, and distributed source models, which are also applied for the source analysis of scalp electroencephalography (EEG) (for review, see Michel et al., 2004; Plummer et al., 2008).

In this article, we review the source analysis methods, describe the techniques of the distributed source analysis, and discuss the feasibility of this method in evaluation of epileptic spikes.

SINGLE EQUIVALENT CURRENT DIPOLE ANALYSIS

Single equivalent current dipole (ECD) analysis has been widely used for source localization of epileptic spikes for decades (Otsubo and Snead, 2001; Stefan et al., 2003; Fischer et al., 2005; Chuang et al., 2006). This model assumes that a single dipole source generates all the neuromagnetic fields recorded on the sensors, and is considered physiologically plausible when a limited area of the cortex is synchronously activated. In the analysis, the measured magnetic fields at a given latency are modeled by the best-fitting single dipole. ECDs are typically calculated by using a standard iterative least-square algorithm (Marquardt, 1963; Iwasaki et al., 2002), and several indicators of their reliability are also calculated, such as goodness of fit (GOF) and correlation coefficient. These indicators reflect the concordance between the magnetic fields calculated from the ECD and the actual measurement MEG data. The current dipole moment is represented by the magnitude of the ECD. These indicators and other metrics are used for selecting adequate sources and discarding inadequate ECDs by setting a threshold. Adequate ECDs are mapped on the patient's MRI, demonstrating the distribution of ECDs (**Figure 1**). Previous studies have validated ECD analysis in temporal lobe epilepsy (Baumgartner et al., 2000; Iwasaki et al., 2002; Assaf et al., 2004; Reinsberger et al., 2010) and frontal lobe epilepsy (Shiraishi et al., 2001; Genow et al., 2004; Ossenblok et al., 2007). Several studies have shown spatial concordance of ECD distribution and interictal spiking area on intracranial EEG (IEEG) (Mikuni et al., 1997; Oishi et al., 2002).

Although ECD analysis is well established procedure for localizing MEG spikes, a few issues remain. First, the criteria of selecting ECDs may vary from laboratory to laboratory. Single ECDs generally do not provide a GOF of 100%, i.e., 100% of measured magnetic fields can not be explained by a single ECD, due to the oversimplification of this model. Some studies accept ECDs with a GOF >80–90% or correlation coefficient >0.90

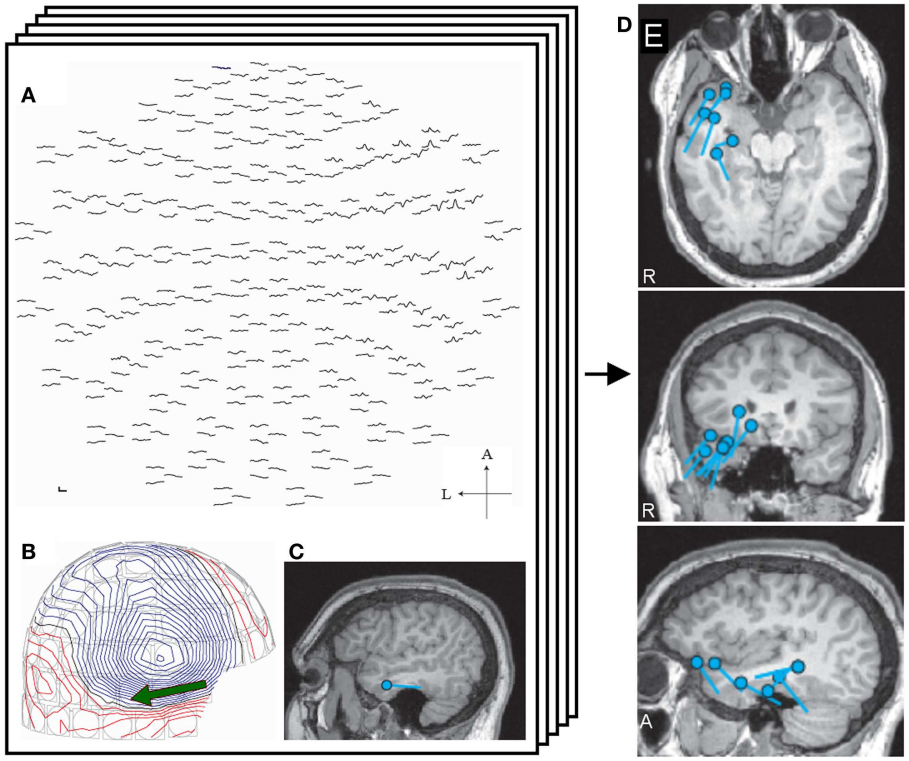

FIGURE 1 | Single equivalent dipole analysis. The full view map of the MEG sensor array shows a right temporal spike **(A)**. The contour map of magnetic fields at the peak demonstrates a dipole pattern in the right temporal area **(B)**. The equivalent current dipole (ECD) is projected on the patient's MRI and is located in the right temporal lobe **(C)**. ECDs obtained from different spikes are collected and mapped on the MRI, providing ECD distribution maps **(D)**.

(Iwasaki et al., 2002; Genow et al., 2004; Pataraia et al., 2004; Oishi et al., 2006; Knowlton et al., 2009), but other use lower thresholds (Shiraishi et al., 2005a,b, 2011; Reinsberger et al., 2010). The criteria dramatically affect the number of adequate ECDs (Tanaka et al., 2009a), although these thresholds are determined subjectively. Several researchers selected certain sensors for calculating ECDs to obtain adequate ECDs (Iwasaki et al., 2002; Pataraia et al., 2004). Such a process adds another assumption that spikes only appear in a group of restricted sensors. Second, the ECD analysis is sometimes inaccurate (Kobayashi et al., 2005) such as when the signal-to-noise ratio (SNR) is low and the spike is widespread (Shiraishi et al., 2005a; Hara et al., 2007). This may obscure the precise localization of early ictal discharges, which usually have a low SNR (Tanaka et al., 2009a). Third, the single ECD model does not always provide an accurate representation of the time course of the epileptiform discharge. When ECDs are sequentially calculated from the onset to the peak of spike, the SNR is low in the early latency. ECDs obtained from the spike onset may have low GOF values and thus an unstable localization (Kanamori et al., 2013). Several clinical studies calculate ECDs at the spike peak (Iwasaki et al., 2002; Oishi et al., 2006; Reinsberger et al., 2010; Jin et al., 2013) for obtaining a high SNR. However, spikes may be widespread or may propagate, and those ECDs may not accurately identify the onset of the discharge. Moreover, recent studies have proposed that epilepsy is a network disease caused by abnormal neural networks (for review, see Spencer, 2002). Spike propagation is required for understanding the abnormal networks (Tanaka et al., 2010), and advanced analysis procedure is necessary for understanding the spike propagation.

SPATIOTEMPORAL DISTRIBUTED SOURCE ANALYSIS

Distributed source models assume that a certain amount of cortical patches are simultaneously activated (Dale and Sereno, 1993; Hämäläinen and Ilmoniemi, 1994). This model calculates the source distribution by deploying numerous unit dipoles on the cortical surface. The source space is created by using a realistic head model, such as the boundary elemental model (Hämäläinen and Sarvas, 1989; Oostendorp and van Oosterom, 1989; Crouzeix et al., 1999; Fuchs et al., 2001), obtained by cortical surface reconstruction derived from MRI (Dale et al., 1999; Fischl et al., 1999). Theoretically, the source solution gives concordance between the simulated and measured magnetic fields by adjusting the strength and orientation of unit dipoles (Dale and Sereno, 1993; Hämäläinen and Ilmoniemi, 1994). The source distribution can be calculated at any time points of spike, and from which dynamic activation maps along with the time course can be created. Thus, the source distribution maps represent the cortical activation generated by the spikes both spatially and temporally. The distributed source analysis does not require an assumption on the number of dipoles and thresholds of likelihood parameters as used in the single dipole analysis. However, an infinite number of source distributions can generate a similar magnetic field

pattern, and further assumption, such as source distribution with minimum overall intensity (L2-norm), is necessary for determining the optimal solution. Thus, many types of analysis have been proposed based on different assumption and modeling, referred as minimum norm estimate (MNE) (Hämäläinen and Ilmoniemi, 1994), dynamic statistical parametric mapping (Dale et al., 2000), Laplacian weighted minimum norm (LORETA) (Pasqual-Marqui et al., 1994), local autoregressive average (LAURA), and EPIFOCUS (Grave de Peralta et al., 2001). Here, we use the MNE as an example of a distributed source solution.

MNE ANALYSIS IN PRACTICE

This section explains spike analysis with MNE software (www.mne.org), which mainly provides an MNE and dSPM solution algorithm.

MEG PREPROCESSING – SPIKE SELECTION AND CLEAN UP

The purpose of preprocessing is to obtain spike data from raw MEG with minimum artifacts. Both individual and averaged spikes can be analyzed by distributed source models. Note that each of these spikes provides identical series of source distribution maps. Visual inspection of spikes is widely performed while automated spike detection is also introduced (Ossadtchi et al., 2004). However, the MEG spike morphology has not been sufficiently described while EEG spikes were well documented in the literature (International Federation of Societies for Clinical Neurophysiology, 1974). A clinical guideline has recommended identifying the MEG spikes based on the principals established for EEG (Bagic et al., 2011). Clarification of MEG spikes will be useful for clinical application of MEG especially in patients with negative EEG findings. Spike selection is critical for obtaining appropriate averaged spikes and spike morphology must be considered.

Artifact reduction is also an important issue for calculating adequate sources of spikes. Exclusion of sensors (channels), which contain continuous artifacts, is helpful for avoiding inadequate affection on the source analysis. Independent component analysis may be useful for removing artifacts specific patterns (e.g., ECG) as used on EEG (Kobayashi et al., 2001). Taulu et al. (2004) (Taulu and Simola, 2006; Taulu and Hari, 2009) proposed signal source separation (SSS) and its temporal extension (tSSS). SSS decomposes MEG signals into two components, which are generated from sources inside and outside of the sensor space, and remove the latter component. The temporally extended SSS also considers temporal signal correlation and is widely used in clinical practice (Medvedovsky et al., 2009; Song et al., 2009; Tanaka et al., 2009b; Jin et al., 2013; Kakisaka et al., 2013) (**Figure 2**). Motion artifacts distort geographic information of the head and sensors, resulting in unreliable source localization. These movements can be compensated by tracking the head position during acquisition, and this technique is useful for analyzing ictal MEG data, where head deviation sometimes occur during seizures (Medvedovsky et al., 2007; Kakisaka et al., 2012).

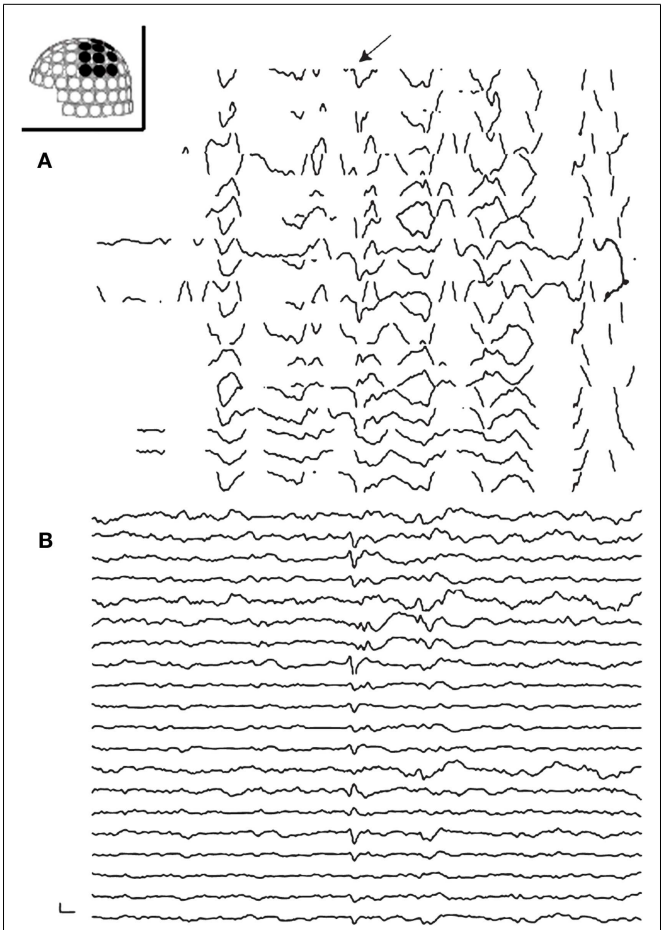

FIGURE 2 | Preprocessing of MEG with tSSS. Panels show MEG waveforms in the left centroparietal sensors recorded on a patient with vagus nerve stimulator (VNS). VNS artifacts contaminate the MEG data **(A)**. MEG processed with tSSS shows a prominent spike-and-wave complex **(B)**.

MRI PREPROCESSING – CREATING A HEAD MODEL

Minimum norm estimate constrains source activities to the cortical surface images. The cortical surface is reconstructed from anatomical T1 MRI data, and the reconstruction is the first step of MRI processing. Various software packages, such as Freesurfer (Dale et al., 1999; Fischl et al., 1999) and Brainstorm (Tadel et al., 2011), provide cortical surface reconstructions. The source space is created by using the cortical surface, deploying grid spacing with numerous cortical patches (Crouzeix et al., 1999; Fuchs et al., 2001). Unit current dipoles are distributed in the source space, and the boundary elemental method (BEM) creates a head model for calculating the activation of these dipoles (Hämäläinen and Sarvas, 1989; Oostendorp and van Oosterom, 1989; Crouzeix et al., 1999; Fuchs et al., 2001). A single-layer BEM model is generally used, since the neuromagnetic signals are not affected by the tissue conductivity (Hämäläinen and Sarvas, 1989).

Coregistration of the patient's MRI with the MEG sensor space is typically performed through the digitization information of the head and head position indicator that generates artificial electric currents in the sensor array. This process estimates the relationship between the source and the sensor spaces (**Figure 3**).

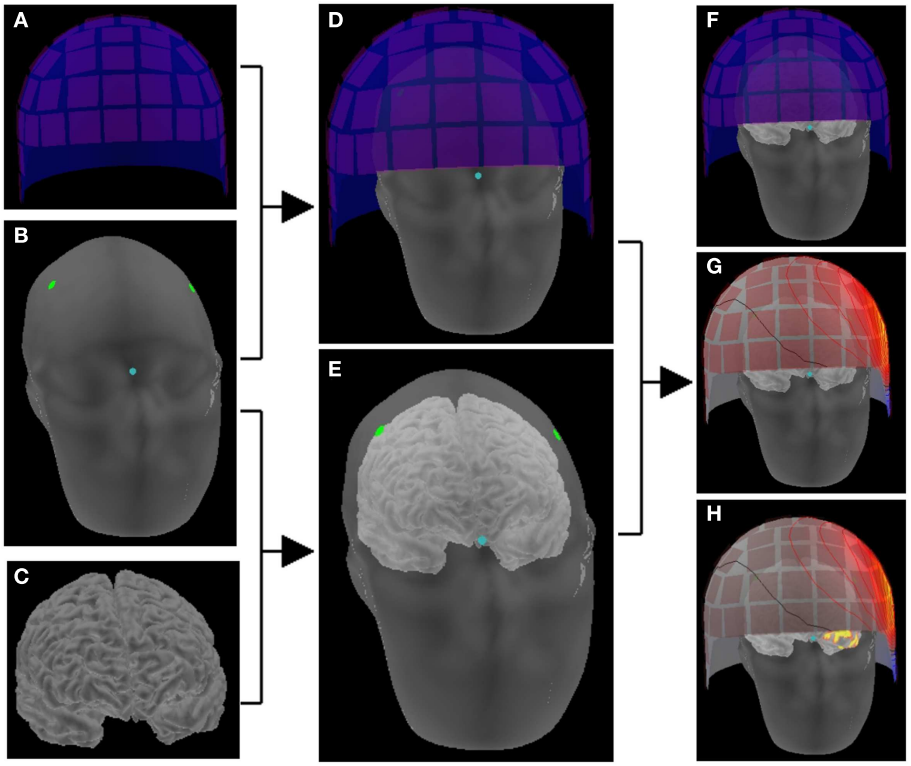

FIGURE 3 | Schematic representation of making a head model. The location correlation of sensors **(A)** and head **(B)** is determined by digitization information (dots) and head position indicator in the sensor array **(D)**. The location information of head **(B)** and brain **(C)** is obtained on the reconstructed images of MRI **(E)**. Thus, the brain and the sensor array are co-registered **(F)**, and magnetic fields on the sensor space provides activation maps on the source space **(G)** that consists of the cortical surface **(H)**.

INVERSE SOLUTION, CREATING SOURCE MAPS

The forward solution, which models the magnetic signals generated by unit current dipoles, is obtained by using the coregistration (Hämäläinen and Sarvas, 1989; Oostendorp and van Oosterom, 1989). Inverse solution is calculated based on the forward solution, mapping the strength of each unit dipole (Dale and Sereno, 1993; Dale et al., 2000). Source activation is projected on the cortical surface by applying a certain threshold, showing the source strength with different colors (**Figure 4**). The strength and extent of activation change along with the time course (**Figure 4**).

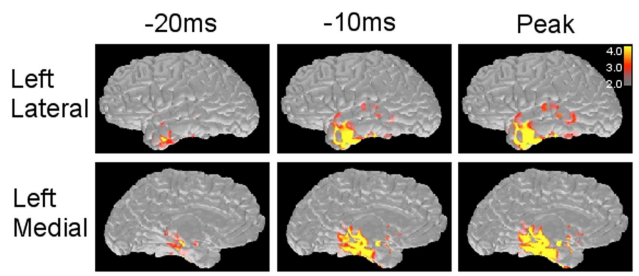

FIGURE 4 | Minimum norm estimate maps obtained from a left temporal spike. MNE solution provides source distribution maps along with the time course of spike at different time points. The scale (right corner) demonstrates that the values above 3.0 × 1e−9 and 4.0 × 1e−9 (nA m) are shown as red and yellow, respectively.

INTERPRETATION OF DISTRIBUTED SOURCE MAPS

Distributed source maps can be examined both spatially and temporally; these maps estimate the spatial source distribution and its time course. A cortical parcellation, provided by Freesurfer (Dale et al., 1999; Fischl et al., 1999), is helpful for understanding detailed anatomical location of activation (**Figure 5**). More importantly, spatial source distribution is considered representing to the cortical extent of spike involvement; activation in a small cortical area suggests that the spiking area is restricted (Hara et al., 2007; Tanaka et al., 2013b). Widespread cortical activation, extending over two lobes or bilaterally, may reflect a large abnormal neural network associated with epilepsy (Shiraishi et al., 2005a,b, 2011).

Time course of source activation provides a way to evaluate spatial source distribution at each time point of the spike (Tanaka et al., 2010, 2012). The interpreter can trace the activation pattern from the spike onset to the peak. The changing pattern along with the time course may reflect physiologic spiking process, such as growing or propagation. Here, several patterns of spatiotemporal source distribution can be recognized; (1) restricted onset activation + restricted peak activation in the onset area, suggesting a highly limited spike involvement, (2) restricted onset activation + widespread peak activation, suggesting broad spike

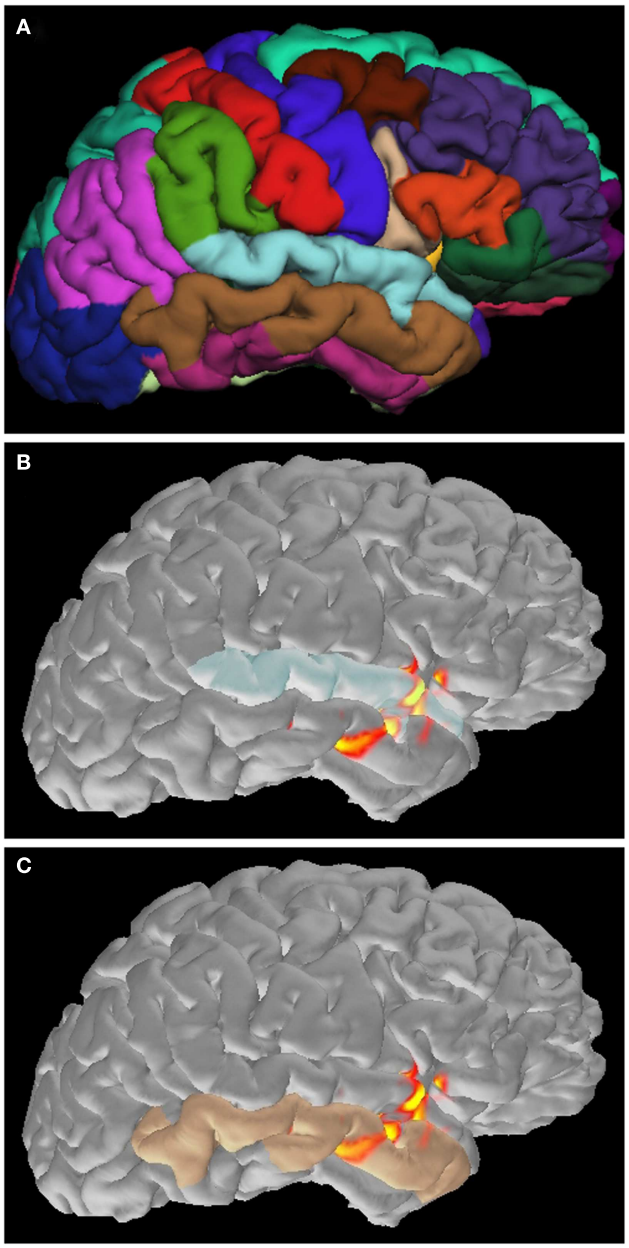

FIGURE 5 | Application of cortical parcellation. Cortical parcellation is obtained by Freesurfer **(A)**. The parcellation is useful to understand that the spike activation is mainly located in the superior **(B)** and inferior **(C)** temporal gyrus.

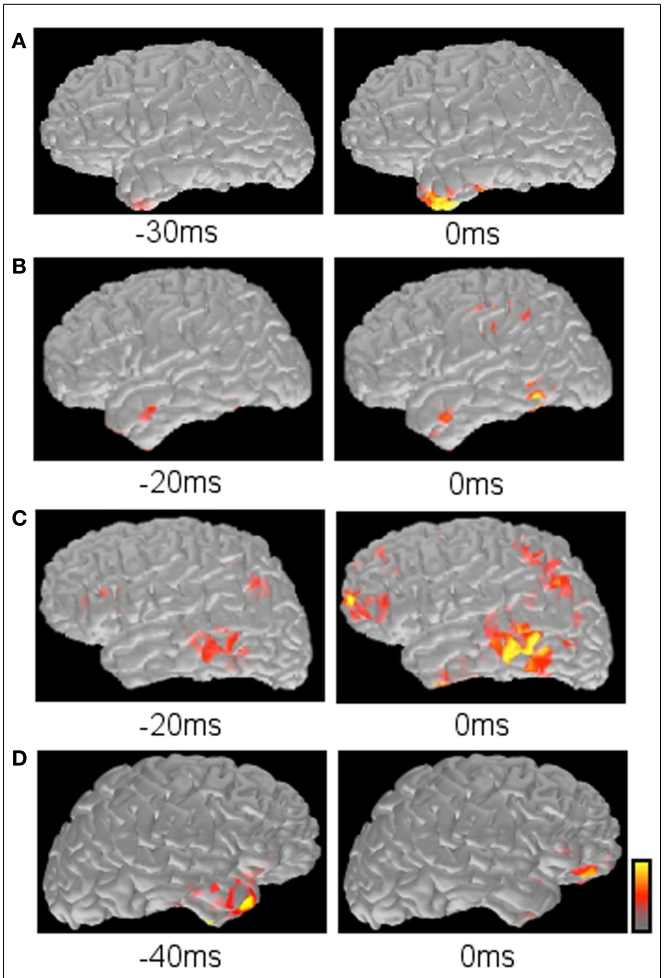

FIGURE 6 | Typical propagation patterns suggested by MNE maps. **(A)** Restricted onset and restricted peak activation in the left anterior temporal lobe. **(B)** Restricted onset in the left anterior temporal lobe and widespread peak in the left posterior temporal and parietal lobes. **(C)** Widespread onset and widespread peak in the left frontal, temporal, and parietal lobes. **(D)** Restricted early activation in the right anterior temporal lobe and late activation in the right inferior frontal lobe.

propagation, (3) widespread onset activation + widespread peak activation, suggesting non-localizing, widespread spiking in the cortex, (4) restricted early activation + restricted late activation in the distant area, suggesting an abnormal propagation pathway (**Figure 6**).

There are still several issues for assuming that the MNE maps accurately show the spike distribution in the whole brain; (1) MEG has different sensitivity to intracranial electric currents depending on regions (de Jongh et al., 2005; Goldenholz et al., 2009), and the information in the region with low sensitivity may be missing. (2) MNE solution does not consider the anatomical connection through white matter tracts. Tractography using diffusion tensor imaging will be useful in combination with MNE maps (Tanaka et al., 2012). (3) There is no established way to determine the threshold objectively, although such a threshold greatly affects the appearance of source maps. Several studies have introduced thresholds which are determined by a quantitative procedure (Gallagher et al., 2012; Tanaka et al., 2013a,b). Further investigation will be necessary to understand how the threshold should be determined.

BENEFITS OF DISTRIBUTED SOURCE MAPS

Previous studies using distributed source analysis mainly focused on providing the evidence of accurate source localization in comparison with IEEG (Waberski et al., 2000; Zumsteg et al., 2006;

Tanaka et al., 2010; Kanamori et al., 2013). There are only a limited number of studies describing the benefit of this method in clinical practice (Tanaka et al., 2009a, 2013b). However, the results of these studies suggest benefits to use this technique in clinical practice.

One of the possible benefits is to obtain accurate spike localization. Distributed source analysis likely provides more reasonable solution than a single dipole model, although there is a localization error still observed in various distributed models (Waberski et al., 2000; Silva et al., 2004; Soufflet and Boeijinga, 2005). Previous studies have shown that MNE (and its derivative, dSPM) provides more accurate source localization than single dipoles, by comparing with single photon emission tomography (Shiraishi et al., 2005a), surgical outcome (Tanaka et al., 2009a), and IEEG (Kanamori et al., 2013) in a small group of patients. By using the distributed source analysis, MEG may contribute to the presurgical evaluation of epilepsy more effectively.

The other benefit is to understand the spike propagation. Some epileptic spikes originate from a restricted onset and propagate to other cortical areas (Alarcon et al., 1994, 1997). In these spikes, source localization of the early phase may be more informative than analyzing the peak for identifying the spike origin. Single dipole method sometimes does not provide adequate sources at the early latency as described above (Kanamori et al., 2013), whereas distributed source analysis provides reliable source distribution which can reconstruct the original, small signals of spikes at the sensor level. This ability is also useful for analyzing ictal MEG, which shows only small discharges in the early phase of seizures (Tanaka et al., 2009a). Distributed source analysis has nicely shown the possible onset of spikes with widespread cortical involvement at the peak in the previous studies (Shiraishi et al., 2005a,b; Kanamori et al., 2013).

FUTURE DIRECTIONS

Single dipole method has been potentially investigated and its benefits and limitations are well understood, and now several laboratories are doing similar studies with MNE and other distributed source solutions. Recent studies have validated MNE source distribution with IEEG. Tanaka et al. (2010) demonstrated that MNE analysis of frontotemporal MEG spikes accurately represents spike propagation as observed in IEEG. Frontoparietal and temporoparietal propagation patterns are also consistent between MEG and IEEG in a series of cases (Kanamori et al., 2013). Such validation will be highly desirable in other propagation involving various regions and in patients with various types of epilepsy.

An important distinction between ECD and MNE is that distributed source maps generally show the source localization of one single spike whereas single dipole maps project many dipoles obtained from different spikes. Thus, the single dipole method provides a viewpoint of a spike population, such as "clustered" or "scattered." Distributed source maps do not have such mapping procedures that are widely used. Therefore, combined use of single dipole maps and distributed source maps is necessary in the current settings of spike analysis. Development of new mapping techniques, which overview numerous distributed source maps, will be useful for analyzing many spike populations.

Another area under active investigation is the surgical implications of distributed source maps. Several studies have demonstrated that MEG affects the planning IEEG placement and interpretation (Sutherling et al., 2008; Knowlton et al., 2009), and correlates with surgical outcomes (Iwasaki et al., 2002) by using a single dipole model. On the other hand, a recent study has shown that these propagation patterns are highly correlated with surgical outcomes in patients with temporal lobe epilepsy by using MNE (Tanaka et al., 2013b). Comparison of these techniques regarding with surgical outcomes is now becoming better understood.

CONCLUSION

Spatiotemporal distributed source analysis is highly useful for understanding epileptic spikes. It provides more accurate source localization than a single dipole model in some situations, and may be informative in presurgical evaluation of epilepsy. However, further observations are necessary for establishing its usefulness in clinical practice.

ACKNOWLEDGMENT

This work was supported by National Institutes of Health (S10RR014978, 1R01NS069696-01A1) and NIBIB (P41EB015896).

REFERENCES

Alarcon, G., Garcia Seoane, J. J., Binnie, C. D., Martin Miguel, M. C., Juler, J., Polkey, C. E., et al. (1997). Origin and propagation of interictal discharges in the acute electrocorticogram. Implications for pathophysiology and surgical treatment of temporal lobe epilepsy. *Brain* 120, 2259–2282. doi:10.1093/brain/120.12.2259

Alarcon, G., Guy, C. N., Binnie, C. D., Walker, S. R., Elwes, R. D., and Polkey, C. E. (1994). Intracerebral propagation of interictal activity in partial epilepsy: implications for source localisation. *J. Neurol. Neurosurg. Psychiatry* 57, 435–449. doi:10.1136/jnnp.57.4.435

Assaf, B. A., Karkar, K. M., Laxer, K. D., Garcia, P. A., Austin, E. J., Barbaro, N. M., et al. (2004). Magnetoencephalography source localization and surgical outcome in temporal lobe epilepsy. *Clin. Neurophysiol.* 115, 2066–2076. doi:10.1016/j.clinph.2004.04.020

Bagic, A. I., Knowlton, R. C., Rose, D. F., Ebersole, J. S., and ACMEGS Clinical Practice Guideline (CPG) Committee. (2011). American clinical magnetoencephalography society clinical practice guideline 1: recording and analysis of spontaneous cerebral activity. *J. Clin. Neurophysiol.* 28, 348–354. doi:10.1097/WNP.0b013e3182272fed

Baumgartner, C., Pataraia, E., Lindinger, G., and Deecke, L. (2000). Neuromagnetic recordings in temporal lobe epilepsy. *J. Clin. Neurophysiol.* 17, 177–189. doi:10.1097/00004691-200003000-00007

Chuang, N. A., Otsubo, H., Pang, E. W., and Chuang, S. H. (2006). Pediatric magnetoencephalography and magnetic source imaging. *Neuroimaging Clin. N. Am.* 16, 193–210. doi:10.1016/j.nic.2005.11.001

Crouzeix, A., Yvert, B., Bertrand, O., and Pernier, J. (1999). An evaluation of dipole reconstruction accuracy with spherical head model and realistic head models in MEG. *Clin. Neurophysiol.* 110, 2176–2188. doi:10.1016/S1388-2457(99)00174-1

Dale, A. M., Fischl, B., and Sereno, M. I. (1999). Cortical surface-based analysis. I. Segmentation and surface reconstruction. *Neuroimage* 9, 179–194. doi:10.1006/nimg.1998.0395

Dale, A. M., Liu, A. K., Fischl, B. R., Buckner, R. L., Belliveau, J. W., Lewine, J. D., et al. (2000). Dynamic statistical parametric mapping: combining fMRI and MEG for high-resolution imaging of cortical activity. *Neuron* 26, 55–67. doi:10.1016/S0896-6273(00)81138-1

Dale, A. M., and Sereno, M. I. (1993). Improved localization of cortical activity by combining EEG and MEG with MRI cortical surface reconstruction: a linear approach. *J. Cogn. Neurosci.* 5, 162–176. doi:10.1162/jocn.1993.5.2.162

de Jongh, A., de Munck, J. C., Gonçalves, S. I., and Ossenblok, P. (2005). Differences in MEG/EEG epileptic spike yields explained by regional differences in signal-to-noise ratios. *J. Clin. Neurophysiol.* 22, 153–158. doi:10.1097/01.WNP.0000158947.68733.51

Fischer, M. J., Scheler, G., and Stefan, H. (2005). Utilization of magnetoencephalography results to obtain favorable outcomes in epilepsy surgery. *Brain* 128, 153–157. doi:10.1093/brain/awh333

Fischl, B., Sereno, M. I., and Dale, A. M. (1999). Cortical surface-based analysis. II: inflation, flattening, and a surface-based coordinate system. *Neuroimage* 9, 195–207. doi:10.1006/nimg.1998.0396

Fuchs, M., Wagner, M., and Kastner, J. (2001). Boundary element method volume conductor models for EEG source reconstruction. *Clin. Neurophysiol.* 112, 1400–1407. doi:10.1016/S1388-2457(01)00589-2

Gallagher, A., Tanaka, N., Suzuki, N., Liu, H., Thiele, E. A., and Stufflebeam, S. M. (2012). Decreased language laterality in tuberous sclerosis complex: a relationship between language dominance and tuber location as well as history of epilepsy. *Epilepsy Behav.* 25, 36–41. doi:10.1016/j.yebeh.2012.06.013

Genow, A., Hummel, C., Scheler, G., Hopfengärtner, R., Kaltenhäuser, M., Buchfelder, M., et al. (2004). Epilepsy surgery, resection volume and MSI localization in lesional frontal lobe epilepsy. *Neuroimage* 21, 444–449. doi:10.1016/j.neuroimage.2003.08.029

Goldenholz, D. M., Ahlfors, S. P., Hämäläinen, M. S., Sharon, D., Ishitobi, M., Vaina, L. M., et al. (2009). Mapping the signal-to-noise-ratios of cortical sources in magnetoencephalography and electroencephalography. *Hum. Brain Map.* 30, 1077–1086. doi:10.1002/hbm.20571

Grave de Peralta, R., Gonzalez, S., Lantz, G., Michel, C. M., and Landis, T. (2001). Noninvasive localization of electromagnetic epileptic activity. I. Method descriptions and simulations. *Brain Topogr.* 14, 131–137. doi:10.1023/A:1012944913650

Hämäläinen, M. S., and Ilmoniemi, R. J. (1994). Interpreting magnetic fields of the brain: minimum norm estimates. *Med. Biol. Eng. Comput.* 32, 35–42. doi:10.1007/BF02512476

Hämäläinen, M. S., and Sarvas, J. (1989). Realistic conductivity geometry model of the human head for interpretation of neuromagnetic data. *IEEE Trans. Biomed. Eng.* 36, 165–171. doi:10.1109/10.16463

Hara, K., Lin, F. H., Camposano, S., Foxe, D. M., Grant, P. E., Bourgeois, B. F., et al. (2007). Magnetoencephalographic mapping of interictal spike propagation: a technical and clinical report. *AJNR Am. J. Neuroradiol.* 28, 1486–1488. doi:10.3174/ajnr.A0596

International Federation of Societies for Clinical Neurophysiology. (1974). A glossary of terms most commonly used by clinical electroencephalographers. *Electroencephalogr. Clin. Neurophysiol.* 37, 538–548. doi:10.1016/0013-4694(74)90099-6

Iwasaki, M., Nakasato, N., Shamoto, H., Nagamatsu, K., Kanno, A., Hatanaka, K., et al. (2002). Surgical implications of neuromagnetic spike localization in temporal lobe epilepsy. *Epilepsia* 43, 415–424. doi:10.1046/j.1528-1157.2002.30801.x

Jin, K., Alexopoulos, A. V., Mosher, J. C., and Burgess, R. C. (2013). Implanted medical devices or other strong sources of interference are not barriers to magnetoencephalographic recordings in epilepsy patients. *Clin. Neurophysiol.* 124, 1283–1289. doi:10.1016/j.clinph.2013.04.004

Kakisaka, Y., Mosher, J. C., Wang, Z. I., Jin, K., Dubarry, A. S., Alexopoulos, A. V., et al. (2013). Utility of temporally-extended signal space separation algorithm for magnetic noise from vagal nerve stimulators. *Clin. Neurophysiol.* 124, 1277–1282. doi:10.1016/j.clinph.2012.03.082

Kakisaka, Y., Wang, Z. I., Mosher, J. C., Dubarry, A. S., Alexopoulos, A. V., Enatsu, R., et al. (2012). Clinical evidence for the utility of movement compensation algorithm in magnetoencephalography: successful localization during focal seizure. *Epilepsy Res.* 101, 191–196. doi:10.1016/j.eplepsyres.2012.03.014

Kanamori, Y., Shigeto, H., Hironaga, N., Hagiwara, K., Uehara, T., Chatani, H., et al. (2013). Minimum norm estimates in MEG can delineate the onset of interictal epileptic discharges: a comparison with ECoG findings. *Neuroimage Clin.* 2, 663–669. doi:10.1016/j.nicl.2013.04.008

Knowlton, R. C., Razdan, S. N., Limdi, N., Elgavish, R. A., Killen, J., Blount, J., et al. (2009). Effect of epilepsy magnetic source imaging on intracranial electrode placement. *Ann. Neurol.* 65, 716–723. doi:10.1002/ana.21660

Kobayashi, K., Merlet, I., and Gotman, J. (2001). Separation of spikes from background by independent component analysis with dipole modeling and comparison to intracranial recording. *Clin. Neurophysiol.* 112, 405–413. doi:10.1016/S1388-2457(01)00457-6

Kobayashi, K., Yoshinaga, H., Ohtsuka, Y., and Gotman, J. (2005). Dipole modeling of epileptic spikes can be accurate or misleading. *Epilepsia* 46, 397–408. doi:10.1111/j.0013-9580.2005.31404.x

Marquardt, D. W. (1963). An algorithm for least-squares estimation of nonlinear parameters. *SIAM J. Appl. Math.* 11, 431–441. doi:10.1137/0111030

Medvedovsky, M., Taulu, S., Bikmullina, R., Ahonen, A., and Paetau, R. (2009). Fine tuning the correlation limit of spatio-temporal signal space separation for magnetoencephalography. *J. Neurosci. Methods* 177, 203–211. doi:10.1016/j.jneumeth.2008.09.035

Medvedovsky, M., Taulu, S., Bikmullina, R., and Paetau, R. (2007). Artifact and head movement compensation in MEG. *Neurol. Neurophysiol. Neurosci.* 29, 4.

Michel, C. M., Murray, M. M., Lantz, G., Gonzalez, S., Spinelli, L., and Grave de Peralta, R. (2004). EEG source imaging. *Clin. Neurophysiol.* 115, 2195–2222. doi:10.1016/j.clinph.2004.06.001

Mikuni, N., Nagamine, T., Ikeda, A., Terada, K., Taki, W., Kimura, J., et al. (1997). Simultaneous recording of epileptiform discharges by MEG and subdural electrodes in temporal lobe epilepsy. *Neuroimage* 5, 298–306. doi:10.1006/nimg.1997.0272

Oishi, M., Kameyama, S., Masuda, H., Tohyama, J., Kanazawa, O., Sasagawa, M., et al. (2006). Single and multiple clusters of magnetoencephalographic dipoles in neocortical epilepsy: significance in characterizing the epileptogenic zone. *Epilepsia* 47, 355–364. doi:10.1111/j.1528-1167.2006.00428.x

Oishi, M., Otsubo, H., Kameyama, S., Morota, N., Masuda, H., Kitayama, M., et al. (2002). Epileptic spikes: magnetoencephalography versus simultaneous electrocorticography. *Epilepsia* 43, 1390–1395. doi:10.1046/j.1528-1157.2002.10702.x

Oostendorp, T. F., and van Oosterom, A. (1989). Source parameter estimation in inhomogeneous volume conductors of arbitrary shape. *IEEE Trans. Biomed. Eng.* 36, 382–391. doi:10.1109/10.19859

Ossadtchi, A., Baillet, S., Mosher, J. C., Thyerlei, D., Sutherling, W., and Leahy, R. M. (2004). Automated interictal spike detection and source localization in magnetoencephalography using independent components analysis and spatio-temporal clustering. *Clin. Neurophysiol.* 115, 508–522. doi:10.1016/j.clinph.2003.10.036

Ossenblok, P., de Munck, J. C., Colon, A., Drolsbach, W., and Boon, P. (2007). Magnetoencephalography is more successful for screening and localizing frontal lobe epilepsy than electroencephalography. *Epilepsia* 48, 2139–2149. doi:10.1111/j.1528-1167.2007.01223.x

Otsubo, H., and Snead, O. C. III (2001). Magnetoencephalography and magnetic source imaging in children. *J. Child Neurol.* 16, 227–235. doi:10.2310/7010.2001.17982

Pasqual-Marqui, R. D., Michel, C. M., and Lehmann, D. (1994). Low resolution electromagnetic tomography: a new method to localize electrical activity in the brain. *Int. J. Psychophysiol.* 18, 49–65. doi:10.1016/0167-8760(84)90014-X

Pataraia, E., Simos, P. G., Castillo, E. M., Billingsley, R. L., Sarkari, S., Wheless, J. W., et al. (2004). Does magnetoencephalography add to scalp video-EEG as a diagnostic tool in epilepsy surgery? *Neurology* 62, 943–948. doi:10.1212/01.WNL.0000115122.81621.FE

Plummer, C., Harvey, A. S., and Cook, M. (2008). EEG source localization in focal epilepsy: where are we now? *Epilepsia* 49, 201–218. doi:10.1111/j.1528-1167.2007.01381.x

Reinsberger, C., Tanaka, N., Cole, A. J., Lee, J. W., Dworetzky, B. A., Bromfield, E. B., et al. (2010). Current dipole orientation and distribution of epileptiform activity correlates with cortical thinning in left mesiotemporal epilepsy. *Neuroimage* 52, 1238–1242. doi:10.1016/j.neuroimage.2010.04.264

Shiraishi, H., Ahlfors, S. P., Stufflebeam, S. M., Knake, S., Larsson, P. G., Hämäläinen, M. S., et al. (2011). Comparison of three methods for localizing interictal epileptiform discharges with magnetoencephalography. *J. Clin. Neurophysiol.* 28, 431–440. doi:10.1097/WNP.0b013e318231c86f

Shiraishi, H., Ahlfors, S. P., Stufflebeam, S. M., Takano, K., Okajima, M., Knake, S., et al. (2005a). Application of magnetoencephalography in epilepsy patients with widespread spike or slow-wave activity. *Epilepsia* 46, 1264–1272. doi:10.1111/j.1528-1167.2005.65504.x

Shiraishi, H., Stufflebeam, S. M., Knake, S., Ahlfors, S. P., Sudo, A., Asahina, N., et al. (2005b). Dynamic statistical parametric mapping for analyzing the magnetoencephalographic epileptiform activity in patients with epilepsy. *J. Child Neurol.* 20, 363–369. doi:10.1177/08830738050200041601

Shiraishi, H., Watanabe, Y., Watanabe, M., Inoue, Y., Fujiwara, T., and Yagi, K. (2001). Interictal and ictal magnetoencephalographic study in patients with medial frontal lobe epilepsy. *Epilepsia* 42, 875–882. doi:10.1046/j.1528-1157.2001.042007875.x

Silva, C., Maltez, J. C., Trindade, E., Arriaga, A., and Ducla-Soares, E. (2004). Evaluation of L1 and L2 minimum norm performances on EEG localizations. *Clin. Neurophysiol.* 115, 1657–1668. doi:10.1016/j.clinph.2004.02.009

Song, T., Cui, L., Gaa, K., Feffer, L., Taulu, S., Lee, R. R., et al. (2009). Signal space separation algorithm and its application on suppressing artifacts caused by vagus nerve stimulation for magnetoencephalography recordings. *J. Clin. Neurophysiol.* 26, 392–400. doi:10.1097/WNP.0b013e3181c29896

Soufflet, L., and Boeijinga, P. H. (2005). Linear inverse solutions: simulations from a realistic head model in MEG. *Brain Topogr.* 18, 87–99. doi:10.1007/s10548-005-0278-6

Spencer, S. S. (2002). Neural networks in human epilepsy: evidence of and implications for treatment. *Epilepsia* 43, 219–227. doi:10.1046/j.1528-1157.2002.26901.x

Stefan, H., Hummel, C., Scheler, G., Genow, A., Druschky, K., Tilz, C., et al. (2003). Magnetic brain source imaging of focal epileptic activity: a synopsis of 455 cases. *Brain* 126, 2396–2405. doi:10.1093/brain/awg239

Stufflebeam, S. M. (2011). Clinical magnetoencephalography for neurosurgery. *Neurosurg. Clin. N. Am.* 22, 153–167. doi:10.1016/j.nec.2010.11.006

Stufflebeam, S. M., Tanaka, N., and Ahlfors, S. P. (2009). Clinical applications of magnetoencephalography. *Hum. Brain Mapp.* 30, 1813–1823. doi:10.1002/hbm.20792

Sutherling, W. W., Mamelak, A. N., Thyerlei, D., Maleeva, T., Minazad, Y., Philpott, L., et al. (2008). Influence of magnetic source imaging for planning intracranial EEG in epilepsy. *Neurology* 71, 990–996. doi:10.1212/01.wnl.0000326591.29858.1a

Tadel, F., Baillet, S., Mosher, J. C., Pantazis, D., and Leahy, R. M. (2011). Brainstorm: a user-friendly application for MEG/EEG analysis. *Comput. Intell. Neurosci.* 2011, 879716. doi:10.1155/2011/879716

Tanaka, N., Cole, A. J., von Pechmann, D., Wakeman, D. G., Hämäläinen, M. S., Liu, H., et al. (2009a). Dynamic statistical parametric mapping for analyzing ictal magnetoencephalographic spikes in patients with intractable frontal lobe epilepsy. *Epilepsy Res.* 85, 279–286. doi:10.1016/j.eplepsyres.2009.03.023

Tanaka, N., Thiele, E. A., Madsen, J. R., Bourgeois, B. F., and Stufflebeam, S. M. (2009b). Magnetoencephalographic analysis in patients with vagus nerve stimulator. *Pediatr. Neurol.* 41, 383–387. doi:10.1016/j.pediatrneurol.2009.06.007

Tanaka, N., Grant, P. E., Suzuki, N., Madsen, J. R., Bergin, A. M., Hämäläinen, M. S., et al. (2012). Multimodal imaging of spike propagation: a technical case report. *AJNR Am. J. Neuroradiol.* 33, E82–E84. doi:10.3174/ajnr.A2701

Tanaka, N., Hämäläinen, M. S., Ahlfors, S. P., Liu, H., Madsen, J. R., Bourgeois, B. F., et al. (2010). Propagation of epileptic spikes reconstructed from spatiotemporal magnetoencephalographic and electroencephalographic source analysis. *Neuroimage* 50, 217–222. doi:10.1016/j.neuroimage.2009.12.033

Tanaka, N., Liu, H., Reinsberger, C., Madsen, J. R., Bourgeois, B. F., Dworetzky, B. A., et al. (2013a). Language lateralization represented by spatiotemporal mapping of magnetoencephalography. *AJNR Am. J. Neuroradiol.* 34, 558–563. doi:10.3174/ajnr.A3233

Tanaka, N., Peters, J. M., Prohl, A. K., Takaya, S., Madsen, J. R., Bourgeois, B. F., et al. (2013b). Clinical value of magnetoencephalographic spike propagation represented by spatiotemporal source analysis: correlation with surgical outcome. *Epilepsy Res.* doi:10.1016/j.eplepsyres.2013.11.006 Available from: http://dx.doi.org/10.1016/j.eplepsyres.2013.11.006,

Taulu, S., and Hari, R. (2009). Removal of magnetoencephalographic artifacts with temporal signal-space separation: demonstration with single-trial auditory-evoked responses. *Hum. Brain Mapp.* 30, 1524–1534. doi:10.1002/hbm.20627

Taulu, S., Kajola, M., and Simola, J. (2004). Suppression of interference and artifacts by the signal space separation method. *Brain Topogr.* 16, 269–275. doi:10.1023/B:BRAT.0000032864.93890.f9

Taulu, S., and Simola, J. (2006). Spatiotemporal signal space separation method for rejecting nearby interference in MEG measurements. *Phys. Med. Biol.* 51, 1759–1768. doi:10.1088/0031-9155/51/7/008

Waberski, T. D., Gobbelé, R., Herrendorf, G., Steinhoff, B. J., Kolle, R., Fuchs, M., et al. (2000). Source reconstruction of mesial-temporal epileptiform activity: comparison of inverse techniques. *Epilepsia* 41, 1574–1583. doi:10.1111/j.1499-1654.2000.001574.x

Zumsteg, D., Friedman, A., Wieser, H. G., and Wennberg, R. A. (2006). Propagation of interictal discharges in temporal lobe epilepsy: correlation of spatiotemporal mapping with intracranial foramen ovale electrode recordings. *Clin. Neurophysiol.* 117, 2615–2626. doi:10.1016/j.clinph.2006.07.319

Conflict of Interest Statement: The authors declare that the research was conducted in the absence of any commercial or financial relationships that could be construed as a potential conflict of interest.

Received: 30 November 2013; accepted: 25 January 2014; published online: 10 February 2014.

Citation: Tanaka N and Stufflebeam SM (2014) Clinical application of spatiotemporal distributed source analysis in presurgical evaluation of epilepsy. Front. Hum. Neurosci. ***8****:62. doi: 10.3389/fnhum.2014.00062*

This article was submitted to the journal Frontiers in Human Neuroscience.

frontiers in
HUMAN NEUROSCIENCE

ORIGINAL RESEARCH ARTICLE
published: 04 February 2014
doi: 10.3389/fnhum.2014.00036

Do you know what I mean? Brain oscillations and the understanding of communicative intentions

Marcella Brunetti [1,2]*, ***Filippo Zappasodi*** [1,2], ***Laura Marzetti*** [1,2], ***Mauro Gianni Perrucci*** [1,2], ***Simona Cirillo*** [2], ***Gian Luca Romani*** [1,2], ***Vittorio Pizzella*** [1,2] ***and Tiziana Aureli*** [2]

[1] *Institute for Advanced Biomedical Technologies, University "G. d'Annunzio" of Chieti-Pescara, Chieti, Italy*
[2] *Department of Neuroscience and Imaging, University "G. d'Annunzio" of Chieti-Pescara, Chieti, Italy*

Edited by:
Christos Papadelis, Boston Children's Hospital and Harvard Medical School, USA

Reviewed by:
Juliana Yordanova, Bulgarian Academy of Sciences, Bulgaria
William C. Gaetz, The Children's Hospital of Philadelphia, USA

***Correspondence:**
Marcella Brunetti, Department of Neuroscience and Imaging, Institute for Advanced Biomedical Technologies, University "G. d'Annunzio" of Chieti-Pescara, Via dei Vestini 33, Chieti 66013, Italy
e-mail: mbrunetti@itab.unich.it

Pointing gesture allows children to communicate their intentions before the acquisition of language. In particular, two main purposes seem to underlie the gesture: to request a desired object (imperative pointing) or to share attention on that object (declarative pointing). Since the imperative pointing has an instrumental goal and the declarative has an interpersonal one, only the latter gesture is thought to signal the infant's awareness of the communicative partner as a mental agent. The present study examined the neural responses of adult subjects with the aim to test the hypothesis that declarative rather than imperative pointing reflects mentalizing skills. Fourteen subjects were measured in a magnetoencephalographic environment including four conditions, based on the goal of the pointing – imperative or declarative – and the role of the subject – sender or receiver of pointing. Time–frequency modulations of brain activity in each condition (declarative production and comprehension, imperative production and comprehension) were analyzed. Both low beta and high beta power were stronger during declarative than imperative condition in anterior cingulated cortex and right posterior superior temporal sulcus, respectively. Furthermore, high gamma activity was higher in right temporo-parietal junction during the sender than receiving condition. This suggests that communicative pointing modulated brain regions previously described in neuroimaging research as linked to social cognitive skills and that declarative pointing is more capable of eliciting that activation than imperative. Our results contribute to the understanding of the roles of brain rhythm dynamics in social cognition, thus supporting neural research on that topic during developmental both in typical and atypical conditions, such as autism spectrum disorder. In particular, the identification of relevant regions in a mature brain may stimulate a future work on the developmental changes of neural activation in the same regions.

Keywords: declarative pointing, theory of mind, social cognition, beta rhythm, gamma rhythm

INTRODUCTION

According to cognitive pragmatics, interpersonal communication can only be successful if the partners share not just the content of an ongoing message, but also the intention. This sharing is easy to achieve when language is used, but it is more difficult when only gestures are available. If a friend of mine points at a salt bottle when looking at me, I could think that he/she wants me to pass it to him/her, or to remember the day before when I spilled the salt on the table. The gesture is the same but the intention differs: to obtain something or to share attention on something.

Pointing represents a milestone in the construction of language and meaning in early development and, indeed, it remains a crucial accompaniment of adults' deictic speech in many languages. This gesture is typically achieved at around the end of the first year of life, when it is thought to signal the beginning of intentional communication, thereby providing the first evidence of the infant' recognizing of the other person as endowed with mental states. In particular, two main purposes are identified as motivating the infant pointing: to request a desired object from another person (imperative pointing) or to share attention with his/her on that object (declarative pointing). The former pointing has an instrumental purpose (but, see Tomasello et al., 2007 for a broader view) and the latter an interpersonal one. A longstanding, however, lively question in developmental literature is whether only declarative pointing should be considered a true signal of early mentalizing skills (Carpenter, 2009) compared to imperative, which would merely signal the infant's understanding of the other person as a causal instead of a mental agent.

Indeed, research data support the uniqueness of declarative pointing. Unlike the imperative, it is very rare, or even absent, in humans affected by impairment of interpersonal function, such as autism spectrum disorders (Sigman et al., 1986; Baron-Cohen, 1995; Camaioni et al., 1997); it is also absent in non-human primates, such as great apes (Call and Tomasello, 1994; Leavens et al., 2005); moreover, it is a reliable precursor of language acquisition (Desrochers et al., 1995); finally, it seems to appear a bit later in development, seeming to require more advanced socio-cognitive skills (Camaioni et al., 2004).

Very few studies on pointing can be found in neuroscience research based on the purpose of the gesture. Henderson et al. (2002), using EEG data with infants aged 14–18 months, showed that frontal regions were involved in declarative but not imperative pointing. Consistent results were also found by a PET study with the same aged infants (Caplan et al., 1993). Both studies support the hypothesis that declarative pointing is related to joint attention instead of behavior regulation.

More quantitative studies were performed on adults (Pierno et al., 2009; de Langavant et al., 2011), but neither of them showed to fully recognize the communicative nature of pointing. Pierno's study compared BOLD signals in subjects observing an hand pointing or grasping, but found no substantial differences between the two conditions. However, the pointing the subjects were presented with had no communicative intention. In a more recent PET study, de Langavant et al. compared pointing gestures with or without a communicative function and found that right posterior superior temporal sulcus (pSTS) and right medial prefrontal cortex (mPFC) were involved in the former but not in the latter condition. However, intentions underlying communication were not distinguished. Indeed, other studies analyzing communicative abilities can be found, even if not directly referring to pointing. Human intentional communication was found to uniquely affect the brain functioning, since it showed to involve neural regions – namely the pSTS area – which were different from those involved in sensorimotor or language processes (Noordzij et al., 2009; Enrici et al., 2011). Furthermore, a magnetoencephalographic (MEG) study explored the brain dynamics involved in imperative vs. declarative communication (Vistoli et al., 2011), finding that the chronometry of neural activation at the early stage of mentalizing process showed a relatively early (before 700 ms post-stimulus) involvement of right temporo-parietal junction (rTPJ) and bilateral pSTS.

With reference to the two communicative functions emphasized by developmental literature as moving pointing gesture, i.e., declarative and imperative, the present study examined adult subjects with the MEG technique, however adapting to this environment is a task specifically devised in fMRI literature to elicit both kinds of pointing. Following the hypothesis that declarative rather than imperative pointing reflects mentalizing skills, we expected the neural network associated to those skills in adults (Saxe et al., 2004; Amodio and Frith, 2006; Becchio et al., 2006; Brüne and Brüne-Cohrs, 2006) and including pSTS, temporo-parietal junction (TPJ), precuneus and mPFC, to be active in declarative but not imperative condition. If so, the critical difference between the two kinds of pointing hypothesized by developmental research could be supported by the adult data and referred to the level of socio-cognitive engagement implied in either case.

Magnetoencephalographic recordings were used to reveal the dynamics of brain activity with high temporal resolution. Specifically, we analyzed the temporal modulation of induced oscillatory activity in the conventional physiological frequency bands (Klimesch, 1996) in a time range including both early and late latencies, the latter more likely related to high-level processes involved in social cognition. Indeed, brain rhythms are the product of synchronized activity among and within neuronal assemblies, and their power modulation is linked to sensory and cognitive functions (Wang, 2010).

To elicit communicative pointing in our sample, we employed the pointing task already used in developmental research (Camaioni et al., 2004; Aureli et al., 2009) and previously arranged for the fMRI environment (Committeri et al., 2012). This paradigm reproduces an interactive situation involving the subject and a virtual character, both of them alternatively producing or observing, pointing either for requesting an object or for sharing attention on it.

EXPERIMENTAL PROCEDURES

SUBJECTS

Fourteen healthy volunteers (6 females and 8 males; mean age: 26.9 ± 3.2 years; age range 22–31 years) were enrolled in the study. Inclusion criteria consisted of right-handedness as assessed with the Edinburgh inventory (Oldfield, 1971), and normal or corrected to normal vision. The exclusion criteria were: progressive neurological and/or systemic disorders; significant unstable concurrent medical illness, hormone replacement therapy; concomitant pharmacological treatment that could alter mood or cerebral metabolism (e.g., benzodiazepines, antidepressants, mood stabilizers, stimulants, or steroids) within the 30-days prior to acquisitions; a history of substance/alcohol abuse or dependence within the past 6 months (nicotine dependence was allowed); incapacities which would have limited understanding or consenting to study procedures.

All volunteers gave written informed consent according to the Declaration of Helsinki (World Medical Association Declaration of Helsinki, 1997). The protocol was approved by the local Ethic Committee (School of Medicine Ethic Committee, University of Chieti, Italy).

RESEARCH DESIGN

The experimental paradigm was devised to reproduce a communicative setting between the subject and a virtual character. Trials were planned to allow pointing production or comprehension, with the gesture fulfilling either declarative or imperative goal. Accordingly, MEG activity was analyzed within a time window including pointing production or pointing comprehension. To improve the subject's feeling of interacting with a real person, feedback pictures representing character's reactions to the trials were also provided and, to prevent the subject from being bored during the session, such a feedback was either positive or negative. Since feedback pictures were introduced only for the purpose of making the interactive situation as plausible as possible, no data analysis was performed following feedback presentation.

Overall, our design comprised two sessions with declarative or imperative pointing goal. Each session included two conditions in which the subject played a producing or comprehending role.

MATERIALS

Home-made pictures were prepared, showing different types of images according to the four different types of communication between the subject and the character (from the subject perspective): imperative production (IP), declarative production (DP), imperative comprehension (IC), and declarative comprehension (DC).

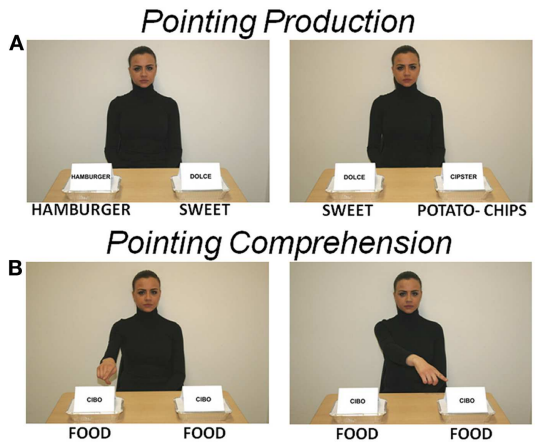

FIGURE 1 | Stimulation pictures. The character looks at the subject. **(A)** Two take-away trays are located on the table. Each tray is marked with a label, one showing the name of a salty food (English translation has been added immediately below each picture) and the other the generic word "dolce" (sweet). Salty and sweet foods represent target and control stimuli, respectively. These pictures were used to elicit an imperative or declarative pointing on subject (POINTING PRODUCTION). **(B)** Both trays show the word "cibo" (food) and the character points with the right index finger toward either the tray on the right or on the left. These pictures were used to elicit an imperative or declarative pointing observation and comprehension on subject (POINTING COMPREHENSION). Subject passively looked at picture, no pointing had to be produced by the subject.

Stimuli pictures

Production (imperative or declarative). Twenty-four pictures were presented, showing a character – the same person who performed subject training – looking at the subject and sitting at a table on which two take-away trays were located. Both trays were marked with a label, one showing the name of a specific salty food (e.g., "hamburger," "potato-chips") and the other showing a generic word, i.e., "dolce" (sweet). Subjects were instructed to point only to the salty food trays, after which the feedback picture followed. The salty food was used as a target stimulus and the sweet food as a control stimulus. Salty food was located on either the left or right side in a counterbalanced random order (**Figure 1A**).

Comprehension (imperative or declarative). Twenty-four pictures were presented. They were identical to the production pictures except for the labels on the two trays, both of them showing the generic word "cibo" (food), and for the character's posture, showing the right index finger pointing toward either the right or left tray (**Figure 1B**). Subjects were instructed to observe the character's pointing, after which the feedback picture followed.

Feedback pictures

Production (imperative or declarative). Twenty-four (12 negative and 12 positive feedback) pictures were presented. To give the subject a feedback after producing an imperative pointing, the picture showed two hands holding either a tray containing the salty food just pointed by the subject or an empty tray, meaning positive or negative feedback, respectively. To give the subject a feedback after a DP, the figure displayed the character, sitting at a table with a tray containing the salty food just pointed by the subject, and showing a smiling or a disgusted expression, meaning that it did or did not appreciate the pointed food, respectively.

Comprehension (imperative or declarative). Twenty-four (12 negative and 12 positive feedback) pictures were used. Feedback pictures to IC depicted either a tray containing the salty food pointed by the character in the previous picture, or an empty tray, meaning positive or negative feedback, respectively. Feedback pictures to DC depicted a tray containing the salty food pointed by the character in the previous picture and the character showing a neutral face expression.

All pictures were presented with Gaglab (Galati et al., 2008), an in-house software implemented in Matlab (The MathWorks, Inc., Natick, MA, USA) using Cogent Graphics toolbox (developed by John Romaya at the LON, Wellcome Department of Imaging Neuroscience, UCL, London, UK), and allowing time-locked presentation of visual and auditory stimuli with millisecond timing accuracy.

Pictures were projected by means of an LCD projector positioned outside of the shielded room. Two response boxes (Lumina, Cedrus Corporation), one for each hand, were used. Subjects' pointing response was provided by means of the right box. At the beginning of the trial, the subject's right index was continuously pressing a key of the right box. Pointing timing was monitored by the release of the key at the onset of the pointing movement. Pointing direction was controlled by the position (right or left) of the object that the subject had to point trial by trial. Two buttons on left box were used to interact with character during feedback.

EXPERIMENTAL DESIGN

All subjects performed a training phase before the MEG session. Training was given by a female operator (the same person appearing in the stimuli/feedback pictures) and included a simulation of the experiment, which lasted until the subject felt confident in her/his ability to perform the task. Soon after, MEG measure was performed. Two main sessions, declarative and imperative, each including two conditions, production and comprehension, were used. The communicative goal of each session was conveyed to the subject at the beginning of the session and maintained throughout the session.

Declarative session

In this session, we investigated pointing as a gesture for sharing intention with another person (**Figure 2** – top). Therefore, the subjects were told that the task was devised either to let the character be informed about their own taste about food (production condition) or to let them informed about the character's taste (comprehension condition).

Pointing production. After the presentation of a fixation cross, a picture for pointing production was shown to the subject for 1500 ms. According to previous instructions, subjects had to point to the tray marked with the label showing the name of a salty food. After a time interval of variable duration (1500/2500/3500 ms), either positive or negative feedback was given to the subject with the character showing a smiling or disgusted expression, respectively.

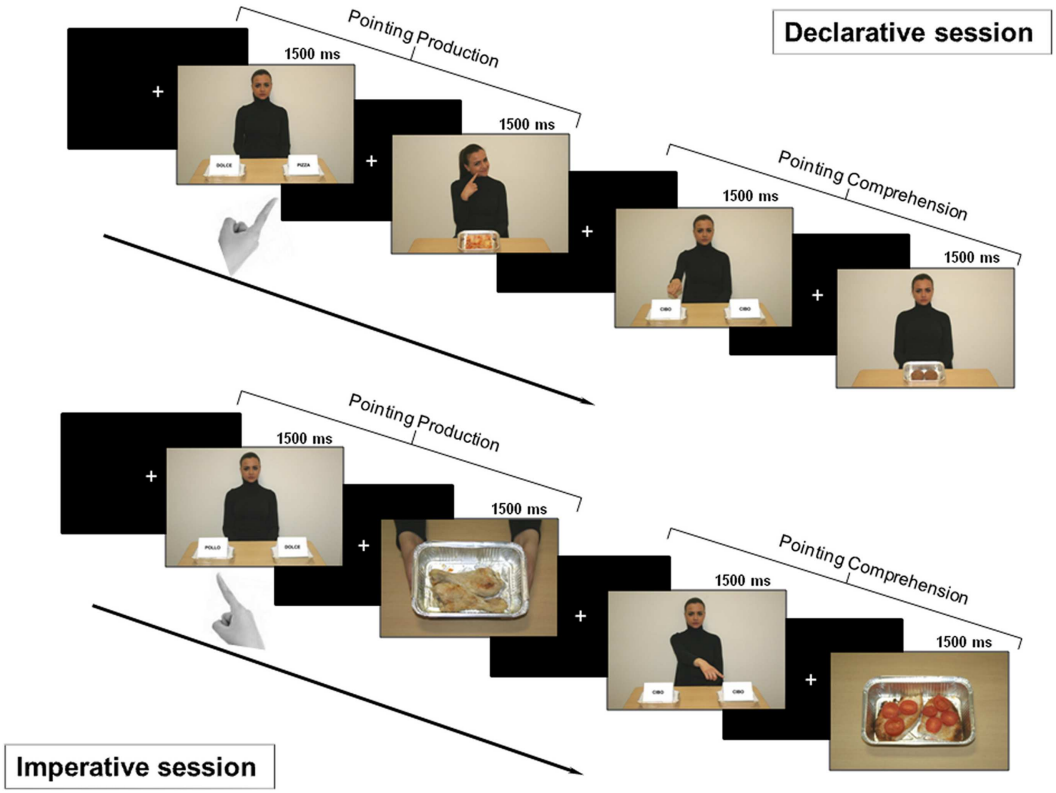

FIGURE 2 | Experimental design. *Top: declarative session.* First part: after a fixation cross, a picture for pointing production was shown for 1500 ms. Subjects were asked to declaratively point with their right hand toward the tray containing salty food. After a variable time interval (1500/2500/3500 ms), either positive or negative feedback was provided (the character showed a smiling or disgusted expression). Second part: after a fixation cross, a picture for pointing comprehension was shown for 1500 ms. Subjects had to carefully observe the side with the food the character was pointing to, in order to provide feedback. After a time interval of variable duration, a picture displaying the food previously pointed to by the character was delivered. If the subject liked that food, she/he had to press the button at the left or the right of the panel, based on the side of the pointed food; if subject did not, no button had to be pressed. *Bottom: imperative session.* First part: after a fixation cross, a picture for pointing production was shown for 1500 ms. Subjects were asked to make an imperative pointing toward the tray containing the salty food. Then, a positive or negative feedback was given to the subject (two hands offering a tray with the pointed food or empty, respectively). Second part: after a fixation cross, a picture for pointing comprehension was shown and subjects were asked to carefully observe which tray the character was pointing to. If the food was available (full tray), the subject had to press the button corresponding to food side (left or right); otherwise (empty tray) no button had to be pressed.

Pointing comprehension. After the presentation of a fixation cross, a picture for pointing comprehension was shown to the subject for 1500 ms. According to previous instructions, subjects had to carefully observe what tray the character was pointing to, i.e., whether it was at the right or left side. After a time interval of variable duration (1500/2500/3500 ms), a feedback picture displaying the character showing a neutral face and the food which the character pointed to in the previous picture was delivered. To have the interaction fulfilled, subjects were asked to press the left or right button of the left box, based on the side of the food previously pointed by the character, if they liked that food. Otherwise, if they did not like the pointed food, no button had to be pressed.

Imperative session

The session investigated pointing as a gesture for requesting something from another person (**Figure 2** – bottom). Therefore, the subjects were told that the task was devised either to obtain the food by the character (production condition) or to give the food to the character (comprehension condition).

Pointing production. After the presentation of a fixation cross, a picture for pointing production was shown to the subject for 1500 ms. According to previous instructions, subjects had to point to the tray marked with the label showing the name of a salty food. After a time interval of variable duration (1500/2500/3500 ms), a positive or negative feedback was given to the subject by showing a picture with two hands holding either a tray with the pointed food or an empty tray, respectively.

Pointing comprehension. After the presentation of a fixation cross, a picture for pointing comprehension was shown to the subject for 1500 ms. According to previous instructions, subjects had to carefully observe what tray the character was pointing to, i.e., whether it was at the right or left side. After a time interval of variable duration (1500/2500/3500 ms), a picture displaying either a

tray with the food pointed by the character in the previous picture or an empty tray was delivered. To have the interaction fulfilled, the subject had to press the button corresponding to the side (left or right) of the tray just pointed by the character, if the food was available (full tray). Otherwise (empty tray) no button had to be pressed.

To summarize, our paradigm included two sessions, imperative and declarative, each of them comprising 24 trials, i.e., 12 "pointing production" trials (one half displaying the target on the right of the display, and the other half on the left) and 12 "pointing comprehension" trials (one half displayed the character pointing to the tray on the right of the display and the other half on the left). Trials were randomly presented at a variable interval (a central white fixation cross on a black screen) of 1500/2500/3500 ms and were balanced with respect to condition order, target location, direction of pointing hand, and positive/negative feedback. Two runs were recorded for the declarative session and other two runs for the imperative session. In summary, four runs, each lasting about 8 min, were recorded for each MEG session, yielding 24 trials for each of the four experimental conditions (total 96 trials) for each subject. Furthermore, a set of 24 pictures was used to provide the character's feedback (12 positive and 12 negative) in declarative as well as in imperative session.

MEG RECORDINGS

Magnetoencephalographic signals were recorded with the 165-channel MEG system installed at the University of Chieti (Pizzella et al., 2001; Chella et al., 2012). This system includes 153 dcSQUID integrated magnetometers arranged on a helmet covering the whole head plus 12 reference channels. Two simultaneous electrical channels [electrocardiogram (ECG) and electro-oculogram (EOG)] were recorded for artifact rejection. All signals were band-pass filtered at 0.16–250 Hz and digitized at 1025 Hz.

An high-resolution MRI structural volume was acquired with a 3-T Philips Achieva MRI scanner (Philips Medical Systems, Best, The Netherlands) via a 3D fast field echo T1-weighted sequence (MP-RAGE; voxel size 1 mm isotropic, TR = 8.1 ms, echo time TE = 3.7 ms; flip angle 8°, and SENSE factor 2).

In order to coregister the head to the MRI volume, four anatomical landmarks (left and right preauricular points and nasion) were identified. Moreover, five coils were placed on the subject's scalp and their position was recovered before and after each MEG run in order to define the subject's head position with respect to the MEG helmet. The positions of the five coils and of the four anatomical landmarks were digitized by means of a 3D digitizer (3Space Fastrak; Polhemus).

MEG DATA ANALYSIS

MEG source-space signal estimation

Magnetoencephalographic data were down-sampled to 341 Hz and analyzed by using an independent components analysis (ICA) approach detailed elsewhere (Mantini et al., 2011). Briefly, the algorithm automatically classifies the ICs and identifies artifactual components and components of brain origin.

The number of artifactual ICs depends on the quality of each recording. On average, the algorithm identified 12 ± 4 artifact related components. Artifact components typically included hardware or environmental-injected noise, bad channels, contamination from high noise levels, and physiologic artifacts such as magnetocardiogram, eye blinks, and movements. To determine which ICs represented artifact, a classification procedure based on: (i) IC spectral properties; (ii) IC statistical properties; and (iii) comparison of the IC time courses with the corresponding time courses of the ECG, EOG, is adopted. See Supplemental Information in de Pasquale et al. (2010) for details. A particularly important advantage of ICA based artifact rejection is that all of the 24 recorded trials for each condition and each subject are preserved, thus a reliable number of trials is maintained for the next step of the analysis. Usually, ICA based pipelines rely on the subtraction of artifactual ICs to increase the signal-to-noise ratio. Here, an alternative approach also used in other works by our group (de Pasquale et al., 2010; Betti et al., 2013; Marzetti et al., 2013) is pursued. The approach is based on reconstructing MEG signals by recombining only the ICs of brain origin. On average, the algorithm identified 15 ± 5 ICs of brain origin, each contributed by the activity of one or more dipole sources or patches (e.g., two sources with no time lag typically contribute to the same IC). Of course, in ICA based approaches a trade-off between including unwanted and excluding wanted signals has to be faced and selecting approximately 15 brain ICs is a reasonable compromise. This strategy has been shown to improve SNR in Mantini et al. (2011).

After the decomposition through the fastICA algorithm with deflation approach and the classification steps, non-artifactual IC topographies were input to the weighted minimum-norm least squares (WMNLSs) linear inverse algorithm (Fuchs et al., 1999) implemented in Curry 6.0 (Neuroscan) and the corresponding source topography was localized. In this step, the volume conductor model was given by an individual boundary element method (BEM) (Fuchs et al., 1998) and the source space was modeled by a Cartesian 3D grid bounded by the subject anatomy as derived from individual MRI.

Single subject source-space topographies were thus mapped onto a standard Montreal Neurological Institute (MNI) stereotaxic space by an affine transformation to allow spatial comparison across subjects. For each grid voxel the activity along each direction, and for each time sample, was obtained as a linear combination of non-artifactual IC time courses weighted by their related source-space topographies.

Source activity magnitude was finally derived from the Cartesian components at each voxel; i.e., square root of the sum of the squared components.

Regions of interest

Band limited MEG power in the whole brain was estimated by using a standard Fast Fourier Transform (FFT) approach after linear detrending and Hanning windowing. The frequency boundaries defining the physiological band ranges, i.e., theta (4–7 Hz), alpha (8–13 Hz), beta (13–30 Hz), and gamma (31–80 Hz) were based on the EEG/MEG literature (Klimesch, 1996; Neuper and Pfurtscheller, 2001; Engel and Fries, 2010; Uhlhaas et al., 2011), and confirmed by visual inspection of the averaged spectra. Stimulus locked maps for each frequency band were estimated for declarative and imperative conditions in a 500-ms time window (from 300 to 800 ms) after the stimulus image presentation. For each

Table 1 | Montreal Neurological Institute coordinates of the maximum activity peak for regions of interest showing significant modulations of band power with respect to baseline (FDR corrected).

Region of interest	MNI coordinates			Frequency band
	x	*y*	*z*	
ACC	6	40	28	β, γ
lOFC	−33	22	−3	β
rOFC	34	19	−10	β
rSFg	15	50	44	β
lPMc	−43	12	48	β
rMFg	40	9	43	γ
rSMA	4	−21	62	β
lpIPS	−25	−62	51	β
rpIPS	25	−64	51	β
lIPS	−33	−54	47	β
rPCC	7	−47	33	β
lAg	−47	−62	17	β
rTPJ	60	−49	28	γ
rpSTS	58	−443	15	β
lpIC	−34	−29	15	β
rCn	4	−80	28	β, γ
rPCn	6	−54	60	β, γ

ACC, anterior cingulate cortex; lOFc/rOFc, left/right orbitofrontal cortex; rSFg, right superior frontal gyrus; lPMc, left premotor cortex; rMFg, right middle frontal gyrus; rSMa, right supplementary motor area; lpIPS/rpIPS, left/right posterior intraparietal sulcus; lIPS, left intraparietal sulcus; rPCC, right posterior cingulate cortex; lAg, left angular gyrus; rTPJ, right temporo-parietal junction; rpSTS, right posterior superior temporal sulcus; lpIC, left posterior insular cortex; rCn, right cuneus; rPCn, right precuneus.

condition, stimulus locked power maps have been contrasted, at a group level, with the power in a baseline period (from −500 to 0 ms) prior to the stimulus image presentation. This contrast was implemented by using a paired *t*-test and the resulting maps were corrected for multiple comparisons by using the false discovery rate (Benjamini and Hochberg, 1995).

This procedure led to the identification of 17 ROIs showing a significant modulation with respect to the baseline in either the declarative or imperative condition in beta and gamma bands (see **Table 1**; **Figure 3**).

TIME–FREQUENCY ANALYSIS

Time–frequency analysis allowed us to investigate whether the four different experimental conditions induced changes of band power in the identified ROIs. To this end, time–frequency representations (TFRs) were estimated in a 1500-ms time window starting 250 ms prior to the image presentation. Specifically, TFRs for each ROI were calculated by Morlet wavelets (Tallon-Baudry et al., 1997; Jensen et al., 2002). The power at a given time t and frequency f_0 is thus provided by the squared value of the convolution of the signal to a Morlet's wavelet:

$$\psi\left(t,\, f_0\right) = Ae^{-\frac{t^2}{2\sigma_t^2}} e^{2\pi i f_0 t} \tag{1}$$

where $A = (\sigma_t\sqrt{\pi})^{-1/2}$. The wavelet width was set to $f_0 2\pi\sigma_t = 7$ as a balance between temporal and frequency resolution (Jensen et al., 2002). Accordingly, power modulation was evaluated by calculating relative changes in TFR of power after the stimulus image presentation (Pow) with respect to mean power in a baseline period of 200 ms (from −250 to −50 ms) prior to the stimulus image presentation (Pow_{bas}) for each experimental condition separately. To this aim, event-related synchronization (ERS) or event-related desynchronization (ERD) (Pfurtscheller and Lopes da Silva, 1999; Neuper and Pfurtscheller, 2001) values were obtained according to:

$$\text{ERD/ERS} = 100\frac{(\text{Pow} - \text{Pow}_{\text{bas}})}{\text{Pow}_{\text{bas}}} \tag{2}$$

Since a high variability in reaction times (RTs) of pointing response across subjects was observed (RTs ranging from 737 to 1332 ms), a normalization of time epochs was performed in order to realign the timing of brain processes underlying the pointing production task. To this aim, for each subject the TFR plot between 100 ms after the stimulus and the individual RT was referenced to a standard time interval between 100 and 900 ms (mean value of the RTs across subjects in the different conditions), by means of a cubic spline interpolation. Consequently, epochs shorter than 900 ms were stretched and those longer than 900 ms were shrunk to fit the standard time epoch. Henceforth, in the TFR plots the motor response occurs exactly at 900 ms. Furthermore, concerning the pointing comprehension task (in which RTs were absent since no pointing response but only pointing observation was required), an analog time window analysis (between 100 and 900 ms after "pointing comprehension stimulus" onset) was applied to analyze the pointing observation processing.

To test the effect of the different conditions on rhythmic activity modulation over time, the whole normalized time epoch was partitioned into five-time intervals. Mean relative power values were estimated by averaging TFR values in a given time interval (t_1 = 101–260 ms; t_2 = 261–420 ms; t_3 = 421–580 ms; t_4 = 581–740 ms; t_5 = 741–900 ms) and physiological frequency band for each ROI and condition. The frequency boundaries defining the physiological bands were chosen according to the EEG/MEG literature (Klimesch, 1996; Neuper and Pfurtscheller, 2001; Engel and Fries, 2010; Uhlhaas et al., 2011): theta (4–7 Hz), alpha (8–13 Hz), low beta (13–20 Hz), high beta (21–30 Hz), low gamma (31–50 Hz), and high gamma (51–80 Hz).

STATISTICAL ANALYSIS

Behavioral data

Reaction time of pointing motor response was analyzed by a one-way ANOVA to identify possible statistical differences within the two communicative goals (declarative vs. imperative). Statistical analysis was performed using Statistica 6.1 software (Statsoft Italia Srl 2003).

MEG data

To assess specificity of ROI reactivity differences between declarative and imperative conditions, we performed a repeated measures ANOVA with *Goal* (declarative, imperative) × *Band* (beta,

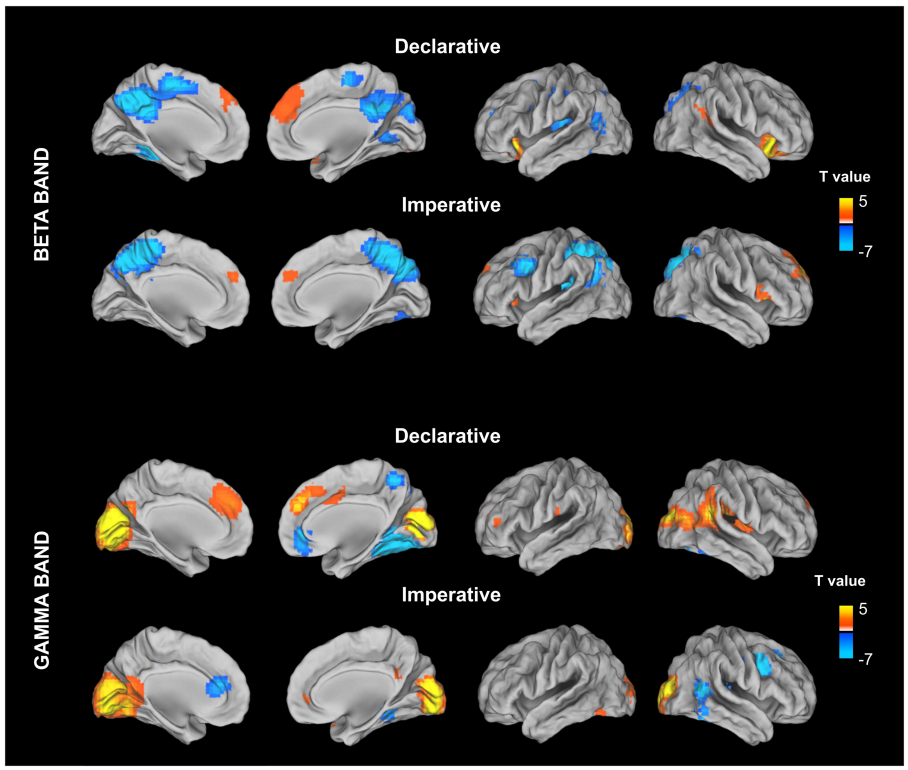

FIGURE 3 | Stimulus locked percentage relative power map in low beta band (13–20 Hz) and gamma (31–80) estimated for declarative and imperative conditions in a 500-ms time window (from 300 to 800 ms) after the stimulus image presentation. For each condition, stimulus locked power maps have been contrasting, at a group level, with the power in a baseline period (from −500 to 0 ms) prior to the stimulus image presentation. This contrast was implemented by using a paired *t*-test and the resulting maps were corrected for multiple comparisons by using the false discovery rate (FDR).

gamma) × *ROI* (listed in **Table 1**). A triple interaction was found [$F(16,208) = 1.948$, $p < 0.02$], indicating specific regional differences between conditions. To further test the effect of conditions on rhythmic activity modulation over time, a repeated measures ANOVA was performed separately for each frequency band and ROI on the time interval averaged TFR values, with *Role* (production, comprehension), *Goal* (declarative, imperative), and *Time* (t_1, t_2, t_3, t_4, t_5) as within subject factors. Bonferroni *post hoc* test was applied when significant interactions were found. Statistical analysis was performed using Statistica 6.1 software (Statsoft Italia Srl 2003).

RESULTS

BEHAVIORAL DATA

No significant differences were found for RTs between goals (one-way ANOVA with *Goal* – declarative and imperative – as within subject factor); mean ± SD: declarative RT: 889 ± 113 ms, imperative RT: 924 ± 163 ms.

MEG DATA

The assessment of the differences between rhythmic activity modulations across conditions in the ROIs by means of ANOVA showed significant effects only for the medial anterior cingulate cortex (ACC), the rTPJ, and the right posterior superior temporal sulcus (rpSTS). These effects were observed in specific frequency bands.

In particular, the repeated measures ANOVA revealed a significant *Goal* effect in low beta for ACC, with the activity being higher in the declarative rather than the imperative session [$F(1,13) = 8.10$, $p < 0.02$]. Furthermore, a significant *Goal* × *Time* interaction was observed [$F(4,52) = 3.81$, $p < 0.01$], indicating a time specific difference of power modulation between the declarative and the imperative sessions. Bonferroni *post hoc* test revealed that this difference was significant at the t_3 ($p < 0.01$), t_4 ($p < 0.001$) and t_5 ($p < 0.001$) (421–580, 580–740, 740–900 ms, respectively; **Figure 4**, right panel) time intervals. Indeed, **Figure 4** (left panel) shows a sustained low beta power modulation after the stimulus onset lasting until the motor response. Low beta power increased during the declarative and decreased during the imperative condition, regardless of the subject role. Furthermore, the difference between declarative and imperative low beta power increased with time and was maximal in the last time interval.

Figure 5 (top left panel) shows power modulations for rTPJ during both comprehension and production conditions. Repeated measures ANOVA revealed a *Role* main effect [$F(1,13) = 9.87$, $p < 0.05$] in high gamma, the power increase being higher during pointing production than comprehension. Furthermore, a *Role* × *Time* interaction was observed [$F(4,52) = 3.52$, $p < 0.05$], indicating a time-specific difference of power modulation between

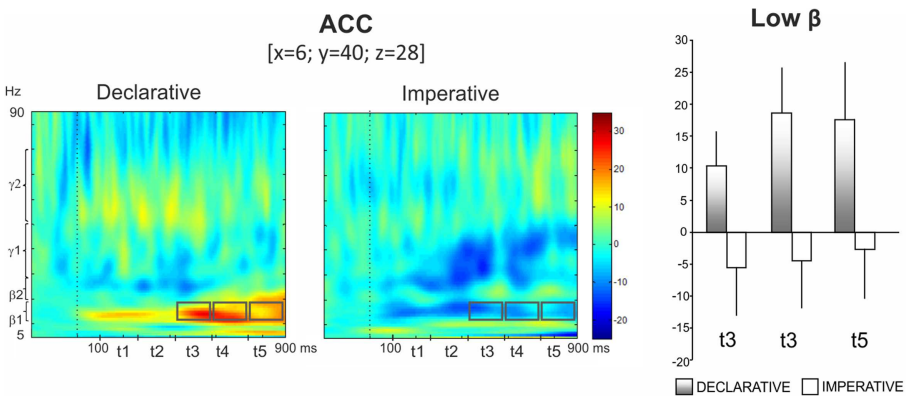

FIGURE 4 | Anterior cingulate cortex (ACC). Group TFRs during declarative and imperative sessions: dotted line indicates the stimulus onset (left). Gray boxes indicate the frequency bands and time intervals where a significant effect of Goal was found in Bonferroni *post hoc* test. Bar plots show average TFR values within gray boxes together with their standard deviations (right). Significant differences as revealed by Bonferroni *post hoc* test were found in t_3 ($p < 0.01$), t_4 ($p < 0.001$) and t_5 ($p < 0.001$).

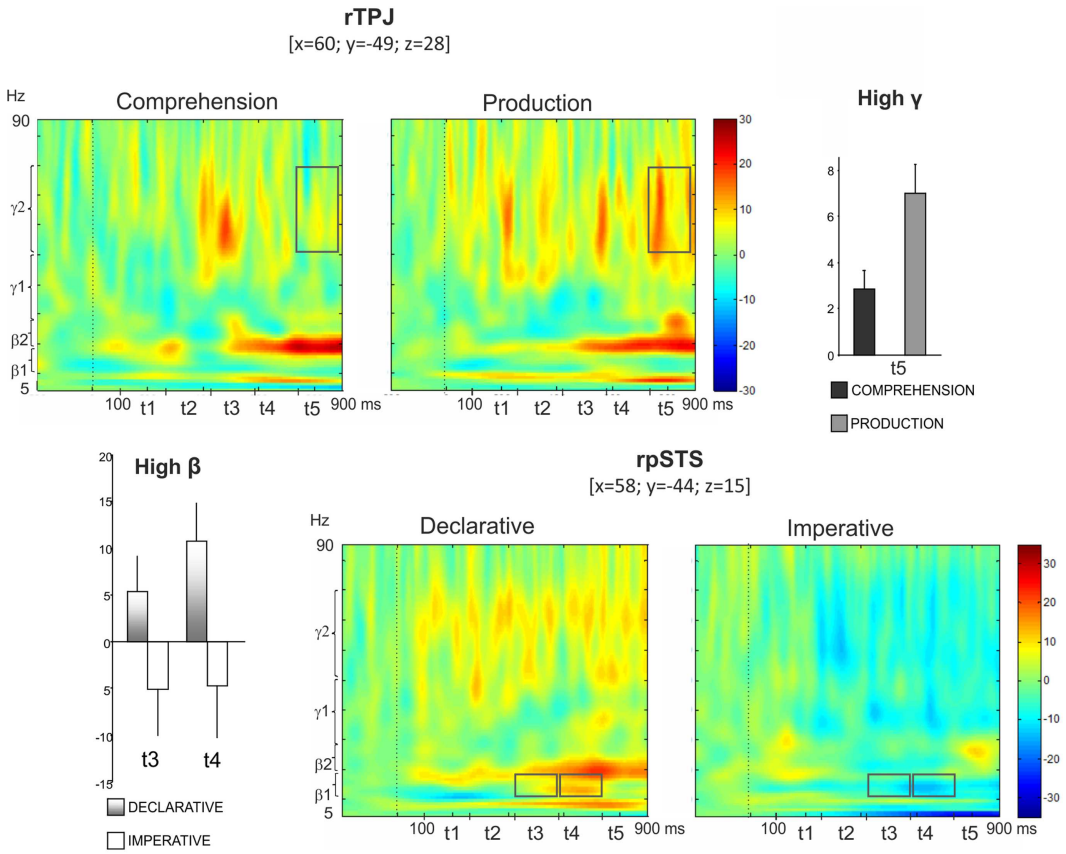

FIGURE 5 | *Top*: right temporo-parietal junction (rTPJ). Group TFRs during pointing comprehension and production: dotted line indicates the stimulus onset (left). In the frequency and time interval marked by superimposed gray boxes (740–900 ms, high gamma), a time specific difference of power modulation between the production and the comprehension sessions was found. Bar plots show results for Bonferroni *post hoc* test: $p < 0.01$ (right). *Bottom*: right posterior superior temporal sulcus (rpSTS). Group TFRs during declarative and imperative sessions (right). Significant increased high beta power during the declarative condition as well as a decreased high beta power during the imperative condition were observed in the frequency and time intervals marked by superimposed gray boxes. Bonferroni *post hoc* evidenced a significant difference during t_3 ($p < 0.05$) and t_4 ($p < 0.01$) (left).

the production and the comprehension sessions. In fact, Bonferroni *post hoc* revealed a significant difference during t_5 ($p < 0.01$) (**Figure 5**, top right panel).

Furthermore, the bottom right panel of **Figure 5** shows TFR plots for rpSTS during both declarative and imperative conditions. High beta power showed an increase during the declarative condition and a decrease during the imperative condition. This effect was specific for the t_3 and t_4 time intervals. Indeed, the repeated measures ANOVA revealed a *Goal* × *Time* significant interaction in high beta [$F(4,52) = 2.96$, $p < 0.05$] and the Bonferroni *post hoc* resulted in a significant difference during t_3 ($p < 0.05$) and t_4 ($p < 0.01$); (**Figure 5**, bottom left panel).

In addition to these significant results, a tendency to a significant *Goal* effect ($p = 0.084$) was found in the low gamma band (31–50 Hz) for ACC.

DISCUSSION

This study used the MEG technique to analyze brain rhythms underlying comprehension and production of pointing as a function of communicative intention, either imperative or declarative. We adapted an interactive task previously used in developmental research (Camaioni et al., 2004; Aureli et al., 2009) and arranged for the fMRI environment (Committeri et al., 2012), with the subject playing alternatively the role of the sender or the addressee of the gesture in two different communicative contexts. The aim was to bring in the subject in a more ecological situation than that usually provided by neuroimaging studies and more similar to that used in social cognition research (Hari and Kujala, 2009). Furthermore, for the first time as far as we are aware, we analyzed the induced oscillatory activity on data elicited by a social cognition task. This strategy allows for the observation of rhythmic modulations of the activity of specific ROIs in a time range which includes late latencies, possibly related to the high-level processes involved in social cognition (Wang et al., 2010). Our results showed different frequency-specific modulations of power based on both the goal of the gesture and the role of the subject.

DECLARATIVE VS. IMPERATIVE GOAL OF POINTING

With respect to the goal of the gesture, in low beta, the declarative pointing elicited higher activity than imperative pointing in dorsal ACC, starting from 421 to 900 ms after the stimulus onset (i.e., the last three periods before motor response). This region is included in the medial frontal cortex (MFC), which was consistently found to play a core role in social cognition. In particular, Amodio and Frith (2006) argued for a functional subdivision of rostral MFC in an anterior and a more posterior section: the former associated with self-knowledge and emotional processing (Lieberman et al., 2004; Steele and Lawrie, 2004; Stern et al., 2009), attribution of mental states (Mitchell et al., 2005), and mentalizing (Brunet et al., 2000; Gallagher et al., 2000; Frith and Frith, 2003; Uchiyama et al., 2012); the latter associated to cognitive processing such as internal action monitoring and decision making (Botvinick et al., 2004; Walton et al., 2004). In this framework, the region identified by our study was localized along this anterior/posterior border of ACC and was activated in the declarative condition, regardless of the subject role (comprehension or production).

A greater beta band functional connectivity between the frontal and right temporal areas during unfamiliar compared to familiar display was showed (Calmels et al., 2012). Furthermore, beta band activity in this cortical area was also recognized as being involved in several cognitive activities, such as learning after positive feedback (van de Vijver et al., 2011), decision making (Cohen et al., 2007), and reward processing (Marco-Pallares et al., 2008). More specifically, the last two studies observed by means of EEG, a reward-related oscillatory activity between 20 and 30 Hz, highlighting the advantage of the use of time–frequency analysis to observe high cognitive processing dynamics. Results from these studies demonstrate that reward processing in the preceding trials could affect oscillatory activity on the next trials. These results were obtained by adequately manipulating positive and negative feedback preceding each trial, and by assigning them a "winner/looser" value. On the contrary, feedback used in our study was devoid of a right/wrong value, since it had the purpose to support the joint attention, over than to prevent the subject from being bored during the session, rather than functioning as a penalty/reward. Consequently, an interpretation of our data in terms of rewards could be speculative.

All these findings suggest a top-down role of beta oscillatory activity in MFC. In particular, Engel and Fries (2010) hypothesize that beta band activity is related to the maintenance of a given cognitive status and that the enhancement of that activity reflects the endogenous vs. exogenous components of subject performance. Looking at our results, we suggest that the enhanced late latency beta band activity, found in ACC-arMFC when the subjects were presented with declarative condition, reflects the endogenous components required by the mentalizing attitude involved in that condition. Conversely, the decreased beta band power, presumed to be involved in causal processes, could reflect exogenous components that interrupted the current cognitive setting during imperative condition.

A second finding concerned the right posterior STS activation in the 20- to 30-Hz frequency range during declarative pointing, in the time interval from 421 to 740 ms post-stimulus. Previous fMRI study demonstrated the role of pSTS in passive viewing of biological motion (Pelphrey et al., 2003), in the extraction of social cues like directional eye gaze (Materna et al., 2008a,b), and in intentional action understanding (Pelphrey et al., 2004). Furthermore, a MEG study by Vistoli et al. (2011) observed a right posterior STS activity 200–600 ms after the stimulus presentation during an intention attribution task. Finally, de Langavant et al. (2011) showed, by means of PET data, the right posterior STS involvement in communicative vs. non-communicative pointing. Our data confirmed the involvement of this region in social interaction when attention is shared with another person as it happens in the declarative condition. Moreover, the observed beta ERS at later latency extends to this region, the above hypothesis on beta band, as reflecting the activity of an endogenous, top-down mechanism.

In conclusion, both right posterior STS and MFC seemed to work in social cognition as high-level processing sites, since they seem to be selectively involved in intentions underlying the declarative pointing. This function was carried out according to different temporal dynamics, since the prefrontal area maintained a sustained activity, whereas right posterior temporal area showed a

time-limited modulation. This suggested that a partial overlap in time, at a middle stage, between these two regions underpins social cognition.

SENDER VS. RECEIVER ROLE IN POINTING

The second goal of our study was to analyze the brain oscillatory activity based on the subject role; i.e., as sender vs. receiver of the pointing gesture. The most important result was provided by the time–frequency modulation in the rTPJ, which showed significant high gamma band ERS during pointing production and not during pointing comprehension, in the 160–0 ms time interval before movement.

Several studies have suggested rTPJ as a critical core for comparing information coming from a self-produced action with those from the environment. Specifically, TPJ has been considered the region which was mostly engaged when the individuals had to distinguish between themselves and the others (Decety and Sommerville, 2003; Uddin et al., 2006), thus playing a predominant role in the sense of agency (Ruby and Decety, 2001; Farrer et al., 2003; Sperduti et al., 2011). The TPJ role was also addressed by Corbetta et al. (2008) with reference to the theory of mind (ToM) ability. According to the authors, TPJ activity could work as an important tool for switching between internal and external signals in the comparison of the self and the other. Our results, showing a gamma band TPJ ERS at a late latency during pointing production regardless of the intention of communication, could suggest a TPJ involvement in agency function. Moreover, since TPJ activation started after the accomplishment of other high-level mental activities localized in posterior STS, such as social information and communicative intention processing (see also Materna et al., 2008a), our data are in accordance with the Decety and Lamm's (2007) quantitative meta-analysis, revealing that the TPJ activation overlaps in different cognitive domains both at high and low level. These data support the evolutionary hypothesis proposed by these authors, according to which high-level mechanisms operate on functionally more primitive levels.

As an additional result, we found that the involvement of TPJ during pointing production was expressed by an enhanced gamma band power. Previous research showed that this frequency range is associated with attention (Jensen et al., 2007), movement preparation (Schoffelen et al., 2011), and conscious awareness (Meador, 2002). Furthermore, this rhythm was observed in the monkey lateral intraparietal area (the putative homologous of human IPS/SPL) during the delay of a delayed saccade task (Pesaran et al., 2002). Finally, gamma band synchronization in parietal cortex was considered to represent the planned direction of the saccade (Van Der Werf et al., 2008). These data, together with the lack of motor responses during pointing comprehension – that prevents from excluding that TPJ activation can be ascribed to motor planning – could drive a possible confound in the TPJ role interpretation. Nevertheless, a previous PET study provided evidence for an increased rCBF in the posterior part of the right STS, close to the TPJ, during communicative pointing contrasted to uncommunicative pointing (de Langavant et al., 2011). The absence of activation in this region during a motor response devoid of communicative intention strongly supports a TPJ involvement in agency rather than in a mere motor process. Interestingly, induced gamma band bursts were observed in 4-month-old infants in right posterior areas (occipital, temporal and parietal EEG channels; Grossmann et al., 2007). This oscillation was elicited during averted vs. directed gaze observation. Averted gaze assumes a central role during social communication by directing the perceiver's attention toward a location. The authors suggest that their finding of gamma burst in response to averted gaze might reflects a shift in spatial attention, highlighting the potential role played by gamma band oscillations in examining the development of social perception.

Taken together, these studies on adults and infants seem to support the interpretation of enhanced rTPJ gamma oscillations observed in our study during pointing production as a sign of the involvement of this region in switching between internal and external aspects and between different spatial locations. In other words, pointing production would require the individual to decide between objects sited in two spatial locations and at the same time to plan a communicative action (pointing) in order to direct the other's attention toward the pointed location.

An alternative view comes from the recent meta-analysis by Kubit and Jack (2013). The authors hypothesize that the overlap of attention reorienting and social cognition on the same cortical region (rTPJ) could be viewed in a new light. They consider the presence of two distinct regions (angular gyrus and supramarginal gyrus) close to rTPJ that could mutually inhibit their activity in response to non-social vs. social tasks. Nevertheless, the comparison between social and non-social tasks is beyond the scope of this work. An *ad hoc* paradigm should be designed to address this issue.

In conclusion, we found that the core of the ToM circuit is active during declarative but not during imperative pointing. This finding suggests that declarative pointing reflects mentalizing skills, thus confirming in human adults the difference between imperative and declarative pointing hypothesized in developmental research. Furthermore, our results suggest that a complex process, such as a communicative interaction, involves a distributed neural circuit in which the modulation of oscillatory activity of different regions is partially overlapped in time. This process may run in parallel with a functional, effect-specific, differentiation between right temporal region and frontal areas, ending in the parietal and medial frontal regions. Our results contribute to the understanding of the roles of brain rhythm dynamics in social cognition, potentially opening the way for a targeted investigation of social interaction and language precursors during development, as well as of alteration of normal social abilities such as those related to autism spectrum disorder. The identification of relevant brain areas and, more importantly, of the frequency bands and the timing of the activation of these regions may greatly contribute to a future work on development, by suggesting to monitor the neural changes occurring in the same regions before the mature form is achieved.

ACKNOWLEDGMENTS

The authors would like to thank Giorgia Committeri and Gaspare Galati for helpful contribution to adaptation of the paradigm to neuroimaging environment.

REFERENCES

Amodio, D. M., and Frith, C. D. (2006). Meeting of minds: the medial frontal cortex and social cognition. *Nat. Rev. Neurosci.* 7, 268–277. doi:10.1038/nrn1884

Aureli, T., Perucchini, P., and Genco, M. (2009). Children's understanding of communicative intentions in the middle of the second year of life. *Cogn. Dev.* 24, 1–12. doi:10.1016/j.cogdev.2008.07.003

Baron-Cohen, S. (1995). Perceptual role-taking and protodeclarative pointing in autism. *Br. J. Dev. Psychol.* 7, 113–127. doi:10.1111/j.2044-835X.1989.tb00793.x

Becchio, C., Adenzato, M., and Bara, B. G. (2006). How the brain understands intention: different neural circuits identify the componential features of motor and prior intentions. *Conscious. Cogn.* 15, 64–74. doi:10.1016/j.concog.2005.03.006

Benjamini, Y., and Hochberg, Y. (1995). Controlling the false discovery rate: a practical and powerful approach to multiple testing. *J. Royal. Stat. Soc. B.* 57, 289–300.

Betti, V., della Penna, S., de Pasquale, F., Mantini, D., Marzetti, L., Romani, G. L., et al. (2013). Natural scenes viewing alters the dynamics of functional connectivity in the human brain. *Nueron* 79, 782–797. doi:10.1016/j.neuron.2013.06.022

Botvinick, M. M., Cohen, J. D., and Carter, C. S. (2004). Conflict monitoring and anterior cingulate cortex: an update. *Trends Cogn. Sci.* 8, 539–546. doi:10.1016/j.tics.2004.10.003

Brüne, M., and Brüne-Cohrs, U. (2006). Theory of mind – evolution, ontogeny, brain mechanisms and psychopathology. *Neurosci. Biobehav. Rev.* 30, 437–455. doi:10.1016/j.neubiorev.2005.08.001

Brunet, E., Sarfati, Y., Hardy-Baylé, M. C., and Decety, J. (2000). A PET investigation of the attribution of intentions with a nonverbal task. *Neuroimage* 11, 157–166. doi:10.1006/nimg.1999.0525

Call, J., and Tomasello, M. (1994). The social learning of tool use by orangutans (*Pongo pygmaeus*). *Hum. Evol.* 9, 297–313. doi:10.1007/BF02435516

Calmels, C., Foutren, M., and Stam, C. J. (2012). Beta functional connectivity modulation during the maintenance of motion information in working memory: importance of the familiarity of the visual context. *Neuroscience* 212, 49–58. doi:10.1016/j.neuroscience.2012.03.045

Camaioni, L., Perucchini, P., Bellagamba, F., and Colonnesi, C. (2004). The role of declarative pointing in developing a theory of mind. *Infancy* 5, 291–308. doi:10.1207/s15327078in0503_3

Camaioni, L., Perucchini, P., Muratori, F., and Milone, A. (1997). Brief report: a longitudinal examination of the communicative gestures deficit in young children with autism. *J. Autism Dev. Disord.* 27, 715–725. doi:10.1023/A:1025858917000

Caplan, R., Chugani, H., Messa, C., Guthrie, D., Sigman, M., Traversay, J., et al. (1993). Hemispherectomy for early onset intractable seizures: presurgical cerebral glucose metabolism and postsurgical nonverbal communication patterns. *Dev. Med. Child Neurol.* 35, 574–581.

Carpenter, M. (2009). Just how joint is joint action in infancy? *Top. Cogn. Sci.* 1, 380–392. doi:10.1111/j.1756-8765.2009.01026.x

Chella, F., Zappasodi, F., Marzetti, L., Della Penna, S., and Pizzella, V. (2012). Calibration of a multichannel MEG system based on the signal space separation method. *Phys. Med. Biol.* 57, 4855–4870. doi:10.1088/0031-9155/57/15/4855

Cohen, M. X., Elger, C. E., and Ranganath, C. (2007). Reward expectation modulates feedback-related negativity and EEG spectra. *Neuroimage* 35, 968–978. doi:10.1016/j.neuroimage.2006.11.056

Committeri, G., Cirillo, S., Costantini, M., Romani, G. L., Galati, G., and Aureli, T. (2012). "Cortical activation during pointing with declarative and imperative intention," in *Proceedings of the 8th FENS Forum of Neuroscience*, Barcelona.

Corbetta, M., Patel, G., and Shulman, G. L. (2008). The reorienting system of the human brain: from environment to theory of mind. *Neuron* 58, 306–324. doi:10.1016/j.neuron.2008.04.017

de Langavant, C. L., Remy, P., Trinkler, I., McIntyre, J., Dupoux, E., Berthoz, A., et al. (2011). Behavioral and neural correlates of communication via pointing. *PLoS ONE* 6:e17719. doi:10.1371/journal.pone.0017719

de Pasquale, F., Della Penna, S., Snyder, A. Z., Lewis, C., Mantini, D., Marzetti, L., et al. (2010). Temporal dynamics of spontaneous MEG activity in brain networks. *Proc. Natl. Acad. Sci. U.S.A.* 107, 6040–6045. doi:10.1073/pnas.0913863107

Decety, J., and Lamm, C. (2007). The role of the right temporoparietal junction in social interaction: how low-level computational processes contribute to meta-cognition. *Neuroscientist* 13, 580–593. doi:10.1177/1073858407304654

Decety, J., and Sommerville, J. A. (2003). Shared representations between self and other: a social cognitive neuroscience view. *Trends Cogn. Sci.* 7, 527–533. doi:10.1016/j.tics.2003.10.004

Desrochers, S., Morissette, P., and Ricard, M. (1995). "Two perspectives on pointing in infancy," in *Joint Attention: Its Origins and Role in Development*, eds C. Moore and P. J. Dunham (Hillsdale, NJ: Lawrence Erlbaum Associates, Inc), 85–101.

Engel, A. K., and Fries, P. (2010). Beta-band oscillations – signalling the status quo? *Curr. Opin. Neurobiol.* 20, 156–165. doi:10.1016/j.conb.2010.02.015

Enrici, I., Adenzato, M., Cappa, S., Bara, B. G., and Tettamanti, M. (2011). Intention processing in communication: a common brain network for language and gestures. *J. Cogn. Neurosci.* 23, 2415–2431. doi:10.1162/jocn.2010.21594

Farrer, C., Franck, N., Frith, C. D., Decety, J., and Jeannerod, M. (2003). Modulating the experience of agency: a positron emission tomography study. *Neuroimage* 18, 324–333. doi:10.1016/S1053-8119(02)00041-1

Frith, U., and Frith, C. D. (2003). Development and neurophysiology of mentalizing. *Philos. Trans. R. Soc. Lond. B Biol. Sci.* 358, 459–473. doi:10.1098/rstb.2002.1218

Fuchs, M., Drenckhahn, R., Wischmann, H. A., and Wagner, M. (1998). An improved boundary element method for realistic volume-conductor modeling. *IEEE Trans. Biomed. Eng.* 45, 980–997. doi:10.1109/10.704867

Fuchs, M., Wagner, M., Kohler, T., and Wischmann, H. A. (1999). Linear and nonlinear current density reconstructions. *J. Clin. Neurophysiol.* 16, 267–295. doi:10.1097/00004691-199905000-00006

Galati, G., Committeri, G., Spitoni, G., Aprile, T., Di Russo, F., Pitzalis, S., et al. (2008). A selective representation of the meaning of actions in the auditory mirror system. *Neuroimage* 40, 1274–1286. doi:10.1016/j.neuroimage.2007.12.044

Gallagher, H. L., Happé, F., Brunswick, N., Fletcher, P. C., Frith, U., and Frith, C. D. (2000). Reading the mind in cartoons and stories: an fMRI study of "theory of mind" in verbal and nonverbal tasks. *Neuropsychologia* 38, 11–21. doi:10.1016/S0028-3932(99)00053-6

Grossmann, T., Johnson, M. H., Farroni, T., and Csibra, G. (2007). Social perception in the infant brain: gamma oscillatory activity in response to eye gaze. *Soc. Cogn. Affect. Neurosci.* 2, 284–291. doi:10.1093/scan/nsm025

Hari, R., and Kujala, M. V. (2009). Brain basis of human social interaction: from concepts to brain imaging. *Physiol. Rev.* 89, 453–479. doi:10.1152/physrev.00041.2007

Henderson, L. M., Yoder, P. J., Yale, M. E., and McDuffie, A. (2002). Getting the point: electrophysiological correlates of protodeclarative pointing. *Int. J. Dev. Neurosci.* 20, 449–458. doi:10.1016/S0736-5748(02)00038-2

Jensen, O., Gelfand, J., Kounios, J., and Lisman, J. E. (2002). Oscillations in the alpha band (9-12 Hz) increase with memory load during retention in a short-term memory task. *Cereb. Cortex* 12, 877–882. doi:10.1093/cercor/12.8.877

Jensen, O., Kaiser, J., and Lachaux, J. P. (2007). Human gamma-frequency oscillations associated with attention and memory. *Trends Neurosci.* 30, 317–324. doi:10.1016/j.tins.2007.05.001

Klimesch, W. (1996). Memory processes, brain oscillations and EEG synchronization. *Int. J. Psychophysiol.* 24, 61–100. doi:10.1016/S0167-8760(96)00057-8

Kubit, B., and Jack, A. I. (2013). Rethinking the role of the rTPJ in attention and social cognition in light of the opposing domains hypothesis: findings from an ALE-based meta-analysis and resting-state functional connectivity. *Front. Hum. Neurosci.* 7:323. doi:10.3389/fnhum.2013.00323

Leavens, D. A., Hopkins, W. D., and Bard, K. A. (2005). Understanding the point of chimpanzee pointing: epigenesis and ecological validity. *Curr. Dir. Psychol. Sci.* 14, 185–189. doi:10.1111/j.0963-7214.2005.00361.x

Lieberman, M. D., Jarcho, J. M., and Satpute, A. B. (2004). Evidence-based and intuition-based self-knowledge: an fMRI study. *J. Pers. Soc. Psychol.* 87, 421–435. doi:10.1037/0022-3514.87.4.421

Mantini, D., Della Penna, S., Marzetti, L., de Pasquale, F., Pizzella, V., Corbetta, M., et al. (2011). A signal processing pipeline for MEG resting state networks. *Brain Connect.* 1, 49–59. doi:10.1089/brain.2011.0001

Marco-Pallares, J., Cucurell, D., Cunillera, T., García, R., Andrés-Pueyo, A., Münte, T. F., et al. (2008). Human oscillatory activity associated to reward processing in a gambling task. *Neuropsychologia* 46, 241–248. doi:10.1016/j.neuropsychologia.2007.07.016

Marzetti, L., Della Penna, S., Snyder, A. Z., Pizzella, V., Nolte, G., de Pasquale, F., et al. (2013). Frequency specific interactions of MEG resting state activity within and across brain networks as revealed by the multivariate interaction measure. *Neuroimage* 2013, 172–183. doi:10.1016/j.neuroimage.2013.04.062

Materna, S., Dicke, P. W., and Thier, P. (2008a). Dissociable roles of the superior temporal sulcus and the intraparietal sulcus in joint attention: a functional magnetic

resonance imaging study. *J. Cogn. Neurosci.* 20, 108–119. doi:10.1162/jocn.2008.20008

Materna, S., Dicke, P. W., and Thier, P. (2008b). The posterior superior temporal sulcus is involved in social communication not specific for the eyes. *Neuropsychologia* 46, 2759–2765. doi:10.1016/j.neuropsychologia.2008.05.016

Meador, K. J. (2002). Gamma coherence and conscious perception. *Neurology* 59, 847–854. doi:10.1212/WNL.59.6.847

Mitchell, J. P., Banaji, M. R., and Macrae, C. N. (2005). General and specific contributions of the medial prefrontal cortex to knowledge about mental states. *Neuroimage* 28, 757–762. doi:10.1016/j.neuroimage.2005.03.011

Neuper, C., and Pfurtscheller, G. (2001). Event-related dynamics of cortical rhythms: frequency-specific features and functional correlates. *Int. J. Psychophysiol.* 43, 41–58. doi:10.1016/S0167-8760(01)00178-7

Noordzij, M. L., Newman-Norlund, S. E., de Ruiter, J. P., Hagoort, P., Levinson, S. C., and Toni, I. (2009). Brain mechanisms underlying human communication. *Front. Hum. Neurosci.* 3:14. doi:10.3389/neuro.09.014

Oldfield, R. C. (1971). The assessment and analysis of handedness: the Edinburgh inventory. *Neuropsychologia* 9, 97–113. doi:10.1016/0028-3932(71)90067-4

Pelphrey, K. A., Morris, J. P., and McCarthy, G. (2004). Grasping the intentions of others: the perceived intentionality of an action influences activity in the superior temporal sulcus during social perception. *J. Cogn. Neurosci.* 16, 1706–1716. doi:10.1162/0898929042947900

Pelphrey, K. A., Singerman, J. D., Allison, T., and McCarthy, G. (2003). Brain activation evoked by perception of gaze shifts: the influence of context. *Neuropsychologia* 41, 156–170. doi:10.1016/S0028-3932(02)00146-X

Pesaran, B., Pezaris, J. S., Sahani, M., Mitra, P. P., and Andersen, R. A. (2002). Temporal structure in neuronal activity during working memory in macaque parietal cortex. *Nat. Neurosci.* 5, 805–811. doi:10.1038/nn890

Pfurtscheller, G., and Lopes da Silva, F. H. (1999). Event-related EEG/MEG synchronization and desynchronization: basic principles. *Clin. Neurophysiol.* 110, 1842–1857. doi:10.1016/S1388-2457(99)00141-8

Pierno, A. C., Tubaldi, F., Turella, L., Grossi, P., Barachino, L., Gallo, P., et al. (2009). Neurofunctional modulation of brain regions by the observation of pointing and grasping actions. *Cereb. Cortex* 19, 367–374. doi:10.1093/cercor/bhn089

Pizzella, V., Della Penna, S., Del Gratta, C., and Romani, G. L. (2001). SQUID systems for biomagnetic imaging. *Supercond. Sci. Tech.* 14, R79–R114. doi:10.1088/0953-2048/14/7/201

Ruby, P., and Decety, J. (2001). Effect of subjective perspective taking during simulation of action: a PET investigation of agency. *Nat. Neurosci.* 4, 546–550. doi:10.1038/87510

Saxe, R., Carey, S., and Kanwisher, N. (2004). Understanding other minds: linking developmental psychology and functional neuroimaging. *Annu. Rev. Psychol.* 55, 87–124. doi:10.1146/annurev.psych.55.090902.142044

Schoffelen, J. M., Poort, J., Oostenveld, R., and Fries, P. (2011). Selective movement preparation is subserved by selective increases in corticomuscular gamma-band coherence. *J. Neurosci.* 31, 6750–6758. doi:10.1523/JNEUROSCI.4882-10.2011

Sigman, M., Mundy, P., Sherman, T., and Ungerer, J. (1986). Social interactions of autistic, mentally retarded and normal children and their caregivers. *J. Child Psychol. Psychiatry* 27, 647–655. doi:10.1111/j.1469-7610.1986.tb00189.x

Sperduti, M., Delaveau, P., Fossati, P., and Nadel, J. (2011). Different brain structures related to self- and external-agency attribution: a brief review and meta-analysis. *Brain Struct. Funct.* 216, 151–157. doi:10.1007/s00429-010-0298-1

Steele, J. D., and Lawrie, S. M. (2004). Segregation of cognitive and emotional function in the prefrontal cortex: a stereotactic meta-analysis. *Neuroimage* 21, 868–875. doi:10.1016/j.neuroimage.2003.09.066

Stern, E. R., Welsh, R. C., Fitzgerald, K. D., and Taylor, S. F. (2009). Topographic analysis of individual activation patterns in medial frontal cortex in schizophrenia. *Hum. Brain Mapp.* 30, 2146–2156. doi:10.1002/hbm.20657

Tallon-Baudry, C., Bertrand, O., Delpuech, C., and Permier, J. (1997). Oscillatory gamma-band (30-70 Hz) activity induced by a visual search task in humans. *J. Neurosci.* 17, 722–734.

Tomasello, M., Carpenter, M., and Liszkowski, U. (2007). A new look at infant pointing. *Child Dev.* 78, 705–722. doi:10.1111/j.1467-8624.2007.01025.x

Uchiyama, H. T., Saito, D. N., Tanabe, H. C., Harada, T., Seki, A., Ohno, K., et al. (2012). Distinction between the literal and intended meanings of sentences: a functional magnetic resonance imaging study of metaphor and sarcasm. *Cortex* 48, 563–583. doi:10.1016/j.cortex.2011.01.004

Uddin, L. Q., Molnar-Szakacs, I., Zaidel, E., and Iacoboni, M. (2006). rTMS to the right inferior parietal lobule disrupts self-other discrimination. *Soc. Cogn. Affect. Neurosci.* 1, 65–71. doi:10.1093/scan/nsl003

Uhlhaas, P. J., Pipa, G., Neuenschwander, S., Wibral, M., and Singer, W. (2011). A new look at gamma? High- (>60 Hz) γ-band activity in cortical networks: function, mechanisms and impairment. *Prog. Biophys. Mol. Biol.* 105, 14–28. doi:10.1016/j.pbiomolbio.2010.10.004

van de Vijver, I., Ridderinkhof, K. R., and Cohen, M. X. (2011). Frontal oscillatory dynamics predict feedback learning and action adjustment. *J. Cogn. Neurosci.* 23, 4106–4121. doi:10.1162/jocn_a_00110

Van Der Werf, J., Jensen, O., Fries, P., and Medendorp, W. P. (2008). Gamma-band activity in human posterior parietal cortex encodes the motor goal during delayed prosaccades and antisaccades. *J. Neurosci.* 28, 8397–8405. doi:10.1523/JNEUROSCI.0630-08.2008

Vistoli, D., Brunet-Gouet, E., Baup-Bobin, E., Hardy-Bayle, M. C., and Passerieux, C. (2011). Anatomical and temporal architecture of theory of mind: a MEG insight into the early stages. *Neuroimage* 54, 1406–1414. doi:10.1016/j.neuroimage.2010.09.015

Walton, M. E., Devlin, J. T., and Rushworth, M. F. (2004). Interactions between decision making and performance monitoring within prefrontal cortex. *Nat. Neurosci.* 7, 1259–1265. doi:10.1038/nn1339

Wang, X.-J. (2010). Neurophysiological and computational principles of cortical rhythms in cognition. *Physiol. Rev.* 90, 1195–1268. doi:10.1152/physrev.00035.2008

Wang, Y. W., Lin, C. D., Yuan, B., Huang, L., Zhang, W. X., and Shen, D. L. (2010). Person perception precedes theory of mind: an event related potential analysis. *Neuroscience* 170, 238–246. doi:10.1016/j.neuroscience.2010.06.055

World Medical Association Declaration of Helsinki. (1997). Recommendations guiding physicians in biomedical research involving human subjects. *Cardiovasc. Res.* 35, 2–3. doi:10.1016/S0008-6363(97)00109-0

Conflict of Interest Statement: The authors declare that the research was conducted in the absence of any commercial or financial relationships that could be construed as a potential conflict of interest.

Received: 18 September 2013; accepted: 17 January 2014; published online: 04 February 2014.

Citation: Brunetti M, Zappasodi F, Marzetti L, Perrucci MG, Cirillo S, Romani GL, Pizzella V and Aureli T (2014) Do you know what I mean? Brain oscillations and the understanding of communicative intentions. Front. Hum. Neurosci. ***8****:36. doi: 10.3389/fnhum.2014.00036*

This article was submitted to the journal Frontiers in Human Neuroscience.

frontiers in
HUMAN NEUROSCIENCE

ORIGINAL RESEARCH ARTICLE
published: 31 December 2013
doi: 10.3389/fnhum.2013.00917

Sensitivity to auditory spectral width in the fetus and infant – an fMEG study

Jana Muenssinger[1]*†, Tamara Matuz[1,2†], Franziska Schleger[1], Rossitza Draganova[3], Magdalene Weiss[1,4], Isabelle Kiefer-Schmidt[4], Annette Wacker-Gussmann[5], Rathinaswamy B. Govindan[6], Curtis L. Lowery[7], Hari Eswaran[7] and Hubert Preissl[1,2]

[1] *fMEG Center, University of Tuebingen, Tuebingen, Germany*
[2] *Institute for Medical Psychology and Behavioral Neurobiology, University of Tuebingen, Tuebingen, Germany*
[3] *Department of Phoniatrics and Pediatric Audiology, Clinic of Otorhinolaryngology, Head and Neck Surgery, St. Elisabeth-Hospital Bochum, Bochum, Germany*
[4] *Department of Obstetrics and Gynecology, University Hospital Tuebingen, Tuebingen, Germany*
[5] *Department of Neonatology, University Children's Hospital Tuebingen, Tuebingen, Germany*
[6] *Division of Fetal and Transitional Medicine, Children's Hospital, Washington, DC, USA*
[7] *Department of Obstetrics and Gynecology, University of Arkansas for Medical Sciences, Little Rock, AR, USA*

Edited by:
Christos Papadelis, Harvard Medical School, USA

Reviewed by:
Minna Huotilainen, University of Helsinki, Finland
Silvia Comani, Università degli Studi "G. d'Annunzio," Italy

****Correspondence:***
Jana Muenssinger, fMEG Center, University of Tuebingen, Otfried-Müller-Strasse 47, Tuebingen 72076, Germany
e-mail: jana.muenssinger@uni-tuebingen.de

†Jana Muenssinger and Tamara Matuz have contributed equally to this work.

Auditory change detection is crucial for the development of the auditory system and a prerequisite for language development. In neonates, stimuli with broad spectral width like white noise (WN) elicit the highest response compared to pure tone and combined tone stimuli. In the current study we addressed for the first time the question how fetuses react to "WN" stimulation. Twenty-five fetuses ($M_{age} = 34.59$ weeks GA, SD ± 2.35) and 28 healthy neonates and infants ($M_{age} = 37.18$ days, SD ± 15.52) were tested with the first paradigm, wherein 500 Hz tones, 750 Hz tones, and WN segments were randomly presented and auditory evoked responses (AERs) were measured using fetal magnetoencephalography (fMEG). In the second paradigm, 12 fetuses ($M_{age} = 25.7$ weeks GA, SD ± 2.4) and 6 healthy neonates ($M_{age} = 23$ days and SD ± 6.2) were presented with two auditory oddball conditions: condition 1 consisted of attenuated WN as standard and 500 Hz tones and WN as deviants. In condition 2, standard 500 Hz tones were intermixed with WN and attenuated WN. AERs to volume change and change in spectral width were evaluated. In both paradigms, significantly higher AER amplitudes to WN than to pure tones replicated prior findings in neonates and infants. In fetuses, no significant differences were found between the auditory evoked response amplitudes of WN segments and pure tones (both paradigms). A trend toward significance was reached when comparing the auditory evoked response amplitudes elicited by attenuated WN with those elicited by WN (loudness change, second paradigm). As expected, we observed high sensibility to spectral width in newborns and infants. However, in the group of fetuses, no sensibility to spectral width was observed. This negative finding may be caused by different attenuation levels of the maternal tissue for different frequency components.

Keywords: WN, spectral width, auditory change detection, magnetoencephalography, auditory evoked responses

INTRODUCTION

Auditory change detection is an important prerequisite for a functional auditory system as well as for the development of language perception and can serve as an indicator for healthy cognitive functioning and development. It has been repeatedly shown that humans possess already at birth the capacity to process acoustic regularities and react to violations of such regularities, meaning that they are able to detect and discriminate different patterns of sound (Carral et al., 2005). Prior studies showed atypical auditory evoked responses (AERs) to auditory changes in pre-maturely born infants (Fellman et al., 2004) as well as in infants with genetic risk for dyslexia (Leppänen et al., 1999). However, the neurophysiological mechanisms underlying early sound perception and discrimination within both, typical and untypical development, are still not fully understood.

Most studies investigating change detection used oddball paradigms and evaluated AERs elicited by individual stimuli and mismatch negativity (MMN) responses determined by the difference between AERs elicited by standard and deviant stimuli. AERs are neurophysiologic indices of sensory functioning and their different components reflect basic cognitive functions. MMN (Näätänen, 2001) – a negative component which in adults peaks at around 150 ms after change onset – is considered as an indicator of automatic change detection reflecting discriminatory capacity. Assessing healthy infants, several studies showed that they were able to distinguish between pure tones of different frequencies (Kushnerenko et al., 2002; Huotilainen et al., 2003; Draganova et al., 2005, 2007). Kushnerenko et al. (2002) studied the development of change detection in neonates over the first 12 months and did not find statistically significant differences between the

responses at different ages on the group level. They also showed that changes between pure tones and novel sounds (clicks, chirps, vowels, syllables) at the age of 2 years elicited significantly higher AER responses to novel sounds compared to pure tones. This effect might be explained by the "novelty" of the stimulus itself or could be caused by the change in spectral width between stimuli, because the novel sounds were composed of different frequencies. To test both hypotheses, Kushnerenko et al. (2007) investigated responses to pure tones, novel sounds, and white noise (WN) segments. WN segments were chosen to match the novel sounds in the broad frequency range but not in the novelty. Results revealed the highest responses for WN segments. This indicates that – unlike adults – neonates are highly sensitive to the effective amount of stimulation, with broader widths eliciting higher AERs. This finding is also supported by behavioral data showing that infants are more sensitive to the amount of stimulation than to the modality of stimulation (Lewkowicz and Turkewitz, 1980; Turkewitz et al., 1983).

However, as shown in several studies using fetal magnetoencephalography, auditory change detection occurs already in the fetal stage (Draganova et al., 2005, 2007; Huotilainen et al., 2005). MMN responses were observed as early as 28 weeks of gestation. In these studies, pure tones with a frequency of 500 Hz were used as standard stimuli, which were intermixed with rarely presented deviants with a frequency of 750 Hz. However, to our best knowledge, fetal responses to more complex stimuli have not been investigated so far. One potential difficulty in using more complex stimuli in fetuses is the sound attenuation caused by maternal tissue. In general, it is known that high frequencies are more attenuated than lower frequencies [for review see Hepper and Shahidullah (1994)]. When using complex stimuli composed of multiple frequencies, the broad difference in attenuation levels between frequencies might result in the fact that fetuses perceive only parts of the whole frequency spectrum. This involves a decrement in the perceived differences between pure tones and complex stimuli by the fetus.

However, studies investigating fetal learning support the assumption that a broad spectrum of sounds reach the fetus *in utero*. Starting at the 29th week of gestational age, music as well as speech sounds were repeatedly presented to fetuses (Partanen et al., 2013a,b). Electroencephalographic (EEG) measurements directly after birth as well as 4 months after birth (Partanen et al., 2013a) showed enhanced AERs to the "learned" stimulus. AERs were significantly higher than in a control group of age-matched infants who were not presented with specific auditory stimulation before birth. This indicates that fetuses are able to perceive and learn a wide range of auditory stimuli *in utero*.

The aim of the first part of the current study (performed in Tuebingen) was to use a simplified paradigm to replicate the findings of Kushnerenko et al. (2007) in neonates and infants and to evaluate if the human fetal brain is able to process and react to differences in spectral width. Similar to newborns and infants, it was expected that fetuses will be sensitive to stimulus energy and will show increased AER amplitudes in reaction to the high spectral width of WN segments compared to those elicited by pure tones. In the second part of the study (performed in Little Rock), a within group oddball paradigm including both changes in volume and spectral width was used to further explore fetal cortical responses to different auditory changes. Higher AERs were expected for changes in frequency than for changes in volume.

MATERIALS AND METHODS

DATA ACQUISITION

Data was recorded using SQUID Array for Reproductive Assessment (SARA) systems installed in two different locations, one at the Department of Obstetrics and Gynecology, University of Arkansas for Medical Sciences, AR, USA and a second one at the fMEG Center, University of Tuebingen. Both systems were built by VSM, Medical Technology Ltd., Canada. To avoid magnetic influences from the environment, the systems are installed in shielded rooms (Vakuumschmelze, Germany). The system in Little Rock contains 151 primary sensors and the system in Tuebingen 156 primary sensors. The primary sensors measure the biomagnetic signals from the physiological sources. Little Rock data were recorded with a sampling rate of 312.5 Hz and the Tuebingen data with 610.352 Hz. The sensor arrangement in both systems is designed to fit the shape of the pregnant women's abdomen. Before each fetal measurement, an ultrasound is performed to determine fetal head position. Afterward, the mothers are seated on the fMEG device in the shielded room. Prior to the recording localization coils are placed at the left side, the right side and the spine of the mother as well as at the position on the abdomen where the fetal head is located. These coils indicate the maternal as well as the fetal position relative to the sensor array which are used in later data analysis.

PARTICIPANTS FROM TUEBINGEN STUDY (FIRST PART)

Twenty-five healthy pregnant women with uncomplicated pregnancies and normally developing fetuses ($M_{age} = 34.59$ weeks, SD $\pm$ 2.35 weeks) between the gestational age of 30 and 38 weeks and 28 healthy newborns and infants without complications during pregnancy and birth between the age of 14 and 67 days ($M_{age} = 37.18$ days SD $\pm$ 15.52) participated in the study. The local ethical committee approved the study and a written consent was obtained.

PROTOCOL USED IN TUEBINGEN STUDY (FIRST PART)

For neonatal/infant measurements, a cradle was attached to the fMEG devise and neonates/infants were lying on their right side with their right hemisphere over the sensor array. Auditory stimulation was generated outside the shielded room and transmitted through flexible, air-filled tubes into the shielded room. Stimulation was presented with a sound pressure level of 65 dB to the left ear using earphones especially developed for neonatal measurements (bio-logic, USA). Stimulation consisted of the random presentation of a 500 Hz tone ($n = 70$), a 750 Hz tone ($n = 70$), and WN ($n = 70$). The stimulus duration was 0.5 s for the 500 Hz tone and the 750 Hz tone and 1 s for the "WN" (80–1000 Hz) segments. The inter-stimulus interval (ISI) between stimulus presentations varied randomly between 2 and 2.5 s. The pure stimulation duration was 8 min (**Figure 1**).

All neonates/infants were measured while sleeping or lying quietly. During the whole measurement, one parent was inside the shielded room with the baby.

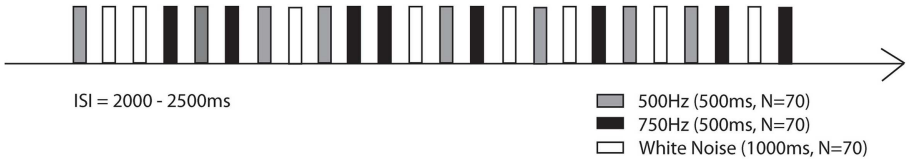

FIGURE 1 | Stimulation paradigm of the first part of the study (Tuebingen).

For the fetal measurements, the same paradigm was applied. Stimulation was presented using an air-filled balloon, which was placed directly on the maternal abdomen. Stimulation intensity was 95 dB, which is attenuated by maternal tissue and amniotic fluid and which the fetus may perceive at a level of approximately 65–70 dB (Querleu et al., 1988).

PARTICIPANTS FROM LITTLE ROCK STUDY (SECOND PART)

Twelve healthy pregnant women with uncomplicated pregnancies and normally developing fetuses ($M_{age} = 25.7$ weeks GA, SD $\pm$ 2.4) and six healthy newborns and infants without complications during pregnancy and birth ($M_{age} = 23$ days and SD $\pm$ 6.2) participated in the study. The local ethical committee approved the study and a written consent was obtained.

PROTOCOL USED IN LITTLE ROCK STUDY (SECOND PART)

Auditory stimulation was generated outside the shielded room and the stimuli were delivered to the inside of the shielded room through Tygon tubing that ended with an air-filled bag. Similar to the first paradigm, for the neonatal measurements a cradle was attached to the fMEG device and neonates/infants were lying on their side with one hemisphere over the sensor array. Stimulation was presented with a sound pressure level of 65 dB at the end of the acoustic emitter, which was attached to the ceiling at a distance of approximately 75 cm from the newborn's head. The stimulation paradigm consisted of two oddball conditions in which a 500 Hz tone, attenuated WN and WN were either standards (probability of 0.8, presented for 560 times) or deviant sounds (each type with a probability of 0.1, presented for 70 times) (see **Figure 2**). Total number of presented stimuli was 700. The stimulus duration was 0.1 s. The ISI was 1 s. The total stimulation duration was about 17 min per condition. All neonates were measured while sleeping or lying quietly. During the measurement, one parent was inside the shielded room with the baby.

For fetal measurements, the same paradigm was used. Sound intensity measured at the end of the tube in the air was 115 dB for the 500 Hz tones as well as for the WN segments. For the attenuated WN segments the sound intensity at the end of the tube was 95 dB.

DATA ANALYSIS

All fMEG recordings were filtered offline using a bandpass filter between 1 and 10 Hz for fetal recordings and between 1 and 15 Hz for neonatal recordings using Butterworth filter with zero phase distortion. Interfering maternal and fetal cardiac signals were attenuated using an orthogonal signal space projection technique (Vrba et al., 2004; McCubbin et al., 2006) or a Hilbert transform method (Wilson et al., 2008). Data was cut in segments according to the test stimulus; the length of the segments was 200 ms before the stimulus (baseline) and 800 ms after the stimulus. All segments including artifacts due to maternal or fetal movement or muscle contractions higher than 2 pT were excluded from further analysis. Evoked responses were determined by visual inspection and quantified by calculating the root-mean squares (RMS) of the five channels with the highest amplitudes. These RMS were used for statistical analysis.

STATISTICAL ANALYSIS

For the Tuebingen Study, the RMSs of all conditions were tested for normal distribution. For normally distributed data, a repeated-measures ANOVA with "tones" as within-subject factor was used to test for main effects and paired t-tests were used for *post hoc* comparisons. For non-normally distributed data, the non-parametric Friedman test was used to test for main effects. Significance levels were adjusted for multiple comparisons using Bonferroni correction.

Due to the explorative nature and the small sample size of the Little Rock study, the statistical analysis of this part had to be limited to descriptive indices and non-parametric comparative tests.

RESULTS

RESULTS FROM TUEBINGEN STUDY (FIRST PART)

Neonatal/infant recordings

Fifteen neonates/infants were excluded from further analysis because either no measurement was possible due to movement/crying or because measurements had to be aborted due to agitation of the neonate/infant. Statistical analysis has been done on the remaining 13 datasets ($M_{age} = 34.08$ days, SD $\pm$ 15.18).

A significant main effect of tones was observed ($F = 11.45$, $p < 0.05$). *Post hoc* analysis revealed significant differences between the 500 Hz tone and WN ($T_{12} = -3.82$, $p < 0.0167$) and the 750 Hz tone and WN ($T_{12} = -3.22$, $p < 0.0167$). No significant differences between the 500 Hz tone and the 750 Hz tone were observed ($T_{12} = -1.05$, $p = 0.317$, see **Figure 3**).

Fetal recordings

Eleven fetuses were excluded from further analysis because they did not show visible evoked responses for all three conditions. All further analysis is based on the remaining 14 fetuses ($M_{age} = 34.57$, SD ≤ 2.34).

No significant main effect of tones was found for fetal recordings ($\chi^2 = 2.71$, $p = 0.26$, see **Figure 4**).

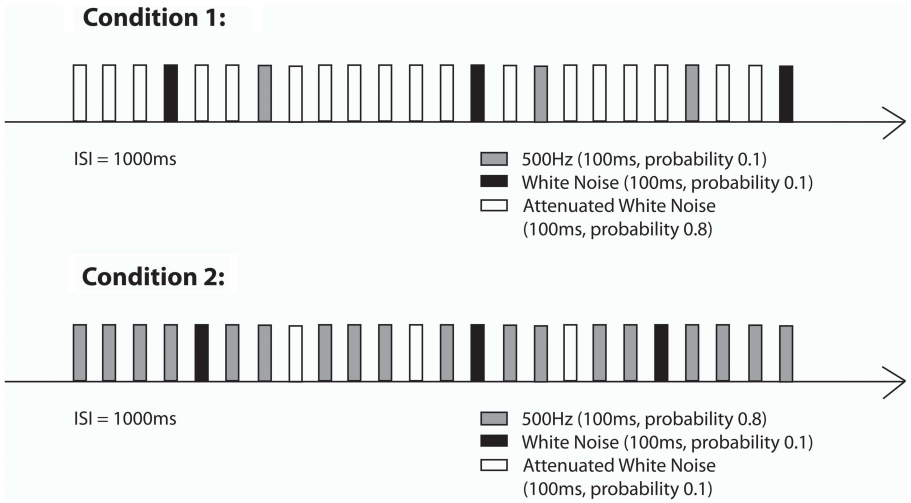

FIGURE 2 | Stimulation paradigms (Condition 1 and Condition 2) of the second part of the study (Little Rock).

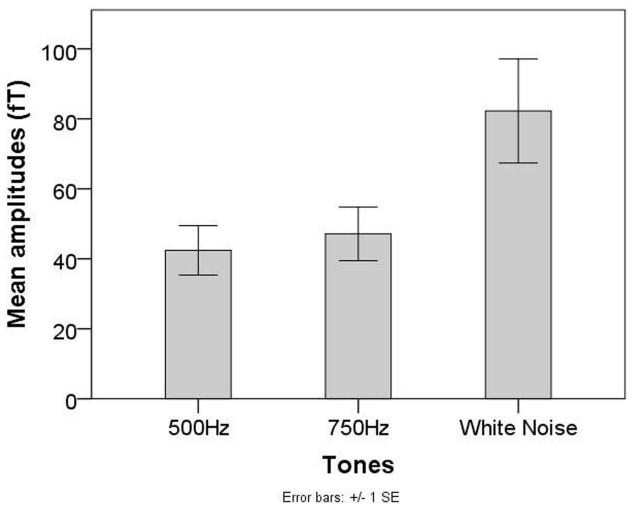

FIGURE 3 | Mean AER amplitudes for the 500 Hz, 750 Hz, and WN stimuli in the group of neonates/infants of the Tuebingen study.

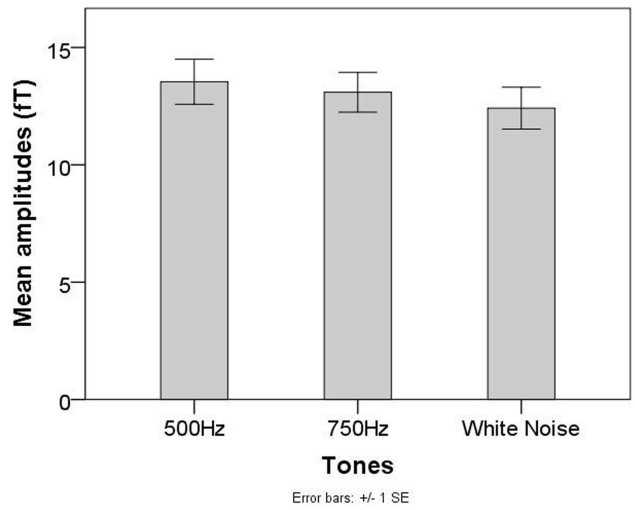

FIGURE 4 | Mean AER amplitudes for the 500 Hz, 750 Hz, and WN stimuli in the group of fetuses of the Tuebingen study.

RESULTS FROM LITTLE ROCK STUDY (SECOND PART)

Neonatal/infant recordings

One out of six neonatal/infant recordings was excluded from the analysis because it was stopped within the first 5 min of the measurement due to newborn crying. The RMS values of the amplitudes of the AERs for the neonates are shown in **Table 1**.

Mean RMS value for the WN segments in the first oddball condition ($M = 37.7$, SD $\pm$ 5.6) was higher than the mean of the RMS values for the 500 Hz tones ($M = 28.7$, SD $\pm$ 9.2). The same was true for the second condition between the amplitudes of the WN segments ($M = 40.6$, SD $\pm$ 18.3) and those of the attenuated WN segments ($M = 27.8$, SD $\pm$ 0.04). Wilcoxon signed ranked tests showed significant differences ($Z = 3.7$, $p < 0.05$) between the median amplitudes of the AERs to the WN and those to the attenuated WN segments as well as between the amplitudes of the cortical responses to the WN and those to the 500 Hz tones of the second condition ($Z = 2.02$, $p < 0.05$).

Fetal recordings

Two out of 12 fetal recordings were excluded from further analysis based on maternal movements and large maternal and fetal heart residuals. AERs on the deviants were detected in 8 out of 10 fetuses in the first oddball condition and in 5 out of 10 fetuses in the second one. Amplitudes of the AERs elicited by infrequent WN segments were not significantly different than those elicited by the infrequent 500 Hz tones ($Z = -0.70$, $p = 0.48$). The difference between RMS values of AERs elicited by infrequent WN segments

Table 1 | RMS values of the neonatal AERs for both oddball conditions applied in the second stimulation paradigm.

Subject	First oddball condition		Second oddball condition	
RMS	WN (fT)	500 Hz (fT)	WN (fT)	WN attenuated (fT)
WN01	30.70	14.99	17.90	11.49
WN02	33.50	27.30	30.70	26.40
WN03	42.20	29.20	67.10	29.32
WN04	38.00	31.10	42.30	35.68
WN05	44.00	40.70	45.00	36.20

and those elicited by infrequent attenuated WN segments showed a tendency toward significance ($Z = -1.8$, $p = 0.08$).

DISCUSSION

The current study aimed to use a simplified paradigm to replicate the increased neonatal reaction to WN stimuli which was already found by Kushnerenko et al. (2007). Moreover, WN segments were used for the first time in fetal recordings to investigate if the human brain is able to detect changes in the spectral width of auditory stimulation during fetal period. An oddball paradigm including changes in volume and spectral width was used to further investigate fetal change detection.

Results of the first paradigm showed, that even when using a simple paradigm wherein pure tones and WN segments were presented in random order with the same probability, infants showed significantly higher reactions to the WN segments than to the pure tones. This replicates prior results showing that infants are sensitive to the effective amount of stimulation with higher reactions to high-energy stimulation (in this case high spectral width) and lower reactions to low-energy stimulation (Kushnerenko et al., 2007). Also earlier behavioral studies support these findings (Lewkowicz and Turkewitz, 1980). Even though our results are in line with other studies, it has to be taken into account that the duration of the WN segments was longer than that of pure tones in the current study. Therefore, the higher reaction to the WN segments might partly be explained by the change in duration rather than in spectral width. However, when studying change detection using a multiple deviant paradigm, Sambeth et al. (2009) found no significant differences between amplitudes of the reaction to standards and duration deviants using magnetoencephalography. This indicates that a change in tone duration plays only a minor role concerning the increment of AER amplitudes. Our results from the second paradigm further support this finding. Neonatal/infant cortical responses to WN segments showed significantly higher amplitudes when compared to pure tones and attenuated WN segments of the same duration. Nevertheless, additional data is needed to thoroughly address this question.

Different from neonates and infants, in both fetal paradigms stimuli consisting of multiple frequencies did not elicit AERs with higher amplitudes than pure tones. Special requirements for fetal measurements might be one important factor concerning the evaluated group differences between neonates and fetuses. While neonates can be stimulated directly at the ear with sounds transmitted through the air, fetal stimulation takes place outside the maternal abdomen. Since the fetus is surrounded by amniotic fluid, the characteristics of sound transmission are different than sound transmission in air. Different studies have been performed to evaluate sound attenuation in fetal measurements [Hepper and Shahidullah (1994) and references therein]. Using a hydrophone near the fetal head at the beginning of labor and after amniotomy, Querleu et al. (1988) recorded an attenuation of 2 dB at 250 Hz, 14 dB at 500 Hz, 20 dB at 1000 Hz, and 26 dB at 2000 Hz. Generally, higher frequencies are more attenuated than lower frequencies, which in some works are even reported to be slightly enhanced in volume (Richards et al., 1992). Since the WN segments in the current study were composed of frequencies in the range between 50 and 1000 Hz, which were all presented with the same sound pressure level, we assume that the higher frequencies were attenuated much more than the lower frequencies before they reached the fetal ear. Compared to neonates/infants who heard the full spectral width of WN segments, fetuses might have perceived only parts of the frequency range, narrowed down to lower and middle frequencies. In this case, due to a narrowed perceived spectral width, also the total energy of the stimulation would have been weakened, leading to AER amplitudes comparable with those of pure tones. Additionally to the differences in sound transmission between fetuses and neonates, the background noise differs between those groups. While neonates are stimulated in a quiet environment, fetuses are surrounded by background noises caused by the maternal heart beat, bowel movements or the maternal voice. Different studies reported background noise intensities of 72 dB measured during labor in the uterus (Bench, 1968), 85 dB measured before labor, and even 95 dB after the R-wave of the maternal heart (Walker et al., 1971). Since these background noises are of low frequencies, we believe that they might have superimposed and masked the lower frequency ranges of WN segments, leaving the higher frequencies nearly unaffected. Since the low frequencies are less attenuated but covered by the background noise, the perceived frequency range is additionally narrowed down. Even though learning studies in fetuses (Partanen et al., 2013a,b) clearly showed that fetuses are able to perceive and learn melodies and speech sounds, these studies did not focus on the effective amount of stimulation. Even if a high range of stimuli can be perceived when presented separately, no clear conclusion can be drawn concerning the frequencies perceived by the fetus when a broad range of frequencies are presented at the same time with the same intensity. Further research is needed to entirely solve this question.

Taken together, we assume that fetuses probably did not perceive the full frequency range of the WN stimulus, which weakened stimulus energy and made it less distinguishable from the pure tone stimuli. The results of the second study suggest that the neonates are sensitive to both spectral and volume changes, whereas the fetuses are rather sensitive to loudness change.

It has to be stressed that the two studies were performed with two separate systems for fMEG recordings and the results were comparable, providing further support for the fMEG as a reliable method to assess fetal brain development.

In summary, the current study showed that newborns are able to differentiate between pure tones and WN segments even in simple paradigms, where tones are randomly presented with the same probability. This enables shorter measurement times, which is an important point in neonatal measurements since movement artifacts are highly probable especially in long measurements. To

thoroughly evaluate fetal ability to distinguish between high- and low-energy stimulation, stimulation methods need to be developed which are not attenuated by the maternal abdomen and amniotic fluid and therefore ensure that the fetus receives the complete spectrum of the WN.

AUTHORS CONTRIBUTION

Jana Muenssinger was involved in the development of the design, data acquisition and analysis, statistical analysis, and wrote the manuscript. Tamara Matuz was involved in the development of the design, data acquisition and analysis, statistical analysis, and writing of the manuscript. Franziska Schleger was involved in data acquisition and analysis and revised the manuscript. Rossitza Draganova was involved in the data analysis and revised the manuscript. Magdalene Weiss was involved in the recruitment of subjects, data acquisition, and revised the manuscript. Isabelle Kiefer-Schmidt and Annette Wacker-Gussmann were involved in the recruitment of subjects and revised the manuscript. Rathinaswamy B. Govindan was involved in the development of the paradigm, data analysis, and revised the manuscript. Curtis L. Lowery was involved in the conceptual design of the study and revised the manuscript. Hari Eswaran was involved in designing the study, analyzing and interpreting results, and revised the manuscript. Hubert Preissl was involved in the development of the design, data analysis and revised the manuscript.

ACKNOWLEDGMENTS

We thank all families for their participation. The fetal MEG and the authors in Tuebingen were supported by the Deutsche Forschungsgemeinschaft (DFG BI 195-50), the Ministry of Science, Baden-Württemberg, the Werner Reichardt Center for Integrative Neuroscience (CIN, Pool-Project 2009–2013) and the Open Access Publishing Fund of Tuebingen University (provided by the "Deutsche Forschungsgemeinschaft"). The Little Rock study was partially supported by grants from the National Institutes of Health (NIH) R01EB007826 and 5R01NS036277-03, USA.

REFERENCES

Bench, J. (1968). Sound transmission to the human foetus through the maternal abdominal wall. *J. Genet. Psychol.* 113, 85–87. doi:10.1080/00221325.1968.10533811

Carral, V., Huotilainen, M., Ruusuvirta, T., Fellman, V., Näätänen, R., and Escera, C. (2005). A kind of auditory 'primitive intelligence' already present at birth. *Eur. J. Neurosci.* 21, 3201–3204. doi:10.1111/j.1460-9568.2005.04144.x

Draganova, R., Eswaran, H., Murphy, P., Huotilainen, M., Lowery, C., and Preissl, H. (2005). Sound frequency change detection in fetuses and newborns, a magnetoencephalographic study. *Neuroimage* 28, 354–361. doi:10.1016/j.neuroimage.2005.06.011

Draganova, R., Eswaran, H., Murphy, P., Lowery, C., and Preissl, H. (2007). Serial magnetoencephalographic study of fetal and newborn auditory discriminative evoked responses. *Early Hum. Dev.* 83, 199–207. doi:10.1016/j.earlhumdev.2006.05.018

Fellman, V., Kushnerenko, E., Mikkola, K., Ceponiene, R., Leipälä, J., and Näätänen, R. (2004). Atypical auditory event-related potentials in preterm infants during the first year of life: a possible sign of cognitive dysfunction? *Pediatr. Res.* 56, 291–297. doi:10.1203/01.PDR.0000132750.97066.B9

Hepper, P. G., and Shahidullah, B. S. (1994). Development of fetal hearing. *Arch. Dis. Child.* 71, F81–F87. doi:10.1136/fn.71.2.F81

Huotilainen, M., Kujala, A., Hotakainen, M., Parkkonen, L., Taulu, S., Simola, J., et al. (2005). Short-term memory functions of the human fetus recorded with magnetoencephalography. *Neuroreport* 16, 81–84. doi:10.1097/00001756-200501190-00019

Huotilainen, M., Kujala, A., Hotakainen, M., Shestakova, A., Kushnerenko, E., Parkkonen, L., et al. (2003). Auditory magnetic responses of healthy newborns. *Neuroreport* 14, 1871–1875. doi:10.1097/00001756-200310060-00023

Kushnerenko, E., Ceponiene, R., Balan, P., Fellman, V., and Näätänen, R. (2002). Maturation of the auditory change detection response in infants: a longitudinal ERP study. *Neuroreport* 13, 1843–1848. doi:10.1097/00001756-200210280-00002

Kushnerenko, E., Winkler, I., Horvath, J., Naatanen, R., Pavlov, I., Fellman, V., et al. (2007). Processing acoustic change and novelty in newborn infants. *Eur. J. Neurosci.* 26, 265–274. doi:10.1111/j.1460-9568.2007.05628.x

Leppänen, P., Pikho, E., Eklund, K. M., and Lyytinen, H. (1999). Cortical responses of infants with and without a genetic risk for dyslexia: II. Group effects. *Neuroreport* 10, 969–973. doi:10.1097/00001756-199904060-00014

Lewkowicz, D. J., and Turkewitz, G. (1980). Cross-modal equivalence in early infancy: auditory – visual intensity matching. *Dev. Psychol.* 16, 597–607. doi:10.1037/0012-1649.16.6.597

McCubbin, J., Robinson, S. E., Cropp, R., Moiseev, A., Vrba, J., Murphy, P., et al. (2006). Optimal reduction of MCG in fetal MEG recordings. *IEEE Trans. Biomed. Eng.* 53, 1720–1724. doi:10.1109/TBME.2006.876619

Näätänen, R. (2001). The perception of speech sounds by the human brain as reflected by the mismatch negativity (MMN) and its magnetic equivalent (MMNm). *Psychophysiology* 38, 1–21. doi:10.1111/1469-8986.3810001

Partanen, E., Kujala, A., Tervaniemi, M., and Huotilainen, M. (2013a). Prenatal music exposure induces long-term neural effects. *PLoS ONE* 8:e78946. doi:10.1371/journal.pone.0078946

Partanen, E., Kujala, T., Näätänen, R., Liitola, A., Sambeth, A., and Huotilainen, M. (2013b). Learning-induced neural plasticity of speech processing before birth. *Proc. Natl. Acad. Sci. U.S.A.* 110, 15145–15150. doi:10.1073/pnas.1302159110

Querleu, D., Renard, X., Versyp, F., Paris-Delrue, L., and Crepin, G. (1988). Fetal hearing. *Eur. J. Obstet. Gynecol. Reprod. Biol.* 28, 191–212. doi:10.1016/0028-2243(88)90030-5

Richards, D. S., Frentzen, B., Gerhardt, K. J., McCann, M. E., and Abrams, R. M. (1992). Sound Levels in the Human Uterus. *Obstet. Gynecol.* 80, 186–190.

Sambeth, A., Pakarinen, S., Ruohio, K., Fellman, V., Van Zuijen, T. L., and Huotilainen, M. (2009). Change detection in newborns using a multiple deviant paradigm: a study using magnetoencephalography. *Neurophysiol. Clin.* 120, 530–538. doi:10.1016/j.clinph.2008.12.033

Turkewitz, G., Lewkowicz, D. J., and Gardner, J. M. (1983). "Determinants of infant perception," in *Advances in the Study of Behavior*, eds C. Rosenblatt, C. Beer, R. Hinde, and M. Busnel (New York: Academic Press), 39–62.

Vrba, J., Robinson, S. E., McCubbin, J., Lowery, C. L., Eswaran, H., Wilson, J. D., et al. (2004). Fetal MEG redistribution by projection operators. *IEEE Trans. Biomed. Eng.* 51, 1207–1218. doi:10.1109/TBME.2004.827265

Walker, D., Grimwade, J., and Wood, C. (1971). Intrauterine noise: a component of the fetal environment. *Am. J. Obstet. Gynecol.* 109, 91–95.

Wilson, J. D., Govindan, R. B., Hatton, J. O., Lowery, C. L., and Preissl, H. (2008). Integrated approach for fetal QRS detection. *IEEE Trans. Biomed. Eng.* 55, 2190–2197. doi:10.1109/TBME.2008.923916

Conflict of Interest Statement: The authors declare that the research was conducted in the absence of any commercial or financial relationships that could be construed as a potential conflict of interest.

Received: 01 October 2013; paper pending published: 13 October 2013; accepted: 15 December 2013; published online: 31 December 2013.
Citation: Muenssinger J, Matuz T, Schleger F, Draganova R, Weiss M, Kiefer-Schmidt I, Wacker-Gussmann A, Govindan RB, Lowery CL, Eswaran H and Preissl H (2013) Sensitivity to auditory spectral width in the fetus and infant – an fMEG study. Front. Hum. Neurosci. 7:917. doi: 10.3389/fnhum.2013.00917
This article was submitted to the journal Frontiers in Human Neuroscience.

frontiers in
HUMAN NEUROSCIENCE

ORIGINAL RESEARCH ARTICLE
published: 15 November 2013
doi: 10.3389/fnhum.2013.00791

Region-specific slowing of alpha oscillations is associated with visual-perceptual abilities in children born very preterm

Sam M. Doesburg[1,2,3,4]*, Alexander Moiseev[5], Anthony T. Herdman[5,6], Urs Ribary[5,7,8,9] and Ruth E. Grunau[8,9]

[1] Department of Diagnostic Imaging, The Hospital for Sick Children, Toronto, ON, Canada
[2] Neurosciences & Mental Health Program, Research Institute, The Hospital for Sick Children, Toronto, ON, Canada
[3] Department of Medical Imaging, University of Toronto, Toronto, ON, Canada
[4] Department of Psychology, University of Toronto, Toronto, ON, Canada
[5] Behavioral and Cognitive Neuroscience Institute, Simon Fraser University, Burnaby, BC, Canada
[6] Department of Audiology and Speech Sciences, The University of British Columbia, Vancouver, BC, Canada
[7] Department of Psychology, Simon Fraser University, Burnaby, BC, Canada
[8] Developmental Neurosciences and Child Health, Child and Family Research Institute, Vancouver, BC, Canada
[9] Department of Pediatrics, The University of British Columbia, Vancouver, BC, Canada

Edited by:
Christos Papadelis, Boston Children's Hospital, USA; Harvard Medical School, USA

Reviewed by:
Paul Sauseng, University of Surrey, UK
Stephanie Jones, Brown University, USA

***Correspondence:**
Sam M. Doesburg, Department of Diagnostic Imaging, The Hospital for Sick Children, 555 University Avenue, Toronto, ON M5G 1X8, Canada
e-mail: sam.doesburg@sickkids.ca

Children born very preterm (≤32 weeks gestational age) without major intellectual or neurological impairments often express selective deficits in visual-perceptual abilities. The alterations in neurophysiological development underlying these problems, however, remain poorly understood. Recent research has indicated that spontaneous alpha oscillations are slowed in children born very preterm, and that atypical alpha-mediated functional network connectivity may underlie selective developmental difficulties in visual-perceptual ability in this group. The present study provides the first source-resolved analysis of slowing of spontaneous alpha oscillations in very preterm children, indicating alterations in a distributed set of brain regions concentrated in areas of posterior parietal and inferior temporal regions associated with visual perception, as well as prefrontal cortical regions and thalamus. We also uniquely demonstrate that slowing of alpha oscillations is associated with selective difficulties in visual-perceptual ability in very preterm children. These results indicate that region-specific slowing of alpha oscillations contribute to selective developmental difficulties prevalent in this population.

Keywords: preterm, magnetoencephalography, neural oscillation, development, resting state, alpha-band, perception, cognition

INTRODUCTION

Children born very prematurely, even in the absence of brain injury and when intelligence is broadly normal, often experience selective developmental difficulties including problems with visual-perceptual abilities (Rickards et al., 2001; Grunau et al., 2002; Atkinson and Braddick, 2007). The biological basis of these issues remains poorly understood. MR imaging has identified numerous structural and functional atypicalities in very preterm children, many of which have been associated with problems in cognitive and perceptual development (Hart et al., 2008; Ment et al., 2009; Miller and Ferriero, 2009). An approach to understanding preterm child brain development which has received somewhat less attention is the mapping of neural oscillations using magnetoencephalography (MEG). MEG is a neurophysiological imaging modality that is particularly effective for characterizing the development of functional brain systems due to its unique combination of spatial and temporal resolution (Hari and Salmelin, 1997), and has been successfully employed to image brain activation in specific cortical systems in preterm infants and children (Nevalainen et al., 2008; Frye et al., 2010). Neural oscillations are known to be critical for brain activity and network connectivity supporting cognition and perception (Joliot et al., 1994; Varela et al., 2001; Ward, 2003; Ribary, 2005; Uhlhaas et al., 2009a), and are altered in many clinical populations (Llinás et al., 1999; Schnitzler and Gross, 2005; Uhlhaas et al., 2009a), including those affecting child development (Murias et al., 2007; Mazaheri et al., 2010). Both spontaneous neural oscillations and their test-dependent dynamics develop throughout childhood and infancy (Clarke et al., 2001; Uhlhaas et al., 2009b; Xiang et al., 2009), including during the developmental epoch corresponding to very premature birth (Okumura et al., 2006; Gonzalez et al., 2011), and are relevant for the maturation of functional brain networks (Uhlhaas et al., 2010). Spontaneous cortical oscillations are characterized by a distinct peak in the alpha-band, and progressive increases in the frequency of spontaneous brain oscillations have been identified as a reliable marker of childhood neurodevelopment (John et al., 1980). Such developmental acceleration in alpha-band oscillations can be reliably measured using MEG. For example, maturational increases in the peak frequency of the mu rhythm have been reported in infants and school-age children (Berchicci et al., 2011) and deviations from typical patterns of spontaneous oscillations often indicate learning disabilities or increased risk for neurological disorders (Ahn et al., 1980).

Using MEG, we previously demonstrated that spontaneous alpha oscillations (8–14 Hz) in school-age children born very preterm are slowed (Doesburg et al., 2011a). Atypical spontaneous alpha oscillations were also found to be associated with poor visual-perceptual abilities, and linked to extensive neonatal procedural pain, in children born at extremely low gestational age (Doesburg et al., 2013a). Such persistent alterations in the spectral structure of spontaneous brain oscillations may contribute to life-long cognitive difficulties in this group, as adults born at extremely low birth weight express altered ratio of high-frequency to low-frequency oscillations (Miskovic et al., 2009). Pronounced differences in long-range alpha-band MEG connectivity have also been identified in very preterm children during the performance of a visual short-term memory task, and these alterations were associated with selective visuospatial difficulties in this group (Doesburg et al., 2011b). Together, these findings indicate that spontaneous oscillations are slowed in very preterm children, and cortical alpha-band connectivity dynamics supporting task processing are not typically expressed in this group. Our previous research has indicated that altered alpha oscillations are strongly related to selective difficulties with visual-perceptual abilities in very preterm children, rather than to general intellectual ability (Doesburg et al., 2011b, 2013a).

Previous studies of altered MEG alpha oscillations in very preterm children and their relation to cognitive development have analyzed data at the sensor level (Doesburg et al., 2011a,b, 2013a), which does not reveal the contribution of specific brain regions, thus limiting interpretation of the underlying functional systems involved. In the present study we investigated slowing of alpha oscillations in very preterm children within specific brain regions and examined their relation to difficulties in visual-perceptual abilities. To this end, we recorded spontaneous-eyes-open MEG activity from a group of school-age children born very preterm and full-term control children. Beamformer source analysis was employed to reconstruct brain activity from 72 locations distributed throughout the brain. These locations were predicated on an anatomical brain parcellation scheme in order to estimate activity within multiple functionally distinct brain regions. Peak oscillatory frequency was obtained for each analyzed brain region and compared with neuropsychological assessments.

MATERIALS AND METHODS

SUBJECTS

Groups of 27 very preterm (≤32 weeks GA) children and 27 full-term controls were tested as part of a longitudinal study investigating the long-term impact of neonatal procedural pain on the neurocognitive development of very preterm children (i.e., Grunau et al., 2007, 2009). Full-term control children were recruited either through pediatricians in infancy or from the community at school-age. The groups were matched on age, sex, and handedness. Both groups comprised 17 girls and 8 boys. Children had been excluded if they were diagnosed with a major sensory (hearing, vision), motor, or cognitive impairment, or had periventricular leukomalacia (PVL) or grade III–IV intraventricular hemorrhage (IVH) on neonatal ultrasound according to Papile's classification (Papile et al., 1978). Following inspection of movement during the MEG scan, one very preterm child, and one full-term control child were excluded due to excessive motion. The resulting group of 26 preterm children (mean age 7.76 years; SD = 0.46 years) consisted of 8 boys and 16 girls; the group of 26 full-term controls (mean age 7.66 years; SD = 0.28 years) was comprised of 9 boys and 17 girls. Both groups contained 24 right handed children and 2 left handed children. The neonatal characteristics of the preterm group are presented in **Table 1**.

MEG RECORDING

Two minutes of spontaneous-eyes-open MEG activity was recorded using a 151-channel whole-head CTF Omega system (CTF Systems, Coquitlam, BC, Canada). Subjects were supine during recording and were instructed to maintain visual fixation on a "happy face" stimulus which was presented 40 cm above their eyes. A research assistant accompanied each subject within the magnetically shielded room to monitor the subjects. Data were digitized continuously at 1200 Hz, stored offline for analysis, and subsequently downsampled to 600 Hz. Fiducial coils were attached at the nasion as well as the right and left preauricular points, and each was energized at a distinct high narrow-band frequency. T1 weighted volumetric MRI images were also collected (1.5 T). Due to practical limitations imposed by multimodal neuroimaging in special child populations, MRI images were not available for all subjects. For those subjects without usable MRIs, a substitute matching MRI was found using the NIH database. MRIs for 4 very preterm children and 22 typically developing controls were taken from the NIH pediatric database. To obtain matching MRIs for individual subjects several candidate volumetric MRIs were selected from the database based on small differences between MEG and candidate MRI fiducial points. A best-matching structural MRI was then fitted to the subject's digitized head surface manually.

MEG ANALYSIS

Head motion was corrected for by obtaining a dipole source solution for each fiducial coil 30 times/s throughout the recording of spontaneous activity. The MEG data were then transformed to a common position by performing an inverse solution, data rotation, and forward solution 30 times/s (Wilson et al., 2007). To investigate slowing and reduction in the magnitude of spontaneous alpha oscillations in preterm children, we reconstructed the activity of multiple brain regions. The regions of interest for the source reconstruction were based on an anatomical brain parcellation scheme (see Kötter and Wanke, 2005; Bezgin et al., 2008).

Table 1 | Neonatal characteristics of the very preterm group.

Gestational age (weeks)	29.82 (2.17)
Birth weight (g)*	1358.62 (402.68)
Singleton (# subjects)	18
Early illness severity (SNAP-II)*	10 (11)
Days on mechanical ventilation*	13 (7)
IVH (Grade I–II; # subjects)	2

**One very preterm child was recruited from outside the longitudinal cohort, excluding scores for certain neonatal variables.*

This approach was chosen because it provides multiple functionally distinct regions which are distributed throughout the brain, and because this approach was successfully employed by a MEG study of functional brain activity and its relation to cognition, from which the set of source locations used in the present study were obtained (Diaconescu et al., 2011). A list of each source location is provided in **Table 2**, and a depiction of each seed location in brain space is available in Doesburg et al. (2013b). Each subject's MRI was warped into a common Talairach space using SPM2. The 72 locations were then warped back into each individual's brain space.

To reconstruct the activity from each analyzed source location, a minimum variance beamformer method was employed (Sekihara et al., 2001). This method has been shown to be very effective in estimating activity of a given source while maximally attenuating signal contributions from all other sources, as well as removing ocular and non-ocular artifacts (Cheyne et al., 2006, 2007). Note that on the sensor level volume currents result in mixing of brain signals from various locations. Source space analysis mostly eliminates the effects of volume currents, because the latter are already taken into account in the beamformer solution. Theoretically, minimum variance beamformers assume that correlations between sources are small, which might pose a problem when synchronous activity of different brain regions is expected. Extensive study of this question has shown that in practice the adverse effects of source correlations on the reconstructed power are significant only if correlations are very strong (Sekihara et al., 2002). Moreover, the signal-to-noise ratio (SNR) also needs to be relatively high for the correlations to introduce significant issues, such as SNRs observed in averaged evoked responses in event-related experimental paradigms. More advanced methods which take correlations into account show that low SNRs (∼0.1), even when strong correlations exist (∼0.8), do not alter reconstructed power significantly (Moiseev et al., 2011; Moiseev and Herdman, 2013). In the case of oscillatory resting state activity, correlations are moderate and SNRs are relatively small. It is for these regions that beamformer techniques have been successfully applied to resting state MEG data in recent years, including in functional connectivity analyses (Gross et al., 2001; Brookes et al., 2011; Hillebrand et al., 2012).

Data reconstructed from each of the 72 source locations were then filtered at 1 Hz intervals from 1 to 60 Hz (passband $= f \pm 0.05f$, where f is the filter frequency), using the eegfilt function from the EEGLAB toolbox, a two-way least-squares FIR filter (Delorme and Makeig, 2004). These methods which has previously been effective for estimating the spectral content of oscillatory signals in M/EEG data (Doesburg et al., 2008, 2011a,b). Power was calculated at each frequency for each data point and sensor, and was subsequently averaged across all time points in the 120 s recording session. Peak oscillatory frequency for each brain region for each subject was defined as the frequency expressing maximum power between 5 and 20 Hz, which included the alpha-band (8–14 Hz), as well as other nearby frequencies. This wider frequency range was selected because peak frequencies of MEG oscillations in specific brain regions in atypically developing children have not been extensively studied. Given this, we did not wish to make strong *a priori* assumptions about frequency content in specific brain regions in very preterm children. Furthermore, slowing of alpha rhythms into the upper theta range has been reported in several other clinical populations (Llinás et al., 1999; Sarnthein et al., 2006; Sarnthein and Jeanmonod, 2007, 2008; Boord et al., 2008). These methods for determining peak oscillatory frequency in MEG data have been previously established (Doesburg et al., 2011a).

To test the hypothesis that peak oscillatory frequency is slowed in very preterm children without statistical challenges imposed by multiple comparisons, peak frequency was averaged across all 72 analyzed regions for each subject to obtain a global measure for each subject. Permutation testing was then used to test for global differences between the very preterm and full-term control groups (see Blair and Karniski, 1993). Permutation tests were one-tailed as the direction these effects were predicted from previous results (Doesburg et al., 2011a). Once global group differences were established we tested whether oscillatory slowing was present in each of the 72 analyzed brain regions. Since our goal at this stage of the analysis was to determine which set of regions contributed to the established global pattern of oscillatory slowing, and type II errors are as misleading as type I errors in determining which brain regions are involved in the global pattern and which are not, these tests were not corrected for multiple comparisons. The rationale for this is that the conservative nature of such corrections would likely underestimate the number of areas expressing atypical alpha oscillations and provide a distorted account of the location and extent of altered brain oscillations in very preterm children. Permutation tests were also used to evaluate regional between-group comparisons.

ASSOCIATIONS BETWEEN MEG ACTIVITY AND PSYCHOMETRIC DATA

Following MEG recording, all children underwent psychometric assessment using the Wechsler Intelligence Scale for Children, 4th Edn. (WISC-IV; Wechsler, 2003) and the Beery–Buktenica Developmental Test of Visual-Motor Integration, 5th Edn. (Beery et al., 2004), administered by a psychometrician. For the present study, we elected to focus on visual-perceptual abilities as previous studies have indicated that altered alpha oscillations in preterm children are strongly associated with visual-perceptual difficulties (Doesburg et al., 2011b, 2013a). The visual perception subscale of the Beery VMI was chosen as an index of visual-perceptual ability, as it has proven to be a sensitive measure in previous studies (Doesburg et al., 2011b, 2013a). The Motor Coordination and Visual-Motor Integration Subscales of the Beery VMI and Full-Scale IQ (FSIQ) from the WISC-IV were also evaluated in relation to the MEG data in order to assess the specificity of relations between altered alpha oscillations and functional abilities in very preterm children, consistent with methods employed in previous research (Doesburg et al., 2011a).

Correlations were examined between each of these psychometric measures, within both the very preterm and full-term groups, and peak oscillatory frequency for each brain region that exhibited slowing. Statistical analysis of correlations between oscillatory slowing and psychometric data were controlled for multiple comparisons using the False Discovery Rate (FDR; see Storey, 2002). The approach taken to multiple comparisons here differs from that in the regional analysis of oscillatory slowing because correlations among oscillatory brain activity and psychometric measures aim

Table 2 | Each source location used in the analysis of spontaneous MEG activity, together with associated Brodmann area and Talairach coordinates.

Source	BA	Hemisphere	X	Y	Z
Anterior cingulate cortex	32	Midline	0	32	24
Posterior cingulate cortex	23	Midline	0	−32	24
Retrosplenial cingulate cortex	30	Midline	0	−48	12
Subgenual cingulate cortex	25	Midline	0	16	−8
A1 (primary auditory)		Left	−40	−14	4
A2 (secondary auditory)	22	Left	−60	−14	4
Frontal eye fields	6	Left	−36	8	56
Anterior insula	13	Left	−36	16	−4
Claustrum		Left	−36	−8	−4
M1 (primary motor)	4	Left	−24	−24	56
Inferior parietal cortex	40	Left	−44	−48	20
Angular gyrus	39	Left	−44	−64	28
Precuneus	7	Left	−8	−64	54
Superior parietal cortex	7	Left	−28	−56	54
Centrolateral prefrontal cortex	46	Left	−48	32	12
Dorsolateral prefrontal cortex	9	Left	−48	36	32
Dorsomedial prefrontal cortex	8	Left	−8	36	40
Medial prefrontal cortex	10	Left	−8	48	20
Orbitofrontal cortex	11	Left	−24	44	−20
Frontal polar	10	Left	−24	64	4
Ventrolateral prefrontal cortex		Left	−48	32	−8
Parahippocampal cortex		Left	−28	−16	−16
Dorsolateral premotor cortex	6	Left	−28	0	60
Medial premotor cortex	6	Left	−4	0	60
Ventrolateral premotor cortex	9	Left	−44	4	24
Pulvinar		Left	−16	−28	4
S1 (primary somatosensory)	3	Left	−40	−28	64
S2 (secondary somatosensory)	43	Left	−56	−16	16
Middle temporal cortex	21	Left	−64	−24	−12
Inferior temporal cortex	20	Left	−64	−24	−24
Temporal pole	38	Left	−52	12	−28
Superior temporal cortex	22	Left	−52	−4	−8
Ventral temporal cortex		Left	−32	−28	−28
Thalamus (ventral lateral nucleus)		Left	−8	−8	4
V1 (primary visual)		Left	−4	−84	−4
V2 (secondary visual)		Left	−4	−96	8
Cuneus	18	Left	−20	−88	20
Fusiform gyrus	19	Left	−20	−84	−12
A1 (primary auditory)		Right	40	−14	4
A2 (secondary auditory)	22	Right	60	−14	4
Frontal eye fields	6	Right	36	8	56
Anterior insula	13	Right	36	16	−4
Claustrum		Right	36	−8	−4
M1 (primary motor)	4	Right	24	−24	56
Inferior parietal cortex	40	Right	44	−48	20
Angular gyrus	39	Right	44	−64	28
Precuneus	7	Right	8	−64	54
Superior parietal cortex	7	Right	28	−56	54
Centrolateral prefrontal cortex	46	Right	48	32	12
Dorsolateral prefrontal cortex	9	Right	48	36	32
Dorsomedial prefrontal cortex	8	Right	8	36	40
Medial prefrontal cortex	10	Right	8	48	20
Orbitofrontal cortex	11	Right	24	44	−20
Frontal polar	10	Right	24	64	4
Ventrolateral prefrontal cortex		Right	48	32	−8
Parahippocampal cortex		Right	28	−16	−16
Dorsolateral premotor cortex	6	Right	28	0	60
Medial premotor cortex	6	Right	4	0	60
Ventrolateral premotor cortex	9	Right	44	4	24
Pulvinar		Right	16	−28	4
S1 (primary somatosensory)	3	Right	40	−28	64
S2 (secondary somatosensory)	43	Right	56	−16	16
Middle temporal cortex	21	Right	64	−24	−12
Inferior temporal cortex	20	Right	64	−24	−24
Temporal pole	38	Right	52	12	−28
Superior temporal cortex	22	Right	52	−4	−8
Ventral temporal cortex		Right	32	−28	−28
Thalamus (ventral lateral nucleus)		Right	8	−8	4
V1 (primary visual)		Right	4	−84	−4
V2 (secondary visual)		Right	4	−96	8
Cuneus	18	Right	20	−88	20
Fusiform gyrus	19	Right	20	−84	−12

Table adapted from Diaconescu et al. (2011).

to determine whether such relationships exist, rather than characterize the location and extent of phenomena which have already been established as statistically significant on a global level.

RESULTS

OSCILLATORY SLOWING IN CHILDREN BORN VERY PRETERM

Analysis of global peak oscillatory frequency (averaged across all 72 analyzed brain regions) revealed statistically significant slowing in school-age children born very prematurely ($p = 0.021$). Regional analysis of oscillatory slowing revealed that this pattern was widespread and encompassed prefrontal, temporal, and parietal areas, as well as aspects of thalamus and cingulate cortex. Complete results of the analysis of regional oscillatory slowing in very preterm children are presented in **Figure 1**. To summarize, slowing was widespread in bilateral temporal cortex, including bilateral in temporal areas implicated in the ventral visual processing stream (i.e., ventral and inferior temporal cortex). Parietal regions associated with visual processing were also implicated (i.e., bilateral inferior parietal cortex). Slowing was also present in secondary somatosensory cortex in both hemispheres, and also encompassed numerous in prefrontal regions (i.e., centrolateral, dorsolateral, ventrolateral, and orbitofrontal cortex).

OSCILLATORY SLOWING ASSOCIATED WITH REDUCED VISUAL-PERCEPTUAL ABILITY IN VERY PRETERM CHILDREN

Visual-perceptual ability, indexed by the visual perception subscale of the Beery VMI, was associated with oscillatory slowing

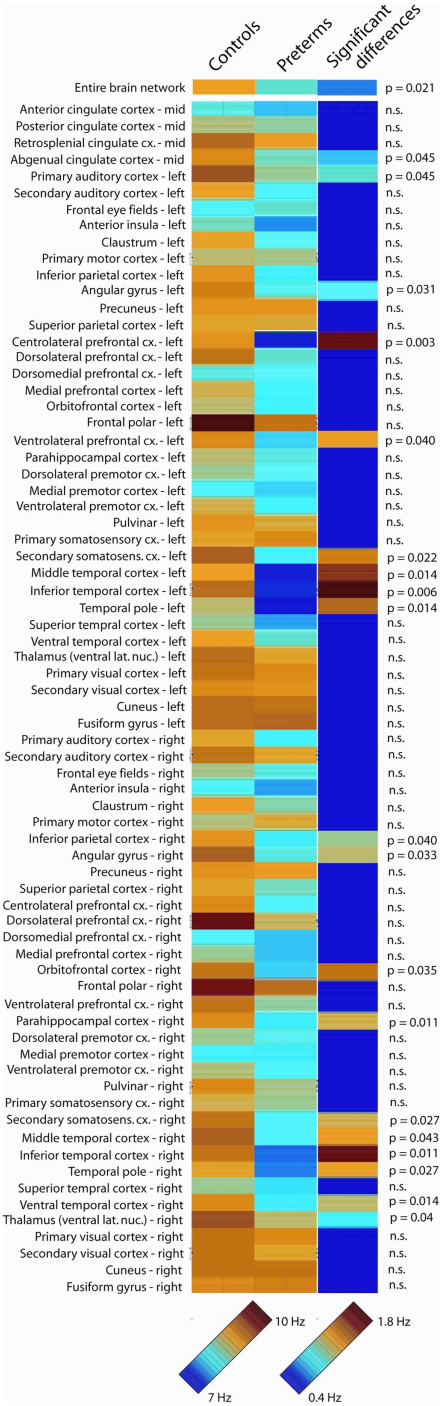

FIGURE 1 | Oscillatory slowing in very preterm children. Peak oscillatory frequency in each of the 72 analyzed brain regions for the full-term control and very preterm groups, as well as statistically significant regional slowing in children born very preterm. The 7- to 10-Hz scale bar corresponds to the peak oscillatory frequency for each analyzed region for the very preterm and typically developing groups. The 0.4- to 1.8-Hz scale bar indicates the difference in peak oscillatory frequency between the very preterm and typically developing groups for regions where statistically significant differences were observed (regions for which no significant group differences were observed are presented in dark blue).

in multiple regions, including several known to be involved in the processing of visual information including inferior parietal cortex, ventral temporal cortex, and thalamus. Regional slowing was not significantly associated with FSIQ or the Motor or Visual-Motor scores on the Beery VMI for the very preterm children. Peak oscillatory frequency was not associated with any of the psychometric tests for full-term children for any region. Complete results of the analysis of associations between regional oscillatory slowing and visual-perceptual ability in preterm children are provided in **Table 3**.

DISCUSSION

We provide the first source-resolved analysis of slowing of alpha oscillations in children born very preterm. Identification of the specific brain regions across thalamocortical systems involved in slowed alpha oscillations in very preterm children represents an important step, as altered alpha oscillations may mediate relations between neonatal procedural pain and cognitive outcome in children born at extremely low gestational age (Doesburg et al., 2013a), and alpha oscillations are particularly relevant for altered network connectivity underlying problems in visual-perceptual abilities in very preterm children (Doesburg et al., 2011b). We observed oscillatory slowing within multiple cortical regions encompassing bilateral temporal, parietal, and prefrontal cortical areas. Many regions expressing oscillatory slowing in preterm children are important for visual processing, including regions involved in both the dorsal visual system (i.e., inferior parietal cortex), and the ventral visual system (i.e., inferior temporal cortex, ventral temporal

Table 3 | Associations between slowing of peak oscillatory frequency and visual-perceptual ability, indexed by the visual perception subscore of the Beery VMI, in children born very preterm.

Source	Correlation coefficient	*P* value (FDR corrected)
Subgenual cingulate cortex (midline)	**0.44**	**0.028**
Primary auditory cortex (left)	n.s.	n.s.
Angular gyrus (left)	**0.53**	**0.019**
Centrolateral prefrontal cortex (left)	n.s.	n.s.
Ventrolateral prefrontal cortex (left)	n.s.	n.s.
Secondary somatosensory cortex (left)	n.s.	n.s.
Middle temporal cortex (left)	n.s.	n.s.
Inferior temporal cortex (left)	n.s.	n.s.
Temporal pole (left)	n.s.	n.s.
Inferior parietal cortex (right)	**0.44**	**0.037**
Angular gyrus (right)	n.s.	n.s.
Orbitofrontal cortex (right)	**0.44**	**0.031**
Parahippocampal cortex (right)	**0.47**	**0.038**
Secondary somatosensory cortex (right)	n.s.	n.s.
Middle temporal cortex (right)	n.s.	n.s.
Inferior temporal cortex (right)	n.s.	n.s.
Temporal pole (right)	n.s.	n.s.
Ventral temporal cortex (right)	**0.54**	**0.035**
Thalamus (right ventral lateral nucleus)	**0.45**	**0.038**

Significant correlations are presented in bold.

cortex). Slowing of alpha oscillations in preterm children was also prevalent in areas of prefrontal cortex involved in executive function (i.e., dorsolateral prefrontal cortex and orbitofrontal cortex).

The present study provides the first evidence that slowing of peak oscillatory frequency is associated with cognitive outcome in very preterm children. Oscillatory slowing was found to be selectively related to visual-perceptual ability, an area of selective developmental vulnerability in very preterm children (Rickards et al., 2001; Grunau et al., 2002; Taylor et al., 2004), and not associated with overall intellectual function, indexed by FSIQ. These results confirmed associations between slowing of alpha oscillations and visual-perceptual ability were typically, but not exclusively, found in regions involved in visual processing including inferior parietal cortex, angular gyrus, ventral temporal, cortex, and thalamus. There were no associations found between peak oscillatory frequency and neuropsychological ability in the full-term children, indicating that this phenomenon corresponds to neural mechanisms underlying selective developmental difficulties prevalent in very preterm children, rather than normal variance in childhood neurocognitive development.

Although not as prevalent as was observed for visual cortical regions, oscillatory slowing was also present in prefrontal cortical areas (i.e., ventrolateral prefrontal cortex and orbitofrontal cortex), congruent with earlier reports of slowed alpha oscillations over frontal MEG sensors (Doesburg et al., 2011a). This may be significant as executive functions are also an area of selective developmental difficulty prevalent in children born very prematurely (Anderson et al., 2004; Marlow et al., 2007; Mulder et al., 2009). Together with our results implicating region-specific slowing of alpha oscillations with selective difficulties in visual-perceptual abilities, the presence of atypical alpha rhythmicity in prefrontal brain regions in very preterm children suggests that region-specific slowing may be associated with developmental difficulties in executive function as well. Stated more generally, alpha slowing within a specific cortical region may be associated with reduced function in the corresponding psychological domain. In this view, specific cortical systems situated in posterior parietal, inferior temporal, and prefrontal regions may be selectively vulnerable to aspects of adverse neonatal experience, impacting the development of brain oscillations underlying the maturation of cognitive and perceptual functions associated with these areas (Benasich et al., 2008; Uhlhaas et al., 2009b, 2010) and causing selective developmental difficulties in the corresponding domains of executive function and visual-perceptual ability.

The perspective that oscillatory slowing is associated with impairment of normal brain function is consistent with observations of MEG slowing in association with neurological insults in other contexts. For example, regional analysis of excessive low-frequency oscillations has been introduced as a method for mapping abnormal functional brain activity following mild traumatic brain injury (Huang et al., 2012), and the anatomical focus of such excessive slow wave activity appears related to the location of white matter injury, measured using diffusion tensor imaging, in this population (Huang et al., 2009). Furthermore, slowing of peak alpha oscillatory frequency toward the theta range in resting state MEG recordings has been reported in diverse pathological conditions including Parkinson's disease, neurogenic pain, tinnitus, and major depression (Llinás et al., 1999). Subsequent combination of methods for the analysis of oscillatory slowing with MEG source analysis techniques have indicated that neuroanatomical systems involved in slowing depend on the pathological condition in question, and likely correspond to the nature of symptoms expressed (Schulman et al., 2011). This finding is consistent with the results of the present study which demonstrates that region-specific slowing of alpha oscillations in visual cortical regions are associated with visual-perceptual difficulties in children born preterm. Slowing of alpha oscillations in neuropathic pain has been confirmed using scalp EEG (Sarnthein et al., 2006; Boord et al., 2008). Slowing of alpha oscillations toward the theta range has also been reported using intracranial EEG in patients with neuropathic pain and Parkinson's disease (Sarnthein and Jeanmonod, 2007, 2008). Oscillatory alpha slowing in M/EEG recordings in numerous pathological conditions is thought to result from deafferentation, particularly in thalamocortical systems (Llinás et al., 2005), and it has been demonstrated that the parameters of alpha oscillations are related to white matter properties revealed using diffusion tensor imaging (Valdés-Hernández et al., 2010).

Slowing of alpha oscillations, together with the purported association of this phenomenon with the loss of integrity in structural brain connectivity, raises questions regarding relations between alpha oscillatory slowing and communication in brain networks. In particular, evidence increasingly indicates that coherence of alpha-band oscillations plays a critical role in communication among brain regions supporting cognition and perception (see Palva and Palva, 2007, 2012 for reviews). Recently, it has been reported that alpha-band oscillatory connectivity is reduced in preterm neonates with brain lesions (Tokariev et al., 2012). Alpha-band oscillatory connectivity during cognitive processing has been found to be slowed and reduced, and associated with selective difficulties in visual-perceptual ability, in very preterm children (Doesburg et al., 2011b). Moreover, this reduced alpha-band phase synchronization was observed in concert with increased interhemispheric theta-band synchronization in the very preterm children, suggesting that task-dependent interactions among brain regions may also be slowed. In light of the prevalence of white matter injury and atypical white matter development in this population (see Khwaja and Volpe, 2008; Miller and Ferriero, 2009), this raises the prospect that increased conduction delays among cortical regions may adversely impact the ability to recruit inter-regional oscillatory network coherence to support task performance.

The observation that slowing of alpha-band oscillations in very preterm children occurred in thalamus is also significant as animal research has demonstrated that thalamocortical mechanisms underlie the generation of alpha oscillations, as well as their slowing under pathological conditions (see Hughes and Crunelli, 2005 for review). Moreover, thalamocortical systems undergo critical phases of development during the gestational epoch corresponding to very premature birth (see Kostovic and Judaš, 2010 for review). The slowing of alpha oscillations, mediated by altered thalamocortical interactions, has been proposed to underlie disruptions of function in several neurological and neuropsychiatric populations (Llinás et al., 1999, 2005). Altered connectivity and white matter development are prevalent in children born very preterm (see Miller and Ferriero, 2009 for review), including

altered development of structural (Anjari et al., 2007; Dudink et al., 2007) and functional (Smyser et al., 2010) connectivity in thalamocortical systems. The importance of thalamus for understanding alterations in cortical development in preterm children is further underscored by recent findings that reduced thalamic volume is predictive of reduced cortical volume in preterm infants (Ball et al., 2012).

Our results showing significant slowing in deep brain structures such as the thalamus should be interpreted with caution. Reconstructing MEG signals from deep structures is not only difficult, but in many cases impossible because the SNR is too small (see Quraan et al., 2011). It should be noted, however, that in terms of power the alpha-band signal is the strongest in the brain, improving the likelihood of accurate source reconstruction in this frequency range (Attal et al., 2007). Moreover, prior MEG source analysis studies have reported task-dependent changes involving thalamus (i.e., Schnitzler et al., 2009). Further investigation will be needed to definitively determine the reliability of MEG measures of oscillations power from deep structures such as thalamus. Future research will also be required to examine relations between the structural and functional development of thalamocortical systems, disruption of the normative structure of cortical alpha oscillations, and functional outcomes in specific psychological domains in children who were born very prematurely. Involvement of specific regions identified in the source space analysis of oscillatory slowing in very preterm children should also be interpreted with some caution, as correction for multiple comparisons was not performed across all analyzed 72 regions. As such, potential false positives for individual regions may have arisen. The consistency of slowing located in regions involved in dorsal and ventral visual pathways, however, together with prefrontal cortical regions, is highly suggestive that region-specific slowing in brain structures is associated with selective developmental difficulties prevalent in children born very prematurely.

CONCLUSION

We demonstrate that slowing of spontaneous alpha oscillations is evident in widespread brain regions in very preterm children. These alterations of alpha oscillations were concentrated in regions involved in visual processing including thalamus, posterior parietal cortex, and interior temporal cortex, as well as in prefrontal regions relevant for executive functions. We provide the first evidence that slowing of spontaneous alpha oscillations is associated with functional outcome in preterm children. This association between slowing of alpha oscillations in particular brain regions and function was specific for visual-perceptual abilities, and was typically found in posterior parietal and inferior temporal brain regions implicated in visual processing. These results indicate that area-specific atypicalities in alpha oscillatory brain activity are associated with selective difficulties in children born very prematurely.

ACKNOWLEDGMENTS

We would like to thank Dr. Ivan Cepeda and Gisela Gosse for coordinating the study, Katia Jitlina, Amanda Degenhardt, Cecil Chau, Teresa Cheung, and Julie Unterman for their help in data collection. This work was supported by grant RO1 HD039783 from The Eunice Kennedy Shriver National Institute of Child Health and Human Development of the National Institutes of Health (NICHD/NIH) to Ruth E. Grunau, who received salary support from the Child and Family Research Institute (CFRI). Urs Ribary holds a BC LEEF Leadership Chair in Cognitive Neuroscience in Early Childhood Health and Development supported by the BC Leading Edge Endowment Fund (BC LEEF), and the MEG facility infrastructure was supported by the CFI grant to Urs Ribary and the Behavioral and Cognitive Neuroscience Institute (BCNI). Research support for Sam M. Doesburg is from the Natural Sciences and Engineering Research Council of Canada (NSERC RGPIN 435659) and the EpLink program of the Ontario Brain Institute (OBI).

REFERENCES

Ahn, H., Prichep, L., John, E. R., Baird, H., Trepetin, M., and Kaye, H. (1980). Developmental equations reflect brain dysfunctions. *Science* 210, 1259–1262. doi:10.1126/science.7434027

Anderson, P. J., Doyle, L. W., and Victorian Infant Collaborative Study Group. (2004). Executive functioning in school-aged children who were born very preterm or with extremely low birth weight in the 1990s. *Pediatrics* 114, 50–57. doi:10.1542/peds.114.1.50

Anjari, M., Srinivasan, L., Allsop, J. M., Hajnal, J. V., Rutherford, M. A., Edwards, A. D., et al. (2007). Diffusion tensor imaging with tract-based spatial statistics reveals local white matter abnormalities in preterm infants. *Neuroimage* 35, 1021–1027. doi:10.1016/j.neuroimage.2007.01.035

Atkinson, J., and Braddick, O. (2007). Visual and visuocognitive development in children born very prematurely. *Prog. Brain Res.* 164, 123–149. doi:10.1016/S0079-6123(07)64007-2

Attal, Y., Bhattacharjee, M., Yelnik, J., Cottereau, B., Lefevre, J., Okada, Y., et al. (2007). Modeling and detecting deep brain activity with MEG and EEG. *Conf. Proc. IEEE Eng. Med. Biol. Soc.* 2007, 4937–4940. doi:10.1109/IEMBS.2007.4353448

Ball, G., Boardman, J. P., Rueckert, D., Aljabar, P., Arichi, T., Merchant, N., et al. (2012). The effect of preterm birth on thalamic and cortical development. *Cereb. Cortex* 22, 1016–1024. doi:10.1093/cercor/bhr176

Beery, K. E., Buktenica, N. A., and Beery, N. A. (2004). *Beery–Buktenica Developmental Test of Visual-Motor Integration*, 5th Edn. San Antonio: Psychological Corporation.

Benasich, A. A., Gou, Z., Choudhury, N., and Harris, K. D. (2008). Early cognitive and language skills are linked to resting frontal gamma power across the first 3 years. *Behav. Brain Res.* 195, 215–222. doi:10.1016/j.bbr.2008.08.049

Berchicci, M., Zhang, T., Romero, L., Peters, A., Annett, R., Teuscher, U., et al. (2011). Development of mu rhythm in infants and preschool children. *Dev. Neurosci.* 33, 130–143. doi:10.1159/000329095

Bezgin, G., Wanke, E., Krumnack, A., and Kotter, R. (2008). Deducing logical relationships between spatially registered cortical parcellations under conditions of uncertainty. *Neural Netw.* 21, 1132–1145. doi:10.1016/j.neunet.2008.05.010

Blair, R. C., and Karniski, W. (1993). An alternative method for significance testing of waveform difference potentials. *Psychophysiology* 30, 518–524. doi:10.1111/j.1469-8986.1993.tb02075.x

Boord, P., Siddall, P. J., Tran, Y., Herbert, D., Middleton, J., and Craig, A. (2008). Electroencephalographic slowing and reduced reactivity in neuropathic pain following spinal cord injury. *Spinal Cord* 46, 118–123. doi:10.1038/sj.sc.3102077

Brookes, M. J., Hale, J. R., Zumer, J. M., Stevenson, C. M., Francis, S. T., Barnes, G. R., et al. (2011). Measuring functional connectivity using MEG: methodology and comparison with fcMRI. *Neuroimage* 56, 1082–1104. doi:10.1016/j.neuroimage.2011.02.054

Cheyne, D., Bakhtazad, L., and Gaetz, W. (2006). Spatiotemporal mapping of cortical activity accompanying voluntary movements using an event-related beamforming approach. *Hum. Brain Mapp.* 27, 213–229. doi:10.1002/hbm.20178

Cheyne, D., Bostan, A. C., Gaetz, W., and Pang, E. W. (2007). Event-related beamforming: a robust method for presurgical functional mapping using MEG. *Neurophysiol. Clin.* 118, 1691–1704. doi:10.1016/j.clinph.2007.05.064

Clarke, A. R., Barry, R. J., McCarthy, R., and Selikowitz, M. (2001). Age and sex effects in the EEG: development of the normal child. *Neurophysiol. Clin.* 112, 806–814. doi:10.1016/S1388-2457(01)00488-6

Delorme, A., and Makeig, S. (2004). EEGLAB: an open source toolbox for analysis of single-trial EEG dynamics. *J. Neurosci. Methods* 134, 9–21. doi:10.1016/j.jneumeth.2003.10.009

Diaconescu, A. O., Alain, C., and McIntosh, A. R. (2011). The co-occurrence of multisensory facilitation and cross-modal conflict in the human brain. *J. Neurophysiol.* 106, 2896–2909. doi:10.1152/jn.00303.2011

Doesburg, S. M., Chau, C. M., Cheung, T. P., Moiseev, A., Ribary, U., Herdman, A. T., et al. (2013a). Neonatal pain-related stress, functional cortical activity and school-age cognitive outcome in children born at extremely low gestational age. *Pain* 152, 1946–1952. doi:10.1016/j.pain.2013.04.009

Doesburg, S. M., Vidal, J., and Taylor, M. J. (2013b). Reduced theta connectivity during set-shifting in children with autism. *Front. Hum. Neurosci.* 7:785. doi:10.3389/fnhum.2013.00785

Doesburg, S. M., Emberson, L. L., Rahi, A., Cameron, D., and Ward, L. M. (2008). Asynchrony from synchrony: long-range gamma-band neural synchrony accompanies perception of audiovisual speech asynchrony. *Exp. Brain Res.* 18, 11–20. doi:10.1007/s00221-007-1127-5

Doesburg, S. M., Ribary, U., Herdman, A. T., Moiseev, A., Cheung, T., Miller, S. P., et al. (2011a). Magnetoencephalography reveals slowing of resting peak oscillatory frequency in children born very preterm. *Pediatr. Res.* 70, 171–175. doi:10.1038/pr.2011.396

Doesburg, S. M., Ribary, U., Herdman, A. T., Miller, S. P., Poskitt, K. J., Moiseev, A., et al. (2011b). Altered long-range alpha-band synchronization during visual short-term memory retention in children born very preterm. *Neuroimage* 54, 2330–2339. doi:10.1016/j.neuroimage.2010.10.044

Dudink, J., Lequin, M., van Pul, C., Buijs, J., Conneman, N., van Goudoever, J., et al. (2007). Fractional anisotropy in white matter tracts of very-low-birth-weight infants. *Pediatr. Radiol.* 37, 1216–1223. doi:10.1007/s00247-007-0626-7

Frye, R. E., Malmberg, B., McLean, J., Swank, P., Smith, K., Papanicolaou, A., et al. (2010). Increased left prefrontal activation during an auditory language task in adolescents born preterm at high risk. *Brain Res.* 1336, 89–97. doi:10.1016/j.brainres.2010.03.093

Gonzalez, J. J., Manas, S., De Vera, L., Mendez, L. D., Lopez, S., Garrido, J. M., et al. (2011). Assessment of electroencephalographic functional connectivity in term and preterm neonates. *Neurophysiol. Clin.* 122, 696–702. doi:10.1016/j.clinph.2010.08.025

Gross, J., Kujala, J., Hamalainen, M., Timmermann, L., Schnitzler, A., and Salmelin, R. (2001). Dynamic imaging of coherent sources: studying neural interactions in the human brain. *Proc. Natl. Acad. Sci. U.S.A.* 98, 694–699. doi:10.1073/pnas.98.2.694

Grunau, R. E., Haley, D. W., Whitfield, M. F., Weinberg, J., Yu, W., and Thiessen, P. (2007). Altered basal cortisol levels at 3, 6, 8 and 18 months in infants born at extremely low gestational age. *J. Pediatr.* 150, 151–156. doi:10.1016/j.jpeds.2006.10.053

Grunau, R. E., Whitfield, M. F., and Davis, C. (2002). Pattern of learning disabilities in children with extremely low birth weight and broadly average intelligence. *Arch. Pediatr. Adolesc. Med.* 156, 615–620. doi:10.1001/archpedi.156.6.615

Grunau, R. E., Whitfield, M. F., Petrie-Thomas, J., Synnes, A. R., Cepeda, I. L., Keidar, A., et al. (2009). Neonatal pain, parenting stress and interaction, in relation to cognitive and motor development at 8 and 18 months in preterm infants. *Pain* 143, 138–146. doi:10.1016/j.pain.2009.02.014

Hari, R., and Salmelin, R. (1997). Human cortical oscillations: a neuromagnetic view through the skull. *Trends Neurosci.* 20, 44–49. doi:10.1016/S0166-2236(96)10065-5

Hart, A. R., Whitby, E. W., Griffiths, P. D., and Smith, M. F. (2008). Magnetic resonance imaging and developmental outcome following preterm birth: review of current evidence. *Dev. Med. Child Neurol.* 50, 655–663. doi:10.1111/j.1469-8749.2008.03050.x

Hillebrand, A., Barnes, G. R., Bosboom, J. L., Berendse, H. W., and Stam, C. J. (2012). Frequency-dependent functional connectivity within resting-state networks: an atlas-based MEG beamformer solution. *Neuroimage* 59, 3909–3921. doi:10.1016/j.neuroimage.2011.11.005

Huang, M. X., Nichols, S., Robb, A., Angeles, A., Drake, A., Holland, M., et al. (2012). Integrated imaging approach with MEG and DTI to detect mild traumatic brain injury in military and civilian patients. *Neuroimage* 61, 1067–1082. doi:10.1089/neu.2008.0672

Huang, M. X., Theilmann, R. J., Robb, A., Angeles, A., Nichols, S., Drake, A., et al. (2009). Integrated imaging approach with MEG and DTI to detect mild traumatic brain injury in military and civilian patients. *J. Neurotrauma* 26, 1213–1226. doi:10.1089/neu.2008.0672

Hughes, S. W., and Crunelli, V. (2005). Thalamic mechanisms of EEG alpha rhythms and their pathological implications. *Neuroscientist* 11, 357–372. doi:10.1177/1073858405277450

John, E. R., Ahn, H., Prichep, L., Trepetin, M., Brown, D., and Kaye, H. (1980). Developmental equations for the electroencephalogram. *Science* 210, 1255–1258. doi:10.1126/science.7434026

Joliot, M., Ribary, U., and Llinás, R. (1994). Human oscillatory brain activity near 40 Hz coexists with cognitive temporal binding. *Proc. Natl. Acad. Sci. U.S.A.* 91, 11748–11751. doi:10.1073/pnas.91.24.11748

Khwaja, O., and Volpe, J. J. (2008). Pathogenesis of cerebral white matter injury of prematurity. *Arch. Dis. Child. Fetal Neonatal Ed.* 93, F153–F161. doi:10.1136/adc.2006.108837

Kostovic, I., and Judaš, M. (2010). The development of the subplate and thalamocortical connections in the human foetal brain. *Acta Paediatr.* 99, 1119–1127. doi:10.1111/j.1651-2227.2010.01811.x

Kötter, R., and Wanke, E. (2005). Mapping brains without coordinates. *Philos. Trans. R. Soc. Lond. B Biol. Sci.* 360, 751–766. doi:10.1098/rstb.2005.1625

Llinás, R., Urbano, F. J., Leznik, E., Ramirez, R. R., and van Marle, H. J. (2005). Rhythmic and dysrhythmic thalamocortical dynamics: GABA systems and the edge effect. *Trends Neurosci.* 28, 325–333. doi:10.1016/j.tins.2005.04.006

Llinás, R. R., Ribary, U., Jeanmonod, D., Kronberg, E., and Mitra, P. P. (1999). Thalamocortical dysrhythmia: a neurological and neuropsychiatric syndrome characterized by magnetoencephalography. *Proc. Natl. Acad. Sci. U.S.A.* 96, 15222–15227. doi:10.1073/pnas.96.26.15222

Marlow, N., Hennessy, E. M., Bracewell, M. A., Wolke, D., EPICure Study, and Group. (2007). Motor and executive function at 6 years of age after extremely preterm birth. *Pediatrics* 120, 793–804. doi:10.1542/peds.2007-0440

Mazaheri, A., Coffey-Corina, S., Mangun, G. R., Bekker, E. M., Berry, A. S., and Corbett, B. A. (2010). Functional disconnection of frontal cortex and visual cortex in attention-deficit/hyperactivity disorder. *Biol. Psychiatry* 67, 617–623. doi:10.1016/j.biopsych.2009.11.022

Ment, L. R., Hirtz, D., and Huppi, P. S. (2009). Imaging biomarkers of outcome in the developing preterm brain. *Lancet Neurol.* 8, 1042–1055. doi:10.1016/S1474-4422(09)70257-1

Miller, S. P., and Ferriero, D. M. (2009). From selective vulnerability to connectivity: insights from newborn brain imaging. *Trends Neurosci.* 32, 496–505. doi:10.1016/j.tins.2009.05.010

Miskovic, V., Schmidt, L. A., Boyle, M., and Saigal, S. (2009). Regional electroencephalogram (EEG) spectral power and hemispheric coherence in young adults born at extremely low birth weight. *Neurophysiol. Clin.* 120, 231–238. doi:10.1016/j.clinph.2008.11.004

Moiseev, A., Gaspar, J., Schneider, J., and Herdman, A. (2011). Application of multi-source minimum variance beamformers for reconstruction of correlated neural activity. *Neuroimage* 58, 481–496. doi:10.1016/j.neuroimage.2011.05.081

Moiseev, A., and Herdman, A. (2013). Multi-core beamformers: derivation, limitations and improvements. *Neuroimage* 71, 135–146. doi:10.1016/j.neuroimage.2012.12.072

Mulder, H., Pitchford, N. J., Hagger, M. S., and Marlow, N. (2009). Development of executive function and attention in preterm children: a systematic review. *Dev. Neuropsychol.* 34, 393–421. doi:10.1080/87565640902964524

Murias, M., Webb, S. J., Greenson, J., and Dawson, G. (2007). Resting state cortical connectivity reflected in EEG coherence in individuals with autism. *Biol. Psychiatry* 62, 270–273. doi:10.1016/j.biopsych.2006.11.012

Nevalainen, P., Pihko, E., Metsaranta, M., Andersson, S., Autti, T., and Lauronen, L. (2008). Does very premature birth affect the functioning of the somatosensory cortex? A magnetoencephalography study. *Int. J. Psychophysiol.* 68, 85–93. doi:10.1016/j.ijpsycho.2007.10.014

Okumura, A., Kubota, T., Tsuji, T., Kato, T., Hayakawa, F., and Watanabe, K. (2006). Amplitude spectral analysis of theta/alpha/beta waves in preterm infants. *Pediatr. Neurol.* 34, 30–34. doi:10.1016/j.pediatrneurol.2005.06.005

Palva, S., and Palva, J. M. (2007). New vistas for alpha-frequency band oscillations. *Trends Neurosci.* 30, 150–158. doi:10.1016/j.tins.2007.02.001

Palva, S., and Palva, J. M. (2012). Discovering oscillatory interaction networks with M/EEG: challenges and breakthroughs. *Trends Cogn. Sci. (Regul. Ed.)* 16, 219–230. doi:10.1016/j.tics.2012.02.004

Papile, L. A., Burstein, J., Burstein, R., and Koffler, H. (1978). Incidence and evolution of subependymal and intraventricular hemorrhage: a study of infants with birth weights less than 1,500 gm. *J. Pediatr.* 92, 529–534. doi:10.1016/S0022-3476(78)80282-0

Quraan, M. A., Moses, S. N., Hung, Y., Mills, T., and Taylor, M. J. (2011). Detection and localization of hippocampal brain activity using beamformers with MEG: a detailed investigation using simulations and empirical data. *Hum. Brain Mapp.* 32, 812–827. doi:10.1002/hbm.21068

Ribary, U. (2005). Dynamics of thalamo-cortical network oscillations and human perception. *Progr. Brain Res.* 150, 127–142. doi:10.1016/S0079-6123(05)50010-4

Rickards, A. L., Kelly, E. A., Doyle, L. W., and Callanan, C. (2001). Cognition, academic progress, behavior and self-concept at 14 years of very low birth weight children. *J. Dev. Behav. Pediatr.* 22, 11–18. doi:10.1097/00004703-200102000-00002

Sarnthein, J., and Jeanmonod, D. (2007). High thalamocortical coherence in patients with Parkinson's disease. *J. Neurosci.* 27, 124–131. doi:10.1523/JNEUROSCI.2411-06.2007

Sarnthein, J., and Jeanmonod, D. (2008). High thalamocortical coherence in patients with neurogenic pain. *Neuroimage* 41, 985–997. doi:10.1016/j.neuroimage.2007.10.019

Sarnthein, J., Stern, J., Aufenberg, C., Rousson, V., and Jeanmonod, D. (2006). Increased EEG power and slowed dominant frequency in patients with neurogenic pain. *Brain* 129, 55–64. doi:10.1093/brain/awh631

Schnitzler, A., and Gross, J. (2005). Normal and pathological oscillatory communication in the brain. *Nat. Rev. Neurosci.* 6, 285–296. doi:10.1038/nrn1650

Schnitzler, A., Münks, C., Butz, M., Timmermann, L., and Gross, J. (2009). Synchronized brain network associated with essential tremor as revealed by magnetoencephalography. *Mov. Disord.* 24, 285–296. doi:10.1002/mds.22633

Schulman, J. J., Cancro, R., Lowe, S., Lu, F., Walton, K. D., and Llinás, R. R. (2011). Imaging of thalamocortical dysrhythmia in neuropsychiatry. *Front. Hum. Neurosci.* 5:69. doi:10.3389/fnhum.2011.00069

Sekihara, K., Nagarajan, S., Poeppel, D., and Marantz, A. (2002). Performance of an MEG adaptive beamformer technique in the presence of correlated neural activities: effects on signal intensity and time-course estimates. *IEEE Trans. Biomed. Eng.* 49, 1534–1546. doi:10.1109/TBME.2002.805485

Sekihara, K., Nagarajan, S. S., Poeppel, D., Marantz, A., and Miyashita, Y. (2001). Reconstructing spatio-temporal activities of neural sources using an MEG vector beamformer technique. *IEEE Trans. Biomed. Eng.* 48, 760–771. doi:10.1109/10.930901

Smyser, C. D., Inder, T. E., Shimony, J. S., Hill, J. E., Degnan, A. J., Snyder, A. Z., et al. (2010). Longitudinal analysis of neural network development in preterm infants. *Cereb. Cortex* 20, 2852–2862. doi:10.1093/cercor/bhq035

Storey, J. D. (2002). A direct approach to false discovery rates. *J. R. Stat. Soc. Series B Stat. Methodol.* 64, 479–498. doi:10.1111/1467-9868.00346

Taylor, H. G., Minich, N. M., Klein, N., and Hack, M. (2004). Longitudinal outcomes of very low birth weight: neuropsychological findings. *J. Int. Neuropsychol. Soc.* 10, 149–163. doi:10.1017/S1355617704102038

Tokariev, A., Palmu, K., Lano, A., Metsaranta, M., and Vanhatalo, S. (2012). Phase synchrony in the early preterm EEG: development of methods for estimating synchrony in both oscillations and events. *Neuroimage* 60, 1562–1573. doi:10.1016/j.neuroimage.2011.12.080

Uhlhaas, P. J., Roux, F., Rodriguez, E., Rotarska-Jagiela, A., and Singer, W. (2010). Neural synchrony and the development of cortical networks. *Trends Cogn. Sci. (Regul. Ed.)* 14, 72–80. doi:10.1016/j.tics.2009.12.002

Uhlhaas, P. J., Roux, F., Singer, W., Haenschel, C., Sireteanu, R., and Rodriguez, E. (2009a). The development of neural synchrony reflects late maturation and restructuring of functional networks in humans. *Proc. Natl. Acad. Sci. U.S.A.* 106, 9866–9871. doi:10.1073/pnas.0900390106

Uhlhaas, P. J., Pipa, G., Lima, B., Melloni, L., Neuenschwander, S., Nikolic, D., et al. (2009b). Neural synchrony in cortical networks: history, concept and current status. *Front. Integr. Neurosci.* 3:17. doi:10.3389/neuro.07.017.2009

Valdés-Hernández, P. A., Ojeda-González, A., Martínez-Montes, E., Lage-Castellanos, A., Virués-Alba, T., Valdés-Urrutia, L., et al. (2010). White matter architecture rather than cortical surface area correlates with the EEG alpha rhythm. *Neuroimage* 49, 2328–2339. doi:10.1016/j.neuroimage.2009.10.030

Varela, F., Lachaux, J. P., Rodriguez, E., and Martinerie, J. (2001). The brainweb: phase synchronization and large-scale integration. *Nat. Rev. Neurosci.* 2, 229–239. doi:10.1038/35067550

Ward, L. M. (2003). Synchronous neural oscillations and cognitive processes. *Trends Cogn. Sci. (Regul. Ed.)* 7, 553–559. doi:10.1016/j.tics.2003.10.012

Wechsler, D. (2003). *Wechsler Intelligence Scales for Children (WISC-IV)*, 4th Edn. San Antonio: Psychological Corporation.

Wilson, H., Moiseev, A., Podin, S., and Quraan, M. (2007). Continuous head localization and data correction in MEG. *Int. Congr. Ser.* 1300, 623–626. doi:10.1016/j.ics.2007.02.051

Xiang, J., Liu, Y., Wang, Y., Kotecha, R., Kirtman, E. G., Chen, Y., et al. (2009). Neuromagnetic correlates of developmental changes in endogenous high-frequency brain oscillations in children: a wavelet-based beamformer study. *Brain Res.* 1274, 28–39. doi:10.1016/j.brainres.2009.03.068

Conflict of Interest Statement: The authors declare that the research was conducted in the absence of any commercial or financial relationships that could be construed as a potential conflict of interest.

Received: 12 June 2013; accepted: 30 October 2013; published online: 15 November 2013.

Citation: Doesburg SM, Moiseev A, Herdman AT, Ribary U and Grunau RE (2013) Region-specific slowing of alpha oscillations is associated with visual-perceptual abilities in children born very preterm. Front. Hum. Neurosci. 7:791. doi: 10.3389/fnhum.2013.00791

This article was submitted to the journal Frontiers in Human Neuroscience.

frontiers in
HUMAN NEUROSCIENCE

ORIGINAL RESEARCH ARTICLE
published: 14 November 2013
doi: 10.3389/fnhum.2013.00785

Reduced theta connectivity during set-shifting in children with autism

Sam M. Doesburg[1,2,3,4]*, Julie Vidal[5,6] and Margot J. Taylor[1,2,3,4]

[1] Department of Diagnostic Imaging, The Hospital for Sick Children, Toronto, ON, Canada
[2] Neurosciences & Mental Health Program, The Hospital for Sick Children Research Institute, Toronto, ON, Canada
[3] Department of Medical Imaging, University of Toronto, Toronto, ON, Canada
[4] Department of Psychology, University of Toronto, Toronto, ON, Canada
[5] Paris Descartes University, Paris, France
[6] UMR, Centre National de la Recherche Scientifique 3521, Paris, France

Edited by:
Christos Papadelis, Harvard Medical School, USA

Reviewed by:
Tal Kenet, Massachusetts General Hospital, USA
Jeff Anderson, University of Utah, USA

***Correspondence:**
Sam M. Doesburg, Department of Diagnostic Imaging, The Hospital for Sick Children, 555 University Avenue, Toronto, ON M5G 1X8, Canada
e-mail: sam.doesburg@sickkids.ca

Autism spectrum disorder (ASD) is a characterized by deficits in social cognition and executive function. An area of particular difficulty for children with ASD is cognitive flexibility, such as the ability to shift between attentional or response sets. The biological basis of such deficits remains poorly understood, although atypical development of structural and functional brain connectivity have been reported in ASD, suggesting that disruptions of normal patterns of inter-regional communication may contribute to cognitive problems in this group. The present magnetoencephalography study measured inter-regional phase synchronization while children with ASD and typically developing matched controls (6–14 years of age) performed a set-shifting task. Reduced theta-band phase synchronization was observed in children with ASD during extradimensional set-shifting. This reduction in task-dependent inter-regional connectivity encompassed numerous areas including multiple frontal lobe regions, and indicates that problems with communication among brain areas may contribute to difficulties with executive function in ASD.

Keywords: ASD, autism, neural synchrony, neural oscillation, magnetoencephalography, set-shifting, executive function, functional connectivity

INTRODUCTION

Autism spectrum disorder (ASD) is associated with difficulties in cognitive development, particularly in domains such as social cognition and executive functions (Hill and Bird, 2006; O'Hearn et al., 2008). These abilities depend heavily on frontal lobe functions, and atypical frontal lobe development has been linked with cognitive difficulties in ASD (Courchesne and Pierce, 2005; Gilbert et al., 2008; Just et al., 2012). ASD is particularly associated with difficulties in cognitive flexibility, which includes the ability to switch between attentional or response sets (Yerys et al., 2009; Maes et al., 2011). This poor mental flexibility, the tendency to get "stuck" in a set is the underlying cognitive basis of the behavioral rigidity, perseveration, and repetitive behavior symptoms that are one of the definitive hallmarks of ASD (Hill, 2004). Several tasks have been used to assess cognitive flexibility behaviorally in ASD, most commonly being the Wisconsin Card Sorting Task (WCST), and have shown impaired performance for individuals with ASD on the WCST (e.g., Lopez et al., 2005). Evidence for cognitive flexibility impairment in ASD also comes from performance on the Cambridge Neuropsychological Test Automated Battery (CANTAB) Intradimensional-Extradimensional (ID-ED) Shift Task [developed by Dias et al. (1996)]. ED attentional shifts are thought to demand greater cognitive flexibility to successfully make the switch than ID shifts. Some studies have shown that individuals with ASD were impaired on ED shifts, but performed similarly to controls on ID shifts (Hughes et al., 1994; Ozonoff et al., 2004); however, other studies have failed to replicate this finding (e.g., Corbett et al., 2009). The neural basis of executive set-shifting abilities in ASD, however, remains unclear.

In previous neuroimaging studies atypical development of connectivity among cortical regions in ASD has been reported. Diffusion tensor imaging (DTI) studies have found that structural connections among cortical regions are atypical in ASD (see Travers et al., 2012 for review; Mak-Fan et al., 2013). Hemodynamic imaging has also demonstrated that functional connectivity among brain regions is abnormal in ASD, both in resting-state conditions and during the performance of cognitive tasks (see Müller et al., 2011 for review). Such results suggest that disordered development of brain network connectivity is common in autism and authors have suggested that this may lead to atypical interactions among brain regions resulting in social and cognitive impairments in this group (Just et al., 2007, 2012; Gilbert et al., 2008; Noonan et al., 2009).

The coordination of neural oscillations across brain areas is currently understood to underlie communication in distributed brain networks (Varela et al., 2001; Fries, 2005; Uhlhaas et al., 2009a). Neural coherence is related both to the organization of resting-state brain networks (Brookes et al., 2011; de Pasquale et al., 2012; Hipp et al., 2012) as well as to cortical network dynamics underling cognition and perception (see Palva and Palva, 2012 for review). Neural oscillations and their coherence develop throughout infancy, childhood and adolescence (Clarke et al., 2001; Uhlhaas et al., 2009b; Boersma et al.,

2011, 2013a) and are relevant for the maturation of cognitive abilities (Benasich et al., 2008; Gou et al., 2011). Atypical oscillatory responses, including altered expression of local power and inter-regional coherence, have been reported in ASD using electroencephalography (EEG) and magnetoencephalography (MEG) (Sun et al., 2012; Wright et al., 2012; Khan et al., 2013). In resting-state networks atypical oscillatory synchrony has also been reported in ASD (Murias et al., 2007; Maxwell et al., 2013). Accumulating evidence that maturation of oscillatory activity in functional networks underlies cognitive development (see Uhlhaas et al., 2010 for review) highlights the importance of understanding the role of oscillatory neural synchronization during cognitive processing in neurodevelopmental disorders such as ASD.

Overall, the literature shows that frontal and parietal areas are implicated in tasks of cognitive flexibility, and there is some initial evidence for abnormalities in these areas in adults with ASD (Schmitz et al., 2006; Shafritz et al., 2008). However, to determine how these atypical patterns arise, investigation is needed in children with ASD. Previous findings have also suggested that abnormal coordination among brain regions may contribute to dysfunctional network interactions leading to cognitive difficulties in children with ASD (e.g., Just et al., 2007). In the present study, we recorded MEG while children with ASD and matched controls performed a set-shifting task requiring strong engagement of executive processes. In particular, this task places strong demands on cognitive flexibility. Atlas-based source reconstruction was performed and task-dependent changes in inter-regional oscillatory synchrony were assessed to test the hypothesis that children with ASD express atypical coordination of oscillatory activity in large-scale networks in tasks requiring cognitive flexibility and executive functions.

MATERIALS AND METHODS

SUBJECTS

A total of 20 children with ASD and 18 typically developing typically developing children were tested. However, due to too much movement during the MEG study, 4 in each group were excluded from analyses. Thus, 16 children with ASD (13 male; mean age 11.1 years; SD = 2.5) and 14 typically developing controls (12 male; mean age 11.5 years; SD = 2.4) were included in the present study. Intellectual ability was assessed using WASI 2-score IQ and did not differ between groups ($p = 0.81$); mean IQ was 107 (SD = 12.7) for the ASD group and 105.8 (SD = 15.6) for the controls. Subjects were excluded if they had a history of neurological disorders (other than ASD for those in the clinical group), brain injury, were using psychoactive medications, did not have normal or corrected-to-normal vision, an IQ below 75, language skill which made them unable to complete the task, or had other contraindications for MEG or MRI imaging. This research was approved by the Hospital for Sick Children Research Ethics Board. All children gave informed assent and their parents gave informed written consent.

TASK AND DATA ACQUISITION

Magnetoencephalographic data were acquired on a 151 channel whole head CTF/MISL system (Coquitlam, Canada). Children were supine throughout data recording, and three coils placed at the nasion and left and right preauricular points were used to monitor head location during recording. Data were collected continuously at 625 Hz, during which subjects performed a set-shifting task (**Figure 1**). In this task, the children were presented with three stimuli on each trial. Subjects were instructed to match the bottom stimulus to one of the two upper stimuli. There were two dimensions on which the stimuli could vary: shape (triangle, circle, diamond, cross, star, pentagon) and color (cyan,

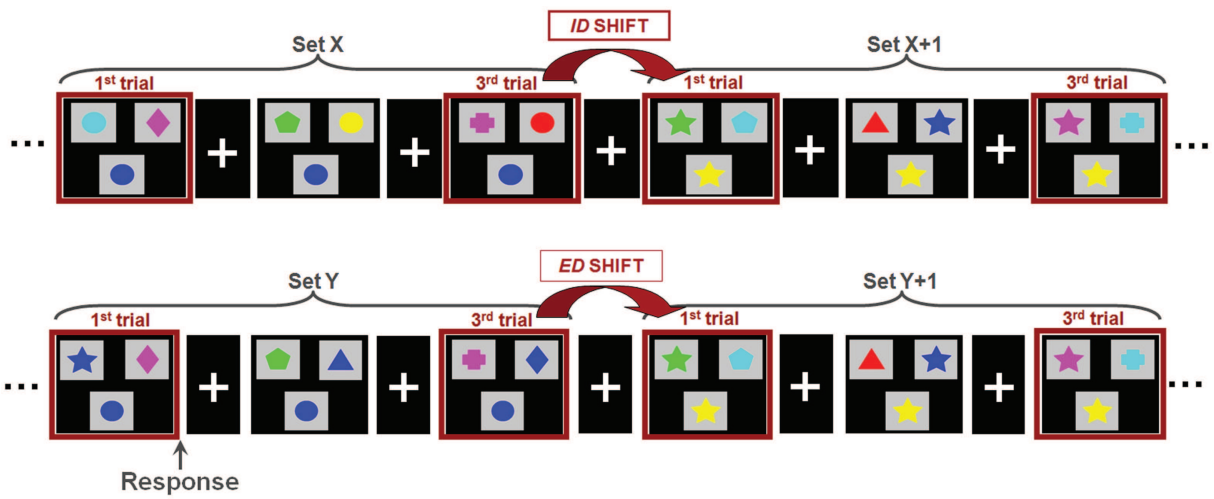

FIGURE 1 | The set-shifting paradigm. Children were instructed to match the stimulus presented at the bottom of each image with one of two options presented at the top; the match was possible only by shape or color, always with only a single correct option. Stimuli were organized into sets, within which the rule for matching is held constant (i.e., green, star). Between sets, the rule for matching changed. In an intradimensional shifts (ID; top), the rule for matching switched within a dimension (i.e., within color; green to red) whereas in extradimensional shifts (ED; bottom) the rule for matching switched between dimensions (i.e., color to shape; green to star).

blue, pink, green, yellow, red). The rule for correctly matching remained constant throughout each "set" and there was always only one correct response. Following three or four consecutive correct trials a "set-shift" occurred, in which the rule for matching would change. In ID shifts the rule would change within a given dimension (e.g., red to green, or star to cross); in ED shifts the rule for matching would change across dimensions, e.g., green to pentagon or triangle to yellow). The order of ID and ED shifts was randomized. Stimulus duration depended on subject response time, with a maximum duration of 4000 ms. The inter-trial interval varied between 1000 and 1500 ms. Two 6 min runs were collected for each subject. To facilitate co-registration of MEG activity to brain anatomy a structural volumetric MR image was collected following MEG recording for each subject using a 1.5-T Signa Advantage system (GE Medical Systems). MEG fiducial coils were replaced by radio-opaque markers for the T1 weighted 3-D SPGR scan to maintain accurate MEG-MRI co-registration.

MEG PREPROCESSING AND SOURCE RECONSTRUCTION

Recording runs were excluded from analysis if more than 1 cm of movement occurred between head localization at the beginning and end of the run, consistent with movement thresholds for MEG studies in child populations (e.g., Pang, 2011; Taylor et al., 2011; Hung et al., 2012). Data epochs were extracted from −1500 to 2500 ms, relative to stimulus onset for trials immediately following extradimensional (ED1) and intradimensional (ID1) shift trials, as well as on the third trials of extradimensional (ED3) and intradimensional (ID3) sets, where task performance but no set-shifting was required. MEG data were co-registered with MRI data by aligning the fiducial markers, and a multisphere head model was constructed for each subject based on their individual MRIs. MRIs were normalized into standard MRI space using SPM2. Seed locations, which were 72 cortical and sub-cortical locations for source-space MEG analysis previously used by Diaconescu et al. (2011) (see **Figure 2**), were then unwarped from standard MRI space into the corresponding location in head space for each individual. The complete list of 72 locations, each Talairach coordinate and anatomical region can be found in Diaconescu et al. (2011) as well as Doesburg et al. (2013). Broadband time-series representing the activity of each of the 72 sources were then reconstructed for each trial using beamformer analysis. Beamformer analysis implements a spatial filter, estimating the activity at each location in the brain while maximally attenuating contributions from other sources, including ocular and muscle artifacts (Robinson and Vrba, 1999; Sekihara et al., 2001; Cheyne et al., 2006).

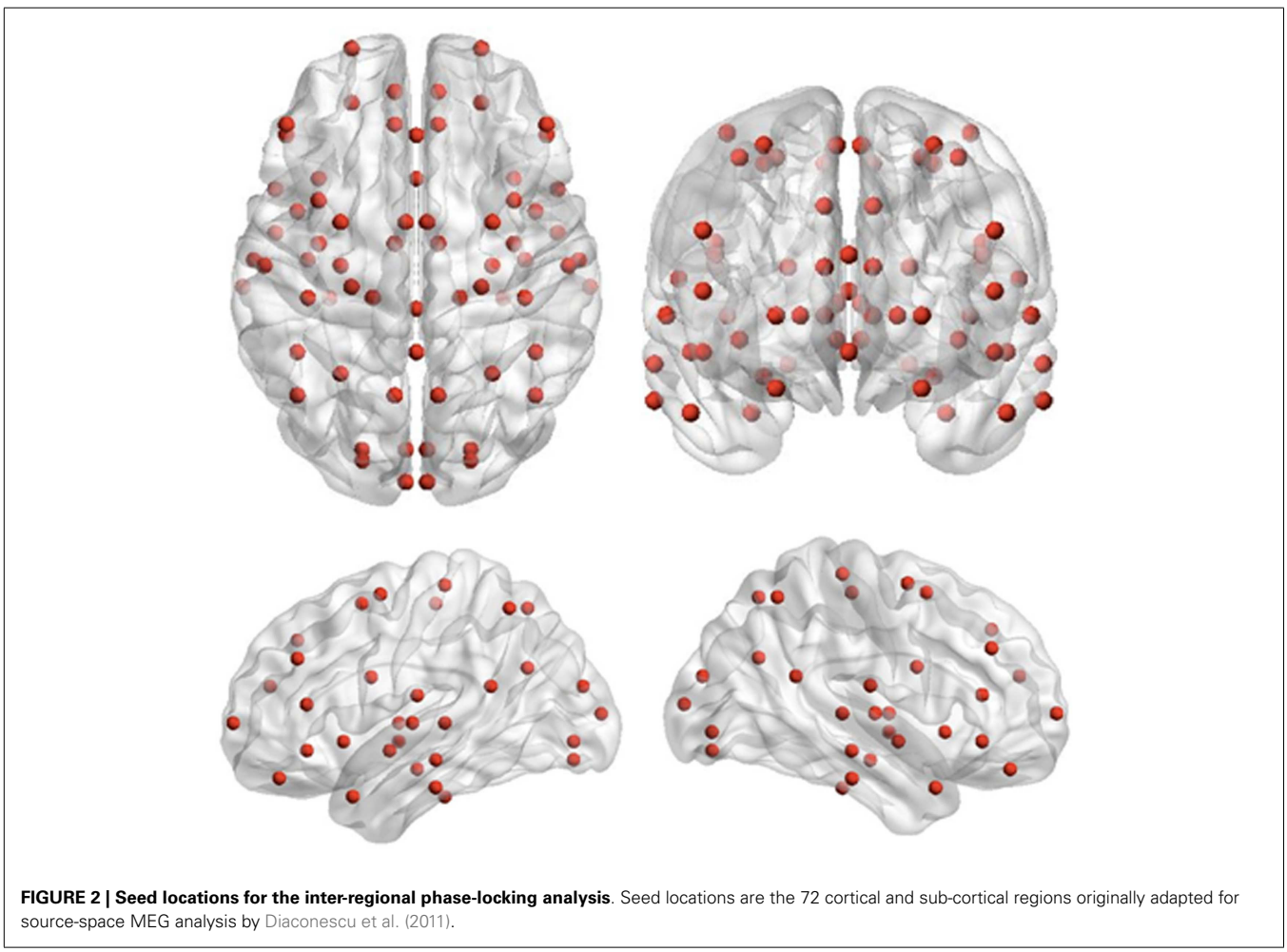

FIGURE 2 | Seed locations for the inter-regional phase-locking analysis. Seed locations are the 72 cortical and sub-cortical regions originally adapted for source-space MEG analysis by Diaconescu et al. (2011).

INTER-REGIONAL PHASE-LOCKING ANALYSIS

Data were filtered into theta (4–7 Hz), alpha (8–14 Hz), beta (15–30 Hz), low gamma (30–80 Hz), and high gamma (80–150 Hz) frequency ranges. Time-series of instantaneous phase values were then obtained for each source and frequency using the Hilbert transform. Inter-regional phase locking was calculated for each source pair and frequency using the phase lag index (PLI) which quantifies the stability of phase relations between source pairs across trials, while removing/attenuating phase locking occurring at zero/near-zero phase lag, thereby providing a measure of inter-regional phase synchronization that is robust against spurious synchronization originating from the activity of common sources (Stam et al., 2007). This strategy of performing phase-locking analysis on time-series of MEG activity reconstructed using beamformer analysis builds on established techniques for investigating oscillatory connectivity dynamics during cognitive processing (Doesburg and Ward, 2009; Doesburg et al., 2012b). This produced a 72-by-72 connectivity matrix for each time point and frequency, for each subject. Time-series of connectivity strengths for each region and frequency band were then calculated using the Brain Connectivity Toolbox (Rubinov and Sporns, 2010). This approach produces a graph metric for each region, for each analyzed time point. Connectivity strength accordingly indexes how functionally connected (phase-locked) a given region is to all other regions in the analyzed network. Time series of average connectivity strength were produced for each frequency by averaging across all 72 analyzed regions, and standardized relative to a −250 to 0 ms baseline interval to reveal the time courses of task-dependent changes in inter-regional phase locking for ED1, ID1, ED3, and ID3 conditions. This approach allowed the determination of dynamics in large-scale connectivity dynamics and the identification of time intervals for further statistical analysis. Time courses of mean connectivity strength averaged across 72 regions distributed across widely separated cortical and subcortical regions reflect fairly global coherence dynamics, whereas connectivity differences in children with ASD during the set-shifting task likely involve more specific subsets of connections, which we evaluated using the Network Based Statistic (NBS; see Zalesky et al., 2010). To this end, time windows exhibiting peaks in networks connectivity were selected, and connectivity matrices representing this task-dependent increase in network connectivity were obtained by averaging the connectivity matrices across time points in the peak window. A baseline connectivity matrix was constructed by averaging across an equivalent number of time points in the pre-stimulus interval. Task-dependent increases in connectivity were indexed by subtracting the baseline connectivity matrix from the active window connectivity matrix for each subject. Group differences in task-dependent phase locking were assessed using the NBS toolbox (Zalesky et al., 2010, 2012). This approach evaluates network differences between groups by first applying a univariate statistical threshold to each element in the connectivity matrix. If a connectivity component (a contiguous set of node pairs which are differentially connected between the compared groups) is discovered, its statistical significance is evaluated by shuffling the group membership, and observing the largest connectivity component observed in the shuffled data. Data surrogation was thus employed to create a null distribution, and the size of observed real connectivity components was considered relative to the surrogate data distribution to evaluate statistical confidence. As such, statistical significance is assigned at the level of the network connectivity component, rather than at the level of individual pair-wise comparisons (see Zalesky et al., 2010). As the largest components in the surrogate data are obtained considering all pair-wise comparisons, NBS controls for false positives due to multiple comparisons (Zalesky et al., 2010, 2012). NBS is a non-parametric technique that is appropriate for analysis of raw connectivity measures (see Zalesky et al., 2010), such as PLI. Seed regions and altered connectivity in children with ASD were plotted using the BrainNet Viewer toolbox (Xia et al., 2013).

RESULTS

BEHAVIORAL PERFORMANCE ON THE SET-SHIFTING TASK

Behavioral data for children with ASD and typically developing controls are presented in **Table 1**. Reaction times for the typically developing control children were significantly longer ($p < 0.02$) on ED1 trials than for ED3 trials, but did not differ significantly between the ID1 and ID3 trials ($p < 0.54$). The children with ASD also exhibited significantly longer reaction times ($p < 0.05$) on ED1 trials than on ED3 trials, but did not express significantly longer RTs ($p = 0.17$) for ID1 relative to ID3 trials. Interestingly, children with ASD and controls did not differ in their reaction times, for either ED (ED1; $p = 0.5$) or ID set-shifting (ID1; $p = 0.49$). This indicates that the ED set-shifting task required additional cognitive resources for both the ASD and control groups, and overall performance did not differ between the groups.

THETA-BAND CONNECTIVITY DYNAMICS DURING SET-SHIFTING

In the theta band, clear increases above baseline values of average network connectivity were seen for both children with ASD and typically developing controls in both the ID1 and ED1 shift conditions, as well as during ED3 and ID3 conditions, in which no set-shifting occurred. **Figure 3** displays the time course of theta-band network connectivity strength, averaged across all 72 analyzed regions, for ASD and controls for each trial condition, standardized relative to a 250 ms pre-stimulus baseline. Time courses of task-dependent theta-band connectivity appeared roughly similar between ASD children and controls, except on ED1 shift trials, where demands on executive function are expected to be greatest. This reduced engagement of network connectivity in children with ASD, relative to typically developing controls, peaked 150–400 ms following stimulus onset. No clear modulations of

Table 1 | Means and standard deviations of reaction times (ms) for children with ASD and typically developing controls for each trial type.

	ASD	Controls
ED1	711 (77)	744 (165)
ED3	697 (68)	699 (141)
ID1	692 (82)	714 (88)
ID3	674 (72)	696 (130)

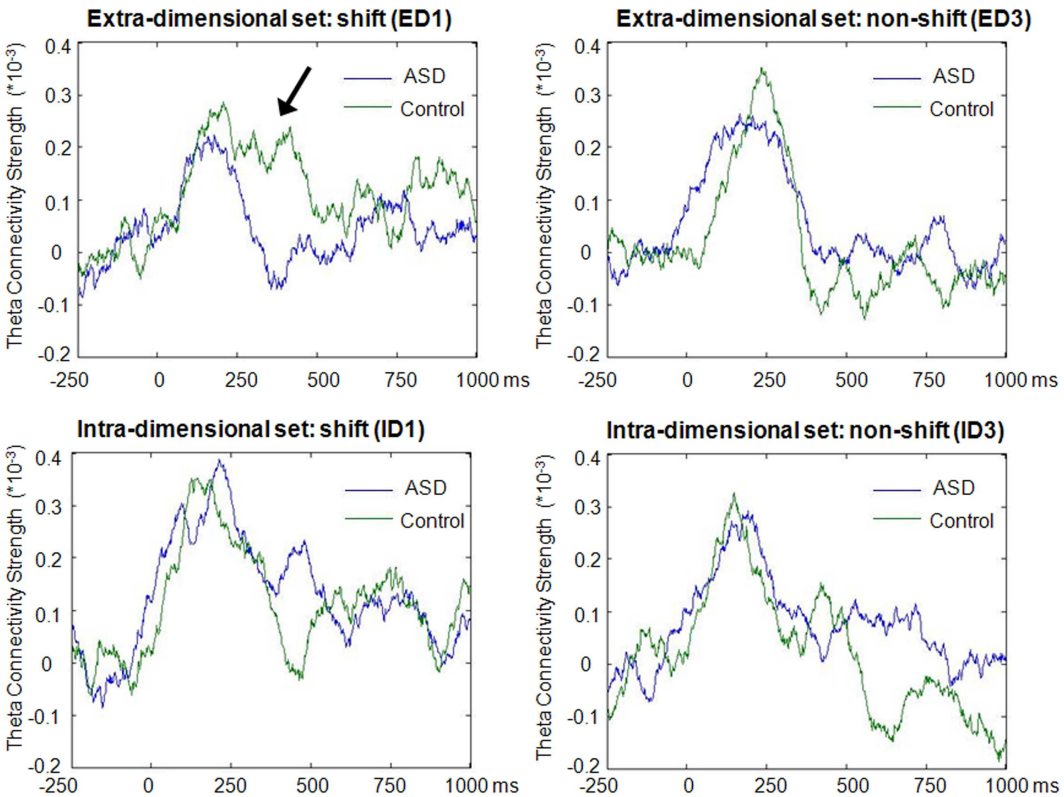

FIGURE 3 | Time-course of theta-band connectivity strength during task performance. Time-courses of connectivity were derived by averaging theta-band (4–7 Hz) connectivity strengths across all 72 analyzed regions for each time point, and subtracting mean baseline (−250 to 0 ms) network connectivity from connectivity strength at each time point. Note the more extensive task-dependent increases in connectivity strengths in both groups during the first block of extradimensional (ED1) and intradimensional (ID1) sets, when increased engagement of executive functions was required, compared to the third trial of each set (ED3 and ID3) when set-shifting did not occur. These task-dependent modulations of network connectivity were observed for both groups, but reduced inter-regional theta connectivity was evident from 150 to 400 ms during extradimensional set-shifting (ED1) in children with ASD (arrow).

inter-regional network synchronization were observed outside the theta frequency range.

REDUCED TASK-DEPENDENT INTER-REGIONAL PHASE-LOCKING IN CHILDREN WITH ASD

The Network Based Statistic was employed to investigate group differences in theta connectivity during the ED1 set-shifting condition. Connectivity matrices reflecting network connectivity 150–400 ms post-stimulus, averaged across time points and bracketing the interval where group differences in connectivity were observed, were compared with connectivity matrices averaged across time points in a −250 to 0 ms pre-stimulus baseline, using a threshold of 2.5. This threshold is a t-statistic and is adapted for the data distribution being analyzed (see Zalesky et al., 2010, 2012). This revealed reduced task-dependent connectivity in children with ASD in a distributed network of brain regions which included strong involvement of frontal, temporal, and occipital brain regions, but also encompassed some sub-cortical and parietal brain areas ($p = 0.01$). **Figure 4** displays the network expressing reduced theta-band connectivity in children with ASD, as well as the magnitude of group differences in regional connectivity strength for each region in this network. A complete list of each region in this network, together with its affiliated anatomical location and Talairach coordinates, is presented in **Table 2**. Comparison of connectivity between baseline and active windows within the ASD and typically developing groups, using NBS, did not reveal any statistically significant differences.

DISCUSSION

Children with ASD expressed reduced theta-band network synchronization during ED set-shifting relative to typically developing controls. The RTs did not differ between the groups, indicating that they were matched on behavioral performance. Thus, differences seen in brain connectivity were not due to performance differences. In studies with adults with ASD, this was also found: despite no differences in behavior, fMRI results showed either increased (Schmitz et al., 2006) or decreased (Shafritz et al., 2008) activation patterns in widespread brain regions, linked to task performance. Our observation that performance differences were seen in the ED but not ID shifts is consistent with the ED task being more difficult and with the prior reports of greater difficulty in ASD with extra rather than ID shifts (e.g., Hughes et al., 1994; Ozonoff et al., 2004). Results from the present study also indicated that ED shifting (ED1 compared with ED3) resulted in significantly longer reaction times

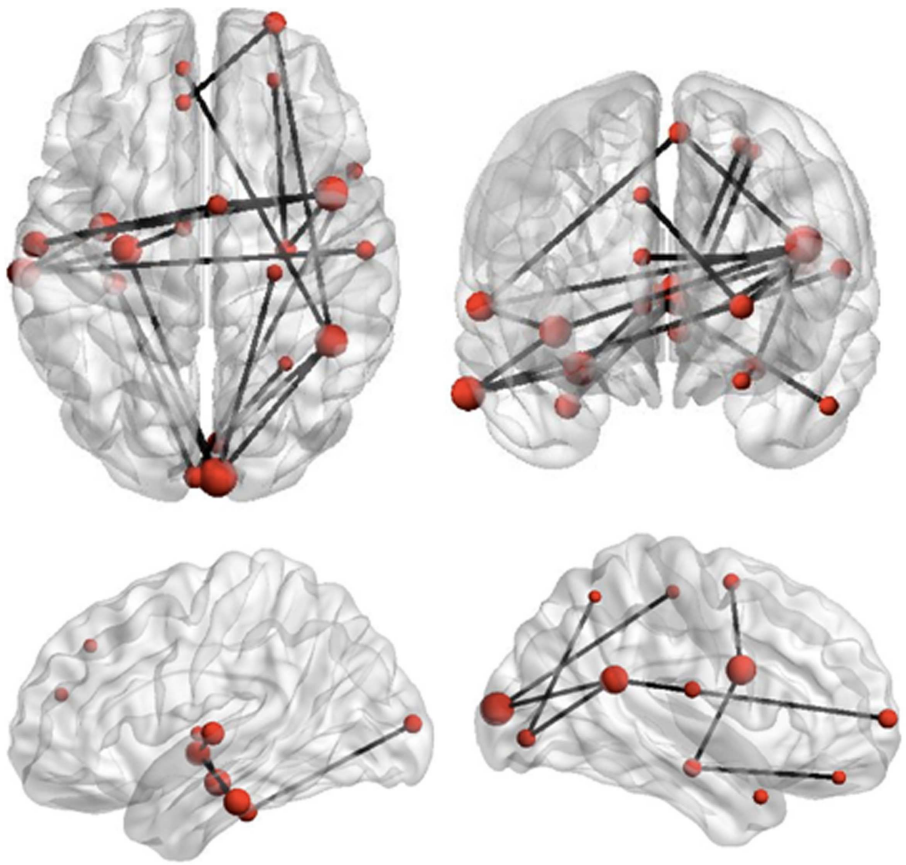

FIGURE 4 | Reduced network synchronization in ASD during set-shifting. Black lines represent connections among regions which expressed reduced task-dependent theta-synchronization during extradimensional set-shifting (ED1) in children with ASD ($p = 0.01$). The size of the regions in this network, indicated by the size of the red dots, represents increasing magnitude of group differences in task-dependent connectivity strength for these regions.

for both children with ASD and controls, whereas ID shifting did not. These findings are consistent with evidence indicating that clinical child populations can achieve comparable behavioral performance by recruiting different patterns of connectivity among brain areas, suggesting that brain systems associated with these functions in controls are impacted in ASD, leading to compensatory reorganization of function (e.g., Schafer et al., 2009).

Alterations in connectivity were widespread and encompassed frontal, parietal, occipital, temporal, and sub-cortical regions. These results add to a growing literature indicating that functional interactions among brain regions are atypical in ASD (Just et al., 2007; Murias et al., 2007; Müller et al., 2011; Sun et al., 2012; Boersma et al., 2013b). These alterations in functional connectivity may be related to abnormal development of underlying structural connections (see Travers et al., 2012 for review), including atypical inter-regional relations in cortical thickness (Shi et al., 2013). Altered structural brain connectivity has been associated with individual differences in cognitive ability in this group (Li et al., 2012). Recent studies, however, have shown that functional connectivity cannot be entirely predicted from brain structure (see Deco et al., 2011). This underscores the importance of understanding how functional interactions are expressed in ASD in the context of specific cognitive tasks. Several frontal regions were implicated in abnormal connectivity during set-shifting including prefrontal cortical areas. This is significant as ASD has been associated with atypical frontal lobe development (i.e., Ecker et al., 2012) as well as atypical connectivity between the frontal lobes and other regions of the brain (see Courchesne and Pierce, 2005). Viewed through this lens, our results suggest that disordered frontal lobe connectivity may impact the ability to marshal task-dependent functional interactions among frontal regions and other areas typically used to perform executive and cognitive tasks. Accordingly, disruptions of the frontal lobes' capacity to orchestrate communication within distributed networks may contribute to selective difficulties in executive function in ASD.

There is a large body of work showing the importance of the prefrontal cortex in executive function in general and cognitive flexibility in particular. This evidence comes from lesion and neuropsychological studies, primate research, and neuroimaging studies. For example, patients with prefrontal lesions have difficulty on neuropsychological measures of flexibility such as the WCST (Stuss and Alexander, 2007). Seminal work by Dias et al. (1996) showed that damage to the dorsolateral prefrontal cortex of monkeys caused specific impairments in set-shifting. A

Table 2 | Each region in the network showing reduced connectivity in children with ASD, together with associated Brodmann areas (BA) and Talairach coordinates.

Region	BA	*X*	*Y*	*Z*
Left medial prefrontal cortex	10	−8	48	20
Left dorsomedial prefrontal cortex	8	−8	36	40
Right orbitofrontal cortex	11	24	44	−20
Right frontal polar	10	24	64	4
Right medial premotor cortex	6	4	0	60
Right ventrolateral premotor cortex	9	44	4	24
Right primary motor cortex	4	24	−24	56
Left inferior temporal cortex	20	−64	−24	−24
Left ventral temporal cortex		−32	−28	−28
Left secondary auditory cortex	22	60	−14	4
Left parahippocampal cortex		−28	−16	−16
Right parahippocampal cortex		28	−16	−16
Right temporal pole	38	52	12	−28
Right inferior parietal cortex	40	44	−48	20
Right superior parietal cortex	7	28	−56	54
Right secondary somatosensory cortex	43	56	−16	16
Left secondary visual cortex		−4	−96	8
Right secondary visual cortex		4	−96	8
Right primary visual cortex		4	−84	−4
Left claustrum		−36	−8	−4
Left thalamus		−8	−8	4

host of neuroimaging studies have confirmed the importance of prefrontal cortex in cognitive flexibility, although specific regions have differed and also include parietal regions (e.g., Konishi et al., 1999; Dove et al., 2000; Sohn et al., 2000; Monchi et al., 2001; Zanolie et al., 2008). In light of this literature, the results of the present study may reflect reduced ability of prefrontal regions to coordinate activity among cortical regions to support set-shifting performance in children with ASD. Right ventrolateral premotor cortex also emerged as an important region in the pattern of reduced inter-regional connectivity during set-shifting in children with ASD, which is intriguing due to the proximity of this seed location to the right insula. Given results implicating right insula in executive abilities and the spatial resolution of MEG, it is possible this is due to reduced network engagement of right insula during ED set-shifting in children with ASD. Although the insula has been less frequently identified in reviews or meta-analyses of executive function, some studies have shown that the insula (specifically the right anterior insula) is functionally connected to other regions important for executive function, and may also play a role in monitoring of task performance. The right insula is part of a network hub responsible for switching between other brain systems during task performance (e.g., Sridharan et al., 2008; Eckert et al., 2009). In addition, a study of cognitive flexibility showed insula activation in a task switch condition (Dove et al., 2000), as well as a region in cuneus/precuneus that was more active with task switching. Accordingly, our findings suggest that reduced incorporation of right insula into distributed task-dependent networks may contribute to difficulties with cognitive flexibility and executive control in children with ASD.

Previous studies have also identified altered expressions of neural oscillations in ASD. This has included atypical local as well as long-range synchrony during cognitive and perceptual processing (i.e., Sun et al., 2012; Khan et al., 2013). Altered resting-state oscillatory coherence has been reported in ASD as well (Murias et al., 2007; Boersma et al., 2013b). Pertinent to the present study, altered long-range theta coherence has been described in ASD using EEG (Murias et al., 2007), and reduced task-dependent inter-regional phase-amplitude coupling has been reported in this population using MEG (Sun et al., 2012). Reduced ability to recruit long-range theta synchronization to support cognitive processing may be particularly pertinent for the ability of frontal regions to coordinate task-dependent activity in large-scale neuronal ensembles, as theta coherence has been proposed to play a primary role in long-distance communication among brain regions (von Stein and Sarnthein, 2000). This view is supported by findings relating long-range theta synchronization to the formation of task-dependent networks (Sarnthein et al., 1998; von Stein et al., 2000), as well as results indicating that theta rhythms are critical for the regulation of oscillations in other frequency ranges relevant for cognition, both within and across cortical regions (Schack et al., 2002; Canolty et al., 2006; Doesburg et al., 2012a,b). In view of this literature, our findings of reduced inter-regional theta-band phase synchronization in children with ASD suggest that inability to express task-dependent coordination of oscillatory coherence in large-scale functional brain networks may contribute to cognitive difficulties in this group. This model is consistent with the notion that inter-regional coherence of neuronal oscillations is a fundamental process which organizes information flow in the brain and supports cognition (Varela et al., 2001; Fries, 2005). Theta oscillations have been suggested to constitute a fundamental element of a "neural code" responsible for the organization of task-relevant information and its communication among brain areas (Lisman and Jensen, 2013). Our results add to growing evidence indicating that disruption of normal patterns of neural synchronization is related to functional impairments in numerous neurological and neuropsychiatric conditions, including neurodevelopmental disorders (Schnitzler and Gross, 2005; Uhlhaas et al., 2009a; Buzsáki and Watson, 2012).

Neural oscillations and their synchronization across brain regions have been proposed to play a key role in neurocognitive development (Uhlhaas et al., 2010). This is particularly pertinent for the present study, which demonstrates reduced inter-regional synchronization during an executive function task in children with ASD. Development throughout childhood and adolescence is associated with progressive shifts in the task-dependent expression of local oscillations (Clarke et al., 2001) and their long-range synchronization (Uhlhaas et al., 2009b). Individual differences in neuronal oscillations have also been related to the emergence of perceptual abilities (Csisbra et al., 2000) and the development of cognitive abilities (Benasich et al., 2008; Gou et al., 2011). Atypical oscillatory synchronization in brain networks has been related

also to functional impairments and cognitive difficulties in other pediatric populations (Doesburg et al., 2011; Ibrahim et al., 2012). These age-dependent changes are understood to reflect changes in the architecture of functional brain networks, reflecting maturation in pathways of information flow in the brain (Boersma et al., 2011, 2013a).

CONCLUSION

This study provides the first evidence for reduced theta-band interregional synchronization during a set-shifting task in children with ASD. This adds to the growing body of literature demonstrating disrupted oscillatory coherence in brain networks in neurodevelopmental disorders. The inability to recruit theta-band synchronization in large-scale networks may contribute to deficits in executive abilities associated with ASD. This altered connectivity included several frontal regions, and including the right insula, suggesting that frontal lobe functions are less effective in coordinating among task-relevant brain regions in ASD, leading to reduced performance on tasks requiring executive abilities.

ACKNOWLEDGMENTS

We would like to thank Travis Mills, Annette Ye, and Carmen Schäfer for their help with data analyses. We would also like to thank CIHR (MOP-81161) for financial support of this project to Margot J. Taylor, and NSERC (RGPIN-435659) for financial support to Sam M. Doesburg.

REFERENCES

Benasich, A. A., Gou, Z., Choudhury, N., and Harris, K. D. (2008). Early cognitive and language skills are linked to resting frontal gamma power across the first 3 years. *Behav. Brain Res.* 195, 215–222. doi:10.1016/j.bbr.2008.08.049

Boersma, M., Smit, D. J., Boomsma, D. I., de Geus, E. J. C., Delemarre-van de Waal, H. A., and Stam, C. J. (2013a). Growing trees in child brains: graph theoretical analysis of electroencephalography-derived minimum spanning tree in 5- and 7-year-old children reflects brain maturation. *Brain Connect.* 3, 50–60. doi:10.1089/brain.2012.0106

Boersma, M., Kemner, C., de Reus, M. A., Collin, G., Snijders, T. M., Hofman, D., et al. (2013b). Disrupted functional brain networks in autistic toddlers. *Brain Connect.* 3, 41–49. doi:10.1089/brain.2012.0127

Boersma, M., Smit, D. J., de Bie, H. M., van Baal, G. C. M., Boomsma, D. I., de Geus, E. J. C., et al. (2011). Network analysis of resting state EEG in the developing young brain: structure comes with maturation. *Hum. Brain Mapp.* 32, 413–425. doi:10.1002/hbm.21030

Brookes, M. J., Woolrich, M., Luckhoo, H., Price, D., Hale, J. R., Stephenson, M. C., et al. (2011). Investigating the electrophysiological basis of resting state networks using magnetoencephalography. *Proc. Natl. Acad. Sci. U.S.A.* 108, 16783–16788. doi:10.1073/pnas.1112685108

Buzsáki, G., and Watson, B. O. (2012). Brain rhythms and neural syntax: implications for efficient coding of cognitive content and neuropsychiatric disease. *Dialogues Clin. Neurosci.* 14, 345–367.

Canolty, R. T., Edwards, E., Dalal, S. S., Soltani, M., Nagarajan, S. S., Kirsch, H. E., et al. (2006). High gamma power is phase-locked to theta oscillations in human neocortex. *Science* 313, 1626–1628. doi:10.1126/science.1128115

Cheyne, D., Bakhtazad, L., and Gaetz, W. (2006). Spatiotemporal mapping of cortical activity accompanying voluntary movements using an event-related beam forming approach. *Hum. Brain Mapp.* 27, 213–229. doi:10.1002/hbm.20178

Clarke, A. R., Barry, R. J., McCarthy, R., and Selikowitz, M. (2001). Age and sex effects in the EEG: development of the normal child. *Clin. Neurophysiol.* 112, 806–814. doi:10.1016/S1388-2457(01)00488-6

Corbett, B. A., Carmean, V., Ravizza, S., Wendelken, C., Henry, M. L., Carter, C., et al. (2009). A functional and structural study of emotion and face processing in children with autism. *Psychiatry Res.* 173, doi:10.1016/j.pscychresns.2008.08.005

Courchesne, E., and Pierce, K. (2005). Brain overgrowth in autism during a critical time in development: implications for frontal pyramidal neuron and interneuron development and connectivity. *Int. J. Dev. Neurosci.* 23, 153–170. doi:10.1016/j.ijdevneu.2005.01.003

Csisbra, G., Davis, G., Spratling, M. W., and Johnson, M. H. (2000). Gamma oscillations and object processing in the infant brain. *Science* 290, 1582–1585. doi:10.1126/science.290.5496.1582

de Pasquale, F., Penna, S. D., Snyder, A. Z., Marzetti, L., Pizzella, V., Romani, G. L., et al. (2012). A cortical core for dynamic integration of functional networks in the resting human brain. *Neuron* 74, 753–764. doi:10.1016/j.neuron.2012.03.031

Deco, G., Jirsa, V. K., and McIntosh, A. R. (2011). Emerging concepts for the dynamical organization of resting-state activity in the brain. *Nat. Rev. Neurosci.* 12, 43–56. doi:10.1038/nrn2961

Diaconescu, A. O., Alain, C., and McIntosh, A. R. (2011). The co-occurrence of multisensory facilitation and cross-modal conflict in the human brain. *J. Neurophysiol.* 106, 2896–2909. doi:10.1152/jn.00303.2011

Dias, R., Robbins, T. W., and Roberts, A. C. (1996). Primate analogue of the Wisconsin card sorting test: effects of exciotoxic lesions of the prefrontal cortex in the marmoset. *Behav. Neurosci.* 110, doi:10.1037/0735-7044.110.5.872

Doesburg, S. M., Green, J. J., McDonald, J. J., and Ward, L. M. (2012a). Theta modulation of inter-regional gamma synchronization during auditory attention control. *Brain Res.* 1431, 77–85. doi:10.1016/j.brainres.2011.11.005

Doesburg, S. M., Moiseev, A., Herdman, A. T., Ribary, U., and Grunau, R. E. (2013). Region-specific slowing of alpha oscillations is associated with visual-perceptual abilities in children born very preterm. *Front. Hum. Neurosci.* 7:791. doi:10.2289/fnhum.2013.00791

Doesburg, S. M., Ribary, U., Herdman, A. T., Miller, S. P., Poskitt, K. J., Moiseev, A., et al. (2011). Altered long-range alpha-band synchronization during visual short-term memory retention in children born very preterm. *Neuroimage* 54, 2330–2339. doi:10.1016/j.neuroimage.2010.10.044

Doesburg, S. M., Vinette, S. A., Cheung, M. J., and Pang, E. W. (2012b). Theta-modulated gamma-band synchronization among activated regions during a verb generation task. *Front. Psychol.* 3:195. doi:10.3389/fpsyg.2012.00195

Doesburg, S. M., and Ward, L. M. (2009). "Synchronization between sources: emerging methods for understanding large-scale functional networks in the human brain," in *Coordinated Activity in the Brain*, eds J. L. Perez-Velazquez and R. Wennberg (New York: Springer), 25–42.

Dove, A., Pollmann, S., Schubert, T., Wiggins, C. J., and von Cramon, D. Y. (2000). Prefrontal cortex activation in task switching: an event-related fMRI study. *Brain Res. Cogn. Brain Res.* 9, doi:10.1016/S0926-6410(99)00029-4

Ecker, C., Suckling, J., Deoni, S. C., Lombardo, M. V., Bullmore, E. T., Baron-Cohen, S., et al. (2012). Brain anatomy and its relationship to behavior in adults with autism spectrum disorder. *Arch. Gen. Psychiatry* 69, 196–209. doi:10.1001/archgenpsychiatry.2011.1251

Eckert, M. A., Menon, V., Walczak, A., Ahlstrom, J., Denslow, S., Horwitz, A., et al. (2009). At the heart of the ventral attention system: the right anterior insula. *Hum. Brain Mapp.* 30, doi:10.1002/hbm.20688

Fries, P. (2005). A mechanism for cognitive dynamics: neuronal communication through neuronal coherence. *Trends Cogn. Sci. (Regul. Ed.)* 9, 474–480. doi:10.1016/j.tics.2005.08.011

Gilbert, S. J., Bird, G., Brindley, R., Frith, C. D., and Burgess, P. W. (2008). Atypical recruitment of medial prefrontal cortex in autism spectrum disorders: an fMRI study of two executive function tasks. *Neuropsychologia* 46, 2281–2291. doi:10.1016/j.neuropsychologia.2008.03.025

Gou, Z., Choudhury, N., and Benasich, A. A. (2011). Resting frontal gamma power at 16, 24 and 36 months predicts individual differences in language and cognition at 4 and 5 years. *Behav. Brain Res.* 220, 263–270. doi:10.1016/j.bbr.2011.01.048

Hill, E. L. (2004). Executive dysfunction in autism. *Trends Cogn. Sci.* 8, 26–32. doi:10.1016/j.tics.2003.11.003

Hill, E. L., and Bird, C. M. (2006). Executive processes in Asperger syndrome: patterns of performance in a multiple case series. *Neuropsychologia* 44, 2822–2835. doi:10.1016/j.neuropsychologia.2006.06.007

Hipp, J. F., Hawellek, D. J., Corbetta, M., Siegel, M., and Engel, A. K. (2012). Large-scale cortical correlation structure of spontaneous oscillatory activity. *Nat. Neurosci.* 15, 884–890. doi:10.1038/nn.3101

Hughes, C., Russell, J., and Robbins, T. W. (1994). Evidence for executive dysfunction in autism. *Neuropsychologia* 32, 477–492. doi:10.1016/0028-3932(94)90092-2

Hung, Y., Smith, M. L., and Taylor, M. J. (2012). Development of ACC-amygdala activations in processing unattended fear. *Neuroimage* 60, 545–552. doi:10.1016/j.neuroimage.2011.12.003

Ibrahim, G. M., Akiyama, T., Ochi, A., Otsubo, H., Smith, M. L., Taylor, M. J., et al. (2012). Disruption of Rolandic gamma-band functional connectivity by seizures is associated with motor impairments in children with epilepsy. *PLoS ONE* 7:e39326. doi:10.1371/journal.pone.0039326

Just, M. A., Cherkassky, V. L., Keller, T. A., Kana, R. J., and Minshew, N. J. (2007). Functional and anatomical cortical underconnectivity in Autism: evidence from an fMRI study of an executive function task and corpus callosum morphometry. *Cereb. Cortex* 17, 951–961. doi:10.1093/cercor/bhl006

Just, M. A., Keller, T. A., Malave, V. L., Kana, R. K., and Varma, S. (2012). Autism as a neural systems disorder: a theory of frontal-posterior underconnectivity. *Neurosci. Biobehav. Rev.* 36, 1292–1313. doi:10.1016/j.neubiorev.2012.02.007

Khan, S., Gramfort, A., Shetty, N. R., Kitzbichler, M. G., Ganesan, S., Moran, J. M., et al. (2013). Local and long-range functional connectivity is reduced in concert in autism spectrum disorders. *Proc. Natl. Acad. Sci. U.S.A.* 110, 3107–3112. doi:10.1073/pnas.1214533110

Konishi, S., Kawazu, M., Uchida, I., Kikyo, H., Asakura, I., and Miyashita, Y. (1999). Contribution of working memory to transient activation in human inferior prefrontal cortex during performance of the Wisconsin card sorting test. *Cereb. Cortex* 9, 745–753. doi:10.1093/cercor/9.7.745

Li, H., Xue, Z., Ellmore, T. M., Frye, R. E., and Wong, S. T. (2012). Network-based analysis reveals stronger diffusion-based connectivity and different correlations with language skills in brains of children with high functioning autism spectrum disorders. *Hum. Brain Mapp.* doi:10.1002/hbm.22185

Lisman, J. E., and Jensen, O. (2013). The theta-gamma neural code. *Neuron* 77, 1002–1016. doi:10.1016/j.neuron.2013.03.007

Lopez, B. R., Lincoln, A. J., Ozonoff, S., and Lai, Z. (2005). Examining the relationship between executive functions and restricted, repetitive symptoms of autistic disorder. *J. Autism Dev. Disord.* 35, 445–460. doi:10.1007/s10803-005-5035-x

Maes, J. H. R., Eling, P. A. T. M., Wezenberg, E., Vissers, C., and Kan, C. C. (2011). Attentional set shifting in autism spectrum disorder: differentiating between the role of perseveration, learned irrelevance, and novelty processing. *J. Clin. Exp. Neurophysiol.* 33, 210–217. doi:10.1080/13803395.2010.501327

Mak-Fan, K. M., Morris, D., Vidal, J., Anagnostou, E., Roberts, W., and Taylor, M. J. (2013). White matter and development in children with an autism spectrum disorder. *Autism* 17, 541–557.

Maxwell, C. R., Villalobos, M. E., Schultz, R. T., Herpertz-Dahlmann, B., Konrad, K., and Kohls, G. (2013). Atypical laterality of resting gamma oscillations in autism spectrum disorders. *J. Autism Dev. Disord.* doi:10.1007/s10803-013-1842-7

Monchi, O., Petrides, M., Petre, V., and Dagher, K. W. A. (2001). Wisconsin card sorting revisited: distinct neural circuits participating in different stages of the task identified by event-related functional magnetic resonance imaging. *J. Neurosci.* 21, 7733–7741.

Müller, R.-A., Shih, P., Keehn, B., Deyoe, J. R., Leyden, K. M., and Shukla, D. K. (2011). Underconnected, but how? A survey of functional connectivity MRI studies in autism spectrum disorders. *Cereb. Cortex* 21, 2233–2243. doi:10.1093/cercor/bhq296

Murias, M., Webb, S. J., Greenson, J., and Dawson, G. (2007). Resting state cortical connectivity reflected in EEG coherence in individuals with autism. *Biol. Psychiatry* 62, 270–273. doi:10.1016/j.biopsych.2006.11.012

Noonan, S. K., Haist, F., and Müller, R. A. (2009). Aberrant functional connectivity in autism: evidence from low-frequency BOLD signal fluctuations. *Brain Res.* 1262, 48–63. doi:10.1016/j.brainres.2008.12.076

O'Hearn, K., Asato, M., Ordaz, S., and Luna, B. (2008). Neurodevelopment and executive function in autism. *Dev. Psychophathol.* 20, 1103–1132. doi:10.1017/S0954579408000527

Ozonoff, S., Cook, I., Coon, H., Dawson, G., Joseph, R. M., Klin, A., et al. (2004). Performance on Cambridge neuropsychological test automated battery subtests sensitive to frontal lobe function in people with autistic disorder: evidence from the collaborative programs of excellence in autism network. *J. Autism Dev. Disord.* 34, 139–150. doi:10.1023/B:JADD.0000022605.81989.cc

Palva, S., and Palva, J. M. (2012). Discovering oscillatory interaction networks with M/EEG: challenges and breakthroughs. *Trends Cogn. Sci. (Regul. Ed.)* 16, 219–230. doi:10.1016/j.tics.2012.02.004

Pang, E. W. (2011). Practical aspects of running developmental studies in the MEG. *Brain Topogr.* 24, 253–260. doi:10.1007/s10548-011-0175-0

Robinson, S. E., and Vrba, J. (1999). "Functional neuroimaging by synthetic aperture magnetometry (SAM)," in *Recent Advances in Biomagnetism*, eds T. Yoshimoto, M. Kotani, S. Kuriki, H. Karibe, and N. Nakasato (Sendai: Tohoku University Press), 302–305.

Rubinov, M., and Sporns, O. (2010). Complex measures of brain connectivity: uses and interpretations. *Neuroimage* 52, 1059–1069. doi:10.1016/j.neuroimage.2009.10.003

Sarnthein, J., Petsche, H., Rappelsberger, P., Shaw, G. L., and von Stein, A. (1998). Synchronization between prefrontal and posterior association cortex during human working memory. *Proc. Natl. Acad. Sci. U.S.A.* 95, 7092–7096. doi:10.1073/pnas.95.12.7092

Schack, B., Vath, N., Petsche, H., Geissler, H. G., and Moller, E. (2002). Phase coupling of theta-gamma EEG rhythms during short-term memory processing. *Int. J. Psychophysiol.* 44, 143–163. doi:10.1016/S0167-8760(01)00199-4

Schafer, R. J., Lacadie, C., Vohr, B., Kesler, S. R., Schneider, K. C., Pugh, K. R., et al. (2009). Alterations in functional connectivity for language in prematurely born adolescents. *Brain* 132, 661–670. doi:10.1093/brain/awn353

Schmitz, N., Rubia, K., Daly, E., Smith, A., Williams, S., and Murphy, D. G. M. (2006). Neural correlates of executive function in autistic spectrum disorders. *Biol. Psychol.* 59, 7–16.

Schnitzler, A., and Gross, J. (2005). Normal and pathological communication in the brain. *Nat. Rev. Neurosci.* 6, 285–296. doi:10.1038/nrn1650

Sekihara, K., Nagarajan, S., Poeppel, D., Marantz, A., and Miyashita, Y. (2001). Reconstructing spatio-temporal activities of neural sources using an MEG vector beamformer technique. *IEEE Trans. Biomed. Eng.* 48, 760–771. doi:10.1109/10.930901

Shafritz, K. M., Dichter, G. S., Baranek, G. T., and Belger, A. (2008). The neural circuitry mediating shifts in behavioral response and cognitive set in autism. *Biol. Psychiatry* 63, 974–980. doi:10.1016/j.biopsych.2007.06.028

Shi, F., Wang, L., Peng, Z., Wee, C.-Y., and Shen, D. (2013). Altered modular organization of structural cortical networks in children with autism. *PLoS ONE* 8:e63131. doi:10.1371/journal.pone.0063131

Sohn, M. H., Ursu, S., Anderson, J. R., Stenger, V. A., and Carter, C. S. (2000). The role of prefrontal cortex and posterior parietal cortex in task switching. *Proc. Natl. Acad. Sci. U.S.A.* 97, 13448–13453. doi:10.1073/pnas.240460497

Sridharan, D., Levitin, D. J., and Menon, V. (2008). A critical role for the right fronto-insular cortex in switching between central-executive and default-mode networks. *Proc. Natl. Acad. Sci. U.S.A.* 105, 12569–12574. doi:10.1073/pnas.0800005105

Stam, C. J., Nolte, G., and Daffertshofer, A. (2007). Phase lag index: assessment of functional connectivity from multi channel EEG and MEG with diminished bias from common sources. *Hum. Brain Mapp.* 28, 1178–1193. doi:10.1002/hbm.20346

Stuss, D. T., and Alexander, M. P. (2007). Is there a dysexecutive syndrome? *Philos. Trans. R. Soc. Lond. B Biol. Sci.* 362, 901–915. doi:10.1098/rstb.2007.2096

Sun, L., Grützner, C., Bölte, S., Wibral, M., Tozman, T., Schlitt, S., et al. (2012). Impaired gamma-band activity during perceptual organization in adults with autism spectrum disorders: evidence for dysfunctional network activity in frontal-posterior cortices. *J. Neurosci.* 32, 9563–9573. doi:10.1523/JNEUROSCI.1073-12.2012

Taylor, M. J., Mills, T., and Pang, E. W. (2011). The development of face recognition; hippocampal and frontal lobe contributions determined with MEG. *Brain Topogr.* 24, 261–270. doi:10.1007/s10548-011-0192-z

Travers, B. G., Adluru, N., Ennis, C., Tromp, D. P. M., Destiche, D., Doran, S., et al. (2012). Diffusion tensor imaging in autism spectrum disorder: a review. *Autism Res.* 5, 289–313. doi:10.1002/aur.1243

Uhlhaas, P. J., Pipa, G., Lima, B., Melloni, L., Neuenschwander, S., and Nikolic, D. (2009a). Neural synchrony in cortical networks: history, concept and current status. *Front. Integr. Neurosci.* 3:1–19. doi:10.3389/neuro.07.017.2009

Uhlhaas, P. J., Roux, F., Singer, W., Haenschel, C., Sireteanu, R., and Rodriguez, E. (2009b). The development of neural synchrony reflects late maturation and restructuring of functional networks in humans. *Proc. Natl. Acad. Sci. U.S.A.* 106, 9866–9871. doi:10.1073/pnas.0900390106

Uhlhaas, P. J., Roux, F., Rodriguez, E., Rotarska-Jagiela, A., and Singer, W. (2010). Neural synchrony and the development of cortical networks. *Trends Cogn. Sci. (Regul. Ed.)* 14, 72–80. doi:10.1016/j.tics.2009.12.002

Varela, F., Lachaux, J., Rodriguez, E., and Martinerie, J. (2001). The brainweb: phase synchronization and large-scale integration. *Nat. Rev. Neurosci.* 2, 229–239. doi:10.1038/35067550

von Stein, A., Chiang, S., and König, P. (2000). Top-down processing mediated by interareal synchronization. *Proc. Natl. Acad. Sci. U.S.A.* 97, 14748–14753. doi:10.1073/pnas.97.26.14748

von Stein, A., and Sarnthein, J. (2000). Different frequencies for different scales of cortical integration: from local gamma to long range alpha/theta synchronization. *Int. J. Psychophysiol.* 38, 301–313. doi:10.1016/S0167-8760(00)00172-0

Wright, B., Alderson-Day, B., Prednergast, G., Bennett, S., Jordan, J., Whitton, C., et al. (2012). Gamma activation in young people with autism spectrum disorders and typically developing controls when viewing emotions on faces. *PLoS ONE* 7:e41326. doi:10.1371/journal.pone.0041326

Xia, M., Wang, J., and He, Y. (2013). BrainNet Viewer: a network visualization tool for human brain connectomics. *PLoS ONE* 8:e68910. doi:10.1371/journal.pone.0068910

Yerys, B. E., Wallace, G. L., Harrison, B., Celano, M. J., Giedd, J. N., and Kenworthe, L. E. (2009). Set-shifting in children with autism spectrum disorders. *Autism* 13, 523–538. doi:10.1177/1362361309335716

Zalesky, A., Cocci, L., Fortino, A., Murray, M. M., and Bullmore, E. (2012). Connectivity differences in brain networks. *Neuroimage* 60, 1055–1062. doi:10.1016/j.neuroimage.2012.01.068

Zalesky, A., Fornito, A., and Bullmore, E. T. (2010). Network-based statistic: identifying differences in brain networks. *Neuroimage* 53, 1197–1207. doi:10.1016/j.neuroimage.2010.06.041

Zanolie, K., Leijenhorst, L. V., Rombouts, S. A. R. B., and Crone, E. A. (2008). Separable neural mechanisms contribute to feedback processing in a rule-learning task. *Neuropsychologia* 46, 117–126. doi:10.1016/j.neuropsychologia.2007.08.009

Conflict of Interest Statement: The authors declare that the research was conducted in the absence of any commercial or financial relationships that could be construed as a potential conflict of interest.

Received: 29 July 2013; paper pending published: 17 September 2013; accepted: 30 October 2013; published online: 14 November 2013.

*Citation: Doesburg SM, Vidal J and Taylor MJ (2013) Reduced theta connectivity during set-shifting in children with autism. Front. Hum. Neurosci. **7**:785. doi: 10.3389/fnhum.2013.00785*

This article was submitted to the journal Frontiers in Human Neuroscience.

frontiers in
HUMAN NEUROSCIENCE

ORIGINAL RESEARCH ARTICLE
published: 24 September 2013
doi: 10.3389/fnhum.2013.00600

Resting-state oscillatory activity in children born small for gestational age: an MEG study

Maria Boersma[1,2]*, Henrica M. A. de Bie[2,3], Kim J. Oostrom[2,4], Bob W. van Dijk[2,5], Arjan Hillebrand[1,2], Bernadette C. M. van Wijk[6], Henriëtte A. Delemarre-van de Waal[3,7†] and Cornelis J. Stam[1,2†]

[1] Department of Clinical Neurophysiology, VU University Medical Center, Amsterdam, Netherlands
[2] Neuroscience Campus Amsterdam, Amsterdam, Netherlands
[3] Department of Pediatrics, VU University Medical Center, Amsterdam, Netherlands
[4] Department of Pediatric Psychology, VU University Medical Center, Amsterdam, Netherlands
[5] Department of Physics and Medical Technology, VU University Medical Center, Amsterdam, Netherlands
[6] Research Institute MOVE, VU University Amsterdam, Amsterdam, Netherlands
[7] Department of Pediatrics, Leiden University Medical Center, Leiden, Netherlands

Edited by:
Hubert Preissl, University of Tübingen, Germany

Reviewed by:
Giancarlo Zito, 'S. Giovanni Calibita' Fatebenefratelli Hospital, Italy
Krunoslav T. Stingl, University of Tübingen, Germany
Fabrice Wallois, Institut National de la Santé et de la Recherche Médicale, France

***Correspondence:**
Maria Boersma, Department of Clinical Neurophysiology/MEG Center, VU University Medical Center, P.O. Box 7057, 1007 MB Amsterdam, Netherlands
e-mail: mariaboersma@gmail.com

[†] Henriëtte A. Delemarre-van de Waal and Cornelis J. Stam have contributed equally to this work.

Growth restriction *in utero* during a period that is critical for normal growth of the brain, has previously been associated with deviations in cognitive abilities and brain anatomical and functional changes. We measured magnetoencephalography (MEG) in 4- to 7-year-old children to test if children born small for gestational age (SGA) show deviations in resting-state brain oscillatory activity. Children born SGA with postnatally spontaneous catch-up growth [SGA+; six boys, seven girls; mean age 6.3 year (SD = 0.9)] and children born appropriate for gestational age [AGA; seven boys, three girls; mean age 6.0 year (SD = 1.2)] participated in a resting-state MEG study. We calculated absolute and relative power spectra and used non-parametric statistics to test for group differences. SGA+ and AGA born children showed no significant differences in absolute and relative power except for reduced absolute gamma band power in SGA children. At the time of MEG investigation, SGA+ children showed significantly lower head circumference (HC) and a trend toward lower IQ, however there was no association of HC or IQ with absolute or relative power. Except for reduced absolute gamma band power, our findings suggest normal brain activity patterns at school age in a group of children born SGA in which spontaneous catch-up growth of bodily length after birth occurred. Although previous findings suggest that being born SGA alters brain oscillatory activity early in neonatal life, we show that these neonatal alterations do not persist at early school age when spontaneous postnatal catch-up growth occurs after birth.

Keywords: magnetoencephalography, spectral power, children, small for gestational age, SGA, IQ

INTRODUCTION

Of all live-born neonates, a small percentage is born small for gestational age (SGA). This percentage depends on the definition used and ranges between 2 and 10%. SGA born children are characterized by a decreased body weight and/or length and diminished head circumference at birth. Children born SGA suffered from suboptimal intra-uterine conditions that lead to underdevelopment of the body and the brain (de Bie et al., 2010; Frisk et al., 2002; Mallard et al., 2000; Rehn et al., 2004; Saenger et al., 2007; Toft et al., 1995; Tolsa et al., 2004). The most common cause of intra-uterine growth restriction (IUGR) is placental insufficiency (Mallard et al., 2000; Rehn et al., 2004). Other factors that influence fetal growth are maternal age and nutrition, placental function and size, smoking, genetic factors, endocrine factors, and sex of fetus. The majority of SGA born children show catch-up growth in the first 2 years of life (SGA+), and approximately 10% lack catch-up growth (SGA−), showing persistent short stature (Saenger et al., 2007). SGA inclusion criteria and definitions are described in the methods section. Besides physical dysregulation, SGA is associated with decreased levels of intelligence and cognitive abilities in children and adults (de Bie et al., 2010; Lundgren et al., 2001; Strauss, 2000). Interestingly, catch-up growth during the first years of life is associated with relatively better cognitive outcome (Frisk et al., 2002; Lundgren et al., 2001; Saenger et al., 2007).

The period during which SGA born children suffer from intra-uterine growth restriction is generally unknown since frequent monitoring of fetal growth with ultrasound echo is not a common procedure. Dependent on the timing of growth restriction, several brain maturation processes can be affected. In the last trimester of pregnancy, proliferation, and migration of neurons is being completed while maturational processes such as synaptogenesis, dendritic aborization, and myelination start to connect the neurons (Dubois et al., 2008; Ment et al., 2009; Rees et al., 2008; Tolsa et al., 2004; Volpe, 2000). Growth restriction might affect these basic maturation processes and can have long-term consequences.

A few studies have investigated the effects of being born SGA on brain anatomy later in life with magnetic resonance imaging (MRI). Martinussen and colleagues reported on lower total brain volume with reduced white matter volume but no significant

differences in gray matter volume for term born SGA 15-year-old adolescents when compared to healthy adolescents (Martinussen et al., 2005, 2009). These results are in line with the results of our recent MRI study in children born SGA at early school age (4- to 7-year-old) (de Bie et al., 2011). This study further differentiated between SGA children with catch-up growth (SGA+) and without catch-up growth (SGA−). Children born SGA demonstrated smaller brains with lower white matter volumes and a smaller cortical surface area. SGA+ children constituted an intermediate between children born appropriate for gestational age (AGA) and SGA− children with respect to these brain parameters with a linear trend ordered from highest volumes and surface area in AGA to SGA− via SGA+ children. Furthermore, both SGA subgroups showed regional differences in cortical thickness most pronounced in the anterior and inferior prefrontal cortex, with SGA− children having the thickest cortex, to intermediate in SGA+ children and lowest in AGA.

Brain oscillatory activity can be recorded with electro- and magnetoencephalography (EEG/MEG). These oscillations are assumed to originate from large neuronal networks that synchronize their activity in the brain areas underlying the sensors. The amplitude of the recorded signals depends on the number of neurons firing in synchrony, which in turn depends on the local connectivity patterns between excitatory and inhibitory neurons as well as on local synaptic density. Development of this oscillatory activity in healthy children is characterized by increases in the amplitude of high frequency oscillations (alpha, beta, and gamma bands) and a reduction in the amplitude of slow oscillations (delta and theta bands) (Okumura et al., 2006; Uhlhaas et al., 2009; Gmehlin et al., 2011). As brain anatomy is affected in SGA children, the development of normal oscillatory activity patterns might also be affected. In an earlier study investigating the effect of being born SGA on brain oscillatory activity, Ozdemir et al. (2009) recorded the EEG of 40 term SGA, and 20 term AGA infants in their first week after birth, and in their first and third month, all during sleep. The authors reported that in all records the amplitude levels were significantly lower for the SGA group than for the AGA group. Furthermore, SGA showed higher relative power for low frequencies and less power for higher frequencies. The authors interpreted their findings as a delay in electrophysiological maturation in term SGA infants.

An advantage of MEG over EEG is that it is a more child-friendly recording technique as the helmet with inbuilt sensors replaces the need to glue electrodes on the head which could be distressing for children. Moreover, the MEG scanner has a 151-sensor array resulting in higher spatial resolution and it is insensitive to the effects of skull-thickness and skin and scalp conductivity, which might have biased the results of Ozdemir and colleagues. In the present study, we used MEG to record brain oscillations during an eyes-closed resting-state condition in SGA and AGA born children at early school age (4–7 years old). The aim of our study was to investigate whether and how oscillatory brain activity is affected in 4- to 7-year-old term born SGA born children in which postnatal catch-up growth has occurred. To answer this question, we calculated the absolute and relative power spectra for several frequency bands and tested for differences between children born SGA and AGA.

MATERIALS AND METHODS

SUBJECTS

This study presents baseline data from a longitudinal project that studies the effects of growth hormone (GH) therapy on brain development and cognition in children born SGA (Dutch Trial Register: NTR 865). The complete project included neuropsychological assessment as well as MRI and MEG investigation and was performed at the VU University Medical Center from March 2007 until April 2010.

Inclusion period of children for MEG scanning ran from March 2008 till October 2009, after which the MEG was replaced by a new system. The study was approved by the ethics committee of the VU University Medical Center. Written informed consent was obtained from the parents or guardians of each child and obtained according to the Declaration of Helsinki (BMJ, 1991; Vol. 302: p. 1194).

Exclusion criteria were: (1) severe prematurity below 34 weeks, (2) complicated neonatal period with signs of severe asphyxia, defined as an Apgar score <7 after 5 min., (3) multiple birth, (4) growth failure caused by somatic or chromosomal disorders or syndromes (except for Silver–Russell syndrome), (5) previous or present use of medication that could interfere with growth or GH treatment, and (6) severe learning disability (IQ < 70). Additional exclusion criteria based on the MEG recordings are described in the data processing section below.

Both SGA and AGA groups were in the age range of 4–7 years old at the moment of the MEG recordings. We included 12 AGA born children and 18 children that were born SGA. Of the 18 SGA children, 14 showed postnatal catch-up growth (SGA+). Following the International Small for Gestational Age Advisory Consensus Board Development Conference Statement (Lee et al., 2003), SGA was defined by a birth weight and/or length less than or equal to −2 SD, adjusted for gender and gestational age; SGA+ was defined as postnatal catch-up growth with an actual height of less than 2 SD below the Dutch population reference mean; and SGA− as persistent postnatal growth failure based on an actual height of less than 2.5 SD below this mean (Fredriks et al., 2000). SGA− children were not included in the current study. AGA was defined as birth weight and length above −2 SD, without known history of prenatal growth restriction. SGA children were selected from the pediatric hospitals in The Netherlands.

Three children (two AGA, one SGA+) were excluded from further processing since they showed minor abnormalities in their MEG recordings (see description in Data Processing); 10 AGA born and 13 SGA+ children were finally included in this study.

MAGNETOENCEPHALOGRAPHY RECORDINGS

Since all children included in our study underwent an MRI dummy scanner training session (de Bie et al., 2010), we used this session to shortly explain the MEG scanning procedure as well. We showed and fitted the MEG helmet to familiarize the children with the helmet and with padding their heads with a foam headband. Padding minimized head movements during recording and placed the small child head in a more centered position in the helmet.

Magnetoencephalography data were acquired during a no-task eyes-closed resting-state condition inside a magnetically shielded room (Vacuumschmelze GmbH, Hanau, Germany) using

a 151-channel whole-head radial gradiometer MEG system (CTF Systems Inc., Port Coquitlam, BC, Canada) at the VU University Medical Center. A sample frequency of 625 Hz was used and the standard preprocessing steps undertaken at our lab to reduce noise are, spatial filtering using third order gradiometers (Vrba et al., 1999), band pass filtering, and visual inspection (see criteria in Data Processing) discarding data contaminated by artifacts. Visual inspection may be preferred over automatic approaches, since, for instance, an independent component analysis may introduce complex new artifacts or biases (Gross et al., 2013). Twelve sensors were not functioning during at least 1 of the recordings, and these were excluded from the analysis for all subjects. At the beginning and end of each recording, the head position relative to the coordinate system of the helmet was recorded by leading small alternating currents through three head position coils attached to the left and right preauricular points and the nasion. Head position changes during the recording of up to 1.5 cm were accepted, to which all children complied. The distance between the cortical mantle and the MEG sensors might have influenced the amplitude of the measured oscillatory signal. As an approximation of the distance of the cortical mantle to the MEG sensors, we calculated the distance of three coils (placed at the nasion, the left ear, and right ear preauricular fiducials) from the center of the MEG helmet.

During the resting-state condition, children were lying comfortably, and were instructed after 1 min to close their eyes for 4 min and move as little as possible. One of the investigators stood nearby the child to control for his/her well-being and one of the parents or caretakers was seated in a corner of the shielded room to comfort the child when necessary.

DATA PROCESSING

For off-line processing, the recordings were converted to ASCII format. Visual inspection and selection of the time segments was done by one of the investigators (MB) with BRAINWAVE software (CS, http://home.kpn.nl/stam7883/brainwave.html). For each child we selected five artifact-free time segments of 4096 samples (∼6.5 s) from the 4 min eyes-closed condition. This has proven to be sufficient to detect clinically relevant differences in power in previous MEG studies (De Haan et al., 2008; Bosboom et al., 2009) and stable over time within healthy subjects (Olde Dubbelink et al., 2013).

Typical artifacts were related to (eye) movement, drowsiness, or muscle contractions. One SGA+ child was excluded from further analysis due to continuous artifacts caused by construction activities near the scanner room. Three children showed minor abnormalities in their MEG recordings (two AGA, one SGA+). These patterns were characterized as spike and wave discharges and sharp waves. Besides these deviant patterns, the background MEG appeared normal in all of these children and these children had no history of epileptic seizures or other clinical symptoms. Since this deviant activity might affect the outcome, we excluded these three children from further analysis.

For each selected time segment, we converted the MEG signal per sensor from the time domain into the frequency domain (Welch periodogram; matlab 7.0; window = 1024 samples; overlap = 512 samples; nfft = 1024; sample frequency = 625 Hz). Per sensor, the absolute power spectrum ranging from 1 to 48 Hz was divided into 78 bins of 0.618 Hz. For relative power spectra construction, the absolute power for each bin was divided by the absolute power of the total spectrum, resulting in values ranging between 0 and 1. It is well known that children at school age show a reduced alpha peak frequency (∼8 Hz) (Marshall et al., 2002; Boersma et al., 2011) compared to adults (∼10 Hz) (Cragg et al., 2011; Smit et al., 2011). Consequently, the alpha frequency would be split up at its peak in case standard definitions of adult lower and upper alpha frequency bands were to be used, which could introduce biases into the results. To ensure that all alpha-like frequencies are captured in children at school age, we chose to use the recorded profile (group averaged) power spectrum (shown in **Figure 1**), which shows clear theta and alpha peaks, to define new boundaries for the theta and alpha band that are appropriate for our population: total spectral power 1–48 Hz, delta 1.0–2.9 Hz, theta 2.9–5.4 Hz, alpha 5.4–11.5 Hz, beta 11.5–27.3 Hz, and gamma 27.3–48 Hz. Subsequently, per sensor, we computed the spectral power within these frequency bands by averaging over bins within these frequency ranges. Then, we averaged these outcomes over all MEG sensors (except 12 noisy or broken sensors), and subsequently, the outcomes were averaged over epochs (five per child) for each child.

To avoid possible biases of the selection of the frequency bands, additional analysis of absolute and relative power in 78 frequency bins was performed. We furthermore performed a region based analysis by grouping sensors in left and right anterior, left and right posterior and left and right temporal areas and subsequently averaged relative and absolute power over the sensors in each region for the different frequency bands.

ESTIMATION OF INTELLIGENCE AND PHYSICAL MEASUREMENT

Both physical examination and estimations of intelligence were performed ranging from 36 weeks before to 23 weeks after MEG investigation. An estimate of the full scale IQ (eIQ) was based on a four-subtest short version of the much used and well standardized Wechsler's scales that would ordinarily be obtained by administration of the complete scales. Estimates of reliability and validity indicate that the abbreviated forms of the Wechsler Preschool and Primary Scale Intelligence – Revised (WPPSI-R, Dutch version), for children under 6 years and the Wechsler Intelligence Scale for Children – third Edition (WISC-III, Dutch version) for children 6 years and older may be used to approximate the Full Scale IQ when time limitations are a consideration (Kaufman et al., 1996; LoBello, 1991). Parental educational levels were classified according to the International Standard Classification of Education (1997).

STATISTICS

Statistical analyses were performed using SPSS 15.0 (Chicago, IL, USA). We used non-parametrical tests for all group comparisons because of the small group sizes and a skewed distribution of spectral power. To test for group differences in subject characteristics, Mann–Whitney *U*-tests were used for continuous data (eIQ, body weight, length, head circumference) and Fisher exact tests were used for categorical variables (gender, handedness, parental education). Mann–Whitney *U*-tests were used to test for differences between AGA and SGA groups in absolute and relative power in

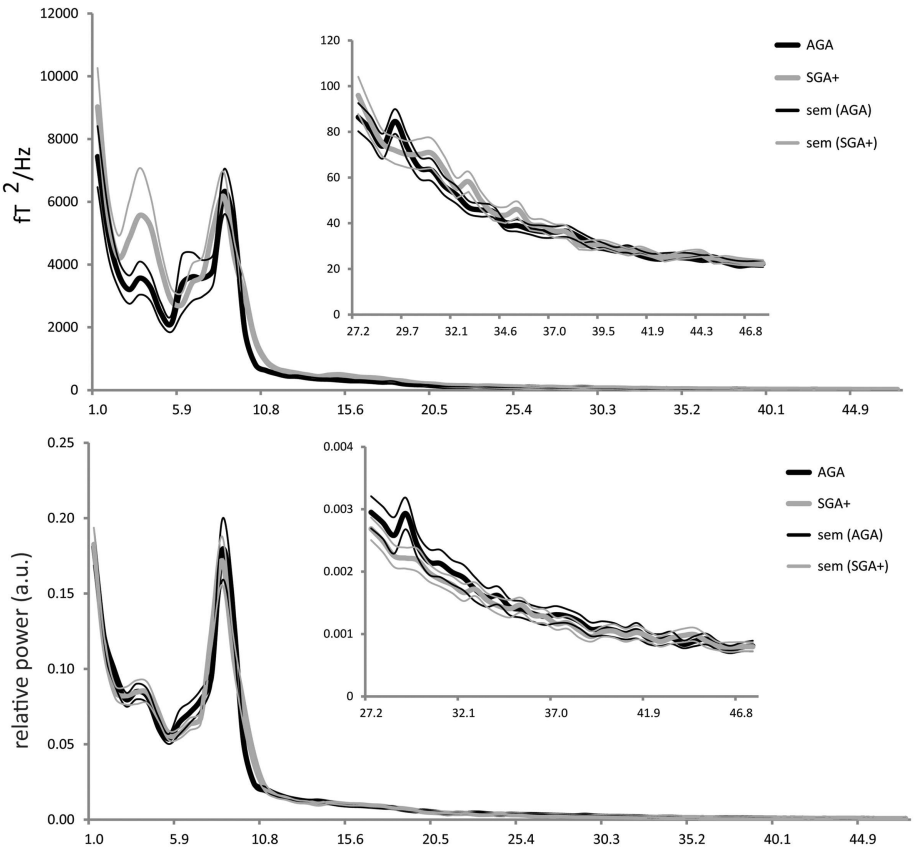

FIGURE 1 | Absolute power (*y*-axis: absolute power in fT2/Hz; *x*-axis: frequency in Hertz) and relative power (*y*-axis: arbitrary units; *x*-axis: frequency in Hertz) averaged for the AGA and SGA born groups, per group averaged over all MEG sensors (five epochs per child). Thick solid black lines represent the average of AGA born children; thick gray lines the SGA+ born children (standard errors of the mean are represented in thin lines).

several frequency bands. *Post hoc* analyses were done to investigate the relationships between total absolute power and continuous variables, which included IQ, head circumference, and the distance between head position coils and the MEG helmet, by using Spearman's rank correlations. For all analyses, p-values < 0.05 (two-tailed) and Z values (ignoring the sign) greater than 1.96 were considered statistically significant.

Additional analysis using log-transformed data and t-tests for independent samples for absolute and relative power for 78 frequency bins were performed to avoid possible biases of the selection of the frequency bands. To statistically test for group differences in region based analysis, we used log-transformed data, t-tests for independent samples and FDR correction for multiple testing.

RESULTS

SUBJECT CHARACTERISTICS

Table 1 lists subject characteristics per group and the significance of the differences between groups. Distributions of handedness and gender did not differ between groups. Twenty-one children were right-handed and the two left-handed children were equally distributed over the subgroups. Groups did not differ in gestational age. Conform the definition, children born SGA had a significantly lower birth weight than AGA born children. Furthermore, although relatively spared compared to body weight and length, head circumference at birth was significantly lower in SGA compared to AGA children. Age at MEG recording did not differ between the groups. Body length at the MEG recording was significantly lower in SGA children compared to AGA. Although catch-up growth had occurred in all SGA+ children, mean length SD was just below population mean. In contrast, complete catch-up of head circumference (mean SD $= -0.08$) had occurred. Nevertheless, head circumference in SGA+ was significantly lower compared to AGA children. This difference is possibly due to AGA children having a head circumference slightly above average compared to the Dutch population mean, whereas SGA+ children showed head circumference comparable to the Dutch population mean. For body length, all SGA+ children stayed within -2 SD of the mean according to definition. A trend toward significance was found with higher eIQ in AGA children compared to SGA+ children. As the control group shows an IQ of 120, the IQ difference (at trend level, $p = 0.058$) between groups indicates that the control group shows intelligence above average instead of reduced intelligence in SGA children. The proportion of parents in the SGA group with an educational level confined to first stage of basic education or lower secondary education did not differ from

Table 1 | Subject characteristics.

	AGA ($n = 10$)	SGA+ ($n = 13$)	AGA vs. SGA+		
	Mean ± SD	Mean ± SD	*U*	*Z*	*p*
Gender (boy: girl)	7:3	6:7			0.428[a]
Handedness (right: left)	9:1	12:1			0.999[a]
Gestational age (weeks)	39.4 ± 1.2	38.4 ± 2.0	46.5	−1.151	0.25
Weight at birth (grams)	3464 ± 489	2144 ± 407	1.0	−3.840	**<0.001**
Weight at birth compared to Dutch population ($SD^{reference}$)	0.10 ± 0.88	−2.61 ± 0.40	0.0	−4.037	**<0.001**
Head circumference at birth compared to Dutch population ($SD^{reference}$)	0.21 ± 0.67	−1.09 ± 0.75	8.0	−3.434	**<0.001**
Age at MEG investigation (years)	5.97 ± 1.2	6.28 ± 0.87	55.5	−0.589	0.556
IQ estimated	114.2 ± 12.2	104.8 ± 11.8	34.5	−1.897	0.058
Length at MEG investigation (cm)	118.1 ± 10.5	111.6 ± 7	44.5	−1.272	0.203
Length at MEG investigation compared to Dutch population ($SD^{reference}$)	0.22 ± 1.02	−0.59 ± 0.75	31.0	−2.110	**0.035**
Weight at MEG investigation (kg)	23.10 ± 8.10	17.2 ± 6.2	28.0	−2.112	**0.035**
Weight at MEG investigation compared to Dutch population ($SD^{reference\ \#}$)	−0.05 ± 0.85	−0.67 ± 1.08	36.0	−1.800	0.072
Head circumference at MEG investigation (cm)	52.0 ± 1.30	51.0 ± 1.2	29.5	−1.749	0.080
Head circumference at MEG investigation compared to Dutch population ($SD^{reference}$)	0.59 ± 0.68	−0.08 ± 0.65	26.5	−2.398	**0.016**

[a] Fisher exact; Body weight and length, as well as head circumference, are expressed in both absolute measures as well as in deviations from the Dutch population mean (where the deviation is expressed as fraction of the SD of the reference population, $SD^{reference}$); # SD according to length. Data (except gender and handedness) are presented as mean (±SD). Bold text indicates a statistical significant difference ($p < 0.05$).

the parents in the AGA group (3 mothers SGA+ vs. 0 mothers AGA, Fisher exact $p = 0.853$; 3 fathers vs. 0 fathers AGA, Fisher exact $p = 0.443$).

POWER SPECTRA

As shown in **Figure 1**, the absolute power spectra for SGA born children and AGA born children largely overlap. Overall, the SGA group has comparable absolute power over the whole frequency range. More specifically, group comparison showed that AGA and SGA+ groups did not differ significantly in absolute power in all frequency bands except for the gamma band, in which SGA+ had lower gamma power (for statistics see **Table 2**).

Figure 1 showed that the relative power spectra for the SGA+ and AGA group largely overlap. Relative power did not differ between groups for the total spectrum, nor for the separate frequency bands (for statistics see **Table 2**). In summary, the SGA group shows similar frequency distributions of the brain oscillations, with similar amplitudes except for the gamma band.

When performing additional analysis testing for group differences in 78 frequency bins, we did not find significant group differences in both absolute and relative power in any of the 78 frequency bins, even when no correction for multiple testing was performed.

We did not find significant group differences when evaluating regional functional differences in left and right anterior, posterior and temporal regions.

POST HOC ANALYSES

We tested whether groups differed in distances between the head and the MEG helmet as this might influence the amplitude of the measured oscillatory signal. AGA and SGA did not show significantly different distances ($U = 95.0$, $Z = -0.310$, $p = 0.757$). We found significant smaller head circumferences (in SD) in SGA children compared to AGA children (**Table 1**), though we did not find a relation between head circumference and total spectral power in both AGA and the SGA group. Furthermore, we did not find significant correlations between eIQ and absolute or relative power in both groups.

Table 2 | Test statistics for absolute and relative power.

	AGA vs. SGA+		
	U	*Z*	*p*
ABSOLUTE POWER			
Total	46.000	−1.18	0.239
Delta	45.000	−1.24	0.215
Theta	51.000	−0.87	0.385
Alpha	43.000	−1.36	0.172
Beta	50.000	−0.93	0.352
Gamma	27.000	−2.36	**0.018**
RELATIVE POWER			
Delta	61.000	−0.25	0.804
Theta	51.000	−0.87	0.385
Alpha	52.000	−0.81	0.420
Beta	61.000	−0.25	0.804
Gamma	58.000	−0.43	0.664

Bold text indicates a statistical significant difference ($p < 0.05$).

DISCUSSION

In this study, we tested if oscillatory brain activity is affected in term born SGA born children at early school age, as suggested by the findings of a previous EEG study. Only SGA born children in which postnatal catch-up growth had occurred were included. SGA+

children showed significantly lower absolute power than AGA children in the gamma band, but not in other frequency bands. The relative power spectra did not significantly differ between AGA and SGA groups. A trend toward significance with higher eIQ in AGA children compared to SGA children was found. Estimated IQ did not correlate with absolute or relative power in both groups. Head circumference differed between AGA and SGA children however HC was not correlating with absolute power in both groups.

In contrast to the EEG-based results by Ozdemir et al. (2009), we found that relative and absolute power did not differ between SGA born children at early school age compared to AGA children, except for lower absolute gamma band power in SGA born children. This frequency band was not examined in the neonates investigated by Ozdemir et al. Furthermore, distinguishing true brain gamma band oscillations from gamma band activity caused by muscle artifacts using EEG is difficult as recently has been shown (Whitham et al., 2007). Unlike EEG, MEG has the advantage of being insensitive to skull-thickness and skin-conductance (Ent et al., 2009), and no reference electrode is required. Possible differences in skull-thickness between AGA and SGA born children, could therefore not have affected our estimated MEG power spectra. On the other hand, MEG might be more influenced by head movements and might favor tangential sources [but see (Hillebrand and Barnes, 2003)]. Although in the present study visual inspection of the lower frequency ranges in the absolute power spectrum might suggest group differences, additional statistical tests based on log-transformed data did not show significant differences between groups in the delta and theta bands. Furthermore, supplemental analyses for log-transformed data did not show significant group differences in both absolute and relative power in any of the 78 frequency bins. Moreover, groups did not significantly differ when evaluating regional functional differences in left and right anterior, posterior and temporal regions.

Few other studies investigated the effect of (extreme) low birth weight on spectral power in neonates and adults (Grieve et al., 2008; Miskovic et al., 2009), however, these studies included preterm births. Distinction between the effects of IUGR and the effect of gestational age and prematurity is difficult since prematurity also affects oscillatory activity as shown in a recent MEG study (Doesburg et al., 2011). They found reduced alpha band power and slowing of the peak frequency in 7-year-old children who were born very premature. Young adults born preterm with a very low birth weight (VLBW) showed significantly higher relative spectral power in the lower frequency bands and lower relative power in higher frequency bands compared to adults born with normal birth weight (NBW) (Miskovic et al., 2009) suggesting a maturational delay of the brain that persists into adulthood. Different from these findings, our groups showed highly overlapping absolute and relative power spectra demonstrating that at early school age the ratios of low and high frequency oscillations are comparable between term born SGA+ and AGA born children. This suggests that the development of brain oscillatory activity is not delayed at early school age in SGA born children born at term.

Strong associations have been described in the literature between IQ and oscillatory activity in resting-state conditions, implicating that the basic resting-state condition is highly informative about a brain's cognitive capabilities. Thatcher et al. (2005) reported positive correlations between IQ and absolute power for all frequency bands in a group of healthy subjects with an age range from 5 to 52 years old. Schmid et al. (2002) found a positive relationship between IQ and relative alpha band power, and a negative correlation between IQ and lower frequency band relative power in school age children. We did not find significant correlations between eIQ and absolute or relative power for both groups. The mean IQ's in our sample are relatively high which may not appear to be typical to SGA once we study larger samples. Future research in larger groups should further investigate the effects of being born SGA and catch-up growth on the association between intelligence and brain oscillatory activity.

This study was limited by a few factors. It has previously been reported that EEG abnormalities of mild nature occur more often in SGA newborns than in a control group (Fitzhardinge and Steven, 1972). One SGA and two AGA born children exhibited (occasional) spikes and/or spike and wave patterns without apparent clinical symptoms. Since deviant activity might have influenced the outcome, we decided to exclude these children from further analysis. Unfortunately, we were not able to enlarge the sample size due to scanner replacement. Furthermore, we only included SGA+ children. Future studies should test for the effect of bodily catch-up growth on oscillatory brain activity in SGA children.

What might be the biological mechanisms that underlie the reduction in absolute gamma power observed in SGA born children? The oscillatory activity measured by MEG is assumed to originate from large networks of spatially and temporally organized neurons and is dependent on local synaptic density and cortical volume, which is shown to be lowered as smaller volumes are found in SGA born children (de Bie et al., 2011). The amplitude of the signal also depends on the synchronizability of the underlying networks, which in turn depends on local connectivity patterns between the excitatory and inhibitory neurons within these networks. In the present study changes in neural mass/local neural circuits might have only led to reductions in the amplitude (absolute power) without changing the frequency of the oscillations (which would have been reflected in the relative power). Especially gamma band activity has previously been associated with perception and attention and cortical local short-distance connections are thought to underlie the high frequency oscillations (Jensen et al., 2007). During pre- and postnatal maturation of the brain, the ability of neurons to migrate, differentiate, and connect to other neurons is important for the formation of optimally organized networks and for the establishment of synchronous activity in these networks. The timing and severity of growth restriction *in utero* determines which brain maturation processes are affected and what the impact of intra-uterine growth restriction will be later in live (Kostovic and Jovanov-Milosevic, 2006; Kostovic and Judas, 2006; Rees et al., 2008). Disturbances of these processes early in life might have affected the ability to synchronize these networks. Future studies should further investigate if severity of IUGR early in life is related to gamma power and for instance attention and behavior later in life.

In conclusion, the great overlap in both relative and absolute power suggests normal development of brain oscillatory activity at early school age in term born SGA children when spontaneous bodily catch-up growth has occurred. An important question that remains to be answered, is how disturbances early in development affect the organization of functional brain networks and its dynamics when SGA born children do not show spontaneous bodily catch-up growth.

ACKNOWLEDGMENTS

We thank Jessica Jeltes, PeterJan Ris, Ndedi Sijsma, and Jeroen Verbunt for their technical assistance and help with data acquisition. We also thank the children and their parents for their motivated participation in this study. This project was financially supported by an educational grant from Pfizer bv, The Netherlands. The Netherlands Organization for Scientific Research (NWO grant # 021-002-047) financially supported the contribution by B. C. M. van Wijk. The authors declare that they have no conflict of interest.

REFERENCES

Boersma, M., Smit, D. J., de Bie, H. M., van Baal, G. C., Boomsma, D. I., de Geus, E. J., et al. (2011). Network analysis of resting state EEG in the developing young brain: structure comes with maturation. *Hum. Brain Mapp.* 32, 413–425. doi:10.1002/hbm.21030

Bosboom, J. L. W., Stoffers, D., Wolters, E. C., Stam, C. J., and Berendse, H. W. (2009). MEG resting state functional connectivity in Parkinson's disease related dementia. *J. Neural Transm.* 116, 193–202. doi:10.1007/s00702-008-0132-6

Cragg, L., Kovacevic, N., McIntosh, A. R., Poulsen, C., Martinu, K., Leonard, G., et al. (2011). Maturation of EEG power spectra in early adolescence: a longitudinal study. *Dev. Sci.* 14, 935–943. doi:10.1111/j.1467-7687.2010.01031.x

de Bie, H. M., Oostrom, K. J., Boersma, M., Veltman, D. J., Barkhof, F., Delemarre-van de Waal, H. A., et al. (2011). Global and regional differences in brain anatomy of young children born small for gestational age. *PLoS ONE* 6:e24116. doi:10.1371/journal.pone.0024116

de Bie, H. M., Oostrom, K. J., and Delemarre-van de Waal, H. A. (2010). Brain development, intelligence and cognitive outcome in children born small for gestational age. *Horm. Res. Paediatr.* 73, 6–14. doi:10.1159/000271911

De Haan, W., Stam, C. J., Jones, B. F., Zuiderwijk, I. M., van Dijk, B. W., and Scheltens, P. (2008). Resting-state oscillatory brain dynamics in Alzheimer disease. *J. Clin. Neurophysiol. Off. Publ. Am. Electroencephalogr. Soc.* 25, 187–193. doi:10.1097/WNP.0b013e31817da184

Doesburg, S. M., Ribary, U., Herdman, A. T., Moiseev, A., Cheung, T., Miller, S. P., et al. (2011). Magnetoencephalography reveals slowing of resting peak oscillatory frequency in children born very preterm. *Pediatr. Res.* 70, 171–175. doi:10.1038/pr.2011.396

Dubois, J., haene-Lambertz, G., Perrin, M., Mangin, J. F., Cointepas, Y., Duchesnay, E., et al. (2008). Asynchrony of the early maturation of white matter bundles in healthy infants: quantitative landmarks revealed noninvasively by diffusion tensor imaging. *Hum. Brain Mapp.* 29, 14–27. doi:10.1002/hbm.20363

Ent, D., Soelen, I., Stam, C. J., De Geus, E. J., and Boomsma, D. I. (2009). Strong resemblance in the amplitude of oscillatory brain activity in monozygotic twins is not caused by "trivial" similarities in the composition of the skull. *Hum. Brain Mapp.* 30, 2142–2145. doi:10.1002/hbm.20656

Fitzhardinge, P. M., and Steven, E. M. (1972). The small-for-date infant. II. Neurological and intellectual sequelae. *Pediatrics* 50, 50–57.

Fredriks, A. M., van Buuren, S., Burgmeijer, R. J., Meulmeester, J. F., Beuker, R. J., Brugman, E., et al. (2000). Continuing positive secular growth change in The Netherlands 1955-1997. *Pediatr. Res.* 47, 316–323. doi:10.1203/00006450-200003000-00006

Frisk, V., Amsel, R., and Whyte, H. E. (2002). The importance of head growth patterns in predicting the cognitive abilities and literacy skills of small-for-gestational-age children. *Dev. Neuropsychol.* 22, 565–593. doi:10.1207/S15326942DN2203_2

Gmehlin, D., Thomas, C., Weisbrod, M., Walther, S., Pfuller, U., Resch, F., et al. (2011). Individual analysis of EEG background-activity within school age: impact of age and sex within a longitudinal data set. *Int. J. Dev. Neurosci.* 29, 163–170. doi:10.1016/j.ijdevneu.2010.11.005

Grieve, P. G., Isler, J. R., Izraelit, A., Peterson, B. S., Fifer, W. P., Myers, M. M., et al. (2008). EEG functional connectivity in term age extremely low birth weight infants. *Clin. Neurophysiol.* 119, 2712–2720. doi:10.1016/j.clinph.2008.09.020

Gross, J., Baillet, S., Barnes, G. R., Henson, R. N., Hillebrand, A., Jensen, O., et al. (2013). Good practice for conducting and reporting MEG research. *Neuroimage* 65, 349–363. doi:10.1016/j.neuroimage.2012.10.001

Hillebrand, A., and Barnes, G. R. (2003). The use of anatomical constraints with MEG beamformers. *Neuroimage* 20, 2302–2313. doi:10.1016/j.neuroimage.2003.07.031

Jensen, O., Kaiser, J., and Lachaux, J. P. (2007). Human gamma-frequency oscillations associated with attention and memory. *Trends Neurosci.* 30, 317–324. doi:10.1016/j.tins.2007.05.001

Kaufman, A. S., Kaufman, J. C., Balgopal, R., and McLean, J. E. (1996). Comparison of three WISC-III short forms: weighing psychometric, clinical, and practical factors. *J. Clin. Child Psychol.* 25, 97–105. doi:10.1207/s15374424jccp2501_11

Kostovic, I., and Jovanov-Milosevic, N. (2006). The development of cerebral connections during the first 20-45 weeks' gestation. *Semin. Fetal Neonatal Med.* 11, 415–422. doi:10.1016/j.siny.2006.07.001

Kostovic, I., and Judas, M. (2006). Prolonged coexistence of transient and permanent circuitry elements in the developing cerebral cortex of fetuses and preterm infants. *Dev. Med. Child Neurol.* 48, 388–393. doi:10.1017/S0012162206000831

Lee, P. A., Chernausek, S. D., Hokken-Koelega, A. C., and Czernichow, P. (2003). International small for gestational age advisory board consensus development conference statement: management of short children born small for gestational age, April 24-October 1, 2001. *Pediatrics* 111, 1253–1261. doi:10.1542/peds.111.6.1253

LoBello, S. G. (1991). A short form of the Wechsler preschool and primary scale of intelligence-revised. *J. Sch. Psychol.* 29, 229–236. doi:10.1016/0022-4405(91)90004-B

Lundgren, E. M., Cnattingius, S., Jonsson, B., and Tuvemo, T. (2001). Intellectual and psychological performance in males born small for gestational age with and without catch-up growth. *Pediatr. Res.* 50, 91–96. doi:10.1203/00006450-200107000-00017

Mallard, C., Loeliger, M., Copolov, D., and Rees, S. (2000). Reduced number of neurons in the hippocampus and the cerebellum in the postnatal guinea-pig following intrauterine growth-restriction. *Neuroscience* 100, 327–333. doi:10.1016/S0306-4522(00)00271-2

Marshall, P. J., Bar-Haim, Y., and Fox, N. A. (2002). Development of the EEG from 5 months to 4 years of age. *Clin. Neurophysiol. Off. J. Int. Fed. Clin. Neurophysiol.* 113, 1199–1208. doi:10.1016/S1388-2457(02)00163-3

Martinussen, M., Fischl, B., Larsson, H. B., Skranes, J., Kulseng, S., Vangberg, T. R., et al. (2005). Cerebral cortex thickness in 15-year-old adolescents with low birth weight measured by an automated MRI-based method. *Brain* 128, 2588–2596. doi:10.1093/brain/awh610

Martinussen, M., Flanders, D. W., Fischl, B., Busa, E., Lohaugen, G. C., Skranes, J., et al. (2009). Segmental brain volumes and cognitive and perceptual correlates in 15-year-old adolescents with low birth weight. *J. Pediatr.* 155, 848–853. doi:10.1016/j.jpeds.2009.06.015

Ment, L. R., Hirtz, D., and Huppi, P. S. (2009). Imaging biomarkers of outcome in the developing preterm brain. *Lancet Neurol.* 8, 1042–1055. doi:10.1016/S1474-4422(09)70257-1

Miskovic, V., Schmidt, L. A., Boyle, M., and Saigal, S. (2009). Regional electroencephalogram (EEG) spectral power and hemispheric coherence in young adults born at extremely low birth weight. *Clin. Neurophysiol.* 120, 231–238. doi:10.1016/j.clinph.2008.11.004

Okumura, A., Kubota, T., Tsuji, T., Kato, T., Hayakawa, F., and Watanabe, K. (2006). Amplitude spectral analysis of theta/alpha/beta waves in preterm infants. *Pediatr. Neurol.* 34, 30–34. doi:10.1016/j.pediatrneurol.2005.06.005

Olde Dubbelink, K. T. E., Stoffers, D., Deijen, J. B., Twisk, J. W. R., Stam, C. J., and Berendse, H. W. (2013). Cognitive decline in Parkinson's disease is associated with slowing of resting-state brain activity: a longitudinal study. *Neurobiol. Aging* 34, 408–418. doi:10.1016/j.neurobiolaging.2012.02.029

Ozdemir, O. M., Ergin, H., and Sahiner, T. (2009). Electrophysiological assessment of the brain function in term SGA infants. *Brain Res.* 1270, 33–38. doi:10.1016/j.brainres.2009.03.008

Rees, S., Harding, R., and Walker, D. (2008). An adverse intrauterine environment: implications for injury and altered development of the brain. *Int. J. Dev. Neurosci.* 26, 3–11. doi:10.1016/j.ijdevneu.2007.08.020

Rehn, A. E., Van Den, B. M., Copolov, D., Briscoe, T., Lambert, G., and Rees, S. (2004). An animal model of chronic placental insufficiency: relevance to neurodevelopmental disorders including schizophrenia. *Neuroscience* 129, 381–391. doi:10.1016/j.neuroscience.2004.07.047

Saenger, P., Czernichow, P., Hughes, I., and Reiter, E. O. (2007). Small for gestational age: short stature and beyond. *Endocr. Rev.* 28, 219–251. doi:10.1210/er.2006-0039

Schmid, R. G., Tirsch, W. S., and Scherb, H. (2002). Correlation between spectral EEG parameters and intelligence test variables in school-age children. *Clin. Neurophysiol.* 113, 1647–1656. doi:10.1016/S1388-2457(02)00212-2

Smit, D. J. A., Geus, E. J. C., de Nieuwenhuijzen, M. E., van de Beijsterveldt, C. E. M., van Baal, G. C. M., van Mansvelder, H. D., et al. (2011). Scale-free modulation of resting-state neuronal oscillations reflects prolonged brain maturation in humans. *J. Neurosci.* 31, 13128–13136. doi:10.1523/JNEUROSCI.1678-11.2011

Strauss, R. S. (2000). Adult functional outcome of those born small for gestational age: twenty-six-year follow-up of the 1970 British Birth Cohort. *JAMA* 283, 625–632. doi:10.1001/jama.283.5.625

Thatcher, R. W., North, D., and Biver, C. (2005). EEG and intelligence: relations between EEG coherence, EEG phase delay and power. *Clin. Neurophysiol.* 116, 2129–2141. doi:10.1016/j.clinph.2005.04.026

Toft, P. B., Leth, H., Ring, P. B., Peitersen, B., Lou, H. C., and Henriksen, O. (1995). Volumetric analysis of the normal infant brain and in intrauterine growth retardation. *Early Hum. Dev.* 43, 15–29. doi:10.1016/0378-3782(95)01657-O

Tolsa, C. B., Zimine, S., Warfield, S. K., Freschi, M., Sancho, R. A., Lazeyras, F., et al. (2004). Early alteration of structural and functional brain development in premature infants born with intrauterine growth restriction. *Pediatr. Res.* 56, 132–138. doi:10.1203/01.PDR.0000128983.54614.7E

Uhlhaas, P. J., Roux, F., Singer, W., Haenschel, C., Sireteanu, R., and Rodriguez, E. (2009). The development of neural synchrony reflects late maturation and restructuring of functional networks in humans. *Proc. Natl. Acad. Sci. U.S.A.* 106, 9866–9871. doi:10.1073/pnas.0900390106

Volpe, J. J. (2000). Overview: normal and abnormal human brain development. *Ment. Retard. Dev. Disabil. Res. Rev.* 6, 1–5. doi:10.1002/(SICI)1098-2779(2000)6:1<1::AID-MRDD1>3.3.CO;2-A

Vrba, J., Anderson, G., Betts, K., Burbank, M. B., Cheung, T., and Cheyne, D. (1999). *151-Channel Whole-Cortex MEG System for Seated or Supine Positions. Recent Advances in Biomagnetism.* Sendai: Tohoku University, 93–96.

Whitham, E. M., Pope, K. J., Fitzgibbon, S. P., Lewis, T., Clark, C. R., Loveless, S., et al. (2007). Scalp electrical recording during paralysis: quantitative evidence that EEG frequencies above 20 Hz are contaminated by EMG. *Clin. Neurophysiol.* 118, 1877–1888. doi:10.1016/j.clinph.2007.04.027

Conflict of Interest Statement: The authors declare that the research was conducted in the absence of any commercial or financial relationships that could be construed as a potential conflict of interest.

Received: 05 March 2013; accepted: 04 September 2013; published online: 24 September 2013.

Citation: Boersma M, de Bie HMA, Oostrom KJ, van Dijk BW, Hillebrand A, van Wijk BCM, Delemarre-van de Waal HA and Stam CJ (2013) Resting-state oscillatory activity in children born small for gestational age: an MEG study. Front. Hum. Neurosci. 7:600. doi: 10.3389/fnhum.2013.00600

This article was submitted to the journal Frontiers in Human Neuroscience.